Final Report 1998-12

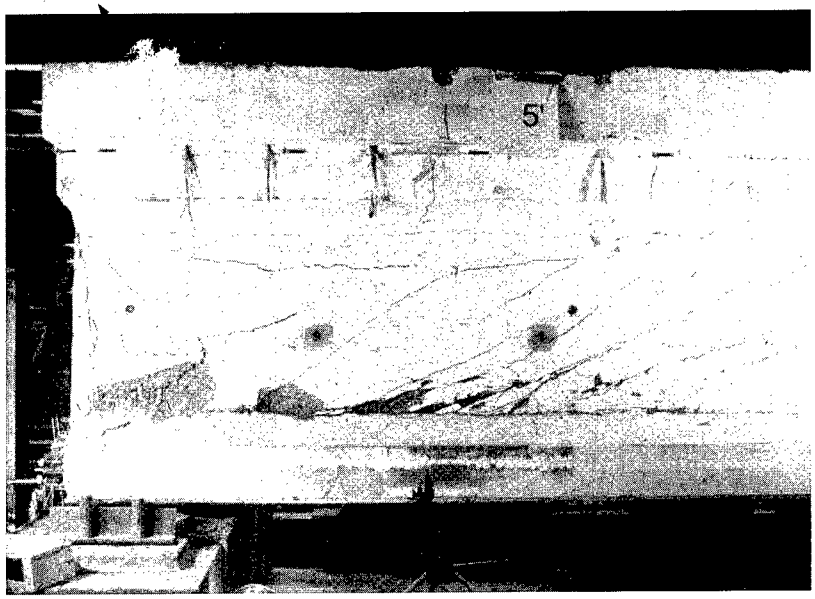

Shear Capacity of High-Strength Concrete Pre-stressed Girders

PB99-104622

UNIVERSITY OF MINNESOTA
CENTER FOR
TRANSPORTATION
STUDIES

This research was made possible with the support and contributions from the Minnesota Prestress Association. Many of its members took a role in the fabrication and testing of the girder specimens.

Technical Report Documentation Page

1. Report No.	2.	3. Recipient's Accession No.
MN/RC - 1998/12		

4. Title and Subtitle	5. Report Date
SHEAR CAPACITY OF HIGH-STRENGTH CONCRETE PRESTRESSED GIRDERS	May 1998
	6.

7. Author(s)	8. Performing Organization Report No.
David A. Cumming Carol K. Shield Catherine E. French	

9. Performing Organization Name and Address	10. Project/Task/Work Unit No.
Department of Civil Engineering University of Minnesota 500 Pillsbury Dr. S.E. Minneapolis, MN 55455-0220	11. Contract (C) or Grant (G) No. (C) 69098 TOC # 83

12. Sponsoring Organization Name and Address	13. Type of Report and Period Covered
Minnesota Department of Transportation 395 John Ireland Boulevard Mail Stop 330 St. Paul, Minnesota 55155	Final Report 1993-1998
	14. Sponsoring Agency Code

15. Supplementary Notes

16. Abstract (Limit: 200 words)

As part of a project at the University of Minnesota to investigate the application of high-strength concrete in prestressed girders, four shear tests were performed on high-strength concrete prestressed girders.

Originally constructed in August 1993, the girders, Minnesota Department of Transportation (Mn/DOT) 45M sections were 45 inches deep. Each girder utilized 46 0.6-inch diameter prestressing strands on 2-inch centers. The girders were designed assuming a 28-day compressive strength of 10,500 psi. Later, a 4-foot-wide and 9-inch-thick composite concrete deck was added to each girder using unshored construction techniques.

The shear test results were compared with predicted results from ACI 318-95 Simplified Method, ACI 318-95 Detailed Method (AASHTO 1989), Modified ACI 318-95 Procedure, Modified Compression Field Theory (AASHTO LRFD 1994), Modified Truss Theory, Truss Theory, Horizontal Shear Design (AASHTO 1989), and Shear Friction (AASHTO LRFD 1994). The calculated shear capacities were in all cases conservative compared to the actual shear capacity.

17. Document Analysis/Descriptors	18. Availability Statement
high performance concrete shear prestressed bridge girders	No restrictions. Document available from: National Technical Information Services, Springfield, Virginia 22161

19. Security Class (this report)	20. Security Class (this page)	21. No. of Pages	22. Price
Unclassified	Unclassified	361	

SHEAR CAPACITY OF HIGH-STRENGTH CONCRETE PRESTRESSED GIRDERS

Final Report

Prepared by:

David A. Cumming
Catherine E. French
Carol Shield

Department of Civil Engineering
University of Minnesota

May 1998

Published by:

Minnesota Department of Transportation
Office of Research Services
Mail Stop 330
395 John Ireland Boulevard
St. Paul, MN 55155

Acknowledgments

The sponsors of the project were the Minnesota Department of Transportation (Mn/DOT), the Minnesota Precast Association (MnPA), the National Science Foundation, the University of Minnesota-Center for Transportation Studies, and the Precast Prestressed Concrete Institute. In addition, the following companies provided goods and services: Elk River Concrete Products fabricated the test girders; LeFebvre & Sons Trucking transported the specimens; and Truck Crane Service Company lifted and maneuvered the test specimens into testing position. In addition, the following University of Minnesota personnel helped out with the project: Tess Ahlborn, Jeffrey Kielb, Paul Bergson, Mike Sondag and Matt Crawford.

Table of Contents

List of Tables

List of Figures

Nomenclature

a	=	horizontal distance from west end to center of support
A_1	=	horizontal distance from west end to applied point load
A_{cs}	=	cross-sectional area of a concrete strut in Strut-and-Tie Model
A_{cv}	=	area of the concrete engaged in shear transfer by AASHTO LRFD 1994 in Interface Shear Model
A_g	=	area of gross girder cross section
A_{gc}	=	area of gross composite cross section
A_{mt}	=	minimum area of required ties for a composite section in AASHTO 1989
A_p	=	area of a prestressing strand
A_{ps}	=	total area of prestressed steel on the flexural tension side of the member, which is reduced if the given section is within the transfer or development length regions
A_{psd}	=	total area of prestressed steel on the flexural tension side of the member, which is reduced if the given section is within the development length region
A_{pst}	=	total area of prestressed steel on the flexural tension side of the member, which is reduced if the given section is within the transfer length region
A_s	=	area of steel of nonprestressed reinforcing steel on the flexural tension side of member, which is reduced for any lack of full development at the given section in Modified Compression Field Theory
A_{st}	=	total area of longitudinal mild steel reinforcement in Strut-and-Tie Model
A_v	=	cross-sectional area of the stirrup
A_{vb}	=	cross-sectional area of the bursting stirrup
A_{vf}	=	area of ties crossing the interface in Interface Shear Model
b	=	horizontal distance from east end to center of support
b_d	=	width of composite deck
b_f	=	width of composite interface
b_m	=	width of the web at the given reference height in Modified ACI Procedure
b_v	=	effective web width taken as the minimum web width within the depth d_v in Modified Compression Field Theory
b_w	=	width of the web
C	=	resultant compressive force
c	=	depth from the top of the girder to the neutral axis
C_d	=	compressive force in the deck
C_f	=	compressive force in the girder
c_f	=	cohesion factor by AASHTO LRFD 1994 in Interface Shear Model
C_h	=	compressive force in the deck haunch
$CorrW$	=	amount of reduction in deflection for West LVDT
$CorrE$	=	amount of reduction in deflection for East LVDT

cs_1 = critical section for ACI Simplified Method, ACI Detailed Method, Modified ACI Procedure, Modified Truss, and Horizontal Shear AASHTO 1989

cs_2 = critical section for Modified Compression Field Theory

d = distance from the extreme compression fiber to the centroid of the longitudinal tension reinforcement of the composite section, but not less than $0.80h$ for prestressed members

d_b = diameter of a prestressing strand

d_c = distance from extreme compression fiber to the resultant compression force

d_p = distance from extreme compression fiber to centroid of the prestressed reinforcement

d_v = flexural lever arm which is the distance between the resultant tension force and resultant compressive force and need not be taken less than $0.9d$ in Modified Compression Field Theory and the Truss Model

$d.f.$ = dead load factor

e = eccentricity from the center of gravity of the gross girder cross section to the centroid of the prestressing strands

$EastCorr$ = corrected deflection on the long shear span

$EastDefl$ = vertical displacement measured by the east LVDT on the long shear span

$EastLVDT$ = horizontal distance from the west end to the east LVDT

E_c = modulus of elasticity of concrete for the girder

E_{cd} = modulus of elasticity of concrete for the deck

E_p = modulus of elasticity of prestressing steel

E_s = modulus of elasticity of nonprestressed reinforcing bars in Modified Compression Field Theory

f_c' = compressive strength of the concrete of the girder

f_{cd}' = compressive strength of the concrete of the deck

f_{cu} = limiting concrete compressive stress in Strut-and-Tie Model

f_d = tensile stress due to unfactored dead load, at the extreme fiber of the given cross section where tensile stress is caused by externally applied loads in ACI Detailed Method

F_e = factor to reduce the strain, ε_x, in the concrete by including an extra term for concrete resistance in Modified Compression Field Theory

f_{pc} = compressive stress at the neutral axis due to effective prestressing force

f_{pcm} = compressive stress at the centroid of the prestressed reinforcement in Modified Compression Field Theory

f_{pd} = average compressive stress in the concrete at the depth of interest due to effective prestressing force and due to applied flexural stresses in Modified ACI Procedure

f_{pe} = compressive stress in the concrete due to the effective prestressing force at the extreme fiber of the given cross section where tensile stress is caused by externally applied loads in ACI Detailed Method

f_{pg} = compressive stress in the concrete at the depth of interest due to applied loads in rosette calculations

f_{pi} = compressive stress in the concrete at the depth of interest due to self weight and prestress without applied loads in rosette calculations

f_{pj} = compressive stress in the concrete at the depth of interest due to self weight, prestress, and applied loads in rosette calculations

f_{po} = stress in the prestressing steel when the stress in the surrounding concrete is zero at the centroid of the prestressed reinforcement in Modified Compression Field Theory

f_{ps} = stress in prestressing reinforcement

f_{pu} = ultimate tensile strength of prestressing steel

F_s = force in stirrup in Truss Model

F_{s8} = yield strength of the eighth stirrup in Interface Shear Model

F_{s9} = yield strength of the ninth stirrup in Interface Shear Model

f_{se} = prestressing stress after all losses

f_{si} = initial prestressing stress

f_t = principal diagonal tension stress in the web of the member

f_y = yield strength of the stirrups

f_{yb} = yield strength of the bursting stirrups

g_8 = horizontal distance from the eighth stirrup to the point load in Interface Shear Model

g_9 = horizontal distance from the ninth stirrup to the point load in Interface Shear Model

g_i = horizontal length of interface between web and lower flange in Interface Shear Model

$g.l.$ = total original girder length

h = depth of the composite section

h_d = height of the deck

h_h = height of the haunch

$h.d.$ = distance to hold down point from end

I_g = gross moment of inertia of the girder cross section

I_{gc} = gross moment of inertia of the composite cross section

j_A = vertical location from the bottom for moment calculations in Interface Shear Model

j_C = vertical distance from resultant compressive force to the top of the web in Interface Shear Model

j_i = location of web and lower flange interface measured from the bottom in Interface Shear Model

j_T = vertical distance from resultant tensile force to the top of the web in Interface Shear Model

K = beneficial effect of the prestressing force on the shear cracking load before diagonal cracking in Modified Truss Model

k = factor for type of prestressing steel

l = specimen length between supports

l_1 = length of prestressing strand debonding which was equal to 0 ft.

l_2 = length of prestressing strand debonding which was equal to 2 ft.

l_3 = length of prestressing strand debonding which was equal to 4 ft.

l_4 = length of prestressing strand debonding which was equal to 12 ft.

l_5 = length of prestressing strand debonding which was equal to 20 ft.

l_d = development length of prestressing strand

l_t = transfer length of prestressing strand

$l.f.$ = live load factor

M_{cr} = moment causing flexural cracking at the given cross section due to externally applied loads in ACI Detailed Method

M_{deck} = moment caused by the self weight of the deck

M_{gird} = moment caused by the self weight of the girder without deck

M_{max} = maximum factored moment at the given cross section due to externally applied loads in ACI Detailed Method

M_{pt} = moment caused by the applied point load

M_u = factored moment at the given cross section

n = number of stirrups in ACI 318-95 Steel Contribution Derivation

$NeoDefl$ = vertical displacement measured by the LVDT monitoring the neoprene pad

$NeoLVDT$ = horizontal distance from the west end to the LVDT at the neoprene support

N_u = applied factored axial force which is taken as positive if compressive in Modified Compression Field Theory

P = horizontal component of effective prestressing force at the given cross section

P_1 = first point live load

P_c = permanent net compressive force normal to the shear plane by AASHTO LRFD 1994 in Interface Shear Model

P_n = strength of struts and ties in Strut-and-Tie Model

$p.l.$ = total prestressing losses

q_{d1} = effective quantity of draped strands

q_{dd} = effective quantity of draped strands based on development length

q_{dn} = total effective quantity of straight strands based on development length

q_{dn1} = effective quantity of straight strands with no debonding based on development length

q_{dn2} = effective quantity of straight strands debonded for 2 ft. based on development length

q_{dn3} = effective quantity of straight strands debonded for 4 ft. based on development length

q_{dn4} = effective quantity of straight strands debonded for 12 ft. based on development length

q_{dn5} = effective quantity of straight strands debonded for 20 ft. based on development length

Q_{gc} = first moment of composite area with respect to a given depth in the cross section in Modified ACI Procedure

q_{n1} = effective quantity of straight strands with no debonding bonding

q_{n2} = effective quantity of straight strands debonded for 2 ft.

q_{n3} = effective quantity of straight strands debonded for 4 ft.

q_{n4} = effective quantity of straight strands debonded for 12 ft.

q_{n5} = effective quantity of straight strands debonded for 20 ft.

q_{td} = effective quantity of draped strands based on transfer length

q_{tn} = total effective quantity of straight strands based on transfer length

q_{tn1} = effective quantity of straight strands with no debonding based on transfer length

q_{tn2} = effective quantity of straight strands debonded for 2 ft. based on transfer length

q_{tn3} = effective quantity of straight strands debonded for 4 ft. based on transfer length

q_{tn4} = effective quantity of straight strands debonded for 12 ft. based on transfer length

q_{tn5} = effective quantity of straight strands debonded for 20 ft. based on transfer length

R_1 = factored left support reaction

s = center-to-center spacing of stirrups

s_b = center-to-center spacing of bursting stirrups

$SuppEnd$ = horizontal distance from the west end to the roller support

s_x = crack spacing parameter in Modified Compression Field Theory

$s.l.$ = total specimen length

T = resultant tensile force

u = horizontal distance in which stirrups yield, based on the depth of the member

U_{ACI} = failure shear divided by the ultimate ACI Detailed Method shear capacity which includes concrete, draping, and stirrup contributions

U_{cw} = cracking shear near the support in the web divided by the ACI Detailed Method shear capacity of the concrete in this region

U_{ci} = cracking shear to start flexural cracking divided by the ACI Detailed Method shear capacity of the concrete in this region

U_{cr} = lowest cracking shear divided by the lowest ACI Detailed Method shear capacity of the concrete at the corresponding section

U_{MCFT} = failure shear divided by the predicted ultimate shear capacity according to Modified Compression Field Theory which includes concrete, draping, and stirrup contributions

v = factored shear stress in Modified Compression Field Theory

V_{bond} = shear capacity based on anchorage bond failure used in Modified Compression Field Theory

V_c = shear carried by the concrete

V_{ci} = nominal shear strength provided by concrete when diagonal cracking results from combined shear and moment (flexure-shear cracking) in ACI Detailed Method

V_{cr} = shear capacity provided by the concrete to cause cracking in Modified Truss Model

V_{cw} = nominal shear strength provided by concrete when diagonal cracking results from excessive principal tensile stress in the web (web-shear cracking) in ACI Detailed Method

V_d = shear force at the given cross section due to unfactored self weight and unfactored superimposed dead loads

V_i = factored shear force at the given cross section due to externally applied loads occurring simultaneously with M_{max} and M_{cr} in ACI Detailed Method

V_{is} = interface shear from the Interface Shear Model

V_{mod} = nominal shear strength provided by concrete when diagonal cracking results from excessive principal tensile stress in the web in Modified ACI Procedure

V_n = nominal shear resistance of the section considered

V_{nh} = nominal horizontal shear resistance of the section considered in AASHTO 1989

V_p = vertical component of effective prestressing force at the given cross section

V_{pt} = shear force at the given cross section due to the applied point load

V_s = shear carried by the stirrups

V_{sf} = shear capacity by Shear Friction in Interface Shear Model

V_{truss} = shear capacity provided by the steel in Modified Truss Model

V_u = shear force due to the factored loads

V_v = interface shear capacity provided when ties are greater than minimum required in AASHTO 1989

w_{dead} = the total of dead loads and self weight of deck and girder

w_{deck} = self weight of deck

w_{dl} = distributed dead load on the composite section

WestCorr = corrected deflection on the short shear span

WestDefl = vertical displacement measured by the west LVDT on the short shear span

WestLVDT= horizontal distance from the west end to the west LVDT

w_{gird} = self weight of girder

w_{ll} = distributed live load on the composite section

$w.s.$ = horizontal width of support

x = horizontal distance from the west end to a given location

y_d = distance from centroid of the draped prestressed reinforcement measured from the extreme tension fiber

y_{d1} = distance from centroid of the draped prestressed reinforcement measured from the extreme tension fiber at the end

y_{d2} = distance from centroid of the draped prestressed reinforcement measured from the extreme tension fiber at the mid-span of the original girder

y_m = distance from a given reference height measured from the extreme tension fiber in Modified ACI Procedure

y_n = resultant distance from centroid of the straight strands measured from the extreme tension fiber

y_{n1} = distance from centroid of the straight strands with no debonded strands measured from the extreme tension fiber

y_{n2} = distance from centroid of the straight strands debonded for 2 ft. measured from the extreme tension fiber

y_{n3} = distance from centroid of the straight strands debonded for 4 ft. measured from the extreme tension fiber

y_{n4} = distance from centroid of the straight strands debonded for 12 ft. measured from the extreme tension fiber

y_{n5} = distance from centroid of the straight strands debonded for 20 ft. measured from the extreme tension fiber

y_t = distance from centroidal axis of the gross girder cross section measured from the extreme tension fiber

y_{tc} = distance from centroidal axis of the gross composite cross section measured from the extreme tension fiber

z = effective truss depth between flexural tension and flexural compression arms, taken as $0.9d$, where d is not less than $0.8h$ in Modified Truss Model

β = factor indicating the ability of diagonally cracked concrete to transmit tension in Modified Compression Field Theory

β_1 = modification factor for neutral axis depth to determine depth of compression block

ε_a = experimental strain in the horizontal direction in rosette calculations

ε_{ag} = theoretical strain in the horizontal direction due to only applied load in rosette calculations

ε_{ai} = corrected experimental strain in the horizontal direction in rosette calculations

ε_{aj} = theoretical strain in the horizontal direction due to self weight, prestress, and applied load in rosette calculations

ε_b = experimental strain at 45° in rosette calculations

ε_{bg} = theoretical strain at 45° due to only applied load in rosette calculations

ε_{bi} = corrected experimental strain at 45° in rosette calculations

ε_{bj} = theoretical strain at 45° due to self weight, prestress, and applied load in rosette calculations

ε_c = experimental strain in the vertical direction in rosette calculations

ε_{cc} = corrected experimental principal compressive strain in rosette calculations

ε_{ce} = experimental principal compressive strain in rosette calculations

ε_{cg} = theoretical principal compressive strain due to only applied load in rosette calculations

ε_{cgg} = theoretical strain in the vertical direction due to only applied load in rosette calculations

ε_{cii} = corrected experimental strain in the vertical direction in rosette calculations

ε_{cj} = theoretical principal compressive strain due to self weight, prestress, and applied load in rosette calculations

ε_{cjj} = theoretical strain in the vertical direction due to self weight, prestress, and applied load in rosette calculations

ε_{ct} = theoretical principal compressive strain due to only applied load in rosette calculations

ε_{tc} = corrected experimental principal tensile strain in rosette calculations

ε_{te} = experimental principal tensile strain in rosette calculations

ε_{tg} = theoretical principal tensile strain due to only applied load in rosette calculations

ε_{tj} = theoretical principal tensile strain due to self weight, prestress, and applied load in rosette calculations

ε_x = longitudinal strain in the reinforcement on the flexural tension side of the member in Modified Compression Field Theory

ε_{x1} = longitudinal strain in the reinforcement on the flexural tension side of the member for first iteration in Modified Compression Field Theory

ε_{x2} = longitudinal strain in the reinforcement on the flexural tension side of the member for two iteration in Modified Compression Field Theory

ε_{x3} = longitudinal strain in the reinforcement on the flexural tension side of the member for third iteration in Modified Compression Field Theory

ϕ = shear strength reduction factor

μ = coefficient of friction by AASHTO LRFD 1994 in Interface Shear Model

θ = angle of diagonal compressive stresses, or angle of inclination of the compression diagonals at failure in Modified Compression Field Theory

θ_1 = crack angle for first iteration in Modified Compression Field Theory

θ_2 = crack angle for second iteration in Modified Compression Field Theory

θ_3 = crack angle for second iteration in Modified Compression Field Theory

θ_4 = final crack angle in Modified Compression Field Theory

θ_{aci} = crack angle in ACI 318-95 Stirrup Contribution Derivation

θ_c = angle of principal compression from the corrected experimental data in rosette calculations

θ_e = angle of principal compression from the experimental data in rosette calculations

θ_g = theoretical angle due to only applied load in rosette calculations

θ_{ism} = crack angle in the web near the applied load in Interface Shear Model

θ_j = theoretical angle due to self weight, prestress, and applied load in rosette calculations

θ_{mtm} = crack angle in Modified Truss Model

θ_{tm} = minimum crack angle in Truss Model

ρ = web reinforcement ratio

τ_g = shear stress in the concrete to applied loads in rosette calculations

τ_i = shear stress in the concrete to self weight and prestress without applied loads in rosette calculations

τ_j = shear stress in the concrete to self weight, prestress, and applied loads in rosette calculations

Executive Summary

Four shear tests were performed on high-strength concrete prestressed girders. This work represents part of an overall project at the University of Minnesota to investigate the application of high-strength concrete to prestressed girders.

Two girders, Mn/DOT 45M sections, were 45 in. deep, originally constructed in August, 1993. Each girder was reinforced with forty-six 0.6 in. diameter prestressing strands on 2 in. centers. The girders were designed assuming a 28-day compressive strength of 10,500 psi. Later, a 4 ft. wide, 9 in. thick composite concrete deck was added to each girder using unshored construction techniques. Prior to shear testing, each girder had been used to evaluate flexural behavior under repeated load, as well as ultimate flexural behavior. After the flexural tests, the two girders were cut in half to provide four shear specimens. Each girder end was instrumented with stirrup strain gages and both internal and external concrete rosette gages to investigate the shear behavior. In addition, linear variable differential transformers (LVDTs) were used to monitor strand slip behavior and girder deflections.

Test variables for the four shear tests included mix design, end strand pattern, and stirrup anchorage. Two specimens were cast from the same limestone aggregate concrete mix, while the other two specimens were cast using a glacial gravel combined with microsilica mix. To relieve end stresses, one of the glacial gravel specimens had 12 draped strands. The other three specimens used 4 draped strands with 8 debonded strands to relieve end stresses. One of the limestone specimens was constructed using standard straight leg Mn/DOT "U" stirrups, while the other three specimens used modified "U" stirrups with leg extensions to increase anchorage.

The shear test results were compared with predicted results from ACI 318-95 Simplified Method, ACI 318-95 Detailed Method, Modified ACI 318-95 Procedure, Modified Compression Field Theory, Modified Truss Theory, Truss Theory, Horizontal Shear Design, and Shear Friction. Based on ACI 318-95 Detailed Method, the girder specimens were expected to carry loads of 340 kips in the case of the specimens with the debonded strands and 380 kips for specimen which contained the 12 draped strands at the end not considering any additional resistance provided by the embedded reinforcement used for handling.

The limestone specimens actually achieved strengths from 500 to 520 kips. The limestone

girder specimens developed diagonal shear cracks which eventually extended into horizontal cracks at the interface between the web and the bottom flange. The enhanced anchorage, provided by the large amount of prestressing reinforcement in the bottom flange, limited the variation in results among the specimen reinforced with standard U-shaped stirrups and the specimens with modified U-shaped stirrups. Both types of stirrups were observed to yield during the tests.

The glacial gravel girders incorporating microsilica exhibited even greater strengths. The girder specimen with the modified U-stirrups and debonded strands carried a load of 614 kips before failure. The investigators were unable to develop a shear failure in the specimen with 12 draped strands with the Universal Testing Machine in the Structural Engineering Laboratory at the University of Minnesota. The girder exhibited nearly elastic behavior even following the peak load level of 676 kips. The glacial gravel specimens eventually developed diagonal cracks which extended towards the support reaction.

The increased capacity of the glacial gravel specimens was attributed to the roughness of the failure surface developed by this mix. The failure of the limestone mix tended to develop relatively smooth planes of failure, whereas the glacial gravel girder tended to have a more uneven failure plane due to the fracture passing around some of the aggregate rather than through all of the aggregate particles. This behavior would tend to increase the aggregate interlock in the case of the glacial gravel girders. It is believed that the compression stresses generated by the large numbers of strand in the bottom flange helped to confine each other, thereby inhibiting strand anchorage failure.

Chapter 1 - Introduction

1.1 Shear Strength Background

The shear strength of prestressed members is an important design consideration. The shear force is most significant near the supports of the member. For simply supported members, the locations of the high-shear forces are usually within the transfer or the development zones of the pretensioned strands. Near the supports, high-shear stresses may cause shear-bond failures and lead to the complete girder failure. Models and equations have been developed to include shear-bond failure and typical shear failure due to the result of a combination of shear and moment. Only limited research has been conducted on high-strength concrete in shear. Therefore, research of prestressed girders with high-strength concrete is important to provide understanding of the girder's response to shear and to verify models, theories, and equations for safe design.

There are several reasons why current shear provisions must be examined or used cautiously for high-strength concrete. Concrete strength is a primary variable in shear capacity calculations, and ACI 318-95 [1] (AASHTO 1989 [2]) shear equations are based on empirical test results which were derived from test structures with concrete strengths less than 6000 psi. Extrapolating empirical equations for concrete with twice the compressive strength of that used in the original empirical studies may be inaccurate.

There has been dissatisfaction with the current method of shear-capacity calculations due to its complexity and lack of a mechanistic basis. Over the last couple of years, a number of shear models have been proposed as replacements for the current models. With the behavioral models, the engineer should be able to visualize the effects of forces acting on the member, resulting in a simpler and more effective design process. The proposed methods are based on the theory of plasticity and on truss models. These provide a visible flow of forces, as opposed to the current empirical methods or models, and need experimental verification to insure accuracy when used to predict the shear capacity of high-strength concrete.

1.2 High-Strength Concrete

Concrete with compressive strengths over 6000 psi are typically considered to be high strength. In recent years high-strength concrete has been produced at competitive prices. High-strength concrete improves the economy of pretensioned girder bridges by increasing allowable span lengths for standard sections or by reducing the number of girders required for a given bridge design.

The physical properties of high-strength concrete are slightly different than those of normal-strength concrete. High-strength concrete typically has smoother crack planes than does normal-strength concrete with fracture occurring through the coarse aggregate and the cement. In normal-strength concrete fracture occurs around the coarse aggregate with a rough plane of fracture. To ensure that the structural behavior is understood, high-strength concrete must be investigated.

1.3 Objectives

The ends of two full-scale prestressed girders were tested to investigate the applicability of current design codes. The main objective of this research was to investigate the mode of failure and the shear capacity of high-strength prestressed girders. Three variables were investigated including two different types of stirrup anchorage, two different high-strength concrete mixes, and two end strand patterns with different amounts of draping and debonding.

1.4 Organization of Report

Chapter 2 contains a literature review of relevant research. This review summarizes other studies of prestressed girders subjected to shear including both high-strength and normal-strength concrete.

Chapter 3 presents the methods and equations by which the shear capacity of the prestressed girders were calculated. Shear capacity models and equations include ACI 318-95 Simplified Method, ACI 318-95 Detailed Method (AASHTO 1989), Modified Compression Field Theory (AASHTO LRFD 1994 [3]), Modified Truss Model, Truss Model, Strut-and-Tie Model, Horizontal Shear Design (AASHTO 1989), and Shear Friction (AASHTO LRFD 1994).

Chapter 4 describes the test setup and includes a discussion of girder and deck materials, transportation, instrumentation, and testing procedures.

Chapter 5 presents the results from data collected from the four shear tests. Results include load-deflection response, crack patterns, stirrup strains, concrete strains, corrected concrete strains, principal compression angle, corrected principal compression angle, bursting stirrup strains, rupture strains in the concrete, strand slip information, and prestressing strands strains in the transfer region.

Chapter 6 presents a detailed comparison of the four shear tests. Each specimen was compared in terms of initial crack pattern, load-deflection curves, measured and predicted crack angles. In addition, the effects of the three shear test variables (stirrup anchorage, concrete mix, and prestressing configurations) are discussed. Each specimen was also compared with the models and theories presented in Chapter 3. Finally, the four specimens were compared with the results of other research.

Chapter 7 presents a final summary and conclusions from the four specimens tested in shear.

Six appendices present information not directly provided in the seven chapters. Appendix A offers a derivation of many models and theories used in Chapter 3. Appendix B presents the concrete cylinder test results which is presented in Chapter 4. Appendix C presents the nominal and measured specimen properties which were used to calculate the shear capacity. Appendix D gives and summarizes the assumptions in the models. Appendix E provides the sample calculations for the models in Chapter 3. Appendix F presents the notes taken during the four shear tests.

Chapter 2 - Literature Review

2.1 Introduction

This chapter summarizes research conducted by other investigators on prestressed members tested in shear. The organization of the chapter is in order of the year of publication. Each summary presents the major variables investigated, number of prestressed girders tested, failure modes, author discussion, and comparison with stated code(s). Table 2.1 shows a comparison of the girders tested grouped by author and some of the major testing parameters.

2.2 Bennett and Balasooriya

In 1971, Bennett and Balasooriya published findings of their testing of 26 prestressed I-beams [4]. Twenty-three beams were prestressed, and three beams were nonprestressed. The concrete strength, cross section, web reinforcement, prestressing force, and shear span were varied. The compressive strengths ranged from 4420 to 6460 psi. The cross section depths of Series A-E and Series F were 10 in. and 18 in., respectively. The web reinforcement ratio was defined as stirrup steel area divided by both web width and stirrup spacing. This ratio varied from 1.64% to 4.90%. The maximum prestressing force for Series A-E was 83 kips and for Series F was 104 kips after losses.

During testing, they found that the appearance of the first cracks occurred when the calculated principal tensile stress was approximately equal to the cylinder splitting strength of the concrete. The cracks were more steeply inclined in the beams with lower prestressing force. The inclination angle of cracking, which ranged from 18° to 48°, was greater than the theoretical angle for an uncracked section by an average of 14%.

Failure of 20 of the 26 beams occurred primarily by crushing of the concrete struts. Warning of impending failure was given by initial flaking of the concrete in the upper half of the web in the central part of the shear span at 85% to 98% of the ultimate load. The method of analyzing the shear strength included the ACI 318-63 Code; however, a table with ACI calculated capacities was not given.

2.3 Elzanaty, Nilson, and Slate

In 1986, Elzanaty, Nilson, and Slate published an extensive investigation of the effects of using high-strength concrete on the shear strength of prestressed concrete beams [5]. They compared the test results to the strength predicted by the ACI 318-83 Detailed Method which is the same procedure described in the ACI 318-95 Code and AASHTO 1989. A total of 34 beams were tested. Seventeen beams had a cross section that was designed to fail due to web-shear cracking, and the other seventeen beams had a cross section that was designed to fail due to flexure-shear cracking. The web-shear members were 18 in. deep with 2 in. thick webs. The flexure-shear members were 14 in. deep with 3 in. thick webs. Also, 18 of these girders were cast without web reinforcement, and the other 16 girders had web reinforcement.

The compressive strength, shear span-to-depth ratio, effective prestressing force, and shear reinforcement ratio were varied. The compressive strengths ranged from 5800 to 11,400 psi. The shear span-to-depth ratio varied from 2.9 to 7.8. The effective prestressing force after losses varied from 97 kips to 138 kips. The shear reinforcement ratio ranged from no reinforcement to 0.79%.

In all beams of the web-shear design, diagonal cracks formed suddenly. During testing, diagonal cracks propagated immediately throughout the depth of the web, usually to points on the web-flange intersection. The cracks ran horizontally from the loading point at the top and to the support at the bottom.

The ACI Code equations for web-shear and flexure-shear were conservative in predicting the shear strength of all the tested beams. The typical observed angle of inclination of the critical diagonal cracks was from 20° to 35° for web-shear and for flexure-shear cracks. The ratio of test-to-predicted values increased with compressive strength of the concrete; whereas, the ratio of test-to-predicted diagonal cracking loads decreased with the increase of prestressing force.

Elzanaty, Nilson, and Slate stated that varying the prestressing force may change the type of shear failure. Increasing the prestressing force will increase the flexural cracking load and the flexure-shear cracking load. Also, the web-shear cracking load increases but at a slower rate. Therefore, with increasing prestressing force, a change failure mode from flexure-shear cracking

to web-shear cracking may take place. In addition, increase in prestressing force may further change the mode of failure from web-shear cracking to web crushing.

2.4 Maruyama and Rizkalla

In 1988, Maruyama and Rizkalla published results from shear tests of 11 single tees with thin-webs [6]. Nine single tees were made of prestressed concrete, and two single tees were made of nonprestressed concrete. The experimental program investigated the behavior of prestressed and nonprestressed concrete beams with low shear span-to-depth ratios. Also, various types of shear reinforcement and the effect of development length were investigated. Compressive strength varied from 5520 to 6480 psi. The shear reinforcement ratios varied from no shear reinforcement to 0.38%.

Strand slip preceded the maximum applied load in all nine of the prestressed concrete beams. After strand slip, all beams exhibited extensive deflection without reduction of the load-carrying capacity. The authors stated that all beams failed prematurely due to slippage of the prestressing strands; although, the table of tested and predicted values shows all the specimens failed at a higher load than predicted by ACI 318-83(95) Detailed Method.

2.5 Kaufman and Ramirez

In 1988, Kaufman and Ramirez published their investigation of six full-scale high-strength concrete prestressed girders [7]. Four Type I AASHTO I-beams and two Type II AASHTO I-beams were tested. The beams were designed and analyzed according to ACI 318-83(95) Detailed Method and tested as noncomposite members.

Many parameters were studied including compressive strength, shear span-to-depth ratio, effective prestressing force, and shear reinforcement. The compressive strength varied from 8340 to 9090 psi. The span-to-depth ratios ranged from 2.2 to 2.7. The total effective prestressing force after losses varied from 298 kips to 425 kips. Shear reinforcement ranged from no shear reinforcement to 0.33%.

The observed failures were explosive due to the brittle nature of the high-strength concrete. The high-strength concrete exhibited flatter cracking angles than typical of normal

strength concrete which resulted in increased efficiency of the web reinforcement through the use of more stirrups, as well as increased capacity of the concrete due to the higher strength.

Three modes of failure were observed: flexural failure occurred in two girders, web-crushing failure occurred in one girder, and shear-bond failure occurred in three girders. The mode of failure identified as shear-bond denotes the case of web-shear cracks that destroy the transfer length bond between the concrete and strand. This failure mode occurred in two of the AASHTO Type I and in one of the AASHTO Type II. ACI 318-83 (95) Detailed Method was very conservative in predicting the strength of members for which shear-bond failure was not the mode of failure. In shear-bond failures, ACI 318-83 (95) Detailed Method overestimated the capacity of two of the three beams.

2.6 Hartmann, Breen, and Kreger

In 1988, Hartmann, Breen, and Kreger reported results of the shear tests of 10 prestressed girders made from concrete with compressive strengths ranging from 10,800 to 13,160 psi [8]. Cast-in-place decks of 3300 or 5350 psi concrete were used. Web reinforcement varied from no shear reinforcement to twice the maximum shear reinforcement allowed by the ACI 318-83 (95) or AASHTO 1989. A total of three girder series were investigated. The major difference between Series 1 and 2 was the number of prestressing strands. Series 3 had a cast-in-place deck which was cast after the strands were cut, as compared to Series 1 and 2 which had a deck that was cast at the same time as the girders were cast. The span-to-depth ratio varied from 3.0 to 3.2. The total effective prestressing force after losses varied from 87 kips to 223 kips. The center of the supports for Series 1 and 2 were 18 in. from the end of the girder. The distance of the center of the supports to the end of the girder for three of the four in Series 3 was 2 in. The forth girder in Series 3 was 8 in. from the end of the girder.

The stirrup gages indicated very small strains until after shear cracking. Bottom rows of strands exhibited little or no slip until shortly before shear-bond failure occurred. Middle rows of strands showed gradual slip throughout the loading. Shear-bond failures were the primary mode of failure of the prestressed concrete beams without sufficient support overhangs. The shear cracks ranged typically from 20° to 35° in most girders.

ACI 318-83 Detailed Method, the 1984 Canadian Code General Method, and the Modified Truss Model by Ramirez and Breen all gave generally conservative predictions of high-strength concrete shear capacity. ACI gave the most accurate results with the least scatter of the three methods.

2.7 Abdalla, Ramirez, and Lee

In 1993, Abdalla, Ramirez, and Lee reported results from five specimens fabricated and tested to failure as simply-supported members [9]. The ACI requirements for flexure and shear design of prestressed bridge girders with debonded strands were examined. Four specimens consisted of Type-I AASHTO girders with a cast-in-place deck. One specimen consisted of an Indiana box girder with a cast-in-place deck. Each girder end had different amounts of strand debonding. Each specimen had two ends that were tested in shear. Therefore, a total of ten ends were tested in shear. The center of the support was 10 in. from the end of the girder.

The compressive strength of the Type-I AASHTO girders varied from 5800 to 7500 psi, and the compressive strength of the cast-in-place deck varied from 2700 to 6300 psi. The effective prestressing force for the Type-I AASHTO girders varied from 87 kips to 309 kips after losses. The compressive strength of the box girder was 7300 psi, and the compressive strength of the corresponding cast-in-place deck was 4200 psi. The effective prestressing force for the Indiana Box girder was 514 kips.

In all of the specimens, large deflections were observed in the beams with debonded strands; although the failure loads of the debonded beams were lower than those of the fully bonded beams. Six of the girder ends failed due to anchorage loss of the required force in the prestressing strands. Cracking in the bottom flange near the ends of the girders disturbed the development length and caused anchorage failure. Close stirrup spacing did not eliminate the anchorage type failure.

All the beams were designed to ensure that shear failure would not occur, and none of the specimens failed in shear. Both web-shear cracking loads and flexure-shear cracking loads were measured in each girder. Comparison of the predicted and observed results indicated that the ACI Code gave conservative estimates of the web-shear cracking for both the debonded and fully bonded I-beams. The flexure-shear cracking developed in all of the debonded I-beams at lower

loads than predicted by the ACI procedures. All flexure-shear cracks in the debonded beams originated at the debonding points.

Strand slip preceded the failure of most of the beams. Abdalla, Ramirez, and Lee concluded that ACI provisions for development length were not adequate in the presence of web-shear cracking. Typically, excessive strand slip occurred when web-shear cracking penetrated into the transfer length of the strand.

2.8 Russell and Burns

In 1993, Russell and Burns published their results of tests done on three Texas Type C prestressed girders fabricated with 10,000 psi concrete [10]. Russell and Burns studied the effects of using high-strength concrete and different amounts of debonding on the shear strength of prestressed girders. The girders were made composite with the addition of an unshored concrete deck cast on each girder. Two of the girders contained debonded strands, and the third girder contained only draped strands. Each girder was 49 ft. in length and contained twenty-four 0.5 in. diameter strands. All three girders were designed for identical strength and serviceability requirements, and the girders varied only slightly in detailing. The compressive strength of the girders varied from 10,100 to 10,400 psi. The compressive strength of the cast-in-place deck varied from 5900 to 8470 psi. The average prestressing force after losses was 598 kips. Two of the girders had shear reinforcement oriented horizontally in the web, and the third girder did not.

Two of the girders failed in flexure, and one girder failed by a horizontal shear failure. The girders with debonded strands developed the horizontal shear crack which effectively separated the bottom flange from the web. The horizontal shear crack may have been caused by web-shear cracking damage, poor detailing of the reinforcement around of the bottom flange, and/or loss of prestressing force due to bursting cracks.

Girders made with debonded strands possessed similar strengths as girders made with draped strands; the behavior of both types of girders was adequately predicted by ACI 318-89 (95) Detailed Method. Russell and Burns recommended that both vertical and horizontal shear reinforcement should be provided in the web to prevent propagation of web-shear cracks into the bottom flange.

2.9 Tawfiq

In 1995, Tawfiq published his findings on the transfer length and the shear capacity of high-strength concrete girders [11]. He tested to failure both ends of six Type II AASHTO girders. The center of the support on the test end was 6 in. from the end of the girder. The girders had concrete strengths varying from 8150 to 11040 psi. The effective prestressing force after losses varied from 401 to 421 kips. The shear span-to-depth ratio varied from 2.1 to 2.5. Near the supports, the shear reinforcement ratio ranged from 1.11% for Series 1R and 2.22% for Series 2R.

Most of the girders failed due to a shear-bond failure between the prestressing strands and the surrounding concrete. The failure of the girder was noted by a sudden increase in the amount of slip and a decrease in the ability of the girders to withstand external loads. In general, the top rows of strands slipped first, but the lower row of strands slipped a larger amount. Increased concrete strength did not significantly affect the shear strength of the test girders; however, the high-strength concrete reduced the deflection of the girders due to the higher modulus of elasticity.

The Modified Compression Field Theory underestimated the shear strength at a horizontal distance from the support equal to the flexural lever arm of the composite section for Series 1R; however, the Modified Compression Field Theory overestimated the shear strength at a horizontal distance from the support equal to the flexural lever arm of the composite section for Series 2R. Tawfiq concluded the Modified Compression Field Theory likely overestimates the effect of the transverse reinforcement contribution and underestimates the effect of the concrete contribution.

The AASHTO 1989 Code overestimated the shear strength at a horizontal distance from the support equal to half the composite section depth for both types of transverse reinforcement patterns. The AASHTO 1989 shear capacity of Series 2R was greatly overestimated; however, the AASHTO 1989 results for Series 2R were closer to actual test results as compared to Modified Compression Field Theory.

2.10 Shahawy and Batchelor

In 1996, Shahawy and Batchelor published results from full-scale tests of 20 Type II AASHTO prestressed girders and compared the measured shear strength with the values predicted by the Modified Compression Field Theory and the ACI 318-89 (95) Detailed Method [12]. The predicted results included in this section were from the original article presented in the *PCI Journal* May-June, 1996.

The girders each had a cast-in-place deck. The design compressive strengths of each girder and each deck were both 6000 psi. The compressive strength of the girders ranged from 7030 to 8480 psi, and the compressive strength of the decks ranged from 4030 to 6700 psi.

The main variables of the study were the shear span, amounts of shear reinforcement, and type of strands. The span-to-depth varied from 1.3 to 3.5. The shear reinforcement varied from no shear reinforcement to three times that required. Seven shear reinforcement series were investigated: 0R had no shear reinforcement, M had minimum shear reinforcement, R/2 had half the required shear reinforcement, R had the required shear reinforcement for design dead and live loads, 3R/2 had 1.5 times the required shear reinforcement, 2R had twice the required shear reinforcement, and 3R had three times the required shear reinforcement. Three types of strands were used: sixteen 0.5 in., fifteen 0.5 in. special, and eleven 0.6 in. strands.

Four modes of failure were observed: shear-bond, shear, flexure, and flexure-bond failure. Shear-bond failures occurred in 18 girders, shear failures occurred in six girders, flexure failures occurred in 14 girders, and flexure-bond failures occurred in two girders.

The ACI 318-89 (95) Detailed Method provided excellent predictions for girders having intermediate amounts of shear reinforcement and conservative estimates for girders with no shear reinforcement. In addition, Shahawy and Batchelor concluded that the effect of shear span-to-depth was also accounted for much better by the ACI 318-89 Detailed Method than by the Modified Compression Field Theory.

The Modified Compression Field Theory considerably overestimated the strength for cases with high amounts of shear reinforcement and grossly underestimated the shear strength of girders with low amounts of shear reinforcement. Therefore, Shahawy and Batchelor concluded

the Modified Compression Field Theory generally overestimates the effect of steel contribution and underestimates the effect of the concrete contribution.

The ACI 318-89 Detailed Method predicted the shear strengths of the girders more accurately than the Modified Compression Field Theory. The authors recognized the appeal of the greater rationality of the Modified Compression Field Theory, but questioned if the increased complexity and the greater discrepancy with test results would justify the use of the Modified Compression Field Theory over the ACI 318-89 (95) Detailed Method.

2.11 Summary

A number of shear tests have been performed on prestressed girders. One of the goals of the testing at the University of Minnesota was to investigate the effect of high-strength concrete on shear capacity. Many of the tests reviewed in the literature included high-strength concrete.

Another of the goals of the shear tests at the University of Minnesota was to test full-scale composite girders. The University of Minnesota girders also had large amounts of prestressing, because they were designed as long-span members. Few tests have been conducted with composite members, and no tests have been performed on prestressed girders with a prestressing force after losses above 600 kips and with an amount of prestressing steel above 4.0 $in.^2$.

A major conclusion of the reported tests was that proper detailing of the web reinforcement and longitudinal steel was essential for prevention of premature shear failure. In addition, slippage of the prestressing strands appeared to be a very common mode of failure. This shear-bond failure caused the girders to lose load carrying capacity prematurely. As noted by Abdalla, Ramirez, and Lee, stirrups placed closely together did not prevent shear-bond failure.

In separate research, Hartmann, Breen, and Kreger and Tawfiq noticed that strand slip began in strands further from the bottom row of the section, and the largest amount of slip occurred in the bottom row of strands.

Table 2.1 gives the average and maximum properties for the girders discussed in the literature review. From these references, ratios of the observed strengths to the strengths predicted by the ACI Detailed Method (AASHTO 1989) and the Modified Compression Field Theory (AASHTO 1994) are presented. No calculations were done to verify the results of the models used by the authors. The ACI Detailed Method results are reported in four columns,

because the authors presented their information in different ways. The column labeled U_{cw} indicates the first observed diagonal cracking shear near the support in the web divided by the ACI shear capacity of the concrete in this region. The column labeled U_{ci} reports the cracking shear to start flexural cracking divided by the ACI shear capacity of the concrete in this region. The column labeled U_{cr} shows the lowest cracking shear divided by the lowest ACI shear capacity of the concrete at the corresponding section. The column labeled U_{ACI} gives the failure shear divided by the ultimate ACI shear capacity which includes concrete, draping, and stirrup contributions. The column labeled U_{MCFT} presents the failure shear divided by the predicted ultimate shear capacity according to the Modified Compression Field Theory which includes concrete, draping, and stirrup contributions.

In most cases, the ACI Code was accurate and conservative in predicting both web-shear or flexure-shear capacity for many different testing variables. Kaufman and Ramirez indicated that ACI 318-95 Detailed Method (AASHTO 1989) may not be conservative for the case of web-shear cracks that destroy the transfer length bond between the concrete and the prestressing strand.

Shahawy and Batchelor and Tawfiq reported that the Modified Compression Field Theory and ACI Code overestimated the strength for cases with high amounts of shear reinforcement. Shahawy and Batchelor showed with low amounts of shear reinforcement that the Modified Compression Field Theory and ACI Code underestimated the strength. As the shear reinforcement increases, the trend from underestimation towards overestimation is much greater in Modified Compression Field Theory than ACI Code. Therefore, the Modified Compression Field Theory likely overestimates the effect of transverse reinforcement contribution more so than the ACI Code.

Chapter 3 - Shear Capacity Models

3.1 Introduction

In the design of long-span prestressed concrete members, flexure is usually a primary consideration. This influences the size of the section and the arrangement of flexural reinforcement needed to provide the necessary moment resistance. Stirrups, also called transverse reinforcement, are required to provide additional shear capacity if the shear capacity of the concrete is not sufficient. In addition, stirrups are typically required to transfer horizontal shear for composite action between the girder and the cast-in-place deck. Generally, flexural failures develop gradually with visible deflection giving warning of failure. Because a shear failure is frequently sudden with minimal deflection, the design for shear capacity should be more conservative than for flexural capacity.

A number of current shear capacity models are presented in this chapter. The models range from empirical to conceptual. The empirical models calculate shear capacity at a given cross section. The conceptual models calculate shear capacity based on the overall length and checking individual components. The five empirical models discussed in this chapter are ACI 318-95 Simplified Method, ACI 318-95 Detailed Method (AASHTO 1989), Modified Compression Field Model (AASHTO LRFD 1994), Modified Truss Model, and Horizontal Shear Design (AASHTO 1989). The three conceptual models discussed here are the Truss Model, the Strut-and-Tie Model, and Shear Friction Theory (AASHTO LRFD 1994).

Most empirical and conceptual equations have been derived from test structures which had concrete compressive strengths less than 6000 psi. In all of the models, compressive strength is a primary variable. The objective of the study was to investigate the applicability of the existing shear capacity models to high-strength concrete in prestressed girders; therefore, the following discussions are limited to shear capacity of prestressed girders.

3.2 ACI 318-95 Simplified Method

In ACI 318-95 Section 11.1 and AASHTO Section 9.20.1, the basic design equation for the shear capacity of a concrete beam is:

$$V_u \le \phi(V_c + V_s), \tag{3.1}$$

where V_u is the shear force due to the factored loads; ϕ is the shear strength reduction factor; V_c is the shear carried by the concrete; and V_s is the shear carried by the stirrups. The code basically superimposes the shear taken by the concrete at cracking and the shear taken by the steel at yielding to predict the ultimate capacity.

3.2.1 Simplified Concrete Contribution

The simplified equation for the shear capacity of the concrete in a prestressed member is (ACI 318-95 Eqn. 11-10):

$$V_c = \left\{ 2\sqrt{f_c'}\, b_w d \le \left(0.6\sqrt{f_c'} + 700\left(\frac{V_u d_p}{M_u}\right)\right)(b_w d) \le 5\sqrt{f_c'}\, b_w d \right\}, \tag{3.2}$$

where f_c' is the compressive strength of the concrete in psi; b_w is the width of the web; and d is the distance from the extreme compression fiber to the centroid of the longitudinal tension reinforcement of the composite section, but not less than $0.80h$ for prestressed members, where h is the overall depth of the composite section. The maximum limit on V_c is an attempt to prevent web crushing. In the above equation,

$$\left(\frac{V_u d_p}{M_u}\right) \le 1.0, \tag{3.3}$$

where V_u is the factored shear force at the given cross section; d_p is the distance from extreme compression fiber to centroid of the prestressed reinforcement and is not limited to $0.80h$; and M_u is the factored moment at the given cross section.

These equations typically provide a conservative estimate of shear capacity. The main advantage of the equation is its simplicity. This equation was added in the ACI 1971 Code. Although there is no term in the equation related explicitly to the prestressing force, this equation can only be applied to members with an effective prestressing force after losses at least equal to 40% of the tensile strength of the flexural reinforcement. This method is not presented in AASHTO 1989 or in AASHTO 1994.

3.2.2 Steel Contribution

In ACI 318-95 Section 11.5.6 and AASHTO Section 9.20.3, the stirrup contribution is based on an assumption of a 45° crack pattern. The stirrup contribution is based on the number of stirrups that cross an inclined shear crack multiplied by the strength of each stirrup. Appendix A.1 has the complete derivation for the steel contribution. The inclined crack length is dependent on the angle of crack inclination, θ_{aci}, and the distance from the extreme compression fiber to the resultant tension arm, d. The angle of inclination is conservatively set to 45°; therefore, the horizontal projection of the crack is taken as d. The resulting equation is conservative for prestressed members, because the effect of prestressing causes the diagonal cracking to form at a shallower angle, thus intercepting more stirrups than predicted by the 45° model. Assuming that the stirrups yield at failure, the shear resisted by the stirrups is (ACI 318-95 Eqn. 11-17 and AASHTO Eqn. 9-30):

$$V_s = \left\{ \frac{A_v f_y d}{s} \le 8\sqrt{f_c'} b_w d \right\}, \tag{3.4}$$

where A_v is the cross-sectional area of the transverse reinforcement; f_y is the yield strength of the transverse reinforcement; and s is the center-to-center spacing of transverse reinforcement. The steel contribution is limited to avoid web crushing.

3.3 ACI 318-95 Detailed Method (AASHTO 1989)

ACI 318-95 Section 11.4.2 and AASHTO Section 9.20.2 provide a more detailed and accurate calculation for the concrete contribution term in Eqn. (3.1). The ACI 318-95 Detailed Method and AASHTO Section 9.20.2 use the same steel contribution equation as given in Section 3.2.2 based on a 45° truss model.

In ACI 318-95 Section 11.4.2 and in AASHTO Section 9.20.2, the shear strength provided by the concrete is a function of the type of shear cracking that controls. Two types of shear cracking exist; the first is flexure-shear concrete cracking, and the second type is web-shear concrete cracking. As shown in Figure 3.1, flexure-shear cracking controls where moment is large and shear exists, and web-shear cracking typically controls in thin web members near the supports where moment is small and shear is large.

3.3.1 Flexural Inclined Cracking

A flexure-shear crack originates as a vertical flexural crack in the member. As the crack penetrates deeper in the cross section it becomes inclined toward the point of load as a result of the shear stresses within the section. Shear capacity controlled by flexure-shear cracking includes three parts: (1) the shear force required to transform a flexural crack into an inclined crack, (2) the unfactored dead load shear force, and (3) the shear force that will cause a flexural crack to initially occur. Appendix A.2 shows a derivation for Eqn. (3.5). The flexure-shear cracking capacity is given by (ACI 318-95 Eqn. 11-11 and AASHTO Eqn. 9-27):

$$V_{ci} = \left\{ 1.7\sqrt{f_c'}\, b_w d \le 0.6\sqrt{f_c'}\, b_w d + V_d + \frac{V_i M_{cr}}{M_{max}} \right\}, \tag{3.5}$$

where for composite members V_d is the shear force at the given cross section due to unfactored self weight and unfactored superimposed dead loads; V_i is the factored shear force at the given cross section due to externally applied loads occurring simultaneously with M_{max} and M_{cr}; and M_{max} is the maximum factored moment at the given cross section due to externally applied loads. The term M_{cr} is the moment causing flexural cracking at the given cross section due to externally applied loads (ACI 318-95 Eqn. 11-12 and AASHTO Eqn. 9-28):

$$M_{cr} = \frac{I_{gc}}{y_{tc}} \left(6\sqrt{f_c'} + f_{pe} - f_d \right), \tag{3.6}$$

where I_{gc} is the gross moment of inertia of the composite cross section; y_{tc} is the distance from centroidal axis of the gross composite section to the extreme tension fiber; f_{pe} is the compressive stress in the concrete due to the effective prestressing force at the extreme fiber of the given cross section where tensile stress is caused by externally applied loads; and f_d is the tensile stress due to the unfactored dead load at the extreme fiber of the given cross section where tensile stress is caused by externally applied loads.

3.3.2 Web-Shear Cracking

The second type of shear failure that occurs in prestressed concrete members is due to web-shear cracking. Web-shear cracks form when the principal tensile stresses from shear exceed the tensile strength of the concrete. In prestressed concrete members, the resistance to web-shear cracking is due to the tensile strength of the concrete and the compressive forces in the

section due to the prestressing force and the applied loads. These compressive forces help keep the web-shear crack closed which in turn provides added shear resistance through aggregate interlock. In addition, the vertical component of the prestressing force due to draped strands provides resistance to the shear. The expression for web-shear strength usually governs for heavily prestressed beams with thin webs, especially when the beam is subject to large concentrated loads near simple supports.

The web-shear equation predicts the shear strength at the onset of web-shear cracking and is given by (ACI 318-95 Eqn. 11-13 and AASHTO Eqn. 9-29):

$$V_{cw} = \left(3.5\sqrt{f_c'} + 0.3f_{pc}\right)b_w d + V_p, \tag{3.7}$$

where f_{pc} is the compressive stress in the concrete at the centroid of the given cross section resisting externally applied loads or at the junction of the web and the flange when the centroid lies within the flange of a composite section and V_p is the vertical component of an effective prestressing force at the given cross section. The junction of the web and the flange statement is only in the ACI Code. Appendix A.3 shows a complete derivation of Eqn. (3.7).

In ACI 318-95 Section 11.4.2, the location of the critical section for a prestressed member is assumed to occur at a distance $h/2$ from the face of the support. When the cross section of interest in the shear analysis is within the transfer length of the prestressing strands, the effective prestressing force must be reduced. The effective prestressing force after losses is assumed to be transferred linearly to the concrete over a transfer length of 50 and 60 strand diameters for the ACI 1995 Code and AASHTO 1989 Code, respectively.

3.3.3 Modified Web Cracking

Modified web cracking was derived from mechanics of materials and was used to calculate the initiation of cracking at any height in the web. A derivation of Eqn. (3.8) is given in Appendix A.4. The principal tensile stress of $3.5\sqrt{f_c'}$ assumed to cause web-shear cracking at the centroid of the section in ACI 318-95 and AASHTO 1989 Code was assumed in this case. The modified web-shear strength calculations give the following equation for web-shear strength:

$$V_{mod} = \frac{I_{gc} b_m}{Q_{gc}} 3.5\sqrt{f_c'}\sqrt{1+\frac{f_{pd}}{3.5\sqrt{f_c'}}} + V_p, \quad (3.8)$$

where b_m is the width of the web at the depth of interest, Q_{gc} is the first moment of gross composite area with respect to a given depth in the cross section, and f_{pd} is the average compressive stress in the concrete at the depth of interest due to the effective prestressing force and the applied flexural stresses. The gross area of the composite section includes the transformation of the deck width based on the ratio of modulus of elasticity of the deck and the girder.

3.4 Modified Compression Field Theory (AASHTO LRFD 1994)

This shear theory, presented in AASHTO LRFD 1994, can be applied equally well to prestressed and to reinforced concrete beams. Also, the beam can be loaded with or without axial forces. The Modified Compression Field Theory assumes that total shear resistance is the sum of the concrete contribution, steel contribution, and prestress draping contribution as given by (AASHTO Eqn. 5.8.3.3-1 & 5.8.3.3-2):

$$\phi V_n = \left\{\phi\left(V_c + V_s + V_p\right) \le \phi\left(0.25 f_c' b_v d_v + V_p\right)\right\}, \quad (3.9)$$

where f_c' is the compressive strength of the concrete in ksi, b_v is the effective web width taken as the minimum web width within the depth d_v, and d_v is the flexural lever arm which is the distance from the resultant tension force to the resultant compressive force and need not be taken less than $0.9d$.

The shear resisted by the concrete can be expressed as (AASHTO Eqn. 5.8.3.3-3):

$$V_c = 0.0316\beta\sqrt{f_c'} b_v d_v, \quad (3.10)$$

where β is the factor indicating the ability of diagonal cracked concrete to transmit tension.

When transverse reinforcement is provided, the term β depends on the average tensile stresses in the cracked concrete and is determined by AASHTO Table 5.8.3.4.2-1, reproduced herein as Table 3.1. The term v is the shear stress at given cross section. To better approximate AASHTO Figure 5.8.3.4.2-1 with transverse reinforcement, the basic table was further refined,

and this detailed table is shown in Table 3.2. The detailed table was used for shear capacity calculations.

The longitudinal strains in the web are related to the concrete capacity. Increasing axial tension increases longitudinal strains in the section, which reduces the concrete ability to resist shear cracking and decreases V_c. The longitudinal strain in the reinforcement on the flexural tension side of the member is calculated by (AASHTO 5.8.3.4.2-2):

$$\varepsilon_x = \frac{\frac{M_u}{d_v} + 0.5N_u + 0.5V_u \cot(\theta) - A_{ps} f_{po}}{E_s A_s + E_p A_{ps}}, \tag{3.11}$$

where N_u is the applied factored axial force which is taken as positive if compressive, A_{ps} is the area of prestressed steel on the flexural tension side of the member, which is reduced if the given section is in the development length; f_{po} is the stress in the prestressing steel when the stress in the surrounding concrete is zero at the depth of the longitudinal reinforcement and is not reduced for development length; E_s is the modulus of elasticity of nonprestressed reinforcing bars; A_s is the area of nonprestressed reinforcing steel on the flexural tension side of the member, which is reduced for any lack of full development at the given section; and E_p is the modulus of elasticity of prestressing steel. As shown in Figure 3.2, the longitudinal strain parameter accounts for the influence of moment, shear, and axial load.

If the value of ε_x is positive, then the value is unchanged. If the value of ε_x is negative, then the concrete section is in compression. In this case, ε_x magnitudes shall be reduced by the factor F_e which includes an extra term for concrete resistance and is given by (AASHTO 5.8.3.4.2-3):

$$F_e = \frac{E_s A_s + E_p A_{ps}}{E_c A_{gc} + E_s A_s + E_p A_{ps}}, \tag{3.12}$$

where E_c is the modulus of elasticity of the concrete and A_{gc} is the gross area of the composite section.

The steel contribution to shear is based on the variable truss model. The shear resisted by the stirrups is (AASHTO C. 5.8.3.3-1):

$$V_s = \frac{A_v f_y d_v}{s} \cot(\theta), \tag{3.13}$$

where θ is the angle of diagonal compressive stresses and is determined using AASHTO Table 5.8.3.4.2-1 when transverse reinforcement is provided. The AASHTO table is reproduced in Table 3.3. To better approximate AASHTO Figure 5.8.3.4.2-1, the basic table was further refined, and this detailed table is shown in Table 3.4. The detailed table for θ was used for calculations.

Both θ and β depend on the longitudinal strain and shear stress. The shear stresses on the concrete section are determined by (AASHTO 5.8.3.4.2-1):

$$\left(\frac{v}{f_c'}\right) = \frac{\left(V_u - \phi V_p\right)}{\phi b_v d_v f_c'}, \tag{3.14}$$

where v is the factored shear stress.

When transverse reinforcement is not provided, the steel contribution is zero, and the term β depends on the average tensile stresses in the cracked concrete which is determined by AASHTO Table 5.8.3.4.2-2, reproduced herein as Table 3.5. To better approximate AASHTO Figure 5.8.3.4.2-2 without transverse reinforcement, the basic table was further divided refined, and this detailed table is shown in Table 3.6. The angle of diagonal compressive stresses, θ, is determined using AASHTO Table 5.8.3.4.2-2. The AASHTO table is reproduced in Table 3.7. To better approximate AASHTO Figure 5.8.3.4.2-2, the basic table was further refined, and this detailed table is shown in Table 3.8. These tables use the same procedure to calculate longitudinal strain; however, the term s_x, crack spacing parameter, is used instead of the shear stresses calculated in Eqn. (3.15).

In addition, the longitudinal reinforcement is checked to ensure the beam will not fail due to bond failure (AASHTO 5.8.3.4.2-1):

$$A_y f_y + A_{ps} f_{ps} \geq \frac{M_u}{d_v \phi} + 0.5\frac{N_u}{\phi} + \left(\frac{V_u}{\phi} + 0.5V_s - V_p\right)\cot(\theta), \tag{3.15}$$

where θ is the crack angle.

In the above calculations, the value of θ must first be assumed, ε_x is calculated, a new value of θ is read from the AASHTO tables, and the new value is used to calculate ε_x. It is a process which requires multiple iterations to find θ and ε_x.

3.5 Modified Truss Model

This shear theory suggested by Ramirez and Breen can be used for both prestressed and reinforced concrete beams [13]. The Modified Truss Model assumes that total shear resistance is the sum of the concrete contribution, steel contribution, and prestress draping contribution as given by:

$$\phi V_n = \left\{ \phi\left(V_{cr} + V_{truss} + V_p\right) \le \phi\left(30\sqrt{f_c'}\sin(\theta_{mtm})\cos(\theta_{mtm})b_w d + V_p\right)\right\}, \qquad (3.16)$$

where V_{cr} is the shear force capacity provided by the concrete; V_{truss} is the shear force capacity provided by the steel; and θ_{mtm} is the angle of inclination of the diagonals at failure which is taken as 25° for prestressed concrete beams (Appendix A.5).

Ramirez and Breen proposed a constant concrete contribution dependent on the level of prestressing. The shear resisted by the concrete can be expressed by:

$$V_{cr} = K f_t b_w z, \qquad (3.17)$$

where K is the prestressing force factor which is given below; f_t is the principal diagonal tension stress in the web of the member; and z equals the effective truss depth between the flexural tension and flexural compression arms, which is taken as $0.9d$, where d is not less than $0.8h$.

The beneficial effect of the prestressing force on the shear cracking load before diagonal cracking is given by the factor K. The expression for K can be derived from a Mohr's circle representation of an element at the neutral axis prior to initial diagonal cracking (Appendix A.6) and is given by:

$$K = \sqrt{1 + \frac{f_{pc}}{f_t}}. \qquad (3.18)$$

where f_{pc} is the compressive stress at the neutral axis due to effective prestressing force and f_t is the principal diagonal tension stress in the web of the member. Ramirez and Breen suggest setting f_t equal to $2\sqrt{f_c'}$.

The value of K is limited to 1.0 when the stress in the extreme tension fiber due to the calculated factored load and prestressing force exceeds $6\sqrt{f_c'}$ which is the extreme fiber cracking stress in bending. Setting K equal to 1.0 avoids detailed calculations for flexure-shear capacity. In this case, the concrete contribution reduces to $2\sqrt{f_c'}b_w z$ which is similar to the lower limit given by the simplified expression in ACI 318-95.

From equilibrium of vertical forces, the shear capacity due to the transverse steel is given as

$$V_{truss} = \frac{A_v f_y z}{s}\cot(\theta_{mtm}), \tag{3.19}$$

where θ_{mtm} is taken as 25° for prestressed concrete beams.

Also, the Modified Truss Model defines the web reinforcement index as

$$\rho f_y = \frac{A_v f_y}{b_w s}, \tag{3.20}$$

where ρ is the web reinforcement ratio.

Ramirez and Breen stated that for 48 prestressed concrete beams with $\rho f_y \leq 200$ psi the Modified Truss Model is more conservative than ACI 318-95 Detailed Method; however, for 15 prestressed concrete beams with ρf_y between 200 psi and 300 psi, both procedures yield similar results. For 14 prestressed concrete beams with ρf_y between 300 psi and 500 psi, the Modified Truss Model predicted better estimates than ACI 318-95 Detailed Method. For prestressed concrete beams with $\rho f_y > 500$ psi, web-crushing is the typical failure mode.

3.6 Truss Model

The Truss Model neglects the concrete contribution and the vertical component of the effective prestressing force. Prestressed concrete is indirectly included by allowing shallower angles of diagonal compression. For beams with large amounts of web reinforcement, the behavior approaches that predicted by this model. On the other hand, the Truss Model predicts zero shear strength for beams without web reinforcement, which could greatly underestimate the shear capacity.

Figure 3.3a shows a beam with inclined cracks. The beam can be replaced by the truss shown in Figure 3.3b. In design, the ideal distribution of stirrups would correspond to all stirrups reaching yield by the time the failure load is reached. The force in each stirrup at yielding is given by:

$$F_s = A_v f_y \tag{3.21}$$

where A_v is the area of the stirrup legs and f_y is the yield strength of the stirrup legs.

Figure 3.3b shows that the truss is formed by lumping all of the stirrups cut by Section A-A into one vertical Member b-c and all the diagonal concrete members cut by Section B-B into one diagonal Member e-f. This diagonal member is stressed in compression to resist the shear on Section B-B. The compression chord along the top of the truss is actually a force in the concrete and is shown as a truss member. The compressive members in the truss are shown with dashed lines to imply that they are really forces in the concrete. The tensile members are shown with solid lines.

Knowing the stirrup forces, $A_v f_y$, the truss becomes statically determinate. This truss is referred to as the Plastic Truss Model because the plasticity in the stirrups makes it statically determinate. The beam is proportioned so that the stirrups yield before the concrete crushes, and sufficient longitudinal steel is provided for horizontal equilibrium; the model does not depend on plastic action of the concrete.

In the Plastic Truss Model shown in Figure 3.4, there are four compression struts to transfer the midspan concentrated load P_1. Likewise at the supports, the reaction force will "fan out," and it takes two compression struts at two angles to transfer the compressive force to each support in the beam. If the concrete stress is below an allowable stress, the truss models ignore additional capacity provided by the concrete, because the concrete is only used to transfer the stirrup forces.

3.7 Strut-and-Tie Model

The Strut-and-Tie Model describes the load-carrying mechanism of a structural member by approximating the flow of internal forces by means of struts representing the flow of compressive stresses and ties representing the flow of tensile stresses. In addition, the Strut-and-Tie Model assists the engineer in determining the size, location, distribution, and anchorage of

the main reinforcement. The Strut-and-Tie Model is covered in AASHTO LRFD 1994 Code Section 5.6.3.

The Strut-and-Tie Model is best-suited for "disturbed" regions, as opposed to "beam" regions. In disturbed regions, complex load paths from concentrated loads converge near the supports. The Strut-and-Tie Model provides insight into the flow of forces in disturbed regions. All stresses are condensed into compression and tension members, and the members are joined by nodes. The model uses concrete compressive struts to represent the concrete in compression, tension ties to model the principal reinforcement, and nodal zones which represent the regions of concrete subjected to multidirectional stresses where the struts and ties meet, see Figure 3.5. AASHTO 5.6.3.1 states that the Strut-and-Tie Model should be considered when the distance between the centers of applied load and the supporting reactions are less than about twice the member thickness. In addition, members with uniform width are better suited for this method.

The first step for using this method is to sketch the location of the nodes and draw the flow of forces. The next step is to determine the size of the elements and forces. After determining the forces, the nodal zones, the compressive struts, and the tension ties are analyzed to ensure that stresses remain below permissible limits.

The concrete compressive stress in the node region should not exceed the values indicated for the following three cases. The maximum compressive stresses in node regions of the strut should not exceed $0.85\phi f_c'$ in node regions bounded by compressive struts and bearing area, $0.75\phi f_c'$ in node regions anchoring only one tension tie, and $0.65\phi f_c'$ in node regions anchoring tension ties in more than one direction.

The strength of unreinforced struts is given by (AASHTO 5.6.3.3.1-1) as

$$P_n = f_{cu} A_{cs}, \tag{3.22}$$

where f_{cu} is the limiting concrete compressive stress and A_{cs} is the effective cross-sectional area of the strut.

The strength of tension ties is given by (AASHTO 5.6.3.4.1-1) as

$$P_n = f_y A_{st} + A_{ps}\left(f_{pe} + f_y\right), \tag{3.23}$$

where A_{st} is the total area of longitudinal mild steel reinforcement.

3.8 Horizontal Shear Design and Shear Friction Theory

A composite beam requires the cast-in-place deck and the girder to act as a single unit. The horizontal shear resulting from bending of the beam must be transferred between the flange and the girder at their interface. The roughness of the top of the precast concrete beam, the amount of steel crossing the joint, and the concrete strength are the major factors affecting the shear strength of the interface.

In some prestressed girders, horizontal shear failures have been observed when the diagonal web crack intersects the bottom flange and develops into a horizontal interface crack. From equations used to calculate horizontal shear capacity of a composite section between a girder and a cast-in-place deck, it was attempted to calculate the horizontal shear capacity of the web and bottom flange.

In the AASHTO 1989 Code Section 9.20.4, for a composite flexural member the factor shear force at any given section should be lower than the horizontal shear strength. From AASHTO 9.20.4.3, when the contact surface is clean, free of laitance, and intentionally roughened, shear strength, V_{nh}, shall not be taken greater than $80b_f d$ in pounds where b_f is the width of composite interface. When minimum ties are provided in accordance with AASHTO . 9.20.4.5, and the contact surface is clean and free of laitance, but not intentionally roughened, shear strength shall not be taken greater than $80b_f d$. When minimum ties are provided in accordance with paragraph AASHTO 9.20.4.5, and contact surface is clean, free of laitance, and intentionally roughened to a full amplitude of approximately 1/4 in., shear strength shall not be taken greater than $350b_f d$ in pounds. For each percent of tie reinforcement crossing the contact surface in excess of the minimum required by AASHTO 9.20.4.5 shear strength may be increased by $\frac{160f_y}{40{,}000b_f d}$.

In AASHTO 1989 Code Section 9.20.4.5, the minimum area of tie reinforcement should be provided between interconnected elements. Tie area should not be less than $\frac{50b_f s}{f_y}$, and tie spacing shall not exceed four times the least web width of support element or 24 inches.

In the AASHTO 1994 Code Section 5.8.4, the nominal shear resistance of the interface plane shall be taken as (AASHTO Eqn. 5.8.4.1-1 and Eqn. 5.8.4.1-2)

$$V_{sf} = c_f A_{cv} + \mu\left(A_{vf} f_y + P_c\right) \leq 0.2 f_c' A_{cv} \tag{3.24}$$

and also should not exceed (AASHTO Eqn. 5.8.4.1-3)

$$V_{sf} \leq 0.8 A_{cv} \tag{3.25}$$

where c_f is the cohesion factor; A_{cv} is the area of the concrete engaged in shear transfer; μ is coefficient of friction; A_{vf} is the area of shear reinforcement crossing the shear plane; and P_c is the permanent net compressive force normal to the shear plane.

3.9 Summary

Accuracy, rationality, and ease of use are important factors in evaluating different models for shear capacity. An accurate model should be applicable for many different cross sections, load types, and amounts of prestressing. A rational model is defined as having a firm physical basis. The model should give a clear indication of the mechanisms and paths used to transfer loads to the supports. For ease of use, the model must give the designer clear understanding of the required procedure, and the parameters used should be simple and easily defined.

The models generally separate shear capacity based on three contributions: concrete, stirrups, and draping. Table 3.9 shows a comparison of the seven presented models with the assumed crack angle measured from a horizontal reference. The stirrup contribution is larger when crack angle is the shallower. ACI 318-95 Detailed Method, Modified ACI 318-95 Procedure, Modified Compression Field Theory, and Modified Truss Theory all include contributions due to concrete, stirrups, and draping. ACI 318-95 Simplified Method, Truss Theory, and Strut-and-Tie Model do not include all three contributions.

ACI 318-95 Simplified Method is generally very conservative and easy to use. Although, the ACI 318-95 Simplified Method does not separately address web-shear cracking, flexure-shear cracking, and shear-bond failure.

ACI 318-95 Detailed Method is more rational than the ACI 318-95 Simplified Method and is based on theoretical relationships containing many parameters. This model provides a

better estimate of shear capacity than ACI 318-95 Simplified Method differentiating between web-shear cracking and flexure-shear cracking. Shear-bond failure is not addressed.

Modified ACI 318-95 Procedure is a modification of ACI 318-95 Detailed Method. This model predicts the shear capacity at any given depth in the cross section; therefore, many depths in cross section must be analyzed to find minimum shear capacity.

The Modified Compression Field Theory is generally described as more rational than the ACI 318-95 Detailed Method. The rationality stems from the allowance of the diagonal compression angle to vary to less than 45° which is more appropriate for prestressed concrete members. With a better estimate of the angle of diagonal compression, the shear strength provided by the steel and concrete should be more accurately calculated. The Modified Compression Field Theory contains many different parameters than the ACI Detailed Method and contains an iterative process to calculate the angle of the cracks. The Modified Compression Field Theory does not address flexure-shear cracking and web-shear cracking as separate phenomena, and shear-bond failure is addressed by the method.

The Modified Truss Model is simpler than ACI 318-95 Detailed Method. The Modified Truss Model for concrete contribution is very similar to web-shear cracking of ACI 318-95 Detailed Method. In the case of sections dominated by flexural cracking, the concrete contribution reduces to $2\sqrt{f_c'}b_w z$. The steel contribution is based on crack angles of 25° for prestressed concrete beams as compared with 45° for ACI Code.

The Truss Model provides a conceptual design method. This model shows the flow of forces and is useful for discontinuities; however, the model neglects the prestressing force. Prestressed concrete is indirectly included by allowing shallower angles of diagonal compression.

The Strut-and-Tie Model is a conceptual method with a visible flow of forces. The size of nodes and struts is very important in calculating the capacity of a member. Also, the level of permissible stresses in the nodes and the struts are important for analysis. This model is better suited for deep beams with short spans, discontinuities, "disturbed" regions, and uniform width.

The Horizontal Shear Design (AASHTO 1989) is a relatively simple method to calculate horizontal shear capacity between a girder and a cast-in-place deck. The horizontal shear

capacity is compared with vertical shear force. The horizontal shear capacity is greatly enhanced when the surface is intentionally roughened and when minimum ties are provided.

The two major methods used today in the United States are the Modified Compression Field Theory and ACI 318-95 Detailed Method. The Modified Compression Field Theory is a relatively new method in the United States, and this method is more difficult to use as an analysis tool. In the ACI 318-95 Detailed Method, the shear capacity for web-shear cracking is unchanged for given load locations as the applied load increases. In the Modified Compression Field Theory, the shear capacity decreases as the applied load increases; therefore, Modified Compression Field Theory is an iterative process to find maximum applied load and shear capacity.

Chapter 4 - Shear Test Specimens and Test Setup

4.1 Introduction

This chapter focuses on the description, transportation, instrumentation, and test setup of the high-strength concrete prestressed girders subjected to shear testing. The description section includes information on the cross section type, concrete mix and strength, prestressing strand, mild reinforcement, and external fiberglass reinforcement. The transportation section provides information on moving the specimens. The instrumentation section includes discussion of the measurement of specimen deflections, stirrup strains, concrete strains, prestressing steel strains, strand slips, and acoustic emissions. The testing and data processing section describes the testing machines, testing procedure, data acquisition, and data reduction.

4.2 Description of Test Specimens

The two girders, Mn/DOT 45M sections, were 45 in. deep, and originally 132 ft. 9 in. long. They were constructed by Elk River Concrete Products in August, 1993. The instrumentation and fabrication of the prestressed bridge girders are described in a thesis written by Jeffrey Kielb [14]. A 4 ft. wide 9 in. thick composite concrete deck was added to each girder in February, 1994, using unshored construction techniques. The cross section of the girders is shown in Figure 4.1 and the composite section is shown in Figure 4.2. Each girder was prestressed with forty-six 0.6 in. diameter prestressing strands on 2 in. centers. Draped strands were harped using two hold down points and located at 40% of the span length from each end. The girders were designed assuming a 28-day compressive strength of 10,500 psi. Detailed information on the material properties of the girders can be found in the thesis written by Jeffrey Kielb [14]. Some of the information is summarized here for completeness.

Prestressing losses, transfer lengths, dynamic response, fatigue life, and flexural strength behavior were investigated and reported by Tess Ahlborn [15]. Following the flexural strength tests, two 43 ft. end sections were cut from each girder. The cutting process resulted in a total of four specimens to be tested in shear.

4.2.1 Test Variables

The specimens were identically designed except for the mix design, the end-strand patterns, and the stirrup-anchorage details. Girder I had a limestone aggregate mix, and Girder II had a glacial gravel with microsilica mix (described in Section 4.2.2). Ends A and B of Girder I and End C of Girder II had 4 draped and 8 debonded strands, while End D of Girder II had 12 draped strands with no debonded strands (described in Section 4.2.3). For stirrup anchorage details, Ends IB, IIC, and IID had modified U stirrups with leg extensions, and End IA contained standard Mn/DOT U stirrups without leg extensions (described in Section 4.2.4). A summary of these variations is given in Figure 4.3.

4.2.2 Concrete

The concrete mix for Ends IA and IB consisted of Type III Portland cement, sand, crushed 5/8 in. limestone aggregate, and superplasticizer. The concrete mix for Ends IIC and IID consisted of Type III Portland cement, sand, superplasticizer, 3/4 in. glacial gravel, and micro silica. Both mixes had a design 28-day compressive strength of 10,500 psi. The complete girder mix designs are given in Table 4.1.

The girder results of the individual cylinder tests measured at the time of the shear tests are given in Appendix B.1, and the cylinder strength history over the life of the girders is given in Appendix B.1. Cylinder compressive strengths were measured at release, 7 days, 28 days, 220 days (approximate age at time of deck cast), 480 days, 1200 days (approximate age at time of flexural tests), and 1240 days (approximate age at time of shear tests). At the time of shear testing, the compressive strength of the 6 x 12 in. cylinders was measured as 11,330 psi and 9315 psi for Girders I and II, respectively. These compressive strengths were lower than the compressive strengths measured at 480 days and 1200 days for both girders. Split tensile strengths were 729 psi and 587 psi for Girders I and II, respectively. These split tensile strengths were lower than the tested values at 28 days. The modulus of rupture was not measured at time of shear testing; however, it was measured at time of flexural testing. At the time of flexural testing, the results for Girders I and II were 1283 psi and 975 psi, respectively, and were higher than the values at 28 days. The modulus of elasticity values for Girders I and II were 5230 ksi

and 4520 ksi, respectively. These values were slightly lower than those recorded at the time of flexural testing.

The deck was fabricated with a concrete mix typical for Mn/DOT bridge decks. The design strength of the deck concrete was 4300 psi. The concrete mix consisted of Type I Portland cement, sand, 3/4 in. gravel, water, and air entrainment. The mix design of the deck concrete is given in Table 4.2.

The deck results of the individual cylinder tests measured at the time of the shear tests are given in Appendix B.2, and the cylinder strength history is given in Appendix B.2. Cylinder compressive strengths were measured at 7 days, 28 days, 1000 days (approximate age at time of flexural tests), and 1040 days (approximate age at time of shear tests). At the time of shear testing, the compressive strength of the cylinders was 5660 psi. This compressive strength was lower than the compressive strengths measured at 28 days and 1000 days. Split tensile strength was 430 psi. The split tensile strength was lower than the measured value at 28 days. The modulus of rupture was not measured at the time of shear testing; however, it was measured at 28 days as 632 psi. At the time of shear testing, the modulus of elasticity was 4480 ksi. This value was approximately the same as the value obtained at the time of flexural testing.

The compressive and tensile strength tests were conducted in accordance with ASTM C39 and ASTM C496, respectively. The modulus of elasticity tests were conducted in accordance with ASTM C469.

At the time of shear testing, many of the properties were lower than results obtained earlier, and this led to concern about calibration of the cylinder testing machine. The cylinder testing machine was calibrated in August, 1996, and the tests were performed in December, 1996. After the cylinder tests, the machine was checked again with a load cell. The results of the load cell showed the calibration to be correct.

4.2.3 Prestressing Strands

The prestressing strands were seven wire strands with a nominal diameter of 0.6 in. The strands were low relaxation Grade 270 ksi. Each girder had 46 strands; however, the pattern varied by the amount of draping and debonding. Test results of the prestressing strands are described in the thesis written by Jeffrey Kielb [14]. The nominal and measured area of the

prestressing tendon was 0.215 and 0.228 $in.^2$, respectively. The nominal and actual initial prestressing stress in each strand was 202.5 ksi and 191.6 ksi, respectively. A total prestressing loss of 35.8% was predicted according to the AASHTO 1989. Consequently, the nominal and expected prestressing force after losses was 130.0 ksi and 123.0 ksi, respectively. The measured transfer length at release of the 0.6 in. diameter strands was 24 in.; whereas the predicted transfer length was 30 in. according to ACI 318-95 and 36 in. according to AASHTO 1989 and 1994.

Centerline strand pattern and the numbering system for the prestressing strands is given in Figure 4.4. The first number refers to the row (from the bottom), and the second number refers to the column (from the left). The numbering system starts with 1-1 at the lower left corner facing the cross section. This means that the numbering system changed half way through the original girders. Figure 4.5 gives the end strand patterns and lengths of debonding.

4.2.4 Mild Reinforcement

Mild reinforcement was used for the stirrups, longitudinal steel in the upper flange of the prestressed member, and longitudinal and transverse steel in the deck. All mild reinforcement was epoxy coated, Grade 60 steel.

Four No. 8 reinforcing bars were used in the longitudinal direction in the upper flange of the girder. Section and elevation views of the girder mild reinforcement are given in Figures 4.6 and 4.7, respectively. Deck reinforcement comprised No. 4 reinforcing bars both in the transverse and longitudinal directions. Figure 4.8 gives the section and elevation views of mild reinforcement in the deck.

Four No. 6 stirrups were placed to control stresses due to the release of the prestressing strand and to provide confinement of the concrete over the support. The stirrup spacing throughout the original girders was primarily controlled by Horizontal Shear Design (AASHTO 1989) and called for No. 4 stirrups at a maximum spacing of 16 in.

The stirrups were double legged with a loop extending out of the top flange of the prestressed member to provide horizontal shear transfer between the prestressed member and the deck. Two different vertical shear stirrup configurations were used. Detailed drawings of the mild reinforcement is given in Figure 4.9. The typical Mn/DOT double leg, straight stirrup without leg extensions was used in End IA. The measured yield strength of the Mn/DOT double

leg stirrups was 75.0 ksi. The stirrup type used in the other ends was a double leg, with a 90° hook at the end of each leg oriented along the length of the specimen. This configuration was termed a stirrup with leg extensions. The leg extensions provided additional anchorage for the stirrup. The measured yield strength of the stirrups with leg extensions was 72.7 ksi.

4.2.5 Lift Hooks

The original girders had eight lift hooks placed in the web and a loop outside of the girder flange. Each lift hook consisted of four bundled 0.5 in. prestressing strands that were unstressed. Four of the lift hooks were used in the prestressing yard to move the original girder. These lift hooks were anchored into the lower flange and were cut at the top of the girder before the deck was cast. The remaining four lift hooks were used to move the specimens with the cast-in-place deck. These lift hooks were the same length as the other lift hooks except placed higher in the cross section of the girder. No tests to determine the strength of the prestressing strands used as lift hooks were performed.

Figure 4.10 shows the three lift hooks near the end of the girder. The first lift hook was anchored outside of the lower flange at approximately 3.8 and 5.2 ft. from the end, the second lift hook was anchored in the lower flange at approximately 7.0 and 8.8 ft. from the end, the third lift hook was anchored in the lower flange at approximately 8.8 and 10.5 ft. from the end, and the fourth lift hook was anchored outside of the lower flange at approximately 36.0 ft.

4.2.6 Fiberglass Reinforcement

The objective of the shear tests was to investigate the capacities of the various end details and concrete mixes. In each of the shear test sections, the end towards midspan of the original section, opposite to the end with the details to be investigated, had been extensively damaged during the flexural tests. To prevent failure of the heavily predamaged ends, supplemental external reinforcement was bonded to the web in the damaged region. The supplemental reinforcement comprised two to three layers of 0°/90° fiberglass reinforcement on each side of the web. The fiberglass-reinforcement system, purchased from Structural Rehabilitation Company, consisted of a woven sheet of fiberglass, epoxy resin, and hardener.

The following procedure was used to apply the fiberglass reinforcement. First, the specimen was scrubbed clean of whitewash and dust to enhance the bond between the specimen and the reinforcement. Then the epoxy resin and the hardener were mixed, placed, and worked to a uniform thickness. A fiberglass sheet was placed over the epoxy layer. The process was continued for two or three layers of fiberglass with a final epoxy layer applied over the last layer of fiberglass. Figure 4.11 shows application of one of the fiberglass sheets onto the specimen, and Figure 4.12 shows the complete reinforcement system on the specimen. No special testing of the composite reinforcement was performed. The total lengths of the fiberglass reinforcement on Ends IA, IB, IIC, and IID were 10 ft., 6 ft., 20 ft., and 12 ft., respectively.

The external-web reinforcement made it difficult to view any new cracks that developed during the shear tests in this area. No failure of the long shear span occurred during testing; it is unknown if these specimens were strong enough to withstand the ultimate shear force without fiberglass reinforcement.

4.3 Transportation

The flexural testing was conducted at an off-campus facility, but it was found that the foundation for the load frame could not resist the forces required for the shear tests. It was decided to transport the specimens to the University of Minnesota Civil Engineering Building to be tested in the 600 kip Universal Testing Machine.

The specimens were transported individually from the Golden Valley facility. Each specimen was lifted onto a flatbed truck using a 40 ton forklift from Truck Crane Company as shown in Figure 4.13. End IIC accidentally rolled over during the loading process at the Golden Valley Facility. The rollover caused additional cracking in the deck and a horizontal crack at the base of the web. In addition, the embedded lift hooks were damaged. LeFebvre & Sons Trucking Company of Elk River, Minnesota, hauled the specimens from Golden Valley to the University of Minnesota Campus.

At the University of Minnesota, the specimens were lifted from the flatbed by a 175 ton truck crane owned by Truck Crane Service Company of Golden Valley, Minnesota, Figures 4.14 and 4.15. In Figure 4.16, the specimen is shown between lifts outside the Civil Engineering Building. Next, the specimen on steel rollers was pushed by the truck crane into the loading

dock area, Figure 4.17. Figure 4.18 shows a view of the specimen from the loading dock looking into the testing laboratory. Figure 4.19 shows a specimen being lowered at a steep angle by the laboratory's 15 ton overhead crane in conjunction with the 175 ton truck crane.

4.4 Instrumentation

Internal shear testing instrumentation, cast into each specimen during fabrication, consisted of a total of 30 stirrup gages, three bursting gages, two rupture gages, five three-armed concrete rosette gages, and a minimum of 12 transfer gages. External instrumentation, attached to each specimen before shear testing, consisted of a maximum of five three-armed concrete rosette gages, nine strand slip linear variable differential transducers (LVDTs), three beam deflection LVDTs, and four acoustic emission transducers. The external rosettes were located as near as possible to the internal rosettes and were used only when the internal rosette had a defective arm(s). In the shear tests, both internal and external instrumentation was used to investigate the flow of forces from the load point to the reactions. The manufacturers of the instrumentation are listed in Table 4.3. The internal stirrup gages and concrete rosette locations are shown in Figure 4.20.

4.4.1 Beam Deflection

For each specimen, two LVDTs were used to measure the beam's vertical deflections on each side of the load point. One LVDT was located on the short shear span, and the other LVDT was located on the long shear span. The location of the LVDTs and testing dimensions are given in Figure 4.21 and Table 4.4, respectively. The displacement measurement obtained from the actuator was not used, because the actuator LVDT included the deformations of the load tube and load pad.

The short shear span, the end with the shortest distance from the load point to the support, had an embedded 15 in. long and 3/4 in. thick steel sole plate which was supported on a steel roller that was assumed not to deform. The long shear span support, the end with the longest distance from the load point to the support, was supported by a neoprene pad. A 1 in. LVDT was used to monitor the vertical deformations of the pad. The deflection of the specimen read by the two beam deflection LVDTs was corrected for changes due to rigid body rotation using the

measurements from the LVDT monitoring the neoprene pad. The rigid body rotation was due to the compression of the neoprene pad.

The correction was done by applying the method of similar triangles as shown in Figure 4.22. The corrected deflection on the short shear span, *WestCorr*, was given by:

$$WestCorr = WestDefl - CorrW, \tag{4.1}$$

with

$$CorrW = NeoDefl\left(\frac{WestLVDT - SuppEnd}{NeoLVDT - SuppEnd}\right), \tag{4.2}$$

where *WestDefl* is the vertical displacement measured by the west LVDT on the short shear span, *NeoDefl* is the vertical displacement measured by the LVDT monitoring the neoprene pad, *WestLVDT* is the horizontal distance from the west end to the west LVDT, *SuppEnd* is the horizontal distance from the west end to the roller support, and *NeoLVDT* is the horizontal distance from the west end to the LVDT at the neoprene support. All distances were measured from the west end of the specimen which was the end supported by the steel roller.

The corrected deflection on the long shear span, *EastCorr*, was given by:

$$EastCorr = EastDefl - CorrE, \tag{4.3}$$

with

$$CorrE = NeoDefl\left(\frac{EastLVDT - SuppEnd}{NeoLVDT - SuppEnd}\right), \tag{4.4}$$

where *EastDefl* is the vertical displacement measured by the east LVDT on the long shear span, and *EastLVDT* is the horizontal distance from the west end to the east LVDT.

4.4.2 Stirrup Strain Gages

A total of 30 stirrup strain gages were distributed among 12 stirrups in each specimen. The strain gages were placed at three possible locations on the stirrups, denoted by letters A, B, and C, corresponding to the top, midpoint, and base of the web, respectively. The strain values were not the actual strains in the stirrups, because the gages were zeroed just prior to the application of the externally applied load. Consequently, the strains in the stirrup represent the strains resulting from the externally applied load. Table 4.5 lists the active stirrup strain gages

for each shear test. The design and actual location of the stirrup gages are given in Tables 4.6-4.9 for Ends IA, IB, IIC, and IID, respectively.

Yielding of an initially unstressed 60 ksi stirrup would be expected to occur at approximately 2000 microstrain; however, because of the initial strain in the stirrups that was not measured, yielding would be expected to occur at strains lower than 2000 microstrain due to the dead load of the specimen.

It was expected that the stirrup strains would not be significant until a crack crossed the stirrup. The three levels of gages enabled "pinpointing" the height at which cracks may have intersected the stirrup. In addition, the gages were used to determine the strain distribution over the length of the stirrup. It was suspected that the less effective anchorage of the standard U-stirrups in End IA would result in lower strain development particularly at location C (bottom of web). Thus the information obtained from the strain gages was used to approximate: (1) when the cracks intersected the stirrups; (2) approximately when the stirrups yielded, and (3) relative stirrup anchorage effectiveness.

4.4.3 Rosette Strain Gages

Internal concrete rosettes were embedded at five locations in all specimens. The rosettes consisted of three arms which measured strains at 0°, 45°, and 90° to the horizontal. The direction of the rosette arms were denoted by A, B, and C corresponding to the horizontal, 45°, and vertical directions, respectively. Table 4.10 lists the active gages for each shear test. The design and actual locations of the internal rosette gages are given in Tables 4.11-4.14.

As for the stirrup strain gages, the measurements of the rosette gages did not represent the actual strain in the concrete; they represented the strains due to the externally applied load in the shear tests. As a result, the calculated values for the principal strains and angles from the concrete rosette measurements did not account for the initial strains in the concrete due to the horizontal prestressing force, the vertical force component of draped strands, and the composite section self weight.

External rosette gages were used to measure strain on the surface of the concrete. Some of the arms of the internal strain gages were not working, so the external rosettes were placed to match the location of the internal rosettes. The positions of the external rosettes were adjusted

slightly to avoid placing the gages over existing cracks in the specimen. As with the internal rosettes, the legs of the external rosettes were oriented at 0°, 45°, and 90° in the vertical plane of the test specimens, and the strains measured were those due to the superimposed external loads. The internal strain gages and the external strain gages were expected to show similar trends. The external rosette gages that were used during the shear tests are given in Table 4.15. The design and actual locations of external rosette gages are given in Tables 4.16-4.19.

Because three different orientations and their strains were measured at each location, the principal strains and directions to the principal strains could be calculated. Combinations of external and internal rosettes were analyzed to better understand the direction and magnitude of the principal stresses.

The experimental principal tensile strains, ε_{te}, and experimental principal compressive strains, ε_{ce}, derived from Mohr's Circle and were calculated from the shear test data by:

$$\varepsilon_{te} = \frac{\varepsilon_a + \varepsilon_c}{2} + \frac{1}{\sqrt{2}}\sqrt{(\varepsilon_a - \varepsilon_b)^2 + (\varepsilon_b - \varepsilon_c)^2}, \tag{4.5}$$

$$\varepsilon_{ce} = \frac{\varepsilon_a + \varepsilon_c}{2} - \frac{1}{\sqrt{2}}\sqrt{(\varepsilon_a - \varepsilon_b)^2 + (\varepsilon_b - \varepsilon_c)^2}, \tag{4.6}$$

where ε_a was the strain in the horizontal direction, ε_b was the strain at 45°, and ε_c was the strain in the vertical direction. The complete derivation of principal strain is given in Appendix A.7.

The angle of principal compression, θ_e, measured from the horizontal direction was also derived from Mohr's Circle and was calculated from the experimental data for external loads by:

$$\cos(2\theta_e) = \left(\frac{(\varepsilon_a - \varepsilon_c)}{\sqrt{2}\sqrt{(\varepsilon_a - \varepsilon_b)^2 + (\varepsilon_b - \varepsilon_c)^2}} \right). \tag{4.7}$$

The derivation of the principal compression angle is given in Appendix A.7.

Corrections to the above principal strain equations include an additional initial axial strain due to prestressing force and self-weight moment and additional initial shear stresses due to self-weight shear and the vertical force component of the draped strands. Axial stresses and shear stresses were resolved into strains in the three directions and added to the above equations.

The corrected principal tensile strains, ε_{tc}, and corrected principal compressive strains, ε_{cc}, were given by:

$$\varepsilon_{tc} = \frac{\varepsilon_a + \varepsilon_c + \frac{f_{pi}}{E_c}}{2} + \frac{1}{\sqrt{2}}\sqrt{\left(\varepsilon_a - \varepsilon_b + \frac{f_{pi}}{2E_c} - \frac{\tau_i}{E_c}\right)^2 + \left(\varepsilon_b - \varepsilon_c + \frac{f_{pi}}{2E_c} + \frac{\tau_i}{E_c}\right)^2}, \qquad (4.8)$$

$$\varepsilon_{cc} = \frac{\varepsilon_a + \varepsilon_c + \frac{f_{pi}}{E_c}}{2} - \frac{1}{\sqrt{2}}\sqrt{\left(\varepsilon_a - \varepsilon_b + \frac{f_{pi}}{2E_c} - \frac{\tau_i}{E_c}\right)^2 + \left(\varepsilon_b - \varepsilon_c + \frac{f_{pi}}{2E_c} + \frac{\tau_i}{E_c}\right)^2}, \qquad (4.9)$$

where f_{pi} represents the initial resultant stress due to the prestressing force and the self-weight moment at the point of interest and τ_i represents the self-weight shear stress at the point of interest. The vertical force component of the draped strands is included by reducing the shear force due to self-weight.

Corrections to Eqn. (4.9) include the additional initial axial stress due to prestressing force and self-weight moment and the additional initial shear stresses due to self-weight shear and the vertical force component of the draped strands. Again, axial stresses and shear stresses were resolved into strains in the three directions and added to above equation. The angle of principal compression, θ_c, measured from the horizontal direction was calculated from the corrected experimental data by:

$$\cos(2\theta_c) = \left(\frac{\left(\varepsilon_a - \varepsilon_c + \frac{f_{pi}}{E_c}\right)}{\sqrt{2}\sqrt{\left(\varepsilon_a - \varepsilon_b + \frac{f_{pi}}{2E_c} - \frac{\tau_i}{E_c}\right)^2 + \left(\varepsilon_b - \varepsilon_c + \frac{f_{pi}}{2E_c} - \frac{\tau_i}{E_c}\right)^2}} \right). \qquad (4.10)$$

4.4.4 Bursting Strain Gages

Near the supports of the original girders, four No. 6 stirrups were placed to control stresses due to the release of prestressing strands and to provide confinement of concrete over the supports. Strain gages were placed on these bursting stirrups near the base of the web. During the shear tests, the bursting gages that were used are given in Table 4.20. The design and actual location of bursting gages are given in Tables 4.21-4.24.

4.4.5 Rupture Strain Gages

Over the supports, a gage was placed to measure concrete strain. The concrete in this area was subject to prestressing force transfer and shear forces. The gages were oriented to measure strain in the horizontal direction. The rupture gages that were used during the shear tests are given in Table 4.25. The design and actual location of rupture gages are given in Tables 4.26-4.29.

4.4.6 Strand Slip

Measurements were taken to determine the existence and amount of strand end slip. Only 9 of the 46 strands were measured for strand slip. It was felt that debonded strands might lead to premature failure in shear due to bond failure. Slip of bonded strands was measured to compare the magnitude of the bonded strand slip to that of the debonded strand slip.

In the last three shear tests, relative slips were monitored between the strands and surrounding concrete at the end of the specimen by attaching the body of an LVDT to the free end of the strand, and the core of the LVDT was epoxied to the concrete specimen near the strand.

In the first shear test on End IB, the setup included a platform clamped to the web. The platform was used to hang the bodies of the LVDTs. The cores of the LVDTs were clamped to the strands. With the mode of failure observed in this test, the setup was determined to be inadequate for measuring strand slip, because the web of the specimen moved relative to the lower flange.

Table 4.30 shows the strands which were measured for slip. The 0.1 in. LVDTs were used to measure strand slip on Strands 1-1, 1-7, 1-8, 1-12, 2-7, and 3-7. The 1 in. LVDTs were used to measure strand slip on Strands 1-4, 1-5, and 1-9. Due to the 12 draped strands in End IID, locations 2-7 and 3-7 did not contain strands, so the LVDTs were moved to Strands 2-8 and 3-8 in this case. On End IA, IB, and IIC, debonded strands that were measured included Strands 1-4, 1-5, 1-8, and 1-9. All strands were bonded for End IID.

4.4.7 Transfer Length Gages

Transfer gages were used to determine the transfer length of prestressing force in the strands after release. To debond specific strands, a plastic sleeve had been placed around the strands for the specified distance to serve as a bond breaker. The length of the sleeves in Ends IA, IB, and IIC used were 2, 4, 12, and 20 ft. The last letter A, B, or C indicates the strain gage location which was 15, 22, and 30 in., respectively, from the bonded end of the particular strand. The transfer length gages monitored during the shear tests are given in Table 4.31. The design and actual locations of transfer length gages are given in Tables 4.32-4.34. No transfer length gages were monitored in End IIC.

4.4.8 Acoustic Emission

Acoustic emission was employed to determine the location and amount of new cracking. The acoustic emission system comprised four transducers, pre-amplifiers, and a signal monitor. Acoustic emission is best for monitoring crack initiation or growth. When the shear cracking was extensive near the ultimate shear strength, the acoustic emission monitoring was less effective in determining locations of new cracking. Although data was taken from three of the four specimens tested, results will not be discussed in this report.

4.5 Testing and Data Processing

This section includes information about the testing equipment used during the shear tests and the testing equipment used for data acquisition. Table 4.35 indicates the manufacturers of this equipment.

4.5.1 Testing Machines

At the Golden Valley test site, two 200 kip actuators with 48 in. stroke were used. It was found that the foundation for the load frame could not resist the necessary force to load the specimens to ultimate shear capacity.

The specimens were moved to the University of Minnesota Structures Lab where a MTS 600 kip universal testing machine was used to apply the load. The MTS machine contained a hydraulic cylinder with a 5 in. stroke. The testing machine is shown in Figure 4.23.

At the University of Minnesota Structures Lab, the cylinder testing machine used was a Forney 400 kip testing machine, which was recalibrated in August, 1996.

4.5.2 Test Procedure

The shear testing was conducted using the actuator in stroke control. Stroke/displacement control was selected for the ability to deflect the specimen after peak load without causing a sudden failure beyond its peak strength. During the shear tests, the displacement was applied incrementally pausing approximately every 20 kips to store data to the hard drive and to locate and mark new cracks and crack extensions. Data was taken again during the hold period and was saved to the hard drive.

The cylinder testing was conducted according to ASTM standards. The compressive and tensile strength tests were conducted in accordance with ASTM C39 and ASTM C496, respectively. Modulus of elasticity tests were conducted in accordance with ASTM C469.

4.5.3 Data Acquisition

The data acquisition system used was an OPTIM MEGADAC system manufactured by OPTIM Electronics. The data was stored to the internal hard drive of a personal computer and later transferred to a spreadsheet for evaluation. Data was taken both during the loading ramps and during the pauses in loading.

4.5.4 Data Reduction

Data taken during the pauses in loading were averaged for that hold period. The initial hold period, when no load was applied, was used to zero the instrumentation. The changes in strain, displacement, and deflection were measured relative to this first hold period.

Data taken during loading had to be reduced due to the vast amount of data. The data was originally read every 0.155, 0.172, 0.447, and 0.167 seconds for the four shear tests. Due to the high rate of data acquisition, the behavior of the specimens was not lost by reducing the data to one eighth of the original data.

Chapter 5- Experimental Results

5.1 Introduction

This chapter summarizes the test data obtained from each specimen. The test setup had approximately the same load-point dimensions, support dimensions, and applied-load steps for each of the specimens. Figure 4.21 shows the test setup, and the actual dimensions are given in Table 4.4. The load was applied in approximately 20 kip increments in the displacement control mode until the peak load was obtained. Loading was continued until a given deflection, as stated in each section, was obtained. Appendix F contains general observations made during each of the shear tests.

During testing, web-shear cracking was observed; flexure-shear cracking through the lower flange was not observed. Three of the four specimens were tested to failure. End IID exceeded the capacity of the 600 kip testing machine without failing. Of the three ends tested to ultimate load, all three exhibited horizontal shear cracks at the base of the web and crushing of the web near the support as the primary failure mode.

5.2 End IA

End IA was fabricated with the limestone aggregate mix and 46 prestressing strands; it contained four draped and eight debonded strands to relieve end stresses; and it had standard U stirrups without leg extensions for transverse reinforcement. Figures 5.1 and 5.2 show photographs of the specimen and setup before testing at the University of Minnesota Structures Lab.

End IA had been previously tested to 324 kips of applied load at the Golden Valley testing facility in February, 1996. The complete shear test was performed August 9, 1996. This was actually the third specimen to be tested in shear at the University of Minnesota Structures Lab. The girder end was one day short of 3 years of age (1095 days), and the slab was about 2 1/2 years of age (896 days).

A complete summary of girder and deck measured concrete strengths is given in Appendixes B.1 and B.2, respectively. At the time of the shear test, 6 x 12 in. cylinder tests

indicated the concrete compressive strength of the girder end was 11300 psi with a modulus of elasticity of 5230 ksi, and the compressive strength of the deck was 5660 psi. The tensile splitting strength of the girder end was 729 psi.

5.2.1 Beam Deflection

Because the test was operated in displacement control, as the deflection was held constant, the load varied to retain the deflection. As a result, load losses of 5 to 10 kips typically occurred during the times the displacement was held constant between load ramps. These load losses may have resulted from load redistribution with new cracking of the concrete section.

The deflection of the specimen read by the two beam deflection LVDTs was corrected for changes due to the rigid body rotation using the measurements from the LVDT monitoring the neoprene pad at the east end. The west end was supported by a steel roller. The respective corrected peak deflections were 6.0% and 7.6% less than the measured peak deflections.

The load-deflection curves for End IA are shown in Figures 5.3 and 5.4 for the West and East LVDTs, respectively. Before the first load peak was reached, the deflection increased linearly with increase in load for both the West and East LVDTs. At first peak load, the West and East LVDTs indicated 0.85 and 0.90 in. of corrected deflection, respectively.

The ultimate load was 503 kips applied 14.1 ft. from the west end. At ultimate load, the West LVDT located 12.1 ft. from the west end indicated 1.07 in. of corrected deflection, and the East LVDT located 15.9 ft. from the west end indicated 1.10 in. of corrected deflection. After the load ramp went to 503 kips, the capacity of the specimen suddenly dropped to 460 kips before the next load ramp. This load loss was due to severe new horizontal cracking. After 4.5 in. of deflection, the specimen had a residual strength of 36% of its ultimate strength, and the test was ended.

5.2.2 Crack Diagrams

After testing at the Golden Valley facility, a single new diagonal crack was observed near the load point in the web. End IA had been tested in shear to 324 kips of applied load in January, 1996. This specimen had the second fewest initial cracks of the four ends upon testing at the University of Minnesota testing facility in August, 1996.

During testing at the University of Minnesota Structural Engineering Lab, the first new cracks occurred after 160 kips. At 360 kips, a large horizontal crack developed near the base of the web. A loud sound was heard, and a new diagonal crack appeared at a load of 440 kips. At the peak load of 503 kips, a loud sound was heard again, and slip along the crack at the base of the web was visible.

After 300 kips, Figure 5.5 shows the increased amount of web-shear cracking. After peak load, the top flange and the web appeared to be sliding relative to the bottom flange, Figure 5.6. No flexure-shear cracks were observed before peak load. The web-shear cracking penetrated the lower flange only over the support, Figures 5.7-5.9. The cracking near the load point is shown in Figures 5.10 and 5.11.

Figure 5.12 shows the crack pattern drawing at the beginning of the shear test. A crack pattern drawing indicating cracking after 300 kips is shown in Figure 5.13. Figure 5.14 shows the crack pattern drawing after peak load at 4.5 in. of deflection.

5.2.3 Stirrup Strains

A total of 30 stirrup strain gages were placed on 12 stirrups. The first letter of each gage label represents the type of gage. For stirrup gages, the first letter is S. The next two or three letters were used to represent the specimen to which the gage belonged, followed by one or two letters to represent the stirrup to which the gage belonged. The strain gages were placed at three possible locations on the stirrup, denoted by the last letters A, B, and C, corresponding to the top, midpoint, and base of the web, respectively.

The stirrup strains were plotted to one data point beyond peak load and are shown in Figures 5.15-5.26. Each figure shows the results of all strain gages located on each respective stirrup. The values given are not the actual strains in the stirrups, the gages were zeroed just prior to the application of the externally applied load. Consequently, the strains in the stirrups represent the change in strains resulting from the externally applied load.

Yielding of an initially unstressed 60 ksi stirrup would be expected to occur at approximately 2000 microstrain; however, because the initial strains in the stirrups were not measured and were assumed tensile, yielding would be expected to occur at measured strains lower than 2000 microstrain.

It was expected that the stirrup strains would not be significant until a crack crossed the stirrup. The three levels of gages enabled "pinpointing" the height at which cracks may have intersected the stirrup. In addition, the gages were used to determine the strain distribution over the length of the stirrup. It was suspected that the less effective anchorage of the standard U-stirrups in End IA would result in lower strain development particularly at location C (bottom of the web). Thus the information obtained from the strain gages was used to approximate: (1) when the cracks intersected the stirrups, (2) when the stirrups yielded, and (3) relative stirrup anchorage effectiveness.

Stirrup 1 contained gages at locations B and C only. Stirrup 1 at location B indicated very little change in strain, 100 microstrain, at ultimate load, Figure 5.15. The Gage 1B region did not indicated any stirrup yielding. The crack drawing indicated that a crack formed below Gage 1B while loading to 300 kips; no cracks were observed above the gage. The stirrup at Gage 1C appeared to yield in tension at approximately 250 kips. This gage indicated that as the load increased, the strain increased at a greater rate compared to Gage 1B. Two preexisting diagonal cracks were present that crossed near the region of Gage 1C. The horizontal crack at the base of the web was preexisting; however, the crack did not visibly cross the gage location until 240 kips. Near ultimate load, the concrete in this area showed spalling due to the lower flange sliding relative to the web.

No strain gage was placed at location 3A. Strains measured with Gage 3B had only half the magnitude of the strains from Gage 3C, Figure 5.16. The stirrup did appear to yield at 420 kips in the 3B region. The nearest crack to this gage occurred at 360 kips. Gage 3C data indicated yielding in tension starting at 360 kips and indicated behavior very similar to Gage 1C. At location 3C, the preexisting horizontal crack at the base of the web crossed the stirrup. Diagonal cracking in this area was limited and did not develop until 440 kips. After ultimate load, visible horizontal displacement was observed at this location.

Gage 4A with a peak strain at 150 kips did not indicate yielding, Figure 5.17. A horizontal crack which developed at 140 kips appeared to be closest to the gage. Gage 4B indicated yielding with a large jump in strain at 440 kips. A diagonal crack which formed at 440 kips was very close to the gage. Near Gage 4C, the stirrup appeared to yield at 200 kips. The

preexisting horizontal crack appeared to cross Gage 4C. This gage indicated odd behavior and possibly may have been damaged. After ultimate load, visible horizontal displacement was observed at this location.

At Gages 5A and B, the stirrup could have yielded, Figure 5.18. Gage 5A indicated the most uniform increase in strain with load, and cracks in this area occurred at 180 kips. Gage 5B indicated the largest initial stiffness with an abrupt change in stiffness at 440 kips. A diagonal crack marked 220 kips appeared to match the location. The data from Gage 5C indicated a reversal from increasing tension to decreasing tension at 300 kips. The preexisting horizontal crack had crossed near Gage 5C. After ultimate load, visible horizontal displacement was observed at this location.

As illustrated in Figure 5.19, all of the stirrup gages at locations 6A-C indicated large increases in strains at 400 to 440 kips. Gage 6A indicated the largest strain of the three gages. The cracks in this area were marked at 220 and 260 kips. A crack marked 380 kips crossed above Gage 6B. The preexisting horizontal crack was observed to cross Gage 6C.

Figure 5.20 indicates the stirrup probably did not yield near Gages 7A and B. Gage 7A indicated greater strain compared to Gage 7B. The closest crack to Gage 7A was marked at 180 kips. The diagonal crack corresponding to Gage 7B was preexisting. No strain gage was placed at location 7C. From this location to the load point at 14.0 ft., a long crack with a large crack width opened in the deck, and cracking was less severe in the web, refer to Figure 5.7.

Figure 5.21 indicates Gages 8A and B probably did not yield; however, Gage 8A indicated greater strain compared to Gage 8B. For Gage 8A, the rate of strain changed at 340 kips; however, no cracks were marked near Gage 8A. The diagonal crack near Gage 8B was marked at 480 kips. No strain gage was placed at location 8C.

Gages 12A and C were damaged before shear testing, and no data from these gages was collected. Gage 12B indicated very little change in strain, about 50 microstrain in compression, Figure 5.22. This stirrup was located within the long shear span where the applied shear was only 1/3 of the applied load compared to 2/3 of the applied load carried by the short shear span. The crack pattern in this area was not recorded. The crack pattern on the long shear span was much less severe than the short shear span due to the decreased shear in that section.

Gages 13A and C were also damaged before shear testing. Gage 13B indicated little strain change until about 400 kips, Figure 5.23. After 400 kips, the strain increased rapidly to 500 microstrain at ultimate load. The crack pattern in this area was not recorded.

Gage 15A indicated very little change in strain at about 50 microstrain, Figure 5.24. Gage 15B indicated the greatest strain of all the gages within the long shear span. As indicated by a rapid increase in strain after 300 kips. The stirrup at location Gage 15B was probably close to yielding. The crack pattern in this area was not recorded. No gage was placed at location 15C.

At Gages 18A and B, the stirrup did not yield, Figure 5.25. Gage 18A indicated only a marginal change in strain of about 150 microstrain. Gage 18B indicated no change in strain throughout the testing. Gage 18C indicated a rapid increase in strain after 400 kips indicating possible yielding. The crack pattern in this area was not recorded.

No gage was placed at location 22A. Gages 22B and C indicated little change in strain, less than 100 microstrain, Figure 5.26. This stirrup was the last stirrup with a strain gage within the long shear span. The crack pattern in this area was not recorded.

In summary, the strains for Stirrups 1-5 at the base of the web were greater than those near midheight or the top of the web during the shear testing. For Stirrups 6-8, the strains at the top of the web were greater than those at midheight or the bottom of the web. Generally, Stirrups 12-22, on the long shear span, indicated much less change in strain than Stirrups 1-8, on the short shear span.

5.2.4 Concrete Rosette Strains

Internal concrete rosettes were embedded at five locations in End IA. End IA had only two of 15 internal arms working during the shear testing. Therefore, external rosettes were placed on the web at approximately the same locations as the internal rosettes. In addition, one arm of the 15 external rosette arms did not work.

For internal gages, the first letter of the label represents the type of gage. For rosette gages, the first letter is R. The next two or three letters were used to represent the specimen to which the gage belonged. Next, one letter was used to represent the area to which the gage belonged. The rosettes consisted of three arms which measured strains at 0°, 45°, and 90° to the

horizontal. The last letter was the direction of the rosette arms which were denoted by A, B, and C corresponding to the horizontal, 45°, and vertical directions, respectively.

For external rosette gages, the first four letters were "extR". Next, one letter was used to represent the specimen to which the gage belonged. The rosettes consisted of three arms which measured strains at 0°, 45°, and 90° to the horizontal. The last letter was the direction of the rosette arms which were denoted by A, B, and C corresponding to the horizontal, 45°, and vertical directions, respectively. The 45° direction pointed from the support on the corresponding shear span to the applied load for all rosettes.

The rosette strains were plotted to one data point past peak load. These values did not represent the actual strain in the concrete; they represented the strains due to the externally applied load in the shear tests only. To compare with the measured values, theoretical strain values were calculated assuming no self weight of the composite section and no prestressing force. The following theoretical values were calculated for comparison: (1) the three directional strains, (2) the principal strains, and (3) the principal compression angle.

The results from each arm are given in Figures 5.27-5.31 for all rosette locations. The solid lines represent the theoretical predicted strain values, and the series with markers show actual test data. The theoretical direction (A) indicated that strain increased as applied load increased, theoretical direction (B) indicated that strain decreased (became more compressive) as applied load increased, and theoretical direction (C) indicated that strain did not change as applied load increased. In all but Rosette 1, for which case the gage along the 45° line was inactive, the largest measured compressive strain was oriented along the 45° arm or direction (B). In all of the rosettes, the horizontal direction (A) appeared to undergo an increase in compressive strain, but smaller in magnitude than recorded by the 45° gages. For experimental Rosettes 3-5, the direction (A) exhibited a greater increase in strain than direction (C) throughout the shear testing.

Figures 5.32-5.35 show the values of the calculated principal strains assuming zero initial conditions. Theoretical and experimental data includes no self-weight of the composite section and no prestressing force. The solid lines represent the theoretical predicted strain values, and the series with markers were combinations of experimental test data. These combinations are

described with letters to represent whether or not the gages in the respective direction A, B, and C were external (E) or internal (I). For example, E I E means the gages were external, internal, and external, in directions (A), (B), and (C), respectively. It was not possible to obtain principal strains for Rosette 1, because one of the three arms had been damaged on the external rosette. In the experimental data, Rosettes 2-5 measured maximum principal tensile strains to be about 125 to 200 microstrain and the maximum principal compressive strains to be approximately -250 microstrain. In Rosettes 3-5, the theoretical principal tension indicated more tensile strain than the experimental data for a majority of the shear testing.

The angles to principal compression were calculated as shown by Eqn. (4.7). The principal angles described in the following paragraph were determined for the case of externally applied loads.

Due to a broken arm on the external gage, the measured direction of principal compression in Rosette 1 was unknown. External Rosette 1 had a crack through the gage at 300 kips. The theoretical principal compression strain orientations due to the external loads were constant at the respective gage locations. In Figures 5.36-5.39, the theoretical angles increased from Rosettes 2-5 as the moment at the respective locations increased. In Figure 5.36, measurements from Rosette 2 indicated the greatest change in principal angle direction of all rosettes from 52° to 30° with increasing applied load. At 440 kips, External Rosette 2 had a crack below the gage. In Figure 5.37, the measured principal angle of Rosette 3 decreased from 52° to 44°, then increased to 52° at peak load, and indicated less scatter than Rosette 2. External Rosette 3 had a crack above 220 kips. With the least scatter, Rosette 4 indicated an initial principal angle of 52°, which flattened to 46°, and then jumped to 56° at 440 kips, Figure 5.38. The principal angle of Rosette 5 started at 47°, increased to 62°, and finished at 59°, Figure 5.39. The crack patterns were not documented in the region of Rosette 5.

In summary, the theoretical value in all four rosettes was greater than the measured principal compression angle calculated from experimental data. Experimental Rosette 3 matched the theoretical calculation the best of the four rosettes.

5.2.5 Corrected Concrete Rosette Strains

The experimental data was corrected to account for initial conditions not measured by the rosettes, using measured properties given in Appendix C. Direction (A) had an initial strain component due to prestressing force and self moment. Direction (B) had an initial component due to prestressing force and shear and moment due to the self weight. Direction (C), the vertical direction, had no initial strain component.

Figures 5.40-5.44 show the experimental data corrected for initial conditions. The corrected and theoretical data matched when no load was applied because the same assumptions were made for initial conditions. The solid lines represent the theoretical predicted strain values, and the series with markers represent the corrected experimental test data. The theoretical direction (A) indicated that strain should increase during the testing. Before peak load, corrected experimental direction (A) data increased only for Rosette 5, Figure 5.44. The theoretical direction (B) indicated that strain should decrease during the testing. This was the case in all four of the corrected experimental direction (B) data. The theoretical direction (C) indicated that there should be no change in strain. In four of the five rosettes, the corrected experimental strains in direction (C) were observed to slightly decrease. In one of the five rosettes, corrected experimental direction (C) data indicated a small increase in strain, Figure 5.41.

Figures 5.45-5.48 show the corrected principal strains using the corrected experimental data. The corrected and theoretical data matched when no load was applied because the same assumptions were made for initial conditions. At peak load, the theoretical predicted principal tension indicated more tensile strains than corrected experimental data.

Figures 5.49-5.52 show the corrected principal compression angle which was calculated for the corrected experimental data. The theoretical and corrected experimental data match very well up to 200 kips. This is due to the large initial condition of prestressing force in the axial direction. The theoretical data indicated that the principal compression angle should increase as the applied load is increased. The corrected experimental data indicated lower values than the theoretical predicted angles at peak load for three of the four rosettes. Corrected experimental angles obtained from Rosette 5 indicated the best agreement with theoretical data.

The theoretical data does not account for section cracking. In the actual specimens after cracking has occurred, the experimental angle does not continue to increase as predicted by the theory; therefore, the theoretical angle is likely larger than experimental angle at peak load.

5.2.6 Bursting Strains

Near the supports of the original girders, four No. 6 stirrups were placed to control stresses due to the release of prestressing strands and to provide confinement of concrete over the support. Gages RIAB1 and RIAB2 were placed on the first bursting stirrup on the west end of the opposite stirrup legs at the base of the web. These two gages should have read similar results. Bursting strains were plotted to one data point past peak load.

Up to peak load, Figure 5.53 shows that the force in the stirrups in this area became more compressive under the externally applied loads with one exception. The exception was Gage RIAB2 at 240 kips which indicated a rapid jump in strain. The bursting stirrups indicated very little change in behavior from 300 kips to peak load. Beyond peak load, the bursting stirrups indicated a rapid change to more tension possibly indicating more cracking or movement along the existing crack interfaces near the base of the web.

5.2.7 Rupture Strains

Over the supports, two gages were placed in the horizontal direction to measure concrete strains. Both gages were located at the same horizontal distance; however, Gage RIAP1 was located vertically 2.5 in. lower in the section as compared to Gage RIAP2. Rupture strains were plotted to one data point past peak load. Note that these measured strains only represent the change in strain observed from the beginning of the shear test; therefore, prestress and self weight effects were not included in the results.

Figure 5.54 shows that the change in strain in the concrete became more tensile, less compressive, up to 300 kips. Gage RIAP2 indicated a much greater increase in tensile strains compared to Gage RIAP1. Beyond peak load, the rupture gages indicated a slight reduction in force acting on the concrete.

5.2.8 Strand Slip

The slips of both debonded and bonded strands were monitored by LVDTs. Only nine of the 46 strands were measured for strand slip of which five of the strands were bonded strands and four were debonded strands. All monitored strands indicated evidence of slip. These slips typically occurred at peak load or 20 kips before peak load and were typically less than 0.08 in. into the specimen. After peak load was reached, the specimen was loaded in deflection control until the specimen could only support 200 kips. In this load region, the strands indicated continued slip into the specimen as deflection increased. After the load was removed, the strands indicated no additional movement. Strand slips were plotted for the entire test.

Strand 1-1 was bonded for the entire length. Strand 1-4 was debonded for 4 ft., and Strand 1-5 was debonded for 2 ft. Figure 5.55 shows Strands 1-4 and 1-5 slipped 0.04 in. at the same load. Strand 1-1 indicated only half the magnitude of slip of Strands 1-4 and 1-5.

Figure 5.56 shows the slip of Strand 1-7 was similar in magnitude to Strand 1-1. Strands 1-8 and 1-9 each indicated a slip of 0.03 in. Strand 1-7 was bonded for the full length, Strand 1-8 was debonded for 2 ft., and Strand 1-9 was debonded for 4 ft.

Strands 1-12, 2-7, and 3-7 were fully bonded. Strand 1-12 indicated behavior and magnitude similar to Strands 1-1 and 1-7, Figure 5.57. Strand 2-7 had the largest measured slip of 0.075 in. The LVDT that measured strand slip for Strand 3-7 had wiring difficulties. Consequently, although Strand 3-7 indicated slip at peak load, the magnitude and direction of slip are suspect.

In summary, the strands farther from the bottom had greater slip than strands in the bottom row. This might have been due to the web sliding relative to the bottom flange. All bonded strands in the bottom row had the same slip which was less than the slip of debonded strands. All debonded strands in the bottom row had the same slip. The magnitude of the slip did not seem related to the length of debonding. Also, debonded strand slip occurred 20 kips earlier than the bonded strand slip.

5.2.9 Transfer Length

The transfer gages were used to determine the transfer length of prestressing force in the strands after release. To debond specific strands, a plastic sleeve had been placed around the

strands for a specified distance to serve as a bond-breaker. The lengths of the sleeves used were 2, 4, 12, and 20 ft. The last letter A, B, or C indicates the strain gage location which was 15, 22, and 30 in., respectively, from the beginning of the bonded end of the particular strand. Transfer strains were plotted to one data point past peak load. Again, these data represent the changes in strain measured relative to the beginning of the shear test.

Figure 5.58 shows the change in strain of Strands 1-5 and 1-8. Strand 1-5 was debonded for 2 ft. and instrumented with Gages TIA25B and TIA25C. Gage TIA25B indicated a linear increase in magnitude of strain without any peaks or reversals that would indicate slip. On the other hand, TIA25C indicated a linear increase in magnitude of strain up to peak load and at peak load the strain increased rapidly. Strand 1-8 was debonded for 2 ft. and instrumented with Gages TIA28B and TIA28C. Both Gages TIA28B and TIA28C indicated similar behavior and magnitude to Gage TIA25B.

Figure 5.59 shows the change in strain of Strands 1-4 and 1-9. Strand 1-4 was debonded for 4 ft. and instrumented with Gage TIA44C. Throughout the shear testing, Gage TIA44C did not change strain value and might have been damaged. Strand 1-9 was debonded for 4 ft. and instrumented with Gage TIA49C. Up to peak load, Gage TIA49C indicated similar behavior to Gages TIA25B, TIA28B, and TIA28C but twice the magnitude. At peak load, Gage TIA49C indicated a dramatic increase in strain.

5.3 End IB

End IB was fabricated with the limestone aggregate mix; it contained four draped and eight debonded strands to relieve end stresses; and it had standard U stirrups with leg extensions for transverse reinforcement.

The shear test was performed on June 6, 1996. This was the first specimen to be tested in shear at the University of Minnesota Structures Lab. The girder end was 2 years and 10 months of age (1031 days), and the slab was approximately 2 years and 3 months of age (832 days).

A complete summary of measured concrete strengths is given in Appendixes B.1 and B.2. At the time of the shear test, 6 x 12 in. cylinder tests indicated the concrete compressive strength of the girder was 11,300 psi with a modulus of elasticity of 5230 ksi, and the compressive strength of the deck was 5660 psi. The tensile splitting strength of the girder end was 729 psi.

5.3.1 Beam Deflection

Because the test was operated in displacement control, load losses of 5 to 10 kips typically occurred during the times the displacement was held constant between load ramps. These load losses resulted from load redistribution with new cracking of the concrete section. After the first load peak of 453 kips, the specimen exhibited reduced stiffness and larger load losses.

The deflection of the specimen read by the two beam deflection LVDTs was corrected for changes due to rigid body rotation using the measurements from the LVDT monitoring the neoprene pad at the east end. The west end was supported by a steel roller. The deflection measurements by the West and East LVDTs were corrected using Eqns. (4.1) and (4.3), respectively. The corrected peak deflections were 6.1% and 7.7% reduction from that of measured peak deflections.

The load-deflection curves for End IB are shown in Figures 5.60 and 5.61 for the West and East LVDTs, respectively. Before the first load peak was reached, the deflection increased linearly with increase in load for both the West and East LVDTs. At first peak load, the West and East LVDTs indicated 0.89 and 0.97 in. of corrected deflection, respectively.

The ultimate load was 520 kips applied 13.82 ft. from the west end. At ultimate load, the West LVDT located 12.0 ft. from the west end indicated 1.24 in. of corrected deflection, and the East LVDT located 15.8 ft. from the west end indicated 1.31 in. of corrected deflection. The ultimate load was the second load peak which occurred after the first load peak of 453 kips. After 2.6 in. of deflection, the specimen had a residual strength of 70% of its ultimate strength, and the test was ended.

5.3.2 Crack Diagrams

Due to camera problems, limited amounts of photos were developed. After peak load, Figure 5.62 shows cracking near the support.

Figure 5.63 shows the crack pattern drawing at the beginning of the shear test. No detailed crack diagrams were taken just after peak load. In addition, photos did not help reconstruct the crack patterns at ultimate load; although, it was noted that a loud sound was heard at 435 kips. Figure 5.64 illustrates a simple sketch taken after the complete testing; however, the

damage and spalling to the girder was so extensive that the information provided by the sketch was minimal.

5.3.3 Stirrup Strains

The stirrup strains, plotted to one data point beyond peak load, are shown in Figures 5.58-5.69. Each figure shows the results of all strain gages located on each respective stirrup. The values given are not the actual strains in the stirrups, the gages were zeroed just prior to the application of the externally applied load. Consequently, the strains in the stirrups represent the change in strains resulting from the externally applied load.

Stirrup 1 contained gages at locations B and C only. Stirrup 1 at location B indicated a maximum change in strain of 250 microstrain, Figure 5.65. The Gage 1B region indicated no signs of yielding. The stirrup at Gage 1C appeared to yield in tension at approximately 290 kips. This gage indicated that as the load increased to 290 kips, the strain increased at the same rate as Gage 1B. The crack pattern in this area was not recorded.

No strain gage was placed at location 3A. Gage 3B had little change in strain up to 200 kips, linear increase in strain from 240 to 430 kips, and rapid increase in strain from 430 kips to peak load, Figure 5.66. The stirrup could have yielded at 430 kips in the 3B region. At the end of the test, data from Gage 3C indicated compression as compared to tension for Gage 3B. The data for Gage 3C indicated a reversal from increasing tension to decreasing tension at 140 kips and again at 430 kips. The crack pattern in this area was not recorded.

Gage 4A did not indicate yielding and indicated a peak strain at ultimate load of 520 kips, Figure 5.67. Gage 4B indicated a large jump in strain and yielding at 300 kips. At Gage 4C, the stirrup appeared to yield in compression at 430 kips. Both Gages 3C and 4C had a behavior that would suggest yielding in compression which could be an indication of damaged gages. The crack pattern in this area was not recorded.

All three gages on Stirrup 5 indicated yielding, Figure 5.68. Gage 5A indicated the most uniform increase in strain with load. Gage 5B indicated little change in strain until 490 kips which was followed by an abrupt increase in strain. At Gage 5C, the stirrup indicated relatively no change in strain until 410 kips and then increased to 700 microstrain. The crack pattern in this area was not recorded.

As illustrated in Figure 5.69, Gages 6A and B indicated similar strains near peak load. The stirrup gages at locations 6A and B probably yielded near 430 kips. Gage 6C indicated little change in strain throughout the shear test. The crack pattern in this area was not recorded.

Figure 5.70 indicated stirrup yielding near Gages 7A and B. Gage 7A indicated greater strain compared to Gage 7B until 450 kips was reached. After 450 kips, the strain in Gage 7B increased much faster than the strain measured by Gage 7A. The stirrup at location 7A probably yielded at 290 kips. Up to 410 kips, the stirrup at location 7B indicated almost no change in strain. After 410 kips, the stirrup strain rapidly increased and indicated yielding. No strain gage was placed at location 7C. The crack pattern in this area was not recorded.

Figure 5.71 indicated Gage 8A probably yielded; however, Gage 8B did not. Gage 8A indicated little change in strain up to 290 kips. After 290 kips, the stirrup at Gage 8A indicated yielding. Gage 8B indicated little change in strain and only showed an increase in strain near peak load. The crack pattern in this area was not recorded.

Gages 12A and B indicated very little change in strain, about 50 microstrain in compression, Figure 5.72. Gage 12C indicated the largest change in strain of the three gages, about 150 microstrain. This stirrup was located within the long shear span where the applied shear was only 1/3 of the applied load compared to 2/3 of the applied load carried by the short shear span. The crack pattern in this area was not recorded.

Gages 13A and B indicated very little change in strain about 50 microstrain, Figure 5.73. Gage 13C indicated little strain change until about 310 kips. After 310 kips, the strain increased at a slightly increasing rate. The crack pattern in this area was not recorded.

Gages 15A and B indicated identical behavior up to 250 kips, Figure 5.74. After 250 kips, the behavior of the two gages diverged; however, at 460 kips the changes in strain were again equal. The crack pattern in this area was not recorded. No gage was placed at location 15C.

At location Gage 18A, the stirrup displayed linear behavior for the entire test, Figure 5.75. Gage 18A indicated the greatest change in strain of any gages on the long shear span. Gage 18B was damaged before shear testing, and no data was collected. Gage 18C indicated a reversal in strain occurring at 450 kips. The crack pattern in this area was not recorded.

No gage was placed at location 22A. Gages 22B and C indicated little change in strain, less than 100 microstrain, Figure 5.76. This stirrup was the last stirrup with a strain gage within the long shear span. The crack pattern in this area was not recorded.

In summary, the strains for Stirrups 1 and 3 at the base of the web were greater than those near midheight or the top of the web for a majority the shear testing. For Stirrups 4-8 to approximately 300 kips, the strains at the top of the web were greater than those at midheight or the bottom of the web. Greater than 300 kips, the strains for Stirrups 4-8 at the midheight were greater than those at the top or the bottom of the web. Only Stirrups 15 and 22, on the long shear span, indicated a strain greater than 500 microstrain.

5.3.4 Concrete Rosette Strains

Internal concrete rosettes were embedded at five locations in End IB. The rosettes consisted of three arms which measured strains at 0°, 45°, and 90° to the horizontal. End IB had only eight of 15 internal arms working during the shear testing. Therefore, three external rosettes were placed on the web at approximately the same locations as the internal rosettes. In addition, two arms of the nine external rosette arms did not work.

The rosette strains were plotted to one data point past peak load. These values were not the actual strains; they represented the strains only due to the externally applied load in the shear tests. The theoretical strain values in this section were the calculated three direction strains, principal strains, and principal compression angle assuming no self weight of the composite section and no prestressing force.

The results from each arm are given in Figures 5.77-5.81 for all rosette locations. The solid lines represent the theoretical predicted strain values, and the series with markers show actual test data. The theoretical direction (A) indicated that strain increased as applied load increased, theoretical direction (B) indicated that strain decreased as applied load increased, and theoretical direction (C) indicated that strain did not change as applied load increased. The internal and external direction (B), 45° arm, indicated the largest change in compression of all directions for Rosettes 1,2,4,5 throughout the shear testing. No comment could be made about Rosette 3 because there were no active direction (B) gages. Except for Rosette 1, the direction (A) and (C) had little change in strain up to more than 300 kips. In all the rosettes, the horizontal

direction (A) appeared to undergo an increase in compressive strain for a majority of the shear testing, but smaller in magnitude than the 45° gages recorded.

Figures 5.82-5.84 show the values of the calculated principal strains assuming zero initial conditions. The solid lines represent the theoretical predicted strain values, and the series with markers were combinations of experimental test data. It was not possible to obtain principal strains for Rosettes 3 and 5, because one of the three directions had been damaged. With four combinations of external and internal arms, Rosette 1 had a wide range of principal strain values at any given applied load. In Rosette 2, the experimental data followed the theoretical data better than Rosette 1. The theoretical principal tension were more tensile than the experimental data up to peak load. The experimental data from Rosette 4 followed the theoretical data the best of the three rosettes up to 410 kips. After 410 kips, a rapid decrease in principal compression and increase in principal tension occurred which could have been due to new cracking in this area. No crack mapping was taken near Rosette 4; therefore, the above conclusion is conjecture.

The angles to principal compression were calculated as shown in Chapter 4. In Figure 5.85, experimental data from Rosette 1 indicated an initial angle around 48° and finished the shear testing around 35°. All four combinations indicated a decrease in angle as load was applied. In Figure 5.86, the angle of Rosette 2 decreased from 47° to 34° and increased to 62° past peak load. It was not possible to obtain principal angles for Rosettes 3 and 5, because one of the three directions had been damaged. The Rosette 4 principal compression angle began at 48° and remained unchanged until 390 kips, Figure 5.87. In Rosettes 2 and 4, the theoretical value was greater than the principal compression angle calculated from experimental data up to peak load.

5.3.5 Corrected Concrete Rosette Strains

Figures 5.88-5.92 show the experimental data corrected for initial conditions. The corrected and theoretical data match with no load applied, because the same assumptions were made for initial conditions. The solid lines represent the theoretical predicted strain values, and the series with markers show corrected experimental test data. The theoretical direction (A) indicated that strain should increase during the testing. The rosettes were placed below the neutral axis of the composite cross section; therefore, the strains due to flexure would be tensile

strains. Up to 400 kips, the experimental data in the direction (A) for Rosettes 1 and 2 indicated a decreasing strain and Rosettes 3 and 4 indicated a relatively constant strain. Due to shear strains and flexural strains, the theoretical direction (B) indicated that strain should decrease during the shear testing. This was the case in all five of the corrected experimental direction (B) data. The theoretical direction (C) should have no change in strain. In four of the six rosettes, corrected experimental direction (C) data indicated a small change, less than 100 microstrain change, up to 400 kips.

Figures 5.93-5.95 show the corrected principal strains using the corrected experimental data. The corrected and theoretical data matched when no load was applied, because the same assumptions were made for initial conditions. For Rosette 1, the corrected experimental principal tension data fell on both sides of the theoretical principal tension data. On the other hand, the corrected experimental principal compression data fell below the theoretical principal compression data from the initial applied load. For Rosettes 2 and 4, the experimental and theoretical principal tension strain agreed better than the experimental and theoretical principal compression strain.

Figures 5.96-5.98 show the corrected principal compression angles which were calculated for corrected experimental data. Up to 390 kips, the corrected experimental data indicated a greater principal compression angle than the theoretical angle for Rosette 1. Afterwards, the theoretical and corrected experimental data agreed well. The theoretical and corrected experimental data match very well up to 200 kips for Rosettes 2 and 4. The theoretical data indicated that the principal compression angle should increase as the applied load is increased. The corrected experimental data indicated lower values than theoretical data at peak load for Rosettes 2 and 4. For applied load less than 200 kips, corrected experimental data for Rosettes 1, 2, and 4 showed good agreement with theoretical data.

The theoretical data does not account for section cracking. In the actual specimens after cracking has occurred, the experimental angle does not continue to increase as predicted by the theory; therefore, the theoretical angle is likely larger than experimental angle at peak load.

5.3.6 Bursting Strains

Near the supports of the original girders, four No. 6 stirrups were placed to control stresses due to the release of prestressing strands and to provide confinement of concrete over the end supports. Gages RIBB2 and RIBB3 were placed on the first and the third bursting stirrups, respectively. Bursting strains were plotted to one data point past peak load.

Figure 5.99 shows that up to 300 kips, the force in the stirrups in this area became more compressive under the externally applied loads with one exception. The exception was Gage RIBB3 which at 120 kips indicated a rapid increase in strain; this may have been due to new cracking near the support. Both bursting stirrups indicated great increase in tension from 440 kips to peak load possibly indicating more cracking or movement along the existing crack interfaces near the base of the web.

5.3.7 Rupture Strains

End IB had two rupture strain gages placed in the original girder; however, neither of the gages were active during testing. Therefore, no results are reported in this section.

5.3.8 Strand Slip

In the first shear test on End IB, the setup included a platform clamped to the web. The platform was used to hang the bodies of the LVDTs. The cores of the LVDT were clamped to the strands. With the mode of failure observed in this test, this setup was found to be inadequate for measuring strand slip, because the web moved relative to the lower flange. Therefore, no results are reported in this section.

5.3.9 Transfer Length

Figure 5.100 shows the change in strain of Strand 3-5. Strand 3-5 was bonded for the entire length of the strand. Gages TIB035A, TIB035B, and TIB035C were placed on Strand 3-5 and located at a distance from the west end of the specimen at 15, 22, and 30 in., respectively. The measured strain for Gages TIB035A and TIB035B was relatively unchanged up to 440 kips, then the strain increased rapidly. Gage TIB035C indicated no change in strain up to 460 kips, then the strain increased rapidly.

Figure 5.101 shows the change in strain of Strand 1-8. Strand 1-8 was debonded for 2 ft. Gages TIB28A, TIB28B, and TIB28C were placed on Strand 1-8 and located at a distance from the beginning of the bonding at 15, 22, and 30 in., respectively. Gage TIB28A indicated no change in strain until 440 kips, then the strain decreased. Gage TIB28B indicated a linear increase in magnitude of strain up to peak load and at peak load the strain increased rapidly. Gage TIB28C indicated a linear increase in magnitude of strain up to 440 kips, then the strain increased rapidly.

Figure 5.102 shows the change in strain of Strand 1-9. Strand 1-9 was debonded for 4 ft. Gages TIB49A, TIB49B, and TIB49C were placed on Strand 1-9 and located at a distance from the beginning of the bonding at 15, 22, and 30 in., respectively. Up to peak load, Gage TIB49A indicated a linear increase in magnitude of strain, and at peak load the strain increased rapidly. Gage TIB49C had almost the same behavior as Gage TIB28C throughout the shear test. Gage TIB49B indicated a larger linear increase in magnitude of strain up to 480 kips compared to Gage TIB28B, then the strain increased rapidly.

5.4 End IIC

End IIC was fabricated with the glacial gravel and microsilica mix; it contained four draped and eight debonded strands to relieve end stresses; and it had standard U stirrups with leg extensions for transverse reinforcement. Figures 5.103 and 5.104 show photographs of the specimen and setup before testing.

The shear test was performed November 23, 1996, and was the fourth specimen to be tested in shear at the University of Minnesota Structures Lab. The girder end was 3 years and 3 months of age (1201 days), and the slab was approximately 2 years and 9 months of age (1002 days).

A complete summary of measured concrete strengths is given in Appendixes B.1 and B.2. At the time of the shear test, 6 x 12 in. cylinder tests indicated the concrete compressive strength of the girder was 9300 psi with a modulus of elasticity of 4520 ksi, and the compressive strength of the deck was 5660 psi. The tensile splitting strength of the girder end was 587 psi.

During the transportation process, End IIC accidentally rolled over during the removal from the Golden Valley Facility. The rollover caused additional cracking in the deck and a horizontal crack at the base of the web. In addition, the embedded lift hooks were damaged.

5.4.1 Beam Deflection

Because the test was operated in displacement control, load losses of 5 to 10 kips typically occurred during the times the displacement was held constant between load ramps. These load losses resulted from load redistribution with new cracking of the concrete section.

The deflection of the specimen read by the two beam deflection LVDTs was corrected for changes due to rigid body rotation using the measurements from the LVDT monitoring the neoprene pad at the east end. The west end was supported by a steel roller. The deflection measurements by the West and East LVDTs were corrected using Eqns. (4.1) and (4.3), respectively. The corrected peak deflections were 8.8% and 11.5% less than the measured peak deflections.

The load-deflection curves for End IIC are shown in Figures 5.105 and 5.106 for the West and East LVDTs, respectively. Before the load peak was reached, the deflection increased nearly linearly with increase in load for both West and East LVDTs.

The ultimate load was 614 kips applied 14.0 ft. from the west end. At ultimate load, the West LVDT located 12.2 ft. from the west end indicated 1.35 in. of corrected deflection, and the East LVDT located 16.0 ft. from the west end indicated 1.44 in. of corrected deflection. After 2.6 in. of deflection, the specimen had a residual strength of 63% of its ultimate strength, and the test was ended.

5.4.2 Crack Diagrams

End IIC had the most initial cracking of the four ends, and the web had many preexisting diagonal cracks. At 100 kips, a detailed look at the cracks indicated only slight growth in length and width of preexisting cracks. First new cracking occurred after 160 kips. At 340 kips, a few new short cracks were found. At 460 kips, the main diagonals indicated growth in crack width. The base of the web near the support started spalling at 500 kips. At 540 and 560 kips, loud

sounds were heard. When peak load was reached at 614 kips, no loud sounds were heard. No flexure-shear cracks were observed before peak load.

After 540 kips, Figure 5.107 shows additional web-shear cracking. After peak load, Figure 5.108 shows the bottom of the web crushing. The web cracking penetrated the lower flange only over the support and occurred with other web diagonal cracking, Figures 5.109 and 5.110. The top flange and the web appeared to be sliding relative to the bottom flange, Figures 5.111 and 5.112. In Figure 5.113, a photograph of the short shear span shows the extent of damage after shear testing.

Figure 5.114 shows a drawing of the crack pattern before the shear testing. Figure 5.115 shows the crack pattern at the end of the shear testing.

5.4.3 Stirrup Strains

The stirrup strains, plotted to one data point beyond peak load, are shown in Figures 5.116-5.124. Each figure shows the results of all strain gages located on each respective stirrup. The values given are not the actual strains in the stirrups; the gages were zeroed just prior to the application of the externally applied load. Consequently, the strains in the stirrups represent the change in strains resulting from the externally applied load.

Stirrup 1 contained only gages at locations B and C. The gages were damaged before shear testing, and no data was collected from the two gages.

No strain gage was placed at location 3A. Although, gages were placed at location 3B and C, the gages were damaged before shear testing.

Gage 4A did not indicate yielding until ultimate load, Figure 5.116. A preexisting diagonal crack appeared to be closest to the gage. Gages 4B and C were damaged before shear testing, and no data was collected from these gages.

At Gage 5A, the stirrup could have yielded, Figure 5.117. Gage 5A indicated strain increased rapidly to 260 kips, started decreasing until 350 kips, and then increased until peak load. A preexisting horizontal crack at the top of the web was identified closest to Gage 5A. Gage 5B indicated an increase in strain to peak load. A diagonal crack marked 220 kips appeared to match the location. Gage 5C indicated increases and decreases in strain with the

trend toward increasing strain. The horizontal preexisting crack at the bottom of the web crossed near Gage 5C.

In Figure 5.118, Gage 6A did not indicate behavior that would suggest yielding. The data shows an approximate linear increase in strain for increase in load. Preexisting cracks were marked above Gage 6A. Gages 6B and C were damaged before shear testing, and no data was collected from these gages.

Figure 5.119 indicates that the stirrup probably did not yield at Gages 7A and B. Gage 7A indicated a rapid increase in strain at 280 kips, and this may have been due to wiring difficulties during shear testing. The cracking near Gage 7A was marked as preexisting. The diagonal crack corresponding to Gage 7B was marked as 200 kips. No strain gage was placed at location 7C.

Figure 5.120 indicates Gages 8A and B probably yielded; however, Gage 8A indicated yielding in tension and Gage 8B yielding in compression. The compression could be an indication of damage to Gage 8B. For Gage 8A, the rate of strain changed at 340 kips, although a diagonal 300 kip crack and a preexisting crack were marked near there. The preexisting diagonal crack near Gage 8B was below the gage. No strain gage was placed at location 8C.

Gage 12A indicated the largest change in strain of the three gages on Stirrup 12, about 600 microstrain at ultimate load, Figure 5.121. Gage 12A indicated similar behavior to Gages 12B and C until 500 kips. Gages 12B and C indicated very little change in strain, about 100 microstrain in compression. This stirrup was located within the long shear span where the applied shear was only 1/3 of the applied load compared to 2/3 of the applied load carried by the short shear span. The crack pattern in this area was not recorded.

Gage 13A indicated a linear decrease in strain until 420 kips and then increased in strain, Figure 5.122. Gage 13B indicated little strain change until about 500 kips. After 500 kips, the strain increased rapidly, and the stirrup at that location likely yielded in tension. Gage 13C indicated very little change in strain, about 100 microstrain in compression. The crack pattern in this area was not recorded.

Gage 15A indicated very little increase in strain, about 150 microstrain, Figure 5.123. Gage 15B indicated the greatest strain of all the gages within the long shear span. The stirrup at

this location probably yielded. The crack pattern in this area was not recorded. No gage was placed at location 15C.

Gage 18A indicated the largest strain of the three gages on this stirrup, Figure 5.124. Gage 18B indicated no change in strain until ultimate load. Gage 18C indicated signs of possible yielding after 500 kips. The crack pattern in this area was not recorded.

No gage was placed at location 22A, and Gages 22B and C were damaged before shear testing. No stirrup data was collected from this location. This stirrup was the last stirrup with a strain gage within the long shear span. The crack pattern in this area was not recorded.

In summary, End IIC had a total of ten damaged stirrups gages which was the most of the four specimens; therefore, the trends between stirrups were limited. The strains for Stirrups 4-15 at the top of the web were greater than those near midheight or the bottom of the web at peak load.

5.4.4 Concrete Rosette Strains

Internal concrete rosettes were embedded at five locations in End IIC. The rosettes consisted of three arms which measured strains at 0°, 45°, and 90° to the horizontal. The direction of the rosette arms were noted by A, B, and C corresponding to the horizontal, 45°, and vertical, respectively. End IIC had only 13 of 15 internal arms working during the shear testing. Therefore, three external rosettes were placed on the web at approximately the same locations as the internal rosettes. Only one arm of the 15 external rosette arms did not work.

The rosette strains were plotted to one data point past peak load. These values were not the actual strains; they represented the strains only due to the externally applied load in the shear tests. The theoretical strain values in this section were the calculated three direction strains, principal strains, and principal compression angle and were found assuming no self weight of the composite section and no prestressing force.

The results from each arm are given in Figures 5.125-5.129 for all rosette locations. The solid lines represent the theoretical predicted strain values, and the series with markers show actual test data. The theoretical direction (A) indicated that strain increased as applied load increased, theoretical direction (B) indicated that strain decreased as applied load increased, and theoretical direction (C) indicated that strain did not change as applied load increased. The

internal and external direction (B) indicated the largest change in compression of all directions for Rosettes 1-5 throughout the shear testing. In Rosettes 1-3, the horizontal direction (A) appeared to undergo an increase in compressive strain for a majority of the shear testing, but smaller in magnitude than the 45° gages recorded.

Figures 5.130-5.134 show the values of the calculated principal strains assuming zero initial conditions. The solid lines represent the theoretical predicted strain values, and the series with markers were combinations of experimental test data. With four combinations of external and internal arms, Rosette 1 had very consistent experimental results. The experimental principal tension strain indicated better agreement to the theoretical principal tension strain than did the experimental principal compression strain to the theoretical principal compression strain. In Rosette 2, eight combinations of principal strain were calculated from three internal and three external arms. The experimental principal compression data appeared to show more compression than calculated by the theoretical equations, and the experimental principal tension indicated a range of values which included the theoretical values. The experimental principal compression and tension values for Rosette 3 correlated well with theoretical compression and tension data until external direction (C) indicated a rapid increase in strain. The experimental principal compression from Rosette 4 indicated about twice the magnitude of theoretical principal compression data. The experimental principal tension indicated much more scatter than the experimental principal compression. In Rosette 5, both experimental principal compression and tension as compared theoretical data indicated more compression and less tension, respectively.

The angles to principal compression were calculated as shown in Chapter 4. In Figure 5.135, experimental data from Rosette 1 indicated an initial angle around 53° and finished the shear testing around 35°. All four combinations indicated a decrease in angle as load was applied. In Figure 5.136, the angle of principal compression obtained from Rosette 2 started at about 56° , decreased to 40° at 340 kips, and increased again near peak load. The eight combinations from Rosette 3 indicated large differences in angle at every applied load, Figure 5.137. Rosette 4 indicated good correlation between the two combinations of experimental angles, Figure 5.138; however, there was a large amount of scatter in the plots. Two

combinations indicated a trend of decreasing angle as applied load increased. In Figure 5.139, the experimental angle combinations from Rosette 5 indicated an increasing trend up to 500 kips.

5.4.5 Corrected Concrete Rosette Strains

Figures 5.140-5.144 show the experimental data corrected for initial conditions. The corrected and theoretical data matched when no load was applied, because the same assumptions were made for initial conditions. The solid lines represent the theoretical predicted strain values, and the series with markers were corrected experimental test data. The theoretical direction (A) indicated that strain should increase during the testing. The rosettes were placed below the neutral axis of the composite cross section; therefore, the strains due to flexure would be tensile strains. The experimental data in the direction (A) for Rosettes 1-4 indicated relatively constant strain until 300 kips and then decreasing strain. Due to shear strains and flexural strains, the theoretical direction (B) indicated that strain should decrease during the shear testing. This was the case in all six of the corrected experimental direction (B) data. The theoretical direction (C) should have no change in strain. In five of the seven rosettes, corrected experimental direction (C) data indicated small change, less than 100 microstrain, up to 300 kips.

Figures 5.145-5.149 show the corrected principal strains using the corrected experimental data. The corrected and theoretical data matched when no load was applied, because the same assumptions were made for initial conditions. For Rosette 1, the corrected experimental principal tension data fell just below the theoretical principal tension data. On the other hand, the corrected experimental principal compression data fell far below the theoretical principal compression data from the initial applied load onward. For Rosette 2, the experimental principal tension strain agreed better with the theoretical tension strain than the experimental principal compression strain to the theoretical principal compression strain. In Rosette 3, one of two trends of experimental principal tension strain agreed very well with the theoretical up to 400 kips when internal direction (C) was damaged. In Rosettes 3-5, the experimental principal compression strain was well below that of theoretical values.

Figures 5.150-5.154 show the corrected principal compression angle which was calculated for corrected experimental data. Up to 250 kips, the corrected experimental data indicated a similar principal compression angle to the theoretical angle for Rosette 1. After 250

kips, the corrected experimental data diverged indicating a shallower angle than predicted by theory. Rosette 2 indicated two trends up to 500 kips, because the internal direction (C) indicated a more tensile strain than did the external direction (C). One trend of the experimental data indicated a shallower angle than the theoretical angle throughout the shear testing The second trend of the experimental data indicated a slightly greater than theoretical angle up to 300 kips at which point the experimental angle became less than the theoretical angle. The theoretical and corrected experimental data matched well up to 250 kips for Rosettes 3 and 4. This was due to the large initial condition of prestressing force in the axial direction. The theoretical data indicated that the principal compression angle should increase as the applied load is increased. The corrected experimental data indicated lower values than theoretical data at peak load for Rosettes 3 and 4. Corrected experimental angles for Rosette 5 indicated the best agreement with theoretical data.

The theoretical data does not account for section cracking. In the actual specimens after cracking has occurred, the experimental angle does not continue to increase as predicted by the theory; therefore, the theoretical angle is likely larger than experimental angle at peak load.

5.4.6 Bursting Strains

End IIC had three bursting gages placed in the original girder; however, none of the gages were active during testing. Therefore, no results are reported in this section.

5.4.7 Rupture Strains

Over the supports, two gages were placed in the horizontal direction to measure concrete strains. Both gages were located at the same horizontal distance; however, Gage RIICP1 was located vertically lower in the section compared to Gage RIICP2. Rupture strains were plotted to one data point past peak load.

Figure 5.155 shows that the change in strain in the concrete at no applied load and at 500 kips to be approximately the same. Gage RIICP1 indicated a rapid increase in compressive strains occurring after 500 kips. On the other hand, Gage RIICP2 indicated a rapid increase in tensile strain occurring after peak load. Because the gages were separated vertically only by 3 in., the two different responses could only a result of damage to one or both the gages. Although

not observed, a crack near or between the two gages is a possible explanation for the different behaviors.

5.4.8 Strand Slip

The slips of both debonded and bonded strands were monitored by LVDTs. Only nine of the 46 strands were measured for strand slip of which five strands were bonded strands and four were debonded strands. All monitored strands indicated evidence of slip. These slips typically occurred at peak load or 60 kips before peak load and were typically less than 0.15 in. into the specimen. After peak load was reached, the specimen was deflected until the specimen could only support 400 kips. In this load region after peak load, the strands indicated continued slip into the specimen as deflection increased. After the load was removed, the strands indicated no additional movement. Strand slips were plotted for the entire test.

Figure 5.156 shows Strands 1-4 and 1-5 had large amounts of signal noise from the LVDTs. Strand 1-1, which was bonded for the entire length, indicated slip only past peak load, and slipped 0.02 in. Strand 1-4, which was debonded for 4 ft., indicated evidence of slip starting at 550 kips, and slipped 0.03 in. Strand 1-5, which was debonded for 2 ft., indicated slip occurring at peak load, and slipped 0.02 in.

In Figure 5.157, Strands 1-7, 1-8, and 1-9 indicated that slip occurred at peak load. Strand 1-7 was bonded for the full length with a final slip of 0.01 in., Strand 1-8 was debonded for 2 ft. with a final slip of 0.10 in., and Strand 1-9 was debonded for 4 ft. with a final slip of 0.03 in.

In Figure 5.158, Strands 1-12, 2-7, and 3-7 were fully bonded and indicated that slip occurred at peak load. Strand 1-12 slipped 0.02 in. Strands 2-7 and 3-7 slipped both 0.14 in.

The strands farther from the bottom had greater slip than strands in the bottom row. This was attributed to the web sliding relative to the bottom flange. All bonded strands in the bottom row indicated similar slips which were less than the slips of debonded strands. The two strands which were debonded for 4 ft. indicated an equal amount of slip. Except for Strand 1-4, strand slip for bonded and debonded strands occurred at peak load.

5.4.9 Transfer Length

End IIC had 30 transfer length gages placed in the original girder; however, none of the gages were active during testing. Therefore, no results are reported in this section.

5.5 End IID

End IID was fabricated with the glacial gravel and microsilica mix. It contained 12 draped and no debonded strands to relieve end stresses, and it had standard U stirrups with leg extensions for transverse reinforcement.

The shear test was performed on July 9, 1996, and July 10, 1996. This was the second specimen tested in shear at the University of Minnesota Structures Lab. This specimen was the only end which was not tested to ultimate load. The 600 kip testing machine used for the shear tests did not have sufficient capacity to load the End IID to failure in shear. At the time of the shear test, the girder end was 2 years and 11 months of age (1064 days), and the slab was approximately 2 years and 4 months of age (865 days).

A complete summary of measured concrete strengths is given in Appendixes B.1 and B.2. At the time of the shear test, 6 x 12 in. cylinder tests indicated that the concrete compressive strength of the girder was 9300 psi with a modulus of elasticity of 4520 ksi, and the compressive strength of the deck was 5660 psi. The tensile splitting strength of the girder end was tested as 587 psi.

5.5.1 Beam Deflection

Because the test was operated in displacement control, load losses of 5 to 10 kips typically occurred during the times the displacement was held constant between load ramps. These load losses resulted from load redistribution with new cracking of the concrete section.

The deflection of the specimen read by the two beam deflection LVDTs was corrected for changes due to rigid body rotation using the measurements from the LVDT monitoring the neoprene pad at the east end. The west end was supported by a steel roller. The deflection measurements by the West and East LVDTs were corrected using Eqns. (4.1) and (4.3), respectively. The corrected peak deflections were 8.5% and 10.2% less than the measured peak deflections.

The corrected load-deflection curves for End IID are shown in Figures 5.159 and 5.160 for the West and East LVDTs, respectively. Before peak load, the deflection increased nearly linearly with an increase in load for both the West and East LVDT.

The peak load was 676 kips applied at 14.0 ft. from the west end. At peak load, the West LVDT, located 12.2 ft. from the west end, indicated 1.20 in. of corrected deflection, and the East LVDT, located 16.1 ft. from the west end, indicated 1.35 in. of corrected deflection. The test was ended after the actuator could not produce additional load to reach ultimate load.

5.5.2 Crack Diagrams

End IID had the least initial cracking of the four ends, and the web had few preexisting cracks. Crack growth appeared to start near the support at the web at 180 kips. At 300 kips, a new crack formed near the support at the top of the web and a new diagonal crack in the web formed 5 ft. from the end of the specimen. At 420 kips, a crack formed at the base of the web and a 15 kips load loss occurred. At 560 and 580 kips, loud sounds were heard. At the base of the web, spalling initiated at 620 kips. After a peak load of 630 kips, the applied load was removed, and the shear testing was suspended for the day.

The following day, the pressure in the actuator lines was boosted to increase the ultimate applied load. At 450 kips, the existing cracks indicated continued spalling. At 640 kips, flaking of the concrete near the support was observed. At 650 and 660 kips, loud sounds were heard again. The actuator reached a maximum applied load of 676 kips, and End IID still had not reached ultimate load.

No flexure-shear cracks were observed. The web cracking near the support is shown in two photographs, Figures 5.161 and 5.162. Figure 5.163 is a photograph of End IID near the applied load.

Before testing, a crack pattern drawing was taken and shown in Figure 5.164. After 340 kips, the crack pattern drawing shows additional cracking, Figure 5.165. After 400 kips and 460 kips, the crack pattern drawings are shown in Figures 5.166 and 5.167, respectively. After peak load, the crack pattern drawing is shown in Figure 5.168.

5.5.3 Stirrup Strains

The stirrup strains are shown in Figures 5.169-5.180. Each figure shows the results of all strain gages located on each respective stirrup. The values given are not the actual strains in the stirrups, the gages were zeroed just prior to the application of the externally applied load. Consequently, the strains in the stirrups represent the changes in strains resulting from the externally applied load.

Stirrup 1 contained only gages at locations B and C. Stirrup 1 at location B indicated a slight increase in compression to peak load of about 250 microstrain, Figure 5.169. Gage 1B region indicated no stirrup yielding. The crack drawing indicated that a 400 kip crack formed below Gage 1B while a preexisting crack was present at the midheight of the web. Gage 1C indicated that as the load increased to 320 kips, the strain increased at the same rate as Gage 1B. The stirrup at Gage 1C appeared to yield in tension at approximately 320 kips. Near the region of Gage 1C, a horizontal crack at the base of the web developed starting at 340 kips.

No strain gage was placed at location 3A. Gage 3B had little change in strain up to 300 kips, a rapid shift in strain at 300 kips, and remained relatively unchanged after 400 kips, Figure 5.170. The stirrup probably did not yield in the 3B region. The nearest crack to this gage occurred at 320 kips. Gage 3C data indicated a rapid change in strain at 400 kips, and the stirrup in this area likely yielded. At location 3C, a horizontal crack at the base of the web did not cross the stirrup until 420 kips.

After 500 kips, the stirrup in the region of Gage 4A probably yielded and indicated a peak strain at peak load, Figure 5.171. A horizontal crack which developed at 460 kips appeared to be closest to the gage. Gage 4B indicated a large jump in strain between 300 and 360 kips, and the stirrup probably yielded. A diagonal crack which formed at 400 kips was very close to the gage. Gage 4C was damaged before shear testing; no data was collected from this gage.

At Gages 5A, B and C, the stirrup indicated yielding, Figure 5.172. Gage 5A indicated a rapid increase in strain at 300 kips, a preexisting crack and a 360 kip crack occurred in the area. Gage 5B indicated little change in strain until 340 kips and then was followed by an abrupt increase. A diagonal crack marked 360 kips appeared to match the location. At Gage 5C, the

stirrup indicated relatively no change in strain until 400 kips and then a sudden increase in strain. A diagonal crack marked 420 kips crossed Gage 5C.

Gage 6A was damaged before shear testing, and no data was collected from this gage. As illustrated in Figure 5.173, the stirrup gage at location 6B indicated a large increase in strain at 400 kips. The diagonal crack near Gage 6B was marked at 360 kips. The stirrup at Gage 6C appeared to yield at 440 kips. A diagonal crack marked 480 kips crossed Gage 6C.

Figure 5.174 indicated that the stirrup at Gage 7A yielded. The stirrup at Gage 7A indicated a rapid increase in strain at 420 kips. The closest crack to Gage 7A was a diagonal crack marked at 340 kips. The stirrup at Gage 7B indicated no change in strain to 320 kips and then an approximate linear increase to peak load. The diagonal crack corresponding to Gage 7B was marked as 460 kips. No strain gage was placed at location 7C.

Figure 5.175 indicates Gages 8A and B yielded. Gage 8A indicated a large increase in strain starting at 400 kips. The diagonal crack near Gage 8A was marked 400 kips. Gage 8B indicated small change in strain up to 540 kips and then an abrupt increase in strain occurred. The diagonal crack near Gage 8B was marked at 440 kips. No strain gage was placed at location 8C.

Gage 12A indicated very little change in strain until 590 kips and then the stirrup indicated yielding, Figure 5.176. Gages 12B and C indicated marginal change in strain of about 200 microstrain. This stirrup was located within the long shear span where the applied shear was only 1/3 of the applied load as compared to 2/3 of the applied load carried by the short shear span. The crack pattern in this area was not recorded.

Gages 13A and B indicated little change in strain until 550 kips and then a change in behavior which could be an indication of the initial process of yielding, Figure 5.177. Gage 13C indicated a maximum change in strain of 170 microstrain at 400 kips. The crack pattern in this area was not recorded.

Gage 15A indicated a small linear increase in strain until 612 kips, Figure 5.178. After 612 kips, Gage 15A indicated the possible start of yielding. Gage 15B indicated no change in strain up to 550 kips, and then a positive shift in strain occurred. The crack pattern in this area was not recorded. No gage was placed at location 15C.

Gages 18A, B, and C indicated minimal changes up to 550 kips, Figure 5.179. After 550 kips, the stirrup at locations 18A and C appeared to yield as shown by the rapid increase in strain. On the other hand, Gage 18B increased only slightly after 550 kips and probably did not yield. The crack pattern in this area was not recorded.

No gage was placed at location 22A. At Gage 22B, the stirrup indicated negligible change in strain to 550 kips, Figure 5.180. Gage 22C was damaged before shear testing, and no data from this gage was collected. This stirrup was the last stirrup with a strain gage within the long shear span. The crack pattern in this area was not recorded.

In summary, the strains for Stirrups 1 and 3 at the base of the web were greater than those near midheight or the top of the web when applied load was greater than 400 kips. For Stirrups 4 and 5, the strains at midheight of the web were greater than those at the top of the web when the applied load was greater than 400 kips. Stirrups 13 and 15 were the only stirrups without any indication of yielding.

5.5.4 Concrete Rosette Strains

Internal concrete rosettes were embedded at five locations in End IID. The rosettes consisted of three arms which measured strains at 0°, 45°, and 90° to the horizontal. The direction of the rosette arms were noted by A, B, and C corresponding to the horizontal, 45°, and vertical, respectively. End IID had only 12 of 15 internal arms working during the shear testing. Therefore, two external rosettes were placed on the web at approximately the same locations as the internal rosettes. All six of the external rosette arms worked during shear testing.

The rosette strains were not the actual strains; they represented the strains only due to the externally applied load in the shear tests. The theoretical strains values in this section were the calculated three direction strains, principal strains, and principal compression angle and were found assuming no self weight of the composite section and no prestressing force.

The results from each arm are given in Figures 5.181-5.185 for all rosette locations. The solid lines represent the theoretical predicted strain values, and the series with markers show actual test data. The theoretical direction (A) indicated that strain increased as applied load increased, theoretical direction (B) indicated that strain decreased as applied load increased, and theoretical direction (C) indicated that strain did not change as applied load increased. The

internal and external direction (B) indicated the largest change in compression of all directions for Rosettes 1-5 throughout the shear testing. Both directions (A) and (C) had less change in strain than did direction (B).

Figures 5.186-5.190 show the values of the calculated principal strains assuming zero initial conditions. The solid lines represent the theoretical predicted strain value, and the series with markers were combinations of experimental test data. For Rosette 1, the two combinations of external and internal arms had good agreement with each other. The experimental data indicated a similar trend to theoretical data, although both experimental principal compression and tension were slightly more compressive or less tensile than the theoretical principal compression and tension. In Rosette 2, the experimental data followed the theoretical data very well until 280 kips. After 280 kips, Rosette 2 was damaged likely due to new cracking. The experimental data from Rosette 3 followed the theoretical data very well up to 340 kips and indicated similar behavior to Rosette 1. The experimental data from Rosette 4 had four combinations of experimental test data. The experimental principal compression combinations were very close together at any given load and were lower than the theoretical principal compression data. On the other hand, the experimental principal tension combinations indicated basically two separate trends. The larger value trend was almost identical to the theoretical data. In Rosette 5, the principal strains indicated a rapid change at 440 kips. The experimental principal compression data matched the theoretical principal compression data better than the experimental principal tension data matched the theoretical principal tension results.

The angles to principal compression were calculated as shown in Chapter 4. In Figure 5.191, experimental data from Rosette 1 indicated an initial angle around 51° and finishing the shear testing around 43°. Both combinations indicated a decrease in angle as load was applied. In Figure 5.192, the angle of Rosette 2 started at about 41° and stayed at that angle until the rosette was damaged at 280 kips. The angle from Rosette 3 started at 33°, increased to 48° at 410 kips, and decreased to 38° just before peak load, Figure 5.193. In Figure 5.194, Rosette 4 indicated two angle trends, because the internal direction (C) indicated a more tensile strain than did the external direction (C). Up to 400 kips, the first angle trend was a constant 55° and was closer to the theoretical angle than the second angle trend which had a constant 45°. In Figure

5.195, the experimental angle from Rosette 5 increased from an initial 40° to 52° at 440 kips. The theoretical angle was much greater than experimental angle up to 440 kips after which the gage was damaged.

5.5.5 Corrected Concrete Rosette Strains

Figures 5.196-5.200 show the experimental data corrected for initial conditions. The corrected and theoretical data matched when no load was applied, because the same assumptions were made for initial conditions. The solid lines represent the theoretical predicted strain values, and the series with markers were corrected experimental test data. The theoretical direction (A) indicated that strain should increase during the testing. The rosettes were placed below the neutral axis of the composite cross section; therefore, the strains due to flexural would be tensile strains. The experimental direction (A) for Rosettes 1 and 2 indicated this trend to 300 kips. Up to rosette damage, the experimental data in direction (A) for Rosettes 3-5 indicated a relatively constant or decrease in strain. Due to shear strains and flexural strains, the theoretical direction (B) indicated that strain should decrease during the shear testing. This was the case in all five of the corrected experimental direction (B) data. The theoretical direction (C) predicted no change in strain. In five of the six rosettes, corrected experimental direction (C) data indicated small changes in strain, less than 100 microstrain, up to 400 kips.

Figures 5.201-5.205 show the corrected principal strains using the corrected experimental data. The corrected and theoretical data matched when no load was applied, because the same assumptions were made for initial conditions. For Rosette 1, the corrected experimental principal tension and principal compression data fell on or below the theoretical principal tension data at any given applied load. On the other hand, the corrected experimental principal compression data for Rosettes 2 and 3 fell below the theoretical principal compression data. The corrected experimental principal tension data for Rosettes 2 and 3 indicated more tension than calculated by the theoretical equations up to 300 kips. For Rosette 4, the experimental principal compression strain indicated more compression than expected by theory. The experimental principal tension strain indicated two trends which bounded the theoretical principal tension strain. The two trends were a result of the differences between the strains in the external and internal rosette in direction (C). The corrected experimental principal tension strain for Rosette 5

was almost identical to theoretical principal tension strain up to 440 kips at which point the rosette was damaged. The corrected experimental principal compression strain for Rosette 5 indicated more compression than predicted by theory.

Figures 5.206-5.210 show the corrected principal compression angle which was calculated for the corrected experimental data. Up to 460 kips, the corrected experimental data was approximately equal to the theoretical principal compression angle for Rosette 1. Afterwards, the theoretical angle was less than the corrected experimental data. The theoretical and corrected experimental data matched well up to 300 kips for Rosettes 2-4. This was due to the large initial condition of prestressing force in the axial direction. The theoretical data indicated that the principal compression angle should increase as the applied load is increased. After 300 kips, corrected experimental data indicated lower values than theoretical data for Rosettes 2-4. Corrected experimental Rosette 1, 2 and 4 indicated good agreement with theoretical data. For Rosette 5, the corrected experimental data indicated the least agreement with theoretical data.

The theoretical data does not account for section cracking. In the actual specimens after cracking has occurred, the experimental angle does not continue to increase as predicted by the theory; therefore, the theoretical angle is likely larger than experimental angle at peak load.

5.5.6 Bursting Strains

Near the supports of the original girders, four No. 6 stirrups were placed to control stresses due to the release of prestressing strands and to provide confinement of concrete over the support. Gages RIIDB1 and RIIDB2 were placed on the first bursting stirrup on opposite stirrup legs, and Gage RIIDB3 was placed on the third bursting stirrup. Bursting strains were plotted to peak load.

Up to 400 kips, Figure 5.211 shows that the force in the stirrups in this area became more compressive under the externally applied loads with one exception. The exception was Gage RIIDB3 at 320 kips which indicated a jump in strain.

5.5.7 Rupture Strains

Over the supports, two gages were placed in the horizontal direction to measure concrete strains. Both gages were located at the same horizontal distance; however, Gage RIIDP1 was located vertically lower in the section compared to Gage RIIDP2. Only Gage RIIDP2 was active during testing. Rupture strains were plotted to peak load. Figure 5.212 shows that the strain in the concrete up to 140 kips became more compressive and after 140 kips become more tensile.

5.5.8 Strand Slip

The slips of both debonded and bonded strands were monitored by LVDTs. Only nine of the 46 strands were measured for strand slip of which all nine were bonded strands. Strand slips were plotted for the entire test. All monitored strands indicated no evidence of slip as shown in Figure 5.213-5.215. The only variation in those three graphs was the amount of signal noise from the LVDTs. The reason for no slip was mostly due to the fact that the ultimate shear capacity was not reached.

5.5.9 Transfer Length

Figure 5.216 shows the change in strain of Strand 3-5. Strand 3-5 was bonded for the entire length of the strand and instrumented with Gage TIID035B. The measured strain for Gage TIID035B was relatively unchanged up to 400 kips, then as the load increased the strain increased at a greater rate.

5.6 Summary

During the shear tests, web-shear cracking was observed; flexure-shear cracking through the lower flange was not observed. Three of the four specimens were tested to failure. End IID exceeded the capacity of the 600 kip testing machine without failing. Of the three ends tested to ultimate load, all three exhibited horizontal shear cracks at the base of the web and crushing of the web near the support as the primary failure mode. In End IIC, the web crushing of the diagonals was observed to develop along a greater length of the web-flange interface compared to Ends IA and IB. This occurrence was attributed to the larger shear forces developed in Ends IIC and End IID which had a lower concrete strength than Ends IA and IB.

Chapter 6 - Discussion and Comparison

6.1 Introduction

This chapter summarizes the results and trends among the four shear test specimens regarding initial crack patterns, load-deflection curves, and measured and predicted crack angles. In addition, the shear test variables including stirrup anchorage, concrete mixes, and prestressing configurations are discussed. Also, the shear capacity of each specimen is compared to the models presented in Chapter 3. Two shear capacities were predicted for each specimen using nominal (design) and measured material properties. The shear friction capacity of the lower web and flange interface was calculated only using measured properties. Finally, the results from the four specimens are compared with the results of other research.

6.2 Initial Crack Pattern Comparison

The types of cracking observed in the four specimens can be classified as diagonal web-shear cracks, reverse diagonal web-shear cracks, and horizontal interface cracks. Typical diagonal web-shear cracks angled between the top of the web near the applied load and the bottom of the web near the support. The reverse diagonal web-shear cracks progressed from the top of the web near the support downward towards the applied load. Horizontal interface cracks occurred at the base of the web at the lower flange intersection.

The short shear span of End IID had the fewest cracks and was in the best condition prior to testing. This was followed by End IB, End IA, and finally End IIC. End IID did not have typical web-shear cracks initially; only one reverse diagonal crack was observed near the location of the draped strands. The reverse diagonal web-shear crack was known to have occurred during the release process of the prestressing strands. Ends IB and IA each had three typical web-shear cracks between the support and the top flange prior to the shear tests. End IIC had one main typical diagonal web-shear crack with numerous additional minor cracks prior to shear testing. Ends IID and IB did not have a preexisting horizontal crack at the base of the web; whereas, Ends IA and IIC had a horizontal crack at the base of the web before testing.

Of the long shear spans, End IID had the fewest cracks and was in the best condition prior to testing. This was followed by End IA, IB, and finally by IIC. Ends IID and IA had cracks in only one direction prior to the shear tests which were in the opposite direction of typical web-shear cracks near a support. This was as a result of flexure-shear cracking during the flexural testing on the original long-span girders. Ends IB and IIC had two directions of diagonal cracking: one direction was in the typical direction of shear cracks near a support, and the second direction was in the reverse direction of shear cracks near a support. The typical-direction cracks were due to additional damage as a result of failure of the original long-span girders after the flexural testing.

6.3 Load-Deflection Curve Comparison

The West LVDT measured the specimen deflections between the short shear span and the applied load. Figure 6.1 shows the West LVDT load-deflection curves for all four tests after correction for rigid body rotation. This rigid body rotation is described more completely in Section 4.4.1. The West end of each specimen was supported by a steel roller, and the East end of each specimen was supported by a neoprene pad. The East LVDT measured the specimen deflections between the applied load and the long shear span. The East LVDT was closer to the midspan of the specimen than the West LVDT. Figure 6.2 shows the East LVDT load-deflection curves for all four tests after correction for rigid body rotation.

The secant stiffness calculated between 100 kips and one-half of the peak load was determined by linear regression and is given in Table 6.1. End IID had the largest stiffness, and End IB had the smallest stiffness. Ends IA and IIC had similar stiffnesses which were between those of Ends IID and IB.

Three comments about measured stiffness are presented herein. First, End IID was the only girder with all 46 strands bonded for the entire length as compared with 8 debonded for the other three specimens. Therefore, End IID had more prestressing force near the West end and should have been more resistant to deflection. With this explanation Ends IA, IB, and IIC should have had similar stiffness; however, the stiffness of End IB was lower than that of Ends IA and IIC by approximately 12%. Second, End IID had the least initial cracking which would explain the greatest stiffness. This conclusion was not supported by End IIC which was the most visibly

damaged specimen and had greater stiffness than End IB. End IIC accidentally rolled over during the loading process for transportation at the Golden Valley Facility. The rollover caused additional cracking in the deck and a horizontal crack at the base of the web. Third, End IB was loaded using a 8.5 in. steel load plate while the other three specimens were loaded using a 12 in. steel load plate. The different load plate may have affected the load distribution. The difference in stiffness is probably some combination of the three possible explanations presented here.

6.4 Measured and Predicted Crack Angle Comparison

Crack angles at the location of the rosettes were determined by uncracked section theory (initial theoretical prestressing force, self weight, and applied load), corrected experimental data including initial conditions (initial theoretical prestressing force, self weight, and test data), and measurements from the crack pattern drawings. The vertical location of the rosettes was at the mid-height of the web and was below the centroid of the composite section. The results of these measurements near the rosettes are shown in Table 6.2. The uncracked section theory and corrected experimental data were used to calculate the principal compression angle. An assumption from uncracked section theory was made that the predicted cracking would occur along the principal compression angle at peak load. Measurements from the crack pattern drawings were made using actual cracks.

The angles from uncracked section theory were based on measured material properties and were between 30° to 41° with steeper angles closer to the applied load for all four specimens. The angles from corrected rosette experimental data varied from 20° to 33° with 25° common. All the specimens were very similar for corrected experimental data. The measured crack angles varied from 14° to 32° with the steepest angles near Rosette 1. End IID had the shallowest measured crack angles of all the specimens.

6.5 Stirrup Anchorage Comparison

Two different vertical shear epoxy-coated stirrup configurations were used and both had nominal yield strengths of 60 ksi. The typical Mn/DOT double leg, straight stirrup without leg extensions used in End IA, had a measured yield strength of 75.0 ksi. The stirrup type utilized in the other specimens had double legs, with a 90° hook at the end of each leg oriented along the

length of the specimen, and had a measured yield strength of 72.7 ksi. This configuration was termed "stirrup with leg extensions." The leg extensions provided additional anchorage to shorten the development length of the stirrup. Figure 4.9 shows the two types of stirrups.

Strain gages were used to determine the strain distribution over the height of the stirrups. Less effective anchorage of the standard U-stirrups in End IA should result in lower strain development particularly at location C (bottom of web). Thus the information obtained from the strain gages was used to approximate relative stirrup anchorage effectiveness.

Even with the reduced development length, four of seven stirrups in End IA at location C (bottom of web) appeared to yield before locations A (top of web) and B (midheight of web) yielded. The behavior at location C in End IA (typical Mn/DOT stirrup) was not dissimilar to that of the other specimens (stirrup with leg extensions).

Ends IA and IB only varied by stirrup anchorage. The maximum applied load that was supported by the specimens was slightly reduced from 520 kips for End IB to 503 kips for End IA. The load difference was minor, because the prestressing steel and prestressing force in the bottom flange helped to anchor both types of stirrups. Stirrup anchorage failure was not observed when subjected to web-shear cracking. Although flexure-shear cracks were not observed in these tests at the University of Minnesota, the flexure-shear cracks could have an effect on the U-stirrup anchorage (typical Mn/DOT stirrup) more so than the stirrups with extensions. Flexure-shear cracks propagate from the bottom flange and progressed upwards into the web. Also, if less prestressing force or less prestressing steel were provided, the anchorage of the U-stirrup anchorage (typical Mn/DOT stirrup) could have been adversely affected.

In each specimen, four separate lift hooks were cast into the original girders and were made of a bundle of four 0.5 in. prestressing strands. Three lift hooks were in the test shear span, and likely performed as transverse reinforcement. Two of these three lift hooks were anchored into the lower flange and through the depth of the web. The third lift hook was only embedded in the web and not into the lower flange.

6.6 Concrete Mix Comparison

All of the measured material properties including compressive strength and split tensile strength for Ends IA and IB (limestone aggregate) were superior to Ends IIC and IID (glacial

gravel); however, the failure plane for split tensile strength was much smoother. Figure 6.3 shows a tested split tensile cylinder with the smooth plane of failure through the limestone aggregate. Figure 6.4 shows a cylinder with the rough plane of failure around the glacial aggregate.

Web-shear cracking in the specimens is caused by a multidirectional state of stress when the concrete reaches a tensile stress that causes cracking. After cracking has occurred, the forces across the crack are transferred primarily through aggregate interlock and dowel action of stirrups or longitudinal reinforcement. At this point, the glacial gravel aggregate concrete was superior to the limestone aggregate concrete, because the additional roughness along the tensile crack plane greatly increased the forces that could be transmitted through aggregate interlock. The limestone concrete in Ends IA and IB appeared to flake into thin sheets. In Ends IIC and IID, the glacial gravel concrete broke into more angular sections.

With all other aspects of the two specimens identical, End IIC with glacial gravel aggregate failed at 614 kips as compared with 520 kips for End IB with limestone aggregate. Even though End IIC had more initial cracks, End IIC failed at a much higher applied load than End IB likely because of the better aggregate interlock of the glacial gravel. In End IIC, the web crushing of the diagonals was observed to develop along a greater length of the web-flange interface compared to Ends IA and IB. This occurrence was attributed to the larger shear forces developed in Ends IIC and End IID which had a lower concrete strength than Ends IA and IB.

6.7 Prestressing Configuration Comparison

Ends IA, IB, and IIC had 4 draped and 8 debonded strands, while End IID had 12 draped strands with no debonded strands. End IID with 12 draped strands had a higher measured shear capacity than all the other ends. The quantifiable difference is unknown, because End IID never obtained ultimate load. In addition, End IID had much shallower crack angles in the web compared to the other three specimens.

Ends IIC and IID only varied by prestressing configuration. The peak applied load that was supported was 676 kips for End IID, and the maximum applied load for End IIC was 614 kips. The difference was at least 62 kips. By increasing the number of strands in the web, the strength of the web was increased by additional local web compression, increased dowel action,

and web confinement. The failure mode in ends with 4 draped strands occurred at the interface between the lower web and the bottom flange with cracking beginning in the web. No failure mode for End IID was observed.

6.8 Shear Model Comparison

This section discusses measured test capacity as compared to the calculated capacities obtained from the methods and models discussed in Chapter 3. For each of the four specimens, shear capacity was calculated for two cases: (1) nominal or design properties for the 43 ft. specimen and (2) measured properties for the 43 ft. specimen. The nominal or design properties and the measured girder and deck properties used to calculate the shear capacity are given in Appendix C. Appendix D includes assumptions used in the models, and Appendix E gives sample calculations of the sectional methods. All loads and resistance factors were taken as unity.

The sectional methods used in calculating shear capacity were ACI 318-95 Simplified Method, ACI 318-95 Detailed Method, Modified Compression Field Theory, Modified ACI 318-95 Procedure, Modified Truss Model, and Horizontal Shear Capacity of AASHTO 1989. The full member methods used in calculating shear capacity were the Truss Model and Shear Friction in AASHTO 1994. Using nominal properties at a given location, the applied point load to cause the shear equal to the capacity was calculated. The applied point loads and shear capacities are given in Tables 6.3 and 6.4, respectively. The ratio of test shear to calculated shear resistance is presented in Table 6.5. Using measured properties at a given location, the applied point load to cause the shear equal to the capacity was calculated and presented in Table 6.6. The applied point loads and shear capacities are given in Tables 6.6 and 6.7, respectively. The ratio of test shear to calculated shear resistance is presented in Table 6.8 for measured properties. The shear capacities given were calculated at the locations of the corresponding code specified critical sections.

Three lift hooks near the end were neglected in each of the shear models. These lift hooks may have had a significant contribution to the shear capacity of all the models. Each lift hook consisted of four bundled 0.5 in. prestressing strands that were unstressed. No tests to determine the strength of the prestressing strands used as lift hooks were performed. The first lift

hook was anchored outside the lower flange at approximately 3.8 and 5.2 ft. from the west end, the second lift hook was anchored in the lower flange at approximately 7.0 and 8.8 ft. from the west end, and the third lift hook was anchored in the lower flange at approximately 8.8 and 10.5 ft. from the west end.

6.8.1 ACI 318-95 Simplified Method

The results of this method yielded the lowest shear resistance among ACI 318-95 Detailed Method, Modified ACI 318-95 Procedure, Modified Truss Model, and Modified Compression Field Theory. The ACI Simplified Method can be used as a lower bound for shear capacities and was found to be very conservative in all cases. The ratio of measured to predicted shear capacities for nominal and measured properties averaged as 1.92 and 1.81, respectively. The average coefficient of variation was 16.5 and 20.0% for nominal and measured properties, respectively. The critical section was at a horizontal location from the west support equal to half the depth of the composite section.

Using nominal properties, this method predicted a lower shear capacity for End IID as compared to the other three specimens. Two reasons for the lower values were: (1) the distance from the extreme compression fiber to centroid of prestressing strand was reduced for End IID with the 12 draped strands, and (2) the vertical component of prestressing force is not included in the simplified method.

Using measured properties, the shear capacity was lower for Ends IIC and IID as compared to Ends IA and IB because of the reduced compressive strength of the concrete. End IA had stirrup yield strengths higher than End IB which explains the difference in predicted shear capacities using measured properties.

6.8.2 ACI 318-95 Detailed Method (AASHTO 1989)

The results for the ACI Detailed Method predicted higher shear capacities than the ACI Simplified Method and generally lower shear capacity than the Modified Truss Model and the Modified Compression Field Theory. The exception was End IID which was predicted to have a higher capacity for nominal and measured properties using ACI Detailed Method as compared with the Modified Compression Field Theory. The ACI Detailed Method was conservative for

all nominal and measured properties cases. The ratios of measured to predicted shear capacities for nominal and measured properties averaged 1.59 and 1.56, respectively. The average coefficient of variation was 10.0 and 12.3% for nominal and measured properties, respectively. The critical section was at a horizontal location from the west support equal to half the depth of the composite section.

Using nominal properties, the ACI Detailed Method predicted a higher shear capacity for End IID as compared to the other three specimens. This method included the vertical component of prestressing force which explains the higher predicted capacity of the specimen with 12 draped strands as compared with the specimens with 4 draped strands.

6.8.3 Modified ACI 318-95 Procedure

This procedure was a modification of ACI 318-95 Detailed Method. It was found that the location through the depth of cross section that produced minimum shear capacity was at the top flange and web intersection (35.5 in. from the bottom of the cross section). At the top flange and web intersection, the results using nominal and measured properties were very similar to ACI Simplified Method for Ends IA, IB, and IIC. The predicted capacities were conservative in all cases. The ratios of measured to predicted shear capacities for nominal and measured properties averaged to be 1.80 and 1.70, respectively. The average coefficient of variation was 8.8 and 11.6% using the nominal and measured properties, respectively. The critical section was at a horizontal location from the west support equal to half the depth of the composite section.

6.8.4 Modified Truss Model

The Modified Truss Model was simpler to apply than the ACI Detailed Method and indicated higher predicted shear capacities in seven of the eight nominal and measured property cases. The Modified Truss Model was conservative for all nominal and measured properties cases. The ratios of measured to predicted shear capacities for nominal and measured properties averaged 1.55 and 1.45, respectively. The average coefficient of variation was 11.7 and 15.5% for nominal and measured properties, respectively. The critical section was at a horizontal location from the west support equal to half the depth of the composite section.

The Modified Truss Model using nominal properties predicted a higher shear capacity for End IID as compared to the other three specimens. The 12 draped strand case had a higher predicted capacity than the cases of the 4 draped strands. This method included the vertical component of prestressing force in the same manner as ACI 318-95 Detailed Method.

6.8.5 Modified Compression Field Theory (AASHTO 1994)

The Modified Compression Field Theory was more complex to apply than the ACI Detailed Method and the Modified Truss Model. For Ends IA, IB, and IIC, the Modified Compression Field Theory provided better shear capacity predictions than ACI Detailed Method using both nominal and measured properties. The Modified Compression Field Theory was conservative for all cases. The ratios of measured to predicted shear capacity for nominal and measured properties averaged 1.59 and 1.50, respectively. The coefficient of variation was 13.6 and 19.5% for nominal and measured properties, respectively. The critical section was at a horizontal location from the west support equal to the centerline flexural lever arm.

Using nominal properties, this method did not predict greater shear capacity for End IID. This method includes the vertical component of prestressing force; however, the smaller distance from the extreme compression fiber to the centroid of prestressing strand reduced the shear capacity more than the extra draping contribution.

6.8.6 Truss Model

For every case, the Truss Model was the most conservative of all methods. The concrete contribution was used only to transfer the stirrup forces, and self weight of the specimens was neglected. The angle of cracking was limited to a minimum angle of 30°. Also, the method did not include the vertical component of prestressing force. The distance from the resultant compression force to the centroid of the prestressing strands was taken at midspan of the original composite girders. Near the end of the specimens, the distance from the resultant compression force to the centroid of the prestressing strands would be smaller than at midspan of the original composite girder; therefore, this assumption is unconservative, because deeper trusses allow for more stirrups to be crossed with the same minimum angle. The ratios of measured to predicted shear capacities for the nominal and measured properties averaged 4.09 and 3.20, respectively.

The average coefficient of variation was 13.8 and 21.5% for nominal and measured properties, respectively. The critical section was at the location of the applied load.

Using measured properties, this method predicted that End IA would have higher capacity than Ends IIC and IID, because the yield strength of stirrups in End IA were slightly higher. End IB had a higher predicted capacity than the other three specimens, because the location of applied load in this specimen was such that the model allowed for two more stirrups to be activated near the applied load. For End IB, the location of applied load was 2.5 in. closer to the steel roller than for the other three specimens; therefore, the shear capacity of girders with uniformly spaced stirrups can jump with slight movements of location of applied point loads.

6.8.7 Strut-and-Tie Model

The Strut-and-Tie Model was intended for shear span-to-depth ratios equal or less than 2.0. In this study, the shear span-to-depth ratios were approximately equal to 3.0 and 5.6. This model was not intended for this type of cross section or this type of load pattern; therefore, no results are reported for the Strut-and-Tie Model.

6.8.8 Horizontal Shear Design (AASHTO 1989)

The Horizontal Shear Capacity for composite flexural members given in AASHTO 1989 controlled the stirrup spacing over ACI 318-89 Detailed Method in the original design of the girders. The horizontal shear capacity is much larger when minimum ties are provided with an intentionally roughened surface as compared to just an intentionally roughened surface. Horizontal Shear Capacity of AASHTO 1989 was calculated at the interface of the cast-in-place deck and girder with an intentionally roughened surface. None of the specimens failed at the interface of the cast-in-place deck and girder; therefore, the test-to-predicted ratios are not reported.

Using nominal properties this method predicted a lower shear capacity for End IID as compared to the other three specimens. The reason for the lower capacity is that the shear capacity was based on the distance from the extreme compression fiber to centroid of prestressing strand and this was reduced for End IID with the 12 draped strands.

6.9 Interface Shear Model

During shear tests, diagonal cracks formed in the web and progressed to the intersection of the web and the lower flange. At the intersection, the cracks turned from a diagonal to a horizontal crack along the web-flange interface. The principal mode of failure appeared to be horizontal shear failure at the base of the web at the web-flange interface. This mode of failure was not predicted by any of the sectional shear models or theories.

It was determined that the shear force to cause failure along the bottom interface was lower than the shear force to cause the crack to penetrate through the bottom flange. In order to determine the capacity and load along this interface, a free-body diagram was constructed as shown in Figure 6.5. From equilibrium equations, the forces along the lower interface were calculated, Appendix A.8. In addition, Shear Friction from AASHTO 1994 was used to calculate the horizontal shear capacity.

A few assumptions were necessary to evaluate the free body diagram. The distance between resultant compressive and tensile forces was the same as that used in the Truss Model. The coefficient of friction used for Ends IA and IB was 1.0 and for Ends IIC and IID was 1.4. Ends IIC and IID used a higher coefficient of friction, because the crack surfaces were rougher. The free body diagram neglected the benefits of the horizontal draped strands in the web which would increase the interface shear capacity. This increase would be larger for End IID, because it had 12 draped compared with 4 draped for End IA, IB, and IIC. Also, self weight of composite section was neglected.

The crack angle was varied to produce minimum shear resistance which occurred at 30°. The predicted interface shear capacities for Ends IA, IB, IIC, and IID were 588, 570, 606, and 603 kips, respectively. The applied point load was calculated to be 268, 261, 274, and 275 kips, respectively.

6.10 Comparison with Other Research

Using measured properties, the shear capacities of the four specimens were compared to other research. Table 6.9 gives the average and maximum properties for the girders discussed in the literature review given in Chapter 2 and for this research. From these references, ratios of the observed strengths to the strengths predicted by the ACI Detailed Method (AASHTO 1989) and

the Modified Compression Field Theory (AASHTO 1994) are presented. No calculations were done to verify the results of the models used by the other authors. The ACI Detailed Method results are reported in four columns, because the authors presented their information in different ways. The column labeled U_{cw} indicates the cracking shear near the support in the web divided by the ACI shear capacity of the concrete in this region. The column labeled U_{ci} reports the cracking shear to start flexural cracking divided by the ACI shear capacity of the concrete in this region. The column labeled U_{cr} presents the lowest cracking shear divided by the lowest ACI shear capacity of the concrete at the corresponding section. The column labeled U_{ACI} gives the failure shear divided by the ultimate ACI shear capacity which includes concrete, draping, and stirrup contributions. The column labeled U_{MCFT} presents the failure shear divided by the predicted ultimate shear capacity according to Modified Compression Field Theory which includes concrete, draping, and stirrup contributions.

At the University of Minnesota, the four specimens had at least twice the effective prestressing force as compared to the beams presented in Chapter 2. In addition, the specimens had at least three times the strand area as compared to the beams presented in Chapter 2. In all cases, both methods were conservative in predicting shear capacity and generally more conservative than other research; however, the mode of failure, the horizontal shear failure, was not predicted. The degree of conservatism may have increased by the placement of three separate lift hooks in the short shear span which were not included in the shear capacity equations.

Horizontal shear failures were observed in three of the four specimens tested at the University of Minnesota. In separate research conducted by Elzanaty, Nilson, and Slate, and by Russell and Burns, horizontal shear failures also developed. The failure mode is likely dependent on the shape of the girder cross section and the amount of prestressing steel in the bottom flange as compared to the amount of prestressing steel in the web. During testing, diagonal web-shear cracks developed in the web and progressed to the bottom flange and web intersection. At this intersection point, the cracks turned and ran horizontally along the bottom flange-web intersection. This change in crack direction was most likely due to the increased concrete area in the cross section and the increased prestressing steel in the bottom flange.

Chapter 7 - Summary and Conclusions

Shear tests were conducted on the ends of two long-span high strength concrete girders. The two original girders, Mn/DOT 45M sections, were 45 in. deep and 132 ft. 9 in. long. A composite concrete deck 4 ft. wide and 9 in. thick was added to each girder using unshored construction techniques. Each girder was prestressed with forty-six 0.6 in. diameter prestressing strands on 2 in. centers. Draped strands were harped using two hold down points located at 40% of the span length from each end. The girders were designed assuming a 28-day compressive strength of 10,500 psi. Four 43 ft. specimens were cut from the ends of the original girders after flexural testing to be used in the shear study.

The specimens were designed identically except for the mix design, the end strand patterns, and the stirrup anchorage details. Ends IA and IB had a limestone aggregate mix, and Ends IIC and IID had a glacial gravel with microsilica mix. Ends IA, IB, and IIC had 4 draped and 8 debonded strands, while End IID had 12 draped strands with no debonded strands. For stirrup anchorage details, Ends IB, IIC, and IID had modified U stirrups with leg extensions, and End IA contained standard Mn/DOT U stirrups without leg extensions.

The specimens were each loaded with a concentrated load located approximately 13.9 ft. from the end. The shear span to total depth ratio was approximately 3.0. The results of the tests were compared with eight shear capacity models: ACI 318-95 Simplified Method, ACI 318-95 Detailed Method (AASHTO 1989), Modified ACI 318-95 Procedure, Modified Truss Model, Horizontal Shear (AASHTO 1989), Modified Compression Field Theory, Truss Model, and Shear Friction. All shear capacity models and theories, using both nominal and measured properties, were conservative in predicting the capacities of all four specimens. The conservative results may have been due to three lift hooks embedded in the tested shear span which were not included in the models. The Modified Truss Model gave the highest prediction, which was closer to the measured shear capacity for the four specimens using nominal and measured properties. The Modified Compression Field Theory gave higher predictions for the specimens with 4 draped strands as compared to the ACI Detailed Method. The Modified Truss Model and

the ACI 318-95 Detailed Method performed better than the Modified Compression Field Theory for the specimen with 12 draped strands.

Although, the Modified Compression Field Theory generally gave slightly better results than the ACI Detailed Method; the calculations were more labor intensive than those of the ACI Detailed Method. A few of the variables used in the Modified Compression Field Theory were open to interpretation which could result in different results among engineers. The ACI Detailed Method was simpler and the variables were more easily calculated than in the Modified Compression Field Theory. The predicted shear capacity obtained from the ACI Detailed Method was slightly lower than the Modified Compression Field Theory. The Modified Truss Model was simpler than the ACI Detailed Method and Modified Compression Field Theory and produced predicted shear capacities similar or better than to those of the Modified Compression Field Theory.

During the shear tests, diagonal cracks formed in the web and progressed to the intersection of the web at the lower flange. At the intersection, the cracks turned from a diagonal to a horizontal crack along the web-flange interface. The principal mode of failure appeared to be horizontal shear failure at the base of the web at the web-flange interface. This mode of failure was not predicted by any shear models or theories; however, a method was developed to calculate the capacity at the lower web-flange interface using a free body diagram.

Three variables were investigated, and conclusions are stated herein.

The typical Mn/DOT double leg, straight stirrup without leg extensions, used in one specimen performed similar to the stirrups with the 90° hook leg extensions oriented along the length of the specimen. In the specimens studied, the large amount of prestressing force in the bottom flange helped to anchor the stirrups. In addition, web-shear cracking controlled the capacity rather than flexure-shear cracking. If flexure-shear cracking controls over web-shear cracking, then leg extensions may be more beneficial.

The 12 draped strands with no debonded strands provided greater shear capacity than the 4 draped strands with 8 debonded strands. The difference in applied load was not fully accounted for by any of the shear models. In addition, the crack angles were much shallower for the 12 draped specimen as compared to the other three specimens.

The performance of the specimens cast with glacial gravel concrete was compared to that of the specimens cast with limestone aggregate concrete. The limestone aggregate had many superior properties, including compressive strength; however, the limestone aggregate had much smoother crack interfaces. The glacial gravel aggregate girders performed better in shear resistance than the limestone girders due to better aggregate interlock of rougher crack surfaces.

References

1. America Concrete Institute, Building Code Requirements for Reinforced Concrete (ACI 318-95), Detroit, 1995.
2. AASHTO, Code for the Design of Highway Bridges, American Association of State Highway and Transportation Officials Washington, D.C., 1989.
3. AASHTO, LRFD Code for the Design of Highway Bridges, American Association of State Highway and Transportation Officials Washington, D.C., 1994.
4. Bennett, E.W. and Balasooriya, B.M.A., "Shear Strength of Prestressed Beams with Thin Webs Failing in Inclined Compression," *ACI Journal*, V. 68, No. 3, March 1971, pp. 204-212.
5. Elzanaty, Ashraf H., Nilson, Arthur H., and Slate, Floyd O., "Shear Capacity of Prestressed Concrete Beams Using High-Strength Concrete," *ACI Journal*, V. 83, No. 3, May-June 1986, pp. 359-368.
6. Maruyama, Kyuichi and Rizkalla, Sami H., "Shear Design Consideration for Pretensioned Prestressed Beams," *ACI Structural Journal*, V. 85, No. 5, September-October 1988, pp. 492-498.
7. Kaufman, M. Keith and Ramirez, Julio A., "Re-evaluation of the Ultimate Shear Behavior of High-Strength Concrete Prestressed I-Beams," *ACI Structural Journal*, V. 85, No. 3, May-June 1988, pp. 295-303.
8. Hartmann, David L., Breen J.E., and Kreger, M.E., "Shear Capacity of High Strength Prestressed Concrete Girders," Research Report 381-2, Center for Transportation Research, The University of Texas at Austin, Jan. 1988.
9. Abdalla, O.A., Ramirez, J.A., and Lee, R.H., "Strand Debonding in Pretensioned Beams-Precast Prestressed Concrete Bridges with Debonded Strands," Report No. FHWA/INDOT/JHRP-92-25, Part 2 Final Report, Purdue University, June 1993.
10. Russell, Bruce W. and Burns, Ned H., "Static and Fatigue Behavior of Pretensioned Composite Bridge Girders Made with High Strength Concrete," *PCI Journal*, V. 38, No. 3, May-June 1993, pp. 116-128.

11. Tawfiq, Kamal S., "Cracking and Shear Capacity of High Strength Concrete Girders," Final Report WPI 0510612, FAMU/FSU College of Engineering, January 1995.

12. Shahawy, Mohsen A. and Batchelor, B., "Shear Behavior of Full-Scale Prestressed Concrete Girders: Comparison Between AASHTO Specifications and LRFD Code," *PCI Journal*, V. 41, No. 3, May-June 1996, pp. 48-62.

13. Ramirez, Julio A. and Breen, John E., "Evaluation of a Modified Truss-Model Approach for Beams in Shear," *ACI Structural Journal*, V. 88, No. 5, September-October 1991, pp. 562-571.

14. Kielb, Jeffrey A., "Instrumentation and Fabrication of Two High Strength Concrete Prestressed Bridge Girders," MS Thesis, Department of Civil Engineering, University of Minnesota, December 1994.

15. Ahlborn, T.M., "Applications of High-Strength Concrete to Long-Span Prestressed Bridge Girders," Ph.D. Thesis, Department of Civil Engineering, University of Minnesota, to be submitted.

Tables

Table 2.1 Experimental Comparison of Prestressed Girders

Reference			Code					Girder					Comp.
Author(s)	Type	Total Tests (number)	ACI U_{cw}	ACI U_{ci}	ACI U_{cr}	ACI U_{ACI}	Mod. C. U_{MCFT}	Web mean (in.)	f_c' max (psi)	P max (kips)	Strand max (number)	Stra. Area max ($in.^2$)	Deck (yes/no)
			(average of test/predicted)										
Bennett & Balasooriya	Series A-E	19	n.a.	n.a.	n.a.	n.a.	n.a.	1	6420	83	10	0.60	no
	Series F	4	n.a.	n.a.	n.a.	n.a.	n.a.	1	5800	104	12	0.72	no
Elzanaty, Nilson, & Slate	CI Series	17	1.17	n.a.	1.17	1.21	n.a.	3	11400	138	4	0.86	no
	CW Series	17	n.a.	1.15	1.15	1.21	n.a.	2	11400	138	4	0.86	no
Maruyama & Rizkalla	Single Tee	9	n.a.	n.a.	1.00	1.03	n.a.	3	6480	n.a.	2	0.31	no
Kaufman & Ramirez	AASHTO I	4	1.07	n.a.	n.a.	1.15	n.a.	6	8370	311	10	1.67	no
	AASHTO II	2	1.04	n.a.	n.a.	1.10	n.a.	6	9090	425	14	2.34	no
Hartmann, Breen, & Kreger	Series 1	3	n.a.	n.a.	1.09	1.39	n.a.	2	11300	87	6	0.51	no
	Series 2	3	n.a.	n.a.	1.02	1.00	n.a.	2	10800	223	17	1.45	no
	Series 3	4	n.a.	n.a.	n.a.	1.16	n.a.	2	13160	173	13	1.11	yes
Abdalla, Ramirez, & Lee	AASHTO I	8	1.36	1.01	n.a.	n.a.	n.a.	6	7500	309	12	1.84	yes
	Indiana Box	2	0.97	0.80	n.a.	n.a.	n.a.	10	7300	514	20	3.06	yes
Russell & Burns	Texas C	6	1.38	n.a.	n.a.	n.a.	n.a.	7	10400	598	24	3.67	yes
Tawfiq	AASHTO II, R	6	n.a.	n.a.	n.a.	0.89	1.05	6	11040	421	18	2.75	yes
	AASHTO II, 2R	6	n.a.	n.a.	n.a.	0.73	0.63	6	11040	421	18	2.75	yes
Shahawy & Batchelor	AASHTO II, 0R	6	n.a.	n.a.	n.a.	1.28	1.67	6	7600	377	18	2.75	yes
	AASHTO II, M	2	n.a.	n.a.	n.a.	1.25	2.67	6	7300	369	18	2.75	yes
	AASHTO II, R/2	2	n.a.	n.a.	n.a.	1.25	2.32	6	7100	369	18	2.75	yes
	AASHTO II, R	12	n.a.	n.a.	n.a.	1.19	1.63	6	8480	377	18	2.75	yes
	AASHTO II, 3R/2	4	n.a.	n.a.	n.a.	1.05	1.41	6	7600	369	18	2.75	yes
	AASHTO II, 2R	8	n.a.	n.a.	n.a.	0.99	0.82	6	7820	377	18	2.75	yes
	AASHTO II, 3R	6	n.a.	n.a.	n.a.	0.96	0.71	6	7680	377	18	2.75	yes

Table 3.1 Values of β for Members with Web Reinforcement

v/f_c' less than or equal	ε_x x 1000 less than or equal										
	-0.20	-0.15	-0.10	0.00	0.125	0.25	0.50	0.75	1.00	1.50	2.00
0.050	6.78	6.17	5.63	4.88	3.99	3.49	2.51	2.37	2.23	1.95	1.72
0.075	6.78	6.17	5.63	4.88	3.65	3.01	2.47	2.33	2.16	1.90	1.65
0.100	6.50	5.87	5.31	3.26	2.61	2.54	2.41	2.28	2.09	1.72	1.45
0.125	2.71	2.71	2.71	2.60	2.57	2.50	2.37	2.18	2.01	1.60	1.35
0.150	2.66	2.61	2.61	2.55	2.50	2.45	2.28	2.06	1.93	1.50	1.24
0.175	2.59	2.58	2.54	2.50	2.41	2.39	2.20	1.95	1.74	1.35	1.11
0.200	2.55	2.49	2.48	2.45	2.37	2.33	2.10	1.82	1.58	1.21	1.00
0.225	2.45	2.38	2.43	2.37	2.33	2.27	1.92	1.67	1.43	1.18	1.14
0.250	2.36	2.32	2.36	2.30	2.28	2.01	1.64	1.52	1.40	1.30	1.25

Table 3.2 Values of β for Members with Web Reinforcement

v/f_c' less than or equal	ε_x x 1000 less than or equal										
	-0.200	-0.188	-0.175	-0.163	-0.150	-0.138	-0.125	-0.113	-0.100	-0.075	-0.050
0.050	6.78	6.63	6.48	6.32	6.17	6.04	5.90	5.77	5.63	5.44	5.26
0.055	6.78	6.63	6.48	6.32	6.17	6.04	5.90	5.77	5.63	5.44	5.26
0.060	6.78	6.63	6.48	6.32	6.17	6.04	5.90	5.77	5.63	5.44	5.26
0.065	6.78	6.63	6.48	6.32	6.17	6.04	5.90	5.77	5.63	5.44	5.26
0.070	6.78	6.63	6.48	6.32	6.17	6.04	5.90	5.77	5.63	5.44	5.26
0.075	6.78	6.63	6.48	6.32	6.17	6.04	5.90	5.77	5.63	5.44	5.26
0.080	6.71	6.56	6.41	6.25	6.10	5.98	5.87	5.75	5.63	5.43	5.24
0.085	6.67	6.52	6.36	6.21	6.05	5.95	5.84	5.74	5.63	5.40	5.17
0.090	6.63	6.47	6.32	6.16	6.00	5.90	5.81	5.71	5.61	5.31	5.01
0.095	6.58	6.42	6.25	6.09	5.92	5.82	5.72	5.62	5.52	5.09	4.66
0.100	6.50	6.34	6.19	6.03	5.87	5.73	5.59	5.45	5.31	4.80	4.29
0.105	6.30	6.10	5.90	5.70	5.50	5.08	4.65	4.23	3.80	3.58	3.35
0.110	6.00	5.78	5.55	5.33	5.10	4.60	4.10	3.60	3.10	3.02	2.94
0.115	5.00	4.85	4.70	4.55	4.40	4.01	3.63	3.24	2.85	2.80	2.75
0.120	3.50	3.38	3.25	3.13	3.00	2.94	2.88	2.82	2.76	2.73	2.69
0.125	2.71	2.71	2.71	2.71	2.71	2.71	2.71	2.71	2.71	2.68	2.66
0.130	2.70	2.70	2.70	2.69	2.69	2.69	2.69	2.69	2.69	2.67	2.64
0.135	2.69	2.69	2.68	2.68	2.67	2.67	2.67	2.67	2.67	2.65	2.63
0.140	2.68	2.67	2.67	2.66	2.65	2.65	2.65	2.65	2.65	2.63	2.61
0.145	2.67	2.66	2.65	2.64	2.63	2.63	2.63	2.63	2.63	2.61	2.60
0.150	2.66	2.65	2.64	2.62	2.61	2.61	2.61	2.61	2.61	2.60	2.58
0.155	2.65	2.64	2.63	2.61	2.60	2.60	2.60	2.59	2.59	2.58	2.57
0.160	2.63	2.62	2.62	2.61	2.60	2.60	2.59	2.59	2.58	2.57	2.56
0.165	2.62	2.61	2.61	2.60	2.59	2.58	2.58	2.57	2.56	2.55	2.54
0.170	2.60	2.60	2.59	2.59	2.58	2.57	2.57	2.56	2.55	2.54	2.53
0.175	2.59	2.59	2.59	2.58	2.58	2.57	2.56	2.55	2.54	2.53	2.52
0.180	2.58	2.58	2.57	2.57	2.56	2.55	2.55	2.54	2.53	2.52	2.51
0.185	2.57	2.56	2.56	2.55	2.54	2.54	2.53	2.53	2.52	2.51	2.50
0.190	2.57	2.56	2.55	2.53	2.52	2.52	2.52	2.51	2.51	2.50	2.49
0.195	2.56	2.55	2.54	2.52	2.51	2.51	2.51	2.50	2.50	2.49	2.48
0.200	2.55	2.54	2.52	2.51	2.49	2.49	2.49	2.48	2.48	2.47	2.47
0.205	2.53	2.52	2.50	2.49	2.47	2.47	2.47	2.47	2.47	2.46	2.46
0.210	2.51	2.50	2.48	2.47	2.45	2.45	2.46	2.46	2.46	2.45	2.44
0.215	2.49	2.47	2.46	2.44	2.42	2.43	2.44	2.44	2.45	2.44	2.43
0.220	2.47	2.45	2.44	2.42	2.40	2.41	2.42	2.43	2.44	2.43	2.42
0.225	2.45	2.43	2.42	2.40	2.38	2.39	2.41	2.42	2.43	2.42	2.40
0.230	2.43	2.42	2.40	2.39	2.37	2.38	2.40	2.41	2.42	2.41	2.39
0.235	2.41	2.40	2.39	2.37	2.36	2.37	2.39	2.40	2.41	2.40	2.38
0.240	2.40	2.39	2.38	2.36	2.35	2.36	2.37	2.38	2.39	2.38	2.36
0.245	2.38	2.37	2.36	2.35	2.34	2.35	2.36	2.36	2.37	2.36	2.34
0.250	2.36	2.35	2.34	2.33	2.32	2.33	2.34	2.35	2.36	2.35	2.33

Table 3.2 (continued)

v/f_c' less than or equal	ε_x x 1000 less than or equal									
	-0.025	0.000	0.031	0.063	0.094	0.125	0.156	0.188	0.219	0.250
0.050	5.07	4.88	4.66	4.44	4.21	3.99	3.87	3.74	3.62	3.49
0.055	5.07	4.88	4.64	4.40	4.16	3.92	3.80	3.68	3.56	3.44
0.060	5.07	4.88	4.64	4.39	4.15	3.90	3.77	3.64	3.51	3.38
0.065	5.07	4.88	4.63	4.37	4.12	3.86	3.72	3.57	3.43	3.28
0.070	5.07	4.88	4.61	4.34	4.07	3.80	3.64	3.49	3.33	3.17
0.075	5.07	4.88	4.57	4.27	3.96	3.65	3.49	3.33	3.17	3.01
0.080	5.04	4.84	4.43	4.02	3.61	3.20	3.10	3.00	2.90	2.80
0.085	4.93	4.70	4.25	3.79	3.34	2.88	2.82	2.77	2.71	2.65
0.090	4.70	4.40	3.98	3.57	3.15	2.73	2.70	2.67	2.63	2.60
0.095	4.23	3.80	3.51	3.22	2.93	2.64	2.62	2.61	2.59	2.57
0.100	3.77	3.26	3.10	2.94	2.77	2.61	2.59	2.58	2.56	2.54
0.105	3.13	2.90	2.83	2.76	2.68	2.61	2.59	2.57	2.55	2.53
0.110	2.85	2.77	2.73	2.69	2.64	2.60	2.58	2.57	2.55	2.53
0.115	2.70	2.65	2.64	2.62	2.61	2.59	2.57	2.56	2.54	2.52
0.120	2.66	2.62	2.61	2.60	2.59	2.58	2.56	2.55	2.53	2.51
0.125	2.63	2.60	2.59	2.59	2.58	2.57	2.55	2.54	2.52	2.50
0.130	2.62	2.59	2.58	2.57	2.56	2.55	2.54	2.52	2.51	2.49
0.135	2.60	2.58	2.57	2.56	2.55	2.54	2.53	2.51	2.50	2.48
0.140	2.59	2.57	2.56	2.55	2.53	2.52	2.51	2.50	2.48	2.47
0.145	2.58	2.56	2.55	2.54	2.52	2.51	2.50	2.49	2.47	2.46
0.150	2.57	2.55	2.54	2.53	2.51	2.50	2.49	2.48	2.46	2.45
0.155	2.55	2.54	2.53	2.51	2.50	2.48	2.47	2.46	2.45	2.44
0.160	2.54	2.53	2.51	2.50	2.48	2.46	2.45	2.45	2.44	2.43
0.165	2.53	2.52	2.50	2.48	2.46	2.44	2.44	2.43	2.43	2.42
0.170	2.52	2.51	2.49	2.47	2.44	2.42	2.42	2.41	2.41	2.40
0.175	2.51	2.50	2.48	2.46	2.43	2.41	2.41	2.40	2.40	2.39
0.180	2.50	2.49	2.47	2.45	2.42	2.40	2.40	2.39	2.39	2.38
0.185	2.49	2.48	2.46	2.44	2.41	2.39	2.39	2.38	2.38	2.37
0.190	2.48	2.47	2.45	2.43	2.41	2.39	2.38	2.37	2.36	2.35
0.195	2.47	2.46	2.44	2.42	2.40	2.38	2.37	2.36	2.35	2.34
0.200	2.46	2.45	2.43	2.41	2.39	2.37	2.36	2.35	2.34	2.33
0.205	2.45	2.44	2.42	2.40	2.38	2.36	2.35	2.34	2.33	2.32
0.210	2.43	2.42	2.41	2.39	2.38	2.36	2.35	2.34	2.32	2.31
0.215	2.41	2.40	2.39	2.38	2.36	2.35	2.34	2.33	2.31	2.30
0.220	2.40	2.39	2.38	2.37	2.35	2.34	2.33	2.32	2.30	2.29
0.225	2.39	2.37	2.36	2.35	2.34	2.33	2.32	2.30	2.29	2.27
0.230	2.38	2.36	2.35	2.34	2.33	2.32	2.30	2.28	2.26	2.24
0.235	2.37	2.35	2.34	2.33	2.32	2.31	2.28	2.25	2.21	2.18
0.240	2.35	2.33	2.32	2.32	2.31	2.30	2.26	2.21	2.17	2.12
0.245	2.33	2.31	2.31	2.30	2.30	2.29	2.24	2.19	2.13	2.08
0.250	2.32	2.30	2.30	2.29	2.29	2.28	2.21	2.15	2.08	2.01

Table 3.2 (continued)

v/f_c' less than or equal	ε_x x 1000 less than or equal									
	0.313	0.375	0.438	0.500	0.563	0.625	0.688	0.750	0.813	0.875
0.050	3.25	3.00	2.76	2.51	2.48	2.44	2.41	2.37	2.34	2.30
0.055	3.21	2.97	2.74	2.50	2.47	2.43	2.40	2.36	2.32	2.29
0.060	3.16	2.94	2.71	2.49	2.46	2.42	2.39	2.35	2.31	2.28
0.065	3.08	2.89	2.69	2.49	2.46	2.42	2.39	2.35	2.31	2.27
0.070	3.00	2.83	2.65	2.48	2.45	2.41	2.38	2.34	2.30	2.26
0.075	2.88	2.74	2.61	2.47	2.44	2.40	2.37	2.33	2.29	2.25
0.080	2.72	2.63	2.55	2.46	2.43	2.39	2.36	2.32	2.28	2.24
0.085	2.60	2.55	2.49	2.44	2.41	2.38	2.34	2.31	2.27	2.22
0.090	2.56	2.52	2.47	2.43	2.40	2.37	2.33	2.30	2.26	2.21
0.095	2.53	2.50	2.46	2.42	2.39	2.36	2.32	2.29	2.25	2.20
0.100	2.51	2.48	2.44	2.41	2.38	2.35	2.31	2.28	2.23	2.19
0.105	2.50	2.47	2.43	2.40	2.37	2.33	2.30	2.26	2.21	2.17
0.110	2.50	2.47	2.43	2.40	2.36	2.32	2.28	2.24	2.20	2.15
0.115	2.49	2.46	2.42	2.39	2.35	2.31	2.26	2.22	2.18	2.13
0.120	2.48	2.45	2.41	2.38	2.34	2.29	2.25	2.20	2.16	2.11
0.125	2.47	2.44	2.40	2.37	2.32	2.28	2.23	2.18	2.14	2.10
0.130	2.46	2.42	2.39	2.35	2.30	2.26	2.21	2.16	2.12	2.08
0.135	2.44	2.41	2.37	2.33	2.28	2.23	2.18	2.13	2.09	2.06
0.140	2.43	2.40	2.36	2.32	2.27	2.21	2.16	2.10	2.07	2.0
0.145	2.42	2.38	2.34	2.30	2.25	2.19	2.14	2.08	2.05	2.(
0.150	2.41	2.37	2.32	2.28	2.23	2.17	2.12	2.06	2.03	2.0
0.155	2.40	2.36	2.31	2.27	2.21	2.16	2.10	2.04	2.00	1.9
0.160	2.39	2.34	2.30	2.25	2.19	2.14	2.08	2.02	1.98	1.95
0.165	2.37	2.33	2.28	2.23	2.17	2.12	2.06	2.00	1.96	1.92
0.170	2.36	2.31	2.27	2.22	2.16	2.10	2.03	1.97	1.93	1.88
0.175	2.34	2.30	2.25	2.20	2.14	2.08	2.01	1.95	1.90	1.85
0.180	2.33	2.28	2.23	2.18	2.12	2.05	1.99	1.92	1.87	1.81
0.185	2.32	2.27	2.21	2.16	2.10	2.03	1.97	1.90	1.84	1.78
0.190	2.30	2.25	2.19	2.14	2.07	2.01	1.94	1.87	1.81	1.75
0.195	2.29	2.23	2.18	2.12	2.05	1.99	1.92	1.85	1.79	1.73
0.200	2.27	2.22	2.16	2.10	2.03	1.96	1.89	1.82	1.76	1.70
0.205	2.26	2.20	2.13	2.07	2.00	1.93	1.85	1.78	1.72	1.66
0.210	2.24	2.18	2.11	2.04	1.97	1.90	1.82	1.75	1.69	1.63
0.215	2.23	2.15	2.08	2.00	1.93	1.87	1.80	1.73	1.67	1.61
0.220	2.21	2.13	2.04	1.96	1.90	1.83	1.77	1.70	1.64	1.58
0.225	2.18	2.10	2.01	1.92	1.86	1.80	1.73	1.67	1.61	1.55
0.230	2.15	2.06	1.97	1.88	1.82	1.76	1.69	1.63	1.58	1.53
0.235	2.09	2.00	1.91	1.82	1.77	1.71	1.66	1.60	1.56	1.51
0.240	2.03	1.93	1.84	1.74	1.70	1.66	1.62	1.58	1.54	1.50
0.245	1.98	1.88	1.78	1.68	1.65	1.62	1.58	1.55	1.52	1.48
0.250	1.92	1.83	1.73	1.64	1.61	1.58	1.55	1.52	1.49	1.46

Table 3.2 (continued)

v/f_c' less than or equal	ε_x x 1000 less than or equal									
	0.938	1.000	1.125	1.250	1.375	1.500	1.625	1.750	1.875	2.000
0.050	2.27	2.23	2.16	2.09	2.02	1.95	1.89	1.84	1.78	1.72
0.055	2.25	2.21	2.14	2.08	2.01	1.94	1.89	1.83	1.78	1.72
0.060	2.24	2.20	2.14	2.07	2.01	1.94	1.88	1.82	1.76	1.70
0.065	2.23	2.19	2.12	2.06	1.99	1.92	1.86	1.80	1.74	1.68
0.070	2.22	2.18	2.11	2.05	1.98	1.91	1.85	1.79	1.73	1.67
0.075	2.20	2.16	2.10	2.03	1.97	1.90	1.84	1.78	1.71	1.65
0.080	2.19	2.15	2.08	2.01	1.94	1.87	1.80	1.74	1.67	1.60
0.085	2.18	2.13	2.06	1.98	1.91	1.83	1.77	1.71	1.64	1.58
0.090	2.17	2.12	2.04	1.96	1.88	1.80	1.74	1.68	1.61	1.55
0.095	2.16	2.11	2.02	1.94	1.85	1.76	1.70	1.63	1.57	1.50
0.100	2.14	2.09	2.00	1.91	1.81	1.72	1.65	1.59	1.52	1.45
0.105	2.12	2.07	1.98	1.88	1.79	1.69	1.62	1.56	1.49	1.42
0.110	2.11	2.06	1.96	1.86	1.76	1.66	1.60	1.53	1.47	1.40
0.115	2.09	2.04	1.94	1.84	1.73	1.63	1.57	1.51	1.44	1.38
0.120	2.07	2.02	1.92	1.82	1.71	1.61	1.55	1.49	1.42	1.36
0.125	2.05	2.01	1.91	1.81	1.70	1.60	1.54	1.48	1.41	1.35
0.130	2.04	2.00	1.90	1.79	1.69	1.58	1.52	1.46	1.39	1.33
0.135	2.02	1.98	1.88	1.77	1.67	1.56	1.50	1.43	1.37	1.30
0.140	2.00	1.96	1.86	1.75	1.65	1.54	1.48	1.41	1.35	1.28
0.145	1.98	1.95	1.84	1.74	1.63	1.52	1.46	1.39	1.33	1.26
0.150	1.96	1.93	1.82	1.72	1.61	1.50	1.44	1.37	1.31	1.24
0.155	1.93	1.89	1.79	1.68	1.58	1.47	1.41	1.35	1.28	1.22
0.160	1.91	1.87	1.76	1.66	1.55	1.44	1.38	1.32	1.25	1.19
0.165	1.87	1.83	1.73	1.62	1.52	1.41	1.35	1.29	1.23	1.17
0.170	1.84	1.79	1.69	1.59	1.48	1.38	1.32	1.26	1.20	1.14
0.175	1.79	1.74	1.64	1.55	1.45	1.35	1.29	1.23	1.17	1.11
0.180	1.76	1.70	1.61	1.51	1.42	1.32	1.26	1.21	1.15	1.09
0.185	1.72	1.66	1.57	1.48	1.38	1.29	1.24	1.18	1.13	1.07
0.190	1.69	1.63	1.54	1.45	1.35	1.26	1.21	1.15	1.10	1.04
0.195	1.66	1.60	1.51	1.42	1.33	1.24	1.19	1.13	1.08	1.02
0.200	1.64	1.58	1.49	1.40	1.30	1.21	1.16	1.11	1.05	1.00
0.205	1.60	1.54	1.45	1.36	1.27	1.18	1.14	1.11	1.07	1.03
0.210	1.57	1.51	1.42	1.34	1.25	1.16	1.14	1.11	1.09	1.06
0.215	1.54	1.48	1.40	1.32	1.23	1.15	1.14	1.12	1.11	1.09
0.220	1.51	1.45	1.38	1.31	1.23	1.16	1.15	1.14	1.13	1.12
0.225	1.49	1.43	1.37	1.31	1.24	1.18	1.17	1.16	1.15	1.14
0.230	1.47	1.42	1.37	1.31	1.26	1.20	1.19	1.18	1.17	1.16
0.235	1.47	1.42	1.37	1.33	1.28	1.23	1.22	1.21	1.19	1.18
0.240	1.45	1.41	1.37	1.34	1.30	1.26	1.25	1.23	1.22	1.20
0.245	1.45	1.41	1.38	1.35	1.31	1.28	1.27	1.26	1.24	1.23
0.250	1.43	1.40	1.38	1.35	1.33	1.30	1.29	1.28	1.26	1.25

Table 3.3 Values of θ for Members with Web Reinforcement

v/f_c' less than or equal	ε_x x 1000 less than or equal										
	-0.20	-0.15	-0.10	0.00	0.125	0.25	0.50	0.75	1.00	1.50	2.00
0.050	27.0	27.0	27.0	27.0	27.0	28.5	29.0	33.0	36.0	41.0	43.0
0.075	27.0	27.0	27.0	27.0	27.0	27.5	30.0	33.5	36.0	40.0	42.0
0.100	23.5	23.5	23.5	23.5	24.0	26.5	30.5	34.0	36.0	38.0	39.0
0.125	20.0	21.0	22.0	23.5	26.0	28.0	31.5	34.0	36.0	37.0	38.0
0.150	22.0	22.5	23.5	25.0	27.0	29.0	32.0	34.0	36.0	36.5	37.0
0.175	23.5	24.0	25.0	26.5	28.0	30.0	32.5	34.0	35.0	35.5	36.0
0.200	25.0	25.5	26.5	27.5	29.0	31.0	33.0	34.0	34.5	35.0	36.0
0.225	26.5	27.0	27.5	29.0	30.5	32.0	33.0	34.0	34.5	36.5	39.0
0.250	28.0	28.5	29.0	30.0	31.0	32.0	33.0	34.0	35.5	38.5	41.5

Table 3.4 Values of θ for Members with Web Reinforcement

v/f'_c less than or equal	ε_x x 1000 less than or equal										
	-0.200	-0.188	-0.175	-0.163	-0.150	-0.138	-0.125	-0.113	-0.100	-0.075	-0.050
0.050	27.0	27.0	27.0	27.0	27.0	27.0	27.0	27.0	27.0	27.0	27.0
0.055	27.0	27.0	27.0	27.0	27.0	27.0	27.0	27.0	27.0	27.0	27.0
0.060	27.0	27.0	27.0	27.0	27.0	27.0	27.0	27.0	27.0	27.0	27.0
0.065	27.0	27.0	27.0	27.0	27.0	27.0	27.0	27.0	27.0	27.0	27.0
0.070	27.0	27.0	27.0	27.0	27.0	27.0	27.0	27.0	27.0	27.0	27.0
0.075	27.0	27.0	27.0	27.0	27.0	27.0	27.0	27.0	27.0	27.0	27.0
0.080	26.4	26.4	26.4	26.4	26.4	26.4	26.4	26.4	26.4	26.4	26.4
0.085	25.8	25.8	25.8	25.8	25.8	25.8	25.8	25.8	25.8	25.6	25.4
0.090	25.0	25.0	25.0	25.0	25.0	25.0	25.0	25.0	25.0	25.0	25.0
0.095	24.3	24.3	24.3	24.3	24.3	24.3	24.3	24.3	24.3	24.3	24.3
0.100	23.5	23.5	23.5	23.5	23.5	23.5	23.5	23.5	23.5	23.5	23.5
0.105	22.8	22.9	22.9	23.0	23.0	23.0	23.0	23.0	23.0	23.0	23.0
0.110	22.1	22.2	22.3	22.4	22.5	22.4	22.4	22.3	22.2	22.3	22.4
0.115	21.4	21.6	21.7	21.9	22.0	21.9	21.7	21.6	21.4	21.8	22.2
0.120	20.7	20.9	21.1	21.3	21.5	21.6	21.6	21.7	21.7	22.1	22.5
0.125	20.0	20.3	20.5	20.8	21.0	21.3	21.5	21.8	22.0	22.4	22.8
0.130	20.4	20.6	20.9	21.1	21.3	21.6	21.8	22.1	22.3	22.7	23.1
0.135	20.8	21.0	21.2	21.4	21.6	21.9	22.1	22.4	22.6	23.0	23.4
0.140	21.2	21.4	21.6	21.7	21.9	22.2	22.4	22.7	22.9	23.3	23.7
0.145	21.6	21.8	21.9	22.1	22.2	22.5	22.7	23.0	23.2	23.6	24.0
0.150	22.0	22.1	22.3	22.4	22.5	22.8	23.0	23.3	23.5	23.9	24.3
0.155	22.3	22.4	22.6	22.7	22.8	23.1	23.3	23.6	23.8	24.2	24.6
0.160	22.6	22.7	22.9	23.0	23.1	23.4	23.6	23.9	24.1	24.5	24.9
0.165	22.9	23.0	23.2	23.3	23.4	23.7	23.9	24.2	24.4	24.8	25.2
0.170	23.2	23.3	23.5	23.6	23.7	24.0	24.2	24.5	24.7	25.1	25.5
0.175	23.5	23.6	23.8	23.9	24.0	24.3	24.5	24.8	25.0	25.4	25.8
0.180	23.8	23.9	24.1	24.2	24.3	24.6	24.8	25.1	25.3	25.7	26.0
0.185	24.1	24.2	24.4	24.5	24.6	24.9	25.1	25.4	25.6	25.9	26.3
0.190	24.4	24.5	24.7	24.8	24.9	25.2	25.4	25.7	25.9	26.2	26.5
0.195	24.7	24.8	25.0	25.1	25.2	25.5	25.7	26.0	26.2	26.5	26.8
0.200	25.0	25.1	25.3	25.4	25.5	25.8	26.0	26.3	26.5	26.8	27.0
0.205	25.3	25.4	25.6	25.7	25.8	26.0	26.3	26.5	26.7	27.0	27.3
0.210	25.6	25.7	25.9	26.0	26.1	26.3	26.5	26.7	26.9	27.2	27.5
0.215	25.9	26.0	26.2	26.3	26.4	26.6	26.8	26.9	27.1	27.4	27.8
0.220	26.2	26.3	26.5	26.6	26.7	26.9	27.0	27.2	27.3	27.7	28.0
0.225	26.5	26.6	26.8	26.9	27.0	27.1	27.3	27.4	27.5	27.9	28.3
0.230	26.8	26.9	27.1	27.2	27.3	27.4	27.6	27.7	27.8	28.2	28.5
0.235	27.1	27.2	27.4	27.5	27.6	27.7	27.9	28.0	28.1	28.4	28.8
0.240	27.4	27.5	27.7	27.8	27.9	28.0	28.2	28.3	28.4	28.7	29.0
0.245	27.7	27.8	28.0	28.1	28.2	28.3	28.5	28.6	28.7	29.0	29.3
0.250	28.0	28.1	28.3	28.4	28.5	28.6	28.8	28.9	29.0	29.3	29.5

Table 3.4 (continued)

v/f_c' less than or equal	ε_x x 1000 less than or equal									
	-0.025	0.000	0.031	0.063	0.094	0.125	0.156	0.188	0.219	0.250
0.050	27.0	27.0	27.0	27.0	27.0	27.0	27.4	27.8	28.1	28.5
0.055	27.0	27.0	27.0	27.0	27.0	27.0	27.4	27.7	28.1	28.4
0.060	27.0	27.0	27.0	27.0	27.0	27.0	27.3	27.6	27.9	28.2
0.065	27.0	27.0	27.0	27.0	27.0	27.0	27.3	27.5	27.8	28.0
0.070	27.0	27.0	27.0	27.0	27.0	27.0	27.2	27.4	27.5	27.7
0.075	27.0	27.0	27.0	27.0	27.0	27.0	27.1	27.3	27.4	27.5
0.080	26.4	26.4	26.4	26.4	26.4	26.4	26.6	26.9	27.1	27.3
0.085	25.2	25.0	25.0	25.0	25.0	25.0	25.5	26.1	26.6	27.1
0.090	25.0	25.0	25.0	25.0	25.0	25.0	25.5	26.0	26.4	26.9
0.095	24.3	24.3	24.3	24.3	24.3	24.3	24.9	25.5	26.1	26.7
0.100	23.5	23.5	23.6	23.8	23.9	24.0	24.6	25.3	25.9	26.5
0.105	23.0	23.0	23.4	23.7	24.1	24.4	25.0	25.6	26.2	26.8
0.110	22.4	22.5	23.1	23.7	24.2	24.8	25.4	26.0	26.5	27.1
0.115	22.5	22.9	23.5	24.1	24.6	25.2	25.8	26.3	26.9	27.4
0.120	22.8	23.2	23.8	24.4	25.0	25.6	26.1	26.7	27.2	27.7
0.125	23.1	23.5	24.1	24.8	25.4	26.0	26.5	27.0	27.5	28.0
0.130	23.4	23.8	24.4	25.0	25.6	26.2	26.7	27.2	27.7	28.2
0.135	23.7	24.1	24.7	25.3	25.8	26.4	26.9	27.4	27.9	28.4
0.140	24.0	24.4	25.0	25.5	26.1	26.6	27.1	27.6	28.1	28.6
0.145	24.3	24.7	25.2	25.8	26.3	26.8	27.3	27.8	28.3	28.8
0.150	24.6	25.0	25.5	26.0	26.5	27.0	27.5	28.0	28.5	29.0
0.155	24.9	25.3	25.8	26.3	26.7	27.2	27.7	28.2	28.7	29.2
0.160	25.2	25.6	26.1	26.5	27.0	27.4	27.9	28.4	28.9	29.4
0.165	25.5	25.9	26.3	26.8	27.2	27.6	28.1	28.6	29.1	29.6
0.170	25.8	26.2	26.6	27.0	27.4	27.8	28.3	28.8	29.3	29.8
0.175	26.1	26.5	26.9	27.3	27.6	28.0	28.5	29.0	29.5	30.0
0.180	26.4	26.7	27.1	27.5	27.8	28.2	28.7	29.2	29.7	30.2
0.185	26.6	26.9	27.3	27.7	28.0	28.4	28.9	29.4	29.9	30.4
0.190	26.8	27.1	27.5	27.9	28.2	28.6	29.1	29.6	30.1	30.6
0.195	27.0	27.3	27.7	28.1	28.4	28.8	29.3	29.8	30.3	30.8
0.200	27.3	27.5	27.9	28.3	28.6	29.0	29.5	30.0	30.5	31.0
0.205	27.5	27.8	28.2	28.6	28.9	29.3	29.8	30.3	30.7	31.2
0.210	27.8	28.1	28.5	28.9	29.2	29.6	30.1	30.5	31.0	31.4
0.215	28.1	28.4	28.8	29.2	29.5	29.9	30.3	30.8	31.2	31.6
0.220	28.4	28.7	29.1	29.5	29.8	30.2	30.6	31.0	31.4	31.8
0.225	28.6	29.0	29.4	29.8	30.1	30.5	30.9	31.3	31.6	32.0
0.230	28.9	29.2	29.6	30.0	30.3	30.7	31.0	31.4	31.7	32.0
0.235	29.1	29.4	29.8	30.1	30.5	30.8	31.1	31.4	31.7	32.0
0.240	29.3	29.6	29.9	30.3	30.6	30.9	31.2	31.5	31.7	32.0
0.245	29.5	29.8	30.1	30.4	30.7	31.0	31.3	31.5	31.8	32.0
0.250	29.8	30.0	30.3	30.5	30.8	31.0	31.3	31.5	31.8	32.0

Table 3.4 (continued)

v/f_c' less than or equal	ε_x x 1000 less than or equal									
	0.313	0.375	0.438	0.500	0.563	0.625	0.688	0.750	0.813	0.875
0.050	28.6	28.8	28.9	29.0	30.0	31.0	32.0	33.0	33.8	34.5
0.055	28.6	28.8	29.0	29.2	30.2	31.2	32.1	33.1	33.8	34.6
0.060	28.5	28.8	29.1	29.4	30.4	31.3	32.3	33.2	33.9	34.6
0.065	28.4	28.8	29.2	29.6	30.5	31.5	32.4	33.3	34.0	34.7
0.070	28.2	28.8	29.3	29.8	30.7	31.6	32.5	33.4	34.1	34.7
0.075	28.1	28.8	29.4	30.0	30.9	31.8	32.6	33.5	34.1	34.8
0.080	28.0	28.7	29.4	30.1	31.0	31.9	32.7	33.6	34.2	34.8
0.085	27.9	28.7	29.4	30.2	31.1	32.0	32.8	33.7	34.3	34.9
0.090	27.8	28.6	29.5	30.3	31.2	32.1	32.9	33.8	34.4	34.9
0.095	27.6	28.6	29.5	30.4	31.3	32.2	33.0	33.9	34.4	35.0
0.100	27.5	28.5	29.5	30.5	31.4	32.3	33.1	34.0	34.5	35.0
0.105	27.8	28.8	29.7	30.7	31.5	32.4	33.2	34.0	34.5	35.0
0.110	28.1	29.0	30.0	30.9	31.7	32.5	33.2	34.0	34.5	35.0
0.115	28.3	29.3	30.2	31.1	31.8	32.6	33.3	34.0	34.5	35.0
0.120	28.6	29.5	30.4	31.3	32.0	32.7	33.3	34.0	34.5	35.0
0.125	28.9	29.8	30.6	31.5	32.1	32.8	33.4	34.0	34.5	35.0
0.130	29.1	29.9	30.8	31.6	32.2	32.8	33.4	34.0	34.5	35.0
0.135	29.2	30.1	30.9	31.7	32.3	32.9	33.4	34.0	34.5	35.0
0.140	29.4	30.2	31.0	31.8	32.4	32.9	33.5	34.0	34.5	35.0
0.145	29.6	30.4	31.1	31.9	32.4	33.0	33.5	34.0	34.5	35.0
0.150	29.8	30.5	31.3	32.0	32.5	33.0	33.5	34.0	34.5	35.0
0.155	29.9	30.7	31.4	32.1	32.6	33.1	33.5	34.0	34.5	34.9
0.160	30.1	30.8	31.5	32.2	32.7	33.1	33.6	34.0	34.4	34.8
0.165	30.3	31.0	31.6	32.3	32.7	33.2	33.6	34.0	34.4	34.7
0.170	30.5	31.1	31.8	32.4	32.8	33.2	33.6	34.0	34.3	34.6
0.175	30.6	31.3	31.9	32.5	32.9	33.3	33.6	34.0	34.3	34.5
0.180	30.8	31.4	32.0	32.6	33.0	33.3	33.7	34.0	34.2	34.5
0.185	31.0	31.6	32.1	32.7	33.0	33.4	33.7	34.0	34.2	34.4
0.190	31.2	31.7	32.3	32.8	33.1	33.4	33.7	34.0	34.2	34.4
0.195	31.3	31.9	32.4	32.9	33.2	33.5	33.7	34.0	34.2	34.3
0.200	31.5	32.0	32.5	33.0	33.3	33.5	33.8	34.0	34.1	34.3
0.205	31.7	32.1	32.6	33.0	33.3	33.5	33.8	34.0	34.1	34.2
0.210	31.8	32.2	32.6	33.0	33.3	33.5	33.8	34.0	34.1	34.2
0.215	32.0	32.3	32.7	33.0	33.3	33.5	33.8	34.0	34.1	34.2
0.220	32.1	32.4	32.7	33.0	33.3	33.5	33.8	34.0	34.1	34.2
0.225	32.3	32.5	32.8	33.0	33.3	33.5	33.8	34.0	34.1	34.3
0.230	32.3	32.5	32.8	33.0	33.3	33.5	33.8	34.0	34.2	34.4
0.235	32.3	32.5	32.8	33.0	33.3	33.5	33.8	34.0	34.2	34.5
0.240	32.3	32.5	32.8	33.0	33.3	33.5	33.8	34.0	34.3	34.6
0.245	32.3	32.5	32.8	33.0	33.3	33.5	33.8	34.0	34.3	34.7
0.250	32.3	32.5	32.8	33.0	33.3	33.5	33.8	34.0	34.4	34.8

Table 3.4 (continued)

v/f_c' less than or equal	ε_x x 1000 less than or equal									
	0.938	1.000	1.125	1.250	1.375	1.500	1.625	1.750	1.875	2.000
0.050	35.3	36.0	37.3	38.5	39.8	41.0	41.5	42.0	42.5	43.0
0.055	35.3	36.0	37.3	38.5	39.8	41.0	41.5	42.0	42.4	42.9
0.060	35.3	36.0	37.2	38.4	39.6	40.8	41.3	41.8	42.3	42.8
0.065	35.3	36.0	37.2	38.3	39.5	40.6	41.1	41.6	42.1	42.6
0.070	35.4	36.0	37.1	38.2	39.2	40.3	40.8	41.3	41.8	42.3
0.075	35.4	36.0	37.0	38.0	39.0	40.0	40.5	41.0	41.5	42.0
0.080	35.4	36.0	36.9	37.8	38.7	39.6	40.0	40.5	40.9	41.3
0.085	35.4	36.0	36.8	37.6	38.3	39.1	39.5	39.9	40.3	40.7
0.090	35.5	36.0	36.7	37.4	38.0	38.7	39.0	39.4	39.7	40.0
0.095	35.5	36.0	36.6	37.2	37.7	38.3	38.6	38.9	39.2	39.5
0.100	35.5	36.0	36.5	37.0	37.5	38.0	38.3	38.5	38.8	39.0
0.105	35.5	36.0	36.5	36.9	37.4	37.8	38.1	38.3	38.6	38.8
0.110	35.5	36.0	36.4	36.8	37.2	37.6	37.9	38.1	38.4	38.6
0.115	35.5	36.0	36.4	36.7	37.1	37.4	37.7	37.9	38.2	38.4
0.120	35.5	36.0	36.3	36.6	36.9	37.2	37.5	37.7	38.0	38.2
0.125	35.5	36.0	36.3	36.5	36.8	37.0	37.3	37.5	37.8	38.0
0.130	35.5	36.0	36.2	36.5	36.7	36.9	37.1	37.4	37.6	37.8
0.135	35.5	36.0	36.2	36.4	36.6	36.8	37.0	37.2	37.4	37.6
0.140	35.5	36.0	36.2	36.4	36.5	36.7	36.9	37.1	37.2	37.4
0.145	35.5	36.0	36.2	36.3	36.5	36.6	36.8	36.9	37.1	37.2
0.150	35.5	36.0	36.1	36.3	36.4	36.5	36.6	36.8	36.9	37.0
0.155	35.4	35.8	35.9	36.1	36.2	36.3	36.4	36.6	36.7	36.8
0.160	35.2	35.6	35.7	35.9	36.0	36.1	36.2	36.4	36.5	36.6
0.165	35.1	35.4	35.5	35.7	35.8	35.9	36.0	36.2	36.3	36.4
0.170	34.9	35.2	35.3	35.5	35.6	35.7	35.8	36.0	36.1	36.2
0.175	34.8	35.0	35.1	35.3	35.4	35.5	35.6	35.8	35.9	36.0
0.180	34.7	34.9	35.0	35.1	35.2	35.3	35.5	35.6	35.8	35.9
0.185	34.6	34.8	34.9	35.0	35.1	35.2	35.4	35.5	35.7	35.8
0.190	34.5	34.7	34.8	34.9	35.0	35.1	35.3	35.4	35.6	35.7
0.195	34.5	34.6	34.7	34.8	34.9	35.0	35.2	35.5	35.7	35.9
0.200	34.4	34.5	34.6	34.8	34.9	35.0	35.3	35.5	35.8	36.0
0.205	34.3	34.4	34.6	34.8	35.0	35.2	35.5	35.9	36.2	36.5
0.210	34.3	34.4	34.7	35.0	35.2	35.5	35.9	36.3	36.6	37.0
0.215	34.2	34.3	34.7	35.1	35.4	35.8	36.3	36.8	37.2	37.7
0.220	34.3	34.4	34.8	35.3	35.7	36.1	36.7	37.2	37.8	38.3
0.225	34.4	34.5	35.0	35.5	36.0	36.5	37.1	37.8	38.4	39.0
0.230	34.5	34.7	35.3	35.8	36.4	36.9	37.6	38.2	38.9	39.5
0.235	34.7	34.9	35.5	36.1	36.7	37.3	38.0	38.7	39.3	40.0
0.240	34.8	35.1	35.8	36.4	37.1	37.7	38.4	39.1	39.8	40.5
0.245	35.0	35.3	36.0	36.7	37.4	38.1	38.8	39.6	40.3	41.0
0.250	35.1	35.5	36.3	37.0	37.8	38.5	39.3	40.0	40.8	41.5

Table 3.5 Values of β for Members without Web Reinforcement

s_x less than or equal	ε_x x 1000 less than or equal								
	-0.200	-0.100	0.000	0.250	0.500	0.750	1.000	1.500	2.000
5	6.90	5.70	4.94	3.78	3.19	2.82	2.56	2.19	1.93
10	6.77	5.53	4.65	3.45	2.83	2.46	2.19	1.87	1.65
15	6.57	5.42	4.47	3.21	2.59	2.23	1.98	1.65	1.45
25	6.24	5.36	4.19	2.85	2.26	1.92	1.69	1.40	1.18
50	5.62	5.24	3.83	2.39	1.82	1.50	1.27	1.00	0.83
100	4.78	4.78	3.47	1.88	1.35	1.06	0.87	0.65	0.52
200	3.83	3.83	3.11	1.39	0.90	0.66	0.53	0.37	0.28

Table 3.6 Values of β for Members without Web Reinforcement

s_x less than or equal	ε_x x 1000 less than or equal										
	-0.200	-0.175	-0.150	-0.125	-0.100	-0.075	-0.050	-0.025	0.000	0.063	0.125
5	6.90	6.60	6.30	6.00	5.70	5.51	5.32	5.13	4.94	4.65	4.36
6	6.87	6.57	6.27	5.97	5.67	5.47	5.27	5.08	4.88	4.59	4.30
7	6.85	6.54	6.24	5.94	5.63	5.43	5.23	5.03	4.82	4.53	4.24
8	6.82	6.52	6.21	5.90	5.60	5.39	5.18	4.97	4.77	4.47	4.17
9	6.80	6.49	6.18	5.87	5.56	5.35	5.14	4.92	4.71	4.41	4.11
10	6.77	6.46	6.15	5.84	5.53	5.31	5.09	4.87	4.65	4.35	4.05
11	6.73	6.42	6.12	5.81	5.51	5.28	5.06	4.84	4.61	4.31	4.01
12	6.69	6.39	6.09	5.79	5.49	5.26	5.03	4.81	4.58	4.27	3.97
13	6.65	6.35	6.06	5.76	5.46	5.23	5.01	4.77	4.54	4.24	3.92
14	6.61	6.32	6.03	5.74	5.44	5.21	4.98	4.74	4.51	4.20	3.88
15	6.57	6.28	6.00	5.71	5.42	5.18	4.95	4.71	4.47	4.16	3.84
17	6.50	6.23	5.96	5.68	5.41	5.16	4.92	4.66	4.41	4.10	3.78
19	6.44	6.18	5.92	5.66	5.40	5.14	4.88	4.62	4.36	4.04	3.71
21	6.37	6.12	5.88	5.63	5.38	5.11	4.85	4.57	4.30	3.98	3.65
23	6.31	6.07	5.84	5.61	5.37	5.09	4.81	4.53	4.25	3.92	3.58
25	6.24	6.02	5.80	5.58	5.36	5.07	4.78	4.48	4.19	3.86	3.52
30	6.12	5.92	5.73	5.53	5.34	5.03	4.73	4.42	4.12	3.78	3.44
35	5.99	5.82	5.65	5.48	5.31	5.00	4.68	4.36	4.05	3.70	3.36
40	5.87	5.73	5.58	5.44	5.29	4.96	4.64	4.30	3.97	3.63	3.27
45	5.74	5.63	5.50	5.39	5.26	4.93	4.59	4.24	3.90	3.55	3.19
50	5.62	5.53	5.43	5.34	5.24	4.89	4.54	4.18	3.83	3.47	3.11
60	5.45	5.38	5.30	5.23	5.15	4.80	4.46	4.10	3.76	3.39	3.02
70	5.28	5.23	5.17	5.12	5.06	4.71	4.38	4.03	3.69	3.31	2.94
80	5.12	5.08	5.04	5.00	4.96	4.63	4.29	3.95	3.61	3.23	2.85
90	4.95	4.93	4.91	4.89	4.87	4.54	4.21	3.88	3.54	3.15	2.77
100	4.78	4.78	4.78	4.78	4.78	4.45	4.13	3.80	3.47	3.07	2.68
120	4.59	4.59	4.59	4.59	4.59	4.29	4.00	3.70	3.40	2.99	2.59
140	4.40	4.40	4.40	4.40	4.40	4.13	3.87	3.60	3.33	2.91	2.51
160	4.21	4.21	4.21	4.21	4.21	3.97	3.73	3.49	3.25	2.84	2.42
180	4.02	4.02	4.02	4.02	4.02	3.81	3.60	3.39	3.18	2.76	2.34
200	3.83	3.83	3.83	3.83	3.83	3.65	3.47	3.29	3.11	2.68	2.25

Table 3.6 (continued)

s_x less than or equal	ε_x x 1000 less than or equal										
	0.188	0.250	0.313	0.375	0.438	0.500	0.563	0.625	0.688	0.750	0.813
5	4.07	3.78	3.63	3.49	3.34	3.19	3.10	3.01	2.91	2.82	2.76
6	4.01	3.71	3.56	3.42	3.27	3.12	3.03	2.94	2.84	2.75	2.69
7	3.94	3.65	3.50	3.35	3.20	3.05	2.96	2.87	2.77	2.68	2.61
8	3.88	3.58	3.43	3.28	3.13	2.97	2.88	2.79	2.69	2.60	2.54
9	3.81	3.52	3.37	3.21	3.06	2.90	2.81	2.72	2.62	2.53	2.46
10	3.75	3.45	3.30	3.14	2.99	2.83	2.74	2.65	2.55	2.46	2.39
11	3.71	3.40	3.25	3.09	2.94	2.78	2.69	2.60	2.50	2.41	2.35
12	3.66	3.35	3.20	3.04	2.89	2.73	2.64	2.55	2.46	2.37	2.30
13	3.62	3.31	3.16	3.00	2.85	2.69	2.60	2.51	2.41	2.32	2.26
14	3.57	3.26	3.11	2.95	2.80	2.64	2.55	2.46	2.37	2.28	2.21
15	3.53	3.21	3.06	2.90	2.75	2.59	2.50	2.41	2.32	2.23	2.17
17	3.46	3.14	2.99	2.83	2.68	2.52	2.44	2.35	2.26	2.17	2.11
19	3.39	3.07	2.92	2.76	2.61	2.46	2.37	2.28	2.20	2.11	2.05
21	3.33	2.99	2.84	2.70	2.55	2.39	2.31	2.22	2.13	2.04	1.98
23	3.26	2.92	2.77	2.63	2.48	2.33	2.24	2.15	2.07	1.98	1.92
25	3.19	2.85	2.70	2.56	2.41	2.26	2.18	2.09	2.01	1.92	1.86
30	3.10	2.76	2.61	2.47	2.32	2.17	2.09	2.00	1.92	1.84	1.78
35	3.01	2.67	2.52	2.38	2.23	2.08	2.00	1.92	1.84	1.75	1.69
40	2.93	2.57	2.43	2.29	2.14	2.00	1.92	1.83	1.75	1.67	1.61
45	2.84	2.48	2.34	2.20	2.05	1.91	1.83	1.75	1.67	1.58	1.52
50	2.75	2.39	2.25	2.11	1.96	1.82	1.74	1.66	1.58	1.50	1.44
60	2.66	2.29	2.15	2.01	1.86	1.73	1.65	1.57	1.49	1.41	1.35
70	2.56	2.19	2.05	1.91	1.77	1.63	1.56	1.48	1.40	1.32	1.27
80	2.47	2.08	1.95	1.82	1.67	1.54	1.46	1.39	1.31	1.24	1.18
90	2.37	1.98	1.85	1.72	1.58	1.44	1.37	1.30	1.22	1.15	1.10
100	2.28	1.88	1.75	1.62	1.48	1.35	1.28	1.21	1.13	1.06	1.01
120	2.19	1.78	1.65	1.53	1.39	1.26	1.19	1.12	1.05	0.98	0.93
140	2.10	1.68	1.56	1.43	1.30	1.17	1.10	1.04	0.97	0.90	0.86
160	2.00	1.59	1.46	1.34	1.20	1.08	1.02	0.95	0.88	0.82	0.78
180	1.91	1.49	1.37	1.24	1.11	0.99	0.93	0.87	0.80	0.74	0.71
200	1.82	1.39	1.27	1.15	1.02	0.90	0.84	0.78	0.72	0.66	0.63

Table 3.6 (continued)

s_x less than or equal	ε_x x 1000 less than or equal										
	0.875	0.938	1.000	1.125	1.250	1.375	1.500	1.625	1.750	1.875	2.000
5	2.69	2.63	2.56	2.47	2.38	2.28	2.19	2.13	2.06	2.00	1.93
6	2.62	2.56	2.49	2.40	2.31	2.21	2.13	2.07	2.00	1.94	1.87
7	2.55	2.48	2.41	2.33	2.24	2.15	2.06	2.01	1.94	1.88	1.82
8	2.47	2.41	2.34	2.25	2.17	2.08	2.00	1.94	1.88	1.83	1.76
9	2.40	2.33	2.26	2.18	2.10	2.02	1.93	1.88	1.82	1.77	1.71
10	2.33	2.26	2.19	2.11	2.03	1.95	1.87	1.82	1.76	1.71	1.65
11	2.29	2.22	2.15	2.07	1.99	1.91	1.83	1.78	1.72	1.67	1.61
12	2.24	2.17	2.11	2.03	1.95	1.86	1.78	1.73	1.68	1.63	1.57
13	2.20	2.13	2.06	1.98	1.90	1.82	1.74	1.69	1.63	1.58	1.53
14	2.15	2.08	2.02	1.94	1.86	1.77	1.69	1.64	1.59	1.54	1.49
15	2.11	2.04	1.98	1.90	1.82	1.73	1.65	1.60	1.55	1.50	1.45
17	2.05	1.98	1.92	1.84	1.77	1.68	1.60	1.55	1.50	1.45	1.40
19	1.99	1.92	1.86	1.79	1.71	1.63	1.55	1.50	1.45	1.40	1.34
21	1.93	1.87	1.81	1.73	1.66	1.57	1.50	1.45	1.39	1.34	1.29
23	1.87	1.81	1.75	1.68	1.60	1.52	1.45	1.40	1.34	1.29	1.23
25	1.81	1.75	1.69	1.62	1.55	1.47	1.40	1.35	1.29	1.24	1.18
30	1.73	1.67	1.61	1.54	1.47	1.39	1.32	1.27	1.22	1.17	1.11
35	1.64	1.58	1.52	1.45	1.39	1.31	1.24	1.19	1.14	1.09	1.04
40	1.56	1.50	1.44	1.37	1.30	1.23	1.16	1.12	1.07	1.02	0.97
45	1.47	1.41	1.35	1.28	1.22	1.15	1.08	1.04	0.99	0.94	0.90
50	1.39	1.33	1.27	1.20	1.14	1.07	1.00	0.96	0.92	0.87	0.83
60	1.31	1.25	1.19	1.12	1.06	1.00	0.93	0.89	0.85	0.81	0.77
70	1.22	1.17	1.11	1.05	0.99	0.93	0.86	0.82	0.79	0.74	0.71
80	1.14	1.08	1.03	0.97	0.91	0.85	0.79	0.76	0.72	0.68	0.64
90	1.05	1.00	0.95	0.90	0.84	0.78	0.72	0.69	0.66	0.61	0.58
100	0.97	0.92	0.87	0.82	0.76	0.71	0.65	0.62	0.59	0.55	0.52
120	0.90	0.85	0.80	0.75	0.70	0.65	0.59	0.57	0.54	0.50	0.47
140	0.82	0.78	0.73	0.69	0.64	0.59	0.54	0.51	0.49	0.45	0.42
160	0.75	0.70	0.67	0.62	0.57	0.53	0.48	0.46	0.43	0.40	0.38
180	0.67	0.63	0.60	0.56	0.51	0.47	0.43	0.40	0.38	0.35	0.33
200	0.60	0.56	0.53	0.49	0.45	0.41	0.37	0.35	0.33	0.30	0.28

Table 3.7 Values of θ for Members without Web Reinforcement

s_x less than or equal	ε_x x 1000 less than or equal								
	-0.200	-0.100	0.000	0.250	0.500	0.750	1.000	1.500	2.000
5	26.0	26.0	27.0	29.0	31.0	33.0	34.0	36.0	38.0
10	27.0	28.0	30.0	34.0	37.0	39.0	40.0	43.0	45.0
15	27.0	30.0	32.0	37.0	40.0	43.0	45.0	48.0	50.0
25	28.0	31.0	35.0	41.0	45.0	48.0	51.0	54.0	57.0
50	31.0	33.0	38.0	48.0	53.0	57.0	59.0	63.0	66.0
100	35.0	35.0	42.0	55.0	62.0	66.0	69.0	72.0	75.0
200	42.0	42.0	47.0	64.0	71.0	74.0	77.0	80.0	82.0

Table 3.8 Values of θ for Members without Web Reinforcement

s_x less than or equal	ε_x x 1000 less than or equal										
	-0.200	-0.175	-0.150	-0.125	-0.100	-0.075	-0.050	-0.025	0.000	0.063	0.125
5	26.0	26.0	26.0	26.0	26.0	26.3	26.5	26.8	27.0	27.5	28.0
6	26.2	26.3	26.3	26.4	26.4	26.7	27.0	27.3	27.6	28.2	28.8
7	26.4	26.5	26.6	26.7	26.8	27.2	27.5	27.9	28.2	28.9	29.6
8	26.6	26.8	26.9	27.1	27.2	27.6	28.0	28.4	28.8	29.6	30.4
9	26.8	27.0	27.2	27.4	27.6	28.1	28.5	29.0	29.4	30.3	31.2
10	27.0	27.3	27.5	27.8	28.0	28.5	29.0	29.5	30.0	31.0	32.0
11	27.0	27.4	27.7	28.1	28.4	28.9	29.4	29.9	30.4	31.5	32.5
12	27.0	27.5	27.9	28.4	28.8	29.3	29.8	30.3	30.8	31.9	33.0
13	27.0	27.6	28.1	28.7	29.2	29.7	30.2	30.7	31.2	32.4	33.5
14	27.0	27.7	28.3	29.0	29.6	30.1	30.6	31.1	31.6	32.8	34.0
15	27.0	27.8	28.5	29.3	30.0	30.5	31.0	31.5	32.0	33.3	34.5
17	27.2	28.0	28.7	29.5	30.2	30.8	31.4	32.0	32.6	33.9	35.2
19	27.4	28.2	28.9	29.7	30.4	31.1	31.8	32.5	33.2	34.6	35.9
21	27.6	28.4	29.1	29.9	30.6	31.4	32.2	33.0	33.8	35.2	36.6
23	27.8	28.6	29.3	30.1	30.8	31.7	32.6	33.5	34.4	35.9	37.3
25	28.0	28.8	29.5	30.3	31.0	32.0	33.0	34.0	35.0	36.5	38.0
30	28.6	29.3	30.0	30.7	31.4	32.5	33.5	34.6	35.6	37.3	39.0
35	29.2	29.9	30.5	31.2	31.8	32.9	34.0	35.1	36.2	38.1	40.0
40	29.8	30.4	31.0	31.6	32.2	33.4	34.5	35.7	36.8	38.9	41.0
45	30.4	31.0	31.5	32.1	32.6	33.8	35.0	36.2	37.4	39.7	42.0
50	31.0	31.5	32.0	32.5	33.0	34.3	35.5	36.8	38.0	40.5	43.0
60	31.8	32.2	32.6	33.0	33.4	34.8	36.1	37.5	38.8	41.5	44.1
70	32.6	32.9	33.2	33.5	33.8	35.3	36.7	38.2	39.6	42.4	45.2
80	33.4	33.6	33.8	34.0	34.2	35.8	37.3	38.9	40.4	43.4	46.3
90	34.2	34.3	34.4	34.5	34.6	36.3	37.9	39.6	41.2	44.3	47.4
100	35.0	35.0	35.0	35.0	35.0	36.8	38.5	40.3	42.0	45.3	48.5
120	36.4	36.4	36.4	36.4	36.4	38.1	39.7	41.4	43.0	46.5	49.9
140	37.8	37.8	37.8	37.8	37.8	39.4	40.9	42.5	44.0	47.7	51.3
160	39.2	39.2	39.2	39.2	39.2	40.7	42.1	43.6	45.0	48.9	52.7
180	40.6	40.6	40.6	40.6	40.6	42.0	43.3	44.7	46.0	50.1	54.1
200	42.0	42.0	42.0	42.0	42.0	43.3	44.5	45.8	47.0	51.3	55.5

Table 3.8 (continued)

s_x less than or equal	ε_x x 1000 less than or equal										
	0.188	0.250	0.313	0.375	0.438	0.500	0.563	0.625	0.688	0.750	0.813
5	28.5	29.0	29.5	30.0	30.5	31.0	31.5	32.0	32.5	33.0	33.3
6	29.4	30.0	30.6	31.1	31.7	32.2	32.7	33.2	33.7	34.2	34.5
7	30.3	31.0	31.6	32.2	32.8	33.4	33.9	34.4	34.9	35.4	35.7
8	31.2	32.0	32.7	33.3	34.0	34.6	35.1	35.6	36.1	36.6	36.9
9	32.1	33.0	33.7	34.4	35.1	35.8	36.3	36.8	37.3	37.8	38.1
10	33.0	34.0	34.8	35.5	36.3	37.0	37.5	38.0	38.5	39.0	39.3
11	33.6	34.6	35.4	36.1	36.9	37.6	38.2	38.7	39.3	39.8	40.1
12	34.1	35.2	36.0	36.7	37.5	38.2	38.8	39.4	40.0	40.6	41.0
13	34.7	35.8	36.6	37.3	38.1	38.8	39.5	40.1	40.8	41.4	41.8
14	35.2	36.4	37.2	37.9	38.7	39.4	40.1	40.8	41.5	42.2	42.7
15	35.8	37.0	37.8	38.5	39.3	40.0	40.8	41.5	42.3	43.0	43.5
17	36.5	37.8	38.6	39.4	40.2	41.0	41.8	42.5	43.3	44.0	44.6
19	37.3	38.6	39.5	40.3	41.2	42.0	42.8	43.5	44.3	45.0	45.6
21	38.0	39.4	40.3	41.2	42.1	43.0	43.8	44.5	45.3	46.0	46.7
23	38.8	40.2	41.2	42.1	43.1	44.0	44.8	45.5	46.3	47.0	47.7
25	39.5	41.0	42.0	43.0	44.0	45.0	45.8	46.5	47.3	48.0	48.8
30	40.7	42.4	43.5	44.5	45.6	46.6	47.4	48.2	49.0	49.8	50.5
35	41.9	43.8	44.9	46.0	47.1	48.2	49.1	49.9	50.8	51.6	52.3
40	43.1	45.2	46.4	47.5	48.7	49.8	50.7	51.6	52.5	53.4	54.0
45	44.3	46.6	47.8	49.0	50.2	51.4	52.4	53.3	54.3	55.2	55.8
50	45.5	48.0	49.3	50.5	51.8	53.0	54.0	55.0	56.0	57.0	57.5
60	46.8	49.4	50.8	52.1	53.5	54.8	55.8	56.8	57.8	58.8	59.4
70	48.0	50.8	52.3	53.7	55.2	56.6	57.6	58.6	59.6	60.6	61.2
80	49.3	52.2	53.8	55.3	56.9	58.4	59.4	60.4	61.4	62.4	63.1
90	50.5	53.6	55.3	56.9	58.6	60.2	61.2	62.2	63.2	64.2	64.9
100	51.8	55.0	56.8	58.5	60.3	62.0	63.0	64.0	65.0	66.0	66.8
120	53.4	56.8	58.6	60.3	62.1	63.8	64.8	65.7	66.7	67.6	68.4
140	55.0	58.6	60.4	62.1	63.9	65.6	66.5	67.4	68.3	69.2	70.0
160	56.6	60.4	62.2	63.9	65.7	67.4	68.3	69.1	70.0	70.8	71.6
180	58.2	62.2	64.0	65.7	67.5	69.2	70.0	70.8	71.6	72.4	73.2
200	59.8	64.0	65.8	67.5	69.3	71.0	71.8	72.5	73.3	74.0	74.8

Table 3.8 (continued)

s_x less than or equal	ε_x x 1000 less than or equal										
	0.875	0.938	1.000	1.125	1.250	1.375	1.500	1.625	1.750	1.875	2.000
5	33.5	33.8	34.0	34.5	35.0	35.5	36.0	36.5	37.0	37.5	38.0
6	34.7	35.0	35.2	35.8	36.3	36.9	37.4	37.9	38.4	38.9	39.4
7	35.9	36.2	36.4	37.0	37.6	38.2	38.8	39.3	39.8	40.3	40.8
8	37.1	37.4	37.6	38.3	38.9	39.6	40.2	40.7	41.2	41.7	42.2
9	38.3	38.6	38.8	39.5	40.2	40.9	41.6	42.1	42.6	43.1	43.6
10	39.5	39.8	40.0	40.8	41.5	42.3	43.0	43.5	44.0	44.5	45.0
11	40.4	40.7	41.0	41.8	42.5	43.3	44.0	44.5	45.0	45.5	46.0
12	41.3	41.7	42.0	42.8	43.5	44.3	45.0	45.5	46.0	46.5	47.0
13	42.2	42.6	43.0	43.8	44.5	45.3	46.0	46.5	47.0	47.5	48.0
14	43.1	43.6	44.0	44.8	45.5	46.3	47.0	47.5	48.0	48.5	49.0
15	44.0	44.5	45.0	45.8	46.5	47.3	48.0	48.5	49.0	49.5	50.0
17	45.1	45.7	46.2	47.0	47.7	48.5	49.2	49.8	50.3	50.9	51.4
19	46.2	46.8	47.4	48.2	48.9	49.7	50.4	51.0	51.6	52.2	52.8
21	47.3	48.0	48.6	49.4	50.1	50.9	51.6	52.3	52.9	53.6	54.2
23	48.4	49.1	49.8	50.6	51.3	52.1	52.8	53.5	54.2	54.9	55.6
25	49.5	50.3	51.0	51.8	52.5	53.3	54.0	54.8	55.5	56.3	57.0
30	51.2	51.9	52.6	53.4	54.2	55.0	55.8	56.6	57.3	58.1	58.8
35	52.9	53.6	54.2	55.1	55.9	56.8	57.6	58.4	59.1	59.9	60.6
40	54.6	55.2	55.8	56.7	57.6	58.5	59.4	60.2	60.9	61.7	62.4
45	56.3	56.9	57.4	58.4	59.3	60.3	61.2	62.0	62.7	63.5	64.2
50	58.0	58.5	59.0	60.0	61.0	62.0	63.0	63.8	64.5	65.3	66.0
60	59.9	60.5	61.0	62.0	62.9	63.9	64.8	65.6	66.3	67.1	67.8
70	61.8	62.4	63.0	63.9	64.8	65.7	66.6	67.4	68.1	68.9	69.6
80	63.7	64.4	65.0	65.9	66.7	67.6	68.4	69.2	69.9	70.7	71.4
90	65.6	66.3	67.0	67.8	68.6	69.4	70.2	71.0	71.7	72.5	73.2
100	67.5	68.3	69.0	69.8	70.5	71.3	72.0	72.8	73.5	74.3	75.0
120	69.1	69.9	70.6	71.4	72.1	72.9	73.6	74.3	75.0	75.7	76.4
140	70.7	71.5	72.2	73.0	73.7	74.5	75.2	75.9	76.5	77.2	77.8
160	72.3	73.1	73.8	74.6	75.3	76.1	76.8	77.4	78.0	78.6	79.2
180	73.9	74.7	75.4	76.2	76.9	77.7	78.4	79.0	79.5	80.1	80.6
200	75.5	76.3	77.0	77.8	78.5	79.3	80.0	80.5	81.0	81.5	82.0

Table 3.9 Model Comparison of Contributions

ACI 318-95 Simplified Method	
concrete =	statistical analysis
stirrups =	45° crack angle
draping =	neglected
ACI 318-95 Detailed Method (AASHTO 1989)	
concrete =	web-shear and flexural-shear
stirrups =	45° crack angle
draping =	included
Modified ACI 318-95 Procedure	
concrete =	web-shear at any depth in the cross section
stirrups =	45° crack angle
draping =	included
Modified Compression Field Theory (AASHTO LRFD 1994)	
concrete =	variable crack angle from 20° to 43° with web reinforcement
stirrups =	variable crack angle from 20° to 43° with web reinforcement
draping =	included
Modified Truss Theory	
concrete =	web-shear
stirrups =	25° crack angle
draping =	included
Truss Theory	
concrete =	neglected
stirrups =	range in crack angles from 30° to 90°
draping =	neglected
Strut-and-Tie Model	
concrete =	allowable stress
stirrups =	neglected
draping =	neglected

Table 4.1 Concrete Mix Design for the Girders

Materials	**Quantity per Cubic Yard**	
	Girder I	Girder II
Type III Cement	750 lb	695 lb
Fine Aggregate (Sand)	1330 lb	1290 lb
Coarse Aggregate (5/8 in. Limestone)	1970 lb	---
Coarse Aggregate (3/4 in. Glacial Gravel)	---	1880 lb
Microsilica	---	56 lb
Water Reducer (WRDA 19)	150 oz.	123.3 oz.
Water / Cement Ratio	0.323	0.359

Design Compressive Strength at 28 days equal to 10,500 psi

Girder I: Crushed Limestone Aggregate Concrete
Girder II: Round Glacial Gravel Concrete with Microsilica

Measured moisture absorption capacity of aggregates, by weight:
limestone = 2.9%, glacial gravel = 2.6%, sand = 3.7%

Table 4.2 Concrete Mix Design for the Deck

Materials	**Quantity per Cubic Yard**
Type I Cement	640 lb
Fine Aggregate (Sand)	1195 lb
Coarse Aggregate (3/4 in. Gravel)	1810 lb
Water	270 lb
Air Entrainment	5.5% ± 1.5%
Water / Cement Ratio	0.42

Design Compressive Strength at 28 days equal to 4300 psi

Design Slump equal to 3 in.

Table 4.3 Type of Instrumentation

Instrumentation	Manufacturer	Model	Description
Deflection LVDTs	Schaevitz Schaevitz	3000 HR 5000 HR	3.0 in. 5.0 in.
Stirrup Strain Gages	Tokyo Sokki Kenkyuto Co	TML Type WFLA-3	-
Internal Concrete Rosettes	Tokyo Sokki Kenkyuto Co	TML Type PMR-60	-
External Rossettes	Tokyo Sokki Kenkyuto Co	TML Type WFRA-6	-
Bursting Stirrup gages	Tokyo Sokki Kenkyuto Co	TML Type WFLA-3	-
Rupture of Concrete	Tokyo Sokki Kenkyuto Co.	TML Type PML-60	-
Strand Slip LVDTs	Schaevitz Schaevitz	100 HR 1000 HR	0.1 in. 1.0 in.
Transfer Gages	Tokyo Sokki Kenkyuto Co	TML Type FLK-1	-
Acoustic Emission	Physical Acoustics	Mistras	8 channel

Table 4.4 Testing Dimensions

Measurements (from West End to cL)	End				
	Nominal (ft.)	IA (ft.)	IB (ft.)	IIC (ft.)	IID (ft.)
Roller (west support)	0.625	0.641	0.625	0.599	0.698
West LVDT	12.00	12.05	12.00	12.15	12.15
Load Point	13.90	14.05	13.80	14.05	14.00
East LVDT	16.00	15.90	15.80	16.00	16.05
Neoprene Pad (East Support)	40.40	40.45	40.35	40.70	40.30
Neoprene LVDT	40.40	41.35	40.35	40.65	40.30
Total Length	43.00	43.00	43.00	43.00	43.00
Total Plate Width	1.00	1.00	0.71	1.00	1.00

Table 4.5 Stirrup Active Gages

Gage	End			
	IA	IB	IIC	IID
S1B	active	active	-	active
S1C	active	active	-	active
S3B	active	active	-	active
S3C	active	active	-	active
S4A	active	active	active	active
S4B	active	active	-	active
S4C	active	active	-	-
S5A	active	active	active	active
S5B	active	active	active	active
S5C	active	active	active	active
S6A	active	active	active	-
S6B	active	active	-	active
S6C	active	active	-	active
S7A	active	active	active	active
S7B	active	active	active	active
S8A	active	active	active	active
S8B	active	active	active	active
S12A	-	active	active	active
S12B	active	active	active	active
S12C	-	active	active	active
S13A	-	active	active	active
S13B	active	active	active	active
S13C	-	active	active	active
S15A	active	active	active	active
S15B	active	active	active	active
S18A	active	active	active	active
S18B	active	-	active	active
S18C	active	active	active	active
S22B	active	active	-	active
S22C	active	active	-	active

number corresponds to stirrup (see Figure 4.19)
letter corresponds to position on stirrup (A = top of web, B = middle of web, C = bottom of web)

Table 4.6 Stirrup Gage Locations (End IA)

Gage	End IA					
	Design			Actual		
	x (ft.)	y (in.)	z (in.)	x (ft.)	y (in.)	z (in.)
S1B	2.25	1.50	22.50	2.10	1.50	22.50
S1C	2.25	1.50	11.50	2.10	1.50	11.00
S3B	4.92	1.50	22.50	4.90	-1.50	21.50
S3C	4.92	1.50	11.50	4.90	-1.50	11.00
S4A	6.25	1.50	35.00	6.15	-1.50	35.00
S4B	6.25	1.50	22.50	6.15	-1.50	22.25
S4C	6.25	1.50	11.50	6.15	-1.50	11.00
S5A	7.58	1.50	35.00	7.40	1.50	34.75
S5B	7.58	1.50	22.50	7.40	1.50	22.50
S5C	7.58	1.50	11.50	7.40	1.50	11.00
S6A	8.92	1.50	35.00	8.75	1.50	35.00
S6B	8.92	1.50	22.50	8.75	1.50	22.00
S6C	8.92	1.50	11.50	8.75	1.50	11.00
S7A	10.25	1.50	35.00	10.15	-1.50	35.00
S7B	10.25	1.50	22.50	10.15	-1.50	22.50
S8A	11.58	1.50	35.00	11.40	-1.50	35.00
S8B	11.58	1.50	22.50	11.40	-1.50	22.50
S12A	16.92	1.50	35.00	16.80	1.50	34.00
S12B	16.92	1.50	22.50	16.80	1.50	22.00
S12C	16.92	1.50	11.50	16.80	1.50	10.50
S13A	18.25	1.50	35.00	18.20	1.50	35.00
S13B	18.25	1.50	22.50	18.20	1.50	23.00
S13C	18.25	1.50	11.50	18.20	1.50	11.00
S15A	20.92	1.50	35.00	20.80	1.50	34.50
S15B	20.92	1.50	22.50	20.80	1.50	22.50
S18A	24.92	1.50	35.00	24.90	1.50	35.00
S18B	24.92	1.50	22.50	24.90	1.50	22.50
S18C	24.92	1.50	11.50	24.90	1.50	11.00
S22B	30.25	1.50	22.50	30.25	1.50	21.50
S22C	30.25	1.50	11.50	30.25	1.50	10.50

x = distance from west end, y = distance from cross section centerline (left is positive)
z = height from bottom of girder

Table 4.7 Stirrup Gage Locations (End IB)

Gage	End IB					
	Design			Actual		
	x (ft.)	y (in.)	z (in.)	x (ft.)	y (in.)	z (in.)
S1B	2.25	1.50	22.50	2.25	-1.50	23.00
S1C	2.25	1.50	11.50	2.25	-1.50	10.50
S3B	4.92	1.50	22.50	4.85	-1.50	23.00
S3C	4.92	1.50	11.50	4.85	-1.50	11.50
S4A	6.25	1.50	35.00	6.20	-1.50	35.25
S4B	6.25	1.50	22.50	6.20	-1.50	23.00
S4C	6.25	1.50	11.50	6.20	-1.50	11.00
S5A	7.58	1.50	35.00	7.60	-1.50	35.25
S5B	7.58	1.50	22.50	7.60	-1.50	23.00
S5C	7.58	1.50	11.50	7.60	-1.50	11.00
S6A	8.92	1.50	35.00	8.95	-1.50	35.50
S6B	8.92	1.50	22.50	8.95	-1.50	23.00
S6C	8.92	1.50	11.50	8.95	-1.50	11.50
S7A	10.25	1.50	35.00	10.30	-1.50	35.50
S7B	10.25	1.50	22.50	10.30	-1.50	22.25
S8A	11.58	1.50	35.00	11.60	-1.50	36.00
S8B	11.58	1.50	22.50	11.60	-1.50	23.00
S12A	16.92	1.50	35.00	17.10	-1.50	35.75
S12B	16.92	1.50	22.50	17.10	-1.50	23.00
S12C	16.92	1.50	11.50	17.10	-1.50	11.50
S13A	18.25	1.50	35.00	18.30	-1.50	35.00
S13B	18.25	1.50	22.50	18.30	-1.50	22.50
S13C	18.25	1.50	11.50	18.30	-1.50	11.00
S15A	20.92	1.50	35.00	21.00	-1.50	36.00
S15B	20.92	1.50	22.50	21.00	-1.50	23.00
S18A	24.92	1.50	35.00	25.10	-1.50	35.25
S18B	24.92	1.50	22.50	25.10	-1.50	23.00
S18C	24.92	1.50	11.50	25.10	-1.50	11.25
S22B	30.25	1.50	22.50	30.50	-1.50	23.00
S22C	30.25	1.50	11.50	30.50	-1.50	11.00

x = distance from west end, y = distance from cross section centerline (left is positive)
z = height from bottom of girder

Table 4.8 Stirrup Gage Locations (End IIC)

Gage	End IIC					
	Design			Actual		
	x (ft.)	y (in.)	z (in.)	x (ft.)	y (in.)	z (in.)
S1B	2.25	1.50	22.50	2.10	1.50	22.75
S1C	2.25	1.50	11.50	2.10	1.50	10.75
S3B	4.92	1.50	22.50	4.65	1.50	23.00
S3C	4.92	1.50	11.50	4.65	1.50	11.00
S4A	6.25	1.50	35.00	6.00	1.50	35.00
S4B	6.25	1.50	22.50	6.00	1.50	23.00
S4C	6.25	1.50	11.50	6.00	1.50	11.00
S5A	7.58	1.50	35.00	7.45	1.50	36.00
S5B	7.58	1.50	22.50	7.45	1.50	23.25
S5C	7.58	1.50	11.50	7.45	1.50	11.25
S6A	8.92	1.50	35.00	8.70	1.50	35.25
S6B	8.92	1.50	22.50	8.70	1.50	23.00
S6C	8.92	1.50	11.50	8.70	1.50	11.00
S7A	10.25	1.50	35.00	10.00	1.50	35.50
S7B	10.25	1.50	22.50	10.00	1.50	23.00
S8A	11.58	1.50	35.00	11.30	1.50	35.50
S8B	11.58	1.50	22.50	11.30	1.50	23.00
S12A	16.92	1.50	35.00	16.90	1.50	35.50
S12B	16.92	1.50	22.50	16.90	1.50	23.00
S12C	16.92	1.50	11.50	16.90	1.50	11.00
S13A	18.25	1.50	35.00	18.20	1.50	35.50
S13B	18.25	1.50	22.50	18.20	1.50	23.00
S13C	18.25	1.50	11.50	18.20	1.50	11.00
S15A	20.92	1.50	35.00	20.90	1.50	35.25
S15B	20.92	1.50	22.50	20.90	1.50	23.00
S18A	24.92	1.50	35.00	24.90	1.50	36.00
S18B	24.92	1.50	22.50	24.90	1.50	23.00
S18C	24.92	1.50	11.50	24.90	1.50	11.50
S22B	30.25	1.50	22.50	30.10	1.50	23.00
S22C	30.25	1.50	11.50	30.10	1.50	11.50

x = distance from west end, y = distance from cross section centerline (left is positive)
z = height from bottom of girder

Table 4.9 Stirrup Gage Locations (End IID)

Gage	End IID					
	Design			Actual		
	x (ft.)	y (in.)	z (in.)	x (ft.)	y (in.)	z (in.)
S1B	2.25	1.50	22.50	2.10	-1.50	22.50
S1C	2.25	1.50	11.50	2.10	-1.50	10.50
S3B	4.92	1.50	22.50	4.80	-1.50	23.00
S3C	4.92	1.50	11.50	4.80	-1.50	11.00
S4A	6.25	1.50	35.00	6.10	-1.50	35.50
S4B	6.25	1.50	22.50	6.10	-1.50	23.00
S4C	6.25	1.50	11.50	6.10	-1.50	11.00
S5A	7.58	1.50	35.00	7.60	-1.50	35.50
S5B	7.58	1.50	22.50	7.60	-1.50	23.50
S5C	7.58	1.50	11.50	7.60	-1.50	11.00
S6A	8.92	1.50	35.00	8.80	-1.50	35.00
S6B	8.92	1.50	22.50	8.80	-1.50	23.00
S6C	8.92	1.50	11.50	8.80	-1.50	11.50
S7A	10.25	1.50	35.00	10.20	-1.50	35.50
S7B	10.25	1.50	22.50	10.20	-1.50	23.00
S8A	11.58	1.50	35.00	11.50	-1.50	35.25
S8B	11.58	1.50	22.50	11.50	-1.50	22.50
S12A	16.92	1.50	35.00	16.95	-1.50	35.50
S12B	16.92	1.50	22.50	16.95	-1.50	23.00
S12C	16.92	1.50	11.50	16.95	-1.50	11.50
S13A	18.25	1.50	35.00	18.30	-1.50	35.75
S13B	18.25	1.50	22.50	18.30	-1.50	23.00
S13C	18.25	1.50	11.50	18.30	-1.50	11.50
S15A	20.92	1.50	35.00	20.90	-1.50	35.50
S15B	20.92	1.50	22.50	20.90	-1.50	23.50
S18A	24.92	1.50	35.00	24.80	-1.50	35.25
S18B	24.92	1.50	22.50	24.80	-1.50	23.00
S18C	24.92	1.50	11.50	24.80	-1.50	11.00
S22B	30.25	1.50	22.50	30.30	-1.50	23.00
S22C	30.25	1.50	11.50	30.30	-1.50	11.50

x = distance from west end, y = distance from cross section centerline (right is positive)
z = height from bottom of girder

Table 4.10 Internal Rosette Active Gages

Gage	End			
	IA	IB	IIC	IID
R1A	-	-	-	active
R1B	-	active	active	-
R1C	-	active	active	-
R2A	-	active	active	active
R2B	-	active	active	active
R2C	-	active	active	active
R3A	-	-	active	active
R3B	-	-	active	active
R3C	-	-	active	active
R4A	active	active	active	active
R4B	-	active	active	-
R4C	-	active	-	active
R5A	active	-	active	active
R5B	-	-	active	active
R5C	-	-	active	active

Table 4.11 Internal Rosette Gage Locations (End IA)

Gage	End IA					
	Design			Actual		
	x (ft.)	y (in.)	z (in.)	x (ft.)	y (in.)	z (in.)
R1A	2.92	0.00	22.50	2.67	1.25	22.50
R1B	2.92	0.00	22.50	2.67	1.25	22.50
R1C	2.92	0.00	22.50	2.67	1.25	22.50
R2A	5.58	0.00	22.50	5.40	1.25	21.50
R2B	5.58	0.00	22.50	5.40	1.25	21.50
R2C	5.58	0.00	22.50	5.40	1.25	21.50
R3A	8.25	0.00	22.50	7.95	1.25	21.88
R3B	8.25	0.00	22.50	7.95	1.25	21.88
R3C	8.25	0.00	22.50	7.95	1.25	21.88
R4A	10.92	0.00	22.50	10.65	1.25	22.00
R4B	10.92	0.00	22.50	10.65	1.25	22.00
R4C	10.92	0.00	22.50	10.65	1.25	22.00
R5A	17.58	0.00	22.50	17.62	1.25	21.38
R5B	17.58	0.00	22.50	17.62	1.25	21.38
R5C	17.58	0.00	22.50	17.62	1.25	21.38

x = distance from west end, y = distance from cross section centerline (left is positive)
z = height from bottom of girder

Table 4.12 Internal Rosette Gage Locations (End IB)

Gage	End IB					
	Design			Actual		
	x (ft.)	y (in.)	z (in.)	x (ft.)	y (in.)	z (in.)
R1A	2.92	0.00	22.50	2.85	1.25	23.13
R1B	2.92	0.00	22.50	2.85	1.25	23.13
R1C	2.92	0.00	22.50	2.85	1.25	23.13
R2A	5.58	0.00	22.50	5.50	1.25	22.75
R2B	5.58	0.00	22.50	5.50	1.25	22.75
R2C	5.58	0.00	22.50	5.50	1.25	22.75
R3A	8.25	0.00	22.50	8.17	1.25	22.75
R3B	8.25	0.00	22.50	8.17	1.25	22.75
R3C	8.25	0.00	22.50	8.17	1.25	22.75
R4A	10.92	0.00	22.50	10.85	1.25	22.50
R4B	10.92	0.00	22.50	10.85	1.25	22.50
R4C	10.92	0.00	22.50	10.85	1.25	22.50
R5A	17.58	0.00	22.50	17.80	1.25	22.63
R5B	17.58	0.00	22.50	17.80	1.25	22.63
R5C	17.58	0.00	22.50	17.80	1.25	22.63

x = distance from west end, y = distance from cross section centerline (left is positive)
z = height from bottom of girder

Table 4.13 Internal Rosette Gage Locations (End IIC)

Gage	End IIC					
	Design			Actual		
	x (ft.)	y (in.)	z (in.)	x (ft.)	y (in.)	z (in.)
R1A	2.92	0.00	22.50	2.70	1.25	22.00
R1B	2.92	0.00	22.50	2.70	1.25	22.00
R1C	2.92	0.00	22.50	2.70	1.25	22.00
R2A	5.58	0.00	22.50	5.30	1.25	22.75
R2B	5.58	0.00	22.50	5.30	1.25	22.75
R2C	5.58	0.00	22.50	5.30	1.25	22.75
R3A	8.25	0.00	22.50	8.00	1.25	23.50
R3B	8.25	0.00	22.50	8.00	1.25	23.50
R3C	8.25	0.00	22.50	8.00	1.25	23.50
R4A	10.92	0.00	22.50	10.50	1.25	23.25
R4B	10.92	0.00	22.50	10.50	1.25	23.25
R4C	10.92	0.00	22.50	10.50	1.25	23.25
R5A	17.58	0.00	22.50	17.60	1.25	22.25
R5B	17.58	0.00	22.50	17.60	1.25	22.25
R5C	17.58	0.00	22.50	17.60	1.25	22.25

x = distance from west end, y = distance from cross section centerline (left is positive)
z = height from bottom of girder

Table 4.14 Internal Rosette Gage Locations (End IID)

Gage	End IID					
	Design			Actual		
	x (ft.)	y (in.)	z (in.)	x (ft.)	y (in.)	z (in.)
R1A	2.92	0.00	22.50	2.70	2.00	23.25
R1B	2.92	0.00	22.50	2.70	2.00	23.25
R1C	2.92	0.00	22.50	2.70	2.00	23.25
R2A	5.58	0.00	22.50	5.45	2.00	23.00
R2B	5.58	0.00	22.50	5.45	2.00	23.00
R2C	5.58	0.00	22.50	5.45	2.00	23.00
R3A	8.25	0.00	22.50	8.10	2.00	22.50
R3B	8.25	0.00	22.50	8.10	2.00	22.50
R3C	8.25	0.00	22.50	8.10	2.00	22.50
R4A	10.92	0.00	22.50	10.80	2.00	22.50
R4B	10.92	0.00	22.50	10.80	2.00	22.50
R4C	10.92	0.00	22.50	10.80	2.00	22.50
R5A	17.58	0.00	22.50	17.65	2.00	23.50
R5B	17.58	0.00	22.50	17.65	2.00	23.50
R5C	17.58	0.00	22.50	17.65	2.00	23.50

x = distance from west end, y = distance from cross section centerline (right is positive)
z = height from bottom of girder

Table 4.15 External Rosette Active Gages

Gage	End			
	IA	IB	IIC	IID
extR1A	active	active	active	active
extR1B	-	active	active	active
extR1C	active	active	active	active
extR2A	active	-	active	-
extR2B	active	-	active	-
extR2C	active	-	active	-
extR3A	active	active	active	-
extR3B	active	-	active	-
extR3C	active	active	active	-
extR4A	active	-	-	active
extR4B	active	-	active	active
extR4C	active	-	active	active
extR5A	active	-	active	-
extR5B	active	active	active	-
extR5C	active	active	active	-

Table 4.16 External Rosette Gage Locations (End IA)

Gage	End IA					
	Design			Actual		
	x (ft.)	y (in.)	z (in.)	x (ft.)	y (in.)	z (in.)
extR1A	2.92	0.00	22.50	2.90	-3.00	-
extR1B	2.92	0.00	22.50	2.90	-3.00	-
extR1C	2.92	0.00	22.50	2.90	-3.00	-
extR2A	5.58	0.00	22.50	5.50	-3.00	-
extR2B	5.58	0.00	22.50	5.50	-3.00	-
extR2C	5.58	0.00	22.50	5.50	-3.00	-
extR3A	8.25	0.00	22.50	8.00	-3.00	-
extR3B	8.25	0.00	22.50	8.00	-3.00	-
extR3C	8.25	0.00	22.50	8.00	-3.00	-
extR4A	10.92	0.00	22.50	10.50	-3.00	-
extR4B	10.92	0.00	22.50	10.50	-3.00	-
extR4C	10.92	0.00	22.50	10.50	-3.00	-
extR5A	17.58	0.00	22.50	17.50	-3.00	-
extR5B	17.58	0.00	22.50	17.50	-3.00	-
extR5C	17.58	0.00	22.50	17.50	-3.00	-

x = distance from west end, y = distance from cross section centerline (left is positive)
z = height from bottom of girder

Table 4.17 External Rosette Gage Locations (End IB)

Gage	End IB					
	Design			Actual		
	x (ft.)	y (in.)	z (in.)	x (ft.)	y (in.)	z (in.)
extR1A	2.92	0.00	22.50	-	-3.00	-
extR1B	2.92	0.00	22.50	-	-3.00	-
extR1C	2.92	0.00	22.50	-	-3.00	-
extR3A	8.25	0.00	22.50	-	-3.00	-
extR3B	8.25	0.00	22.50	-	-3.00	-
extR3C	8.25	0.00	22.50	-	-3.00	-
extR5A	17.58	0.00	22.50	-	-3.00	-
extR5B	17.58	0.00	22.50	-	-3.00	-
extR5C	17.58	0.00	22.50	-	-3.00	-

x = distance from west end, y = distance from cross section centerline (left is positive)
z = height from bottom of girder

Table 4.18 External Rosette Gage Locations (End IIC)

Gage	End IIC					
	Design			Actual		
	x (ft.)	y (in.)	z (in.)	x (ft.)	y (in.)	z (in.)
extR1A	2.92	0.00	22.50	2.75	-3.00	21.50
extR1B	2.92	0.00	22.50	2.75	-3.00	21.50
extR1C	2.92	0.00	22.50	2.75	-3.00	21.50
extR2A	5.58	0.00	22.50	5.33	-3.00	21.50
extR2B	5.58	0.00	22.50	5.33	-3.00	21.50
extR2C	5.58	0.00	22.50	5.33	-3.00	21.50
extR3A	8.25	0.00	22.50	8.00	-3.00	21.50
extR3B	8.25	0.00	22.50	8.00	-3.00	21.50
extR3C	8.25	0.00	22.50	8.00	-3.00	21.50
extR4A	10.92	0.00	22.50	10.50	-3.00	21.75
extR4B	10.92	0.00	22.50	10.50	-3.00	21.75
extR4C	10.92	0.00	22.50	10.50	-3.00	21.75
extR5A	17.58	0.00	22.50	17.58	-3.00	21.75
extR5B	17.58	0.00	22.50	17.58	-3.00	21.75
extR5C	17.58	0.00	22.50	17.58	-3.00	21.75

x = distance from west end, y = distance from cross section centerline (left is positive)
z = height from bottom of girder

Table 4.19 External Rosette Gage Locations (End IID)

Gage	End IID					
	Design			Actual		
	x (ft.)	y (in.)	z (in.)	x (ft.)	y (in.)	z (in.)
extR1A	2.92	0.00	22.50	-	3.00	-
extR1B	2.92	0.00	22.50	-	3.00	-
extR1C	2.92	0.00	22.50	-	3.00	-
extR4A	10.92	0.00	22.50	-	3.00	-
extR4B	10.92	0.00	22.50	-	3.00	-
extR4C	10.92	0.00	22.50	-	3.00	-

x = distance from west end, y = distance from cross section centerline (right is positive)
z = height from bottom of girder

Table 4.20 Bursting Active Gages

Gage	End			
	IA	IB	IIC	IID
B1	active	-	-	active
B2	active	active	-	active
B3	-	active	-	active

Table 4.21 Bursting Gage Locations (End IA)

Gage	End IA					
	Design			Actual		
	x (ft.)	y (in.)	z (in.)	x (ft.)	y (in.)	z (in.)
B1	2.00	1.70	11.50	3.00	1.70	11.00
B2	2.00	-1.70	11.50	3.00	-1.70	11.00
B3	8.00	-1.70	11.50	8.00	-1.70	11.50

x = distance from west end, y = distance from cross section centerline (left is positive)
z = height from bottom of girder

Table 4.22 Bursting Gage Locations (End IB)

Gage	End IB					
	Design			Actual		
	x (ft.)	y (in.)	z (in.)	x (ft.)	y (in.)	z (in.)
B1	2.00	1.70	11.50	2.50	1.70	10.25
B2	2.00	-1.70	11.50	2.50	-1.70	10.25
B3	8.00	1.70	11.50	7.50	1.70	11.25

x = distance from west end, y = distance from cross section centerline (left is positive)
z = height from bottom of girder

Table 4.23 Bursting Gage Locations (End IIC)

Gage	End IIC					
	Design			Actual		
	x (ft.)	y (in.)	z (in.)	x (ft.)	y (in.)	z (in.)
B1	2.00	1.70	11.50	2.50	1.70	11.00
B2	2.00	-1.70	11.50	2.50	-1.70	11.00
B3	8.00	-1.70	11.50	8.00	-1.70	11.50

x = distance from west end, y = distance from cross section centerline (left is positive)
z = height from bottom of girder

Table 4.24 Bursting Gage Locations (End IID)

Gage	End IID					
	Design			Actual		
	x (ft.)	y (in.)	z (in.)	x (ft.)	y (in.)	z (in.)
B1	2.00	1.70	11.50	3.00	1.70	11.25
B2	2.00	-1.70	11.50	2.50	-1.70	11.25
B3	8.00	1.70	11.50	9.00	-1.70	11.75

x = distance from west end, y = distance from cross section centerline (right is positive)
z = height from bottom of girder

Table 4.25 Rupture Active Gages

Gage	End			
	IA	IB	IIC	IID
P1	active	-	active	-
P2	active	-	active	active

Table 4.26 Rupture Gage Locations (End IA)

Gage	End IA					
	Design			Actual		
	x (ft.)	y (in.)	z (in.)	x (ft.)	y (in.)	z (in.)
P1	7.50	0.00	9.50	6.50	-	10.00
P2	7.50	0.00	12.50	6.50	-	12.50

x = distance from west end, y = distance from cross section centerline (left is positive)
z = height from bottom of girder

Table 4.27 Rupture Gage Locations (End IB)

Gage	End IB					
	Design			Actual		
	x (ft.)	y (in.)	z (in.)	x (ft.)	y (in.)	z (in.)
P1	7.50	0.00	9.50	7.00	-	9.75
P2	7.50	0.00	12.50	7.00	-	12.25

x = distance from west end, y = distance from cross section centerline (left is positive)
z = height from bottom of girder

Table 4.28 Rupture Gage Locations (End IIC)

Gage	End IIC					
	Design			Actual		
	x (ft.)	y (in.)	z (in.)	x (ft.)	y (in.)	z (in.)
P1	7.50	0.00	9.50	7.50	-	9.50
P2	7.50	0.00	12.50	7.50	-	12.50

x = distance from west end, y = distance from cross section centerline (left is positive)
z = height from bottom of girder

Table 4.29 Rupture Gage Locations (End IID)

Gage	End IID					
	Design			Actual		
	x (ft.)	y (in.)	z (in.)	x (ft.)	y (in.)	z (in.)
P1	7.50	0.00	9.50	7.00	0.00	8.50
P2	7.50	0.00	12.50	7.00	0.00	12.25

x = distance from west end, y = distance from cross section centerline (right is positive)
z = height from bottom of girder

Table 4.30 Strand Slip Active Gages

Gage	End			
	IA	IB	IIC	IID
1-1	active	-	active	active
1-4	active	-	active	active
1-5	active	-	active	active
1-7	active	-	active	active
1-8	active	-	active	active
1-9	active	-	active	active
1-12	active	-	active	active
2-7	active	-	active	active
3-7	active	-	active	active
2-8	-	-	-	active
3-8	-	-	-	active

Table 4.31 Transfer Length Active Gages

Gage	End			
	IA	IB	IIC	IID
035A	-	active	-	-
035B	-	active	-	active
035C	-	active	-	-
25B	active	-	-	-
25C	active	-	-	-
28A	-	active	-	-
28B	active	active	-	-
28C	active	active	-	-
44C	active	-	-	-
49A	-	active	-	-
49B	-	active	-	-
49C	active	active	-	-

Table 4.32 Transfer Gage Locations (End IA)

Gage	End IA					
	Design			Actual		
	x (ft.)	y (in.)	z (in.)	x (ft.)	y (in.)	z (in.)
25A	3.25	3.00	2.00	3.33	3.00	2.25
25B	3.83	3.00	2.00	4.05	3.00	2.25
25C	4.50	3.00	2.00	4.55	3.00	2.25
28A	3.25	-3.00	2.00	3.12	-1.00	2.25
28B	3.83	-3.00	2.00	3.80	-1.00	2.25
28C	4.50	-3.00	2.00	4.44	-1.00	2.25
44C	6.50	5.00	2.00	6.50	5.00	2.25
49A	5.25	-5.00	2.00	5.24	-5.00	2.25
49C	6.50	-5.00	2.00	6.40	-5.00	2.25

x = distance from west end, y = distance from cross section centerline (left is positive)
z = height from bottom of girder

Table 4.33 Transfer Gage Locations (End IB)

Gage	End IB					
	Design			Actual		
	x (ft.)	y (in.)	z (in.)	x (ft.)	y (in.)	z (in.)
035A	1.25	3.00	6.00	1.00	3.00	6.00
035B	1.83	3.00	6.00	1.77	3.00	6.00
035C	2.50	3.00	6.00	2.46	3.00	6.00
28A	3.25	-3.00	2.00	3.20	-3.00	2.25
28B	3.83	-3.00	2.00	3.72	-3.00	2.25
28C	4.50	-3.00	2.00	4.33	-3.00	2.25
49A	5.25	-5.00	2.00	5.20	-5.00	2.25
49B	5.83	-5.00	2.00	5.60	-5.00	2.25
49C	6.50	-5.00	2.00	6.22	-5.00	2.25

x = distance from west end, y = distance from cross section centerline (left is positive)
z = height from bottom of girder

Table 4.34 Transfer Gage Locations (End IID)

Gage	End IID					
	Design			Actual		
	x (ft.)	y (in.)	z (in.)	x (ft.)	y (in.)	z (in.)
035B	1.83	-5.00	6.00	1.75	-5.00	6.00

x = distance from west end, y = distance from cross section centerline (right is positive)
z = height from bottom of girder

Table 4.35 Type of Equipment

Instrumentation	Manufacturer	Model	Description
Shear Testing	MTS Systems Corporation	810 Material Testing System	Capacity: 600 kips Stroke 5 in.
Concrete Cylinder Testing	Forney	QC-400F-LC1	Calibrated: 8/15/96 Capacity: 400 kips
Data Acquisition	OPTIM Electronics	TCS Version 5.1.1	-
	OPTIM Electronics OPTIM Electronics	MEGADAC 3008AC MEGADAC 0016AC	- -
	Zeos Personal Computer	Ambra	

Table 6.1 Measured Stiffness (100 kips to 1/2 Peak Load)

End	Secant Stiffness		Percent Difference	
	West (kip/in.)	East (kip/in.)	West (%)	East (%)
IA	627	610	2.2	1.6
IB	520	516	-15.2	-13.9
IIC	622	589	1.4	-1.9
IID	685	685	11.6	14.2
Average	614	600		

Table 6.2 Measured and Predicted Crack Angle Comparison

End	Type of Measurement	Rosette 1 (degrees)	Rosette 2 (degrees)	Rosette 3 (degrees)	Rosette 4 (degrees)	Rosette 5 (degrees)
IA	Uncracked Section Theory	30	32	34	37	31
	Corrected Experimental Data	n.a.	20	25	30	33
	Measured from Crack Drawing	28	26	25	24	n.a.
IB	Uncracked Section Theory	31	32	35	38	n.a.
	Corrected Experimental Data	30	25	n.a.	n.a.	n.a.
	Measured from Crack Drawing	22	n.a.	n.a.	n.a.	n.a.
IIC	Uncracked Section Theory	33	35	38	41	39
	Corrected Experimental Data	27	32	25	27	32
	Measured from Crack Drawing	32	25	22	22	n.a.
IID	Uncracked Section Theory	31	34	38	41	41
	Corrected Experimental Data	25	n.a.	25	30	n.a.
	Measured from Crack Drawing	22	15	16	14	n.a.

Table 6.3 Maximum Applied Point Loads Based on Nominal Properties

Models	End IA (kips)	End IB (kips)	End IIC (kips)	End IID (kips)
Peak Applied Load	**503**	**520**	**614**	**676 ***
ACI 318-95 Simplified Method	292	292	292	272
ACI 318-95 Detailed Method	341	341	341	378
Mod. ACI 318-95 Procedure (35.5 in.)	294	294	294	346
Modified Truss Model	357	357	357	374
Horizontal Shear AASHTO 1989	710	710	710	663
Modified Compression Field Theory	355	355	355	353
Truss Model	156	156	156	156

* End IID did not reach ultimate shear capacity; therefore, the applied load was actually higher.

Table 6.4 Shear Capacity Based on Nominal Properties

Models	End IA (kips)	End IB (kips)	End IIC (kips)	End IID (kips)
Critical Location	@ 2.92 ft.	@ 2.92 ft.	@ 2.92 ft.	@ 2.92 ft.
Calculated Peak Shear	355	367	429	471 *
ACI 318-95 Simplified Method	215	215	215	201
ACI 318-95 Detailed Method	248	248	248	272
Mod. ACI 318-95 Procedure (35.5 in.)	216	216	216	251
Modified Truss Model	258	258	258	269
Horizontal Shear AASHTO 1989	494	494	494	462
Critical Location	@ 4.35 ft.	@ 4.35 ft.	@ 4.35 ft.	@ 4.35 ft.
Calculated Peak Shear	354	365	428	469 *
Modified Compression Field Theory	255	255	255	254
Critical Location	@ 13.9 ft.	@ 13.9 ft.	@ 13.9 ft.	@ 13.9 ft.
Calculated Peak Shear	343	354	417	458 *
Truss Model	96	96	96	96

* End IID did not reach ultimate shear capacity; therefore, the capacity was actually higher.

Table 6.5 Test-to-Predicted Ratios Based on Nominal Properties

Models	End IA (Test/Pre)	End IB (Test/Pre)	End IIC (Test/Pre)	End IID (Test/Pre)	Mean (Test/Pre)	Coef. Var. (Test/Pre)
ACI 318-95 Simplified Method	1.65	1.71	2.00	2.34	1.92	16.5
ACI 318-95 Detailed Method	1.43	1.48	1.73	1.73	1.59	10.0
Mod. ACI 318-95 Procedure (35.5 in.)	1.64	1.70	1.99	1.88	1.80	8.8
Modified Truss Model	1.38	1.42	1.66	1.75	1.55	11.7
Horizontal Shear AASHTO 1989			not observed			
Modified Compression Field Theory	1.39	1.43	1.68	1.85	1.59	13.6
Truss Model	3.57	3.69	4.34	4.77	4.09	13.8

Table 6.6 Maximum Applied Point Loads Based on Measured Properties

Models	**End IA** (kips)	**End IB** (kips)	**End IIC** (kips)	**End IID** (kips)
Peak Applied Load	**503**	**520**	**614**	**676 ***
ACI 318-95 Simplified Method	328	321	302	281
ACI 318-95 Detailed Method	361	354	340	381
Mod. ACI 318-95 Procedure (35.5 in.)	327	320	306	358
Modified Truss Model	404	392	384	383
Horizontal Shear AASHTO 1989	723	716	720	673
Modified Compression Field Theory	407	395	364	354
Truss Model	196	218	190	190

* End IID did not reach ultimate shear capacity; therefore, the applied load was actually higher.

Table 6.7 Shear Capacity Based on Measured Properties

Models	**End IA** (kips)	**End IB** (kips)	**End IIC** (kips)	**End IID** (kips)
Critical Location	@ 2.93 ft.	@ 2.92 ft.	@ 2.89 ft.	@ 2.99 ft.
Calculated Peak Shear	354	368	429	470 *
ACI 318-95 Simplified Method	238	236	222	207
ACI 318-95 Detailed Method	260	257	247	274
Mod. ACI 318-95 Procedure (35.5 in.)	237	235	225	259
Modified Truss Model	289	283	276	275
Horizontal Shear AASHTO 1989	501	500	500	468
Critical Location	@ 4.36 ft.	@ 4.35 ft.	@ 4.32 ft.	@ 4.42 ft.
Calculated Peak Shear	353	367	428	468 *
Modified Compression Field Theory	289	283	261	254
Critical Location	@ 14.1 ft.	@ 13.8 ft.	@ 14.1 ft.	@ 14.0 ft.
Calculated Peak Shear	341	355	416	457 *
Truss Model	120	146	116	116

* End IID did not reach ultimate shear capacity; therefore, the capacity was actually higher.

Table 6.8 Test-to-Predicted Ratios Based on Measured Properties

Models	**End IA** (Test/Pre)	**End IB** (Test/Pre)	**End IIC** (Test/Pre)	**End IID** (Test/Pre)	**Mean** (Test/Pre)	**Coef. Var.** (Test/Pre)
ACI 318-95 Simplified Method	1.49	1.56	1.93	2.27	1.81	20.0
ACI 318-95 Detailed Method	1.36	1.43	1.74	1.72	1.56	12.3
Mod. ACI 318-95 Procedure (35.5 in.)	1.49	1.57	1.91	1.81	1.70	11.6
Modified Truss Model	1.22	1.30	1.55	1.71	1.45	15.5
Horizontal Shear AASHTO 1989			not observed			
Modified Compression Field Theory	1.22	1.30	1.64	1.84	1.50	19.5
Truss Model	2.84	2.43	3.59	3.94	3.20	21.5

Table 6.9 Experimental Comparison of Prestressed Girders

Reference			Code					Girder					Comp.
Author(s)	Type	Total Tests (number)	ACI U_{cw}	ACI U_{ci}	ACI U_{cr}	ACI U_{ACI}	Mod. C. U_{MCFT}	Web mean (in.)	f_c' max (psi)	P max (kips)	Strands max (number)	Stra. Area max ($in.^2$)	Deck (yes/no)
			(average of test/predicted)										
Bennett & Balasooriya	Series A-E	19	n.a.	n.a.	n.a.	n.a.	n.a.	1	6420	83	10	0.60	no
	Series F	4	n.a.	n.a.	n.a.	n.a.	n.a.	1	5800	104	12	0.72	no
Elzanaty, Nilson, & Slate	CI Series	17	1.17	n.a.	1.17	1.21	n.a.	3	11400	138	4	0.86	no
	CW Series	17	n.a.	1.15	1.15	1.21	n.a.	2	11400	138	4	0.86	no
Maruyama & Rizkalla	Single Tee	9	n.a.	n.a.	1.00	1.03	n.a.	3	6480	n.a.	2	0.31	no
Kaufman & Ramirez	AASHTO I	4	1.07	n.a.	n.a.	1.15	n.a.	6	8370	311	10	1.67	no
	AASHTO II	2	1.04	n.a.	n.a.	1.10	n.a.	6	9090	425	14	2.34	no
Hartmann, Breen, & Kreger	Series 1	3	n.a.	n.a.	1.09	1.39	n.a.	2	11300	87	6	0.51	no
	Series 2	3	n.a.	n.a.	1.02	1.00	n.a.	2	10800	223	17	1.45	no
	Series 3	4	n.a.	n.a.	n.a.	1.16	n.a.	2	13160	173	13	1.11	yes
Abdalla, Ramirez, & Lee	AASHTO I	8	1.36	1.01	n.a.	n.a.	n.a.	6	7500	309	12	1.84	yes
	Indiana Box	2	0.97	0.80	n.a.	n.a.	n.a.	10	7300	514	20	3.06	yes
Russell & Burns	Texas C	6	1.38	n.a.	n.a.	n.a.	n.a.	7	10400	598	24	3.67	yes
Tawfiq	AASHTO II, R	6	n.a.	n.a.	n.a.	0.89	1.05	6	11040	421	18	2.75	yes
	AASHTO II, 2R	6	n.a.	n.a.	n.a.	0.73	0.63	6	11040	421	18	2.75	yes
Shahawy & Batchelor	AASHTO II, 0R	6	n.a.	n.a.	n.a.	1.28	1.67	6	7600	377	18	2.75	yes
	AASHTO II, M	2	n.a.	n.a.	n.a.	1.25	2.67	6	7300	369	18	2.75	yes
	AASHTO II, R/2	2	n.a.	n.a.	n.a.	1.25	2.32	6	7100	369	18	2.75	yes
	AASHTO II, R	12	n.a.	n.a.	n.a.	1.19	1.63	6	8480	377	18	2.75	yes
	AASHTO II, 3R/2	4	n.a.	n.a.	n.a.	1.05	1.41	6	7600	369	18	2.75	yes
	AASHTO II, 2R	8	n.a.	n.a.	n.a.	0.99	0.82	6	7820	377	18	2.75	yes
	AASHTO II, 3R	6	n.a.	n.a.	n.a.	0.96	0.71	6	7680	377	18	2.75	yes
Cumming, French, & Shield	Minn. 45M, IA	1	n.a.	n.a.	n.a.	1.36	1.22	6	11330	1290	46	10.49	yes
	Minn. 45M, IB	1	n.a.	n.a.	n.a.	1.43	1.30	6	11330	1290	46	10.49	yes
	Minn. 45M, IIC	1	n.a.	n.a.	n.a.	1.74	1.64	6	9315	1290	46	10.49	yes
	Minn. 45M, IID*	1	n.a.	n.a.	n.a.	1.72	1.84	6	9315	1290	46	10.49	yes

* End IID did not reach ultimate shear capacity; therefore, the capacity was actually higher.

Figures

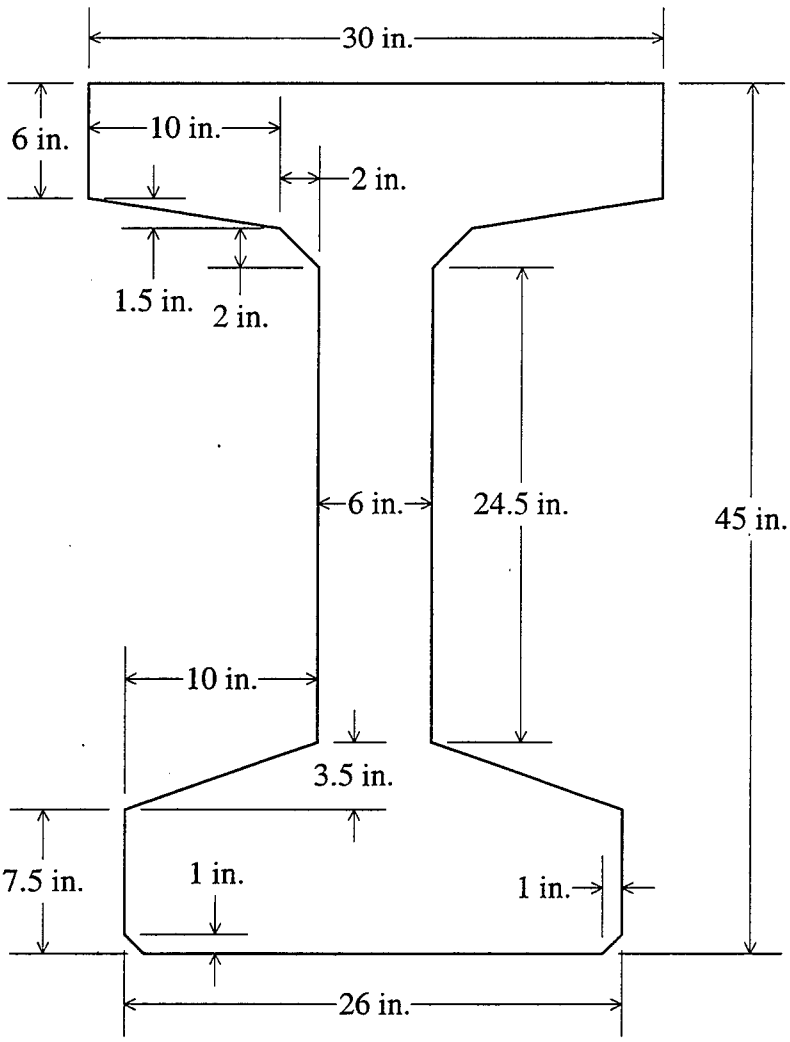

Girder Property	MnDOT *	Actual
moment of interia , I_g =	167048 in.^{4}	166563 in.^{4}
area, A_g =	624 in.^{2}	623 in.^{2}
center of gravity, y_t = (from bottom)	22.34 in.	22.38 in.

* MnDOT neglects the 1 in. chamfer.

Figure 4.1 Girder Cross Section

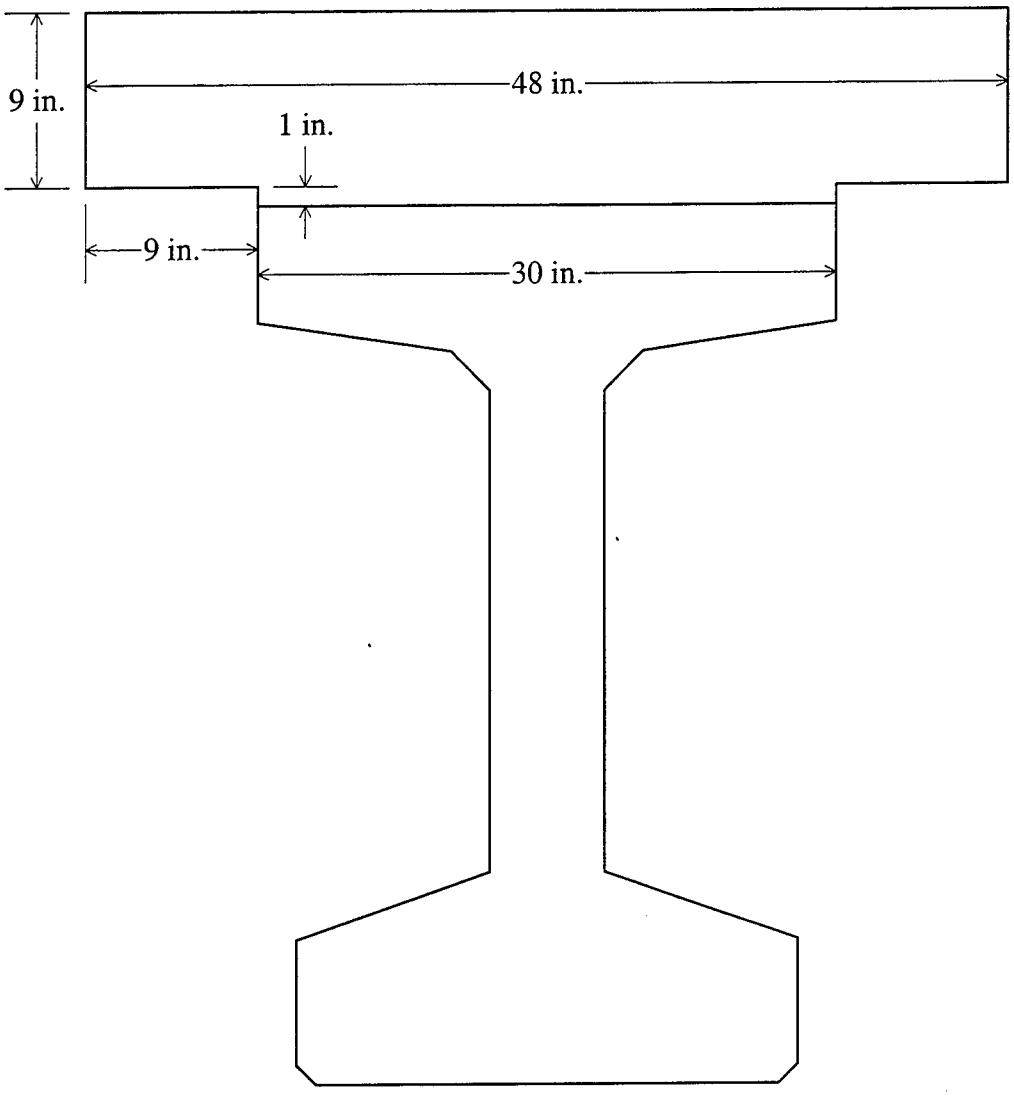

Composite Property *	Nominal	IA & IB	IIC & IID
moment of interia, I_{gc} =	335428 in.^{4}	352880 in.^{4}	353122 in.^{4}
area, A_{gc} =	950 in.^{2}	1006 in.^{2}	1007 in.^{2}
center of gravity, y_{tc} = (from bottom)	31.89 in.	32.97 in.	32.98 in.
chamfer	neglected	included	included

* deck transformed based of the ratio of deck E_{cd} to girder E_c
(no steel transformed)

Figure 4.2 Composite Cross Section

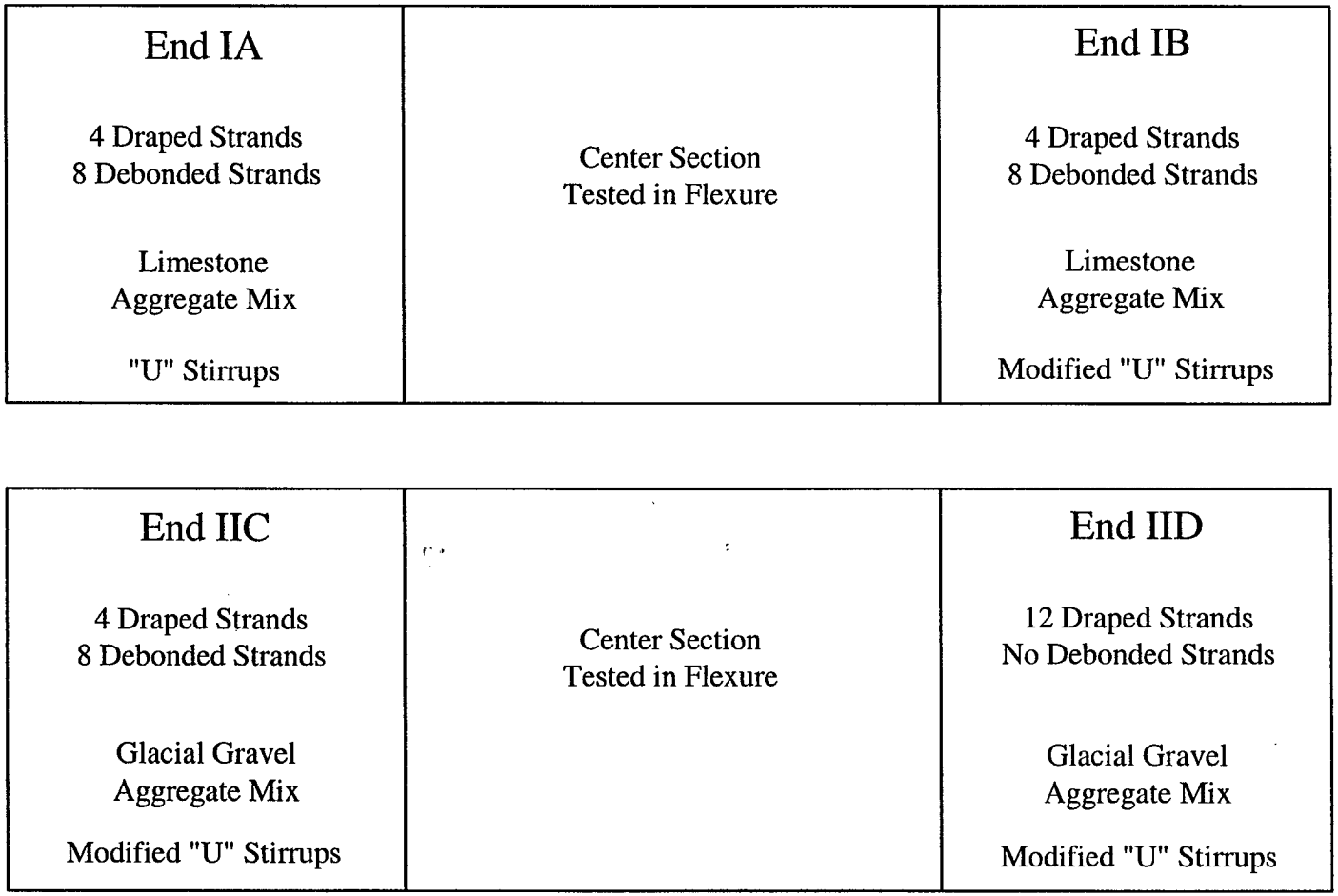

Figure 4.3 End Variables

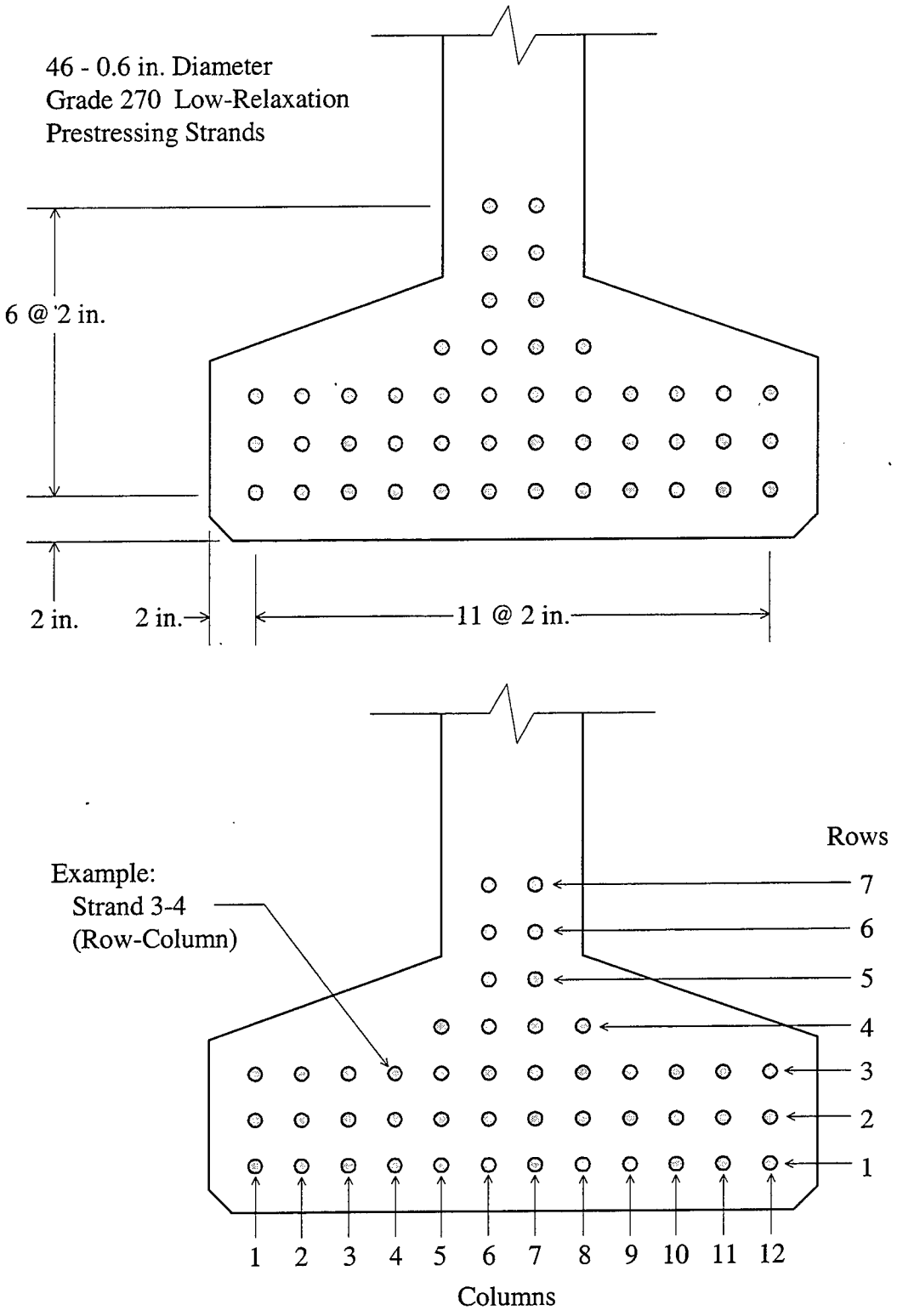

Figure 4.4 Centerline Strand Pattern and Strand Numbering System

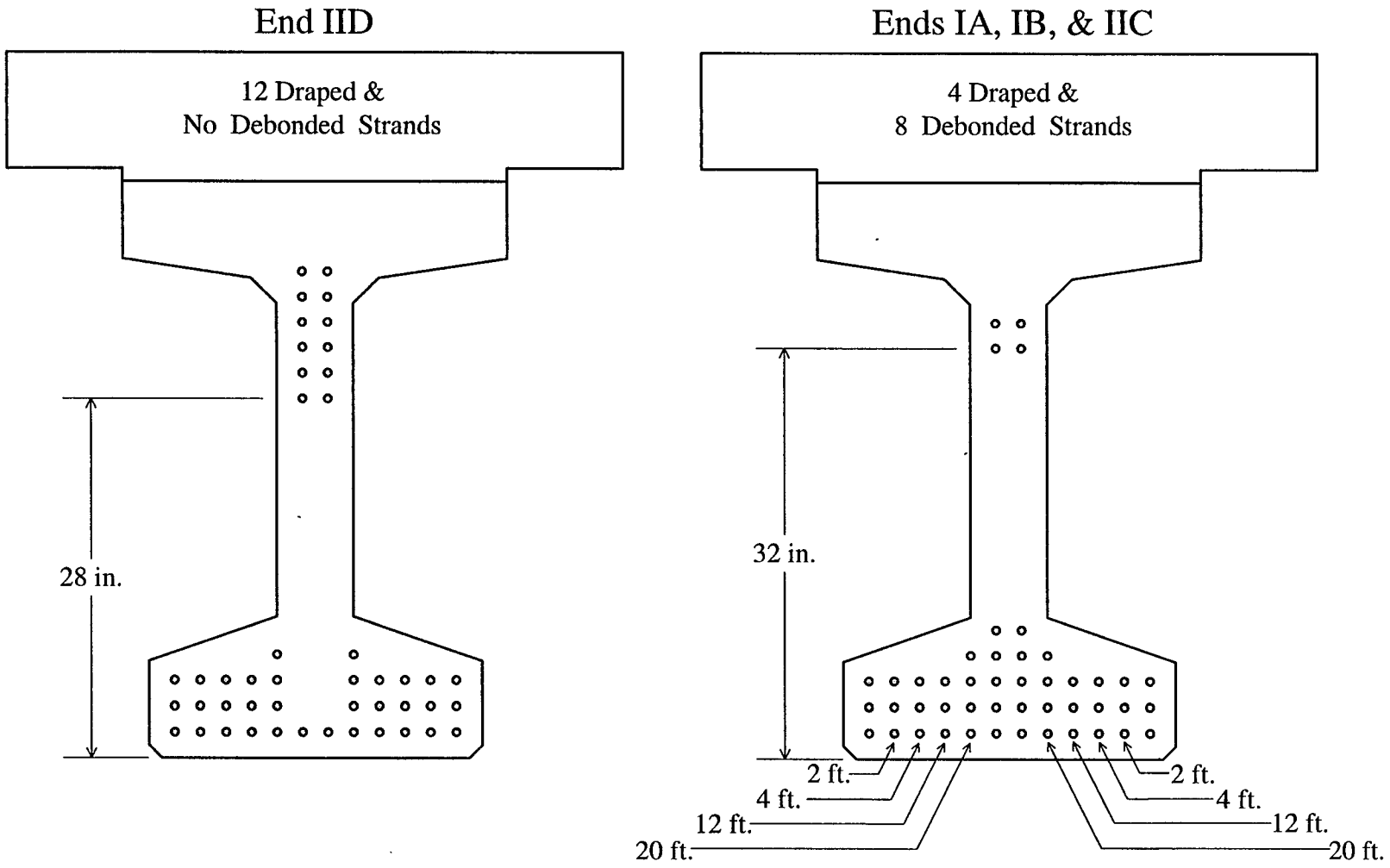

Figure 4.5 End Strand Patterns and Lengths of Strand Debonding

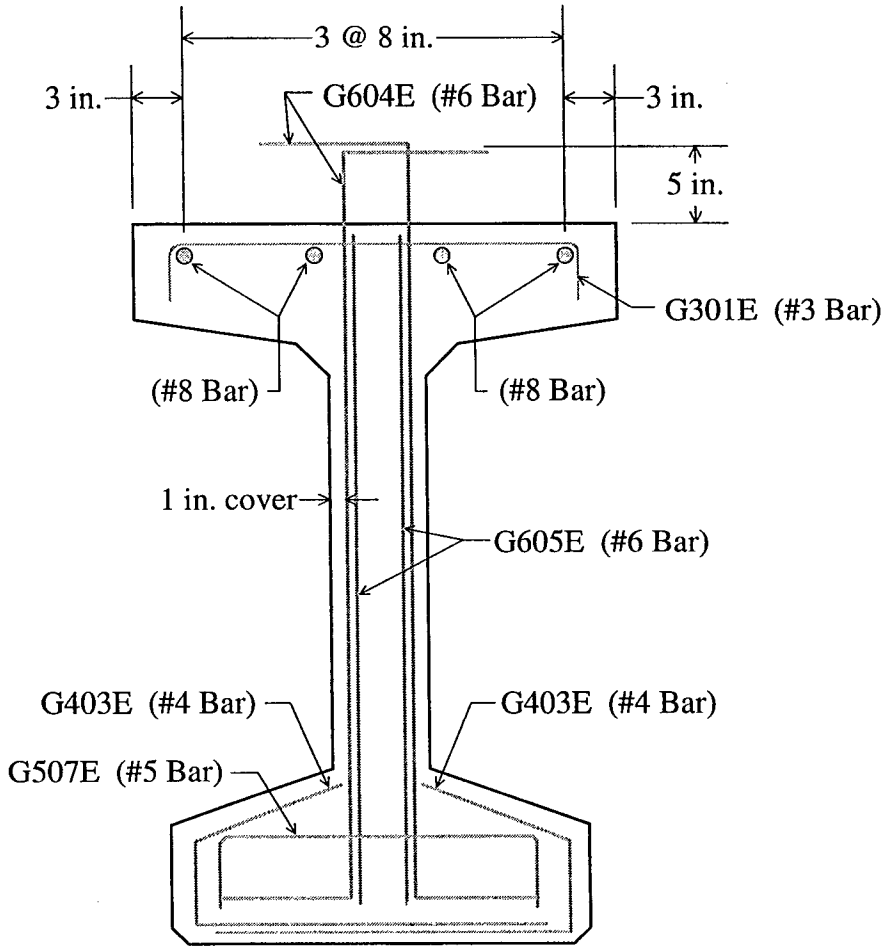

Girder at West End

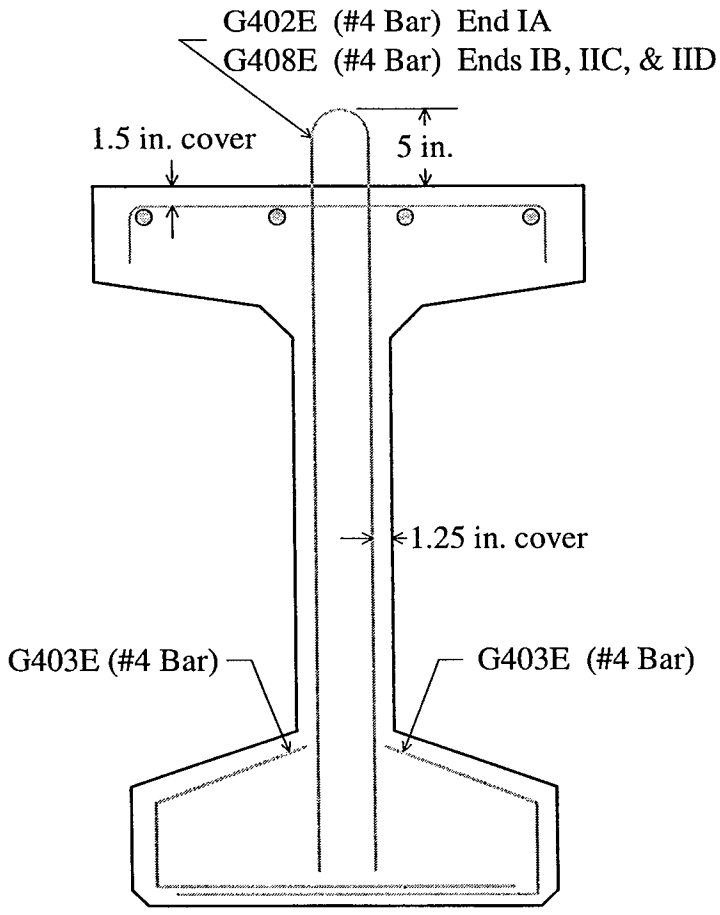

Girder away from West End

Figure 4.6 Section View of Girder Mild Reinforcement

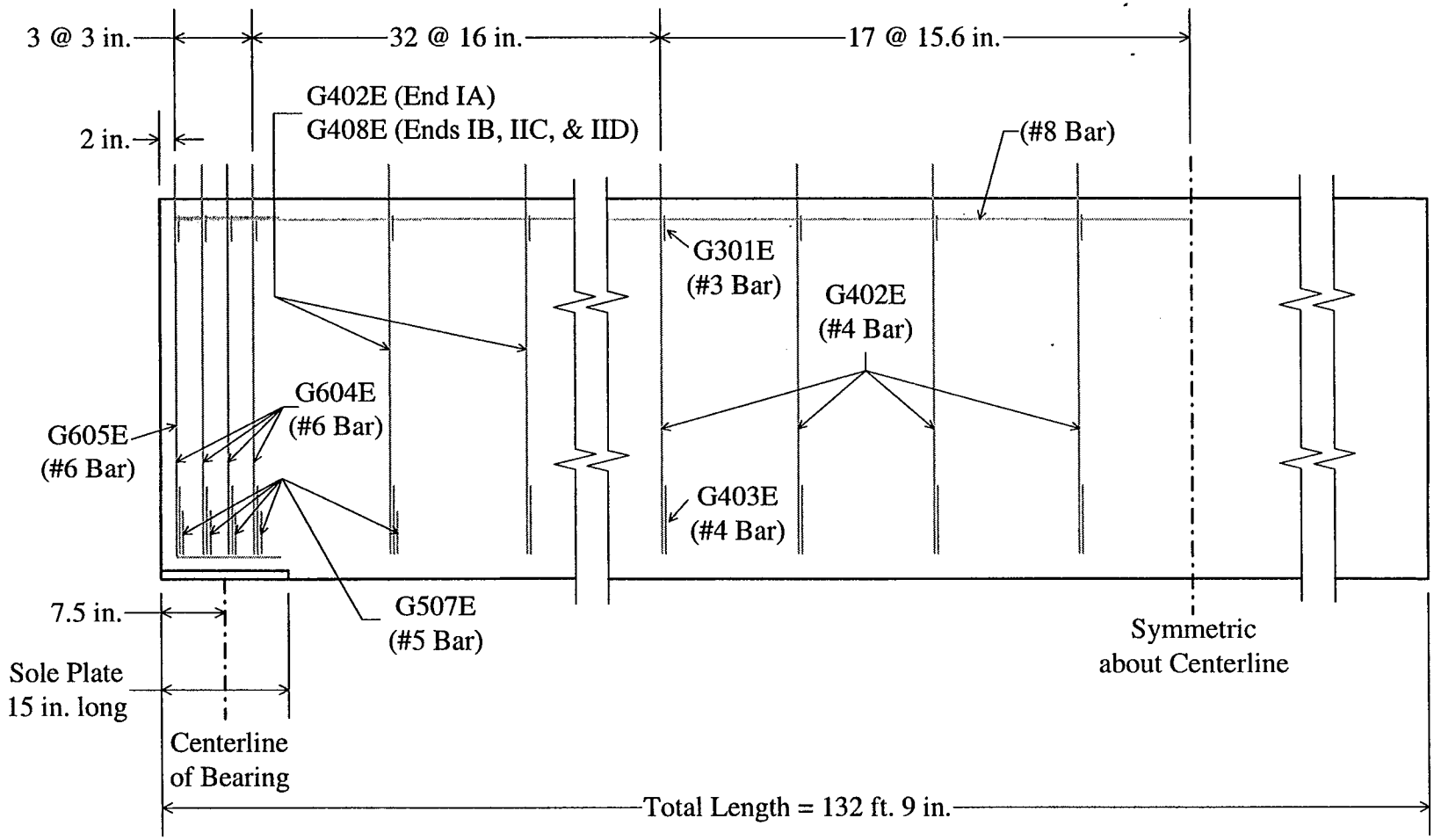

Note: 1-G301E (#3 Bar) and 2-G403E (#4 Bar) per Stirrup

Figure 4.7 Elevation View of Girder Mild Reinforcement

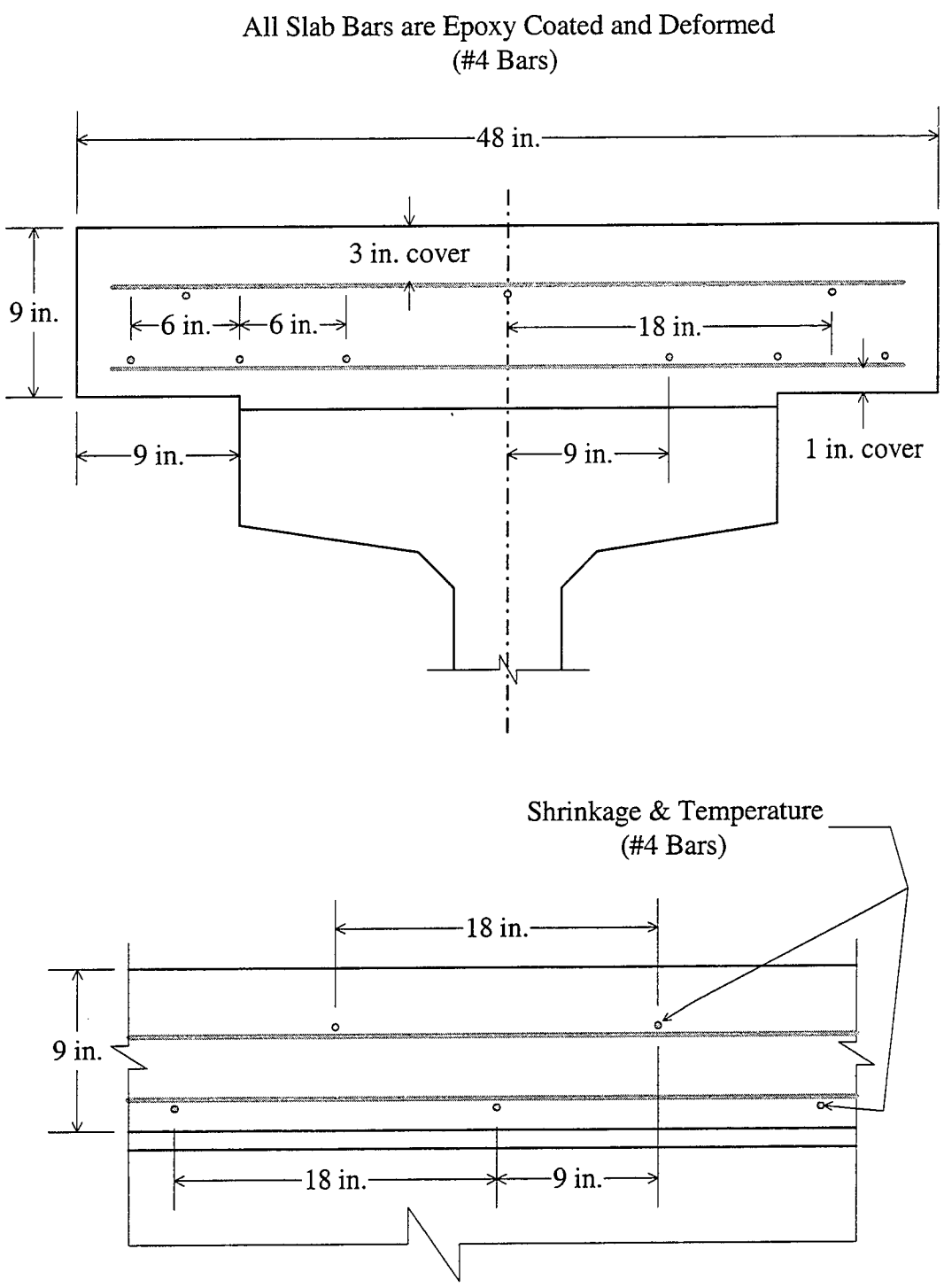

Figure 4.8 Reinforcement Layout in Deck

All Bars are Epoxy Coated and Deformed

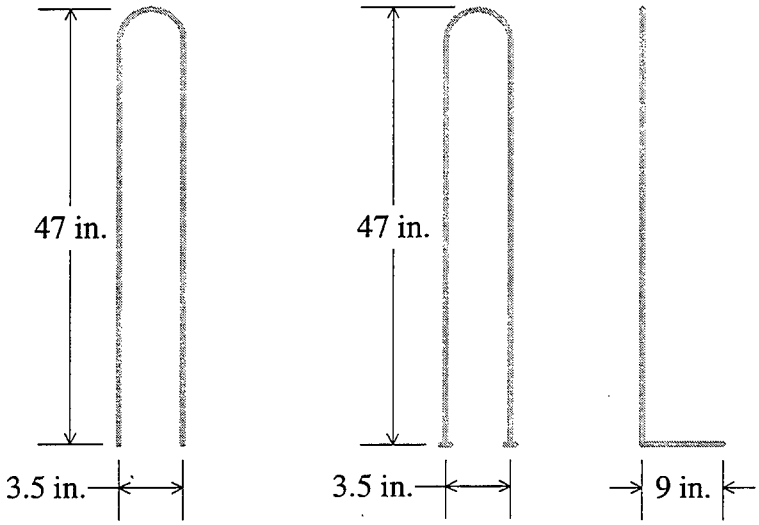

G402E (#4 Bar)
MnDOT "U"

G408E (#4 Bar)
Modified "U"

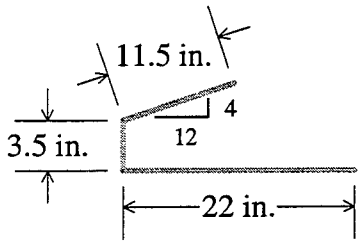

G403E (#4 Bar)

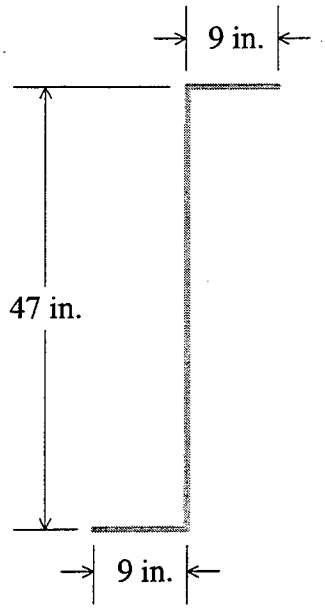

G604E (#6 Bar)

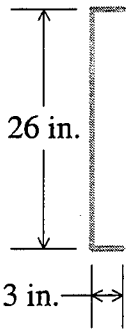

G301E (#3 Bar)

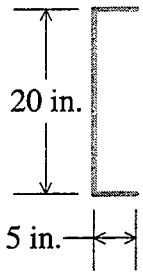

G507E (#5 Bar)

Figure 4.9 Mild Reinforcement Details

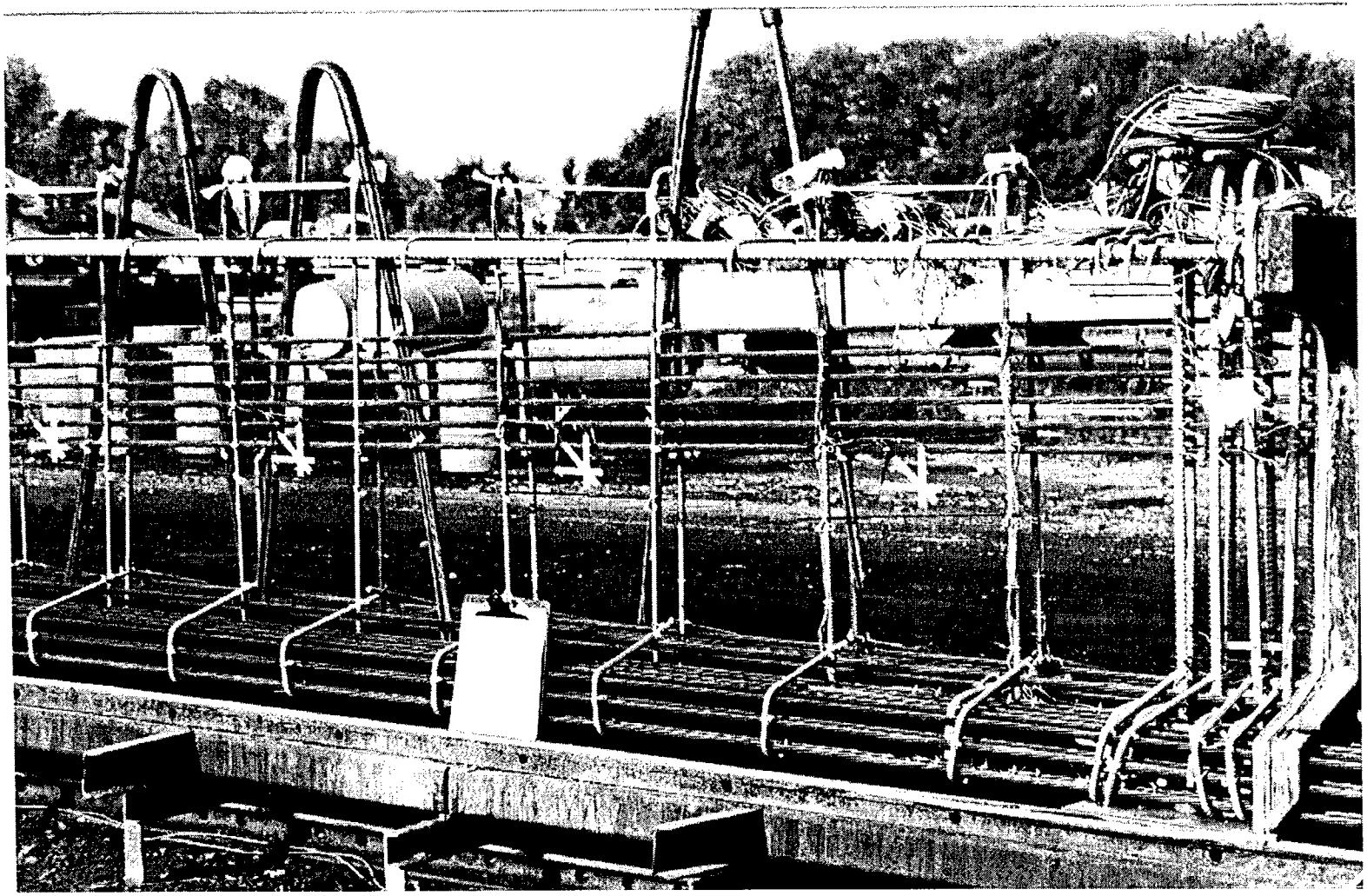

Figure 4.10 Lift Hooks Near the End

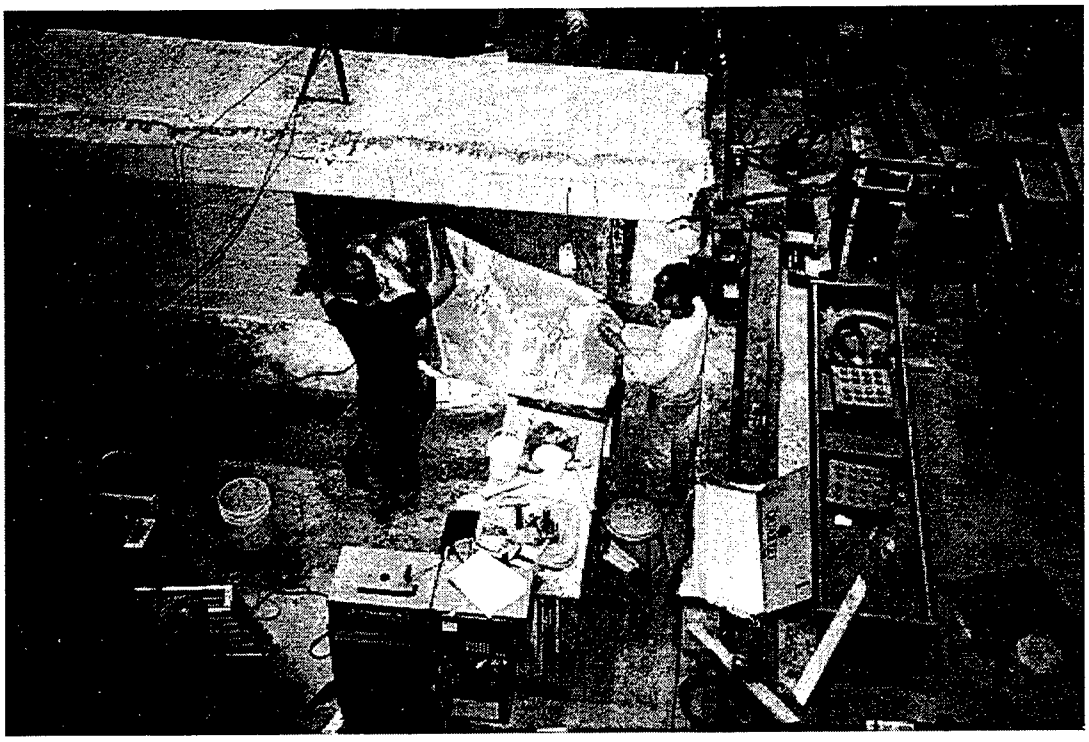

Figure 4.11 Application of Fiberglass Reinforcement

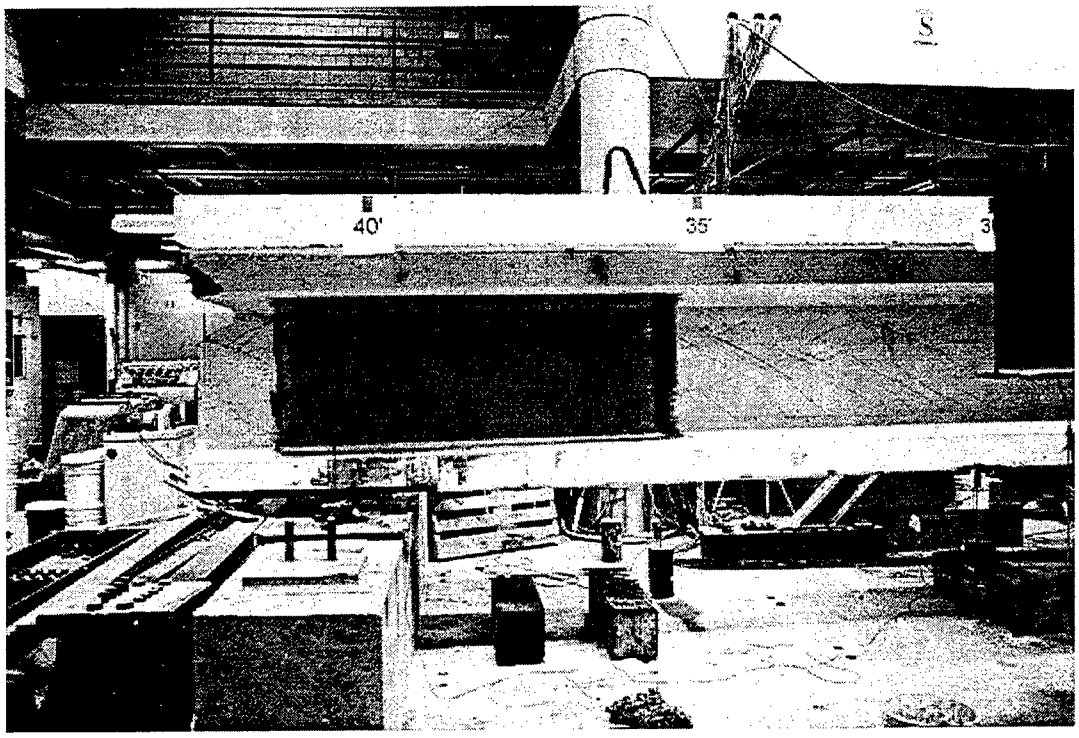

Figure 4.12 Fiberglass Reinforcement

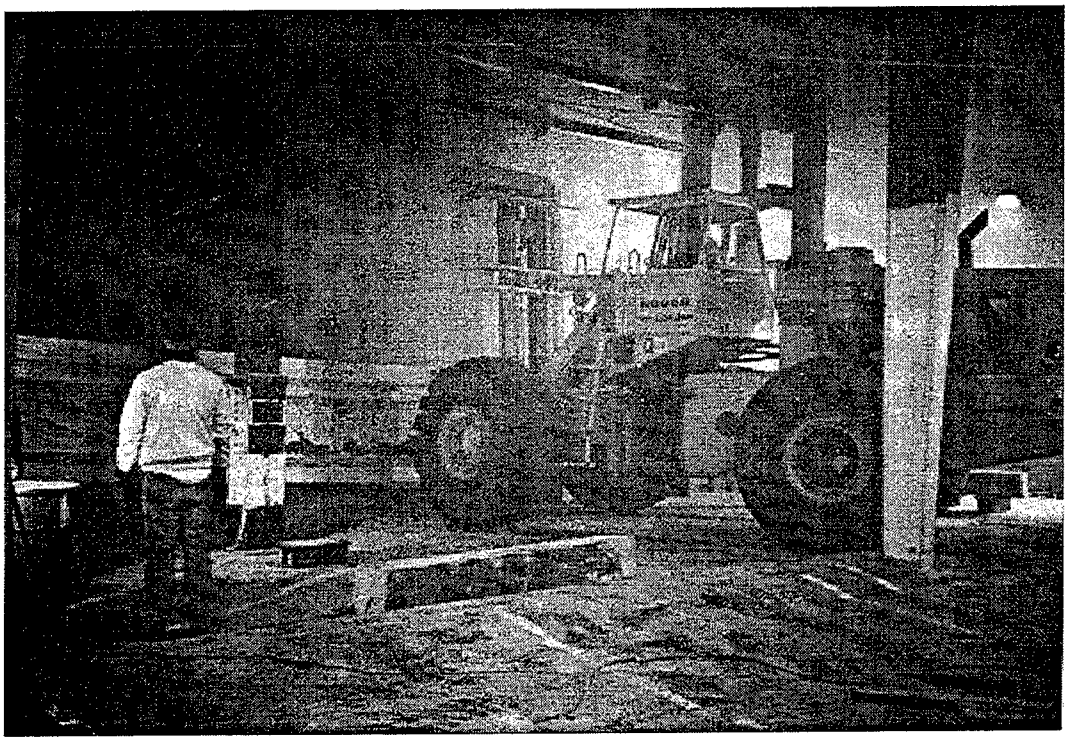

Figure 4.13 Forklift Moving Specimens

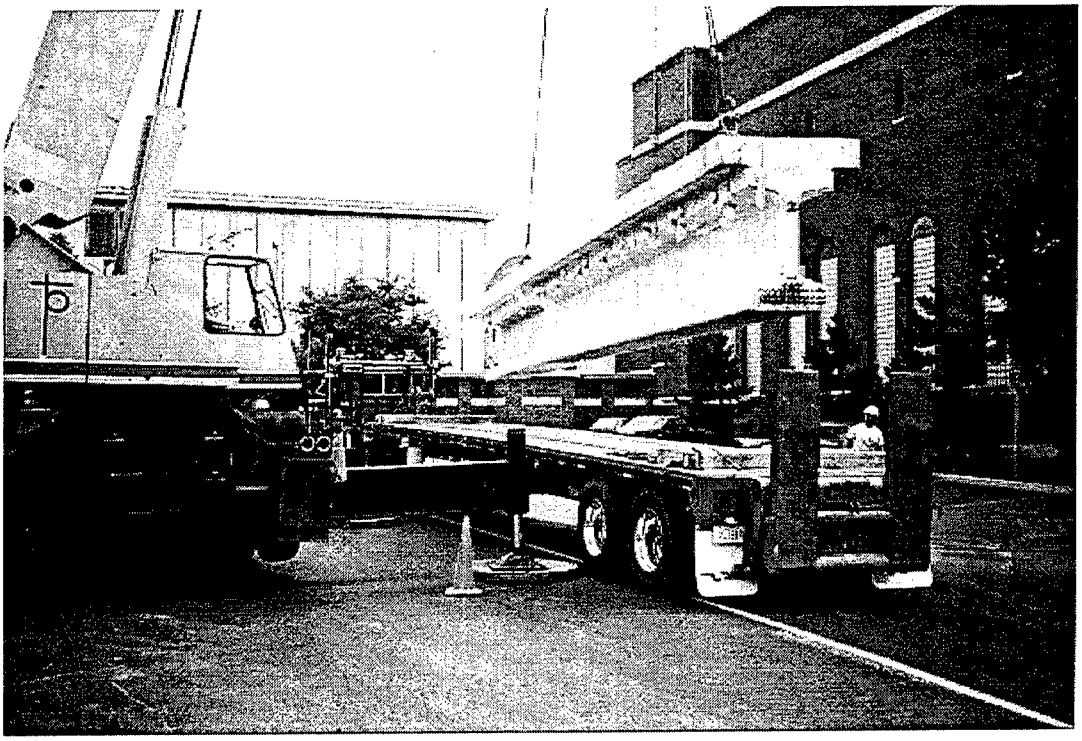

Figure 4.14 Lifting Specimen from Flatbed

Figure 4.15 Crane Lifting the Specimen

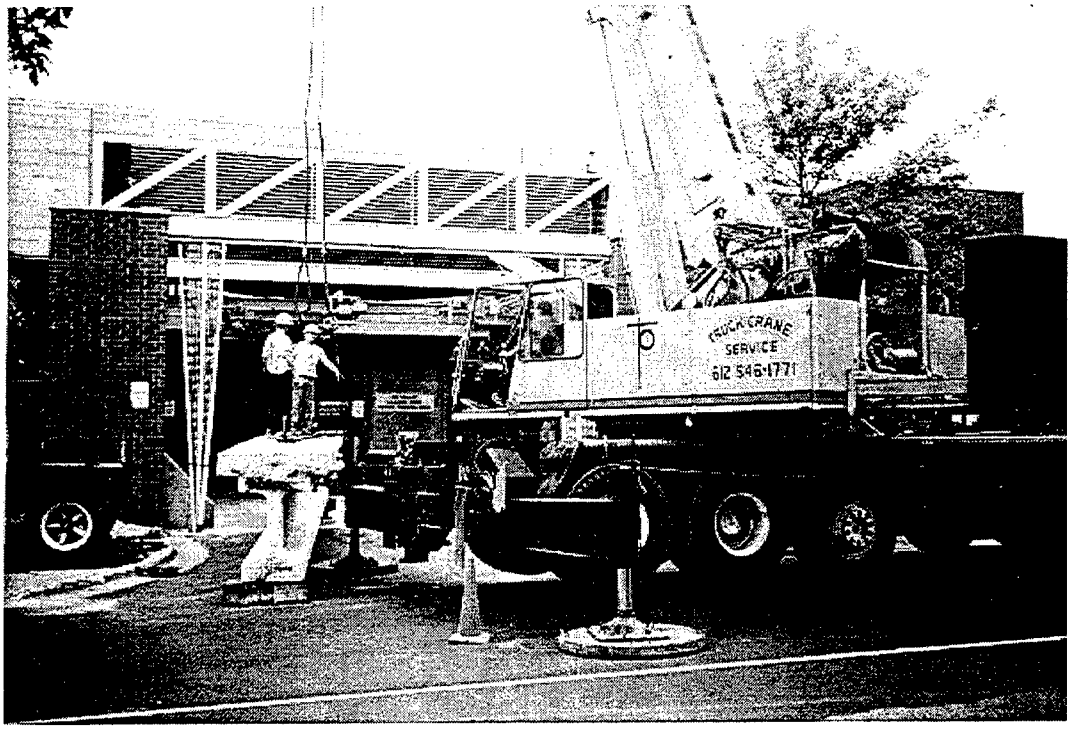

Figure 4.16 Specimen Between Crane Lifts

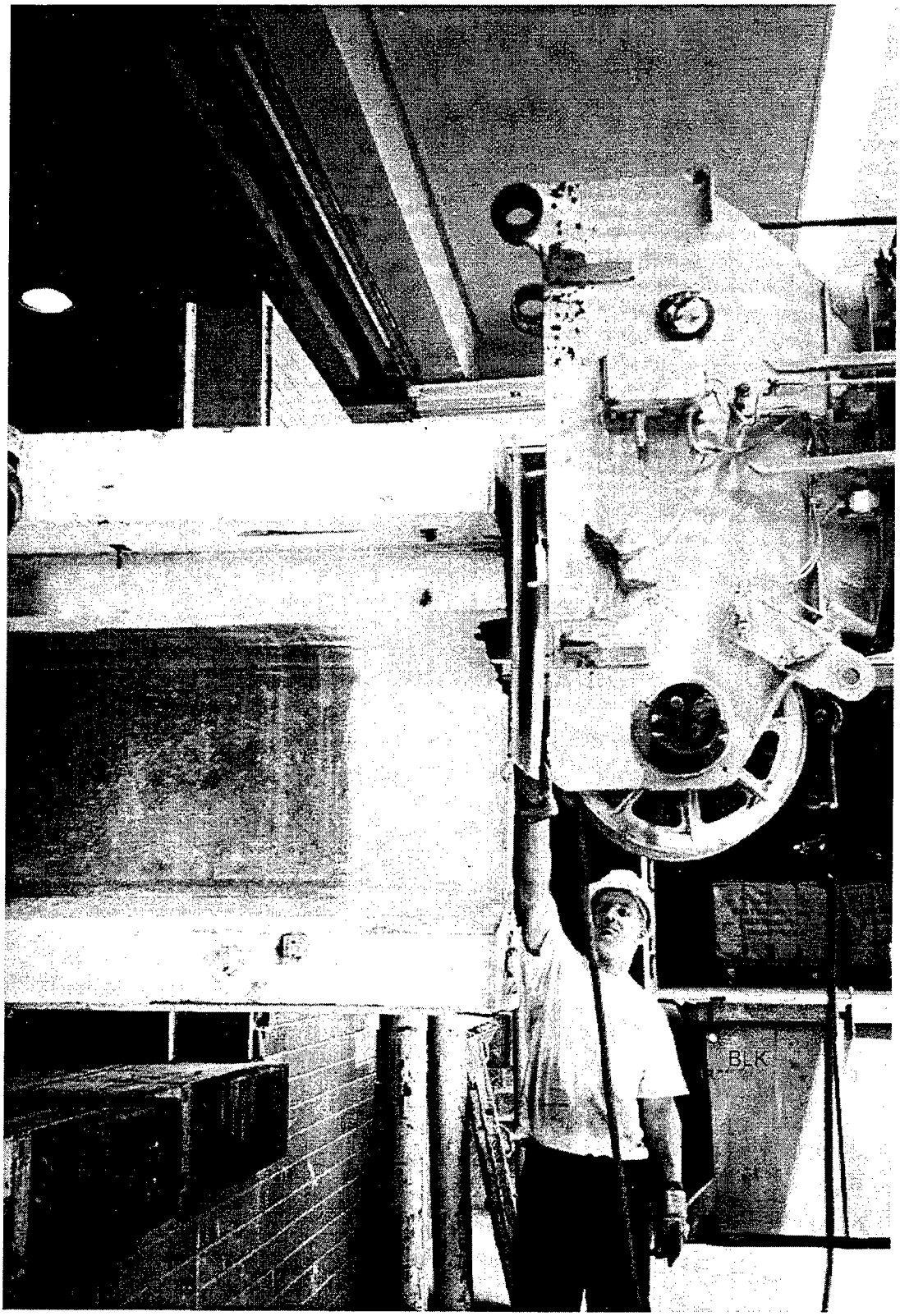

Figure 4.17 Specimen Pushed into Loading Dock Area

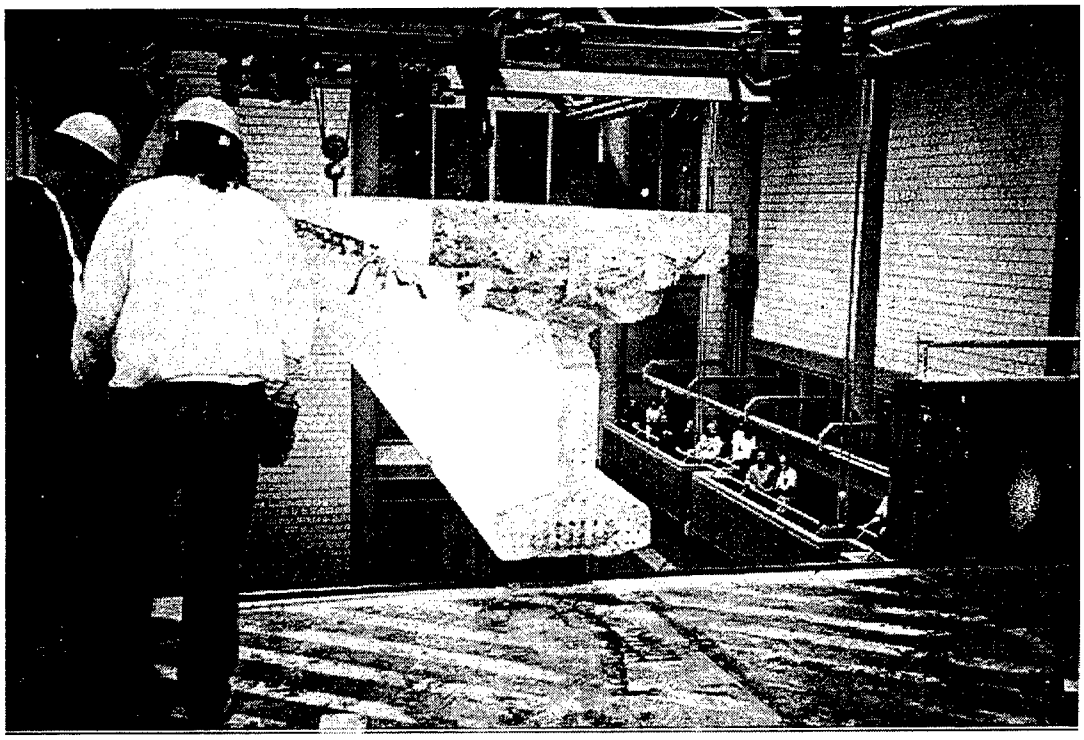

Figure 4.18 Lifting Specimen by Both Cranes

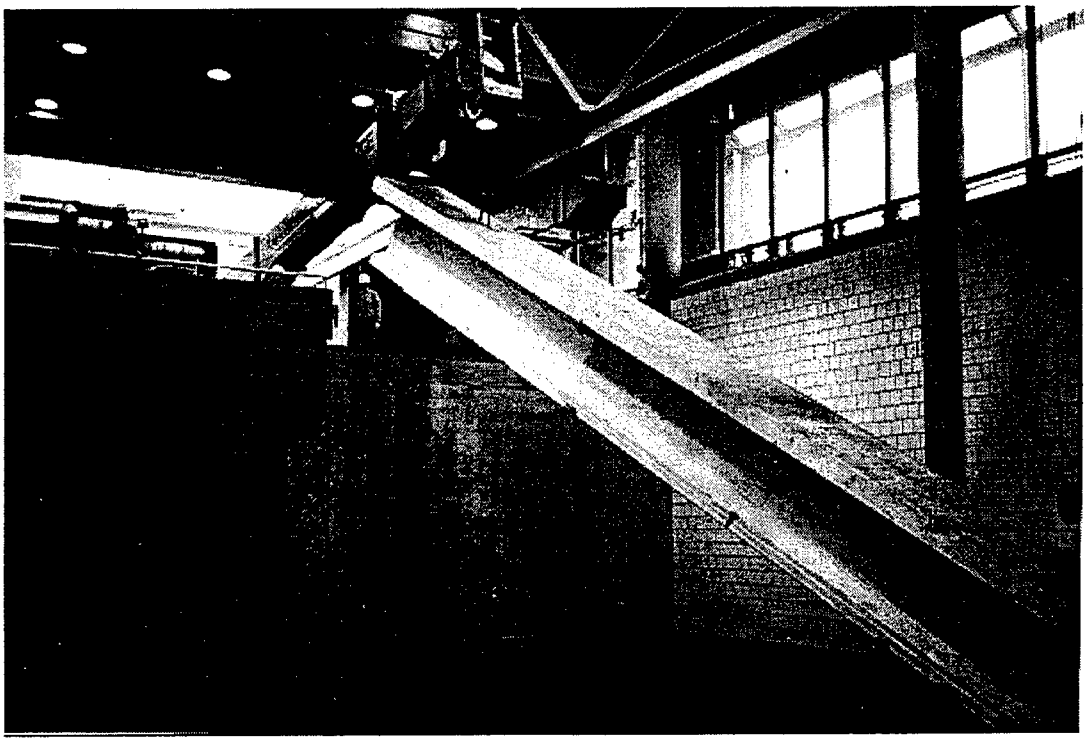

Figure 4.19 Lifting Specimen into Testing Laboratory

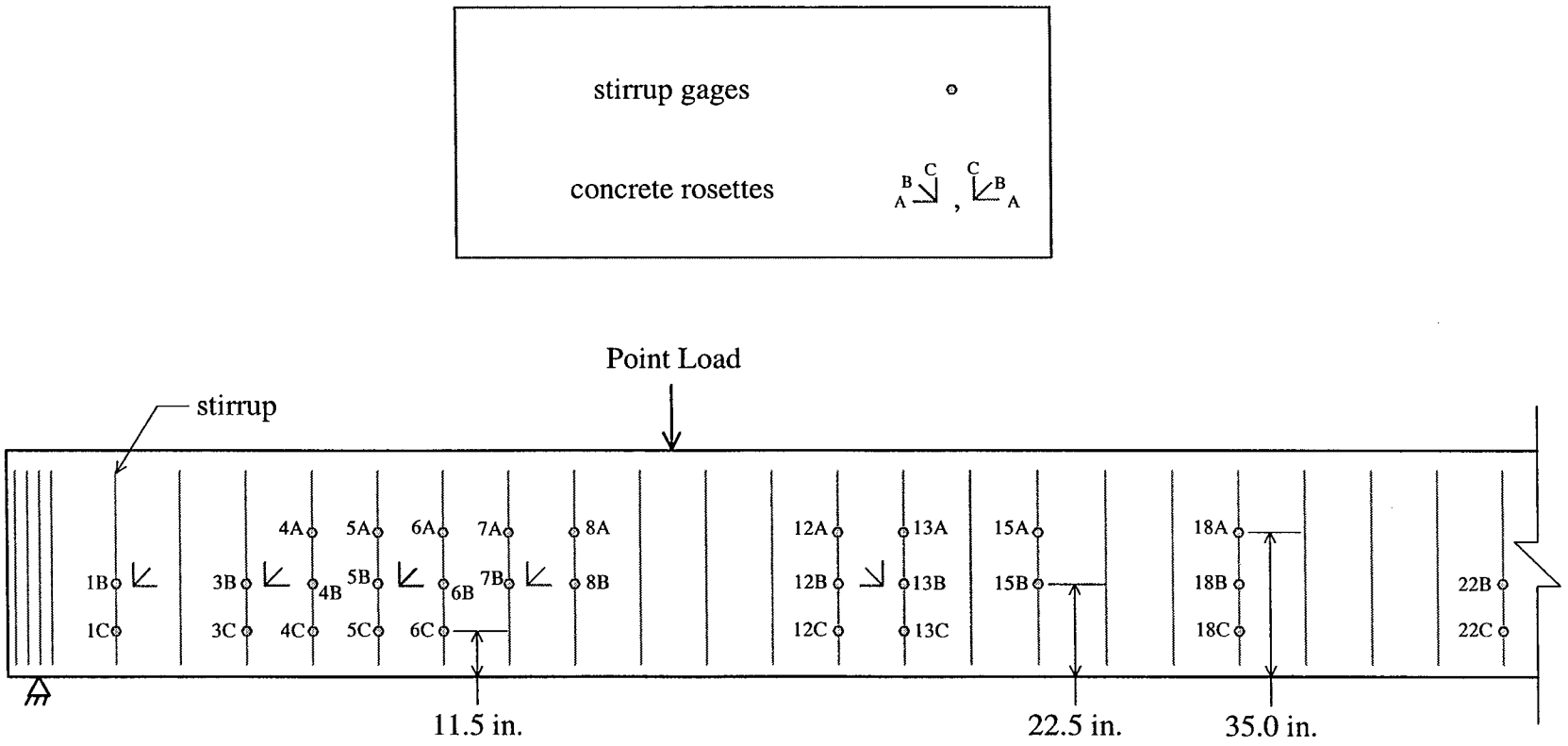

Figure 4.20 Internal Stirrup Gages and Rosette Locations

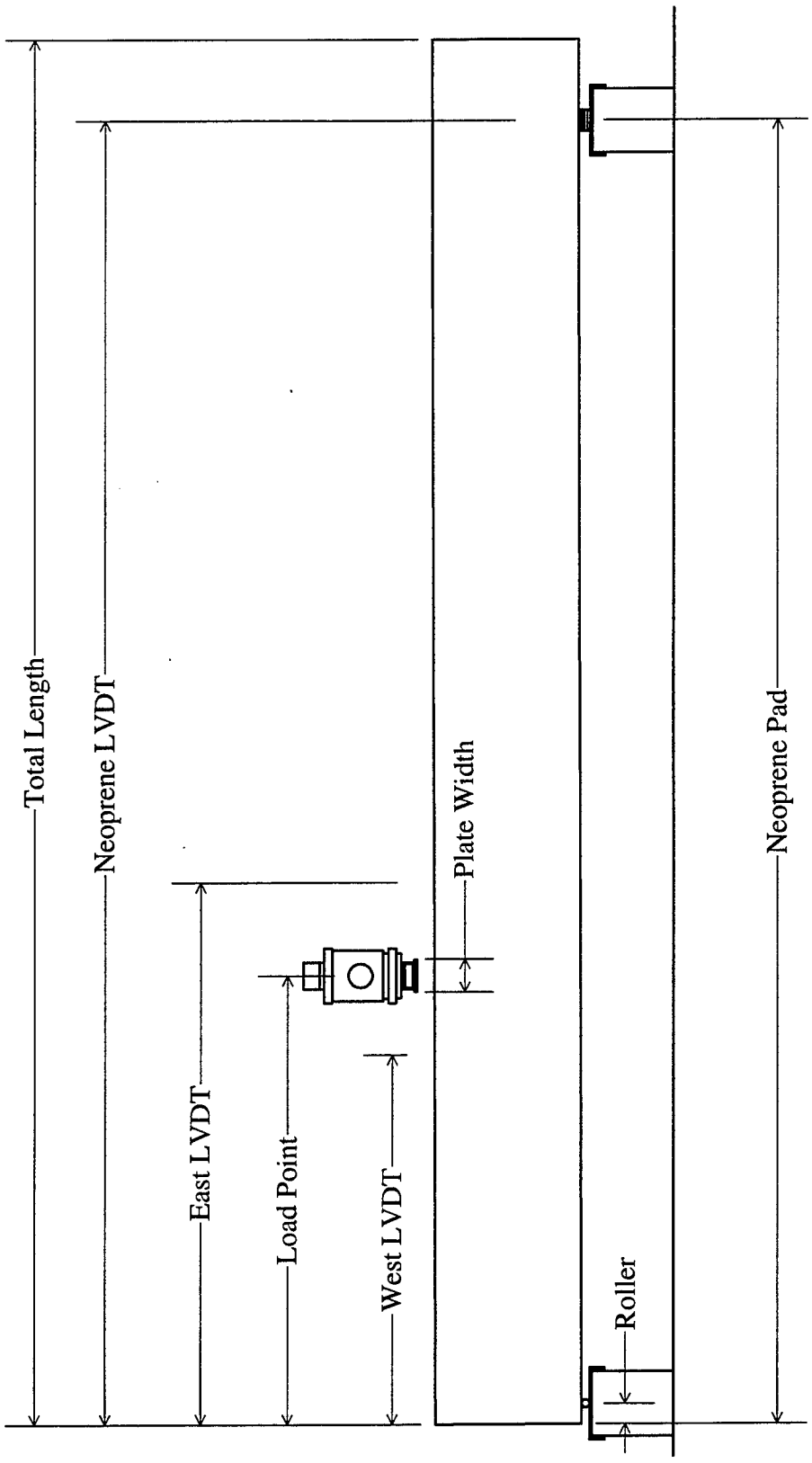

Figure 4.21 Test Setup

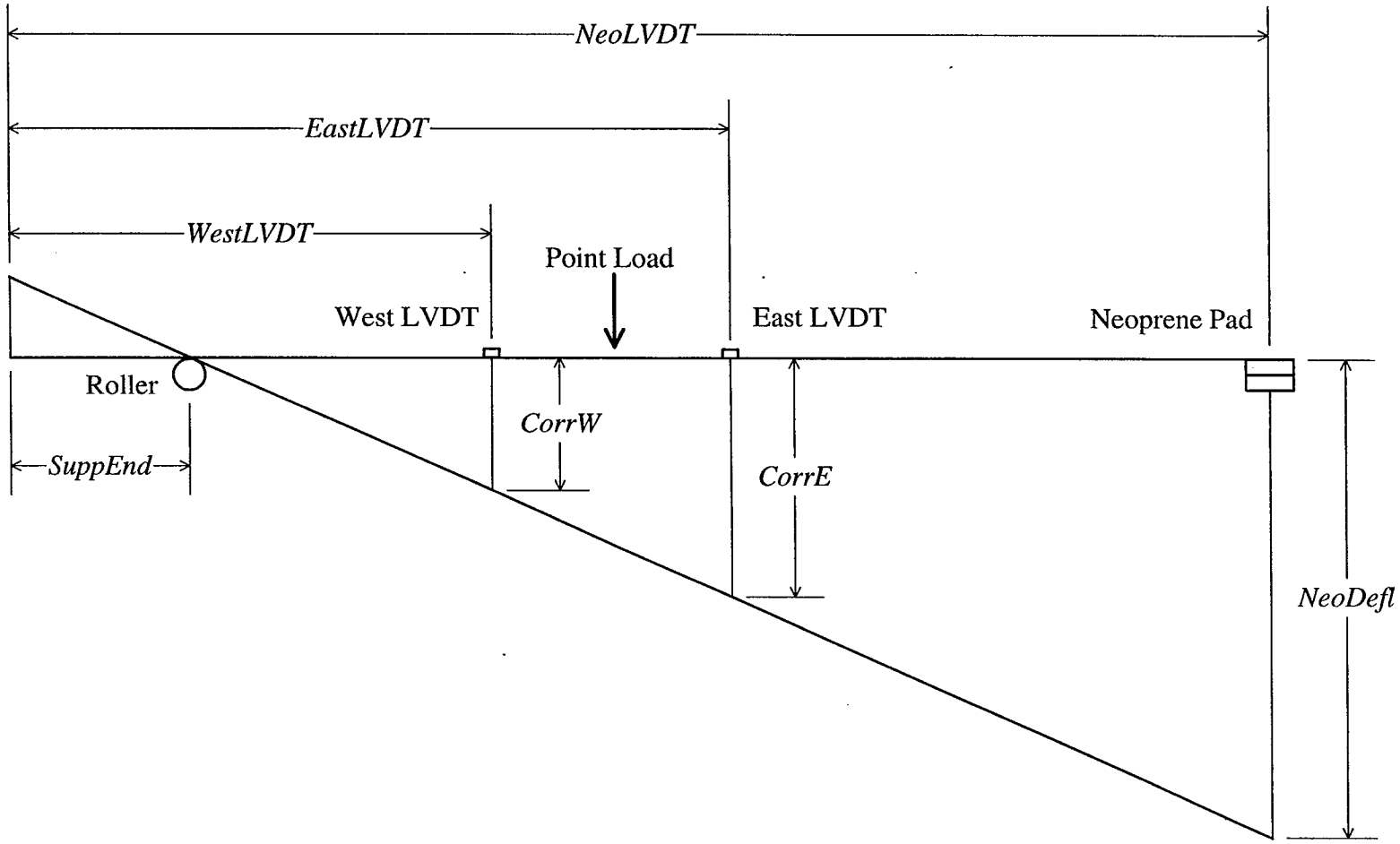

Figure 4.22 Correction in Deflection

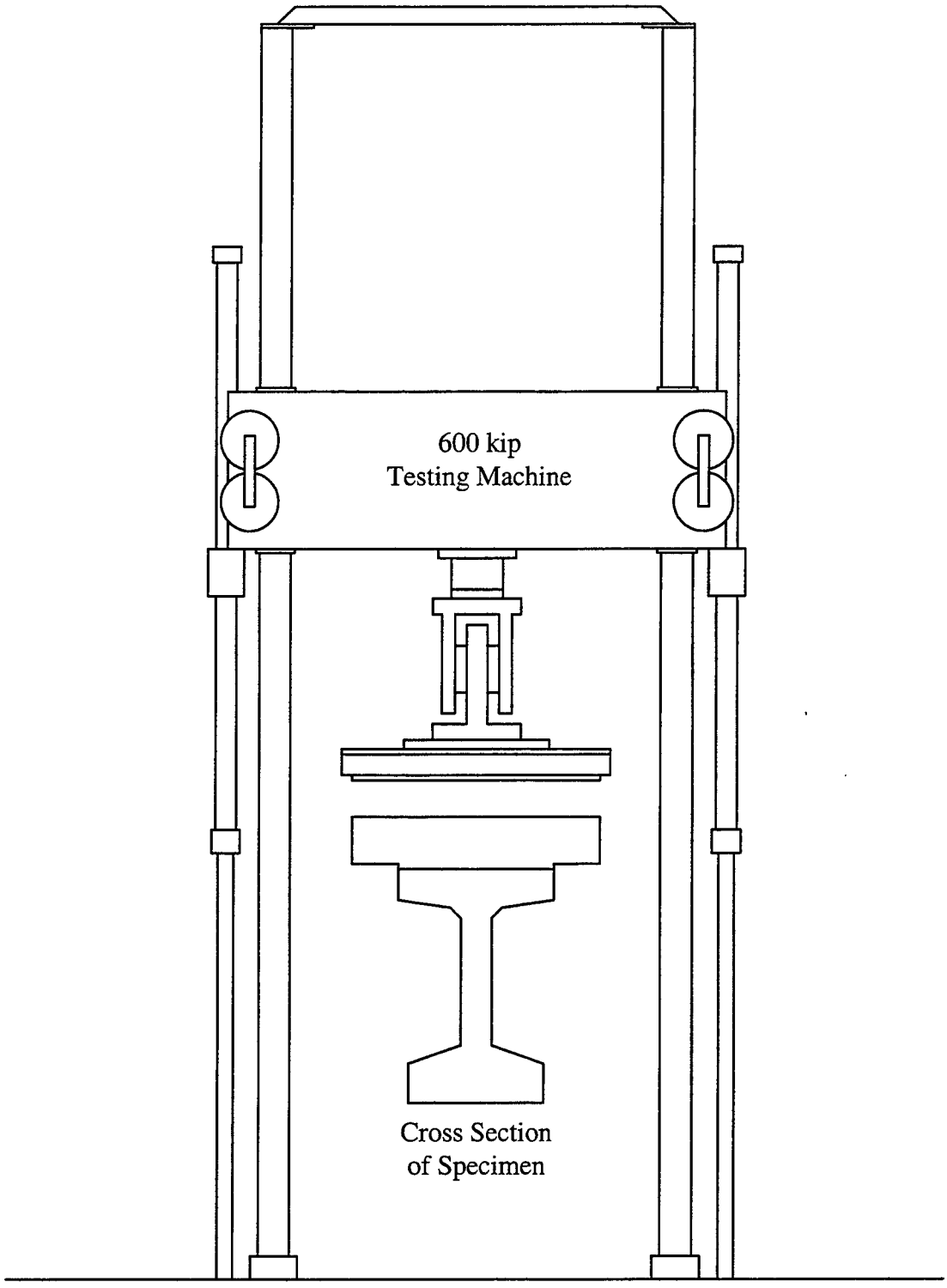

Figure 4.23 Testing Machine

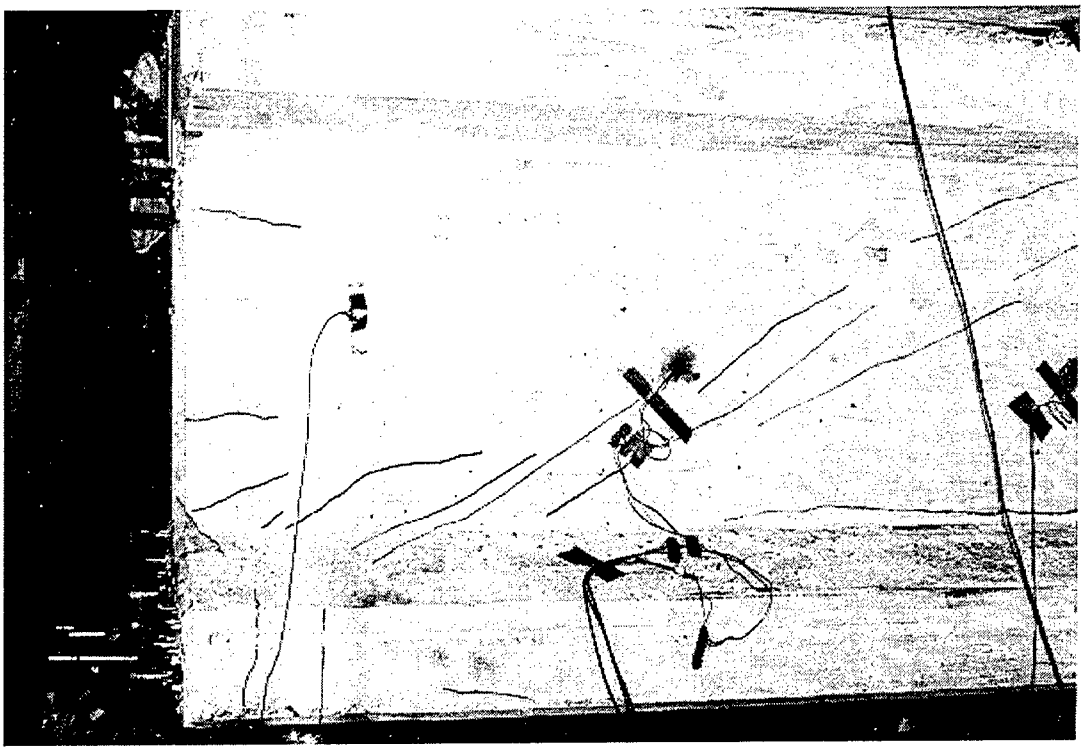

Figure 5.1 Before Testing Near Support (End IA)

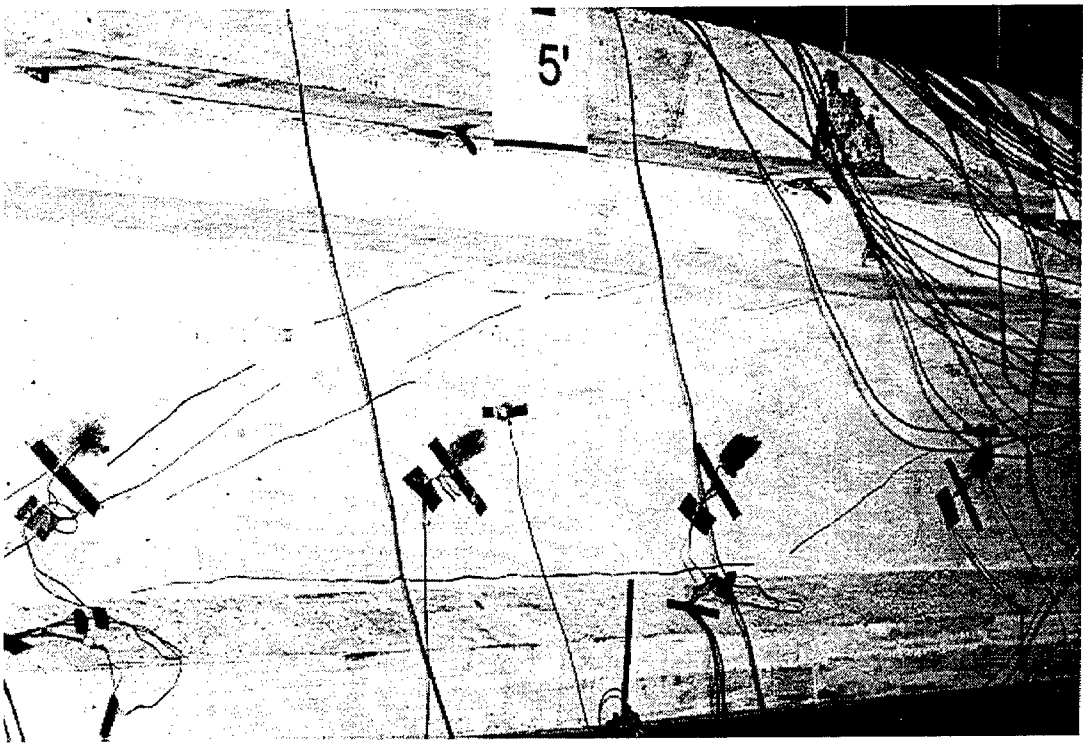

Figure 5.2 Before Testing Near Applied Load (End IA)

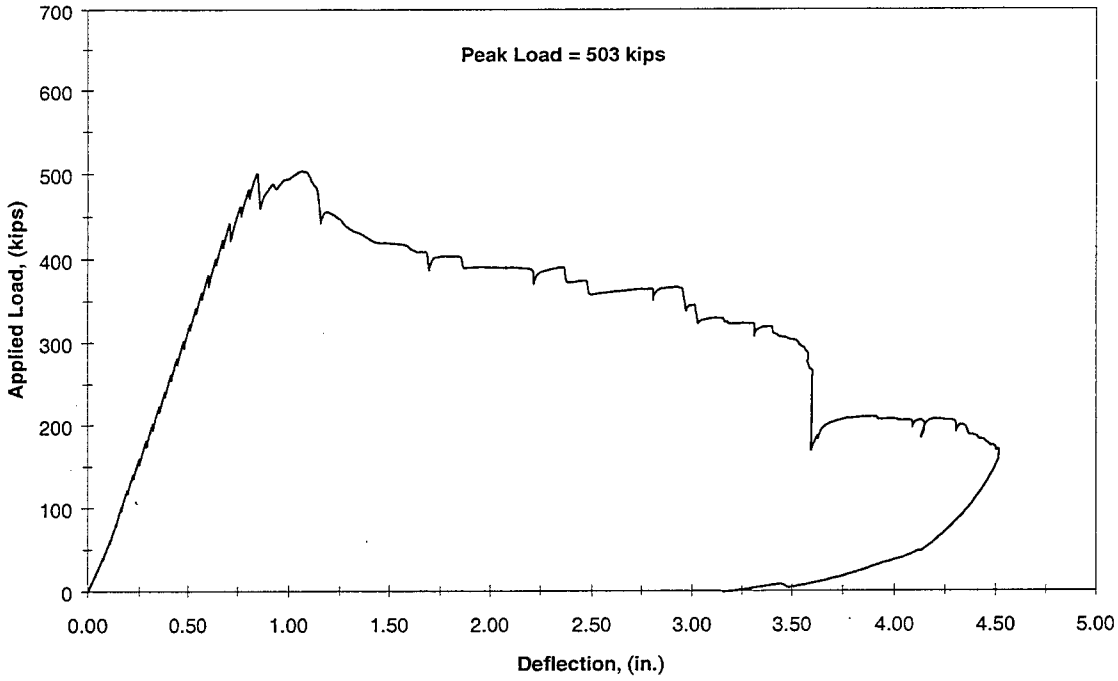

Figure 5.3 Corrected West Load Deflection (End IA)

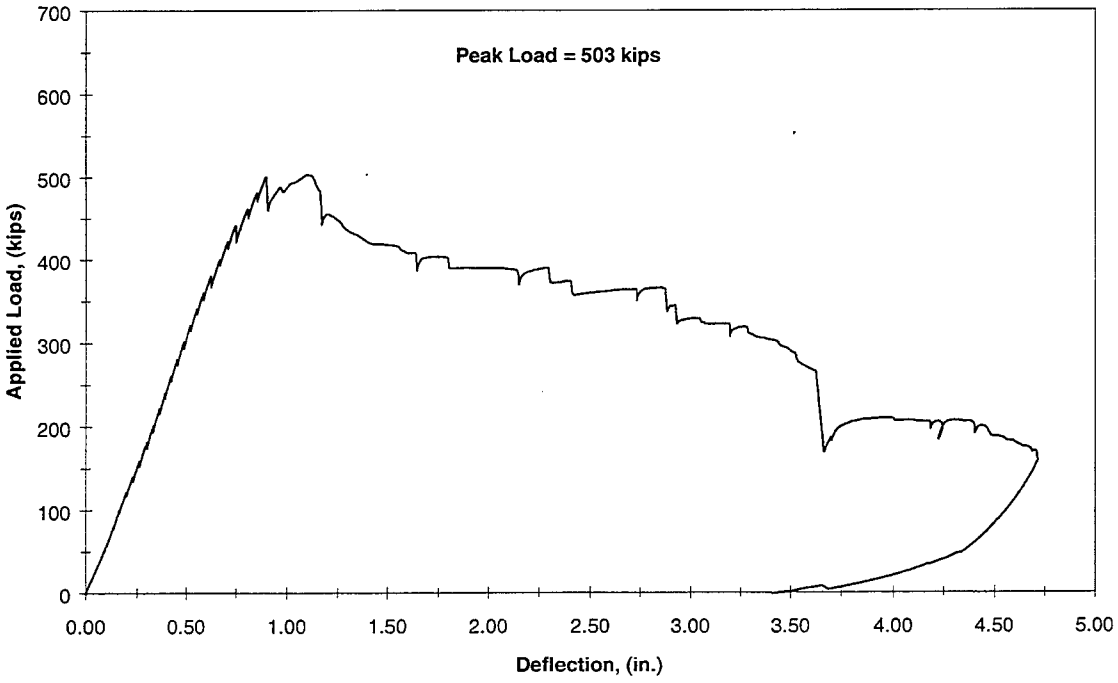

Figure 5.4 Corrected East Load Deflection (End IA)

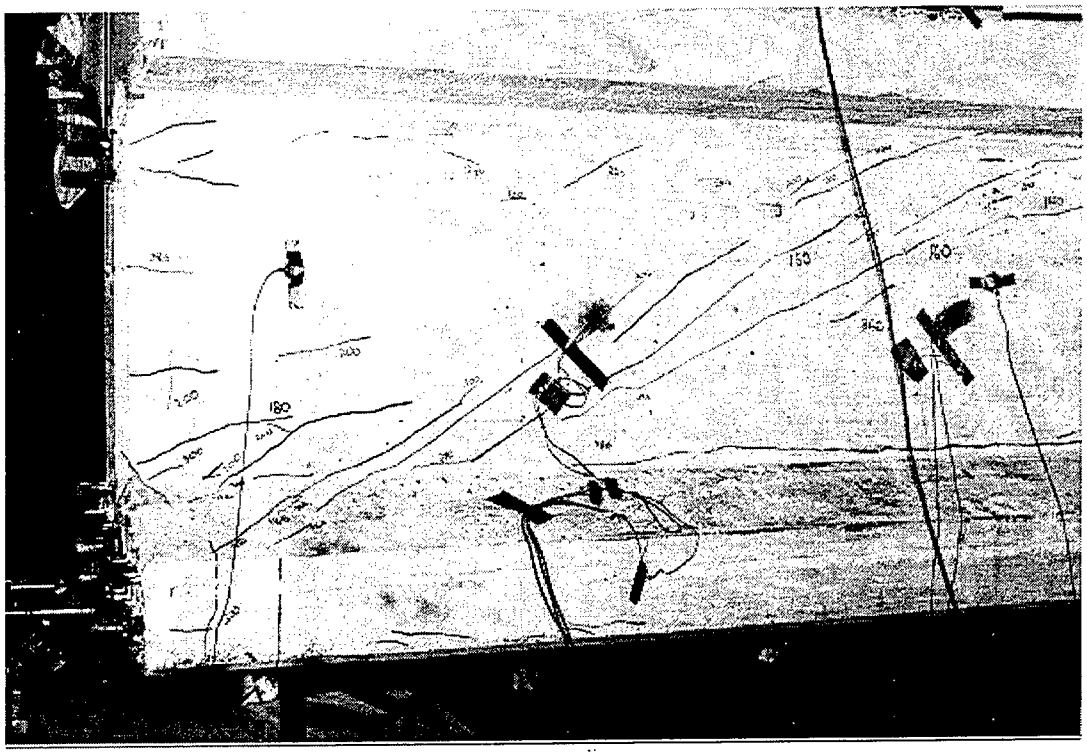

Figure 5.5 After 300 kips, Cracking Near Support (End IA)

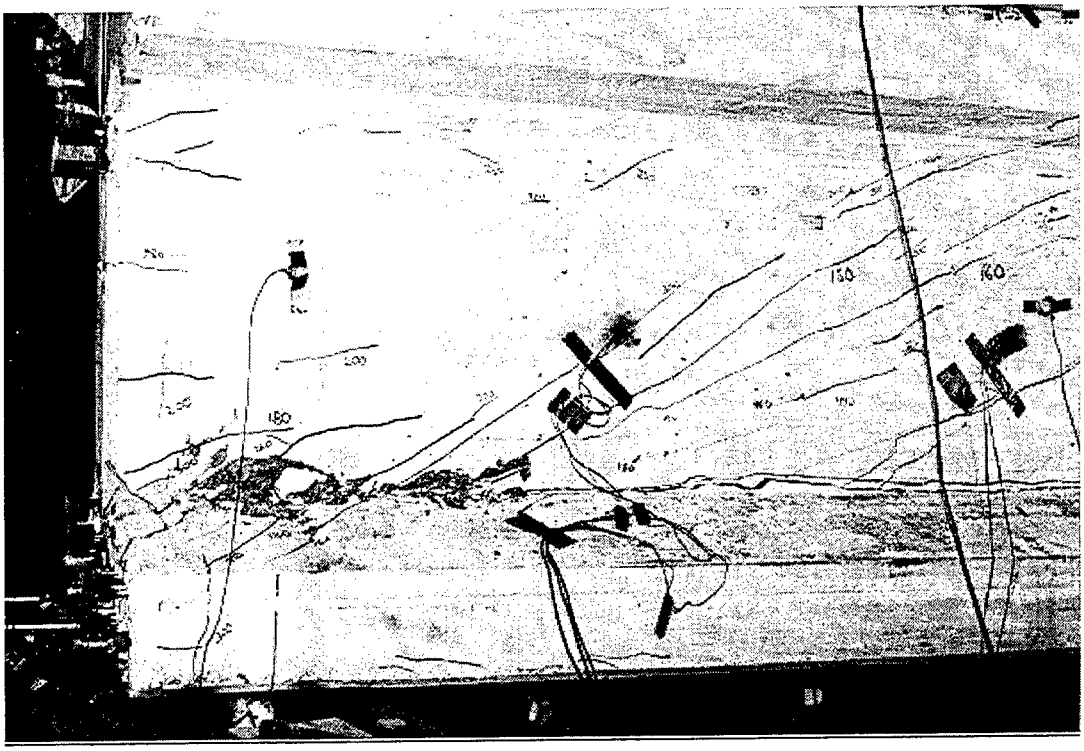

Figure 5.6 After Peak Load, Web Sliding Near Support (End IA)

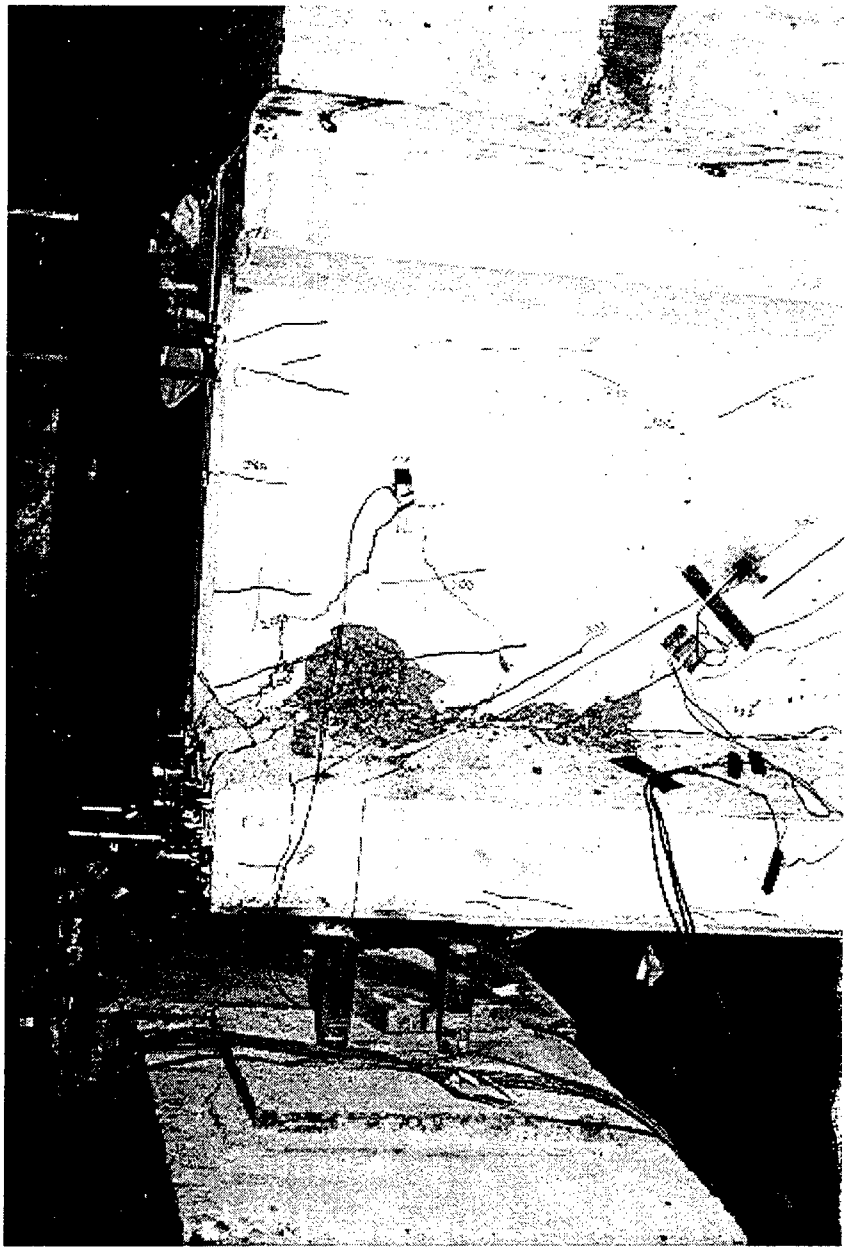

Figure 5.7 After Peak Load, Web Sliding Near Support (End IA)

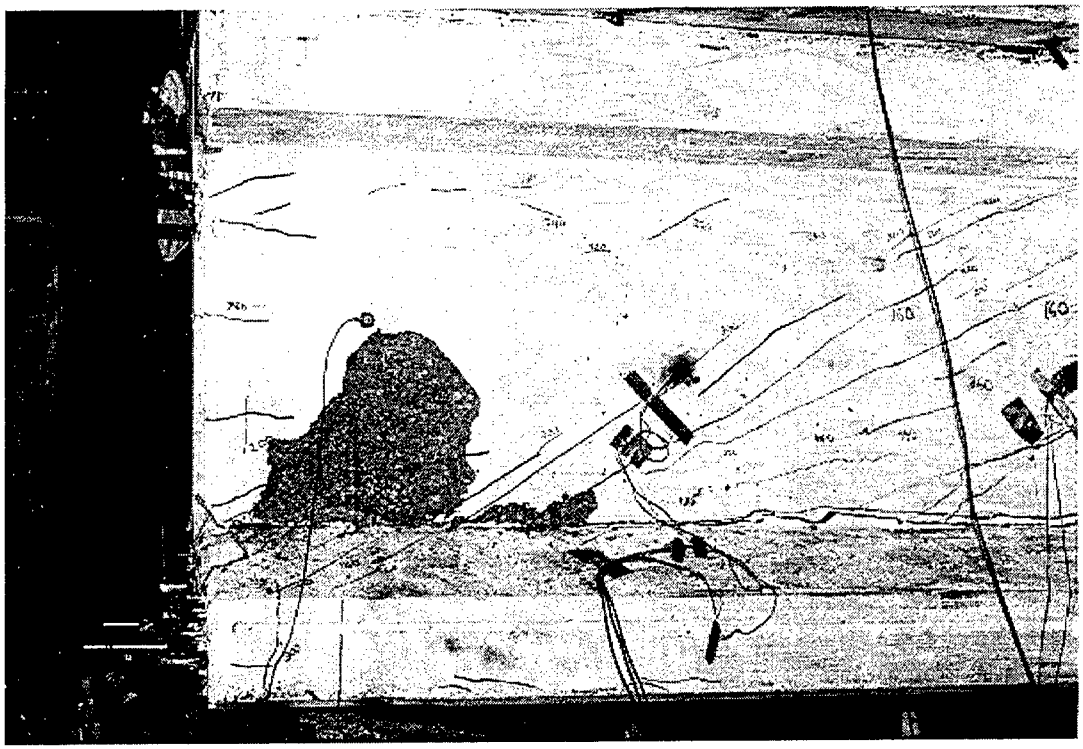

Figure 5.8 After Peak Load, Web Sliding Near Support (End IA)

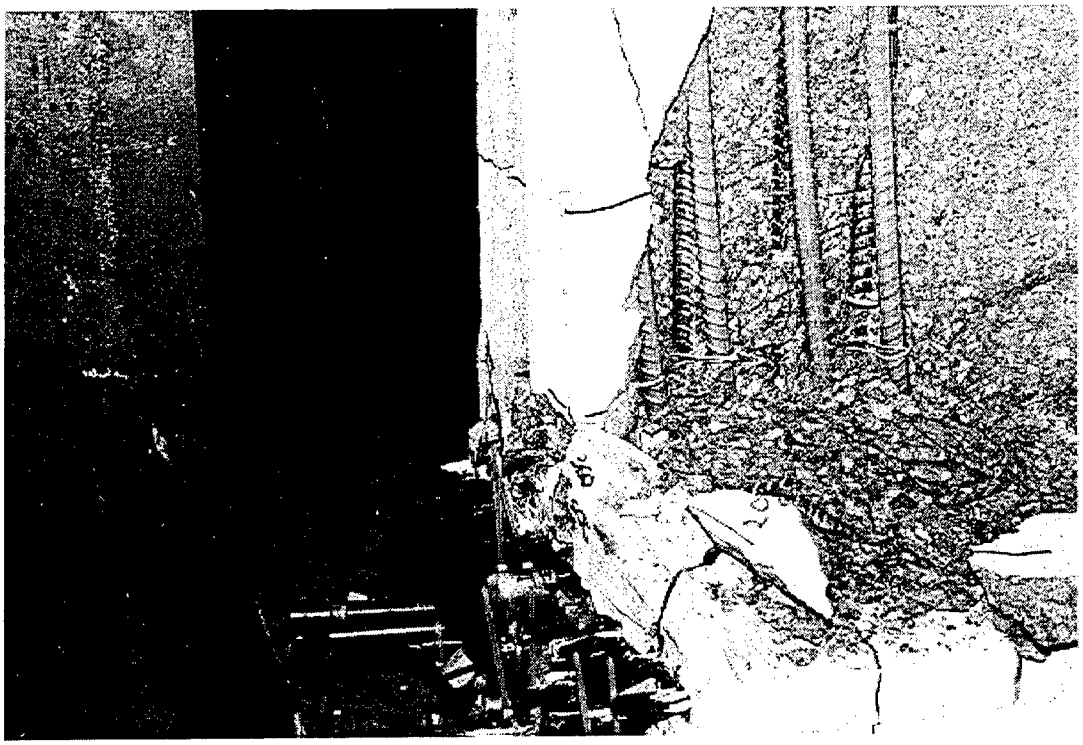

Figure 5.9 After Peak Load, Web Sliding Near Support (End IA)

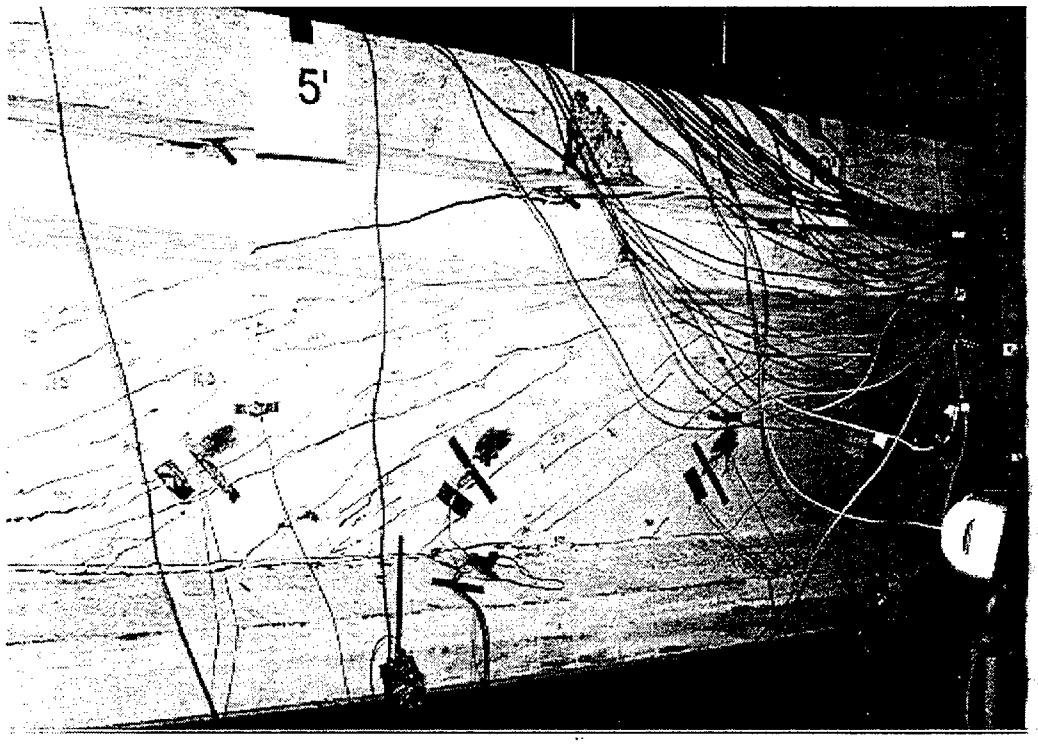

Figure 5.10 After Peak Load, Cracking Near Load Point (End IA)

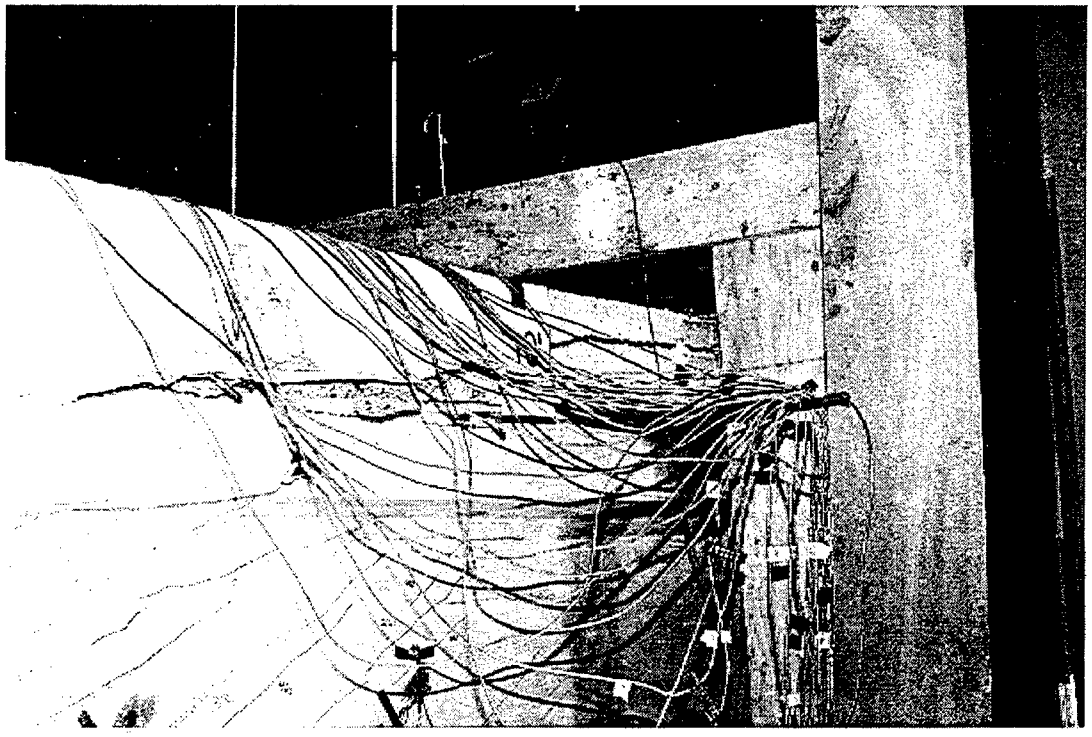

Figure 5.11 After Peak Load, Cracking Near Load Point (End IA)

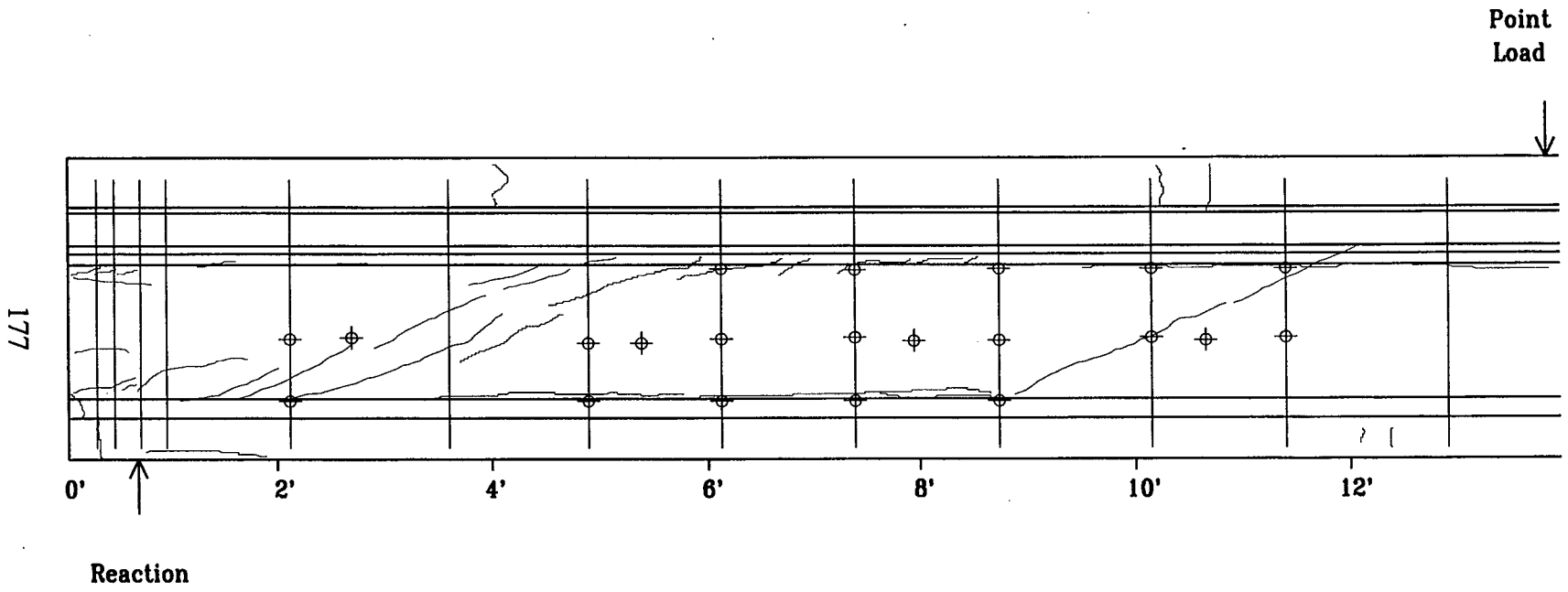

Figure 5.12 Before Testing, Crack Drawing (End IA)

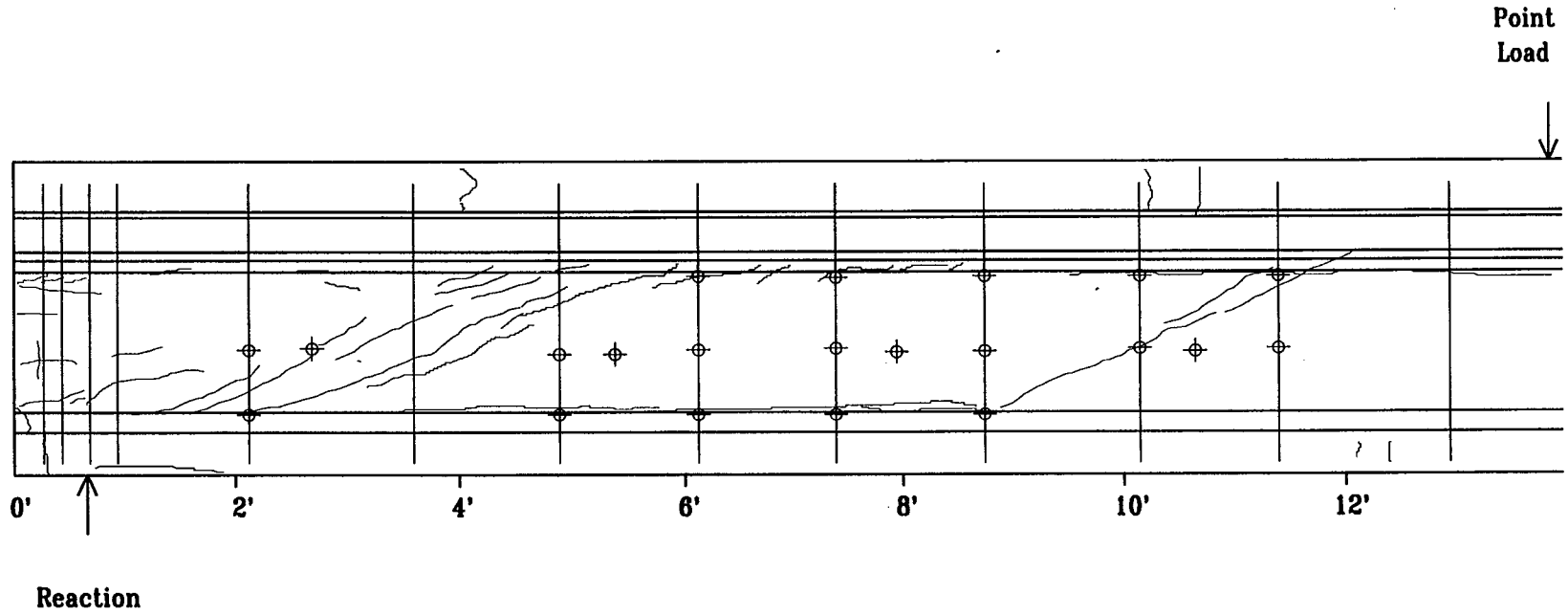

Figure 5.13 After 300 kips, Crack Drawing (End IA)

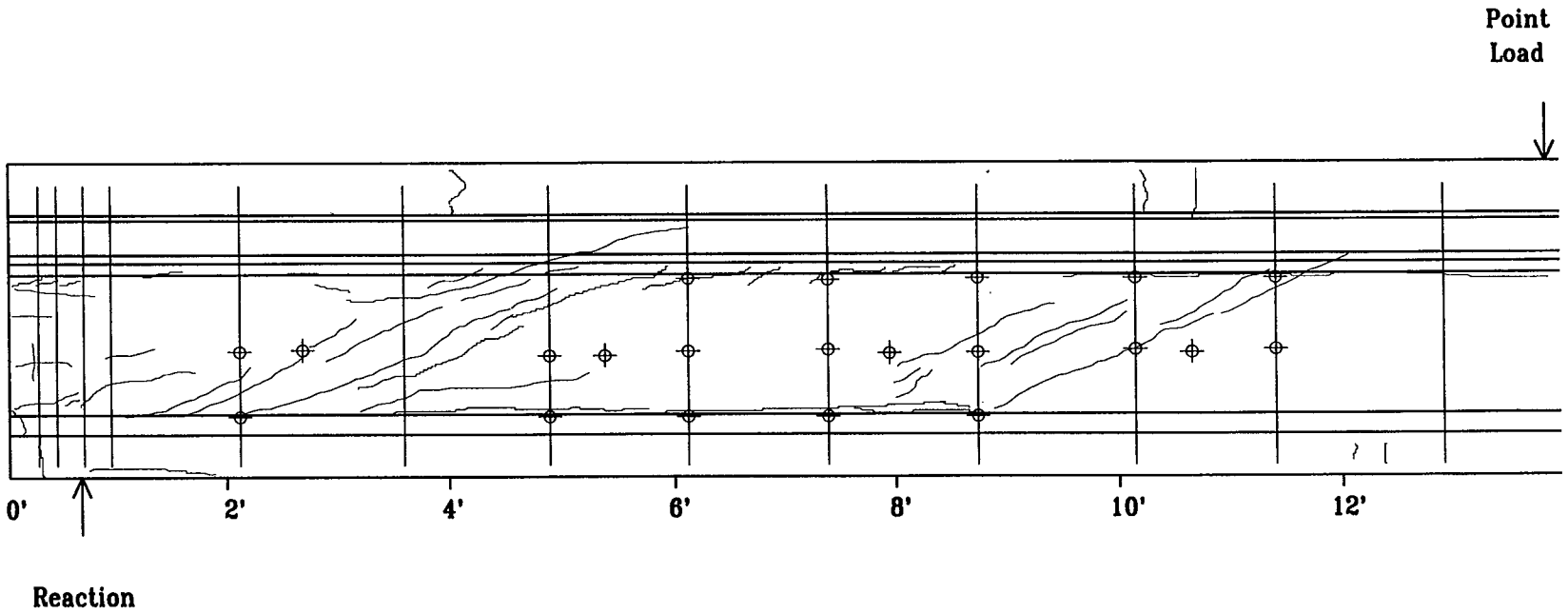

Figure 5.14 After Peak Load, Crack Drawing (End IA)

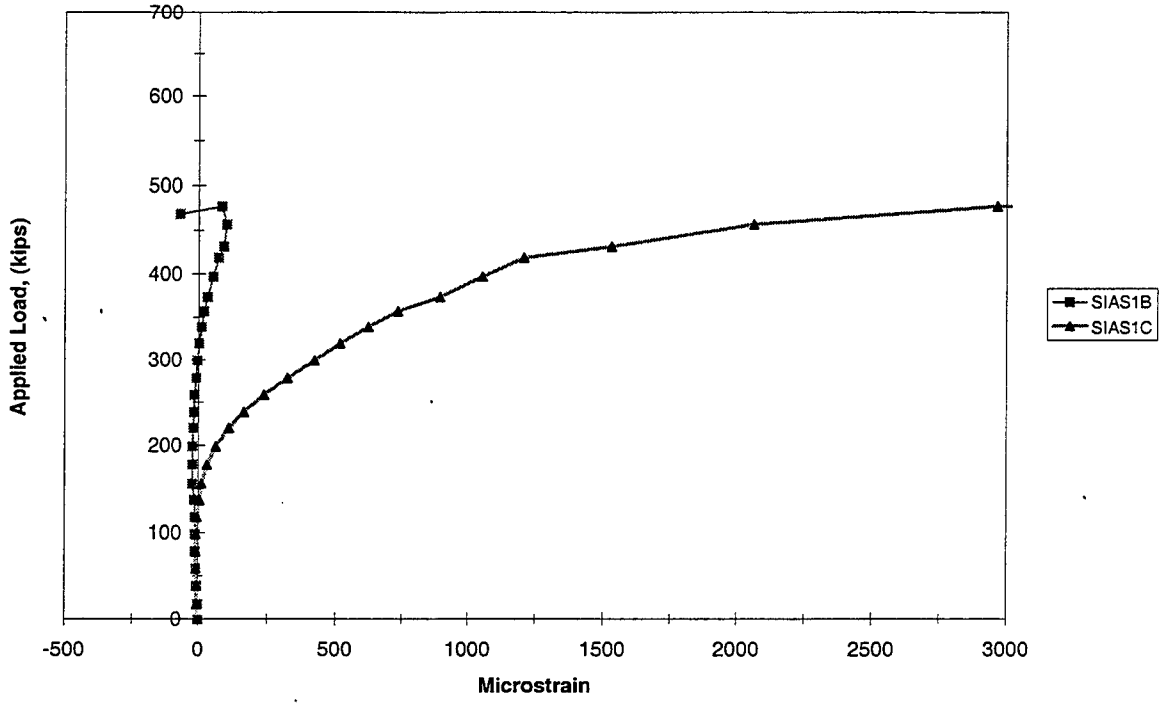

Figure 5.15 Stirrup 1 (End IA)

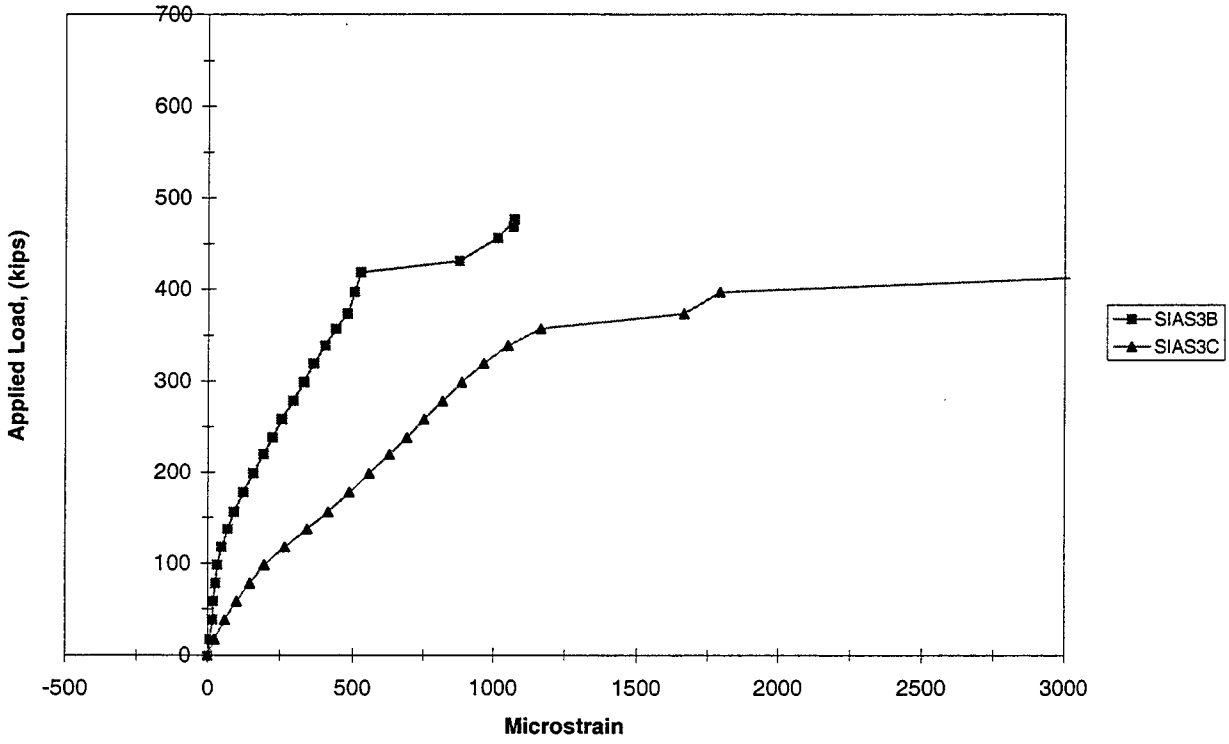

Figure 5.16 Stirrup 3 (End IA)

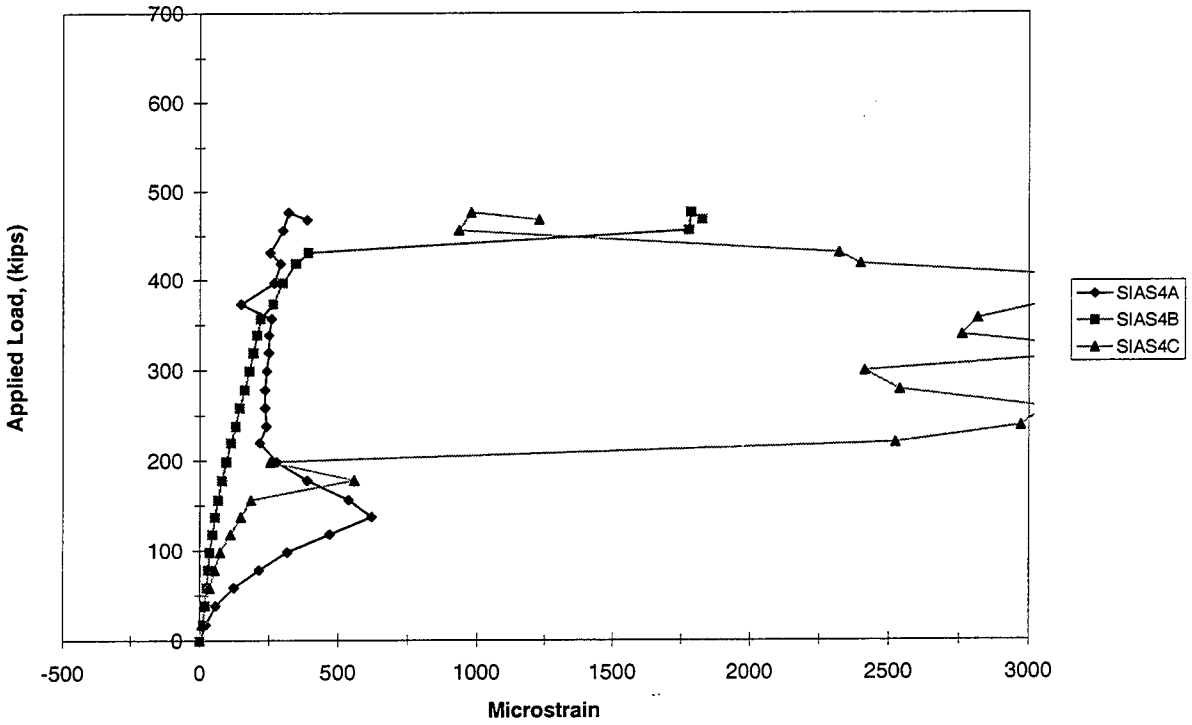

Figure 5.17 Stirrup 4 (End IA)

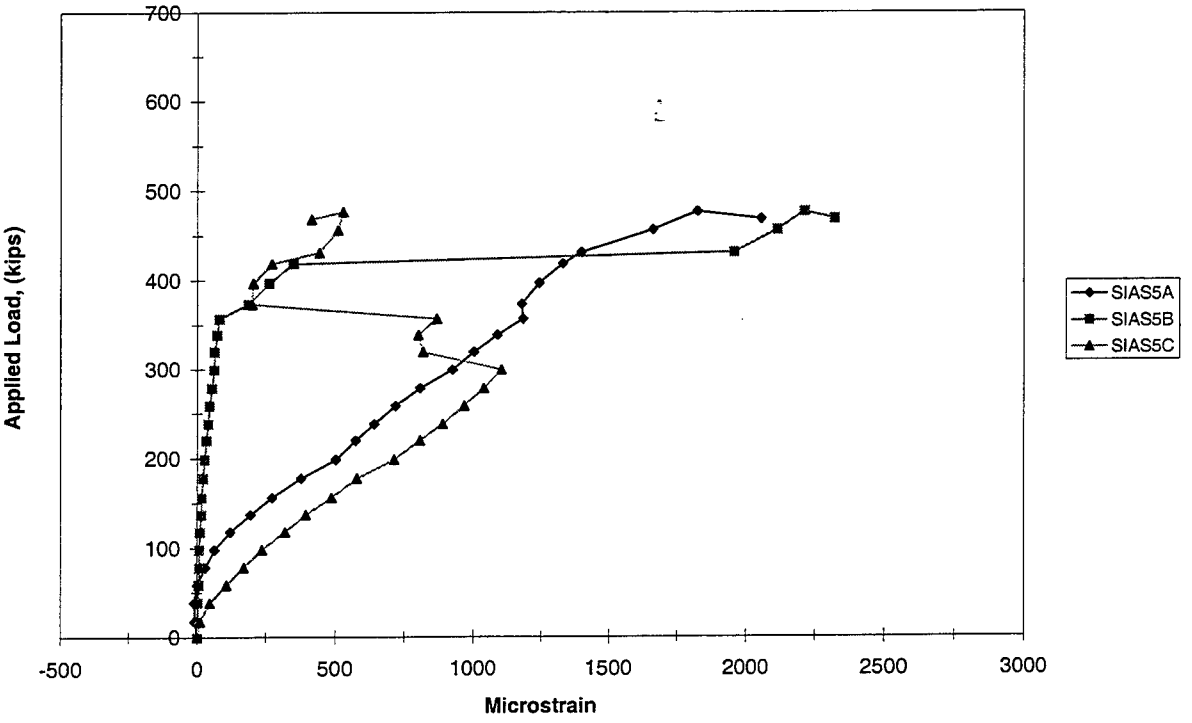

Figure 5.18 Stirrup 5 (End IA)

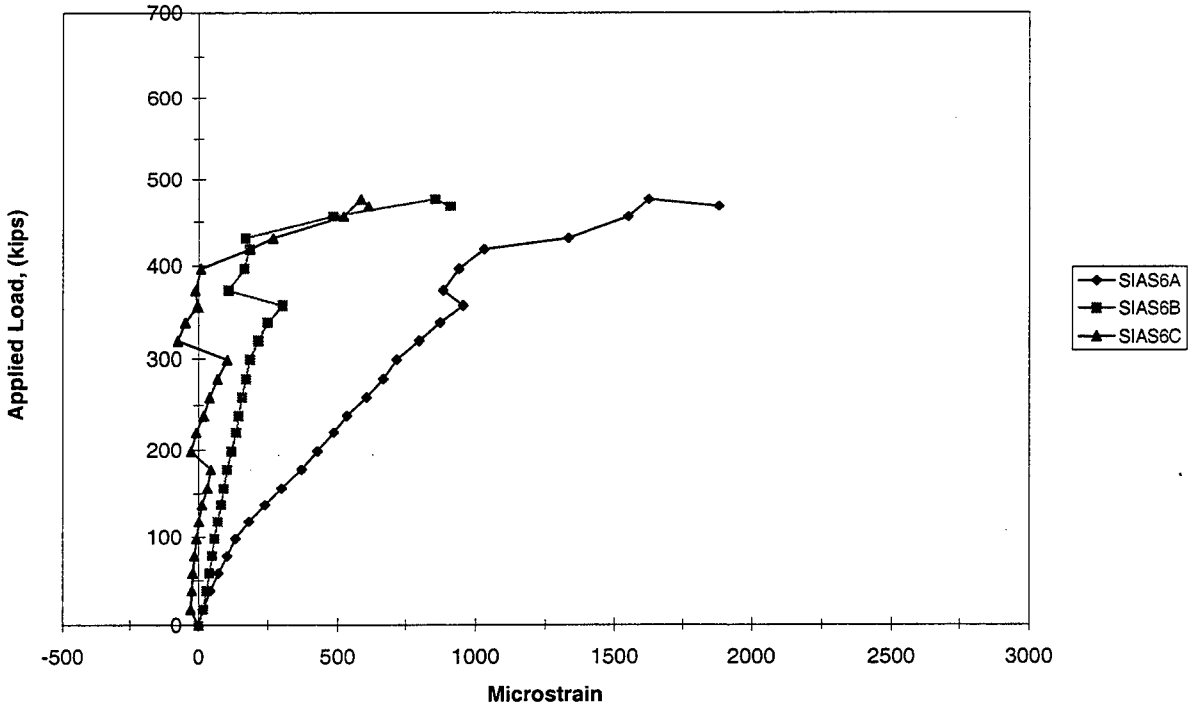

Figure 5.19 Stirrup 6 (End IA)

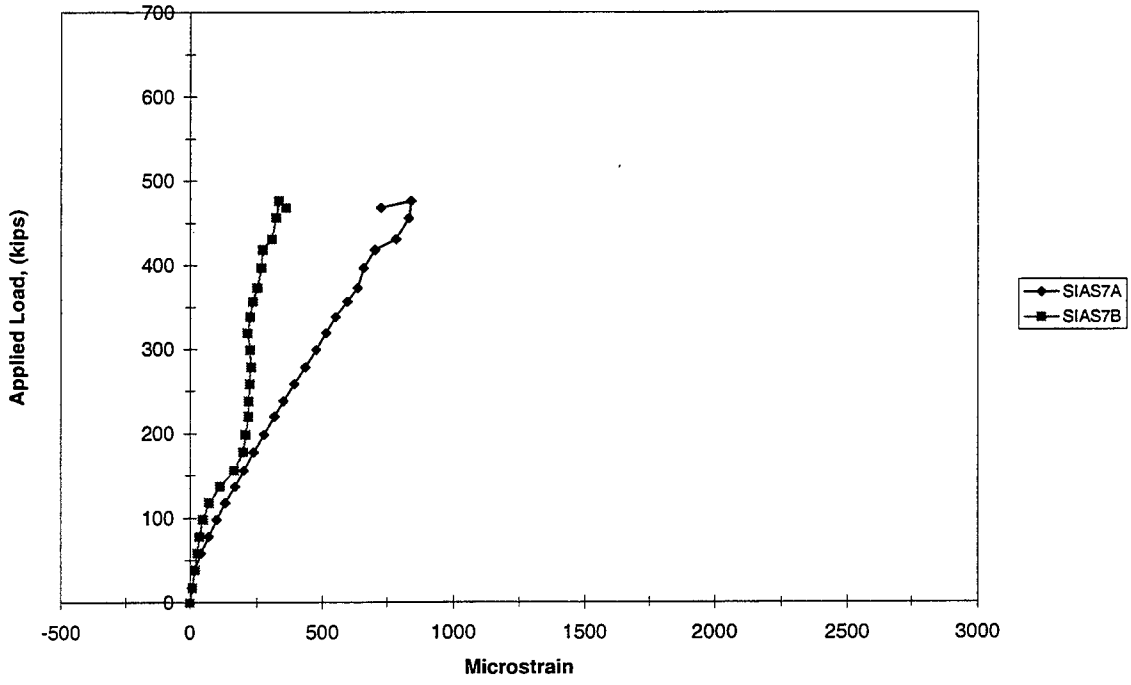

Figure 5.20 Stirrup 7 (End IA)

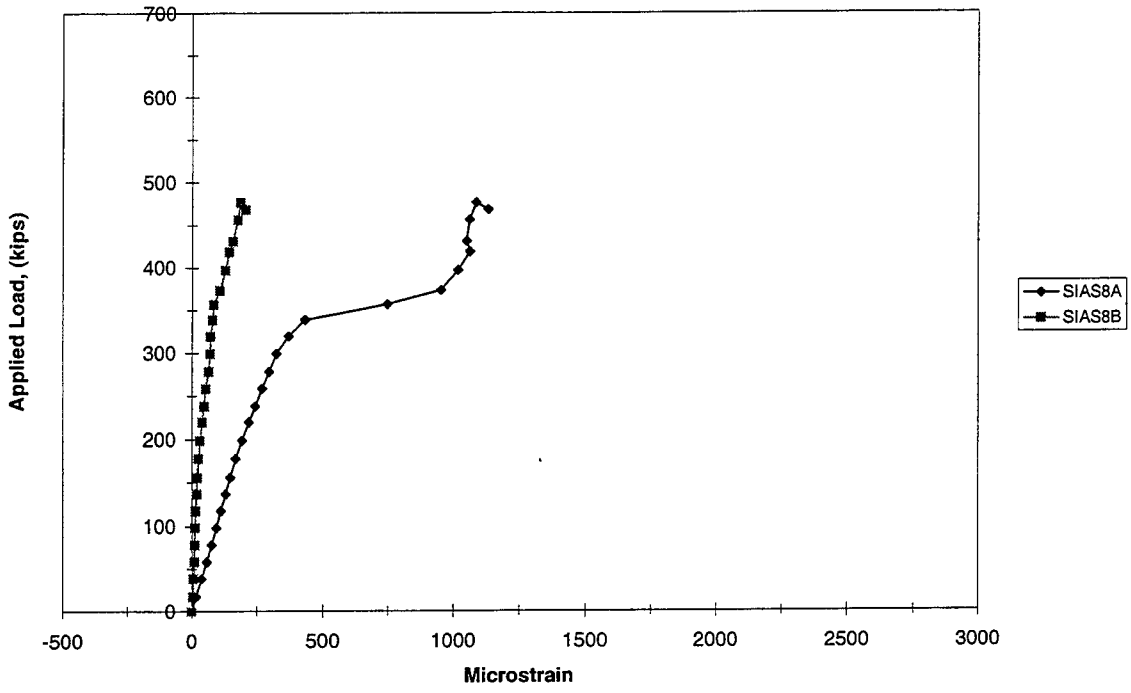

Figure 5.21 Stirrup 8 (End IA)

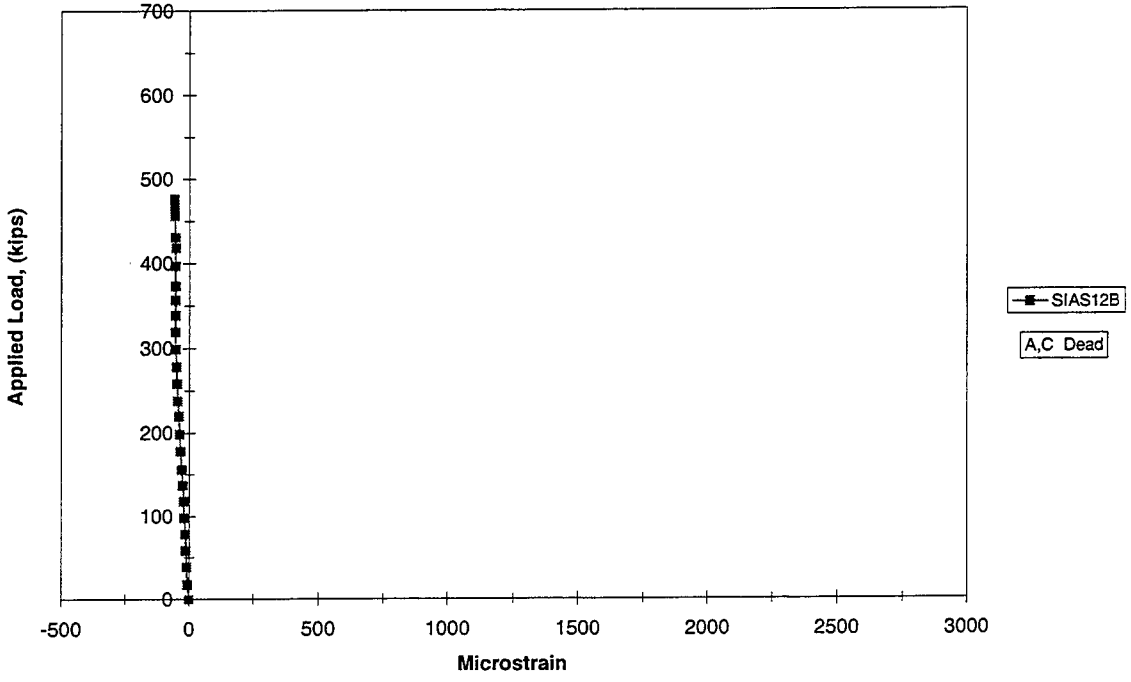

Figure 5.22 Stirrup 12 (End IA)

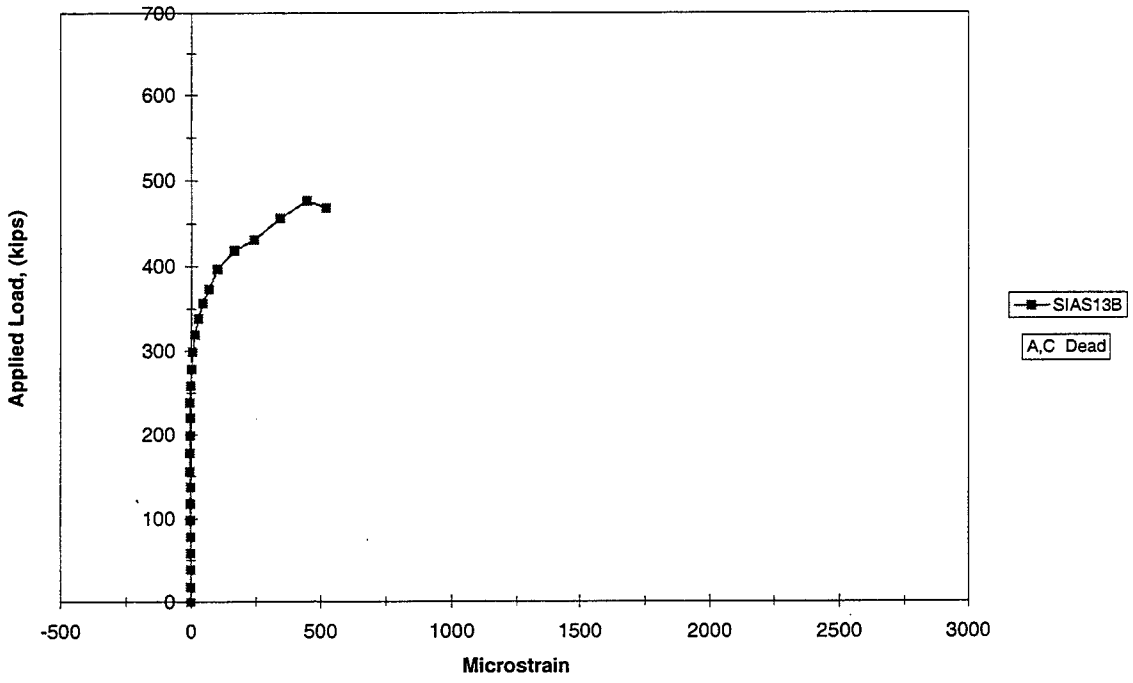

Figure 5.23 Stirrup 13 (End IA)

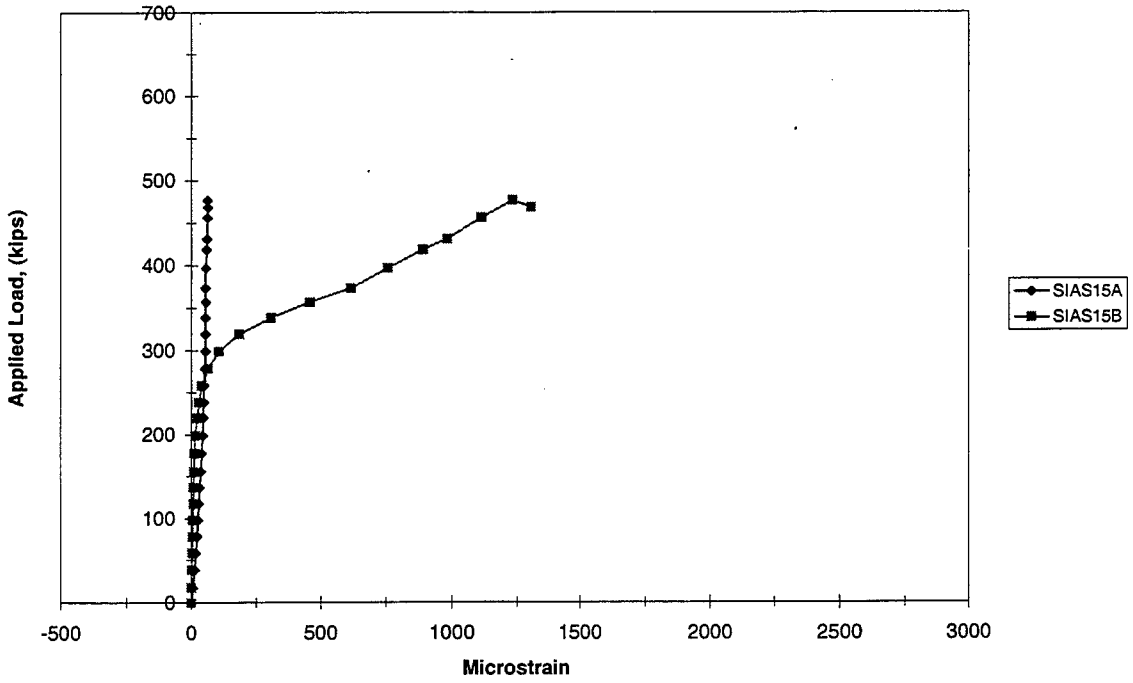

Figure 5.24 Stirrup 15 (End IA)

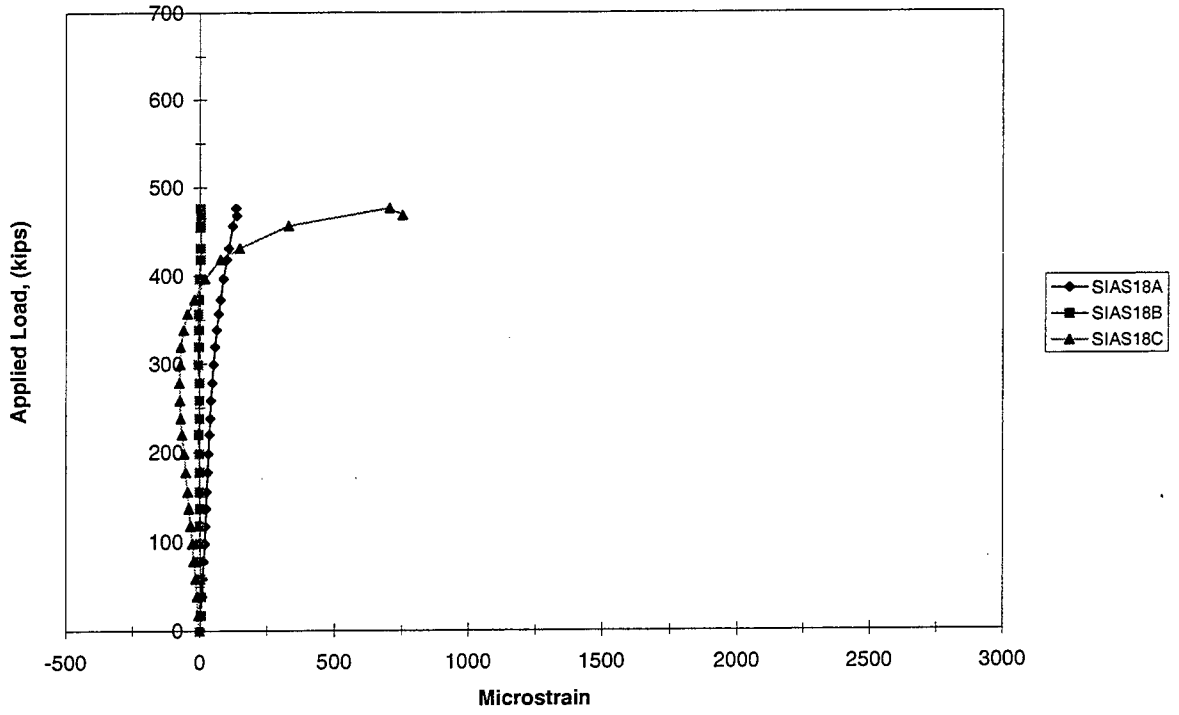

Figure 5.25 Stirrup 18 (End IA)

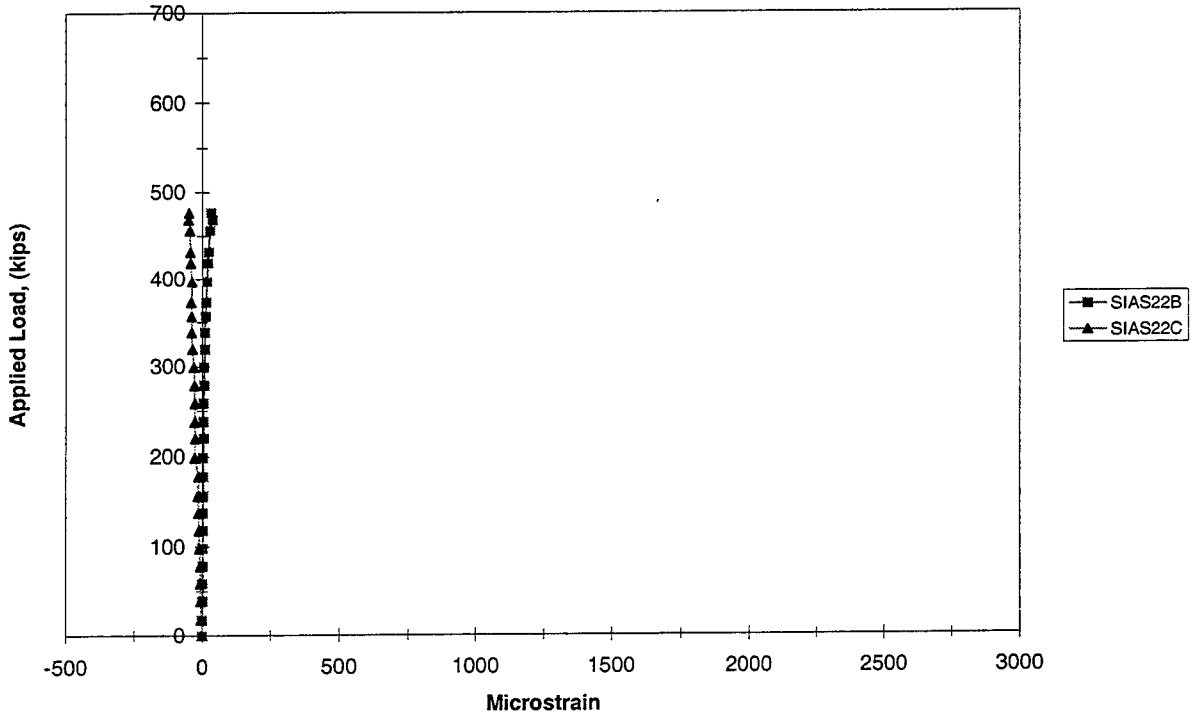

Figure 5.26 Stirrup 22 (End IA)

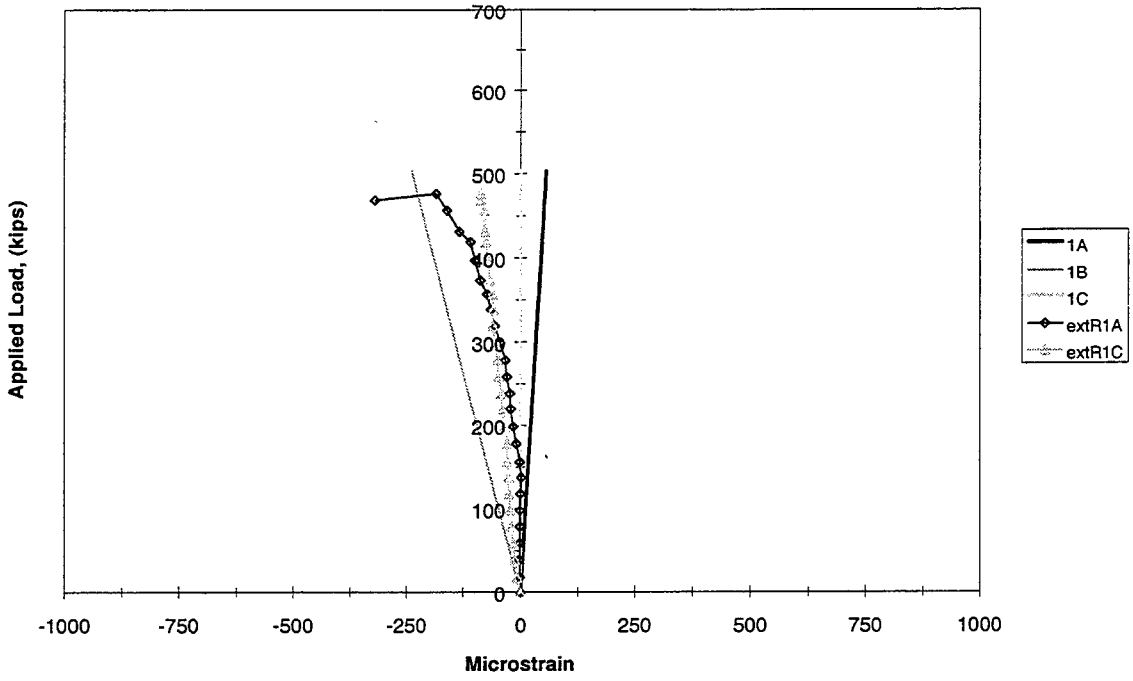

Figure 5.27 Rosette 1 (End IA)

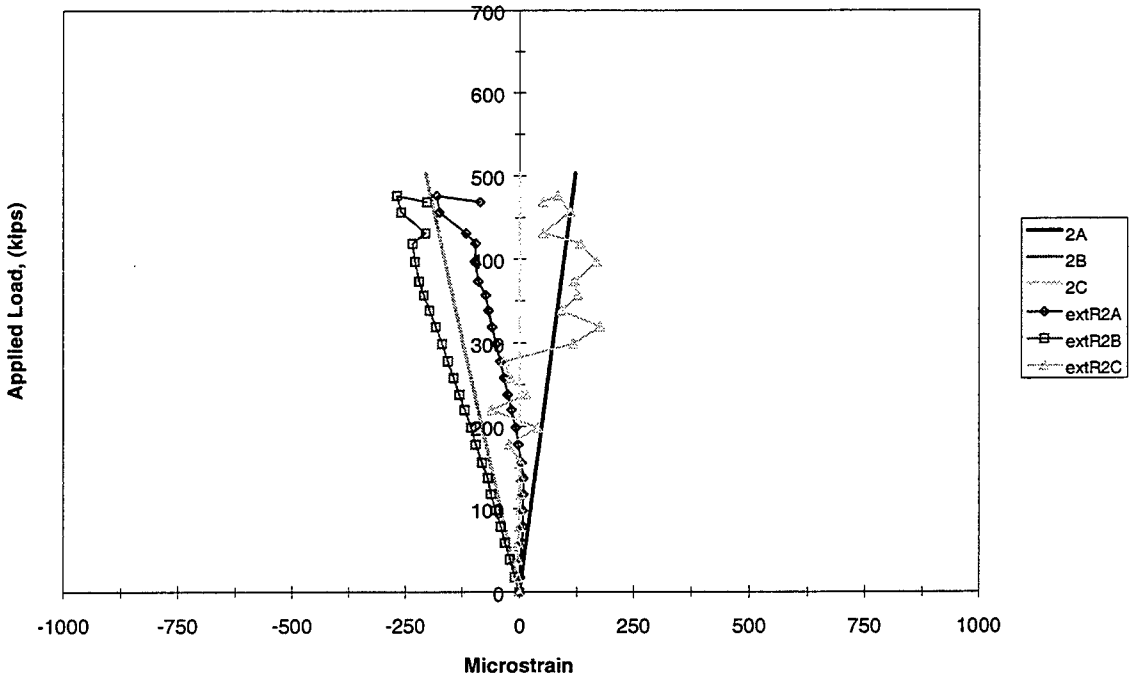

Figure 5.28 Rosette 2 (End IA)

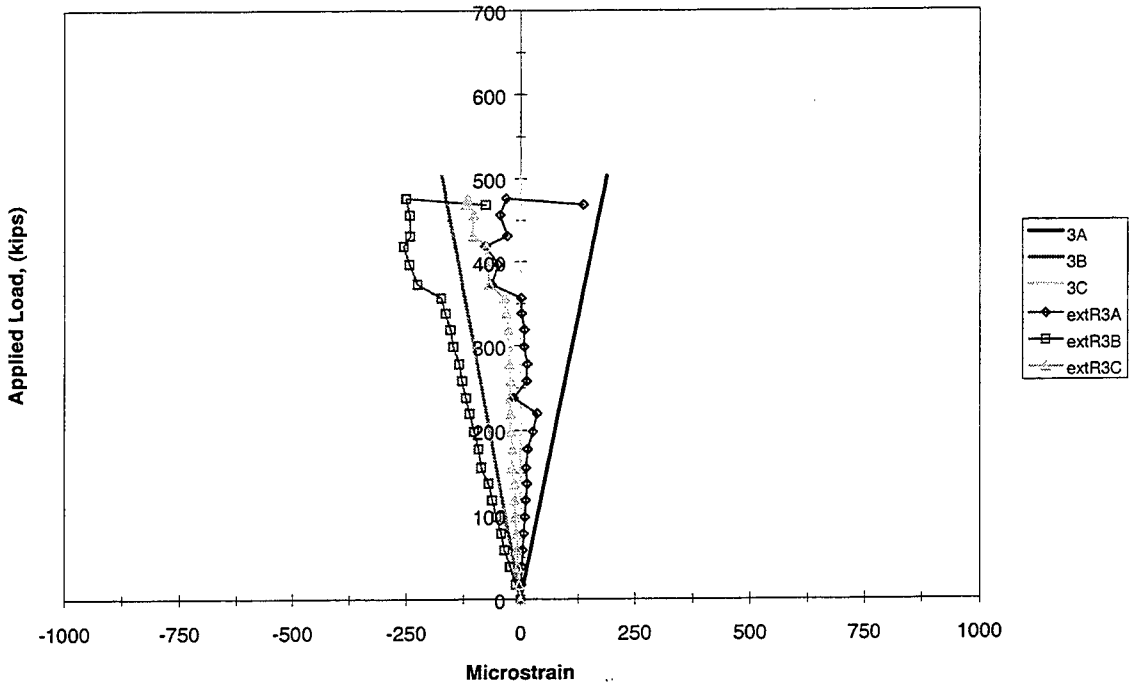

Figure 5.29 Rosette 3 (End IA)

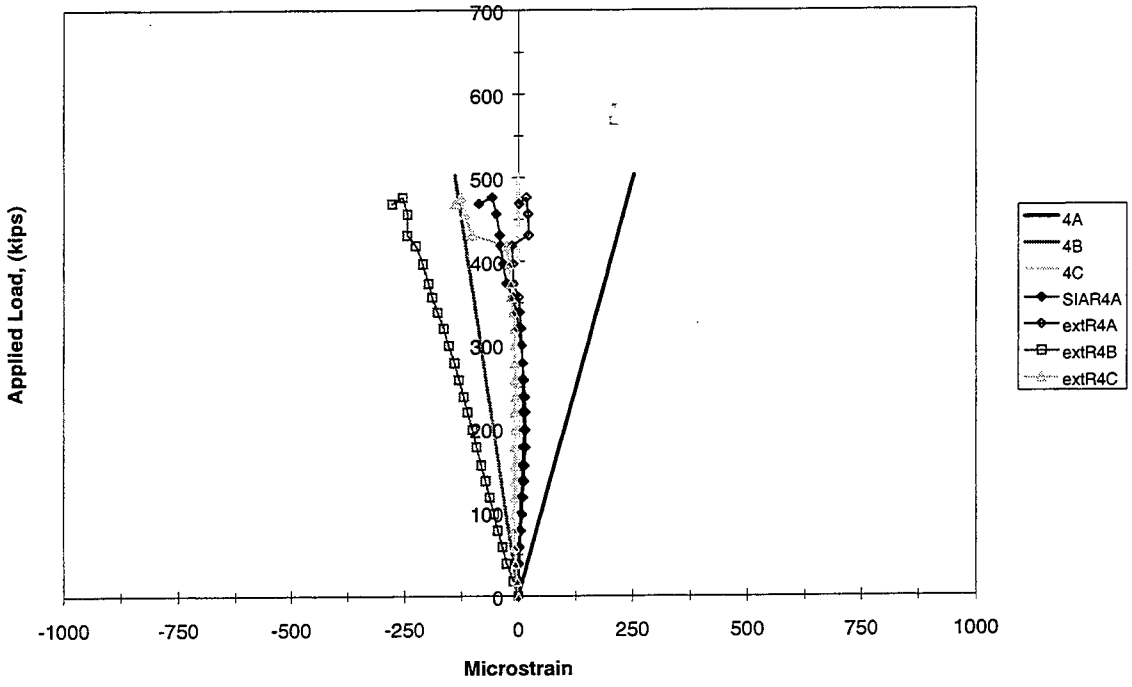

Figure 5.30 Rosette 4 (End IA)

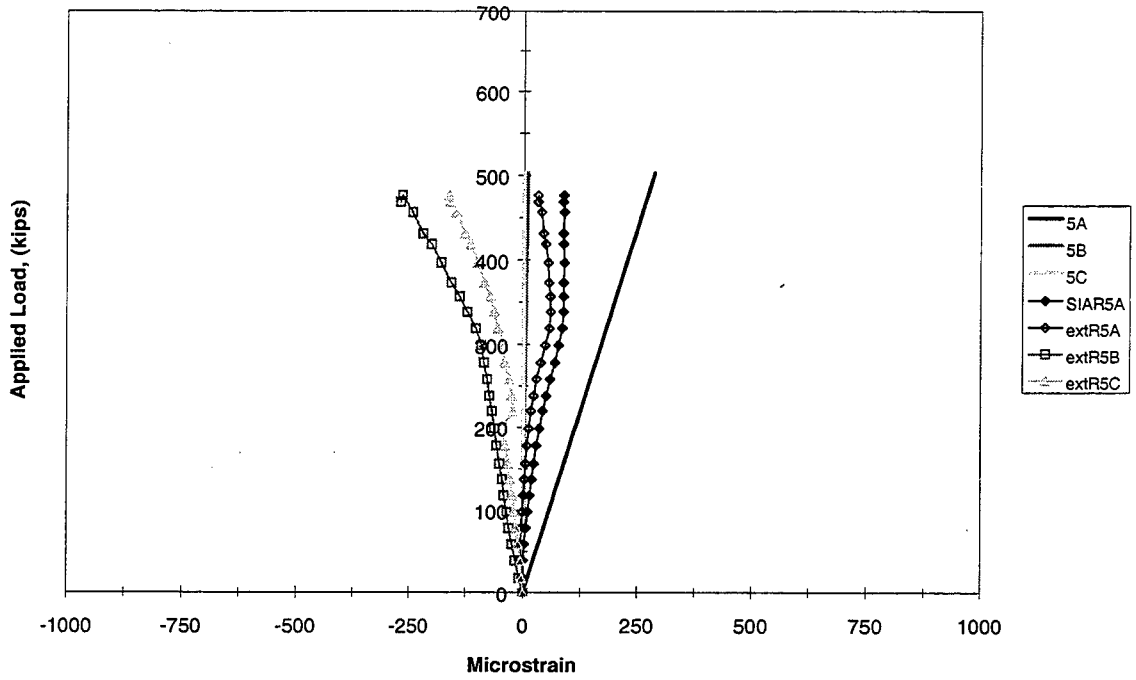

Figure 5.31 Rosette 5 (End IA)

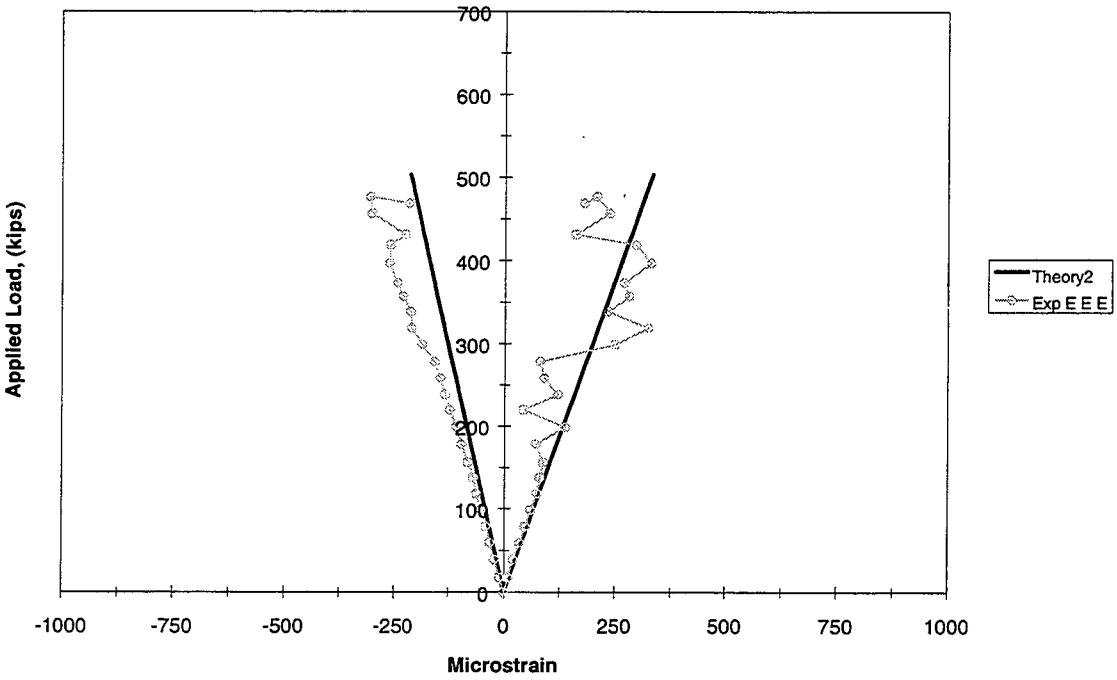

Figure 5.32 Principal Strains Rosette 2 (End IA)

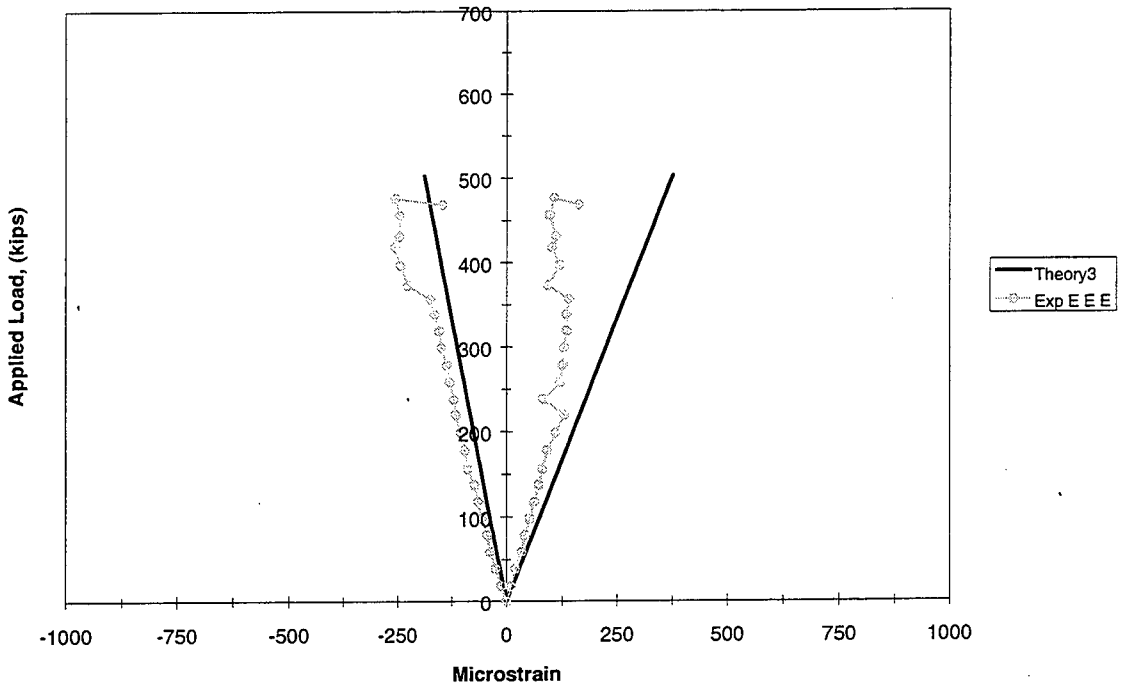

Figure 5.33 Principal Strains Rosette 3 (End IA)

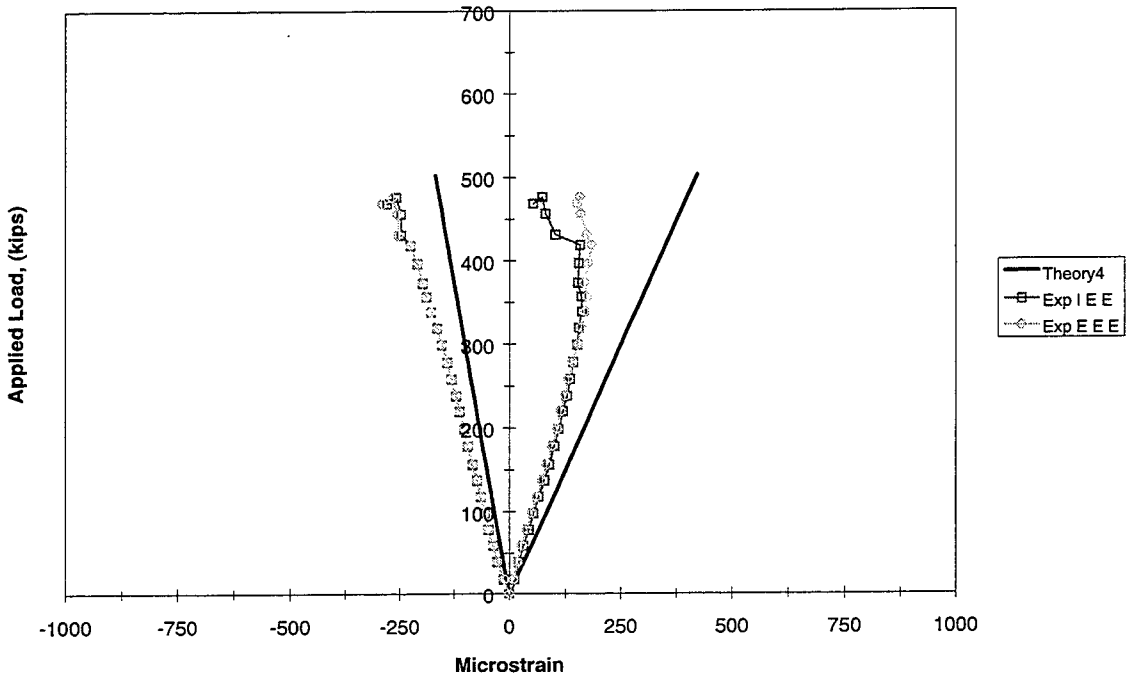

Figure 5.34 Principal Strains Rosette 4 (End IA)

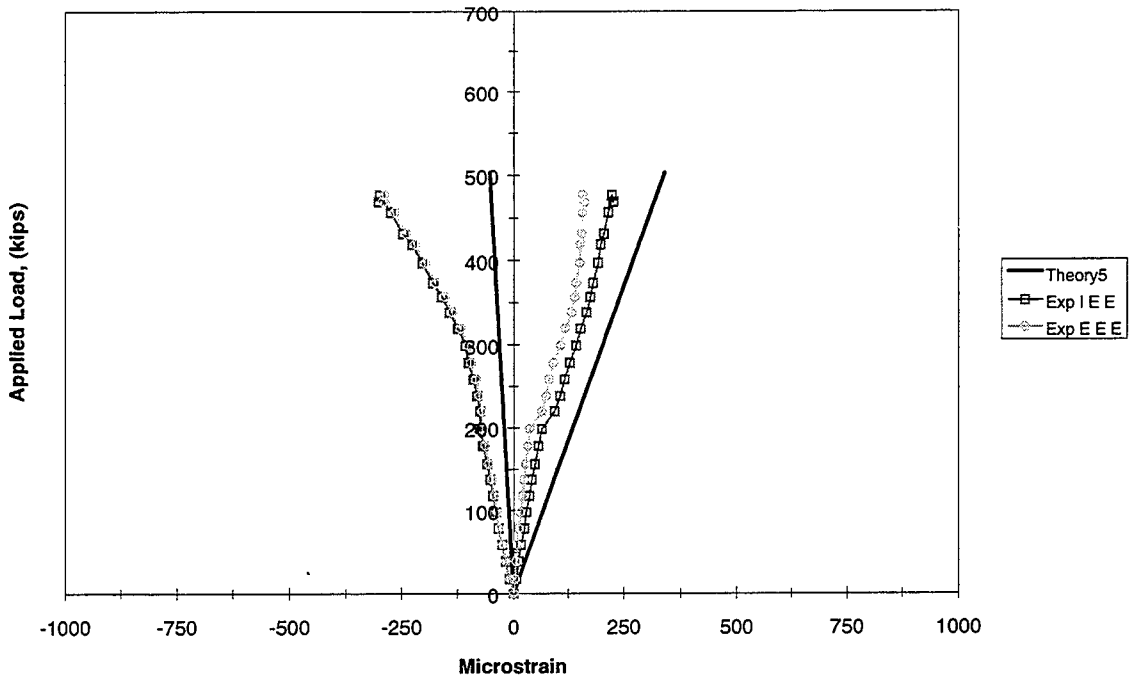

Figure 5.35 Principal Strains Rosette 5 (End IA)

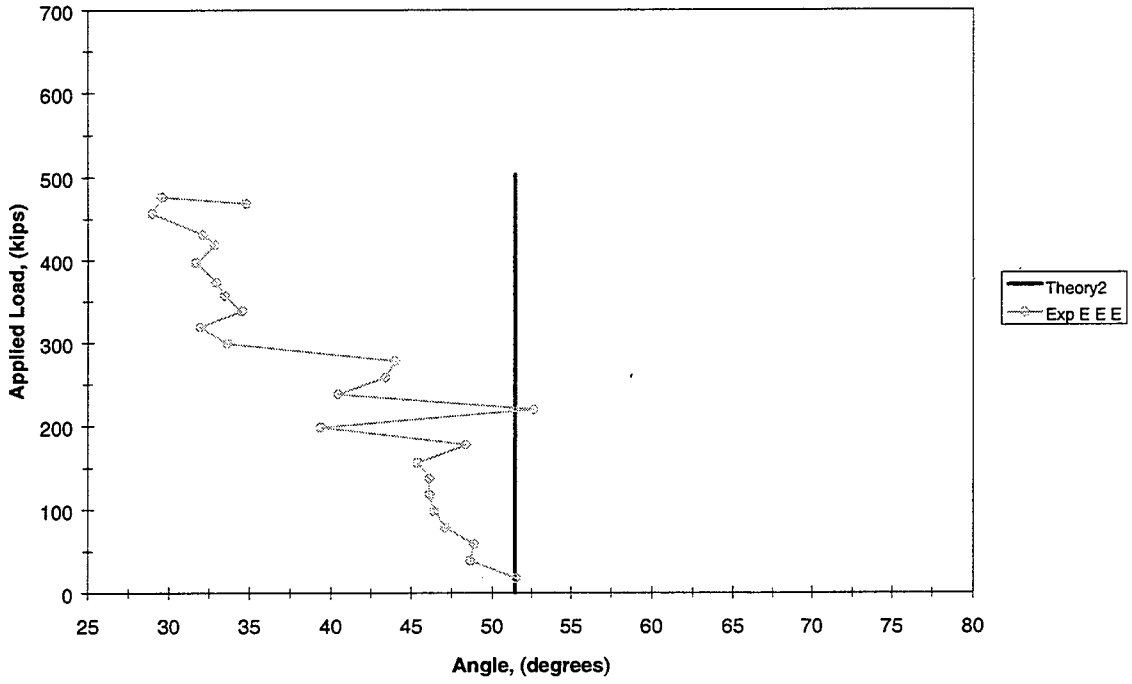

Figure 5.36 Principal Compression Angle Rosette 2 (End IA)

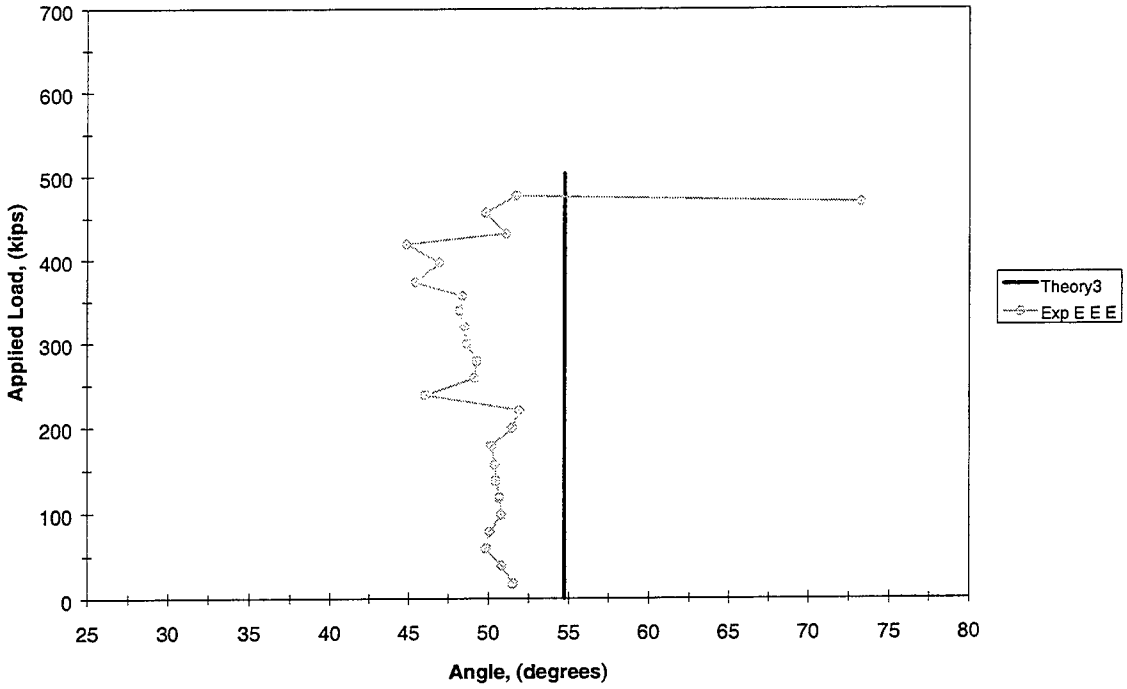

Figure 5.37 Principal Compression Angle Rosette 3 (End IA)

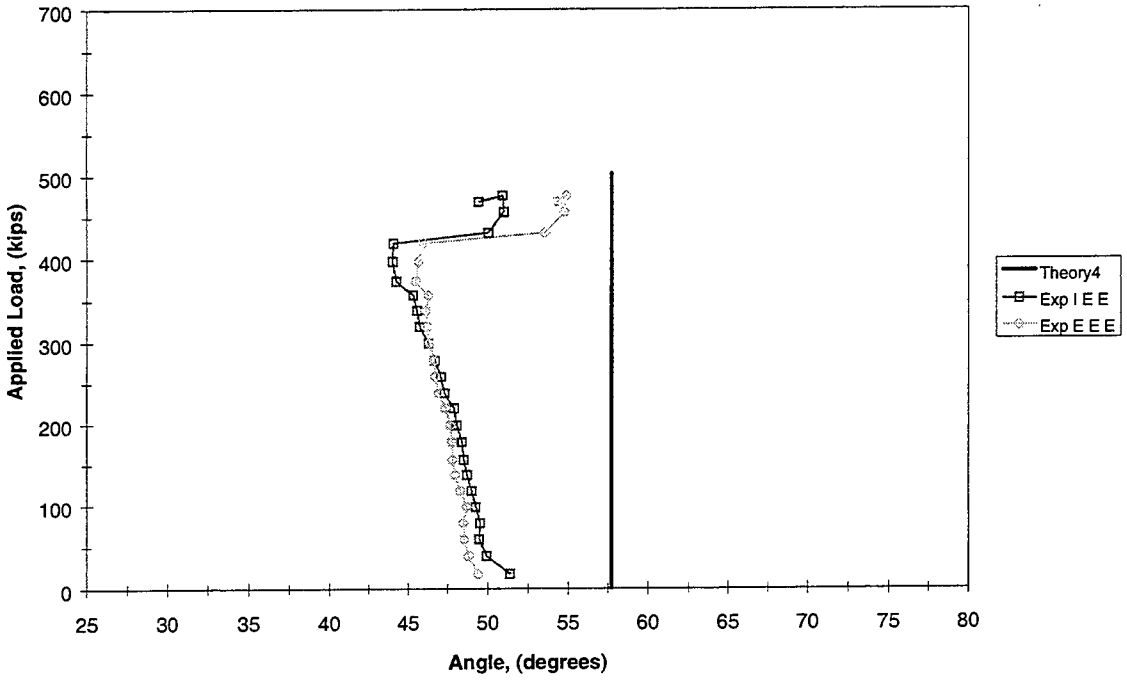

Figure 5.38 Principal Compression Angle Rosette 4 (End IA)

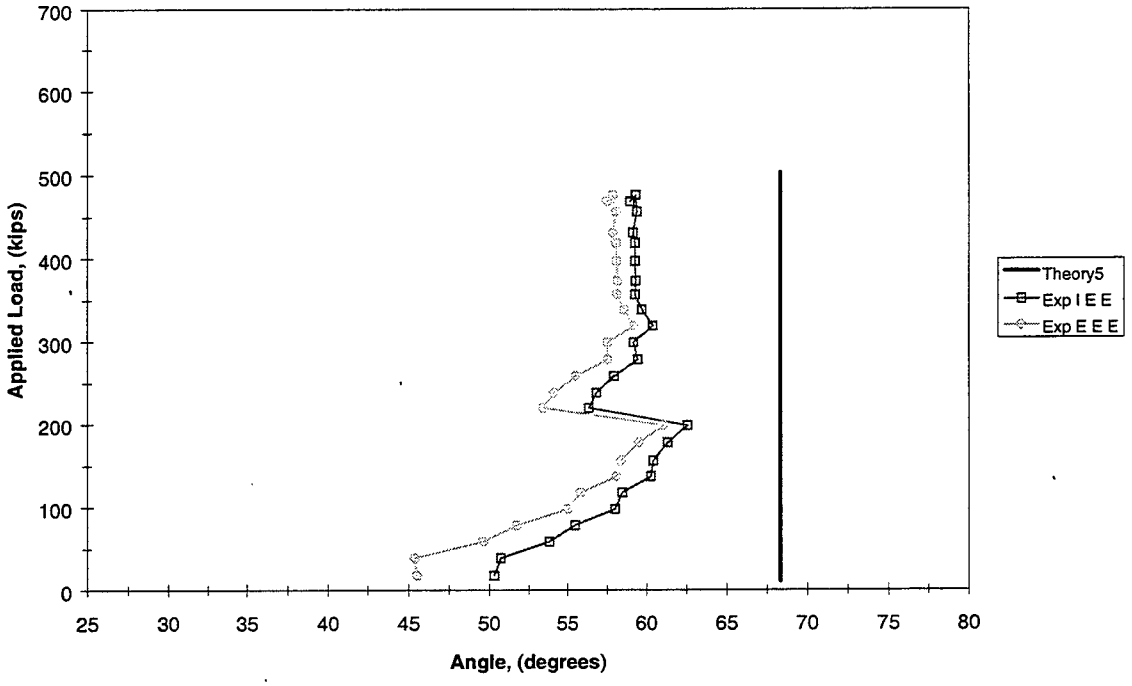

Figure 5.39 Principal Compression Angle Rosette 5 (End IA)

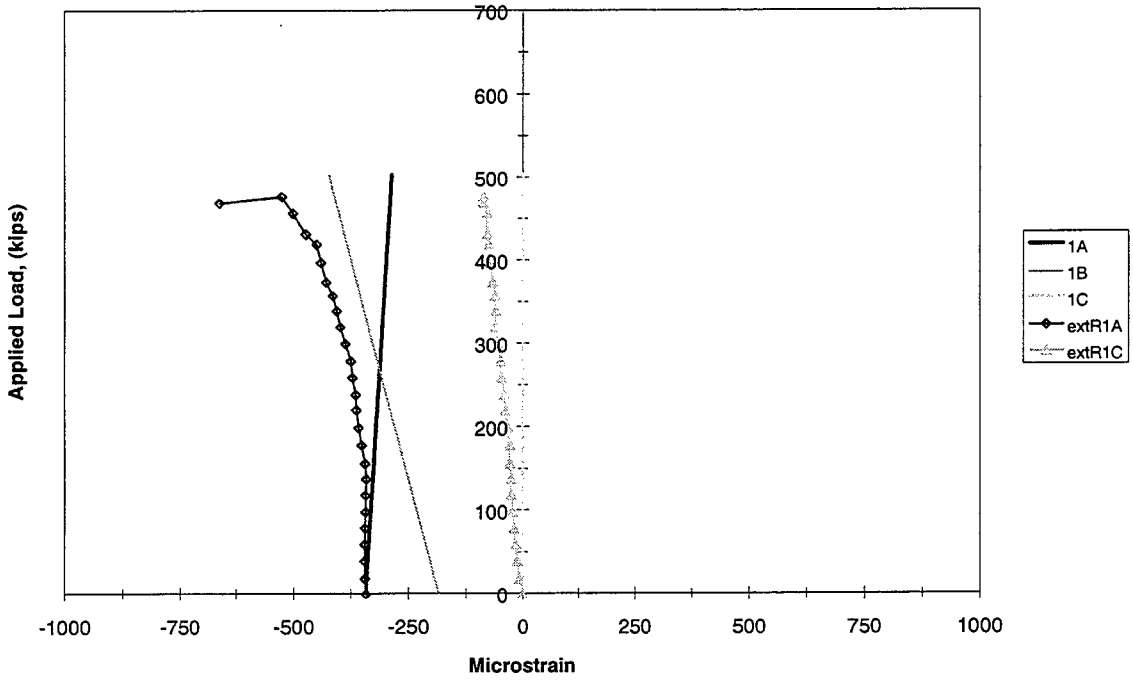

Figure 5.40 Corrected Rosette 1 (End IA)

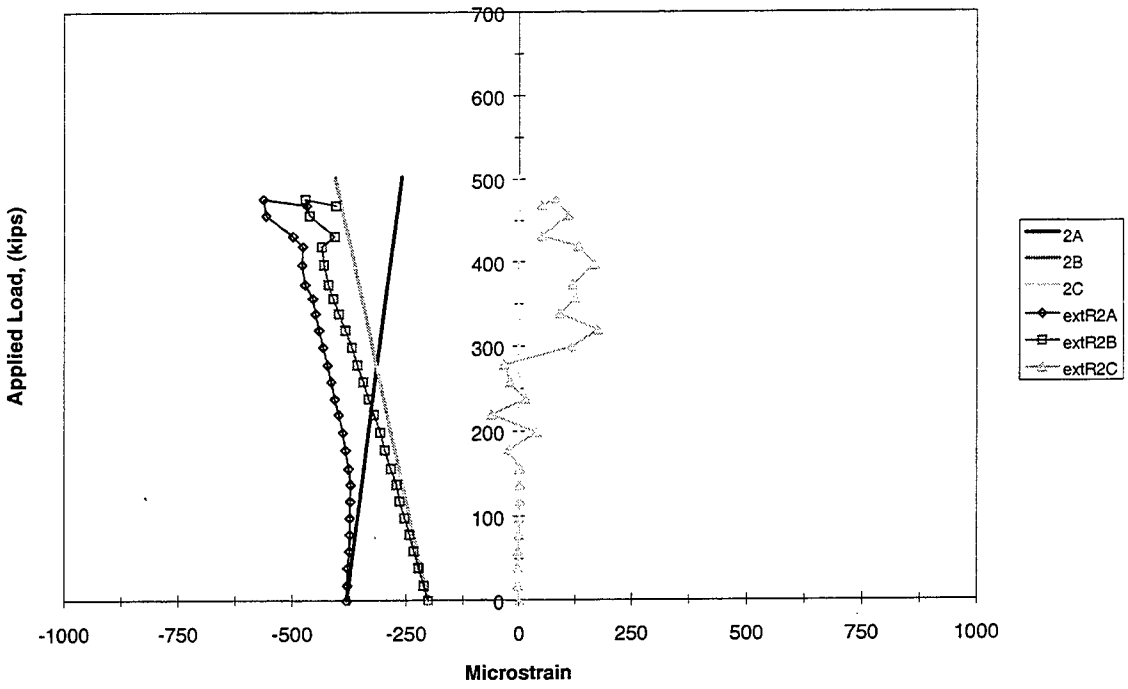

Figure 5.41 Corrected Rosette 2 (End IA)

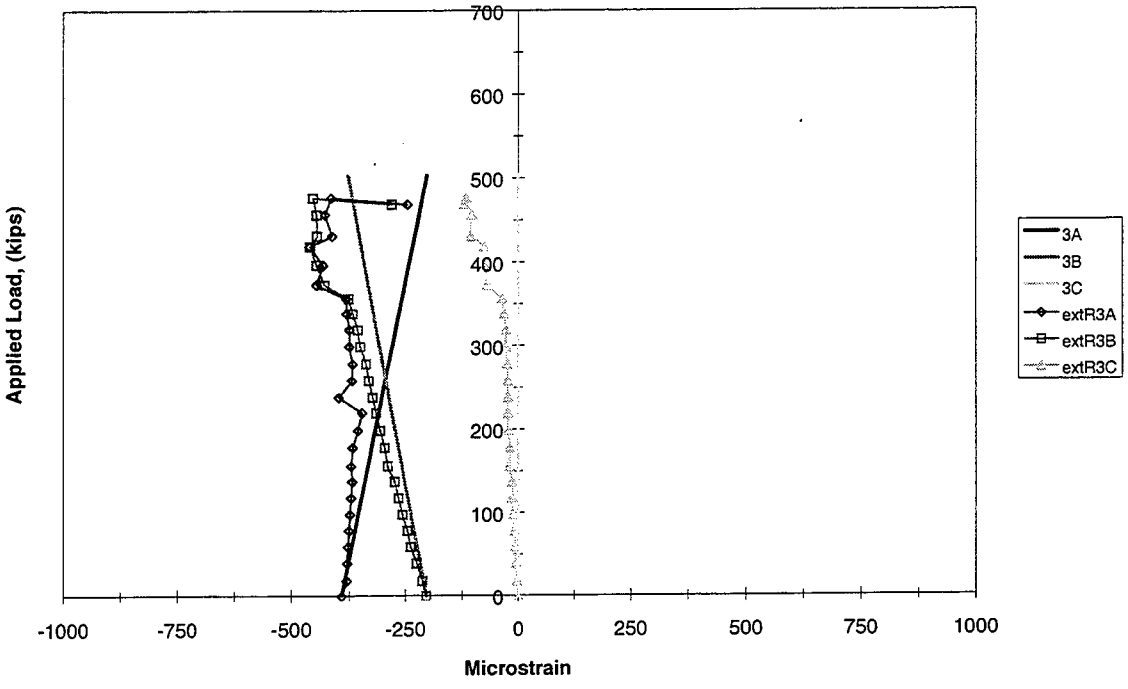

Figure 5.42 Corrected Rosette 3 (End IA)

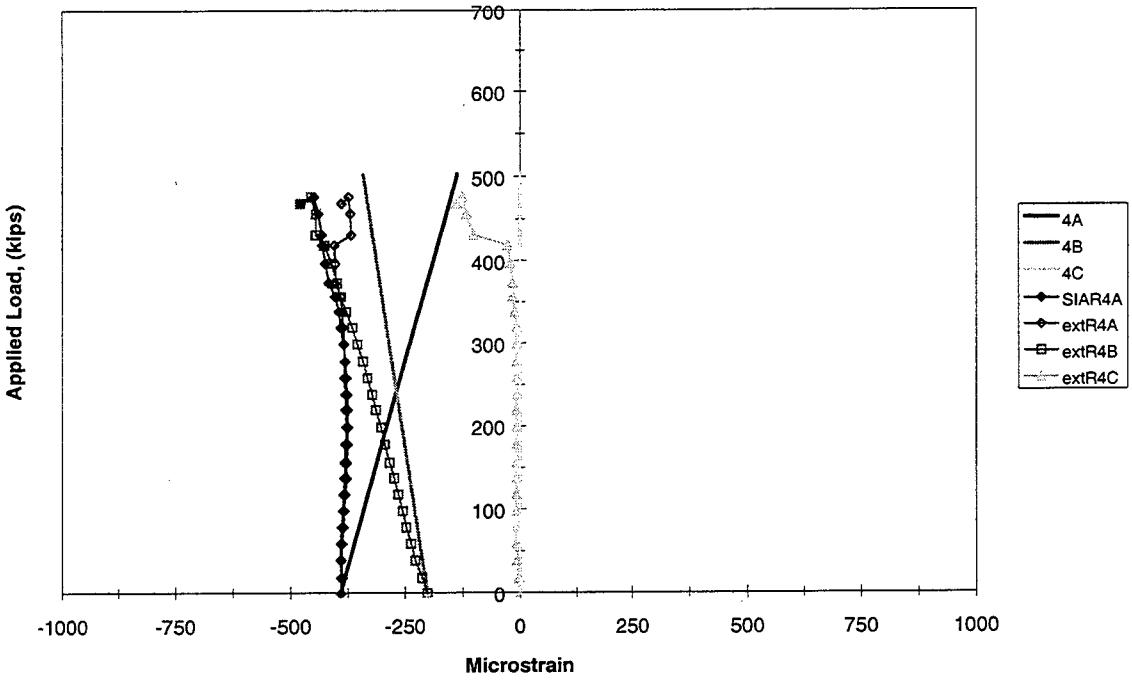

Figure 5.43 Corrected Rosette 4 (End IA)

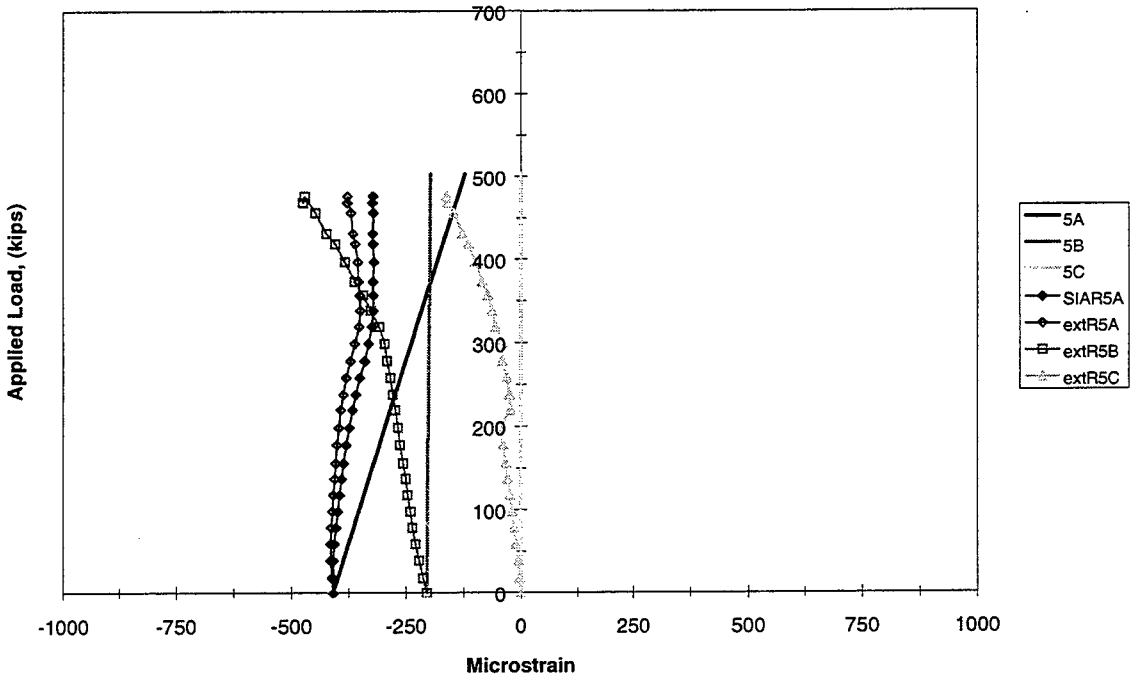

Figure 5.44 Corrected Rosette 5 (End IA)

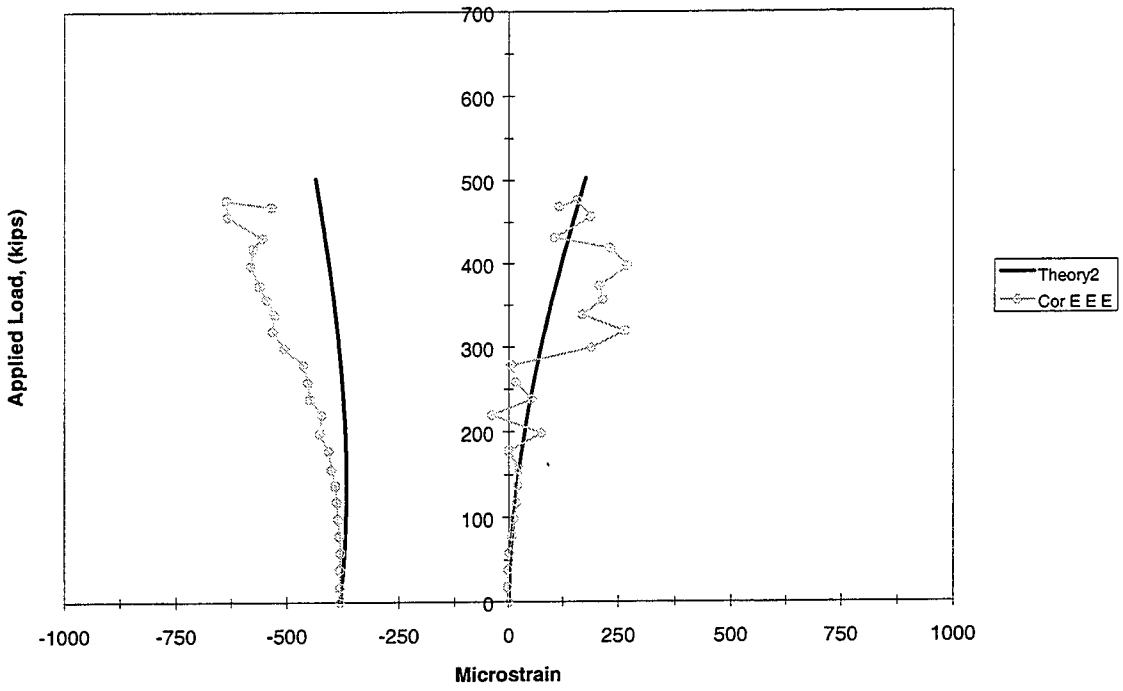

Figure 5.45 Corrected Principal Strains Rosette 2 (End IA)

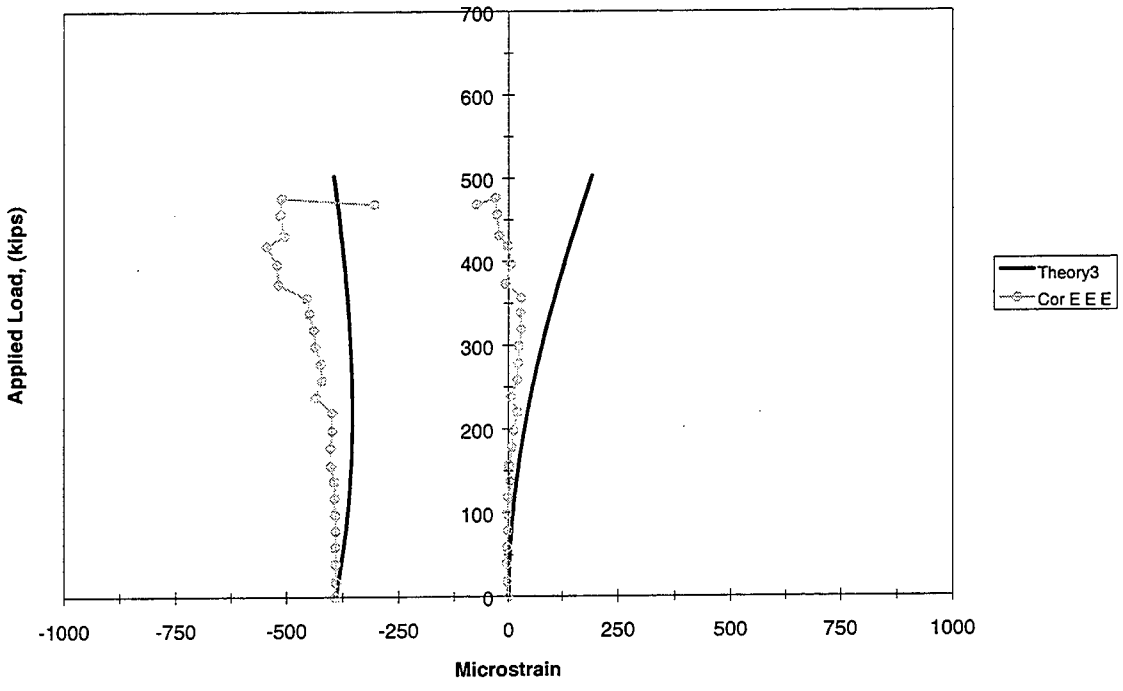

Figure 5.46 Corrected Principal Strains Rosette 3 (End IA)

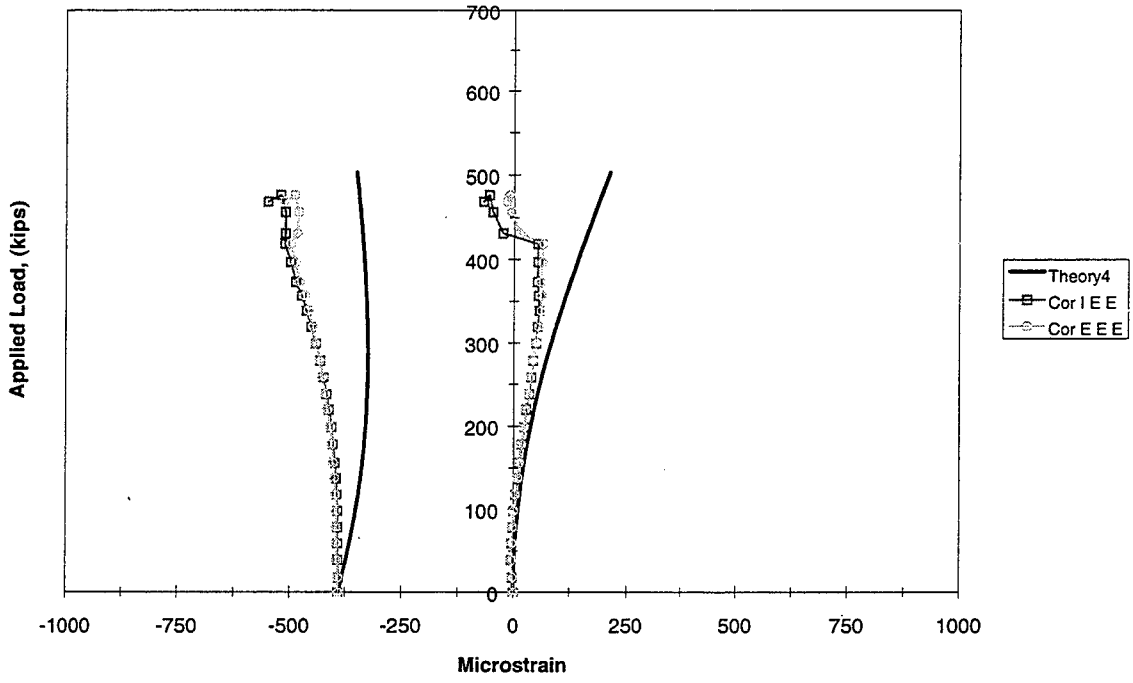

Figure 5.47 Corrected Principal Strains Rosette 4 (End IA)

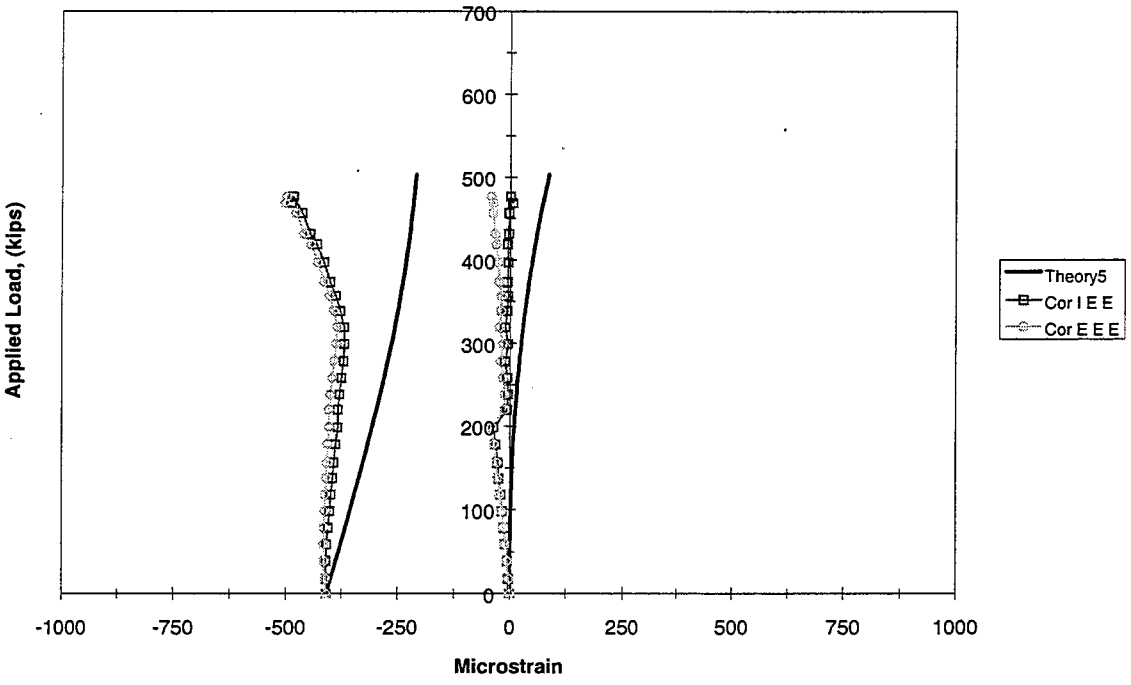

Figure 5.48 Corrected Principal Strains Rosette 5 (End IA)

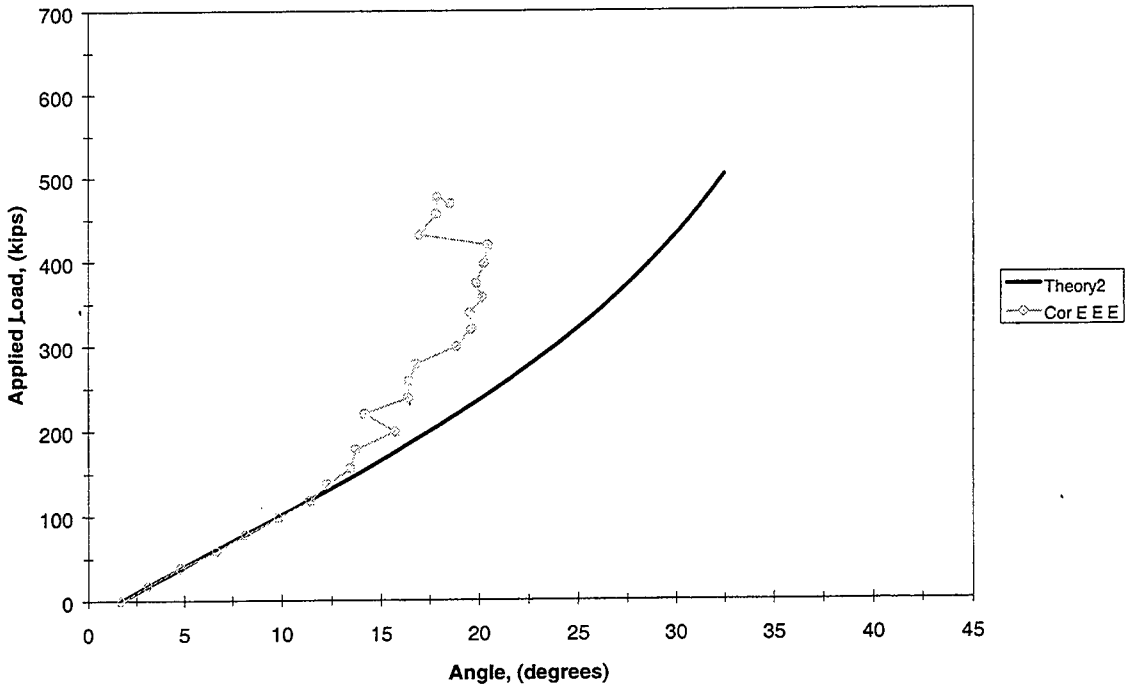

Figure 5.49 Corrected Principal Compression Angle Rosette 2 (End IA)

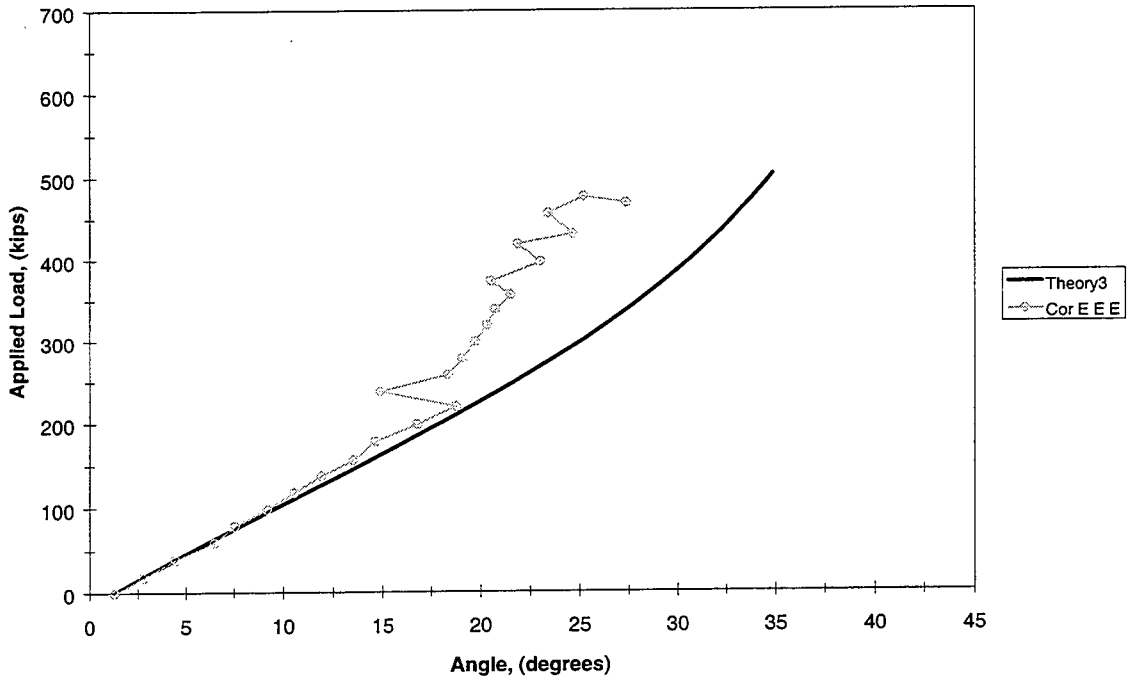

Figure 5.50 Corrected Principal Compression Angle Rosette 3 (End IA)

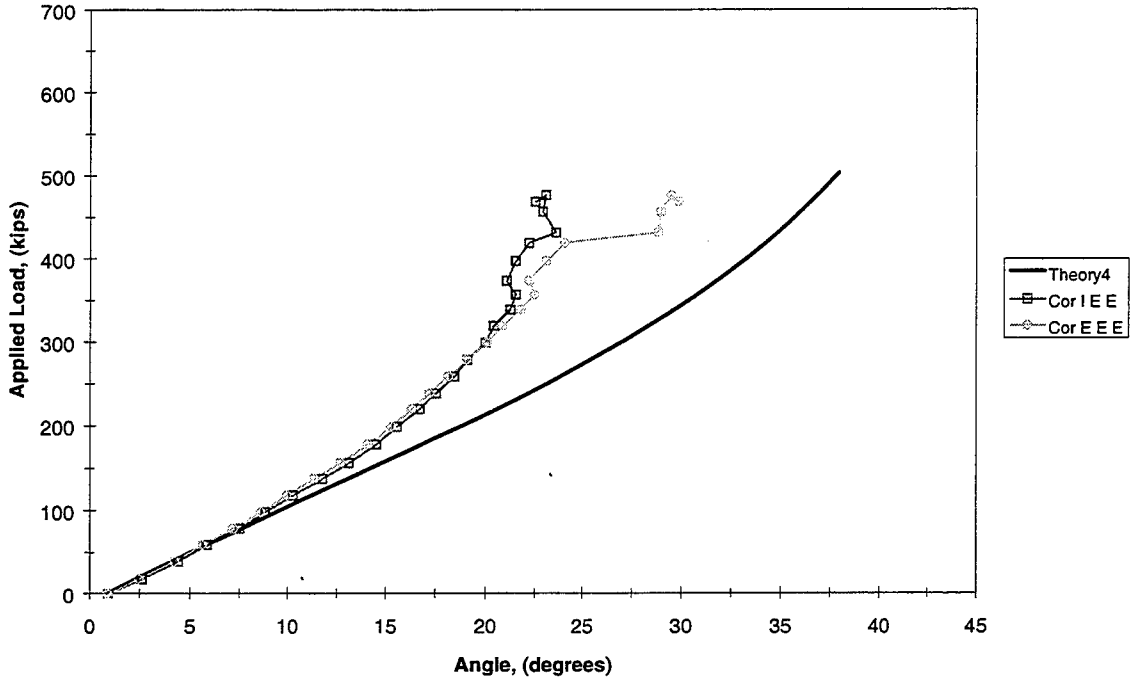

Figure 5.51 Corrected Principal Compression Angle Rosette 4 (End IA)

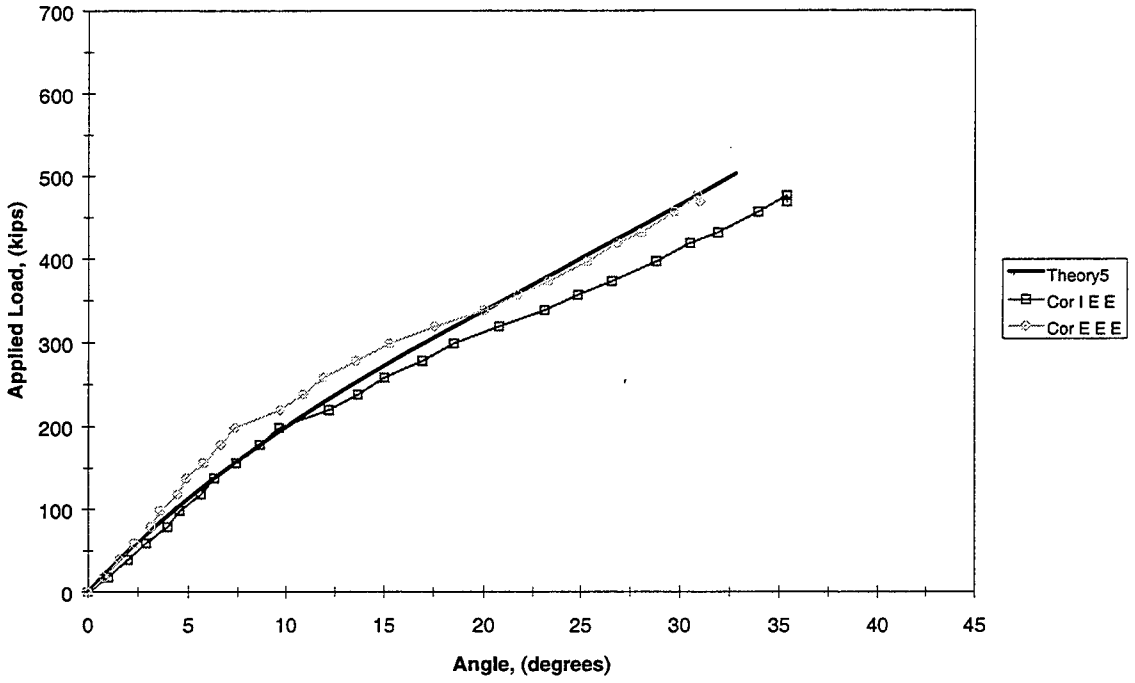

Figure 5.52 Corrected Principal Compression Angle Rosette 5 (End IA)

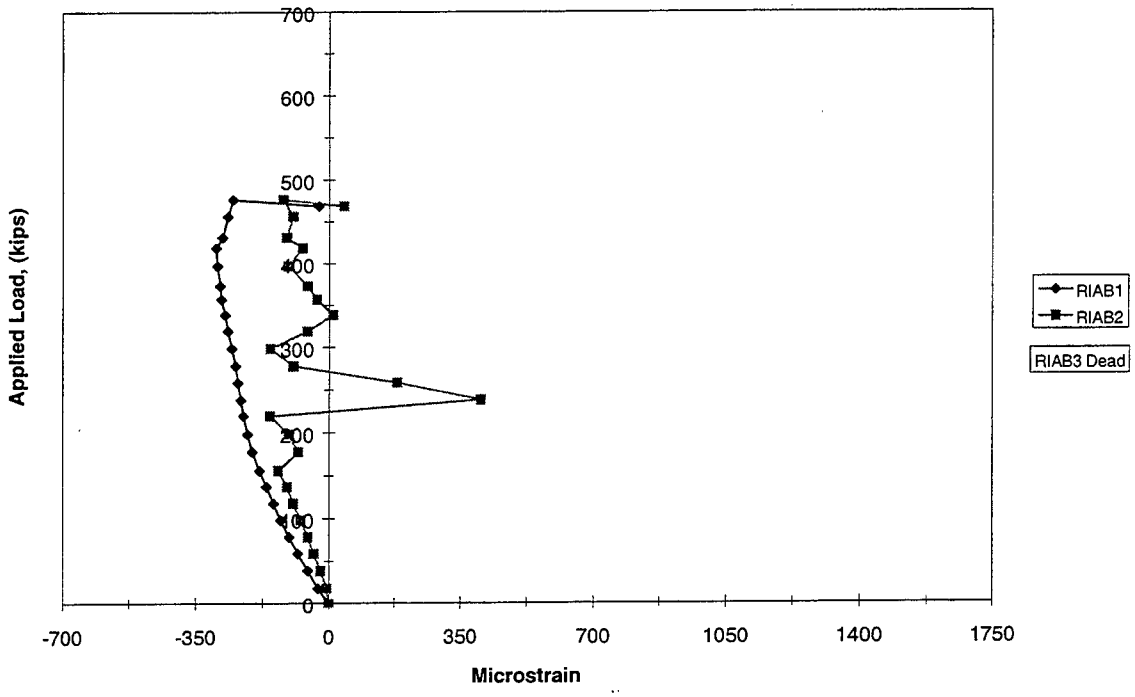

Figure 5.53 Bursting Stirrup (End IA)

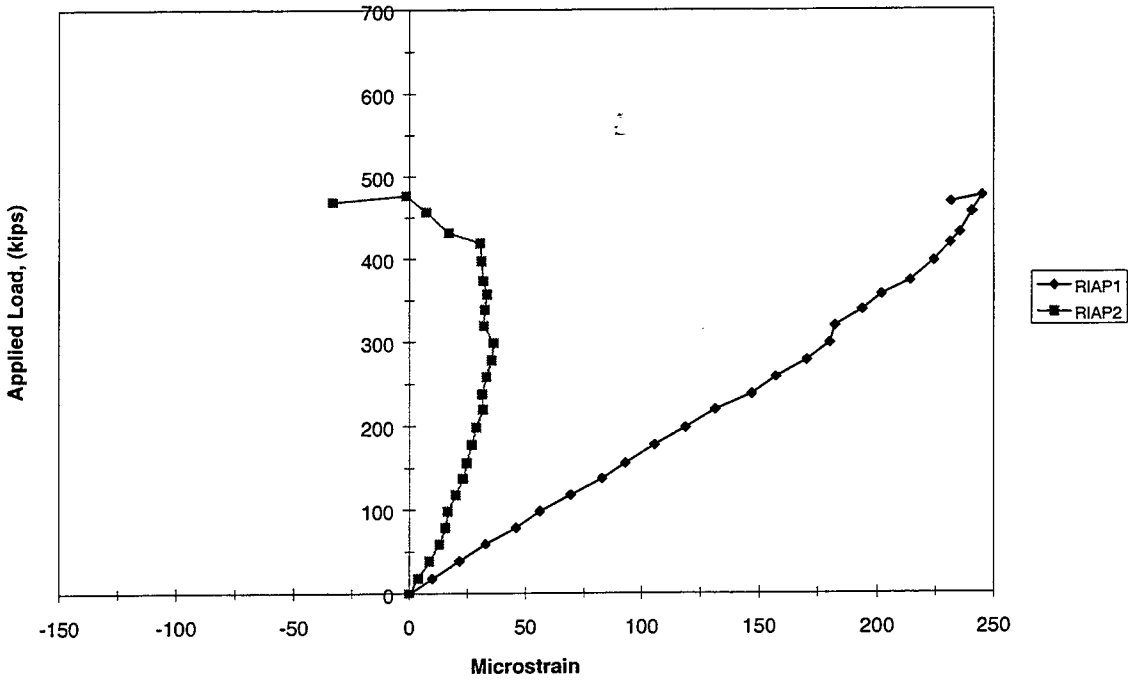

Figure 5.54 Rupture of Concrete (End IA)

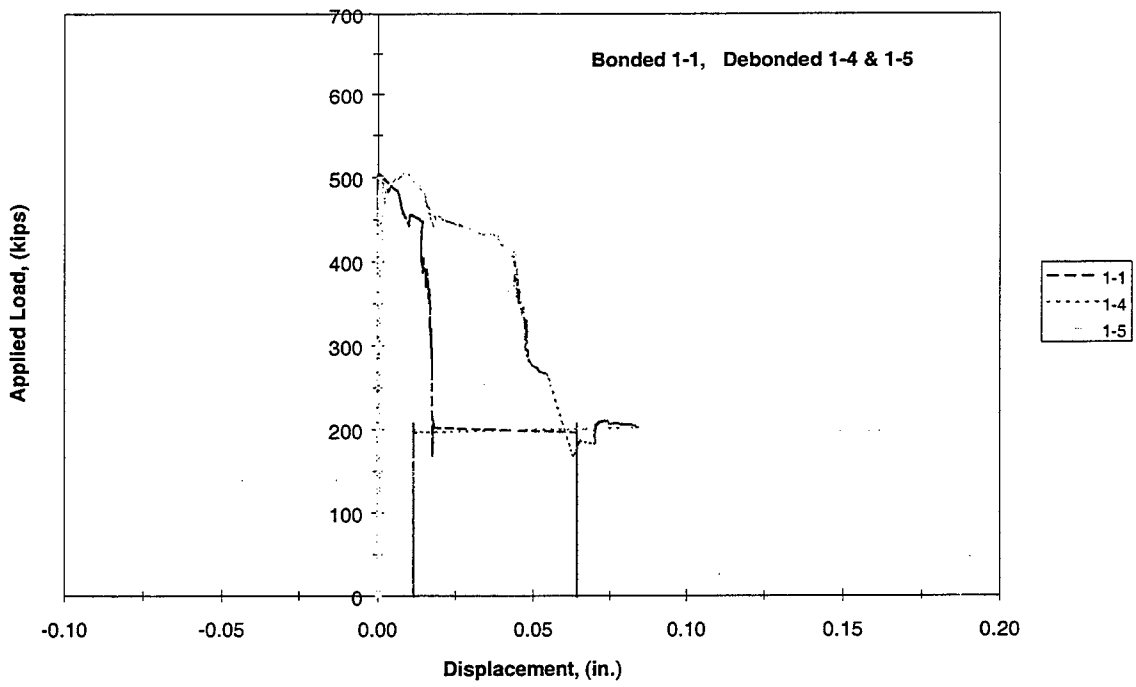

Figure 5.55 Strand Slip for 1-1, 1-4, & 1-5 (End IA)

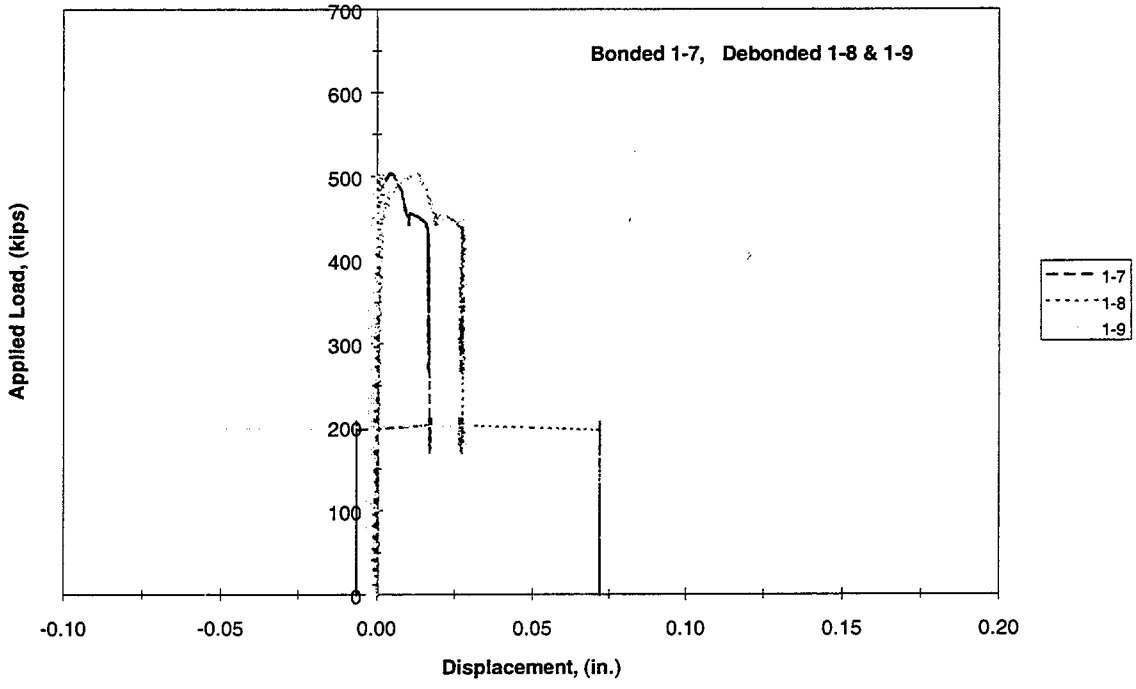

Figure 5.56 Strand Slip for 1-7, 1-8, & 1-9 (End IA)

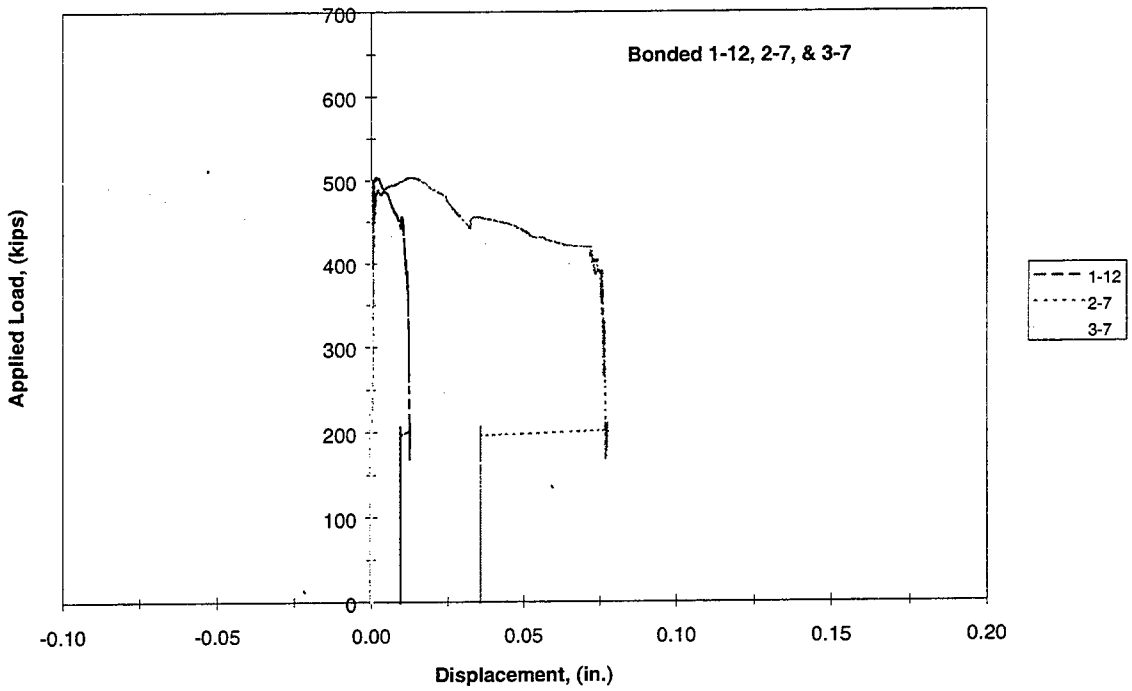

Figure 5.57 Strand Slip for 1-12, 2-7, & 3-7 (End IA)

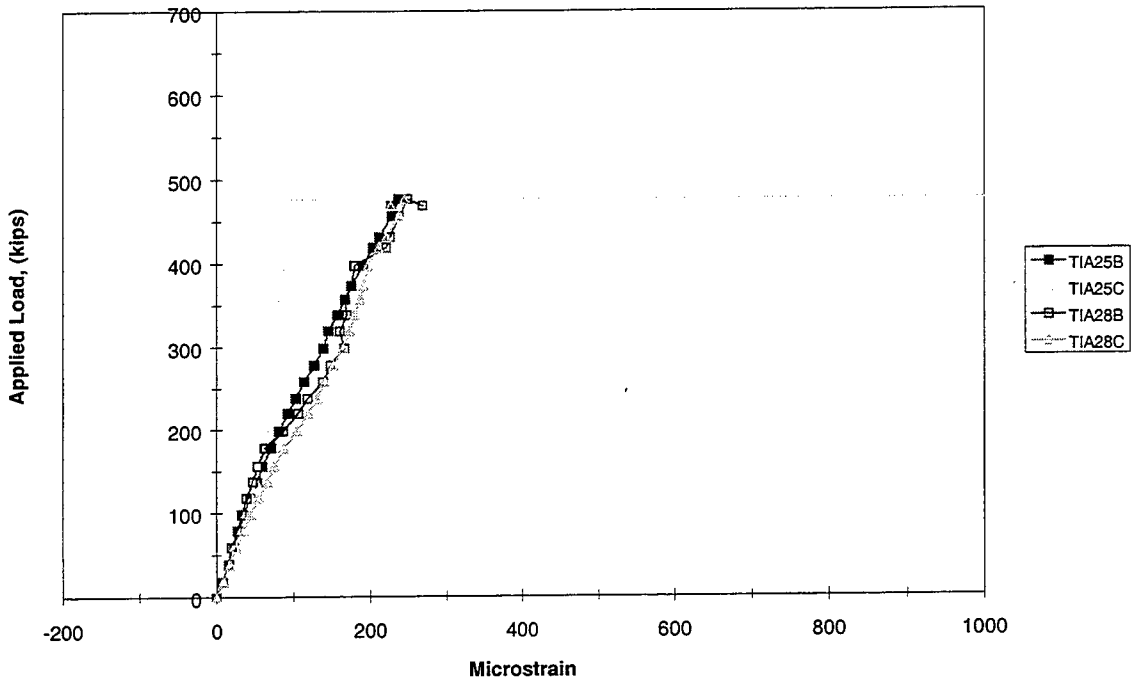

Figure 5.58 Transfer Length 2 ft. (End IA)

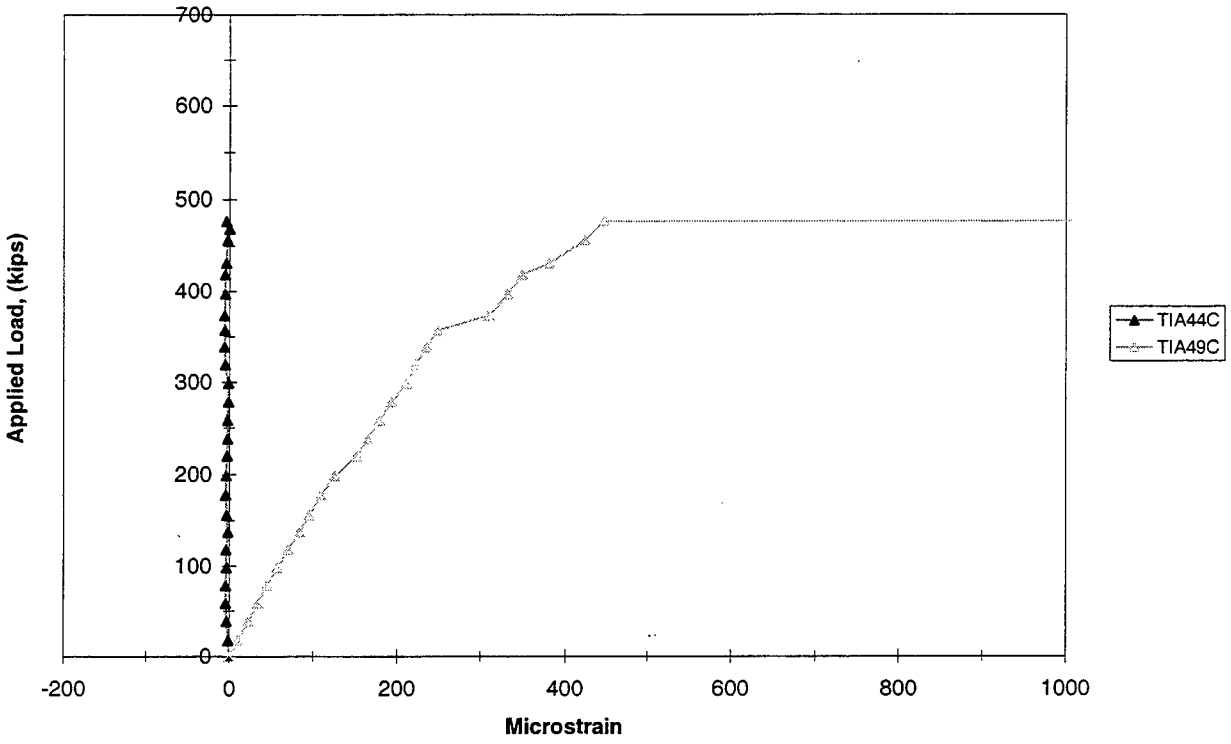

Figure 5.59 Transfer Length 4 ft. (End IA)

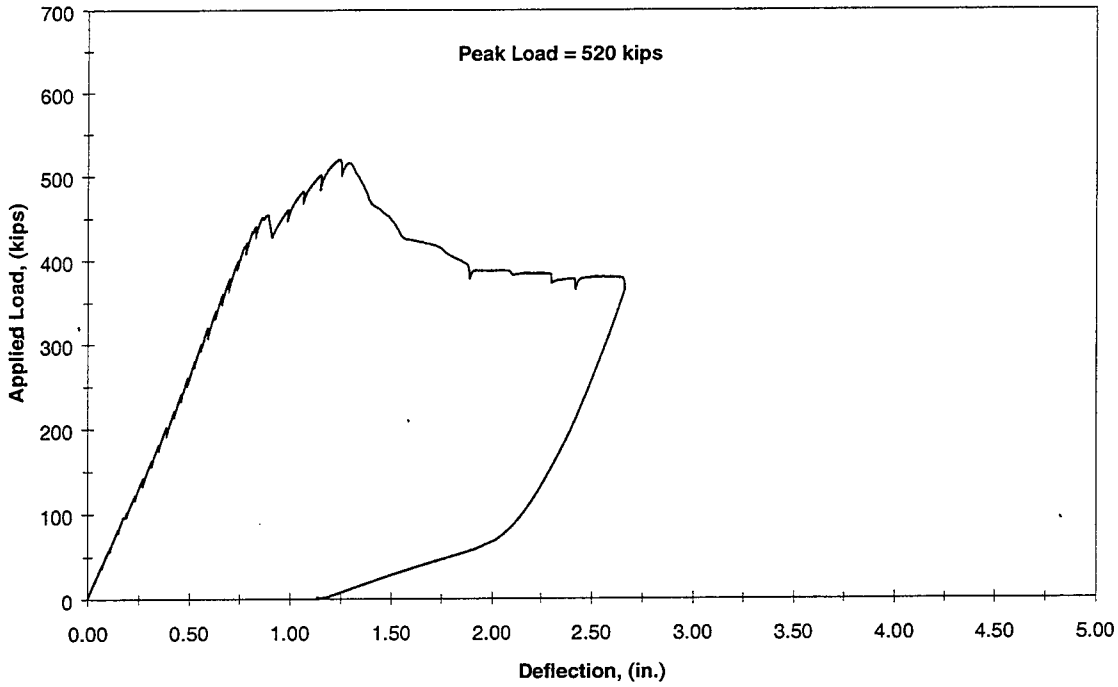

Figure 5.60 Corrected West Load Deflection (End IB)

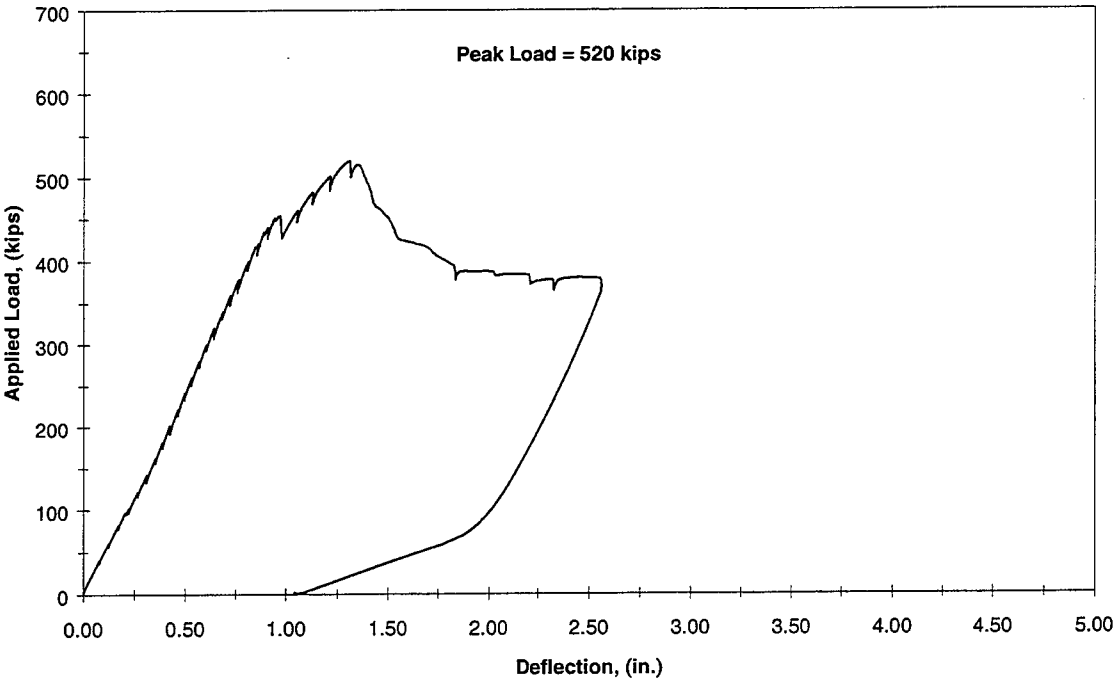

Figure 5.61 Corrected East Load Deflection (End IB)

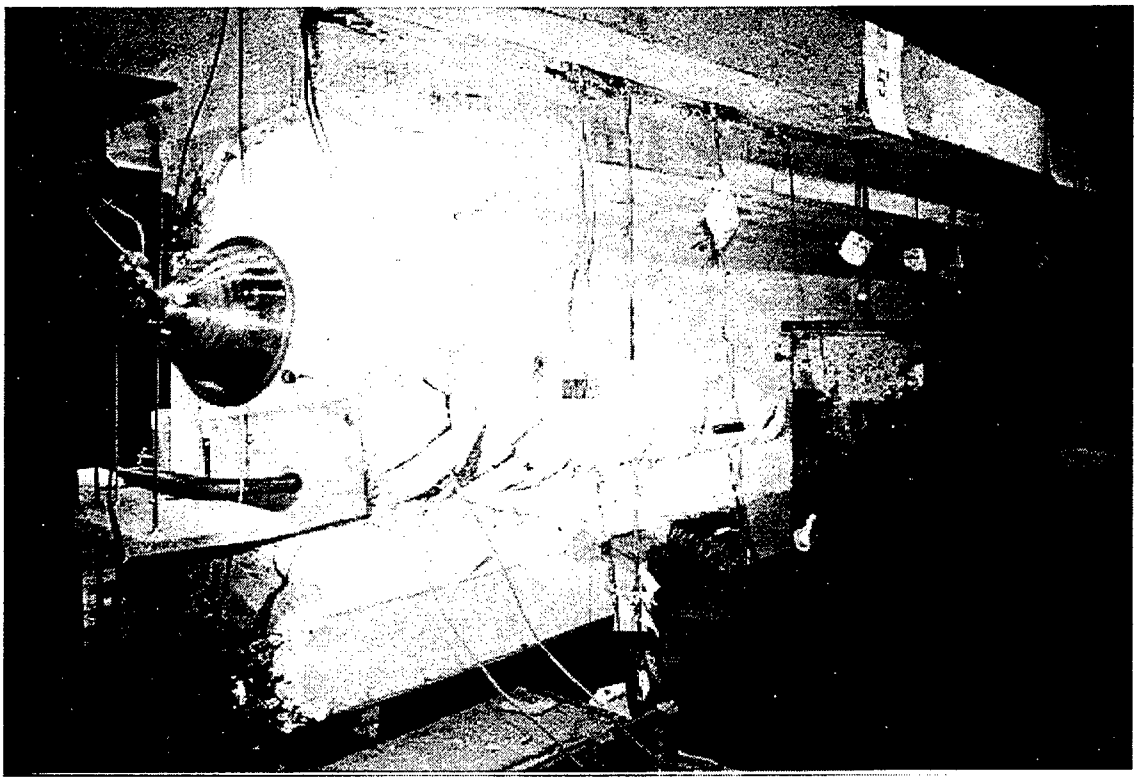

Figure 5.62 After Peak Load, Cracking Near Support (End IB)

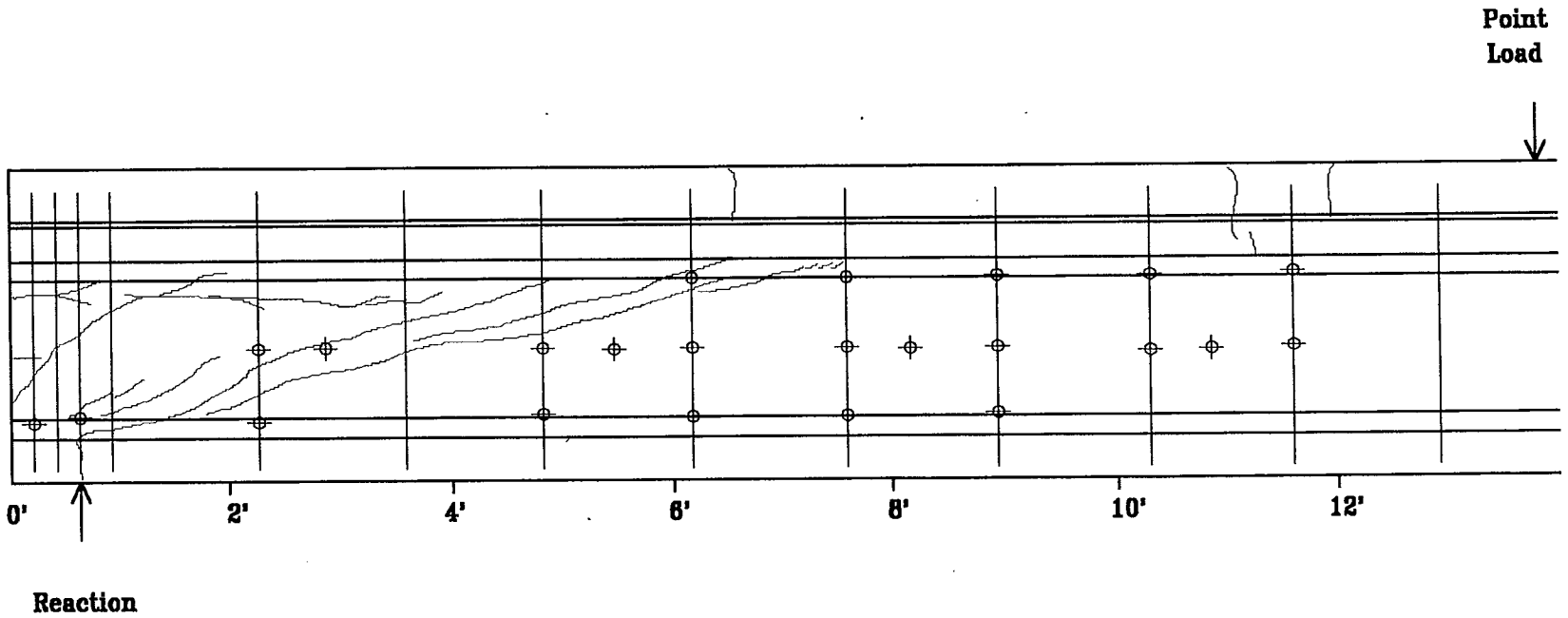

Figure 5.63 Before Testing, Crack Drawing (End IB)

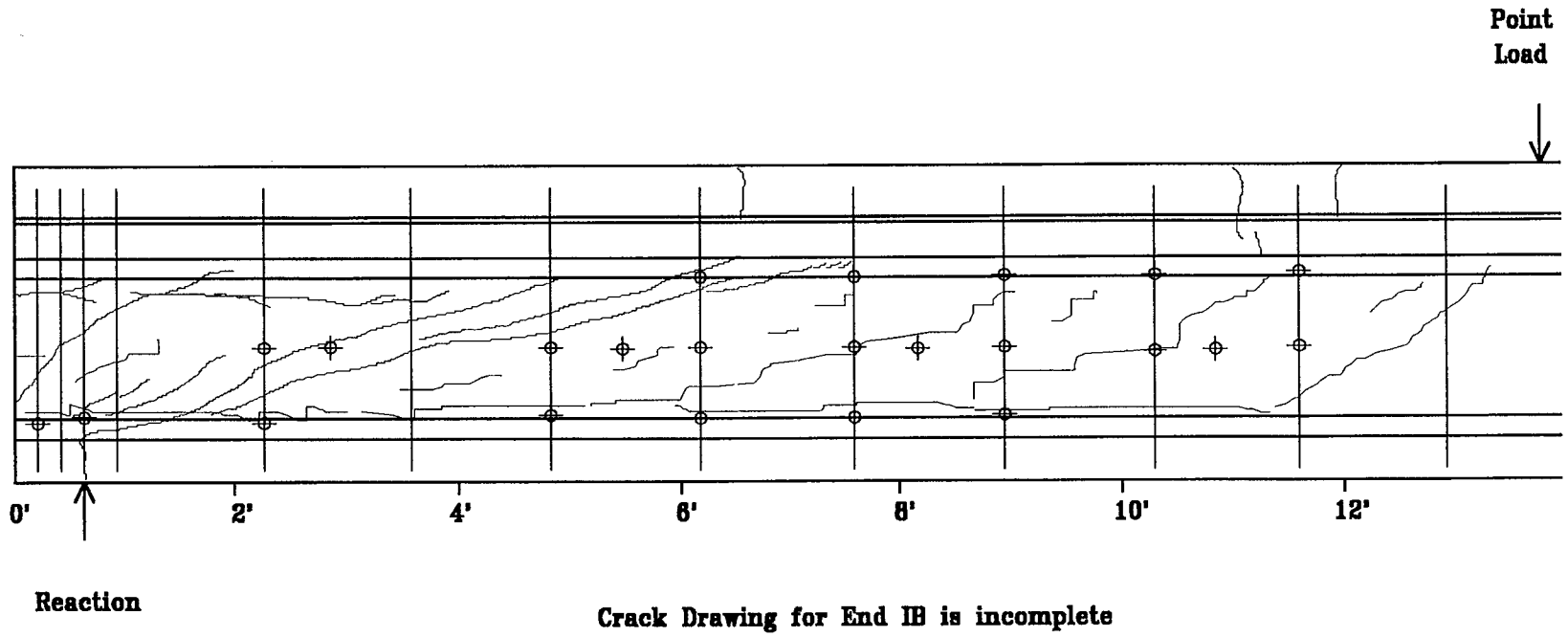

Figure 5.64 After Peak Load, Crack Drawing (End IB)

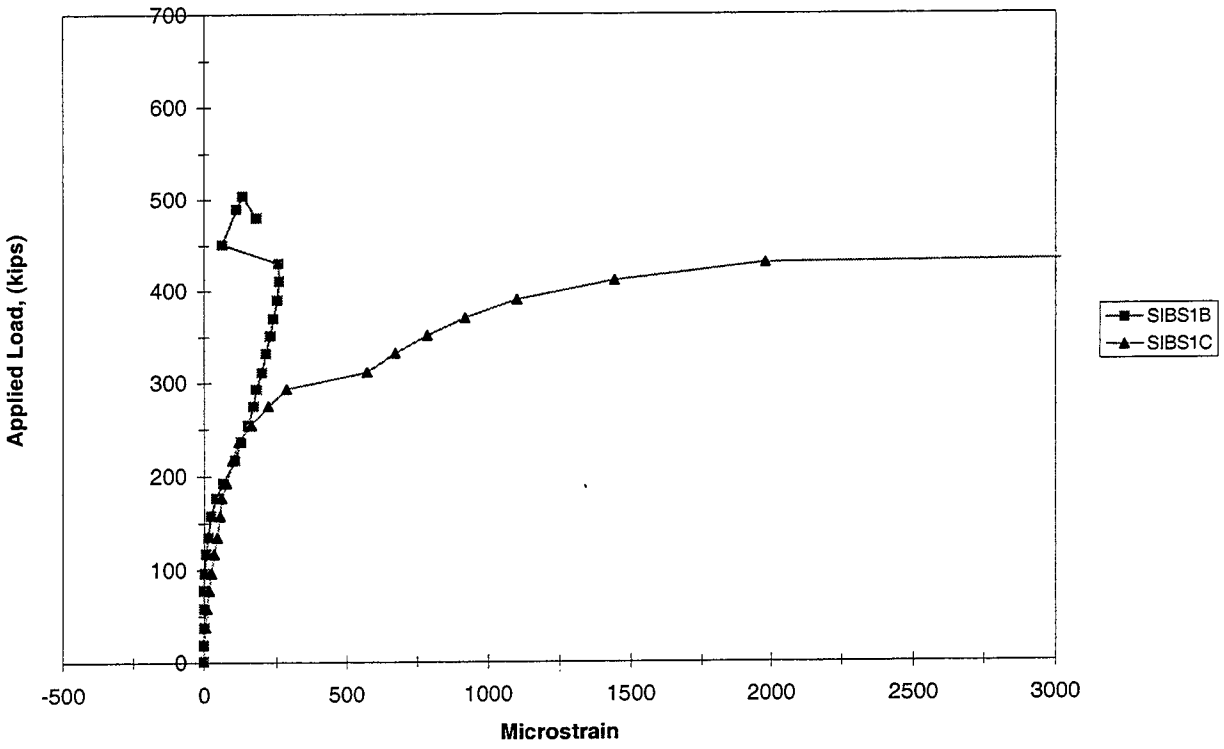

Figure 5.65 Stirrup 1 (End IB)

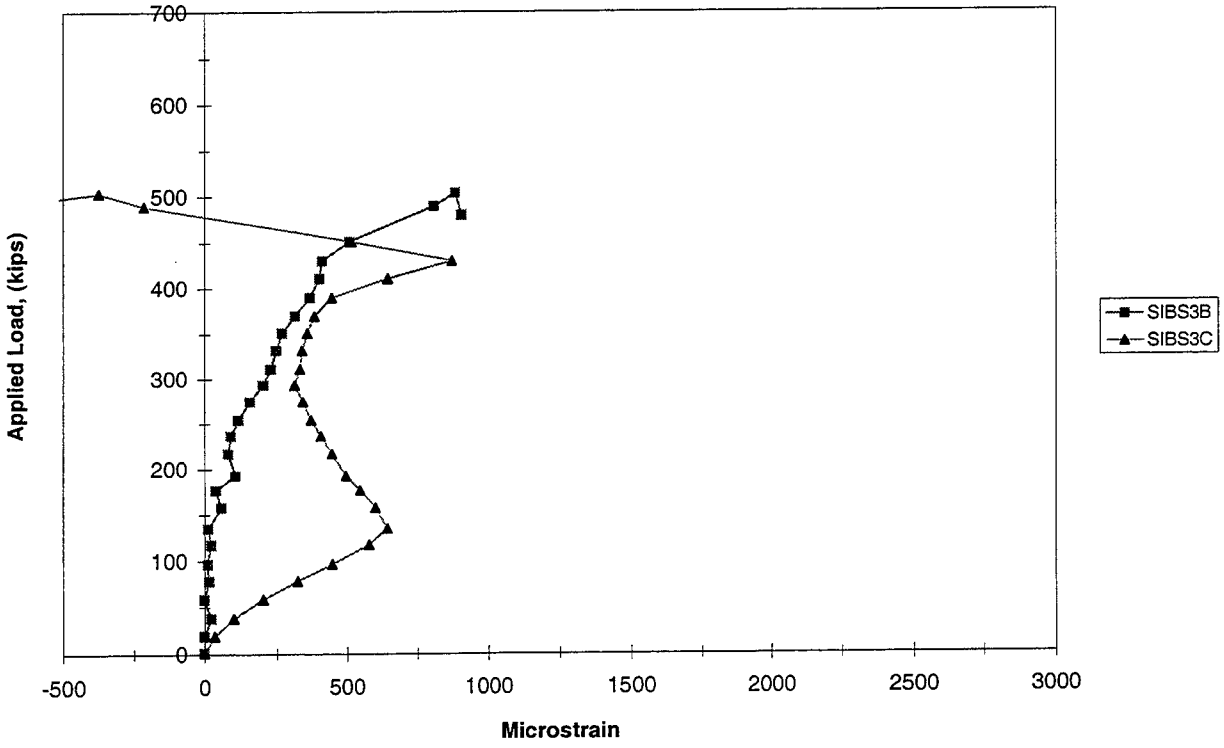

Figure 5.66 Stirrup 3 (End IB)

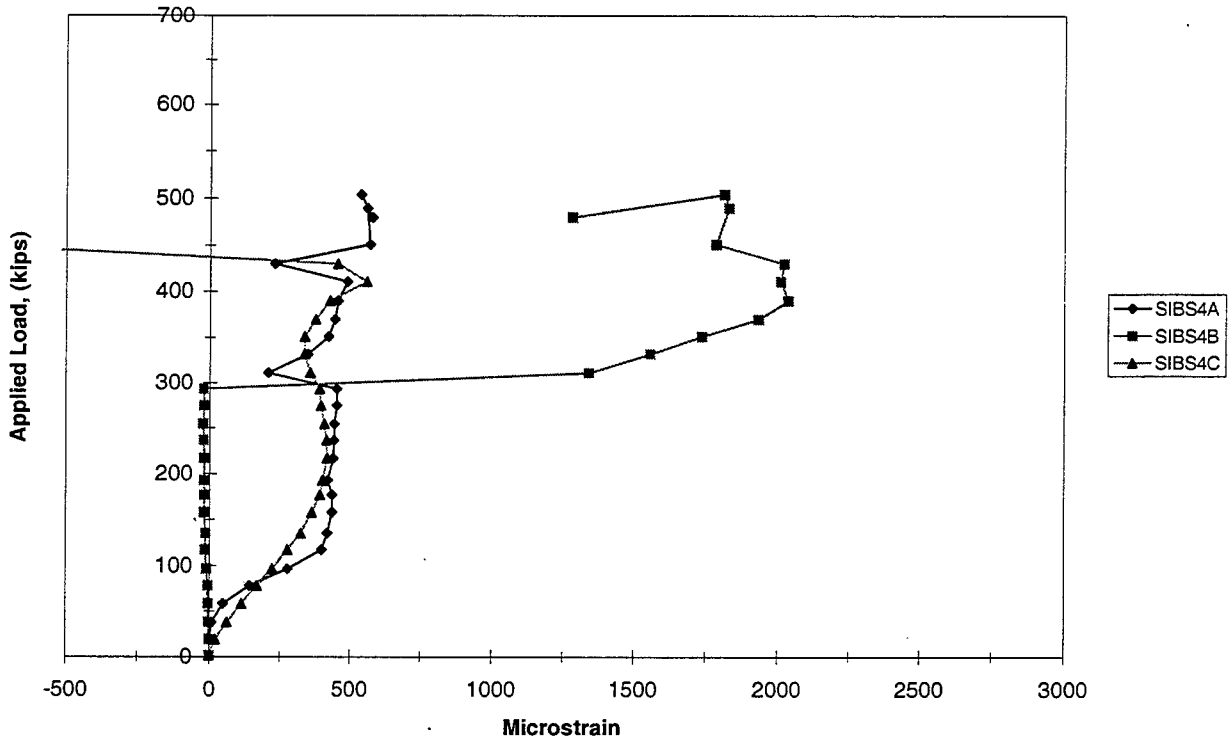

Figure 5.67 Stirrup 4 (End IB)

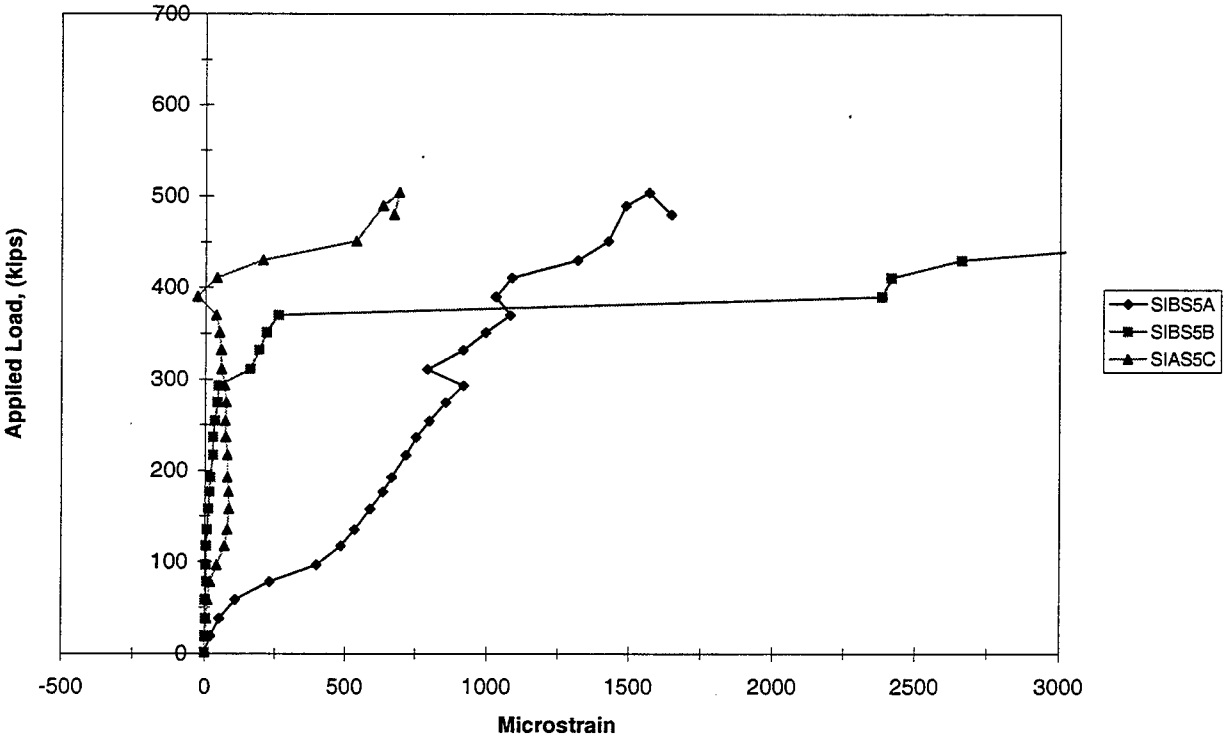

Figure 5.68 Stirrup 5 (End IB)

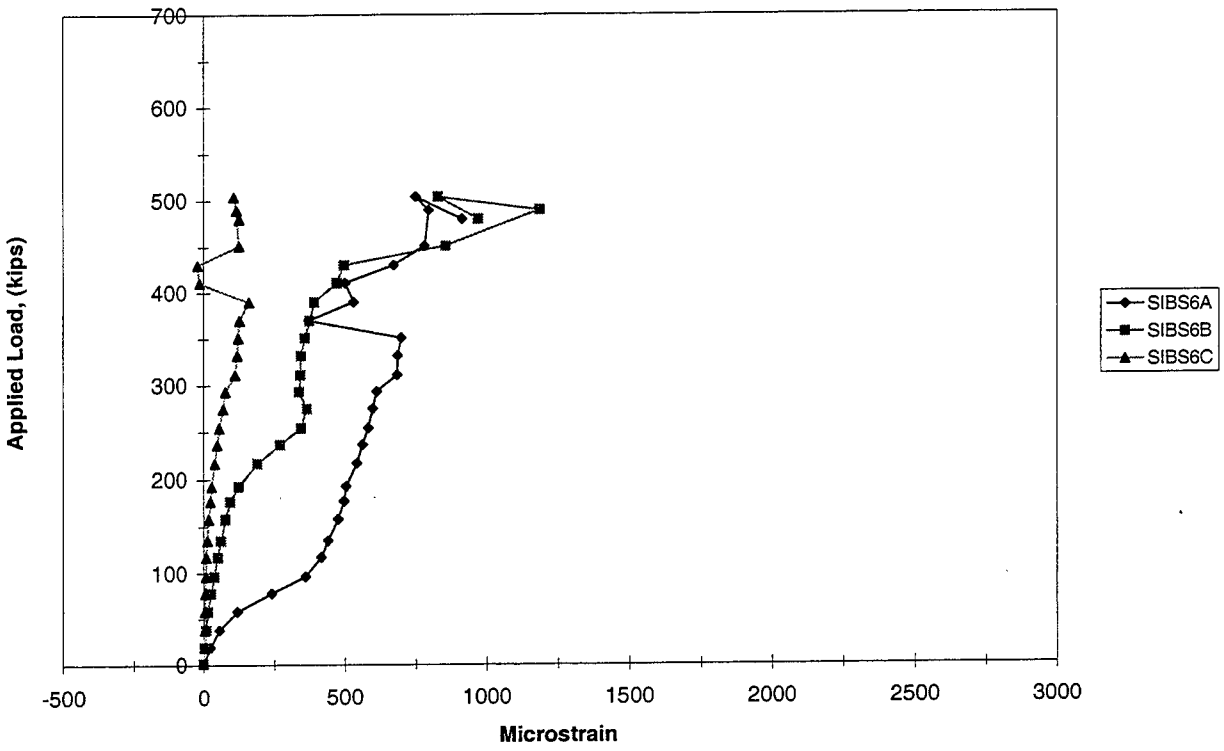

Figure 5.69 Stirrup 6 (End IB)

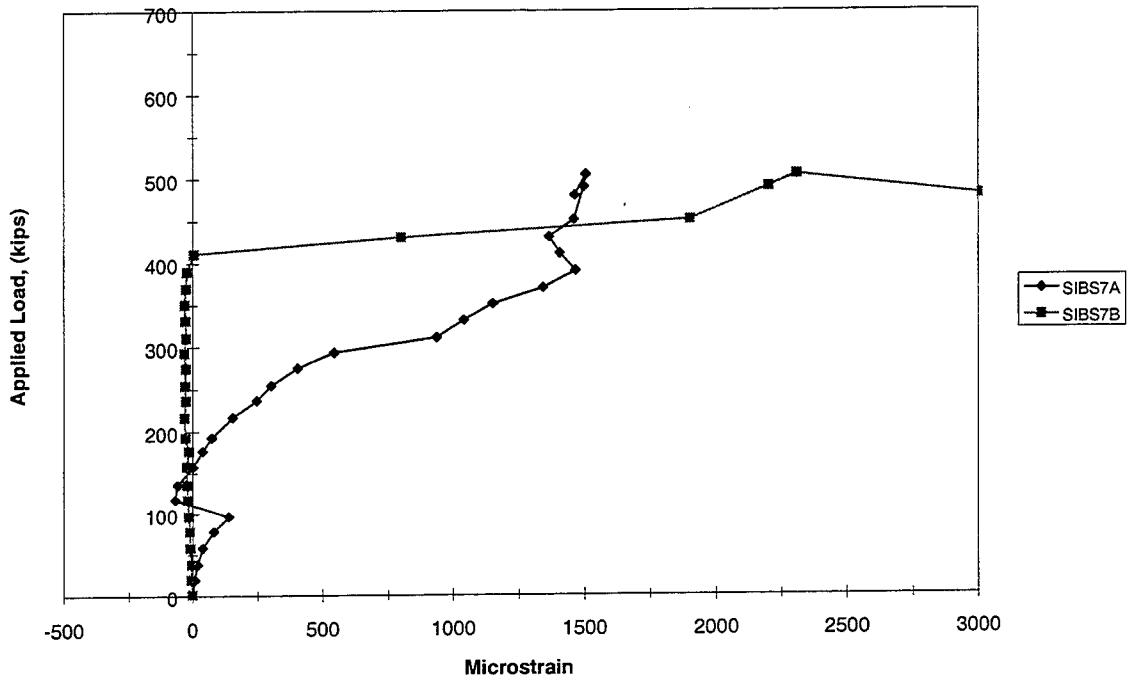

Figure 5.70 Stirrup 7 (End IB)

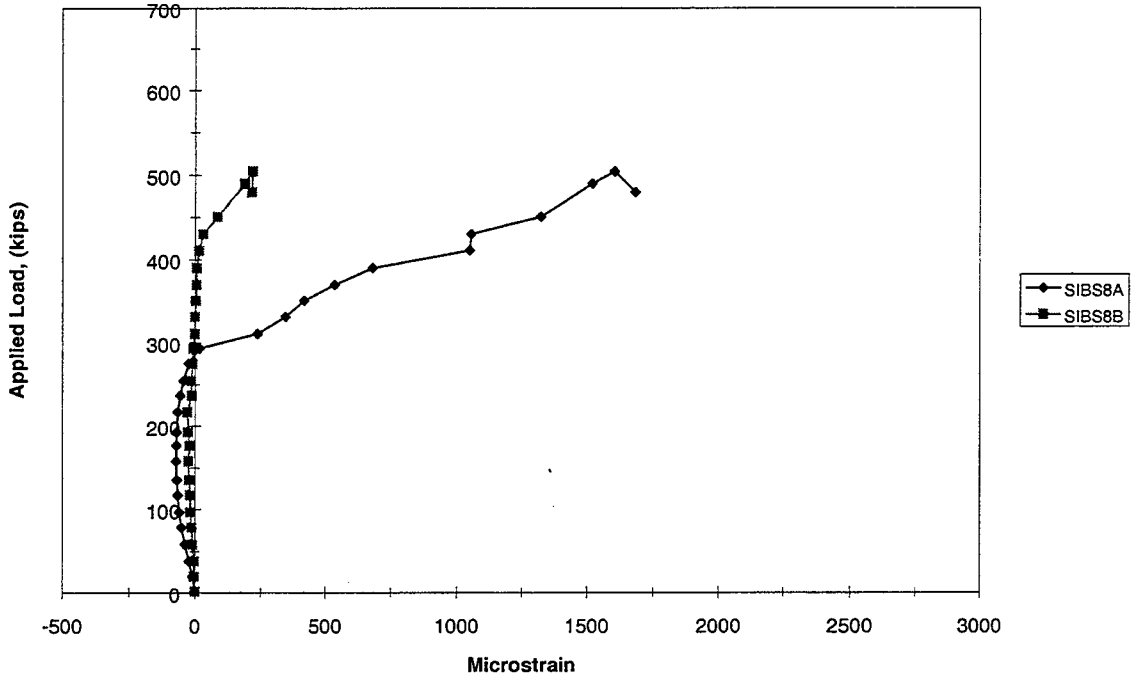

Figure 5.71 Stirrup 8 (End IB)

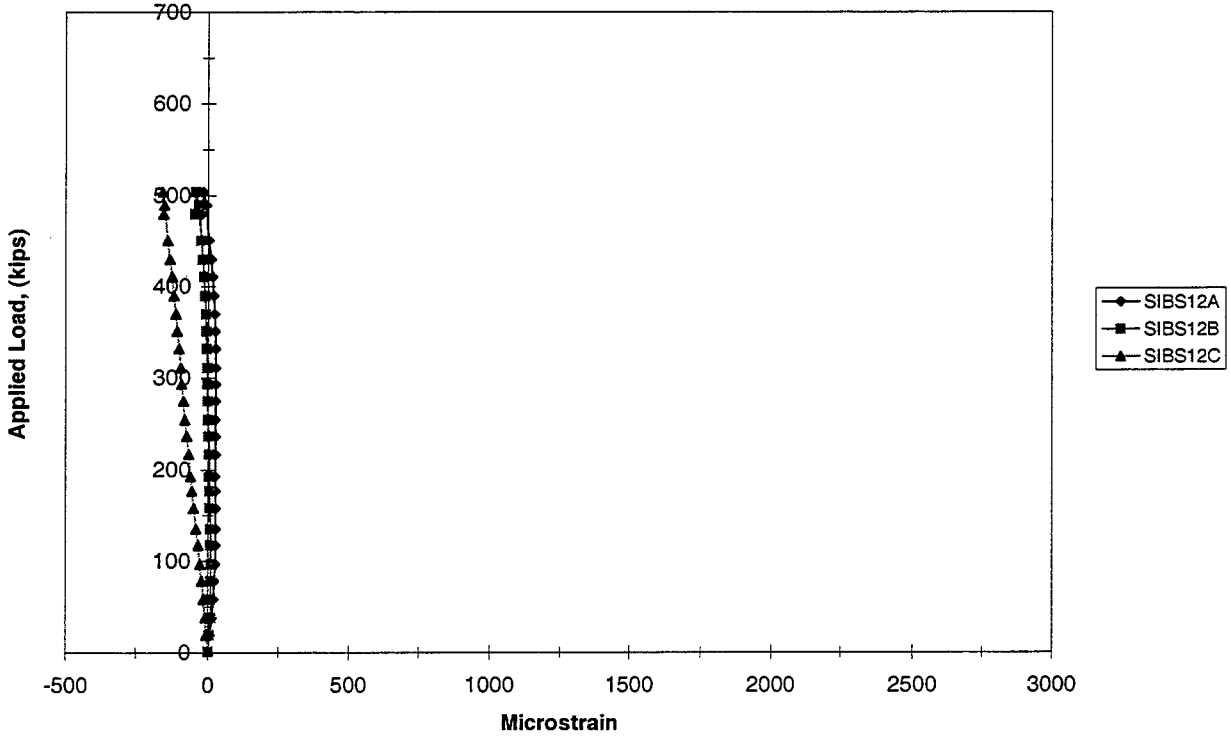

Figure 5.72 Stirrup 12 (End IB)

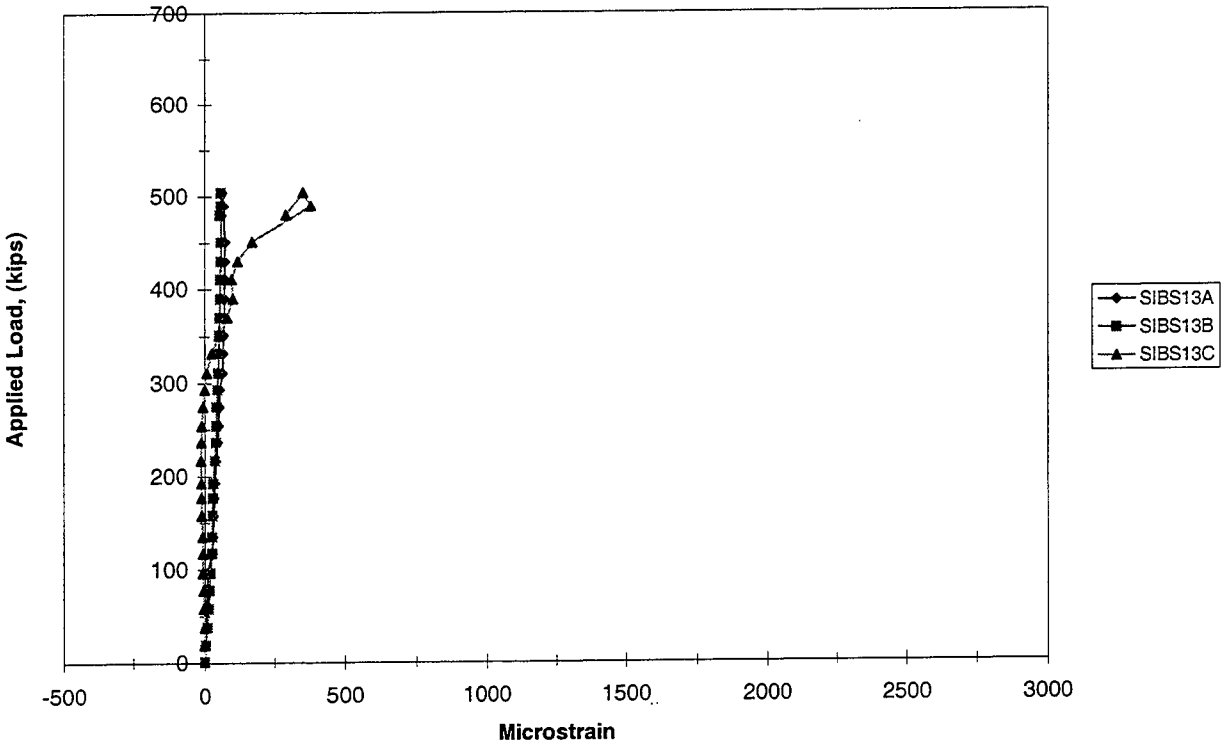

Figure 5.73 Stirrup 13 (End IB)

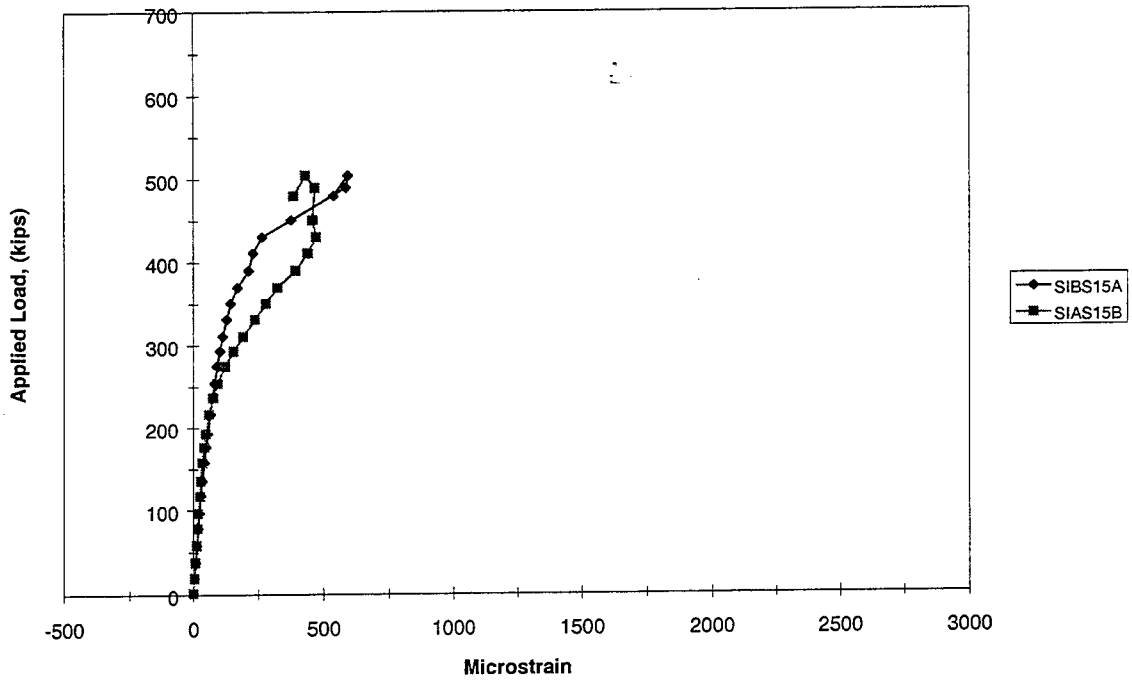

Figure 5.74 Stirrup 15 (End IB)

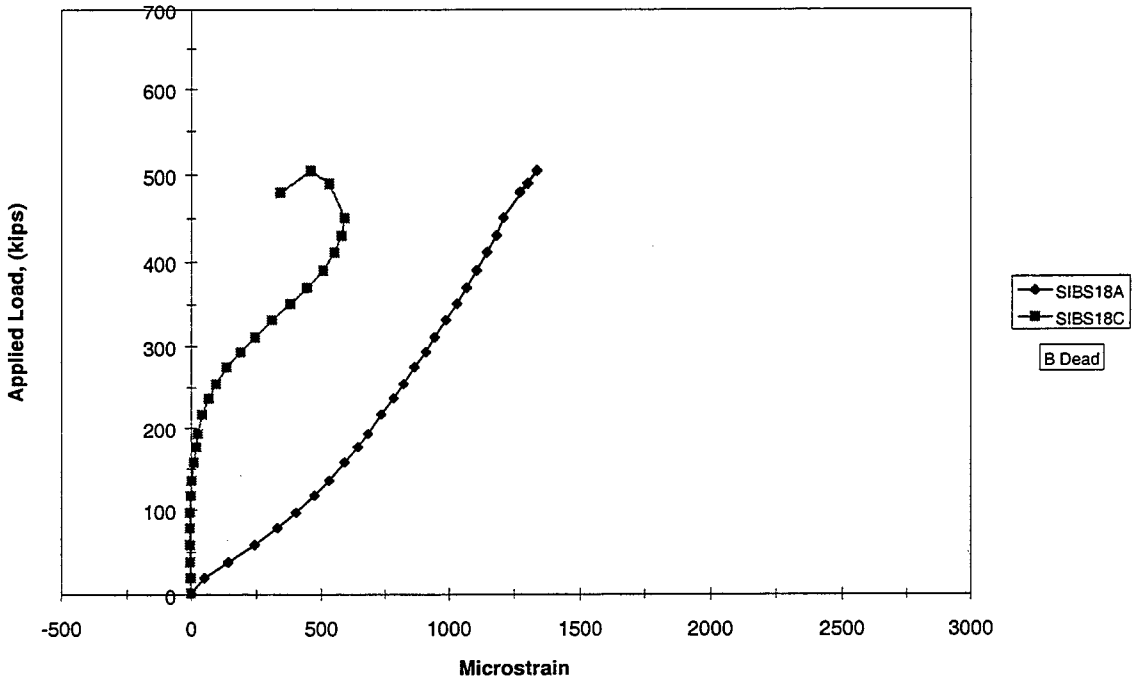

Figure 5.75 Stirrup 18 (End IB)

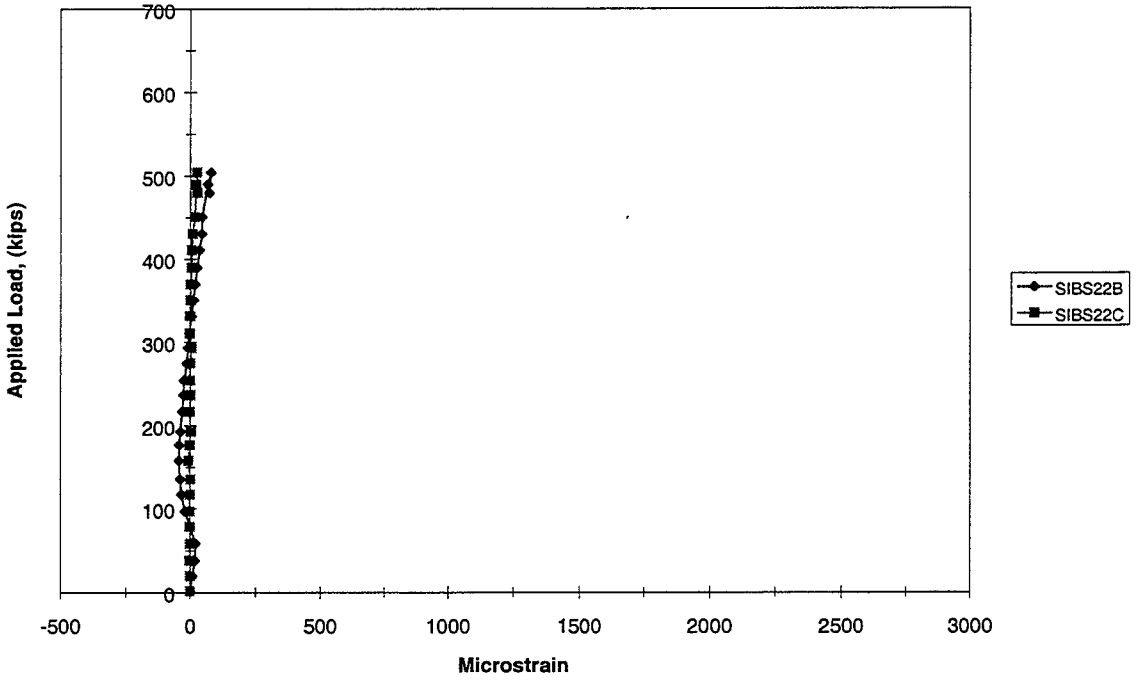

Figure 5.76 Stirrup 22 (End IB)

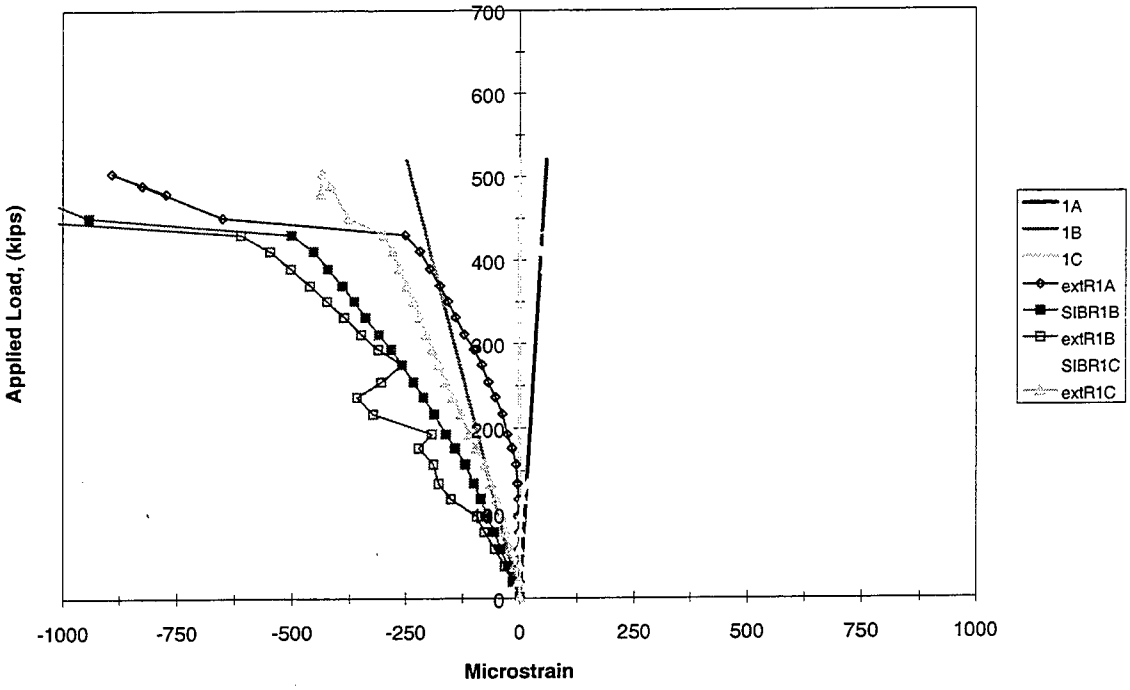

Figure 5.77 Rosette 1 (End IB)

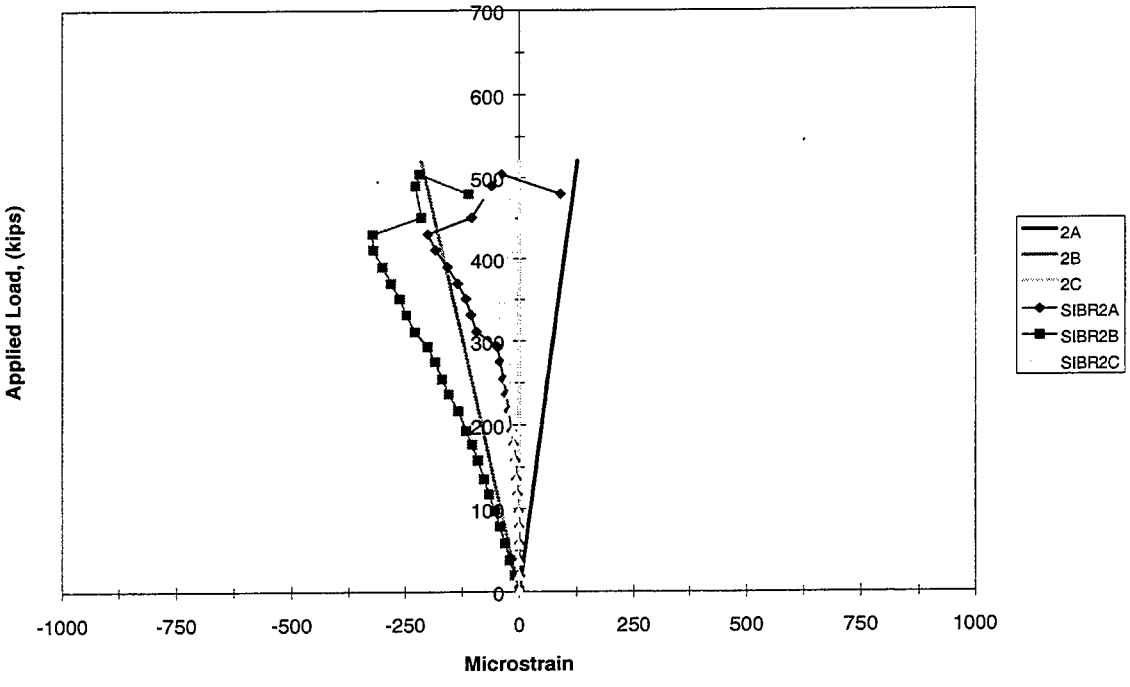

Figure 5.78 Rosette 2 (End IB)

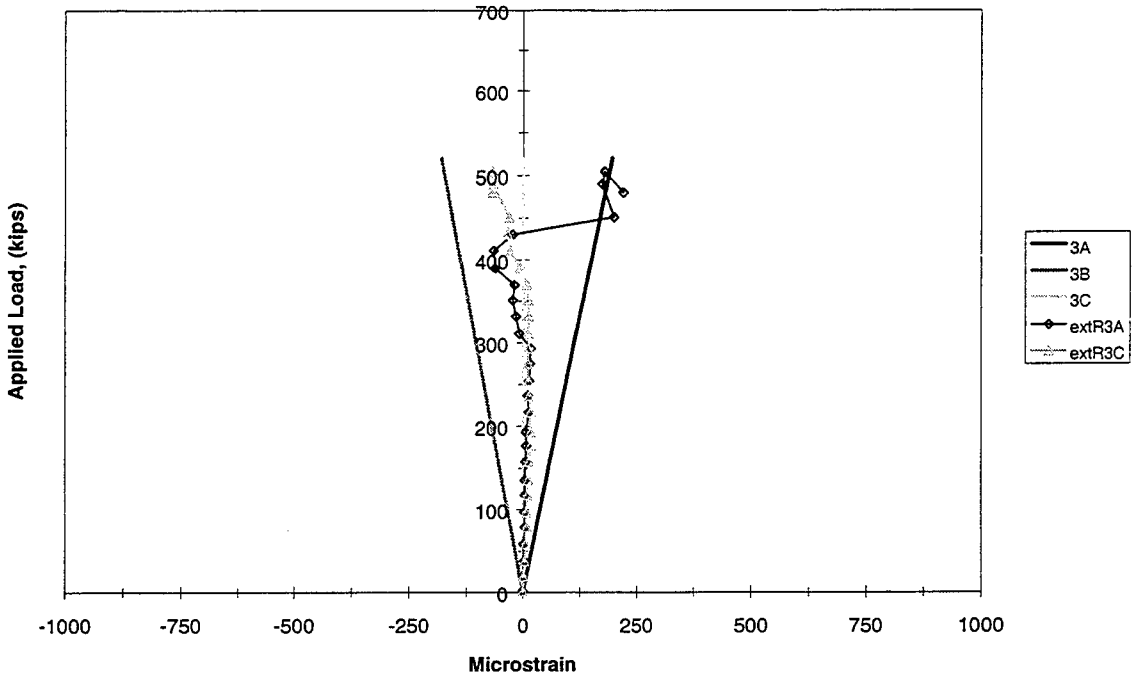

Figure 5.79 Rosette 3 (End IB)

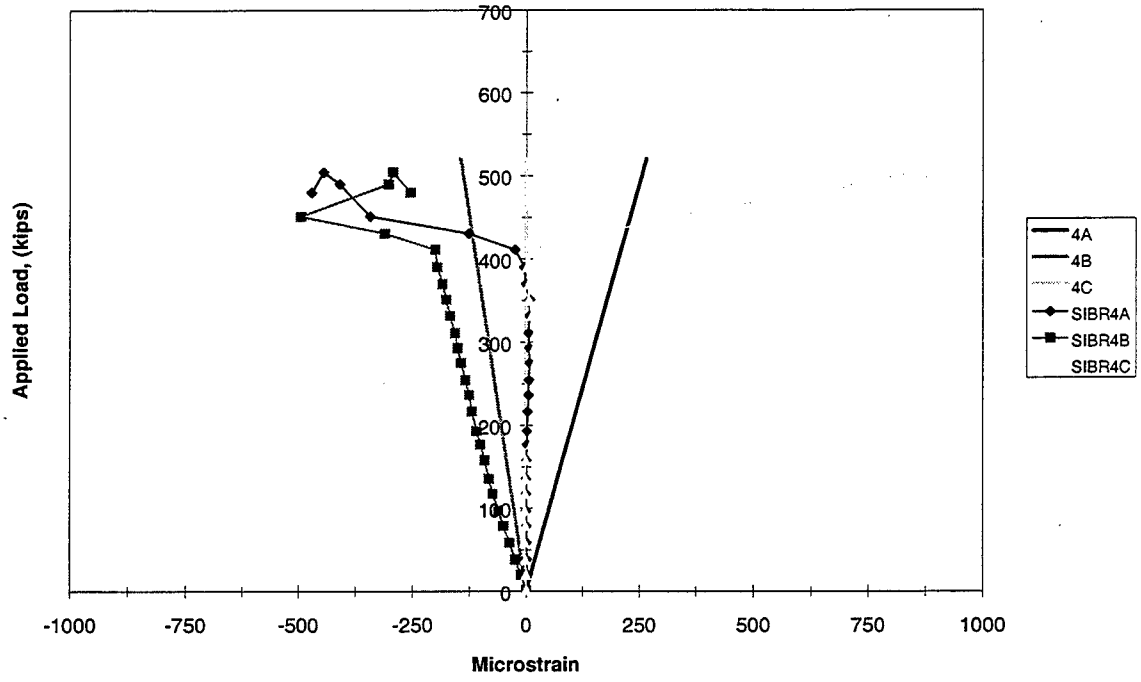

Figure 5.80 Rosette 4 (End IB)

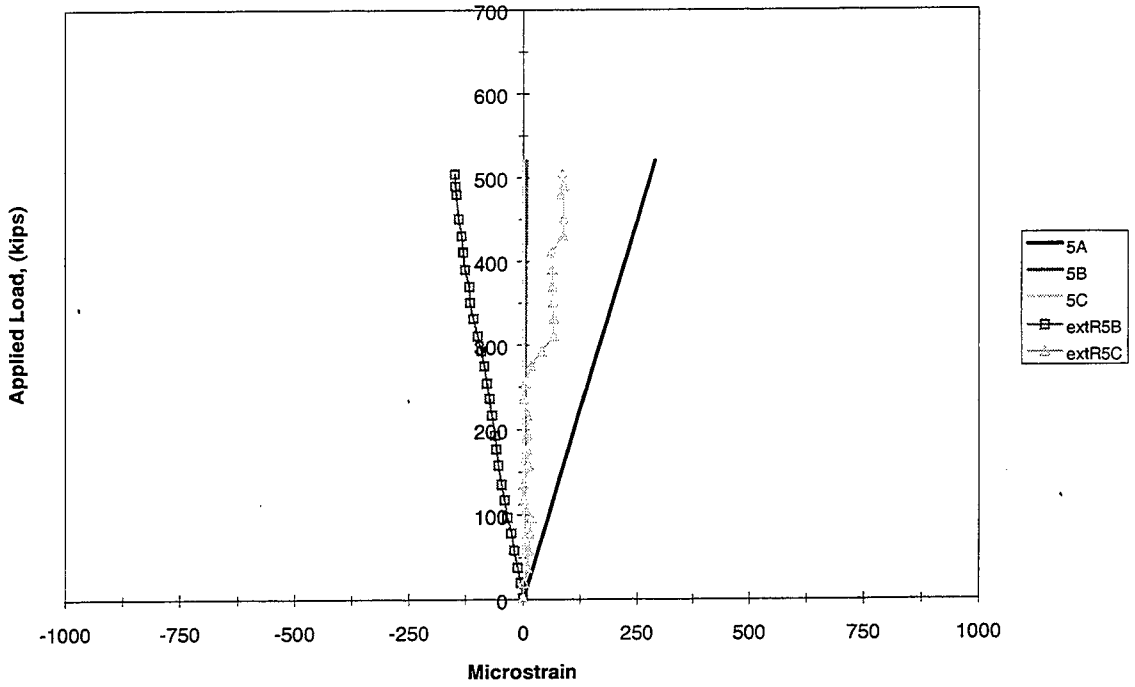

Figure 5.81 Rosette 5 (End IB)

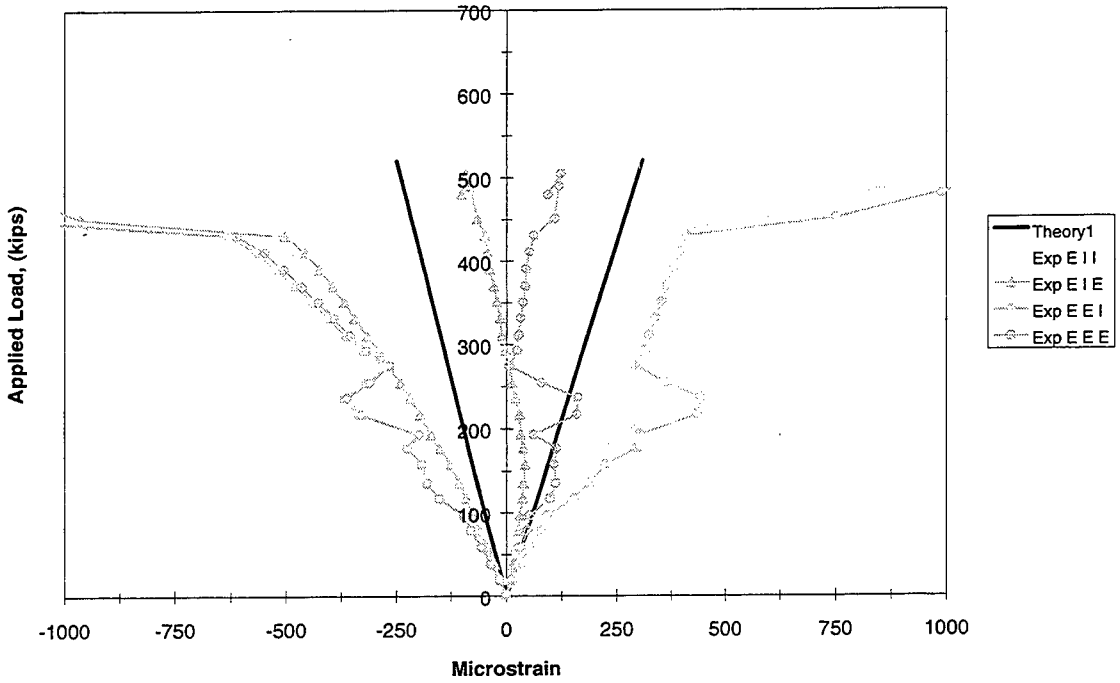

Figure 5.82 Principal Strains Rosette 1 (End IB)

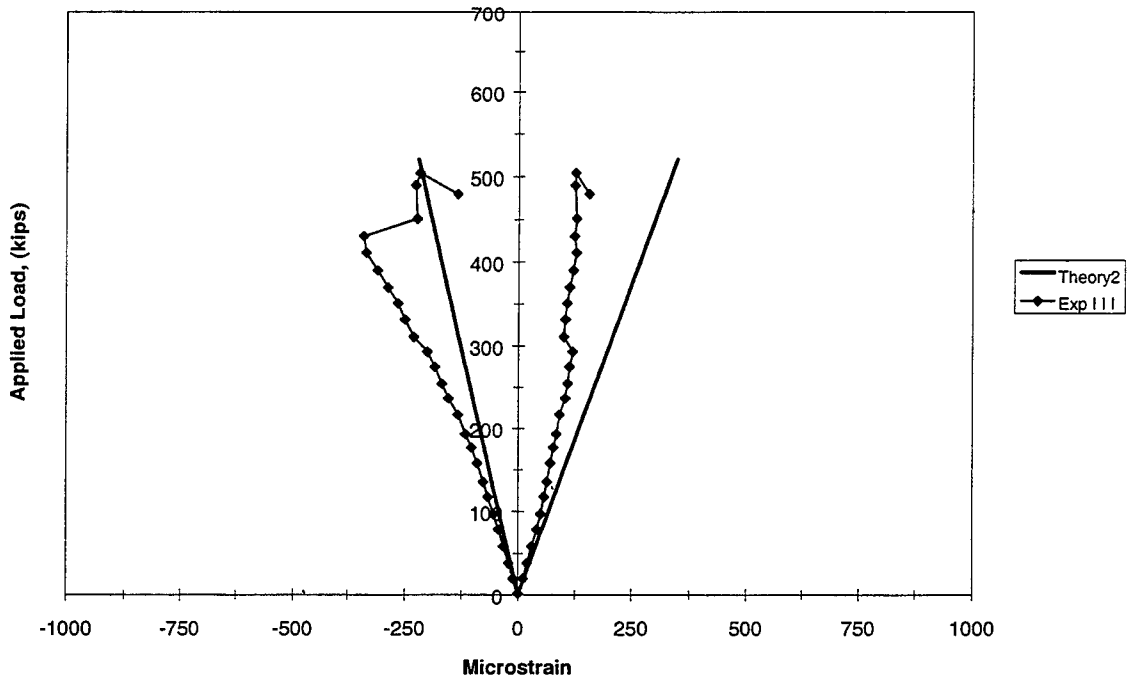

Figure 5.83 Principal Strains Rosette 2 (End IB)

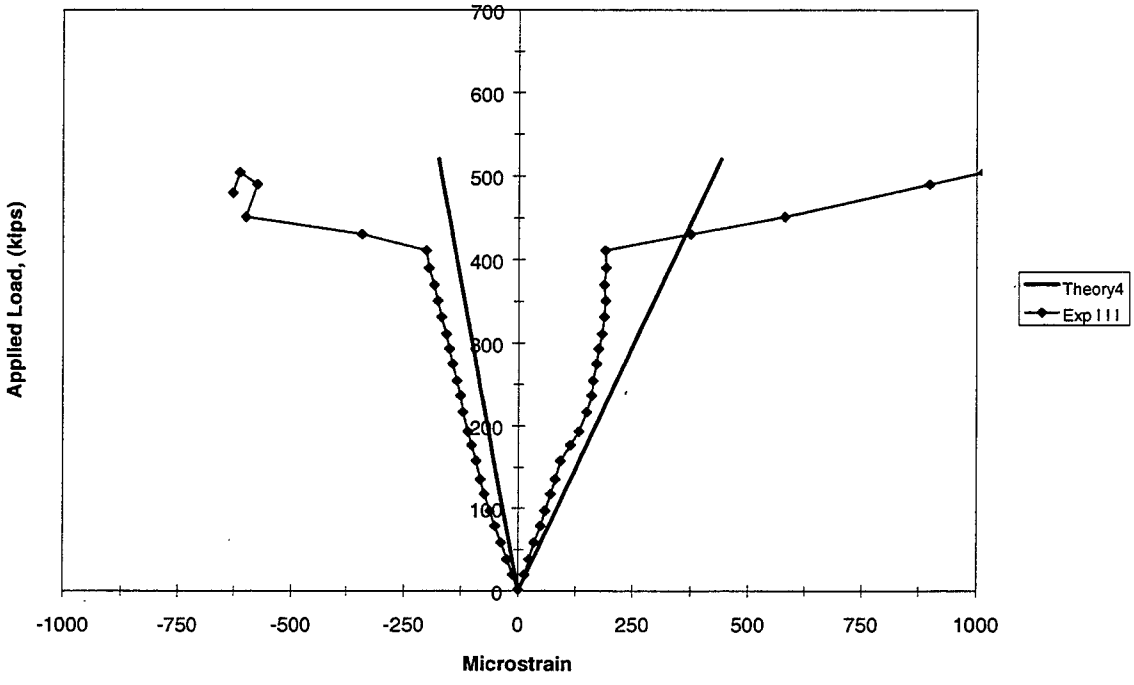

Figure 5.84 Principal Strains Rosette 4 (End IB)

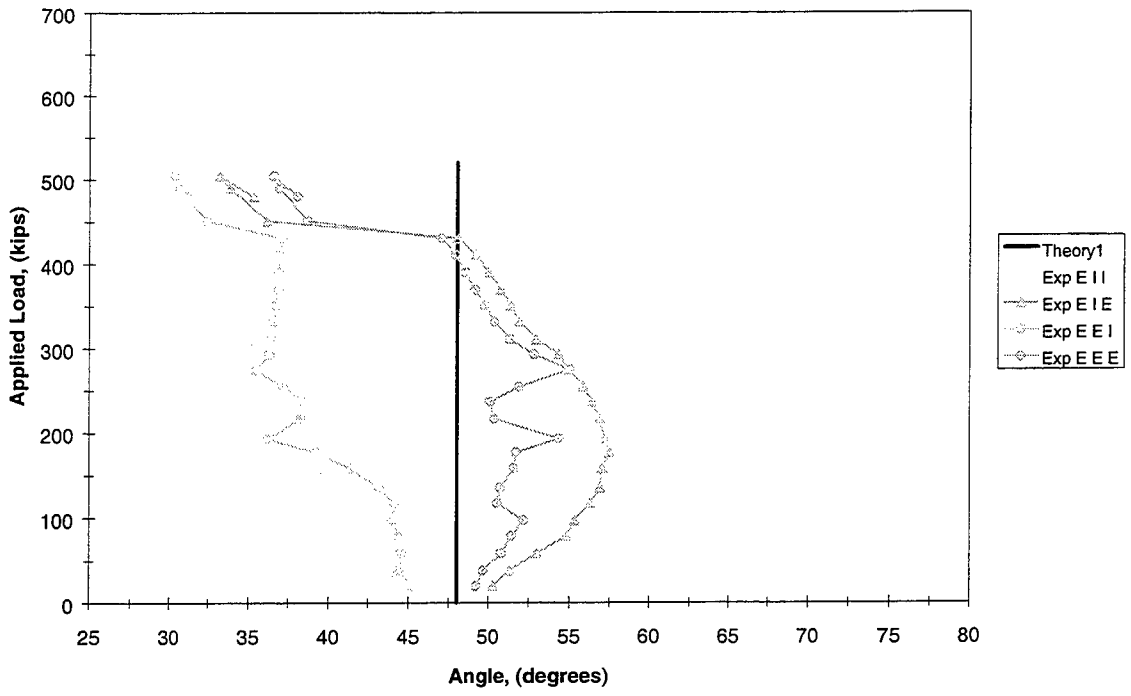

Figure 5.85 Principal Compression Angle Rosette 1 (End IB)

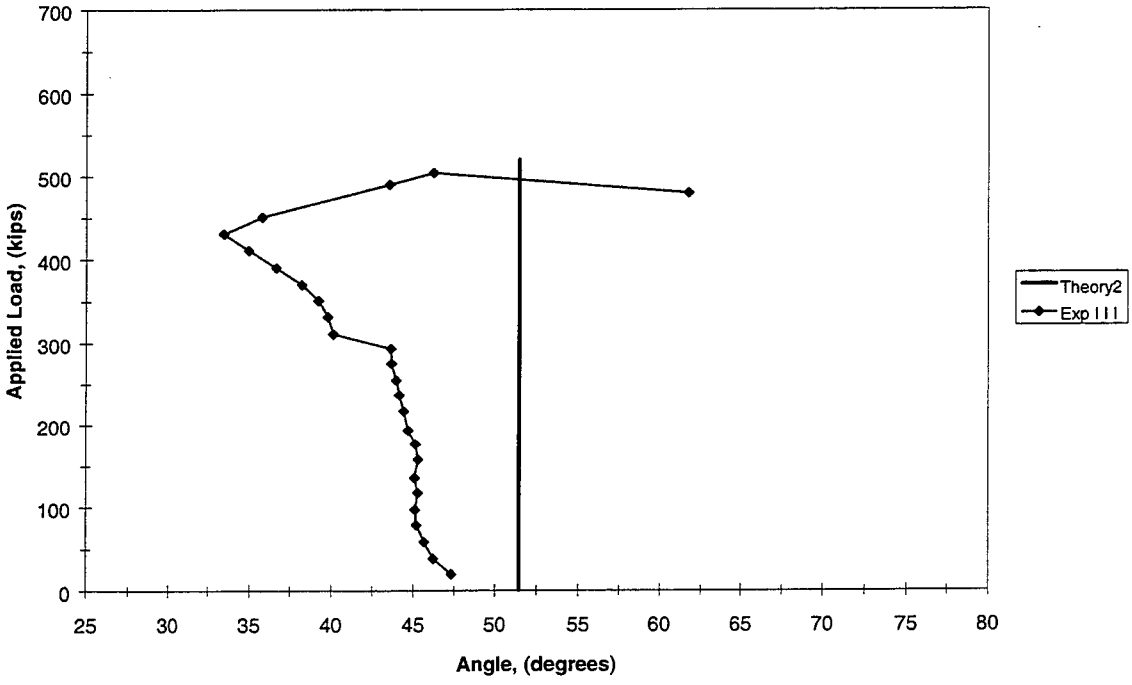

Figure 5.86 Principal Compression Angle Rosette 2 (End IB)

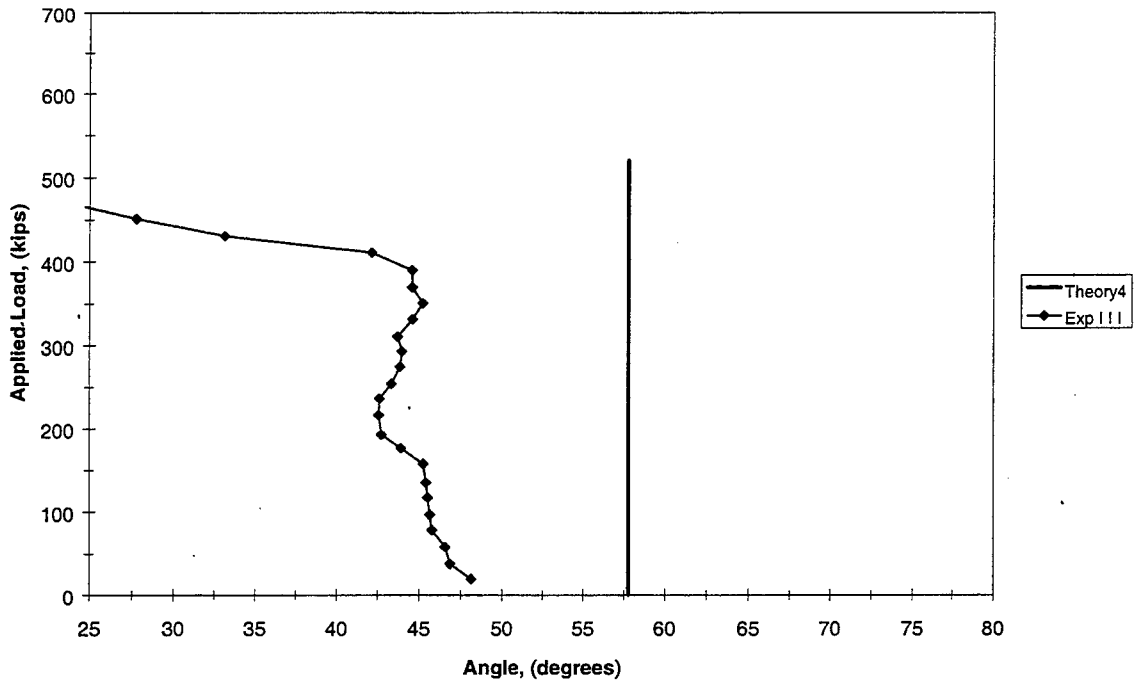

Figure 5.87 Principal Compression Angle Rosette 4 (End IB)

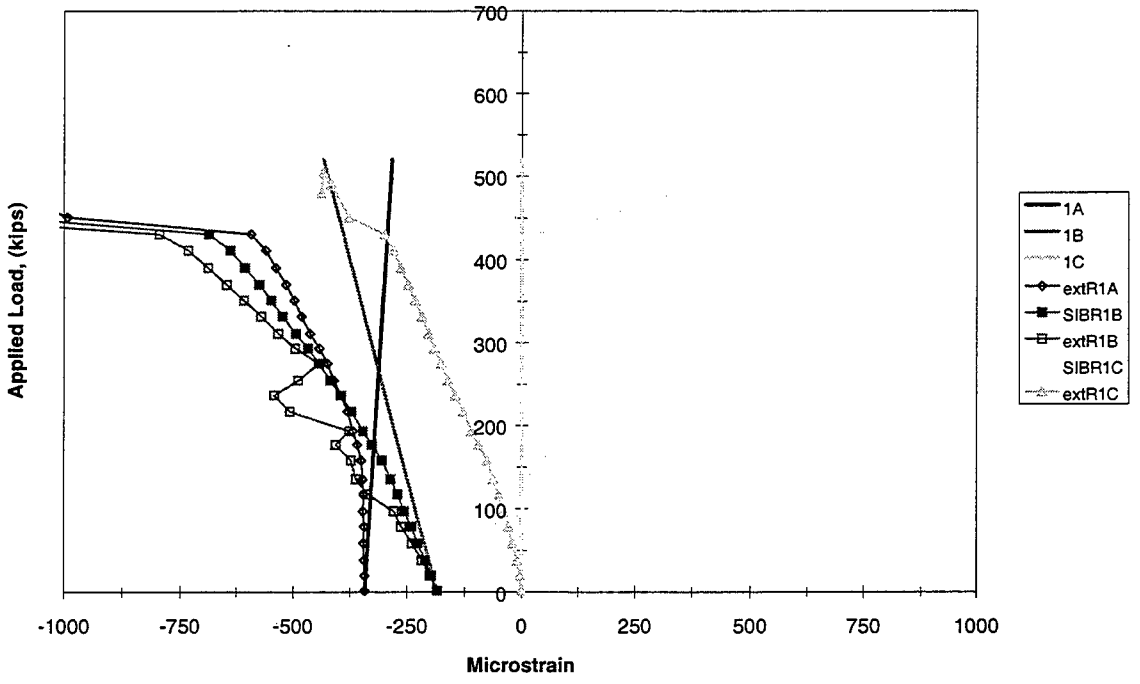

Figure 5.88 Corrected Rosette 1 (End IB)

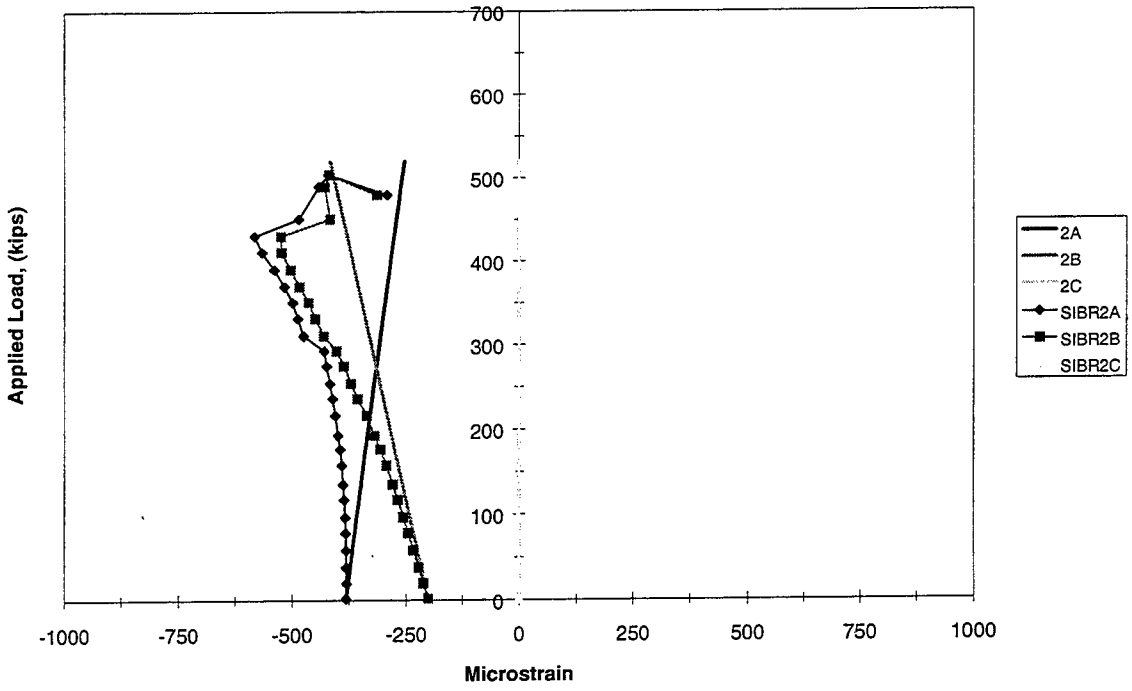

Figure 5.89 Corrected Rosette 2 (End IB)

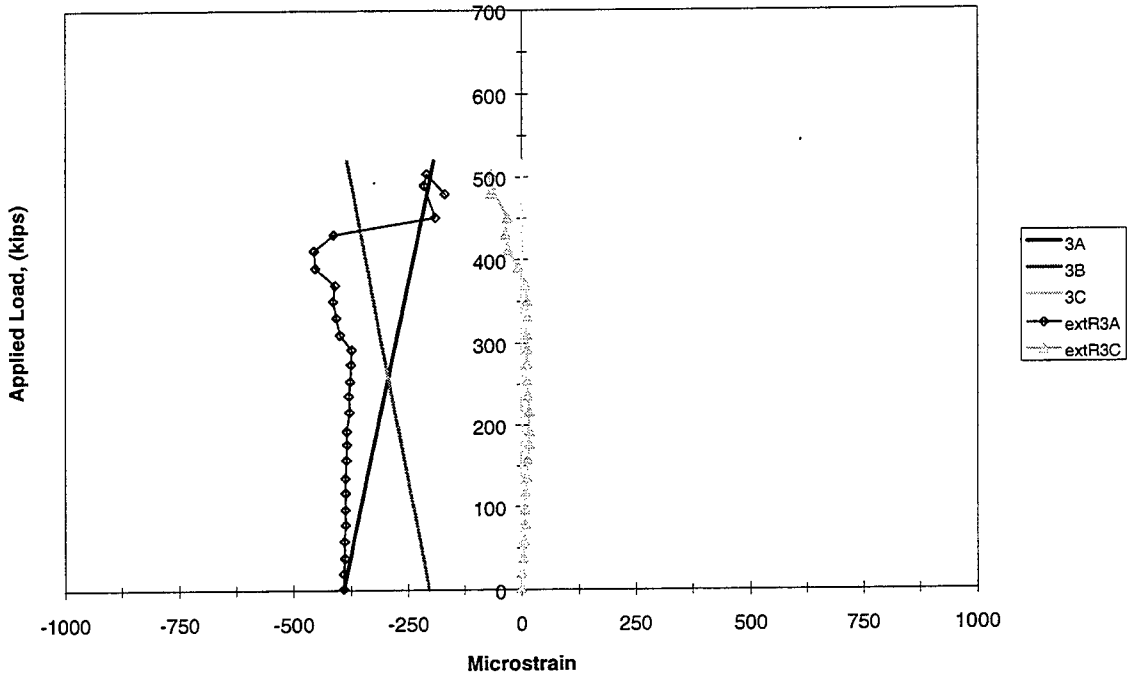

Figure 5.90 Corrected Rosette 3 (End IB)

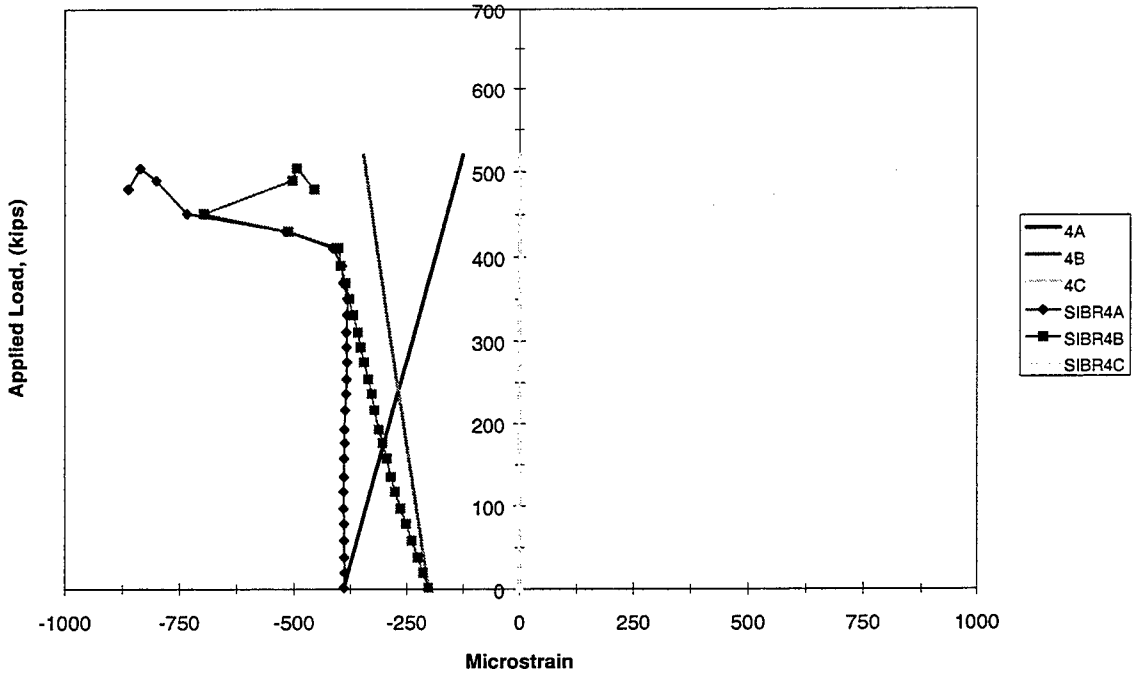

Figure 5.91 Corrected Rosette 4 (End IB)

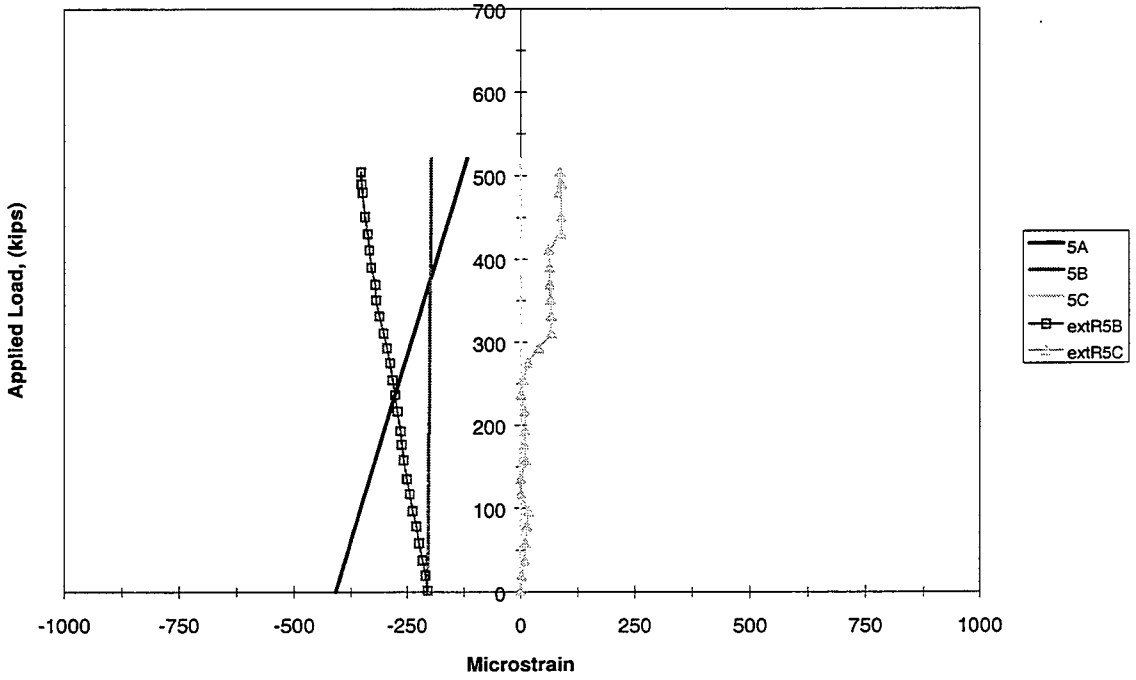

Figure 5.92 Corrected Rosette 5 (End IB)

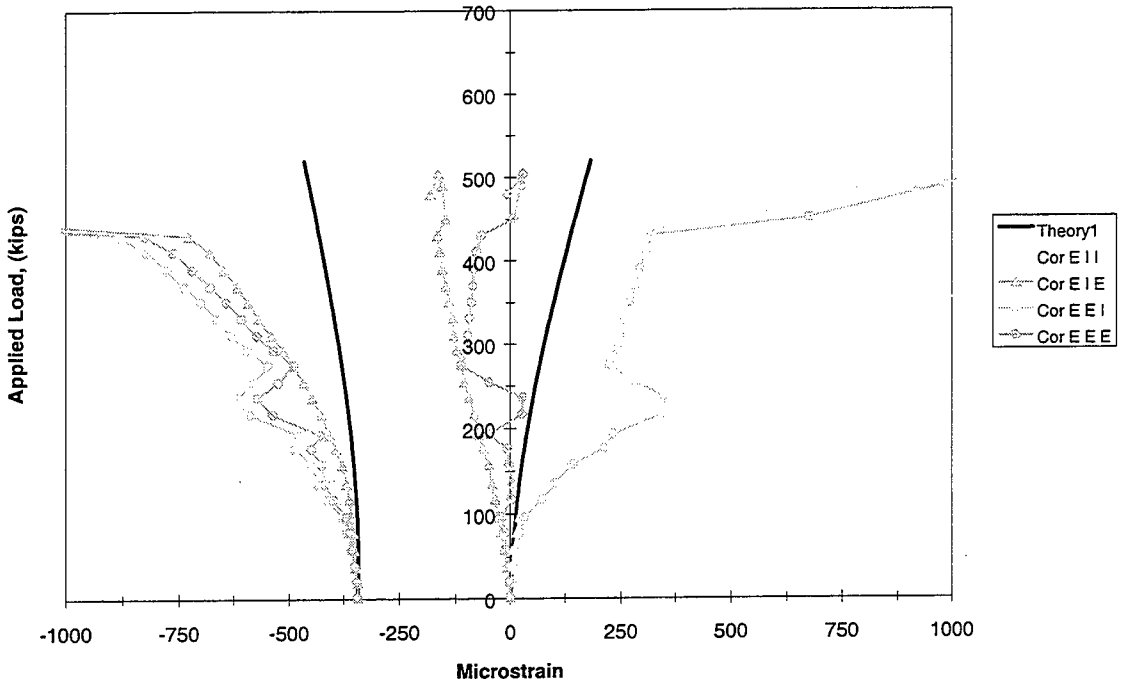

Figure 5.93 Corrected Principal Strains Rosette 1 (End IB)

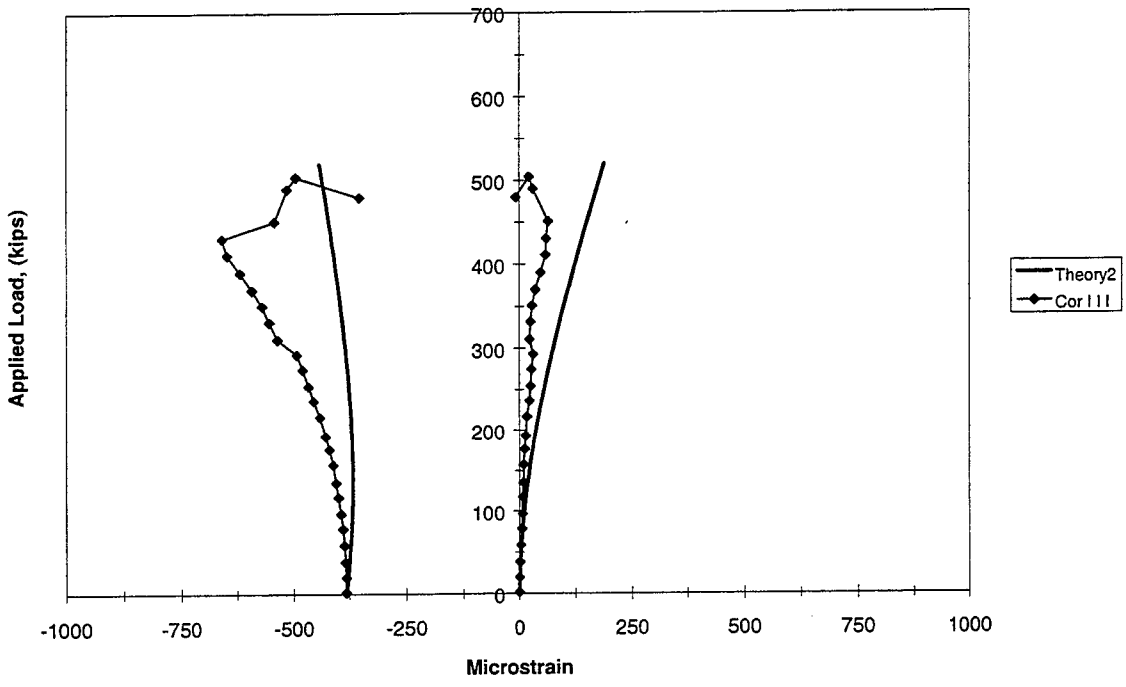

Figure 5.94 Corrected Principal Strains Rosette 2 (End IB)

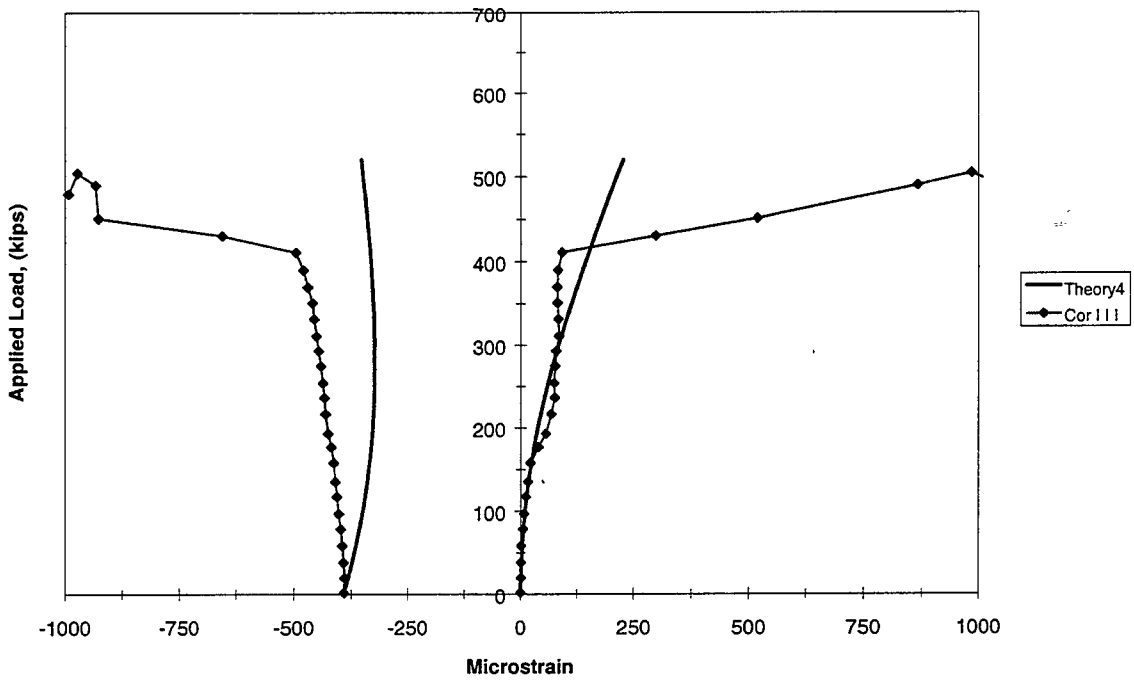

Figure 5.95 Corrected Principal Strains Rosette 4 (End IB)

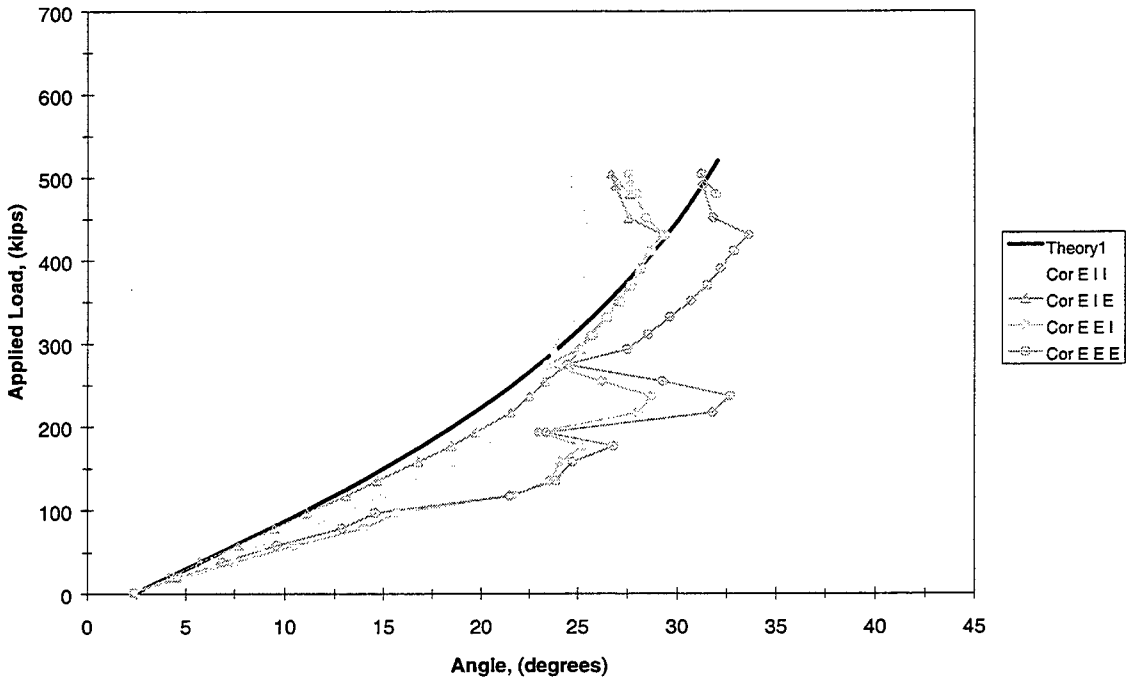

Figure 5.96 Corrected Principal Compression Angle Rosette 1 (End IB)

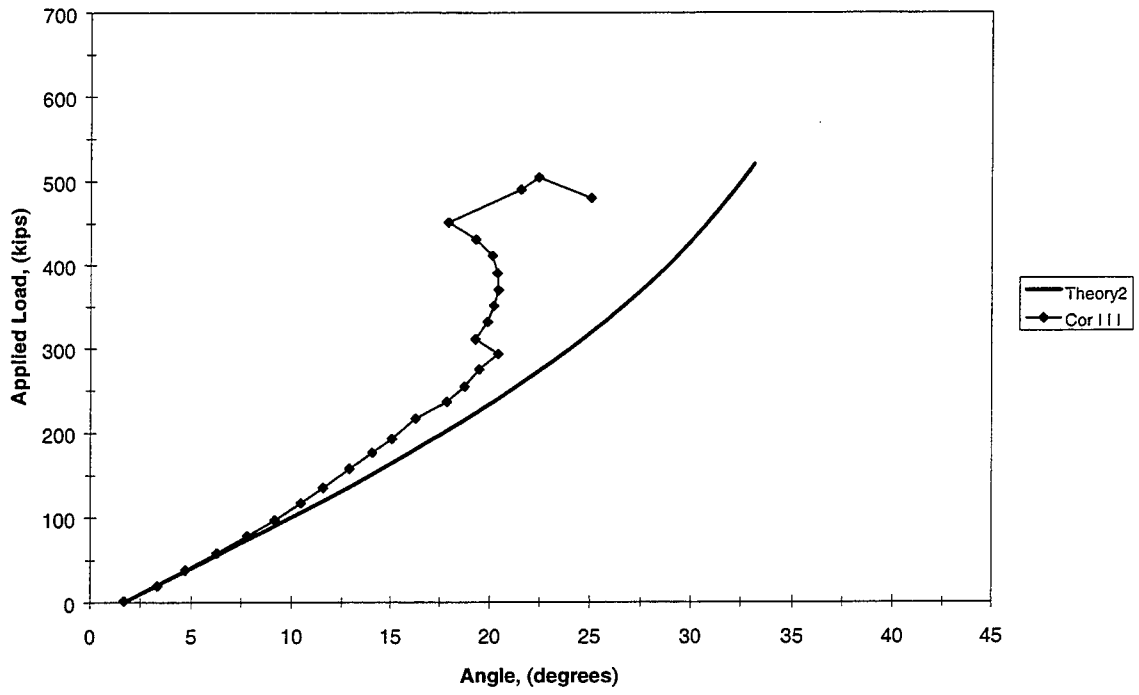

Figure 5.97 Corrected Principal Compression Angle Rosette 2 (End IB)

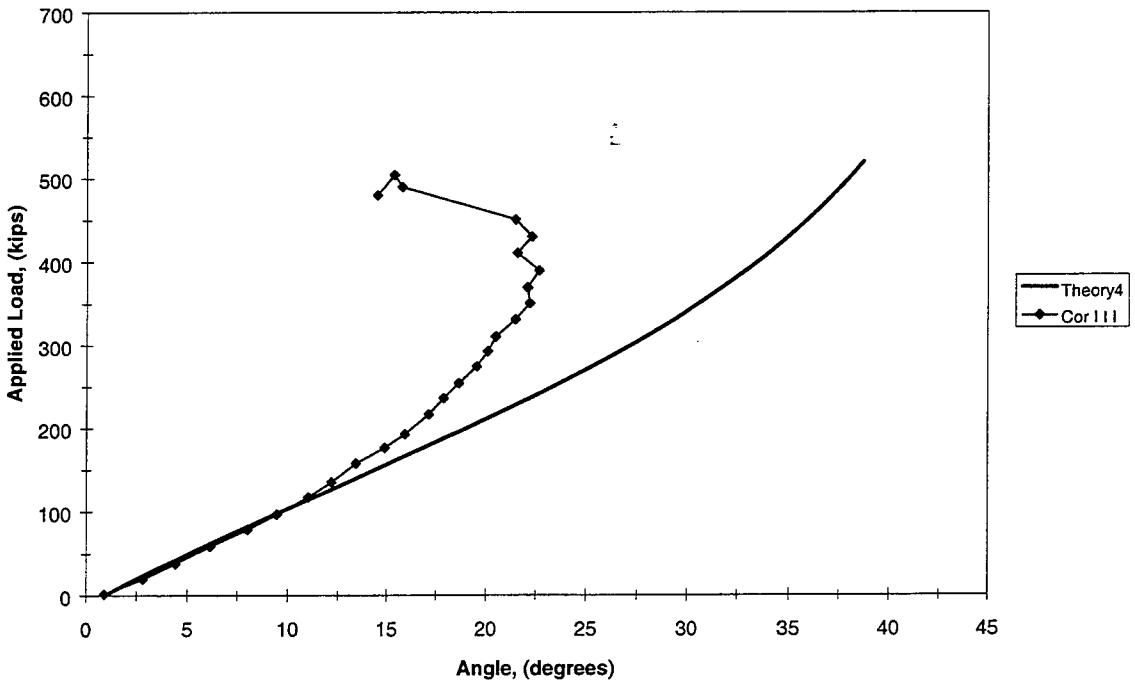

Figure 5.98 Corrected Principal Compression Angle Rosette 4 (End IB)

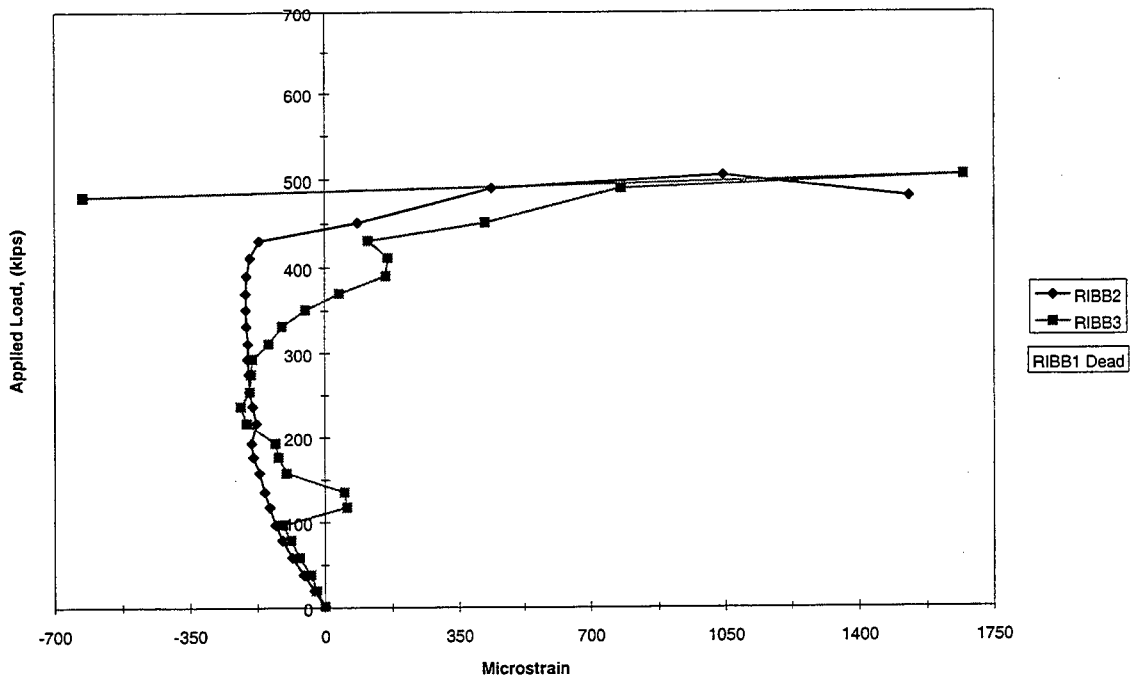

Figure 5.99 Bursting Stirrup (End IB)

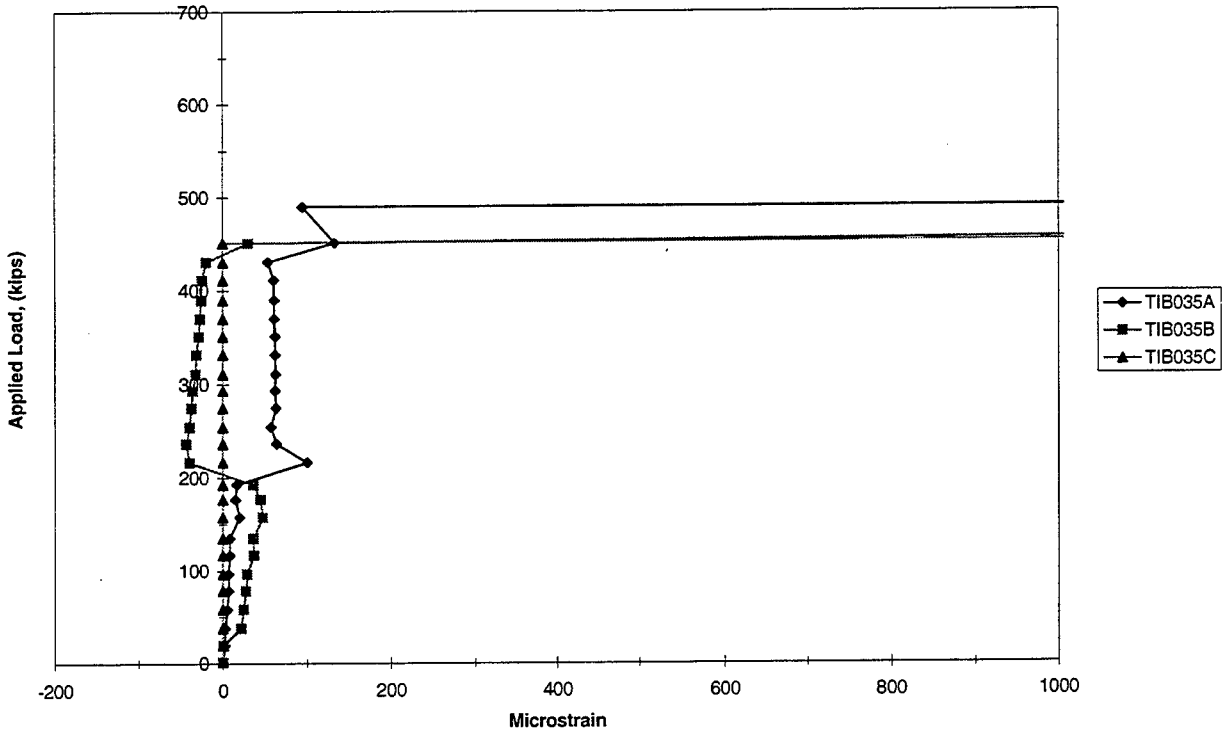

Figure 5.100 Transfer Length 0 ft. (End IB)

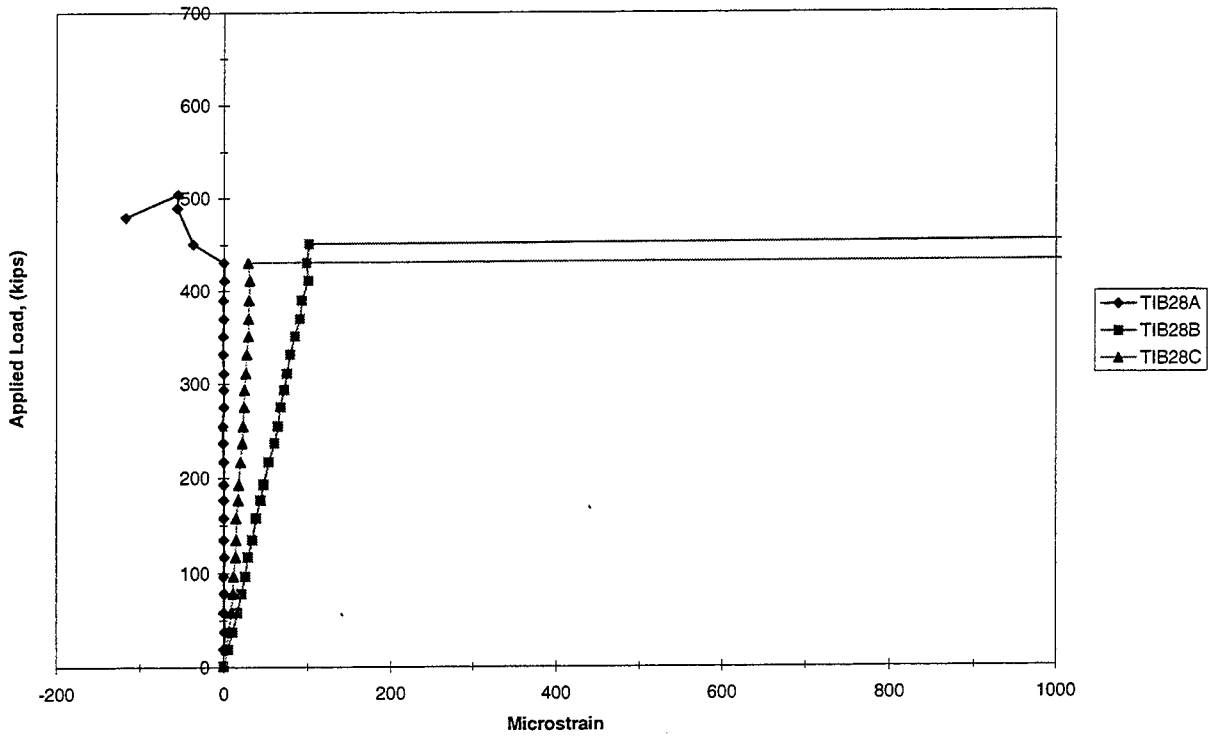

Figure 5.101 Transfer Length 2 ft. (End IB)

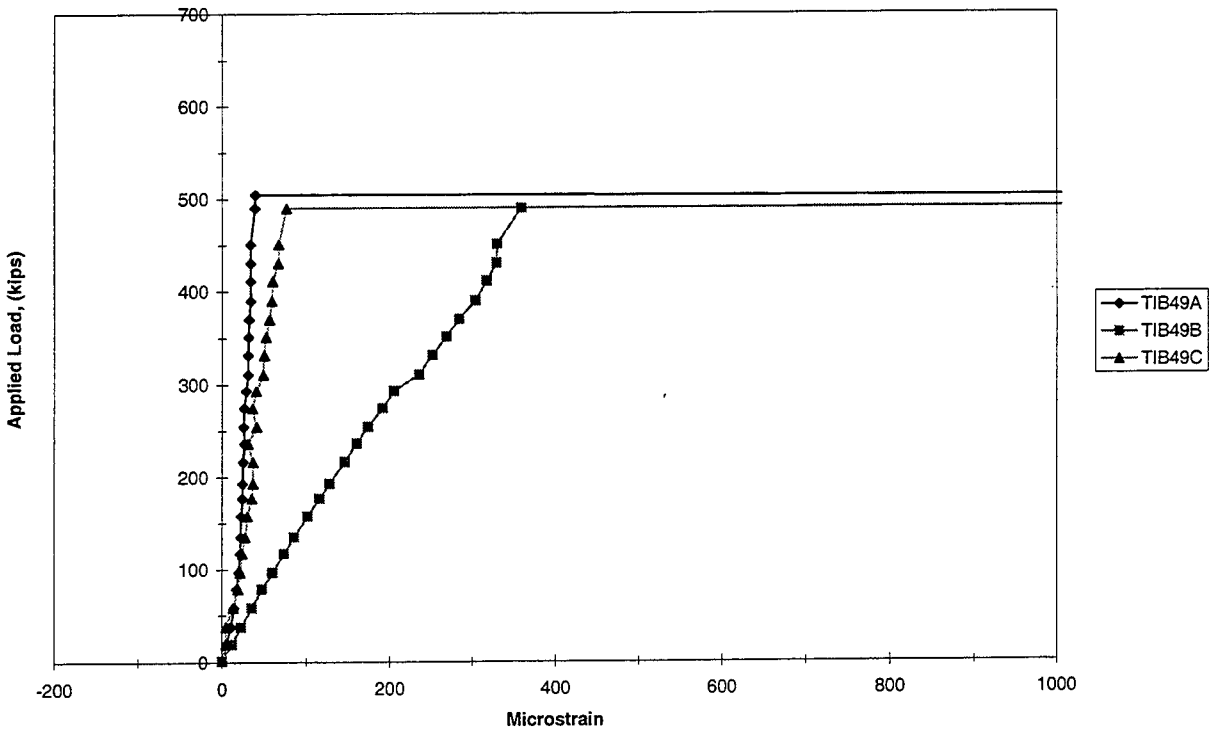

Figure 5.102 Transfer Length 4 ft. (End IB)

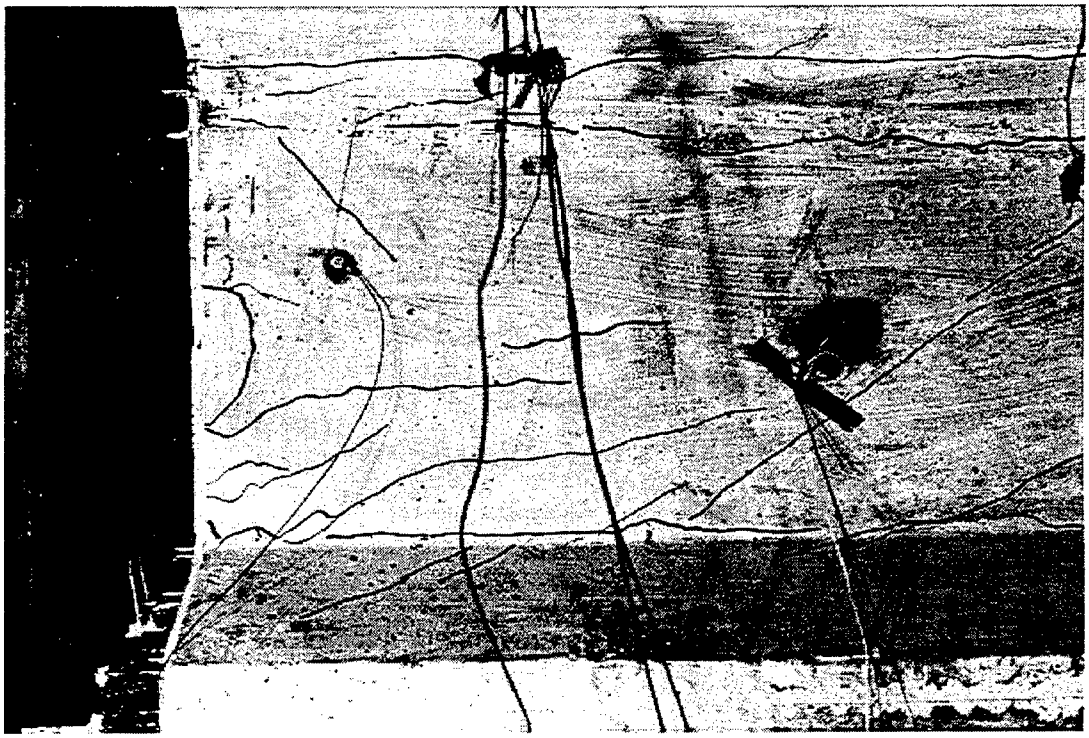

Figure 5.103 Before Testing (End IIC)

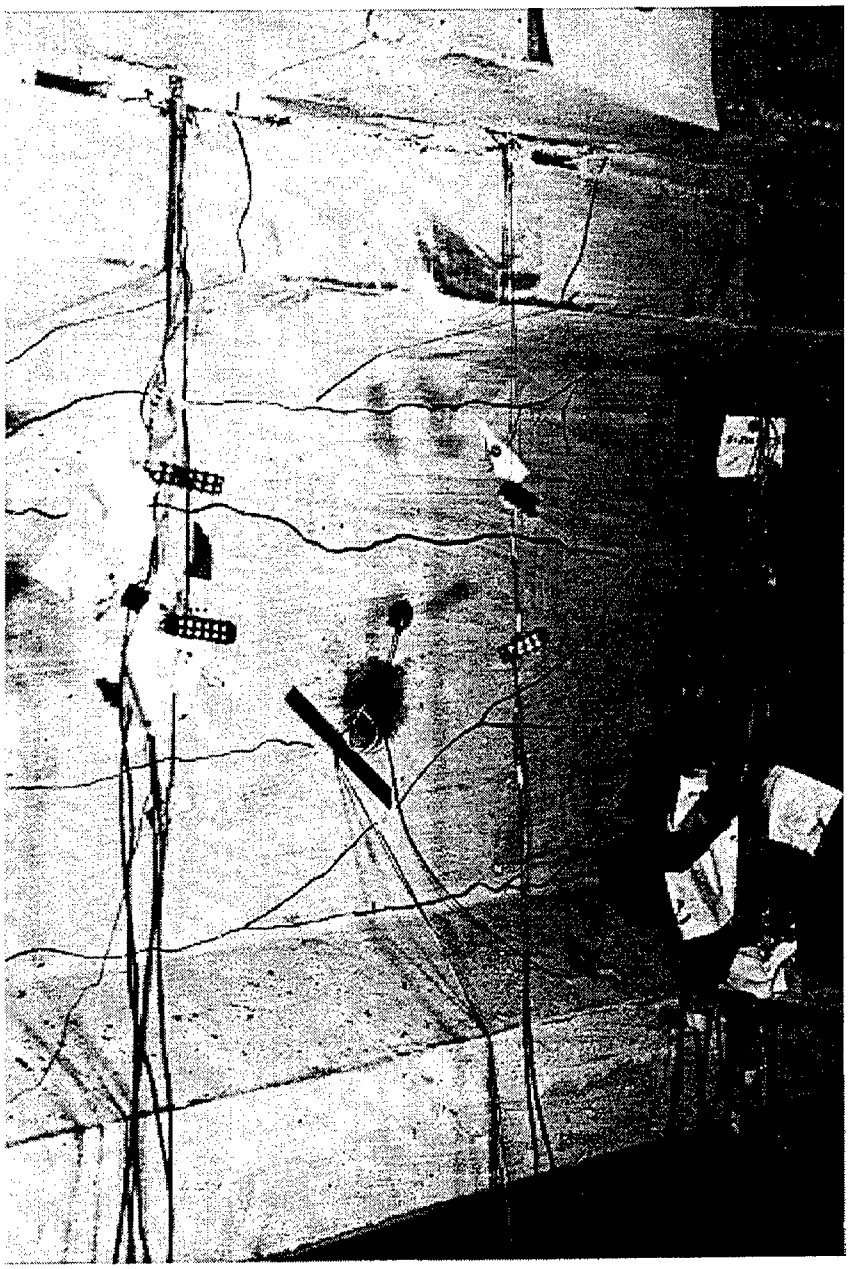

Figure 5.104 Before Testing (End IIC)

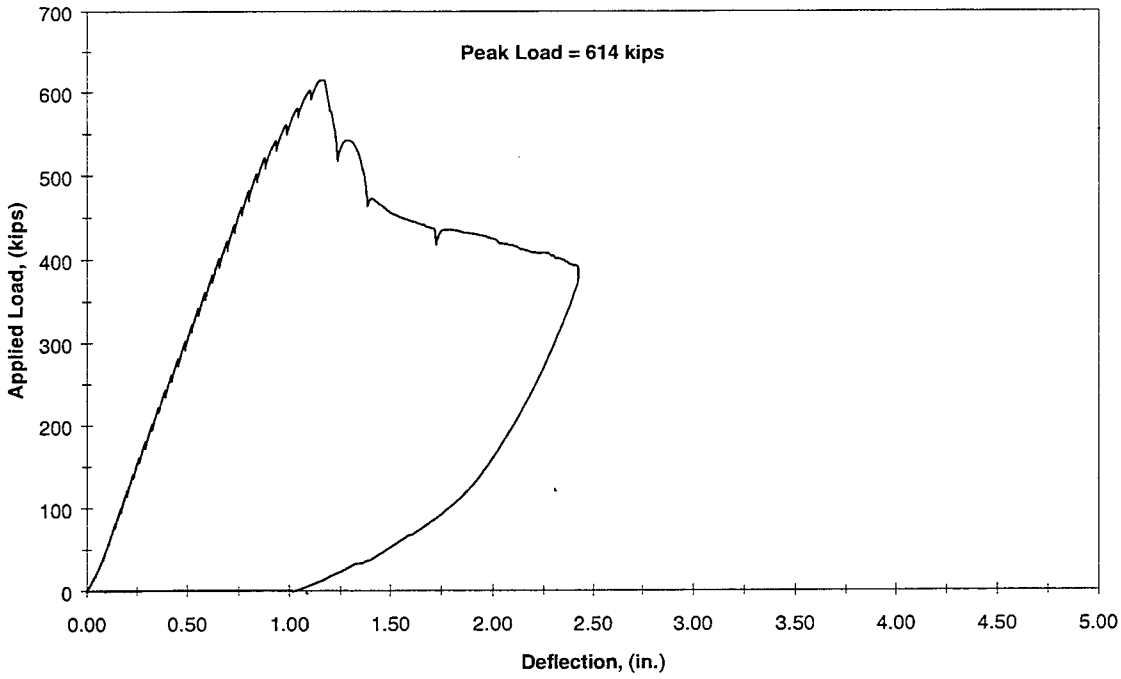

Figure 5.105 Corrected West Load Deflection (End IIC)

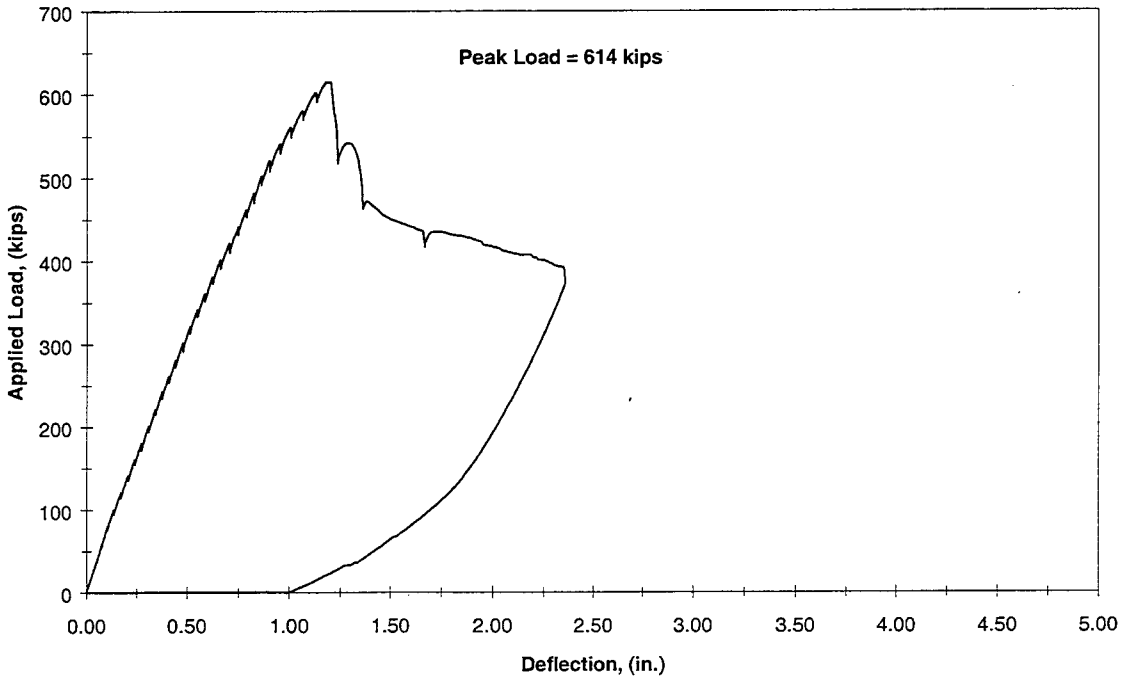

Figure 5.106 Corrected East Load Deflection (End IIC)

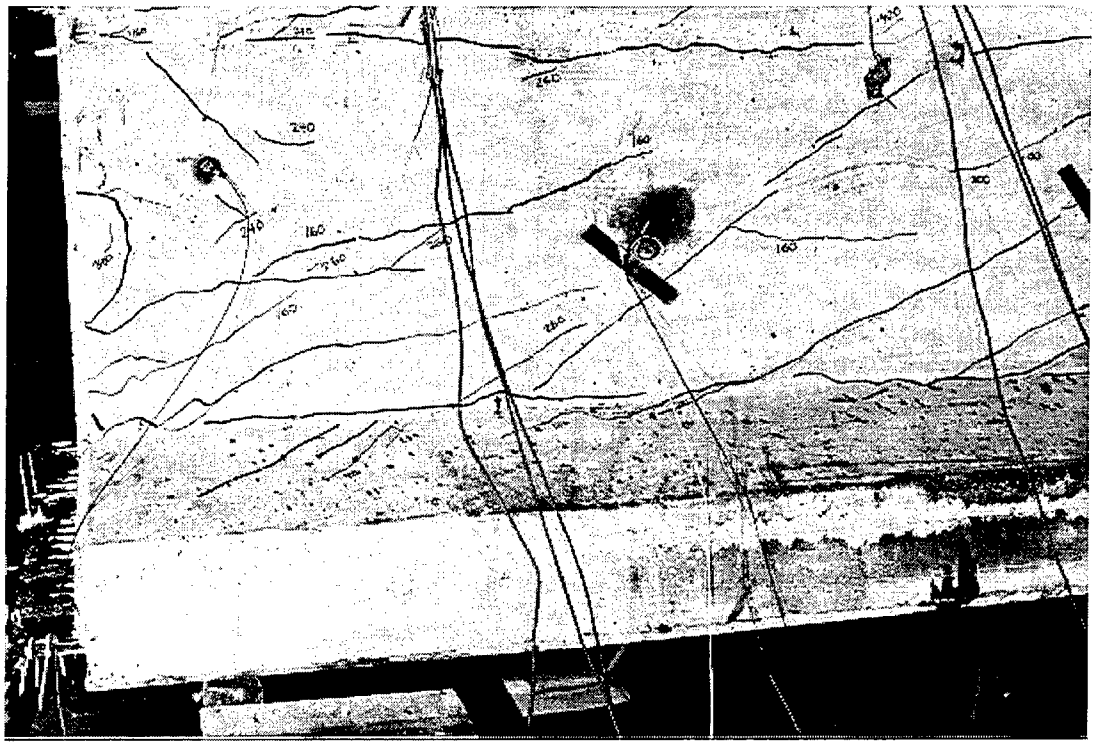

Figure 5.107 After 540 kips, Cracking Near Support (End IIC)

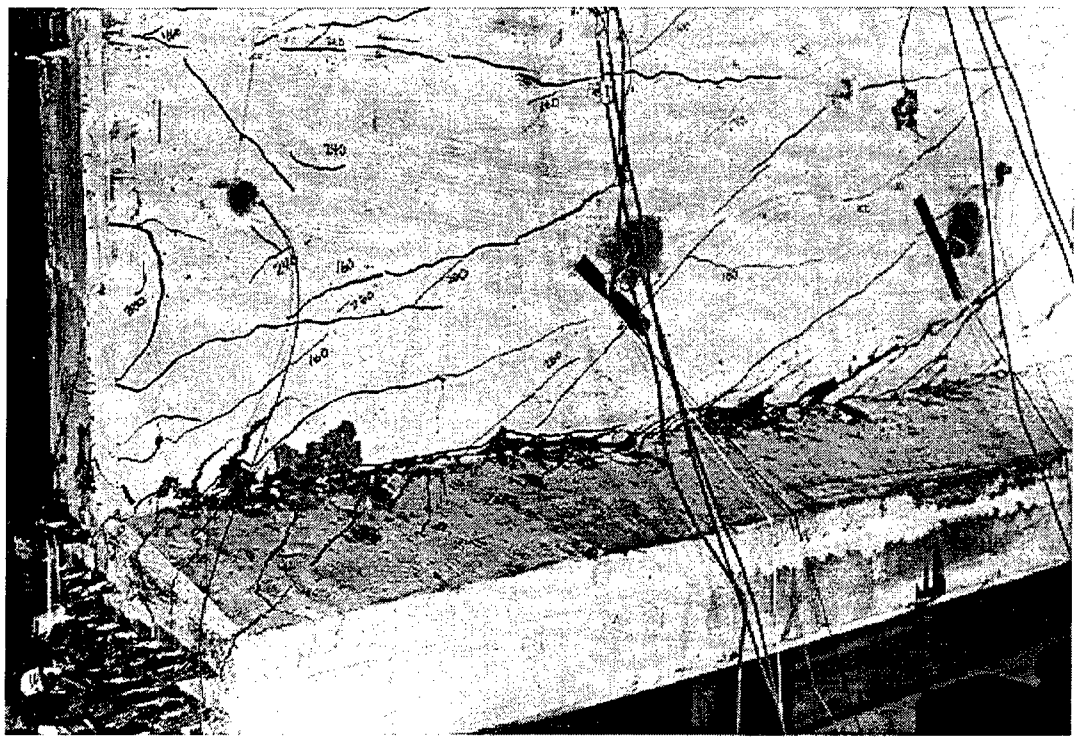

Figure 5.108 After Peak Load, Cracking Near Support (End IIC)

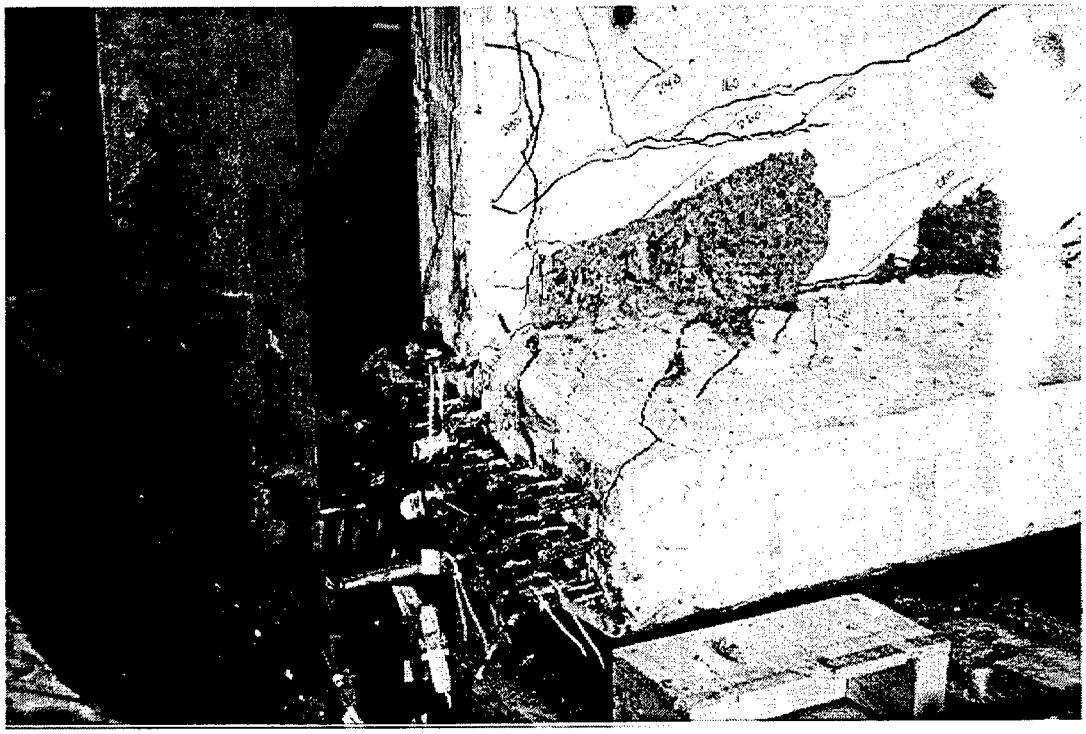

Figure 5.109 After Peak Load, Cracking Near Support (End IIC)

Figure 5.110 After Peak Load, Cracking Near the Support (End IIC)

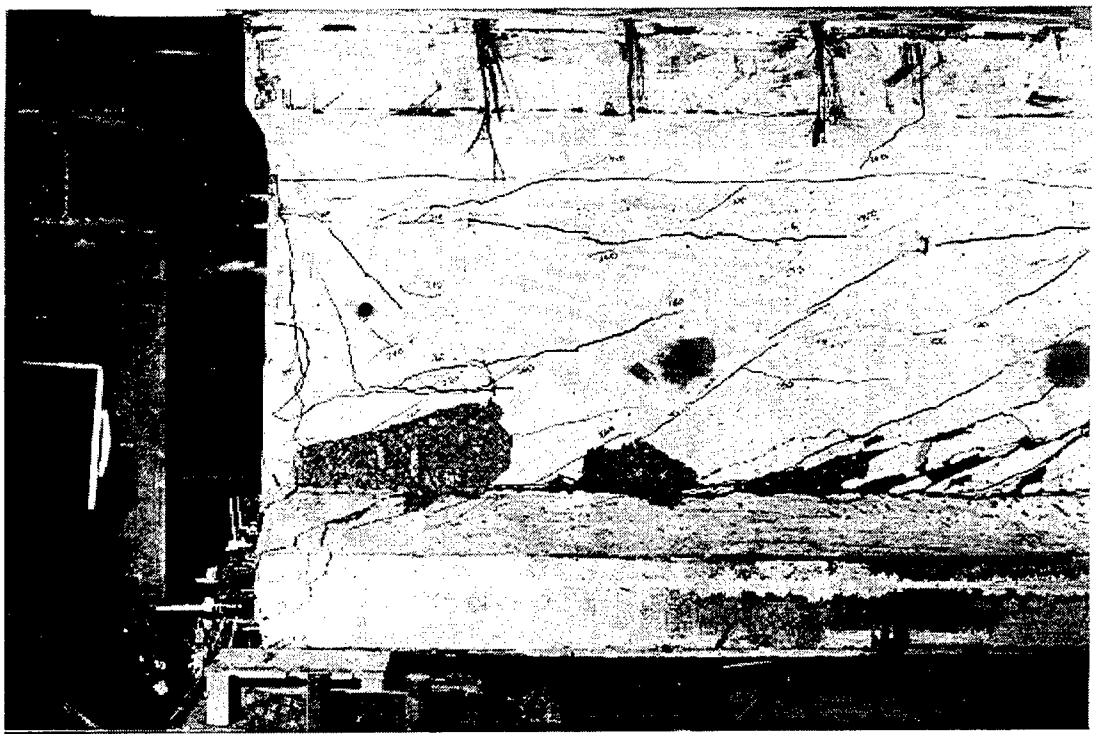

Figure 5.111 After Peak Load, Cracking Near the Support (End IIC)

Figure 5.112 After Peak Load, Cracking Near the Load Point (End IIC)

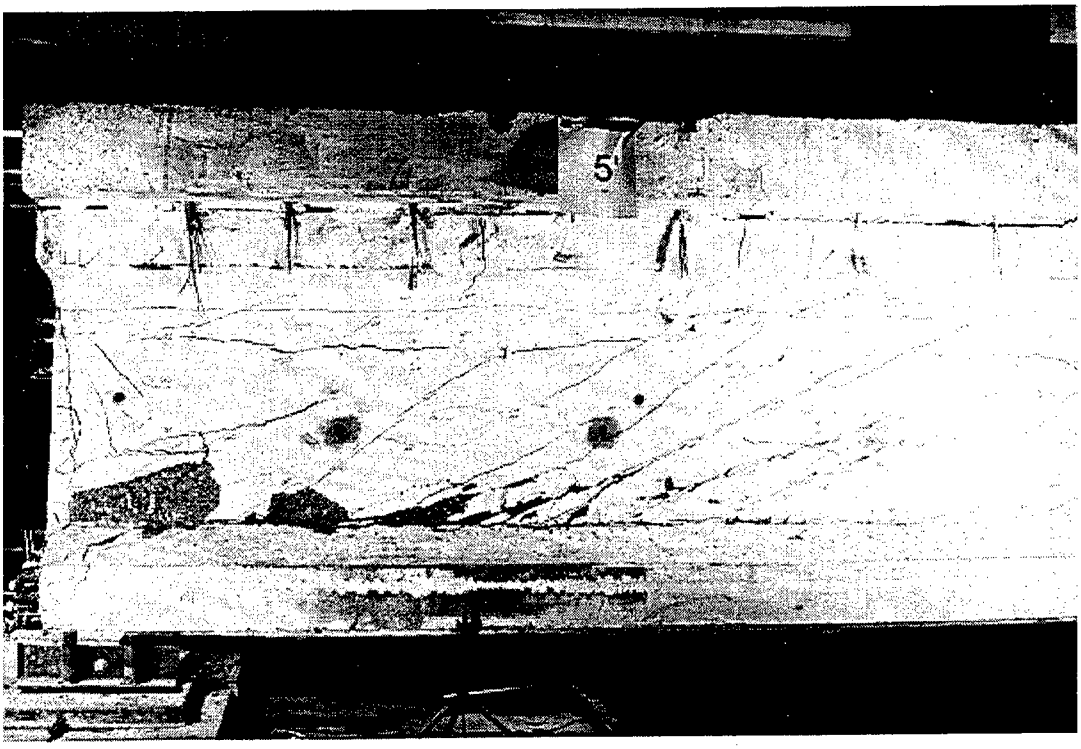

Figure 5.113 After Testing, Cracking (End IIC)

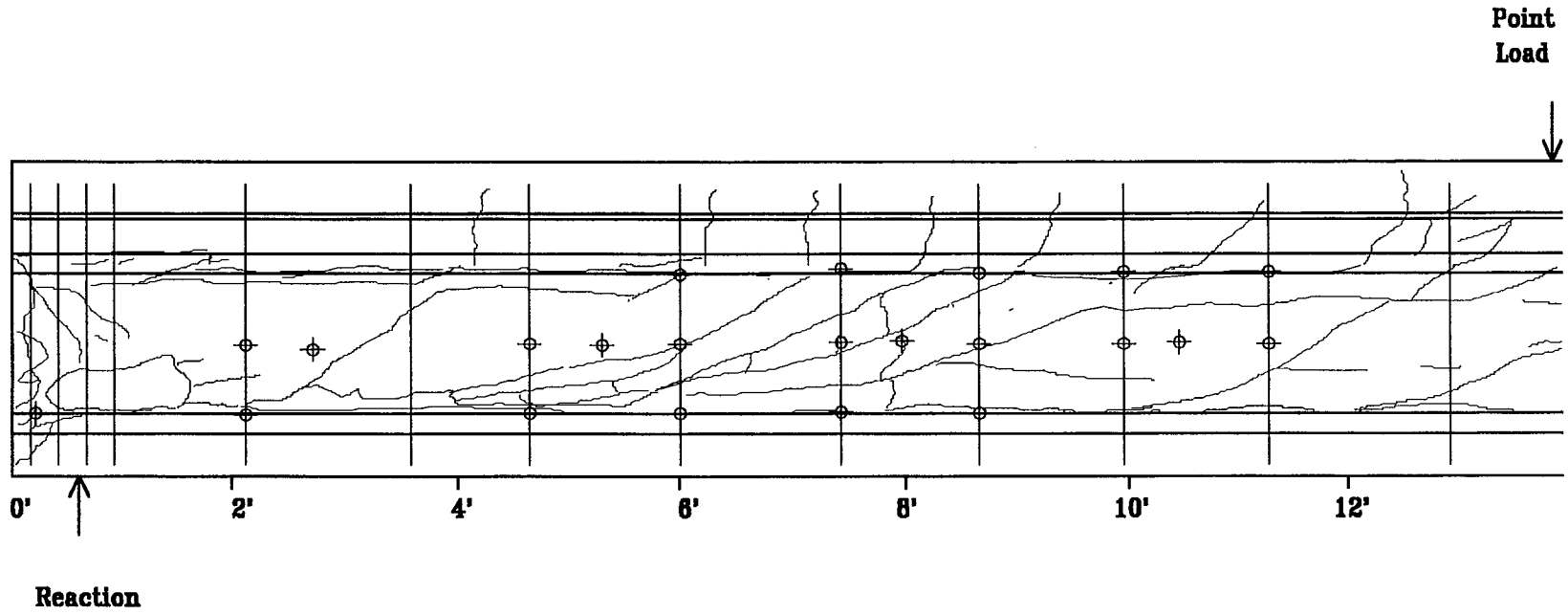

Figure 5.114 Before Testing, Crack Drawing (End IIC)

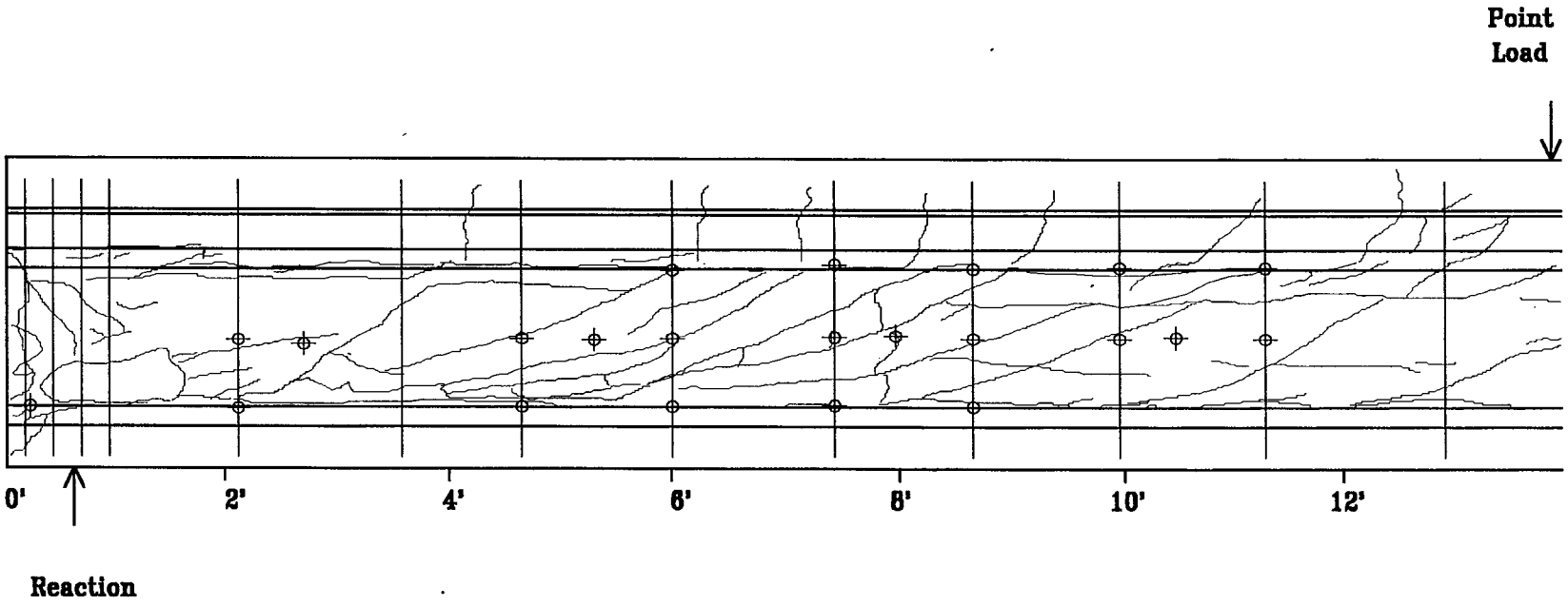

Figure 5.115 After Peak Load, Crack Drawing (End IIC)

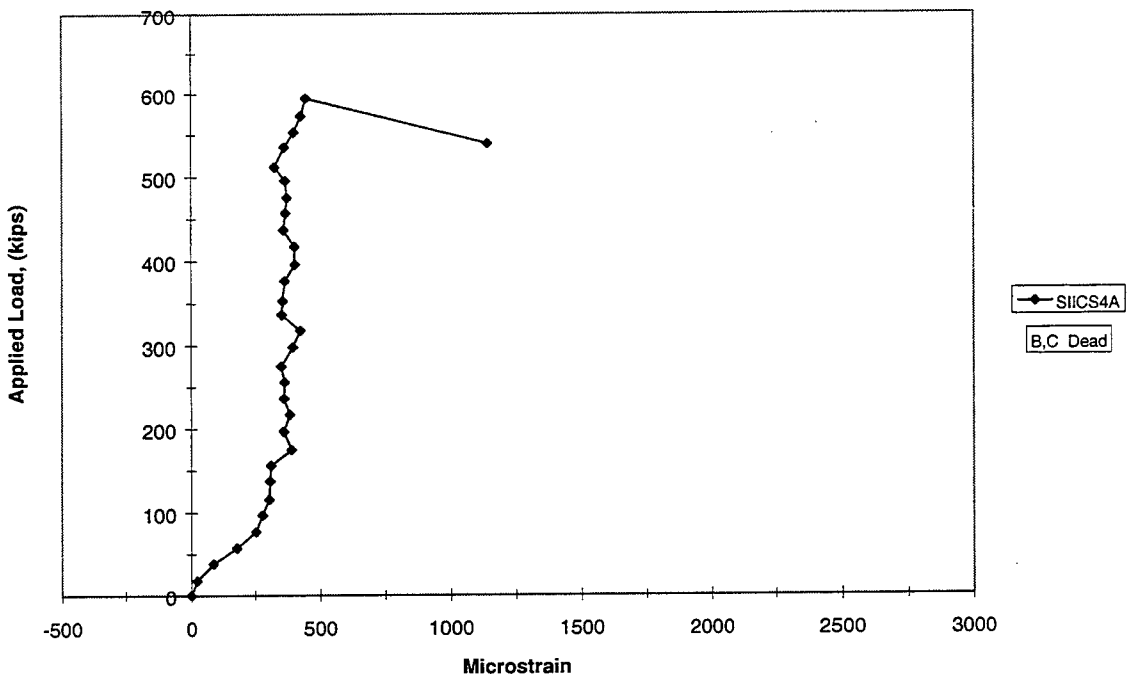

Figure 5.116 Stirrup 4 (End IIC)

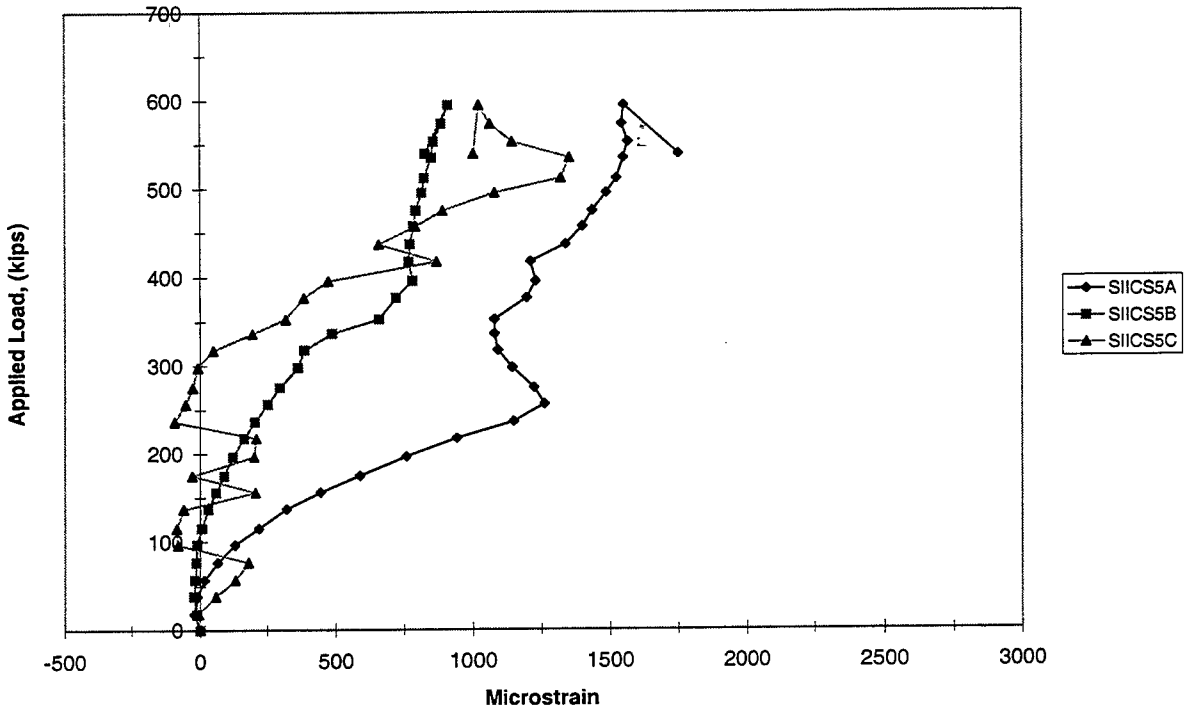

Figure 5.117 Stirrup 5 (End IIC)

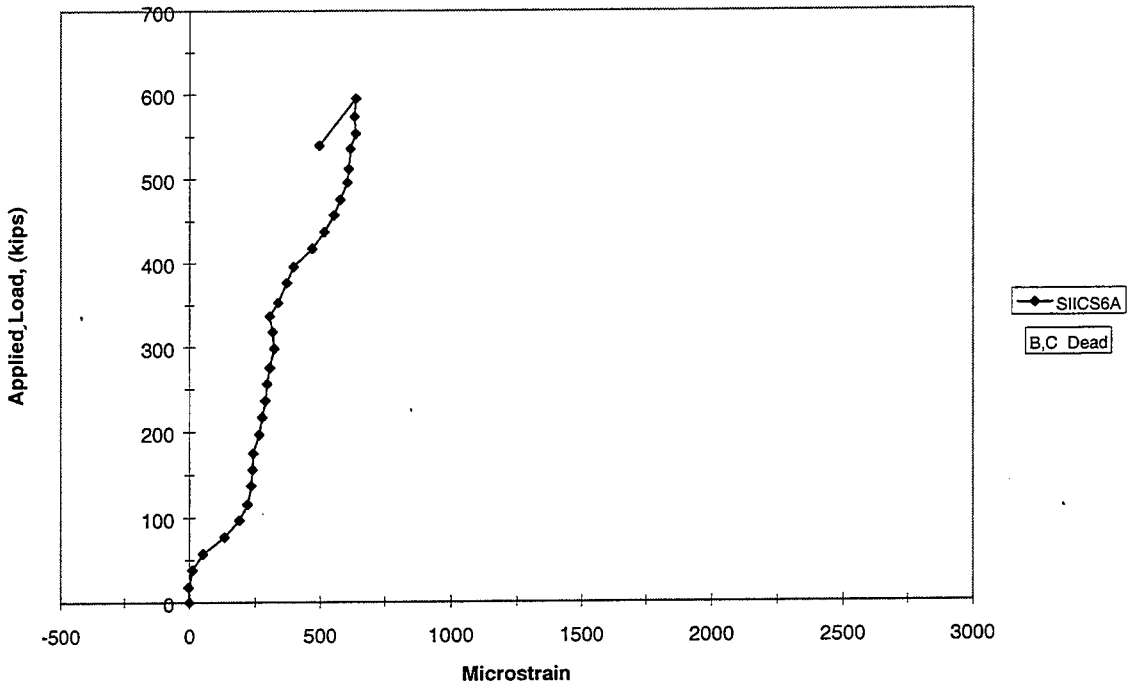

Figure 5.118 Stirrup 6 (End IIC)

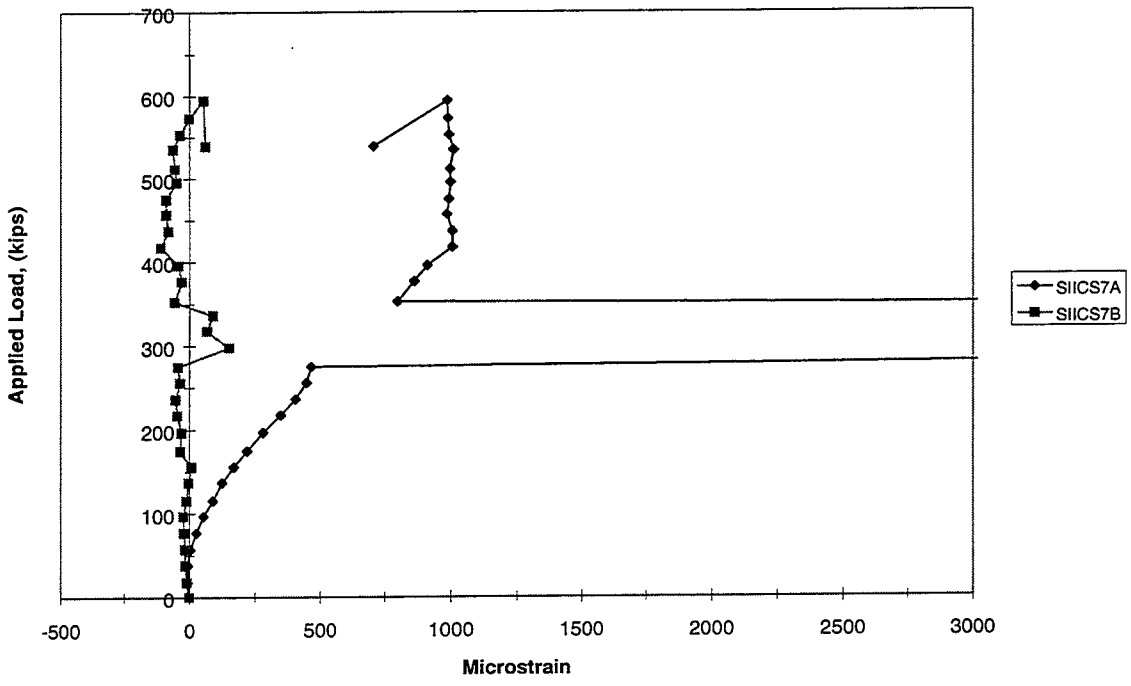

Figure 5.119 Stirrup 7 (End IIC)

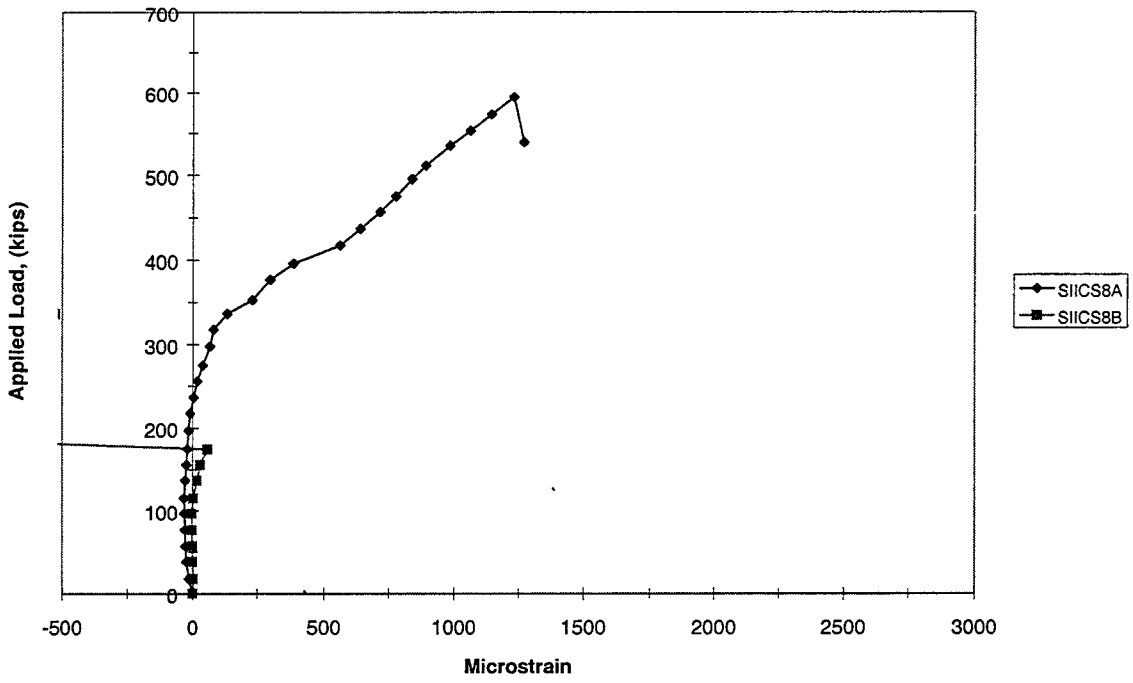

Figure 5.120 Stirrup 8 (End IIC)

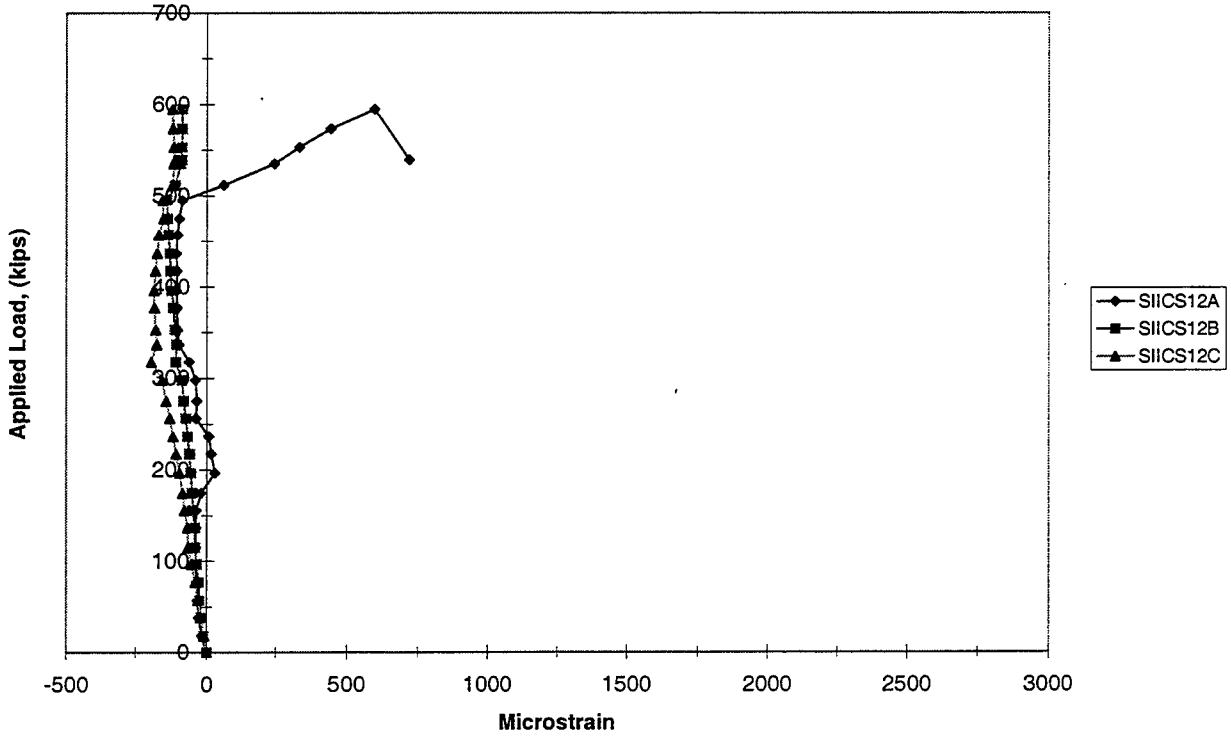

Figure 5.121 Stirrup 12 (End IIC)

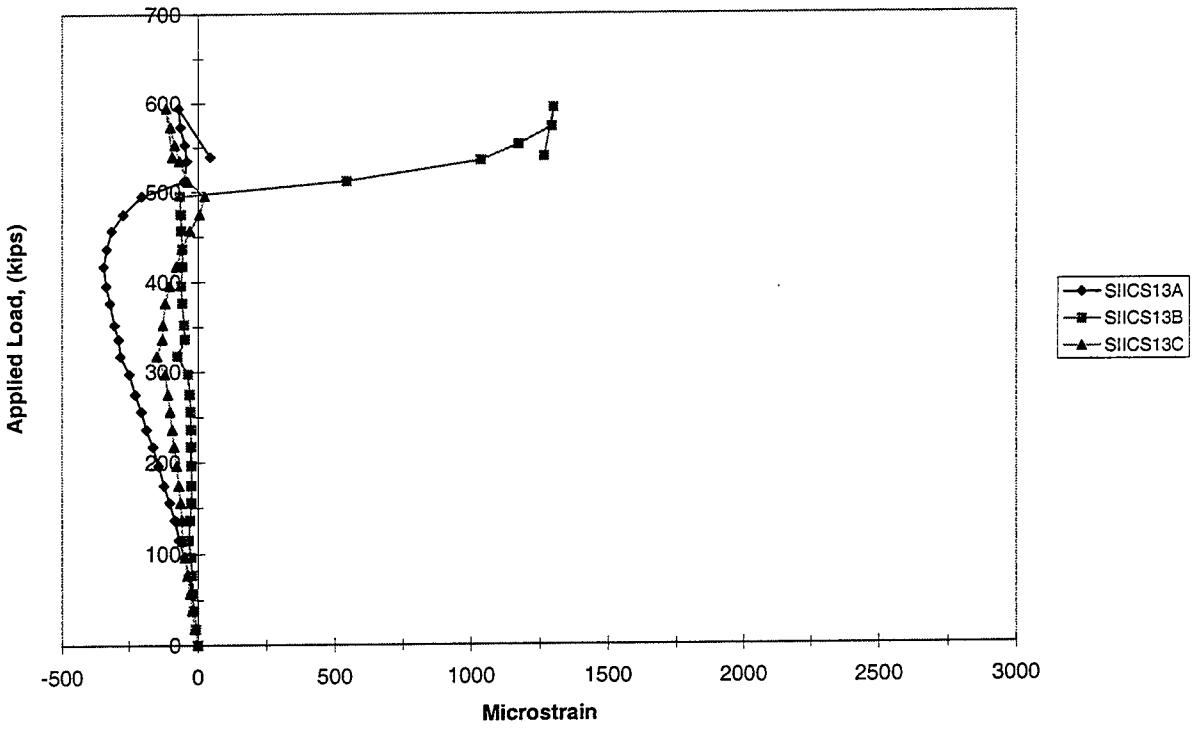

Figure 5.122 Stirrup 13 (End IIC)

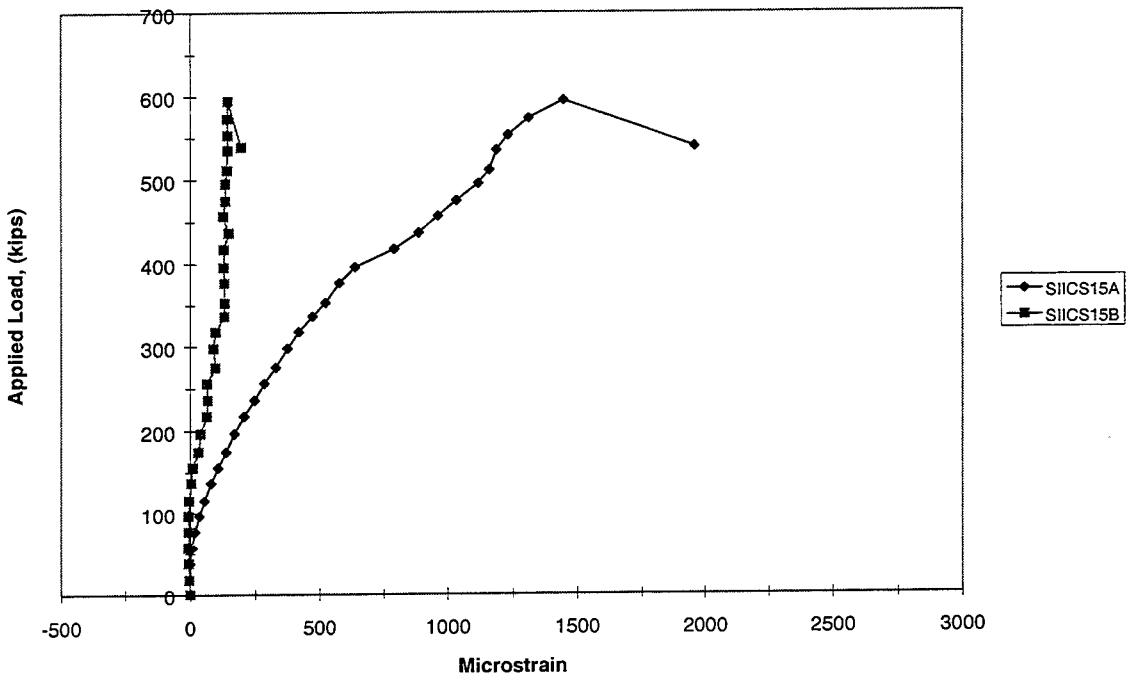

Figure 5.123 Stirrup 15 (End IIC)

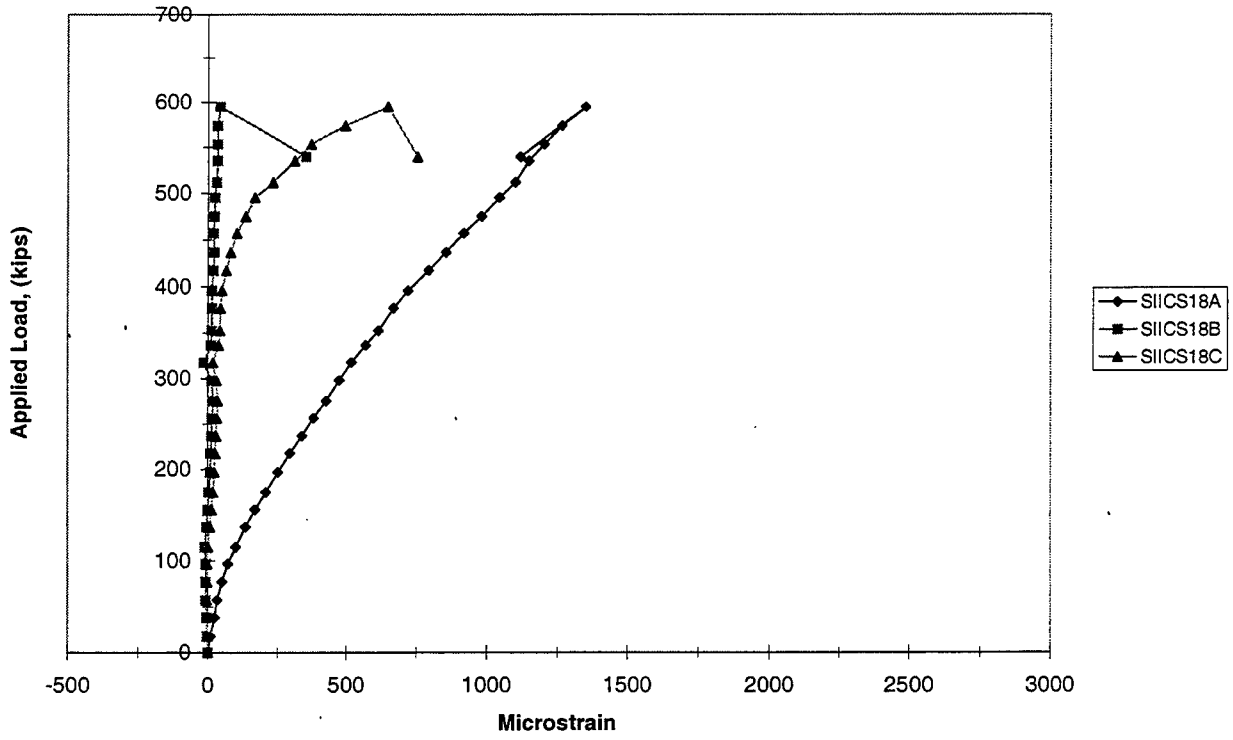

Figure 5.124 Stirrup 18 (End IIC)

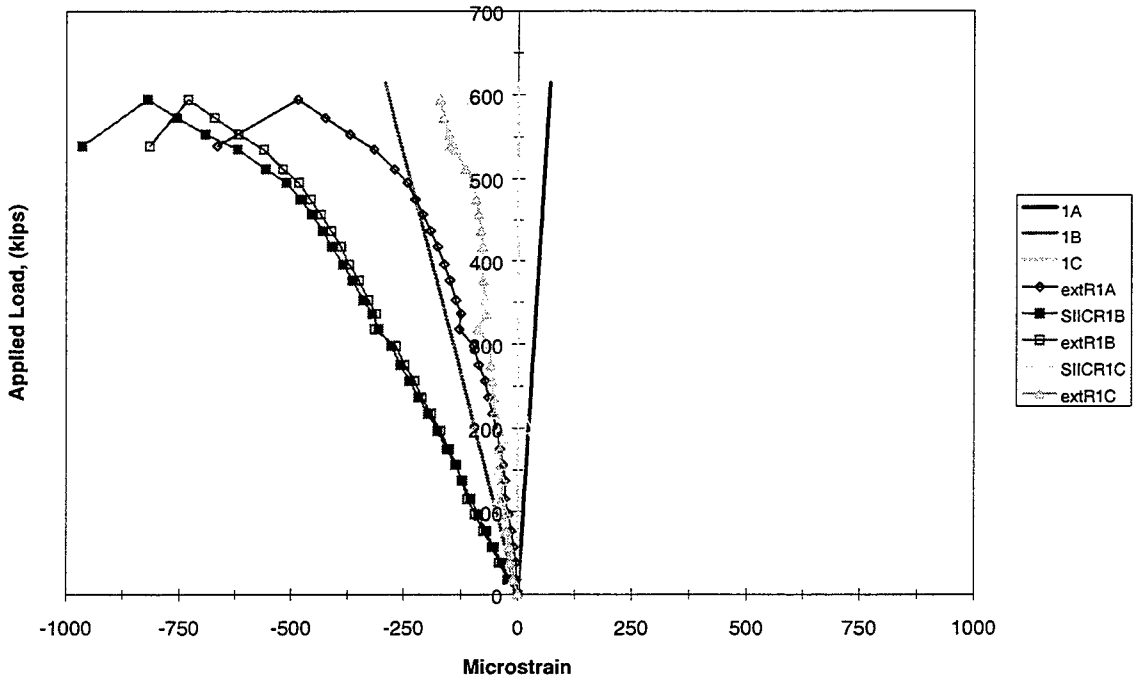

Figure 5.125 Rosette 1 (End IIC)

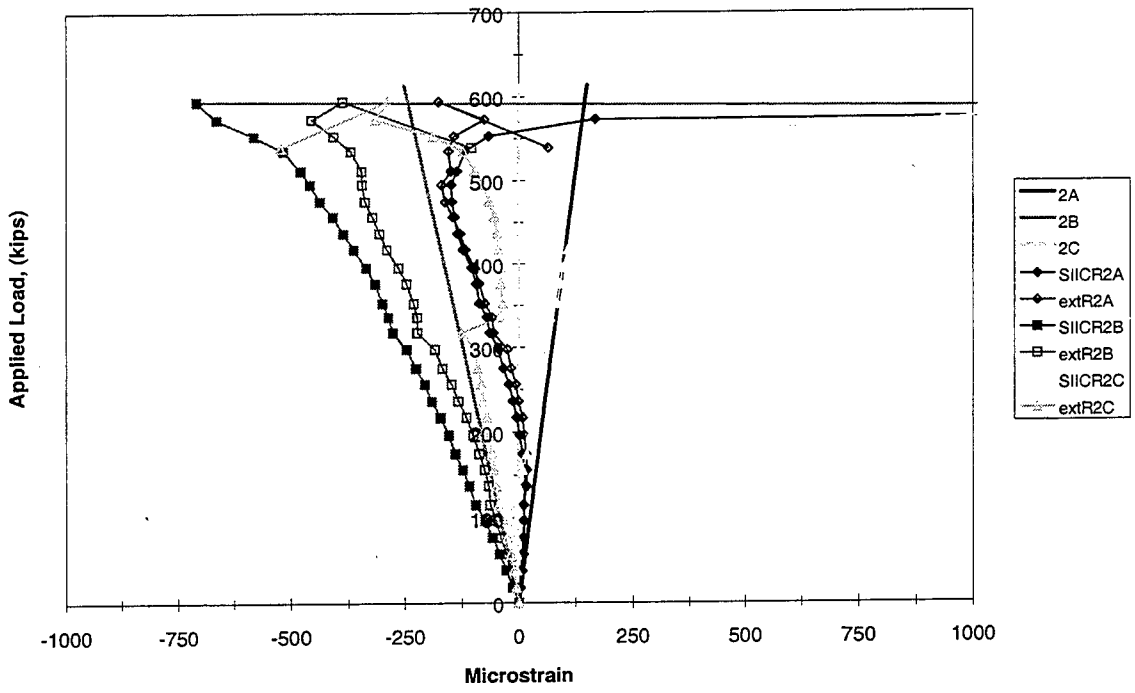

Figure 5.126 Rosette 2 (End IIC)

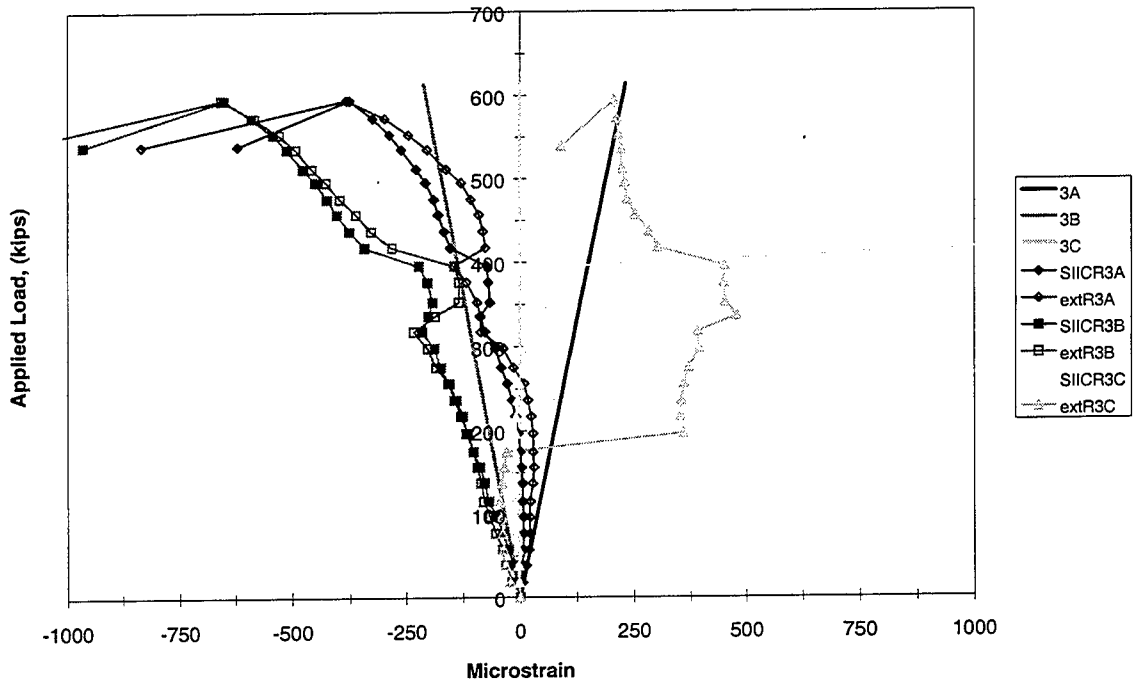

Figure 5.127 Rosette 3 (End IIC)

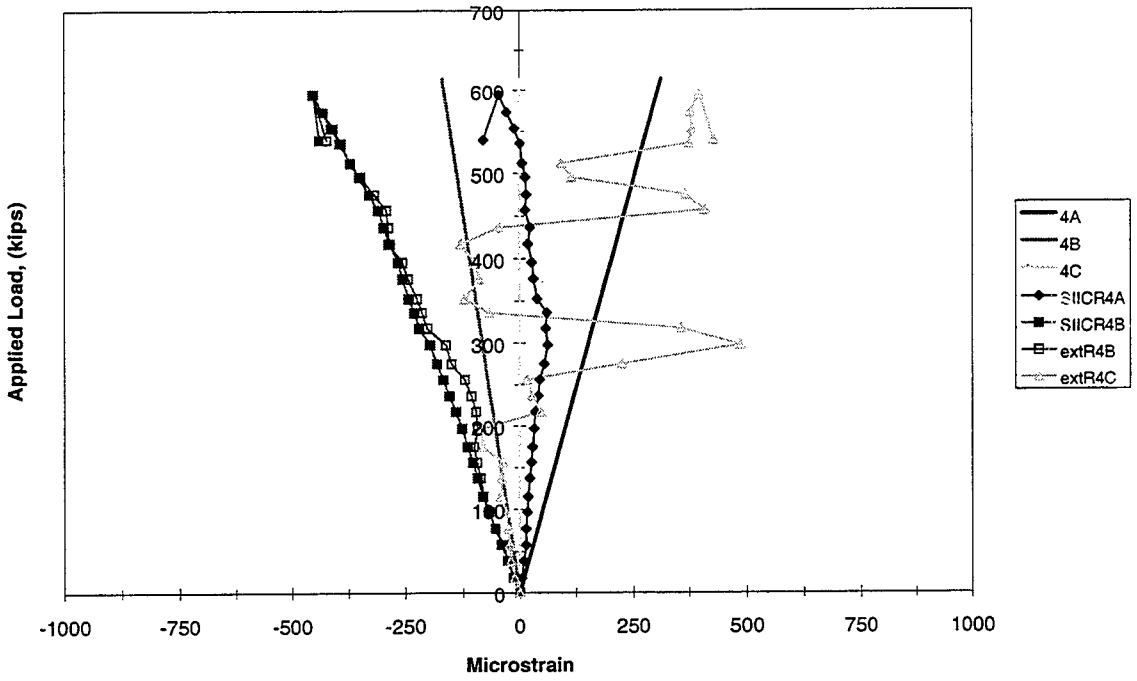

Figure 5.128 Rosette 4 (End IIC)

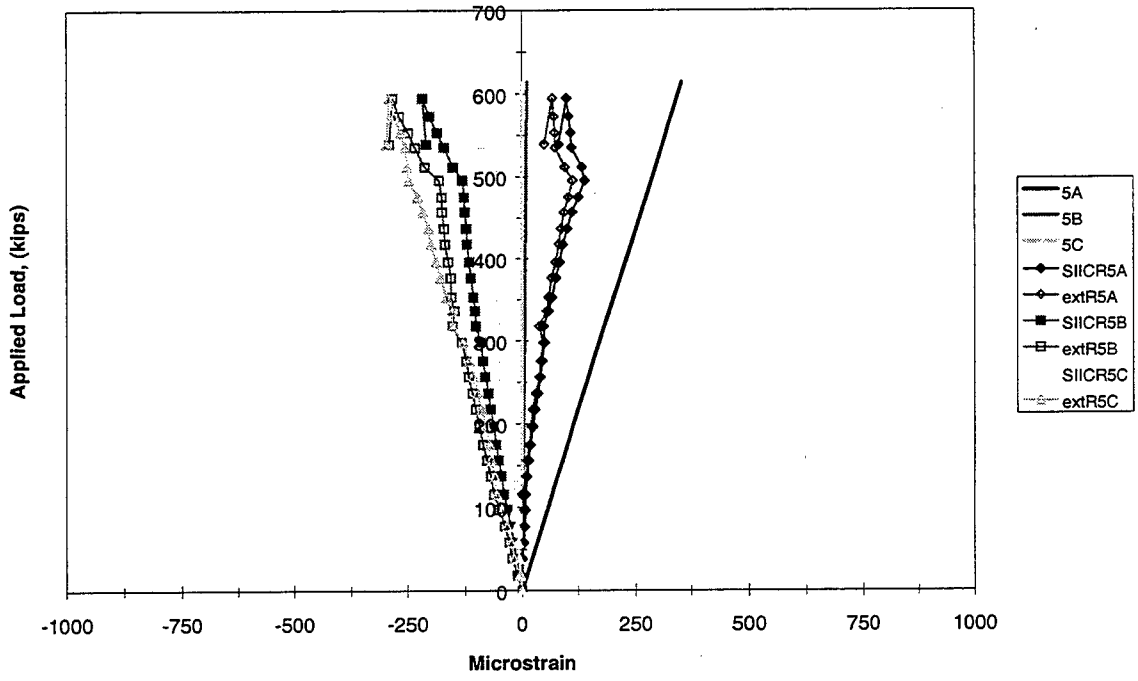

Figure 5.129 Rosette 5 (End IIC)

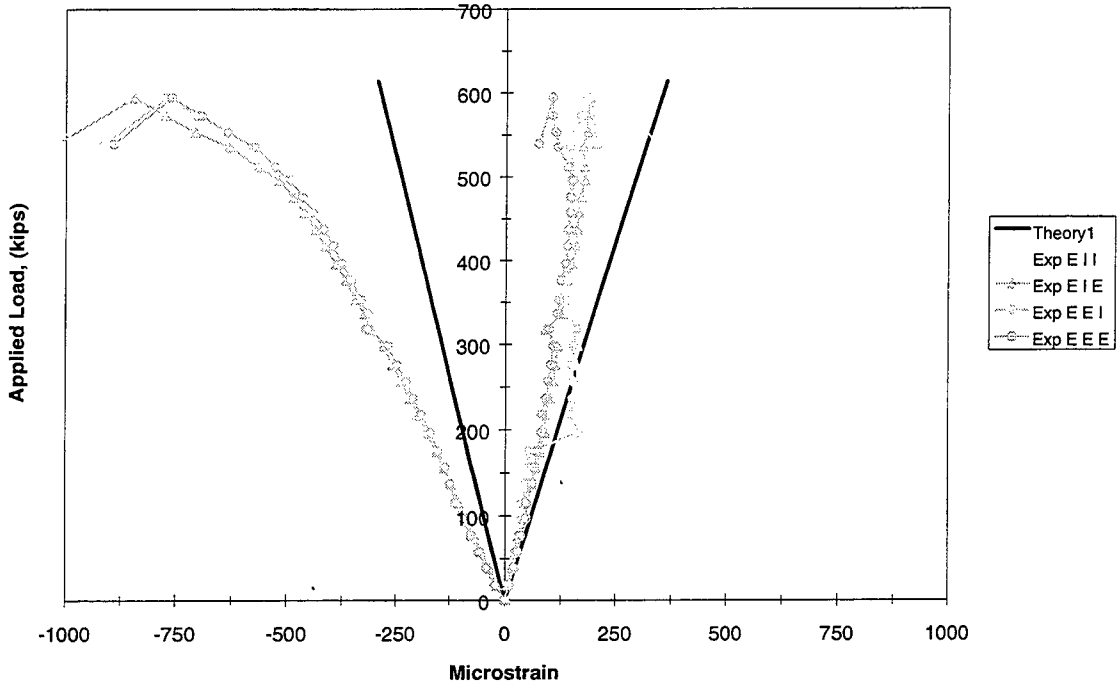

Figure 5.130 Principal Strains Rosette 1 (End IIC)

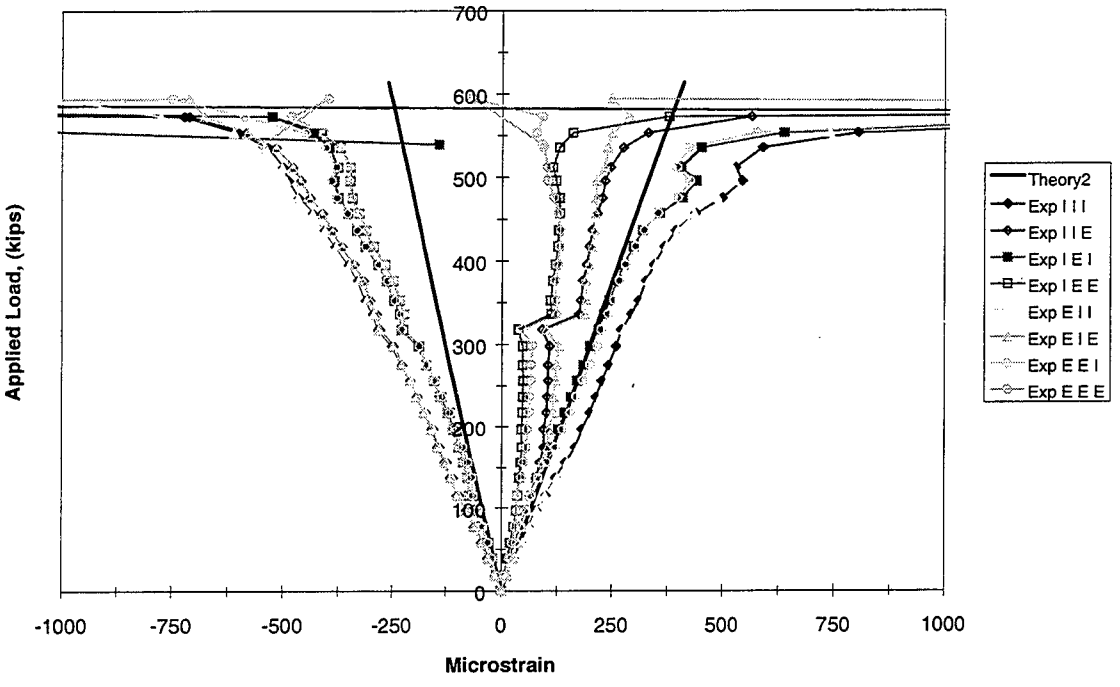

Figure 5.131 Principal Strains Rosette 2 (End IIC)

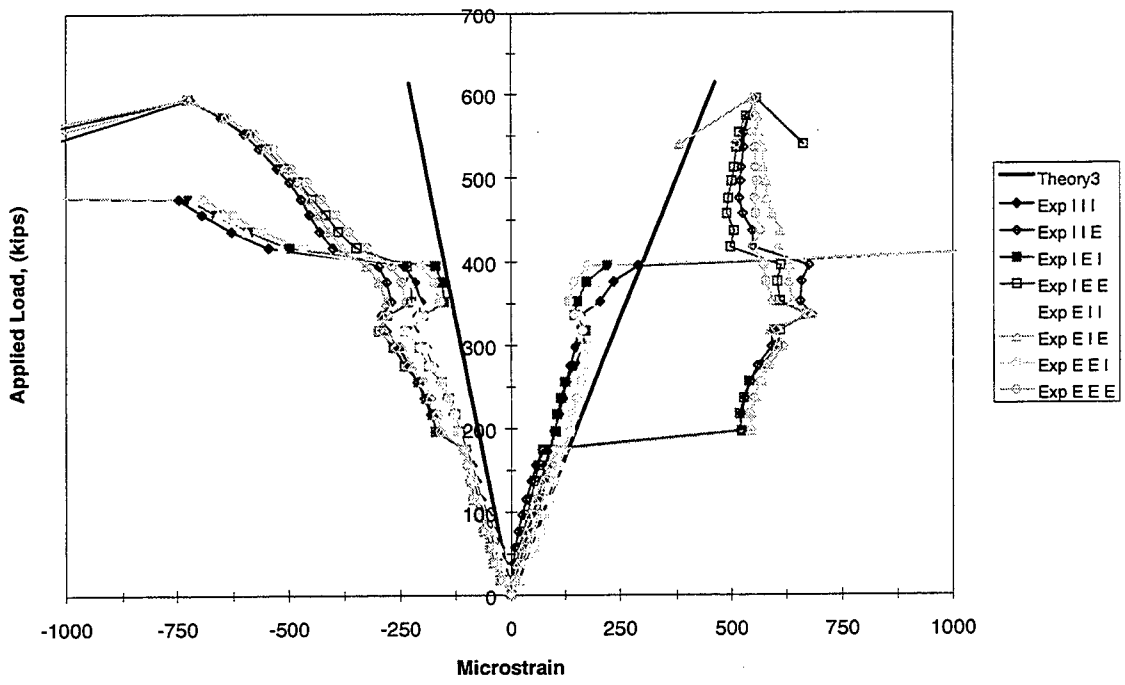

Figure 5.132 Principal Strains Rosette 3 (End IIC)

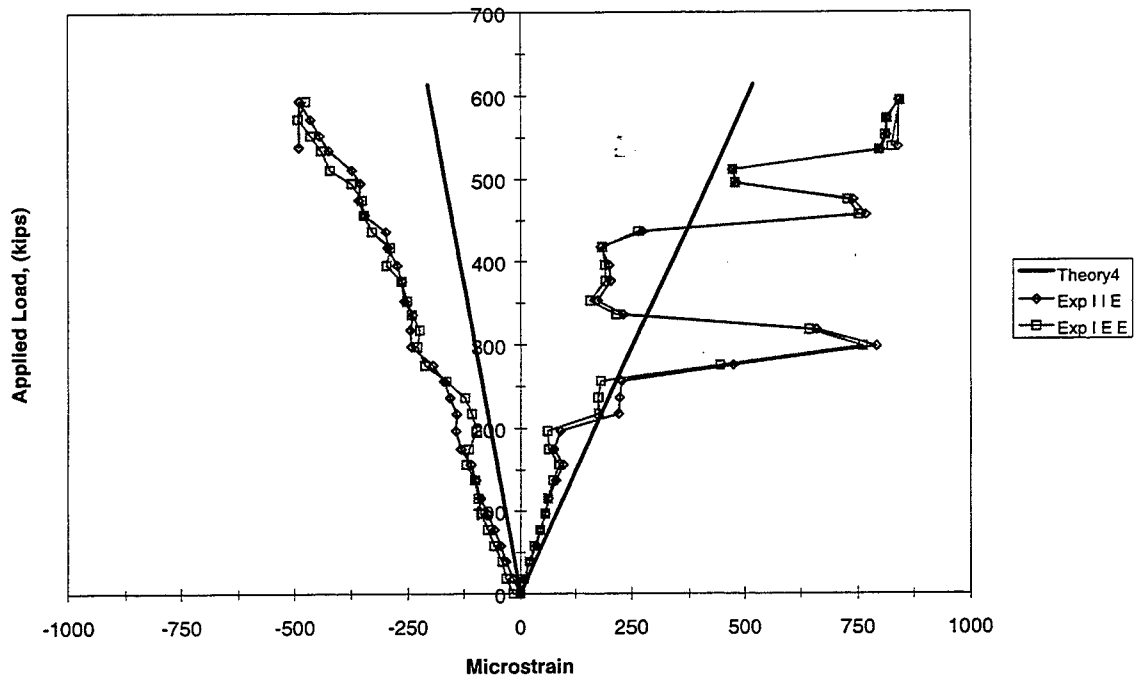

Figure 5.133 Principal Strains Rosette 4 (End IIC)

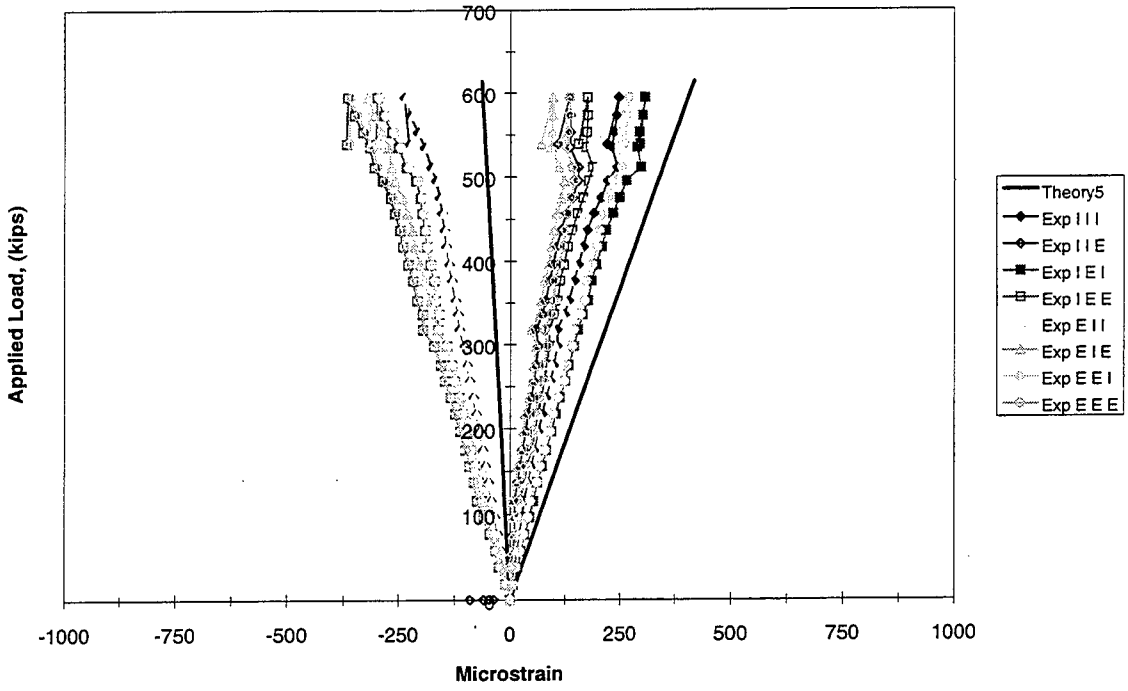

Figure 5.134 Principal Strains Rosette 5 (End IIC)

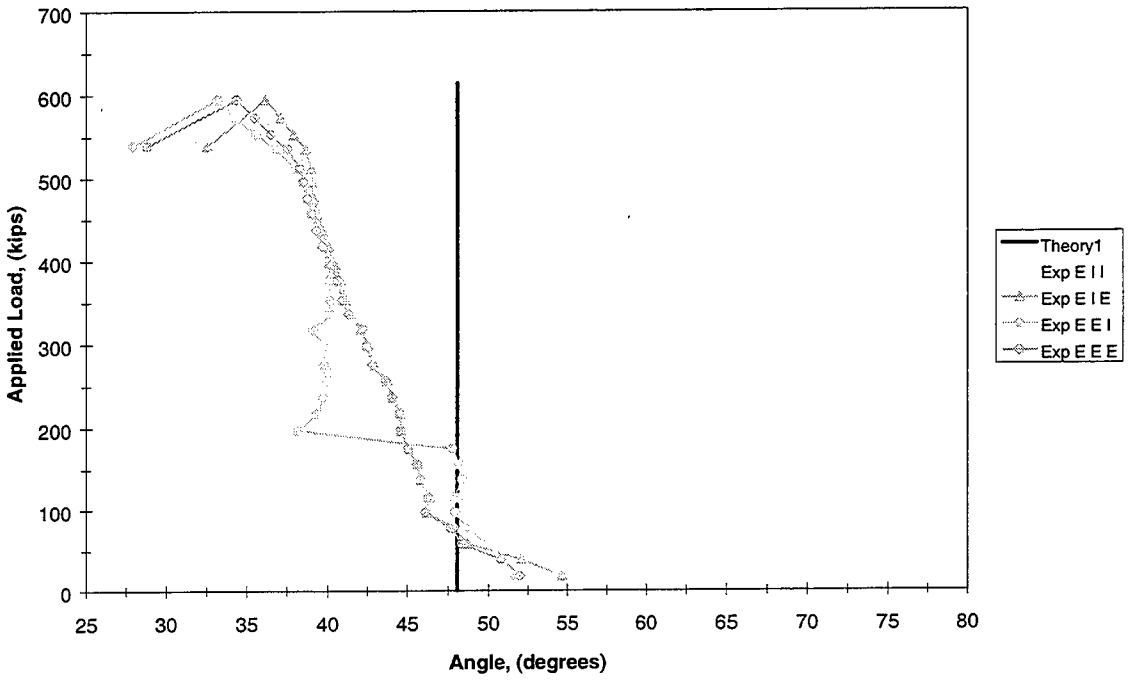

Figure 5.135 Principal Compression Angle Rosette 1 (End IIC)

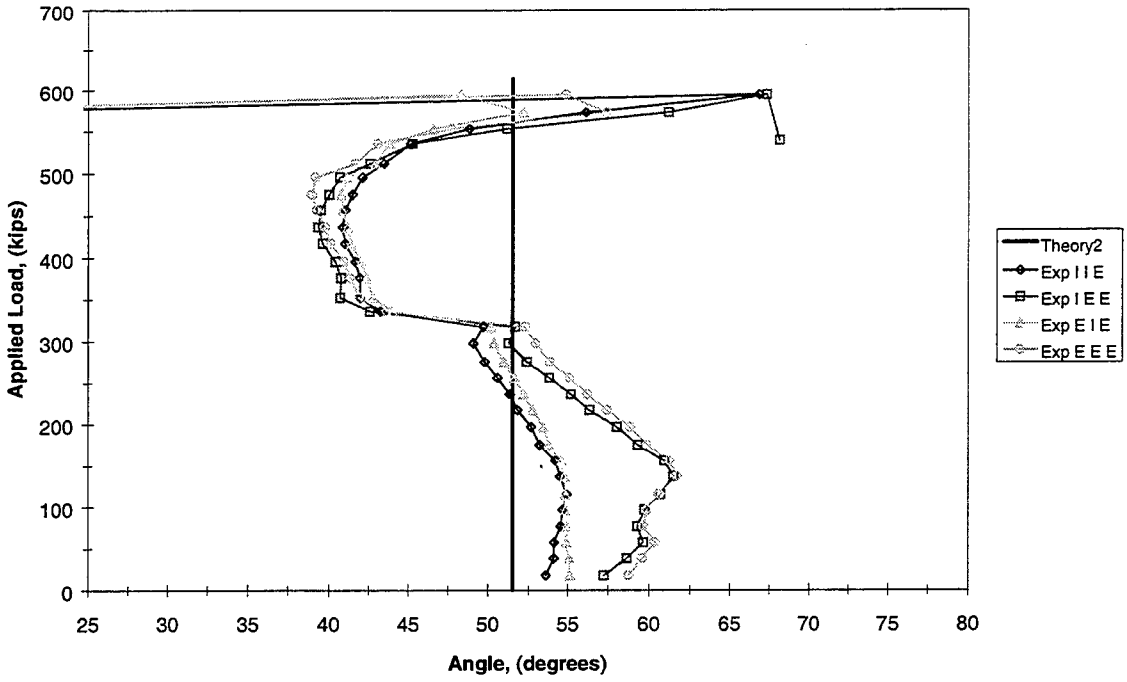

Figure 5.136 Principal Compression Angle Rosette 2 (End IIC)

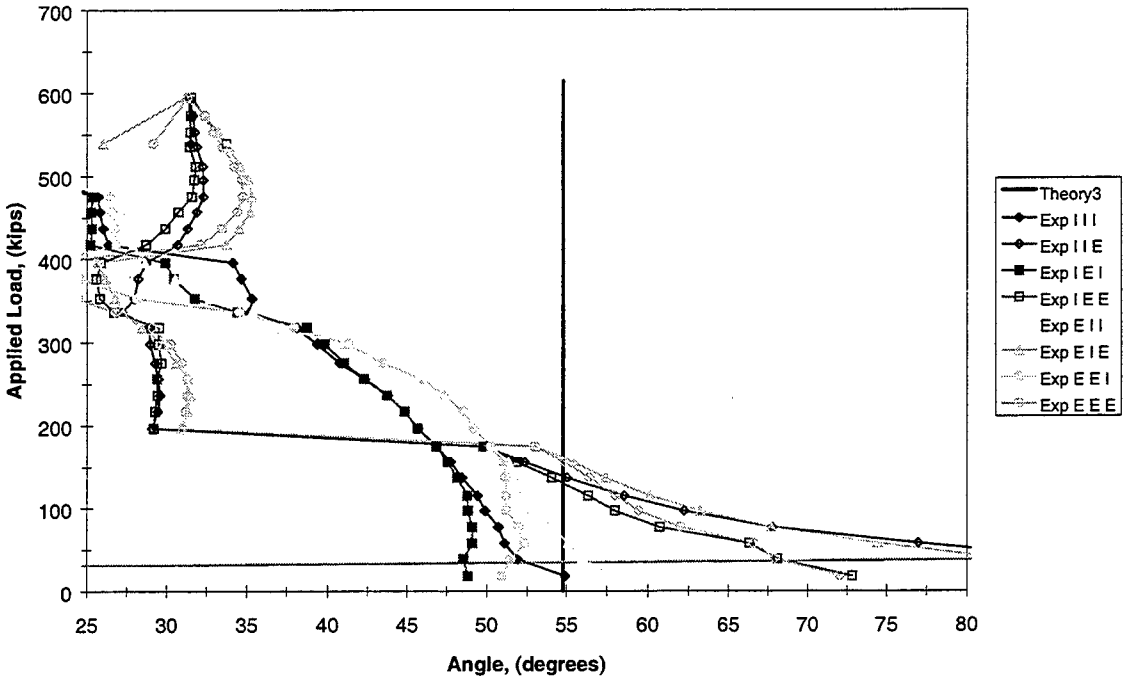

Figure 5.137 Principal Compression Angle Rosette 3 (End IIC)

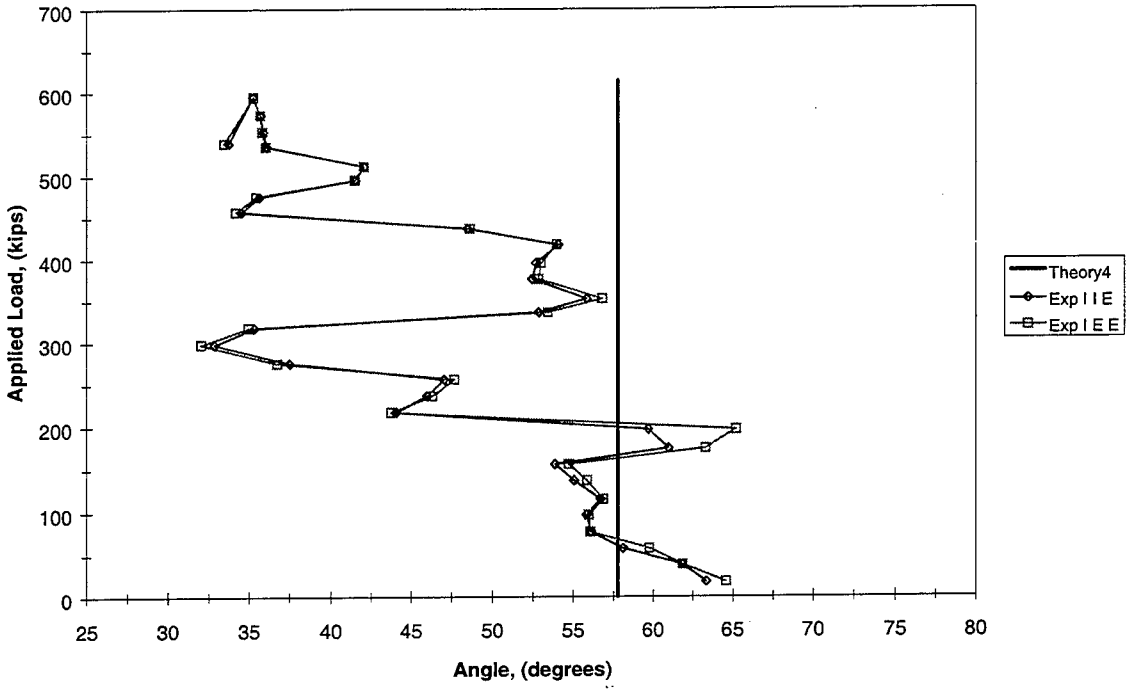

Figure 5.138 Principal Compression Angle Rosette 4 (End IIC)

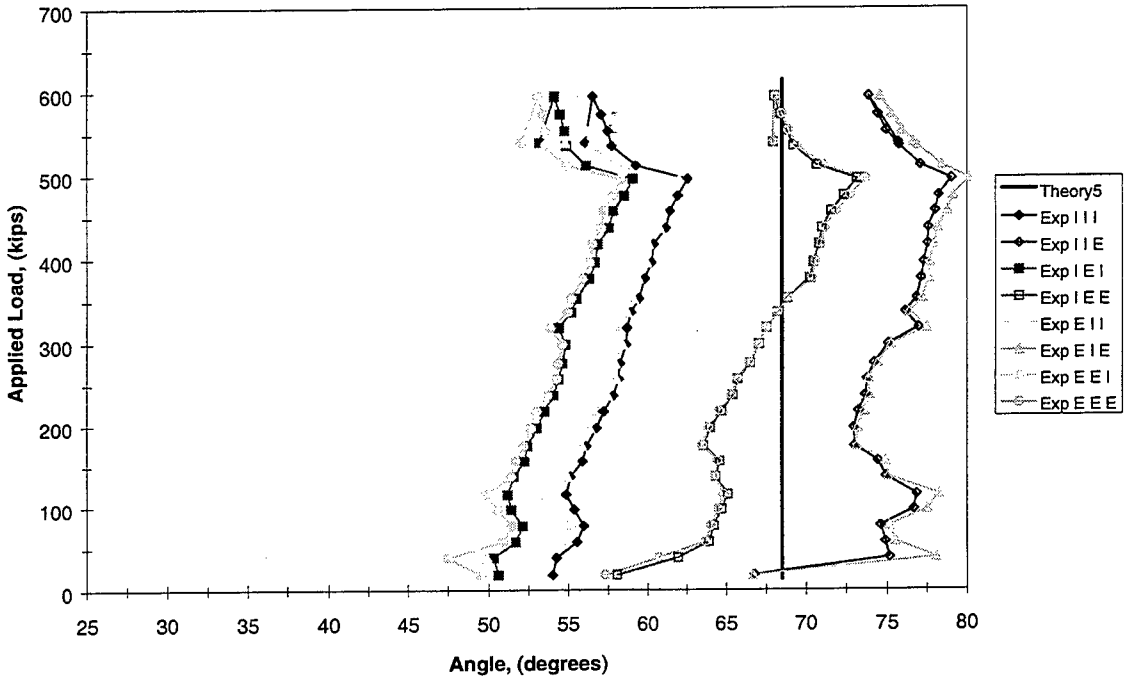

Figure 5.139 Principal Compression Angle Rosette 5 (End IIC)

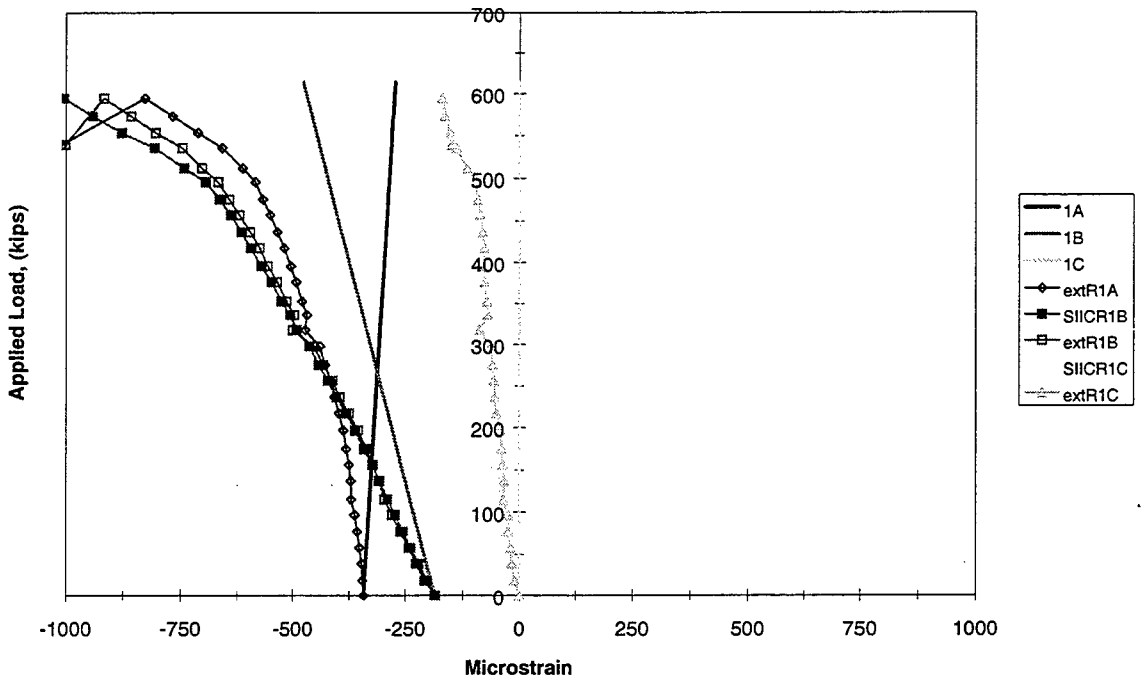

Figure 5.140 Corrected Rosette 1 (End IIC)

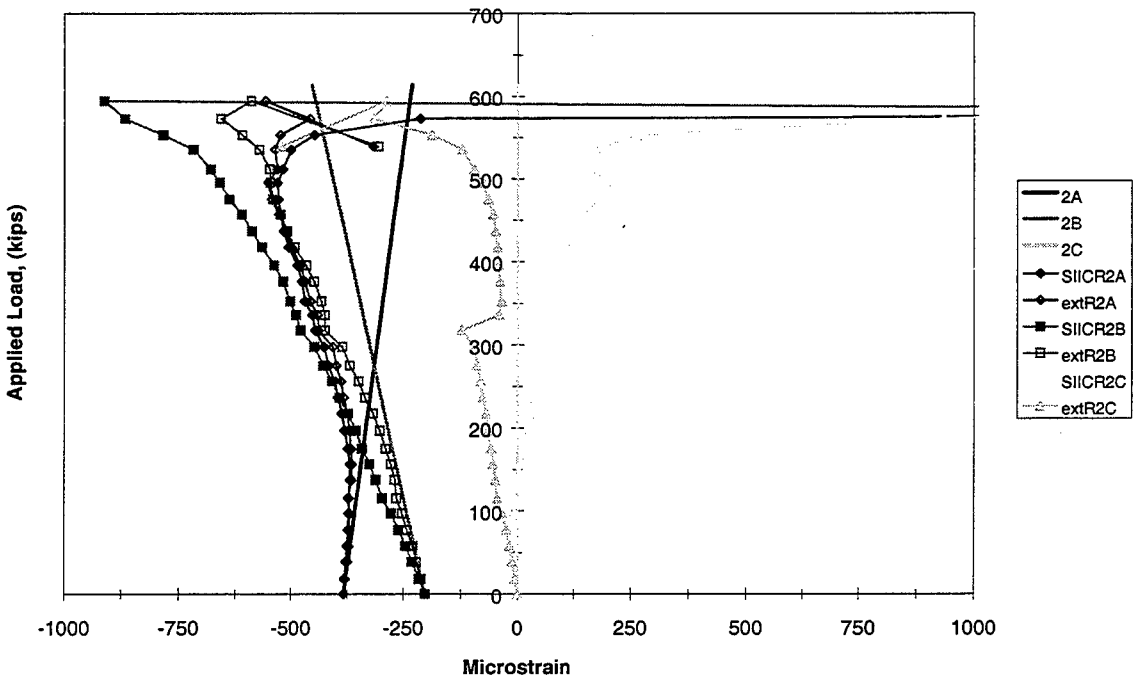

Figure 5.141 Corrected Rosette 2 (End IIC)

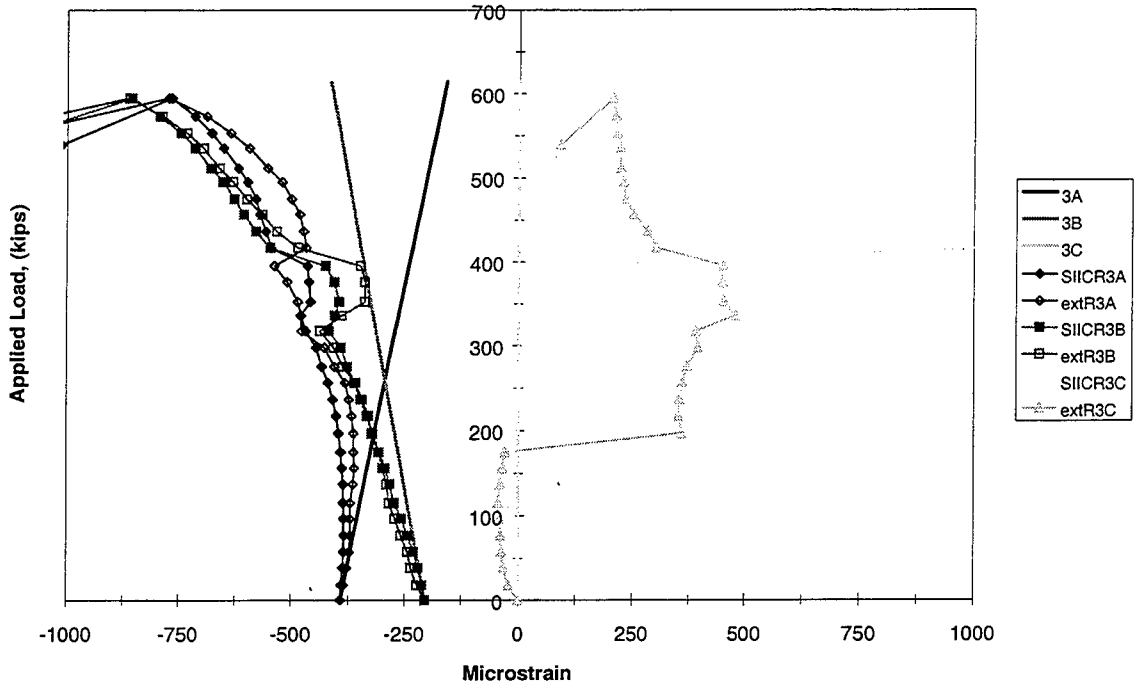

Figure 5.142 Corrected Rosette 3 (End IIC)

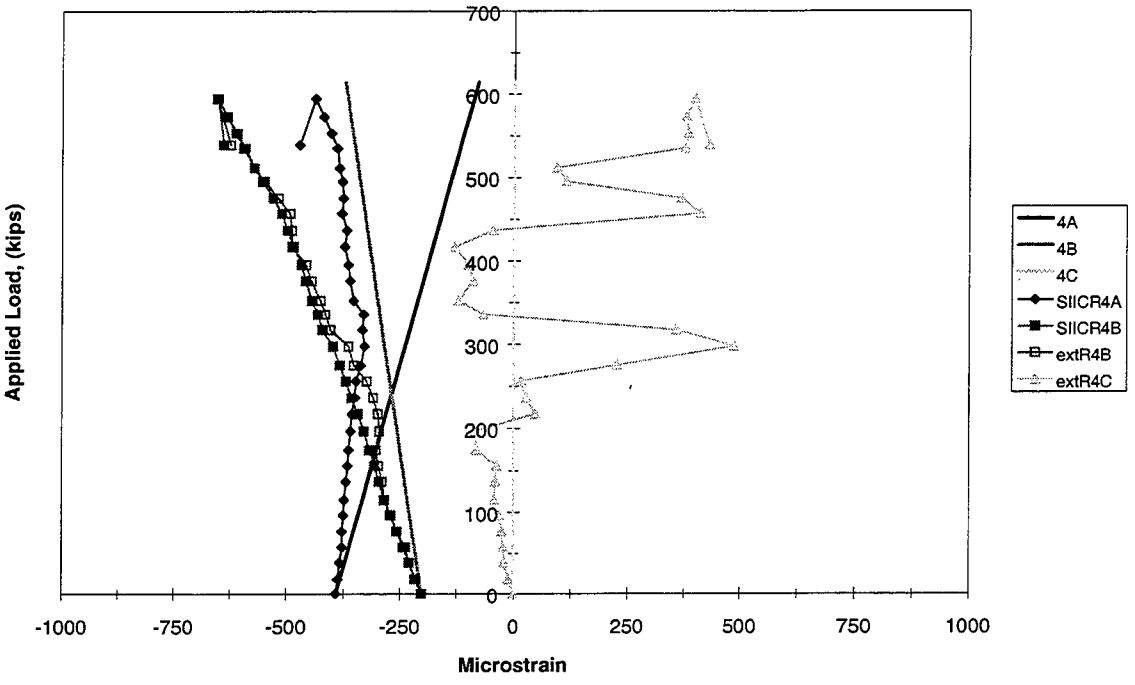

Figure 5.143 Corrected Rosette 4 (End IIC)

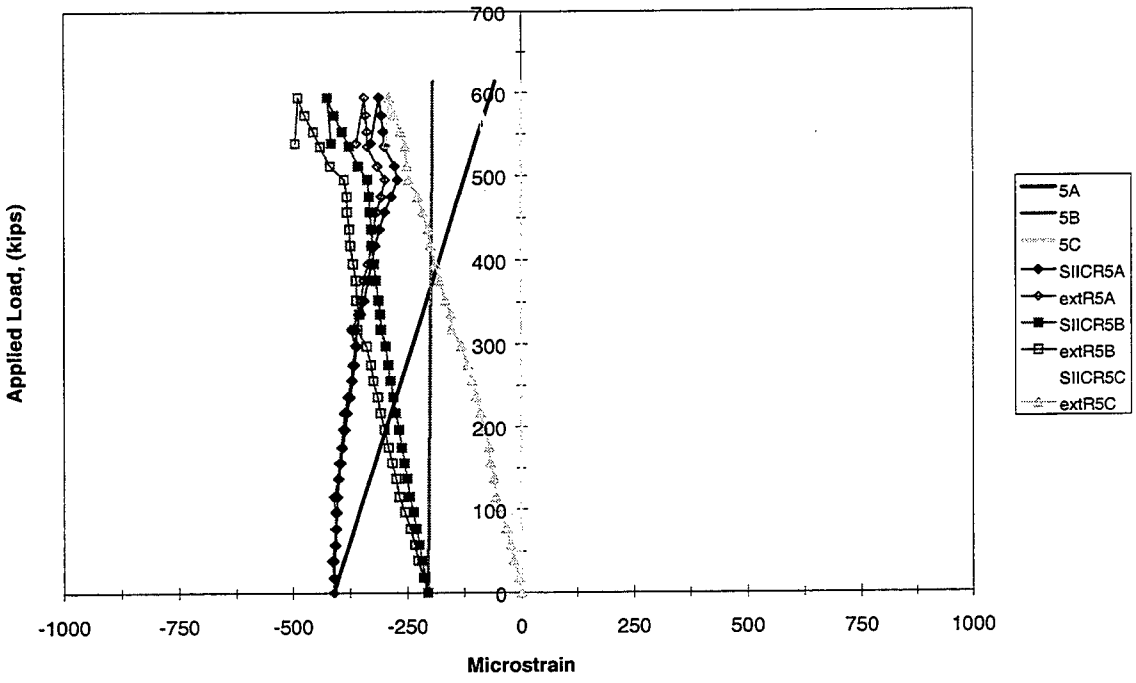

Figure 5.144 Corrected Rosette 5 (End IIC)

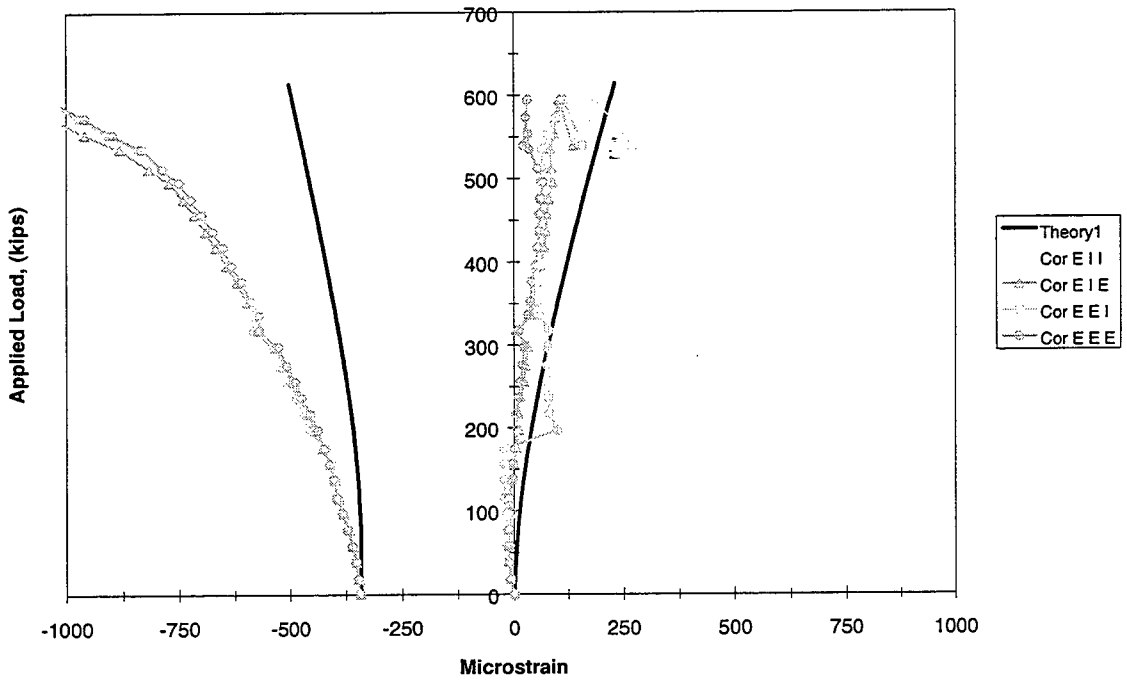

Figure 5.145 Corrected Principal Strains Rosette 1 (End IIC)

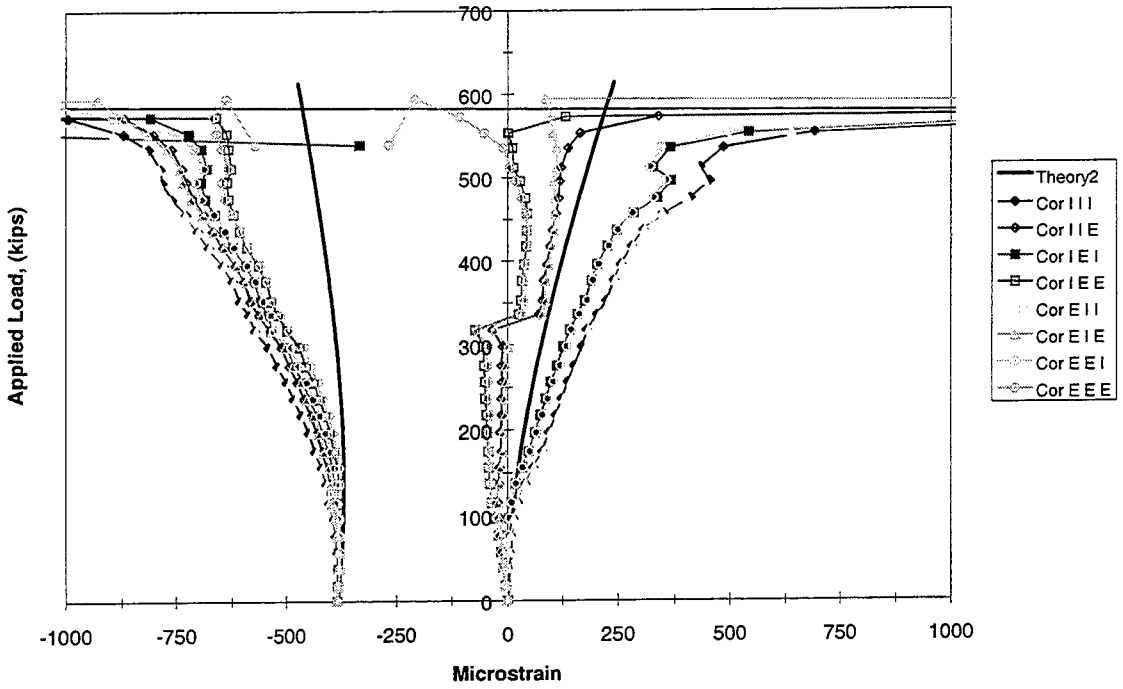

Figure 5.146 Corrected Principal Strains Rosette 2 (End IIC)

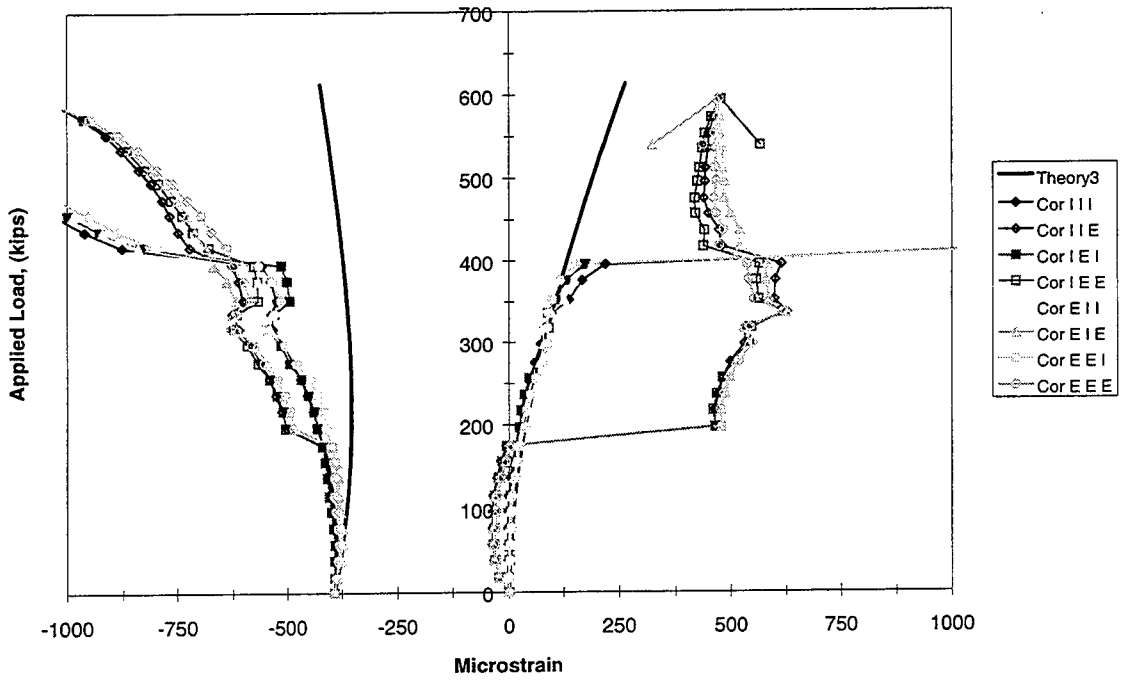

Figure 5.147 Corrected Principal Strains Rosette 3 (End IIC)

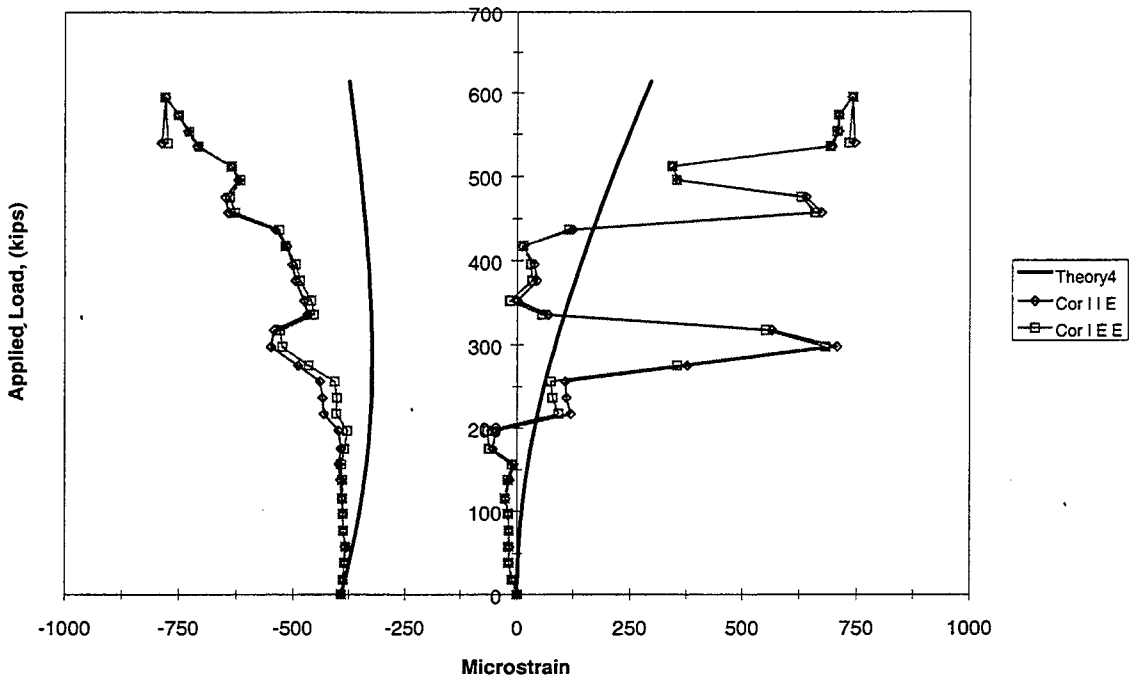

Figure 5.148 Corrected Principal Strains Rosette 4 (End IIC)

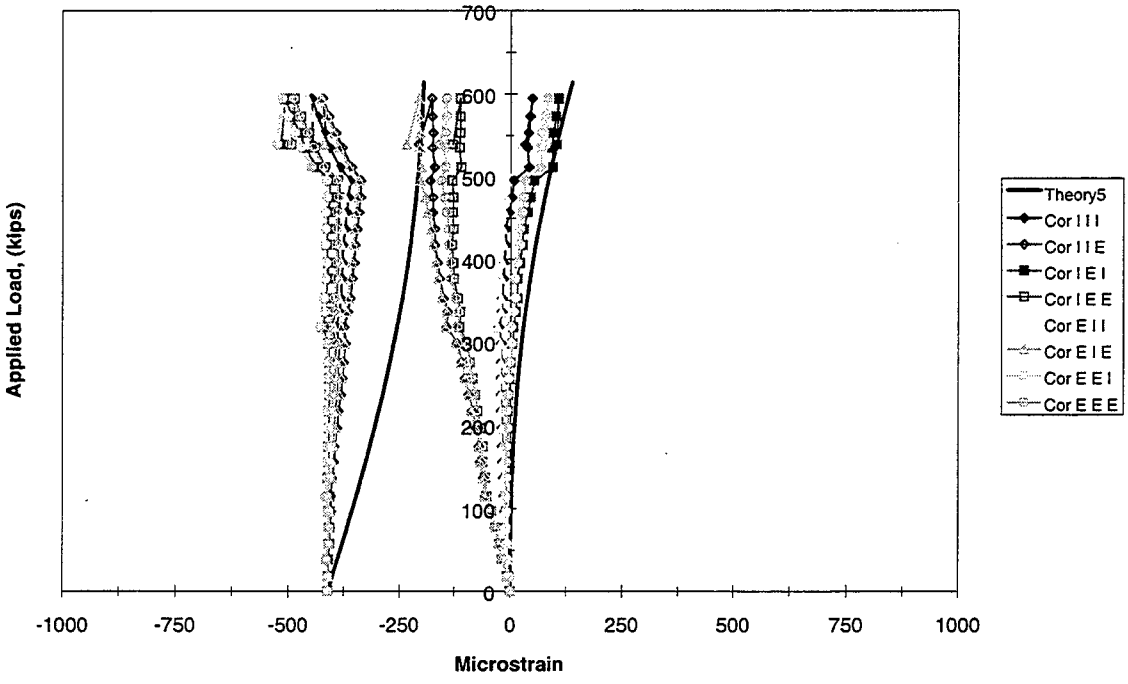

Figure 5.149 Corrected Principal Strains Rosette 5 (End IIC)

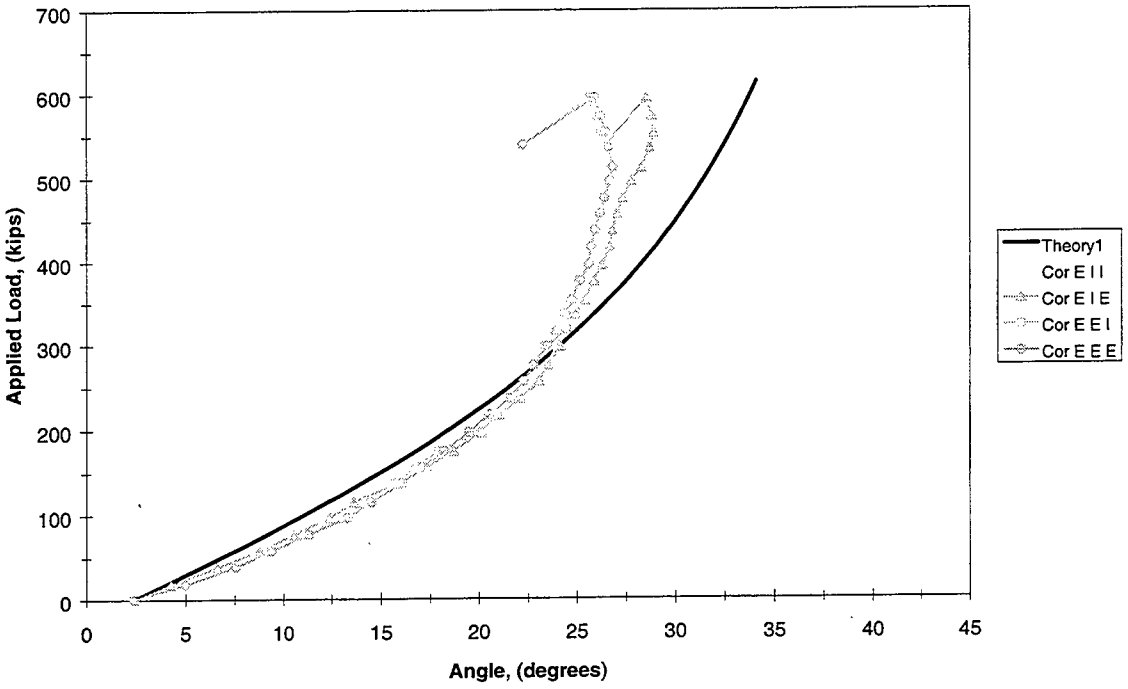

Figure 5.150 Corrected Principal Compression Angle Rosette 1 (End IIC)

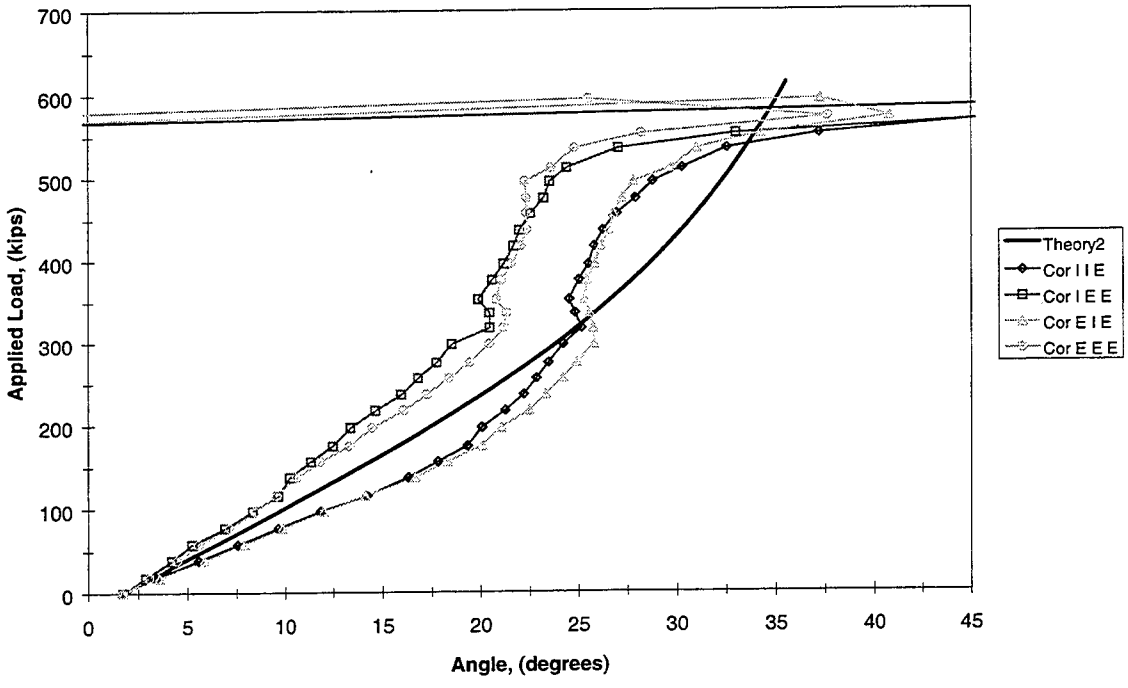

Figure 5.151 Corrected Principal Compression Angle Rosette 2 (End IIC)

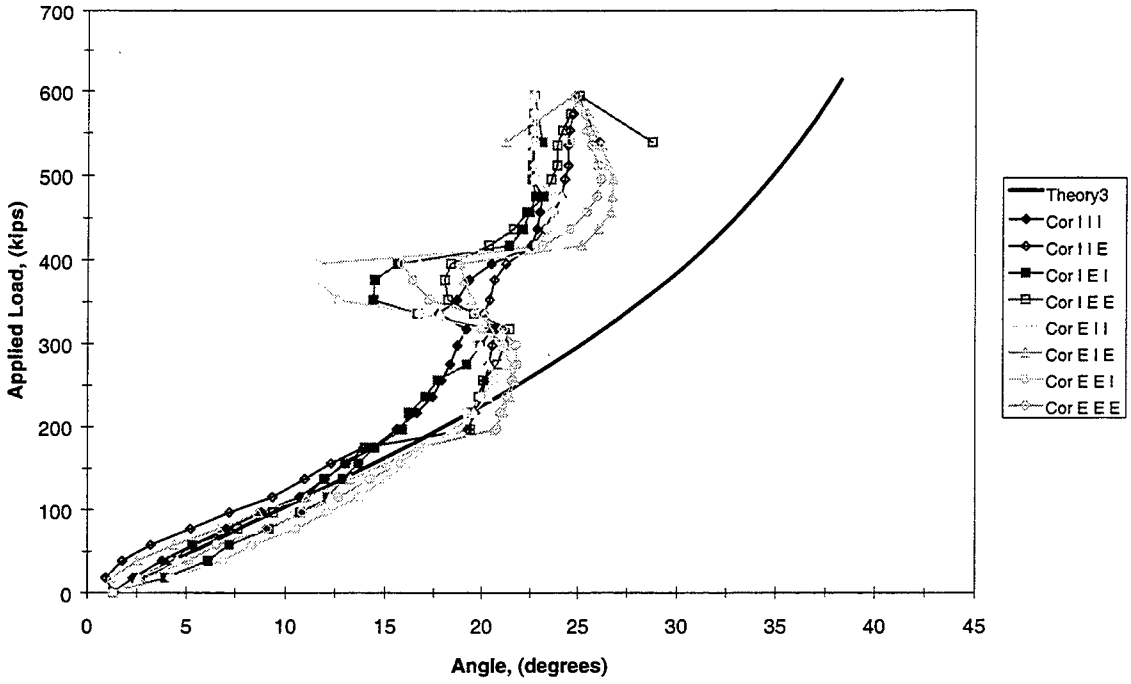

Figure 5.152 Corrected Principal Compression Angle Rosette 3 (End IIC)

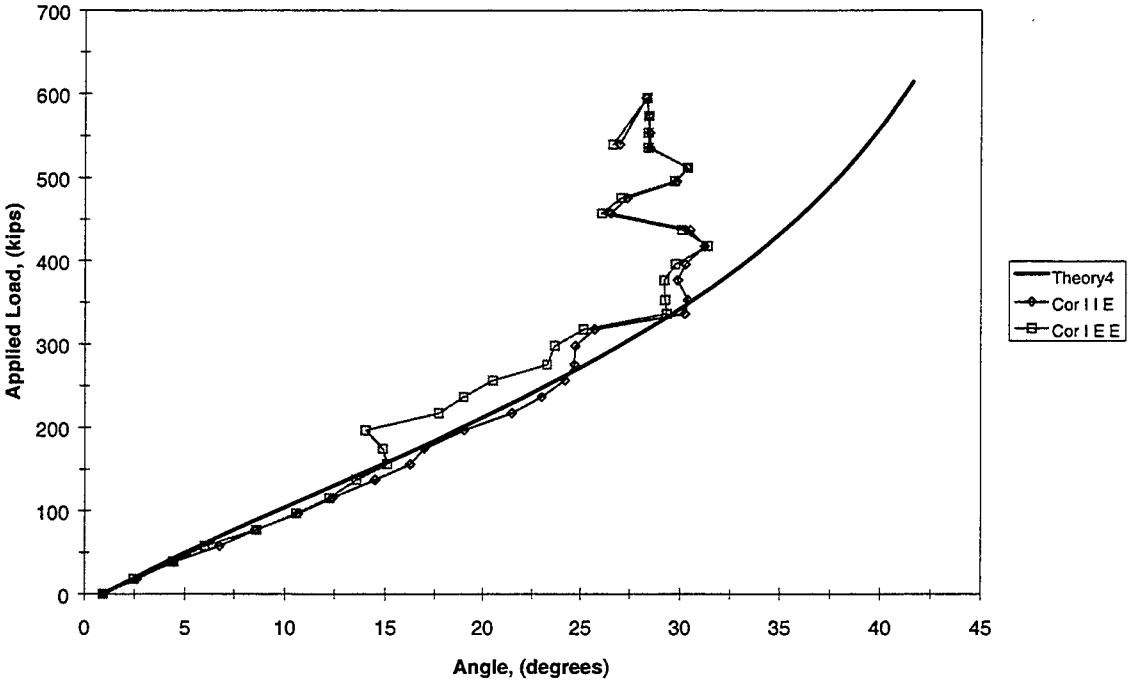

Figure 5.153 Corrected Principal Compression Angle Rosette 4 (End IIC)

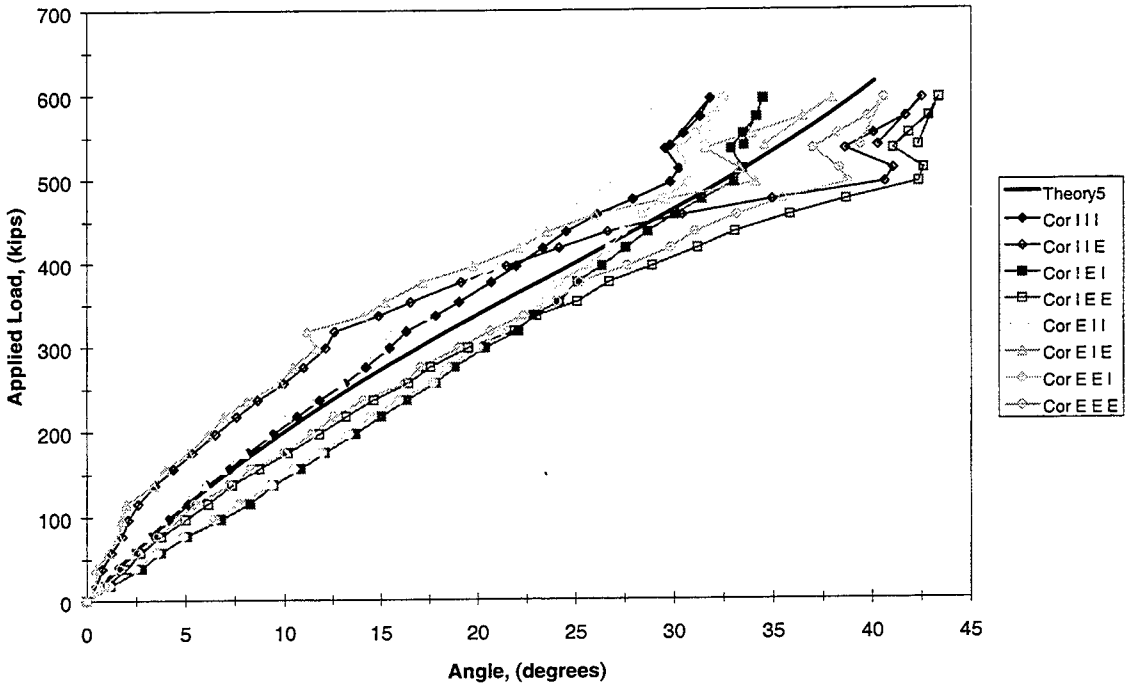

Figure 5.154 Corrected Principal Compression Angle Rosette 5 (End IIC)

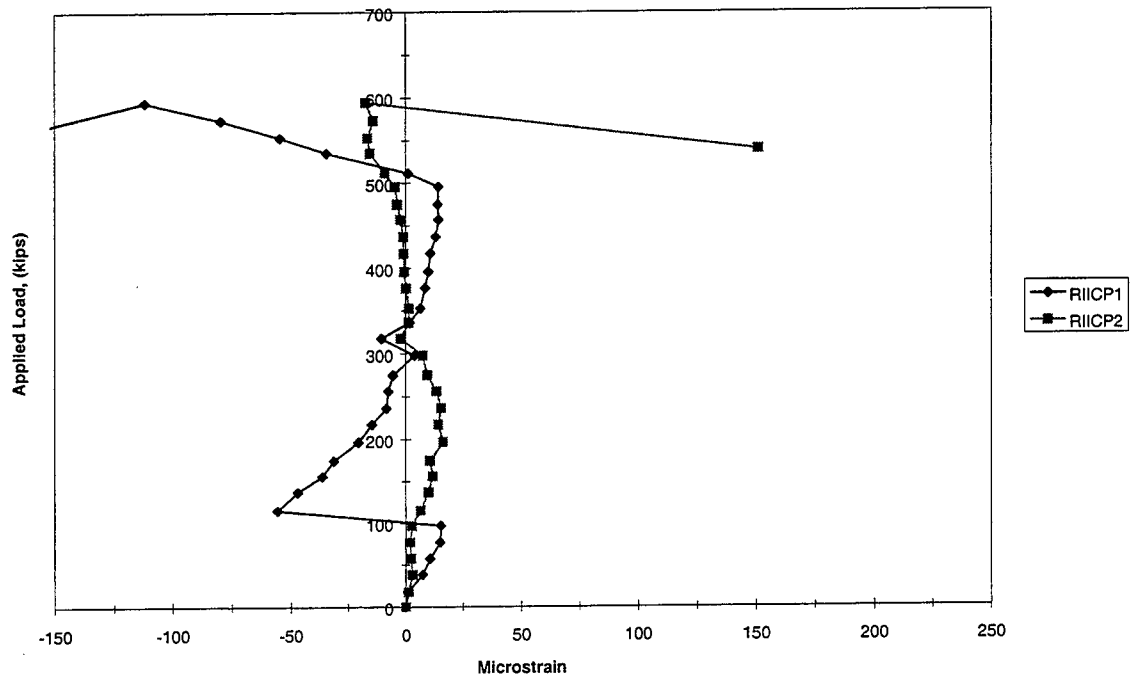

Figure 5.155 Rupture of Concrete (End IIC)

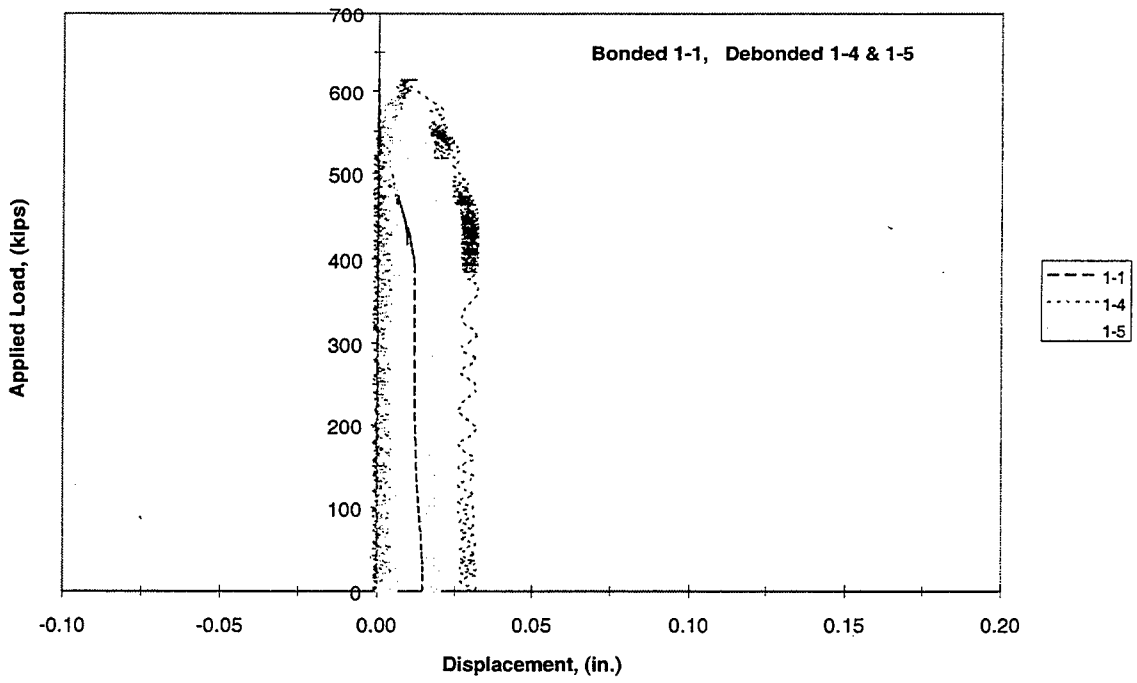

Figure 5.156 Strand Slip for 1-1, 1-4, & 1-5 (End IIC)

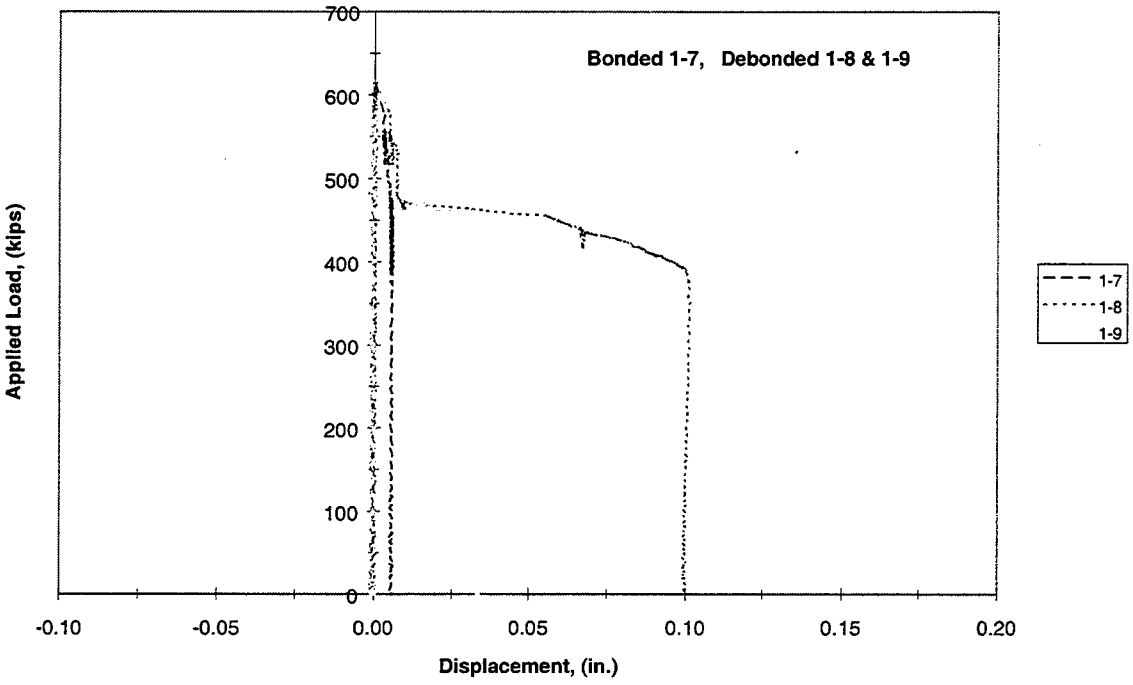

Figure 5.157 Strand Slip for 1-7, 1-8, & 1-9 (End IIC)

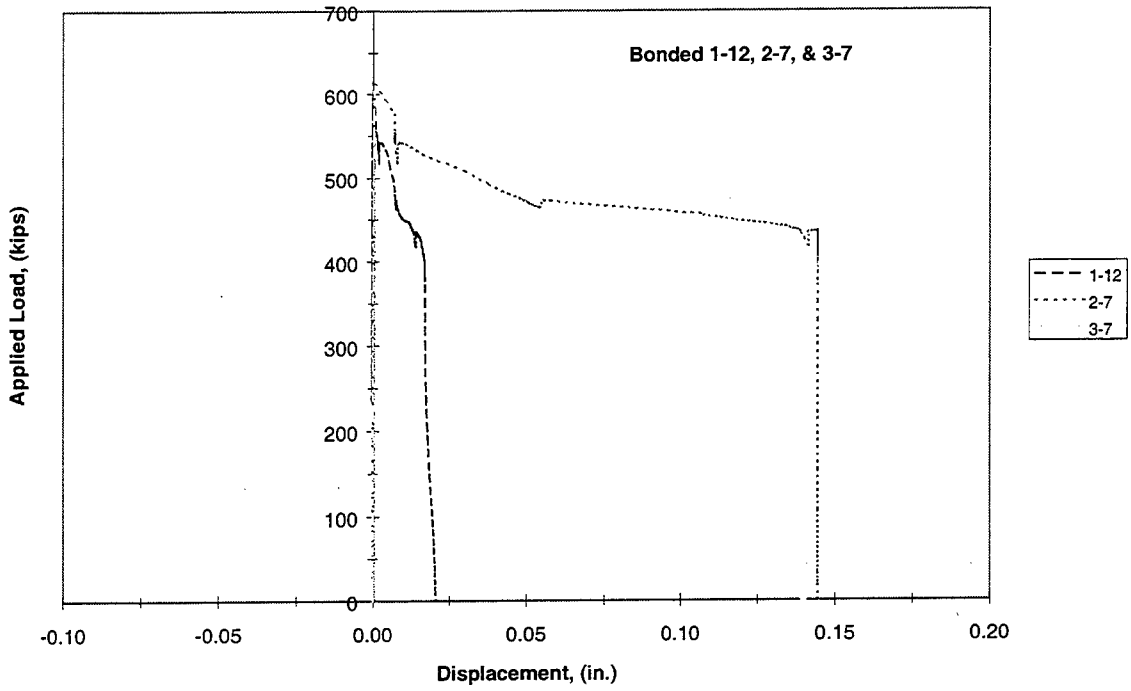

Figure 5.158 Strand Slip for 1-12, 2-7, & 3-7 (End IIC)

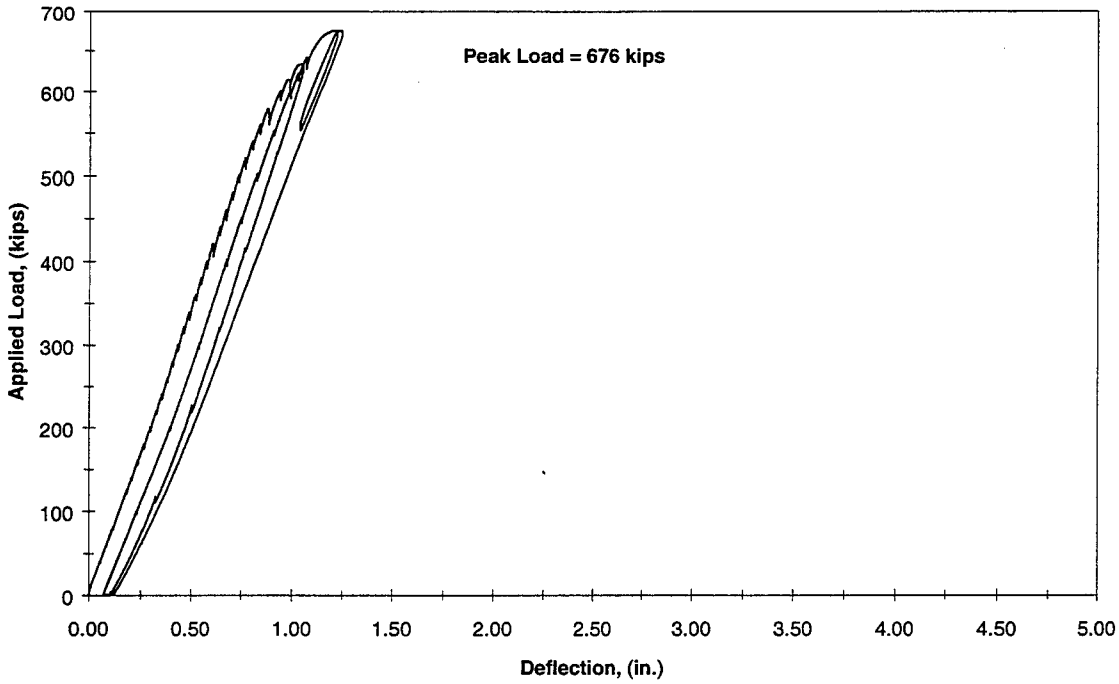

Figure 5.159 Corrected West Load Deflection (End IID)

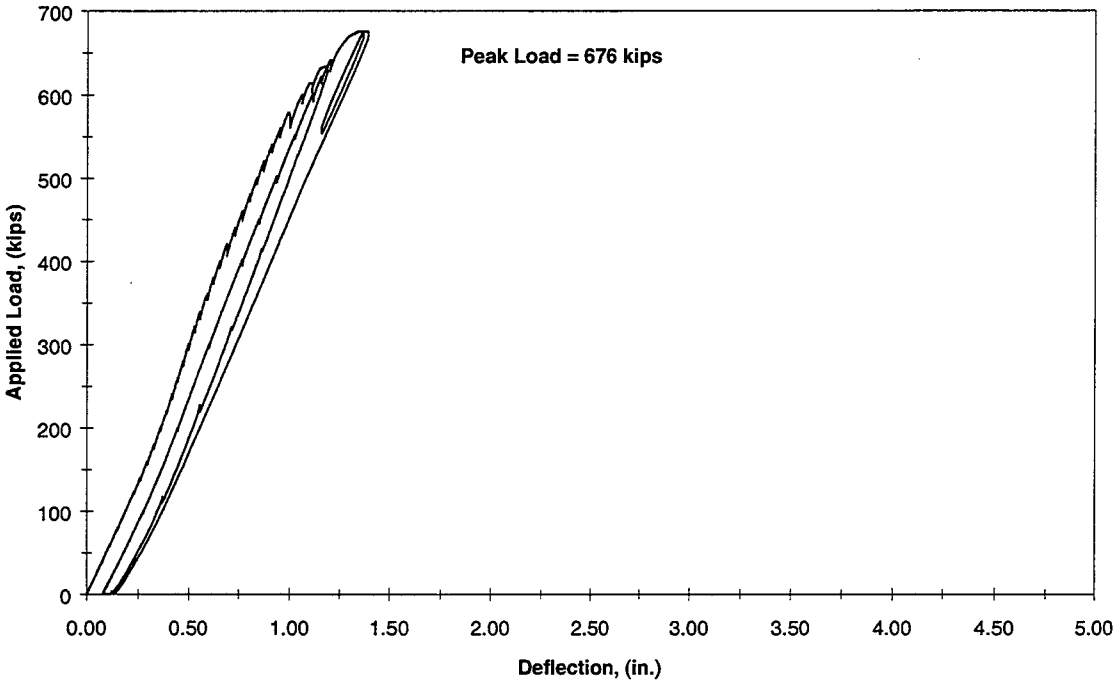

Figure 5.160 Corrected East Load Deflection (End IID)

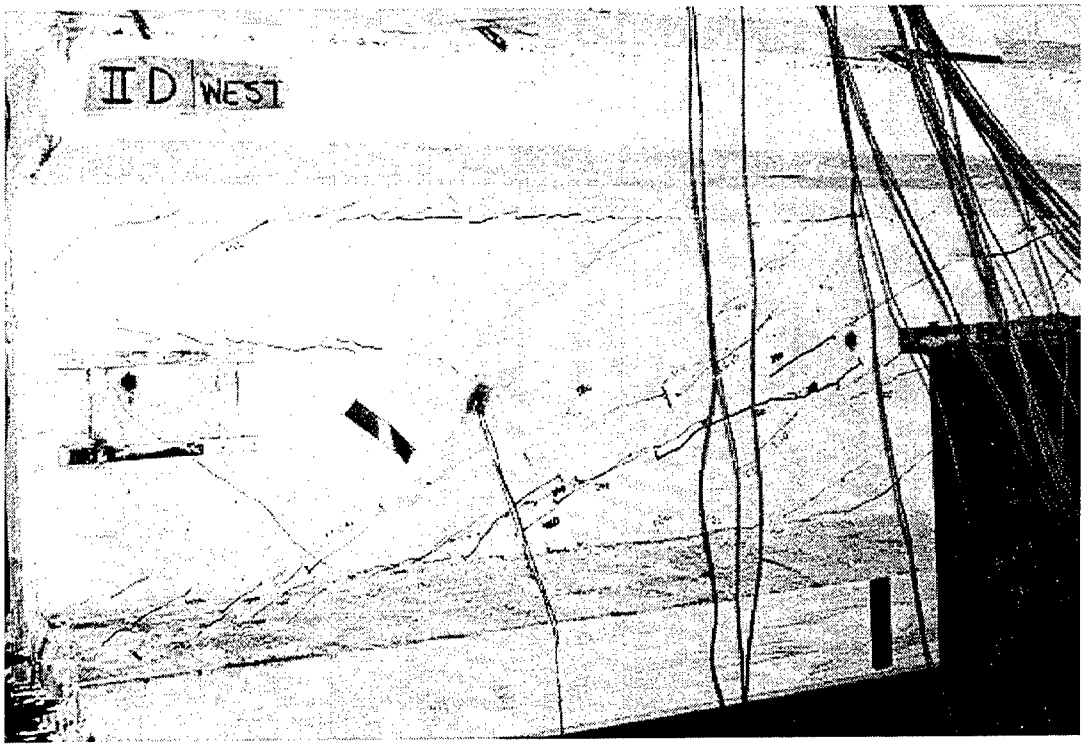

Figure 5.161 After Peak Load, Cracking Near Support (End IID)

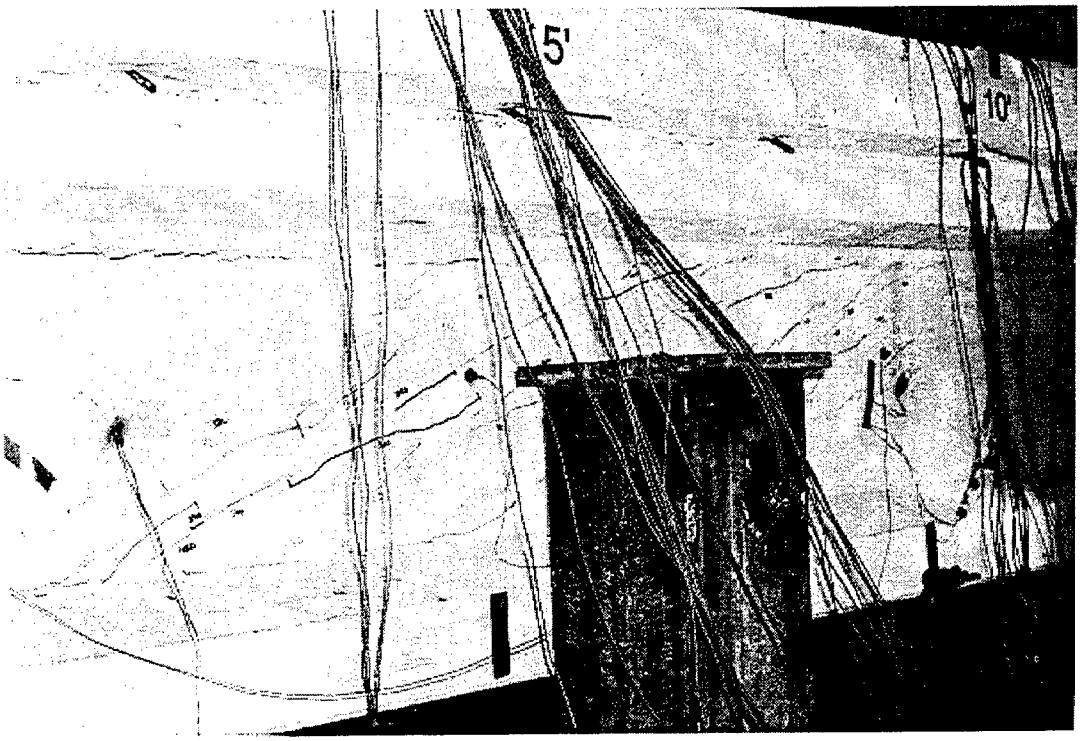

Figure 5.162 After Peak Load, Cracking Near Support (End IID)

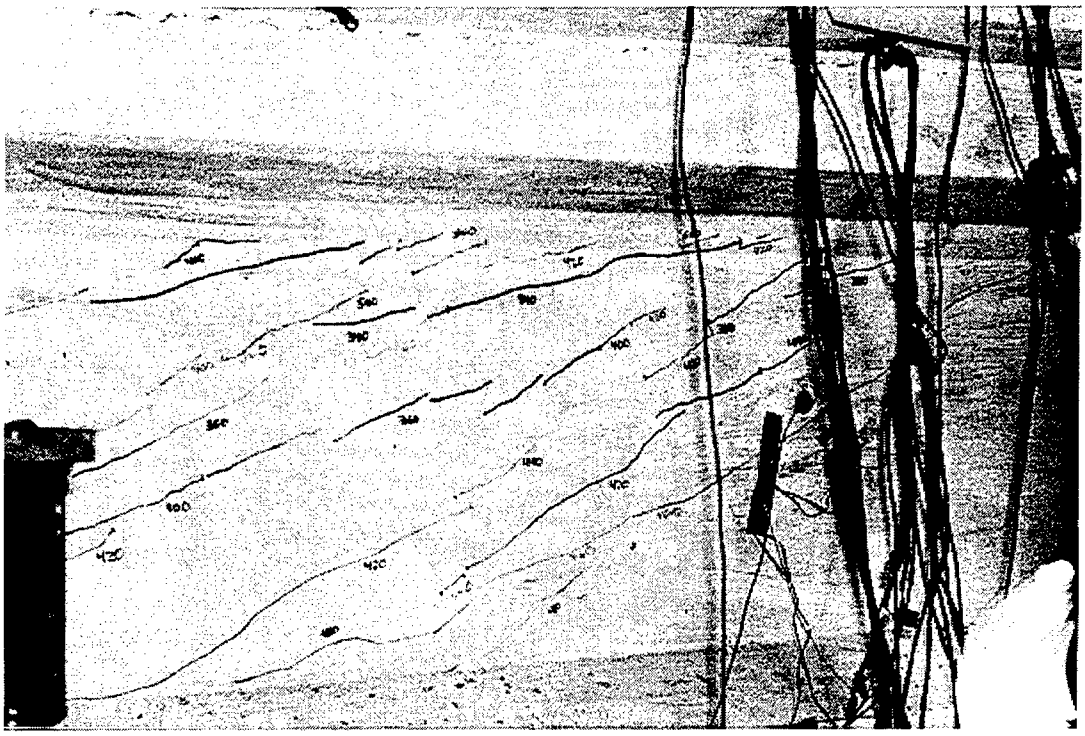

Figure 5.163 After Peak Load, Cracking Near Load Point (End IID)

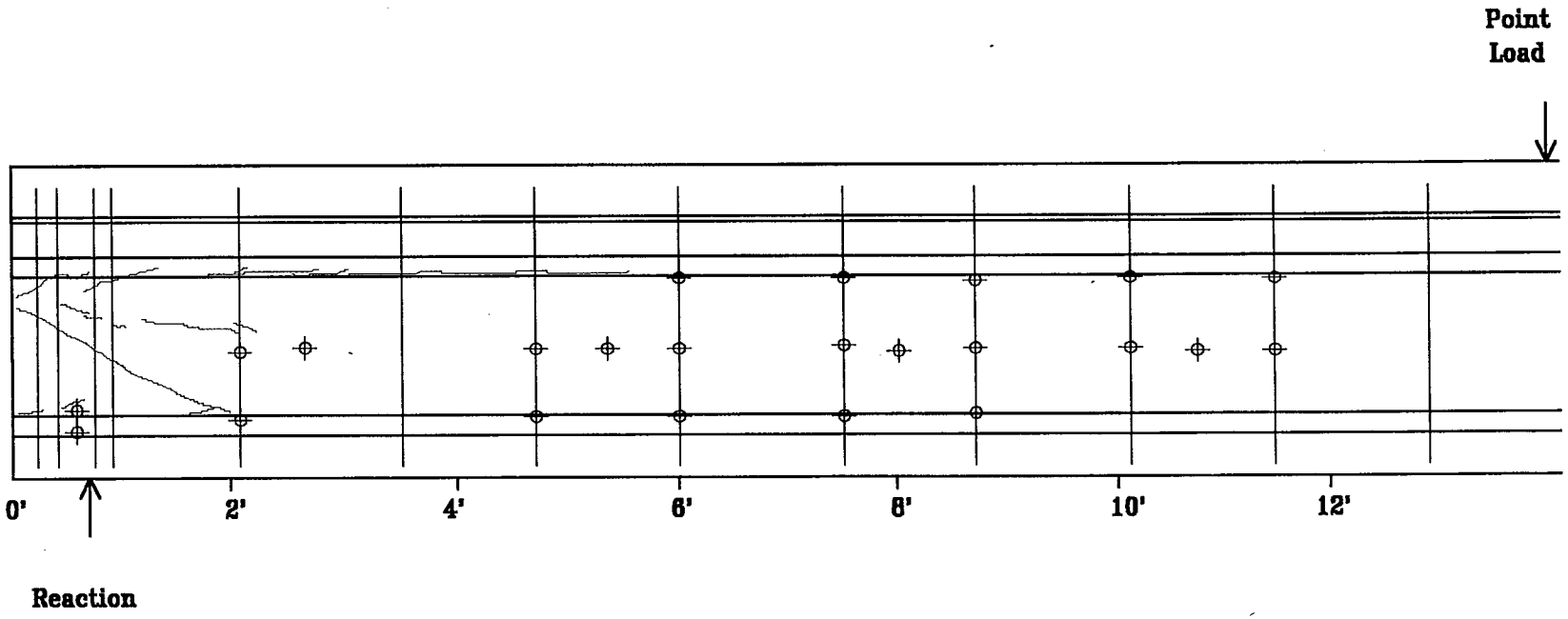

Figure 5.164 Before Testing, Crack Drawing (End IID)

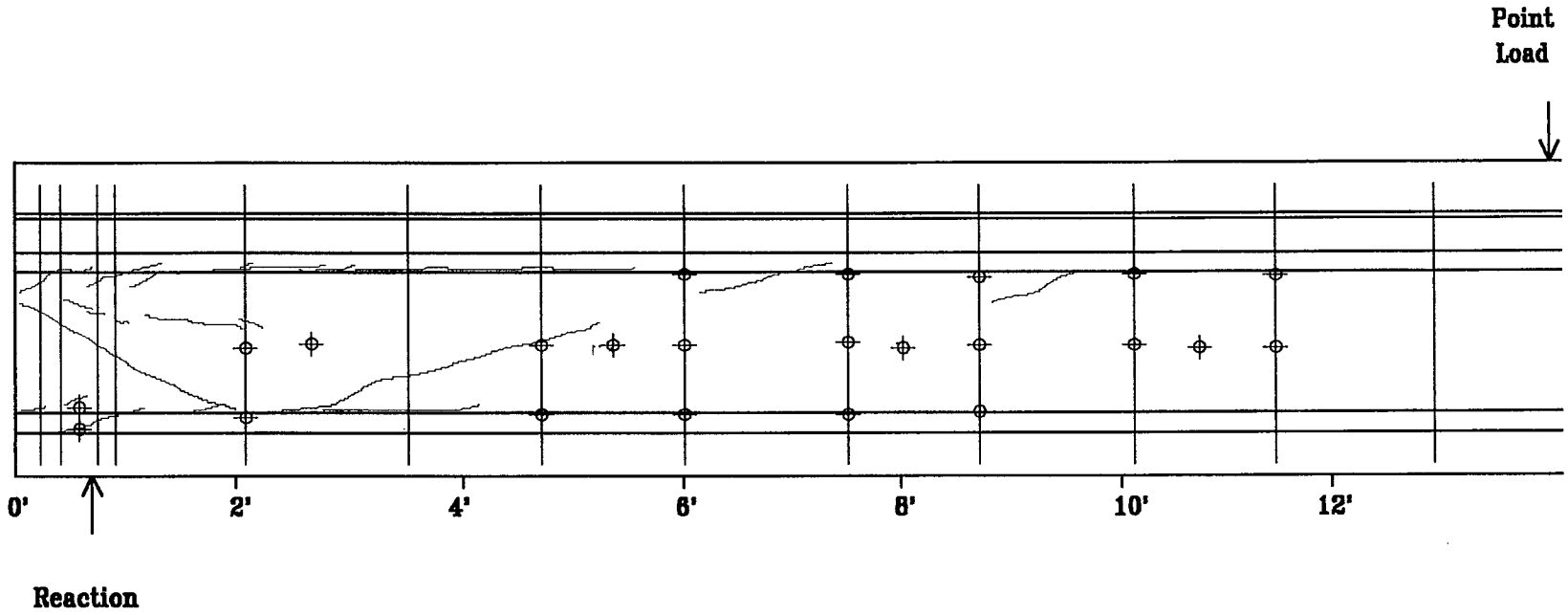

Figure 5.165 After 340 kips, Crack Drawing (End IID)

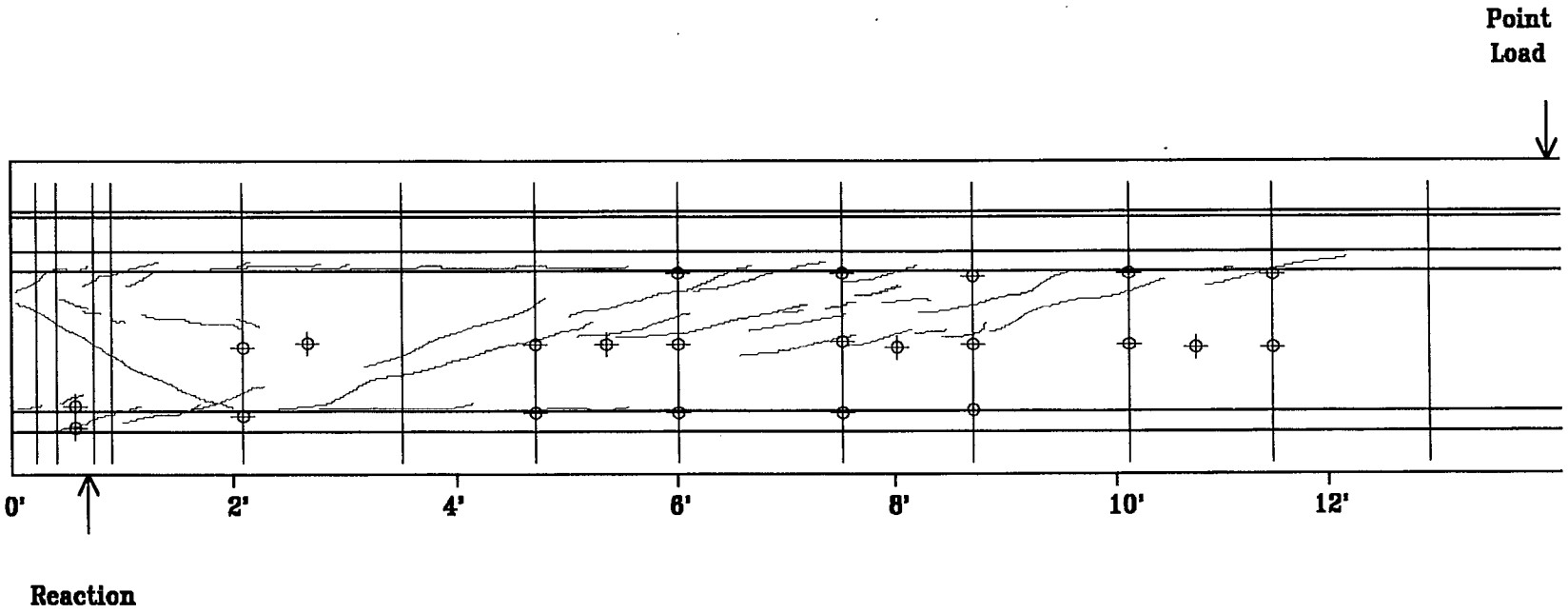

Figure 5.166 After 400 kips, Crack Drawing (End IID)

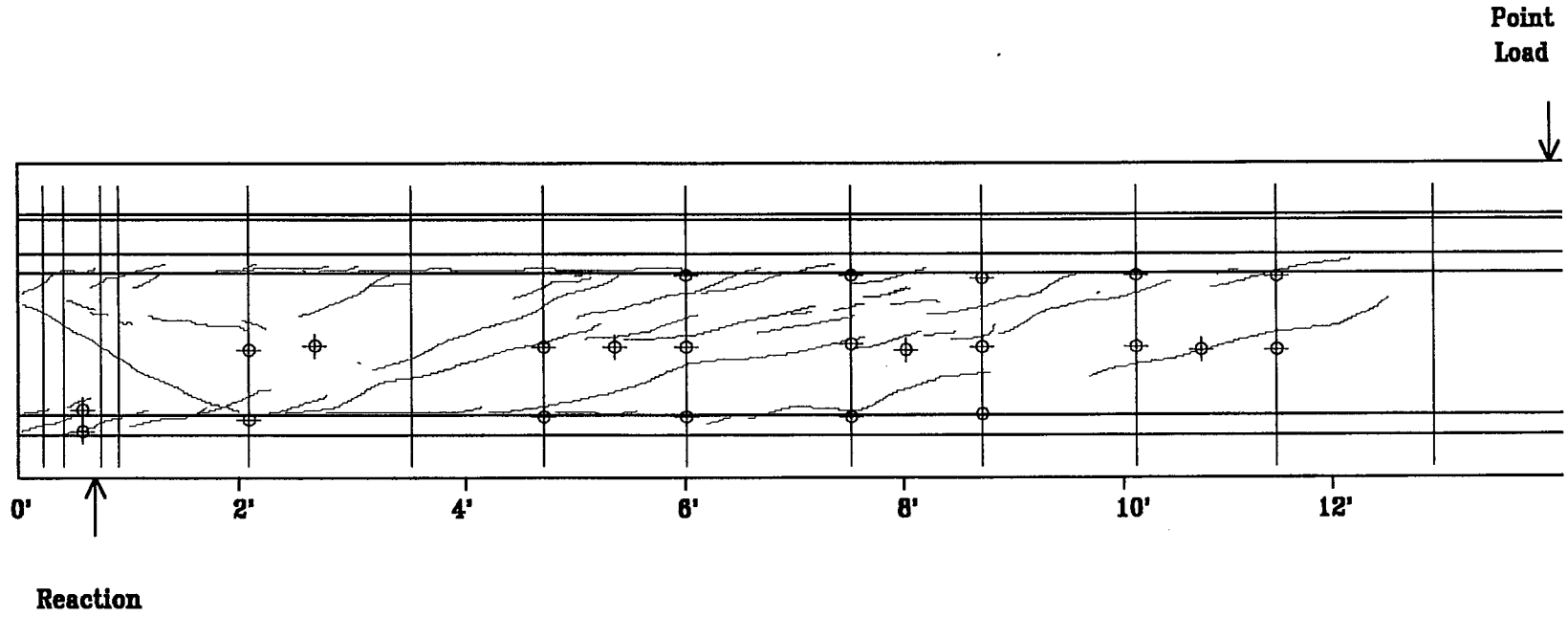

Figure 5.167 After 460 kips, Crack Drawing (End IID)

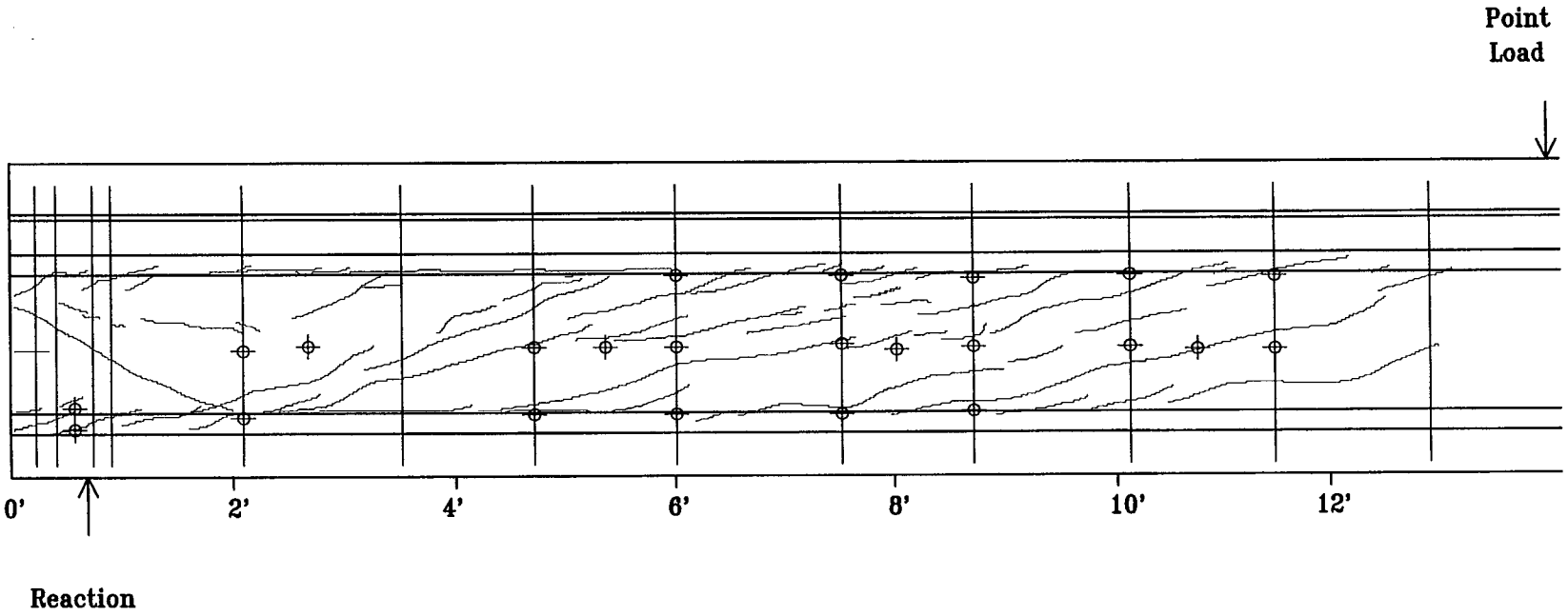

Figure 5.168 After Peak Load, Crack Drawing (End IID)

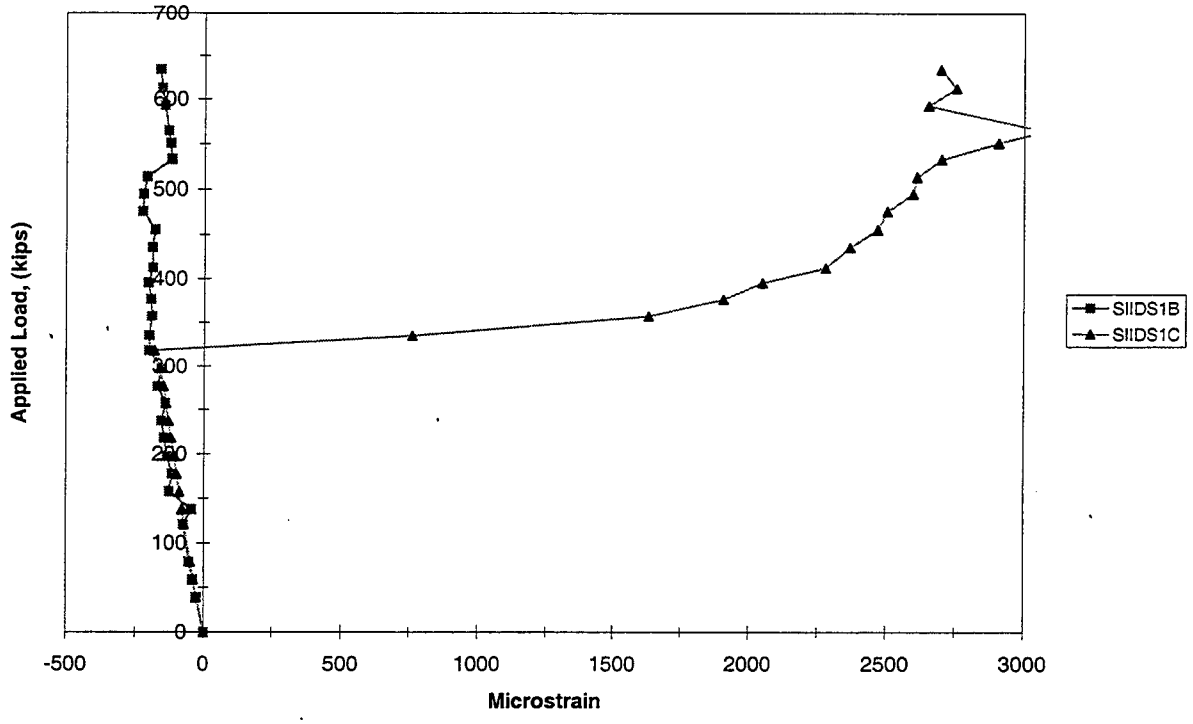

Figure 5.169 Stirrup 1 (End IID)

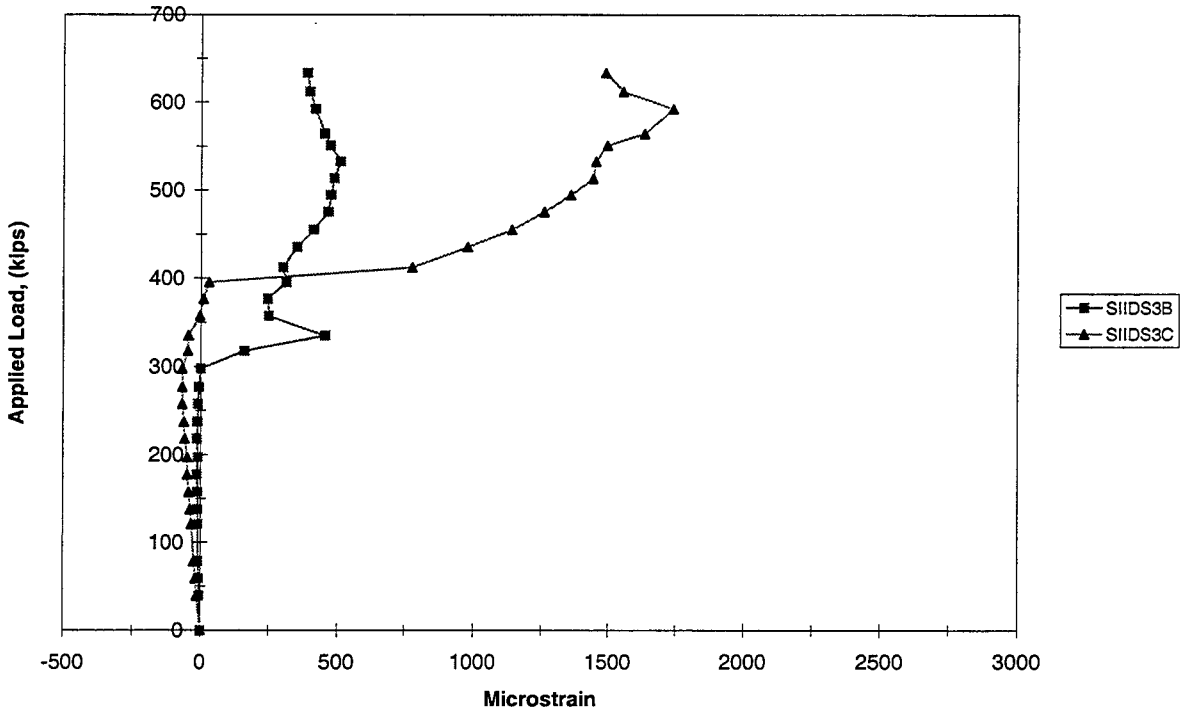

Figure 5.170 Stirrup 3 (End IID)

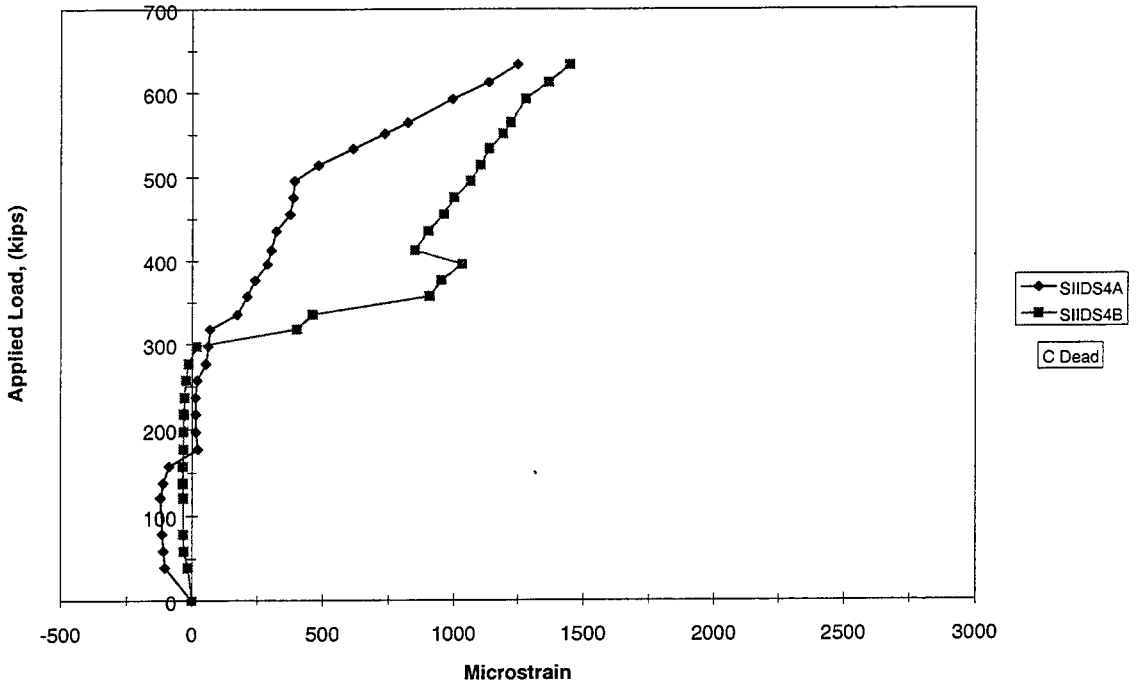

Figure 5.171 Stirrup 4 (End IID)

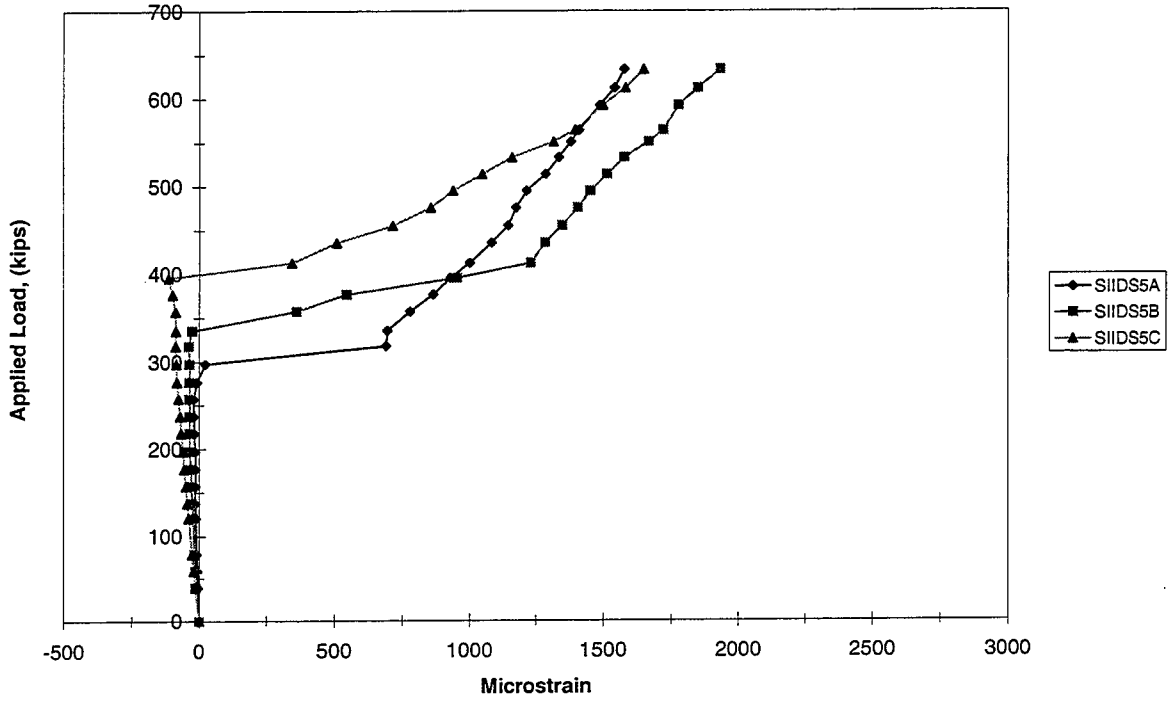

Figure 5.172 Stirrup 5 (End IID)

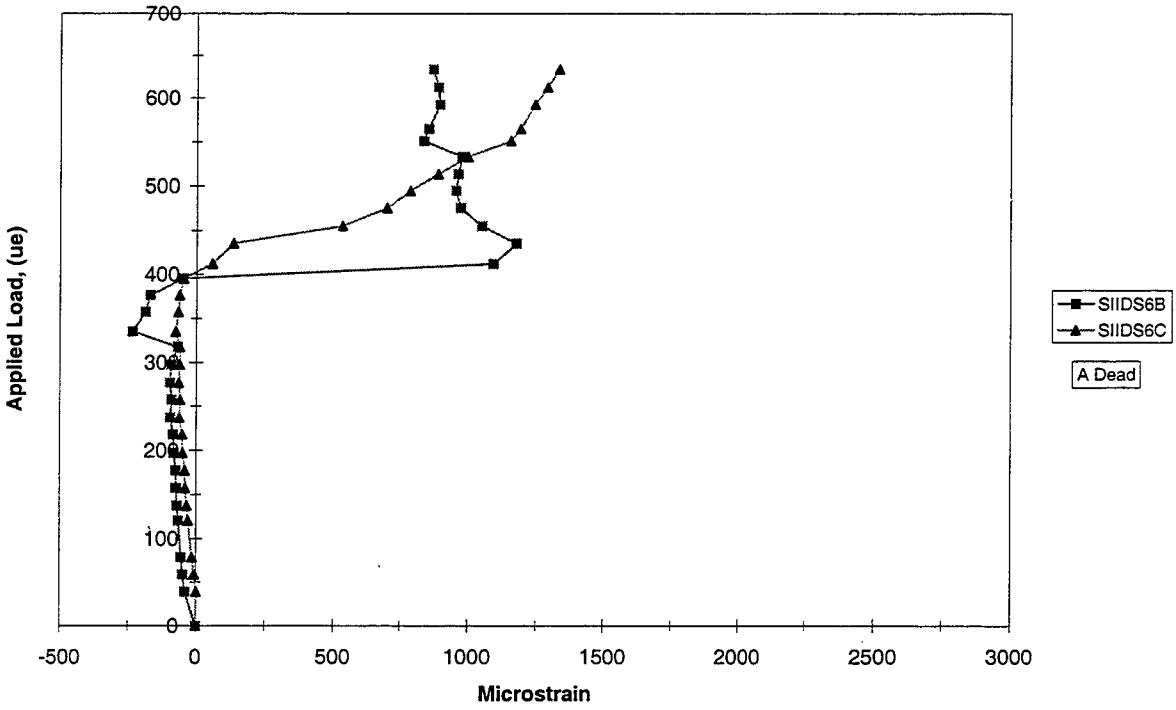

Figure 5.173 Stirrup 6 (End IID)

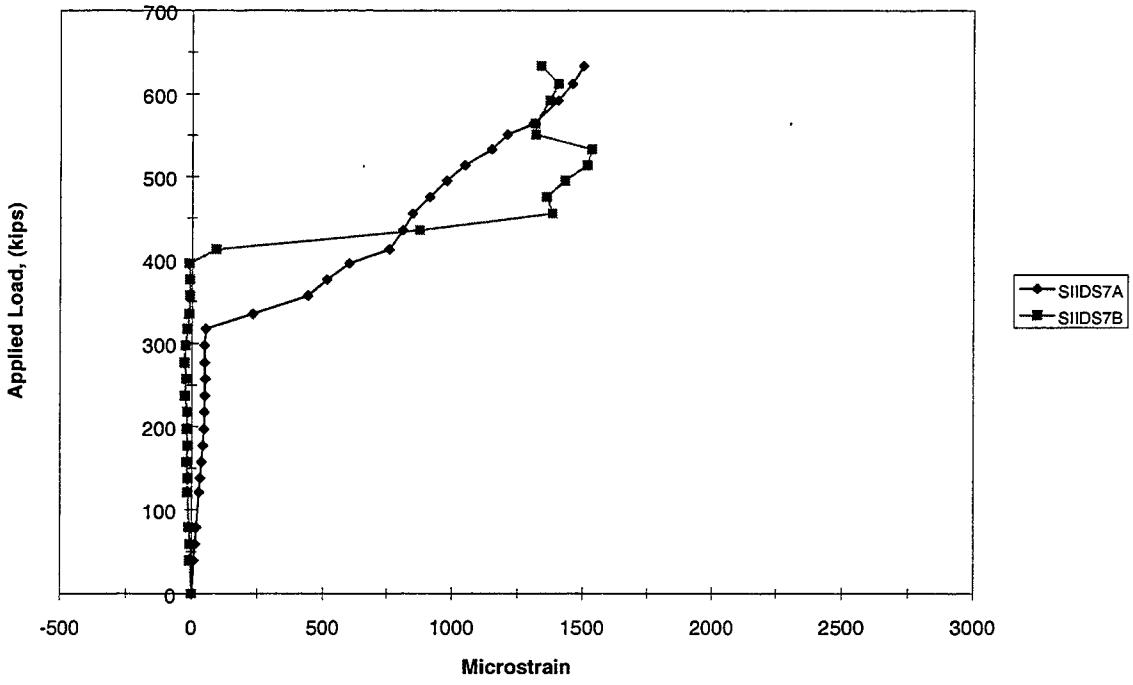

Figure 5.174 Stirrup 7 (End IID)

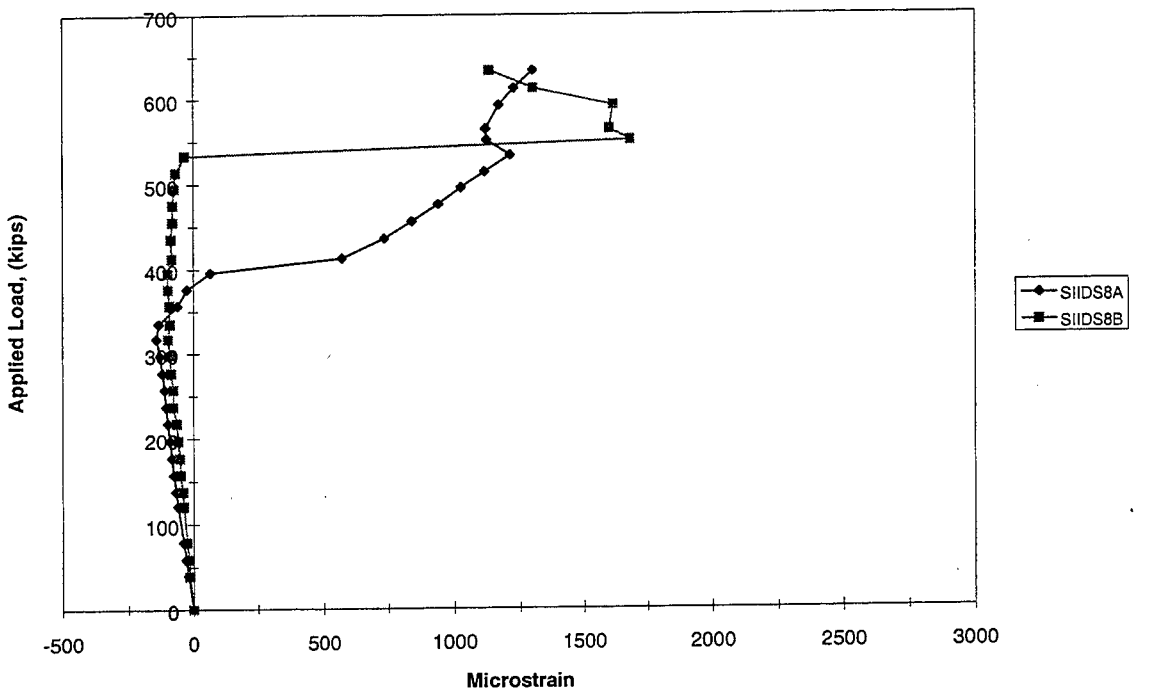

Figure 5.175 Stirrup 8 (End IID)

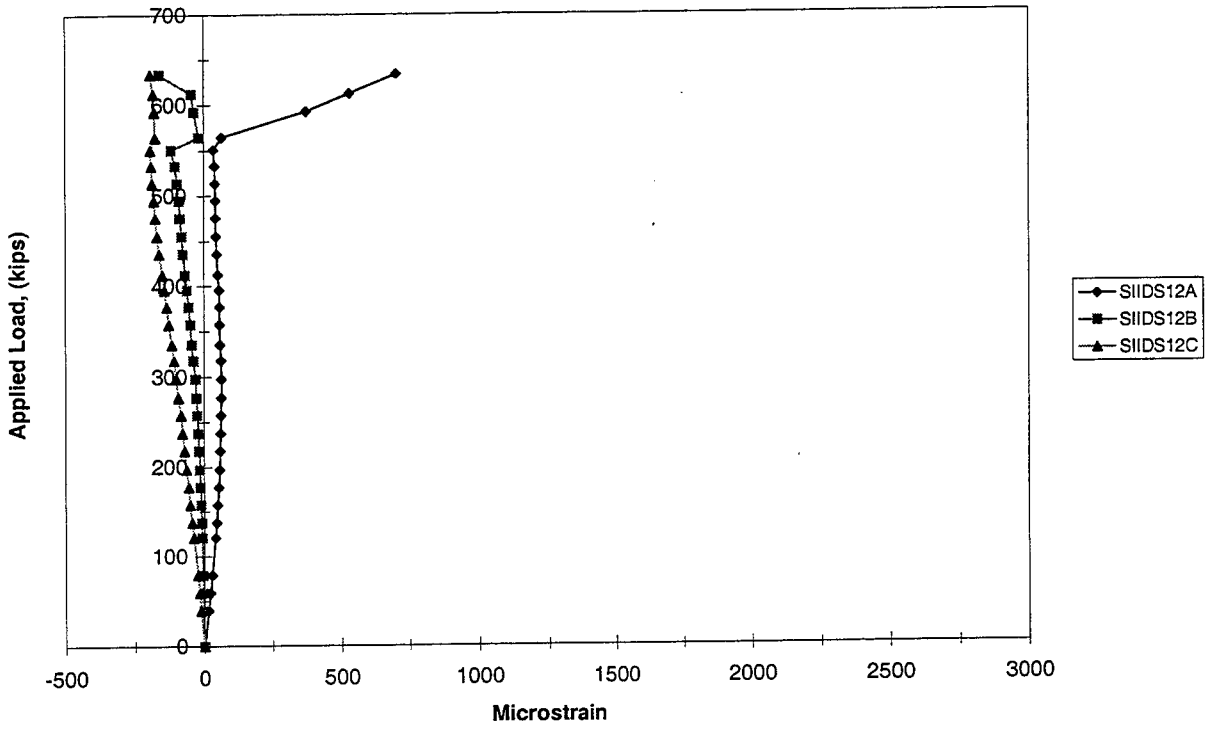

Figure 5.176 Stirrup 12 (End IID)

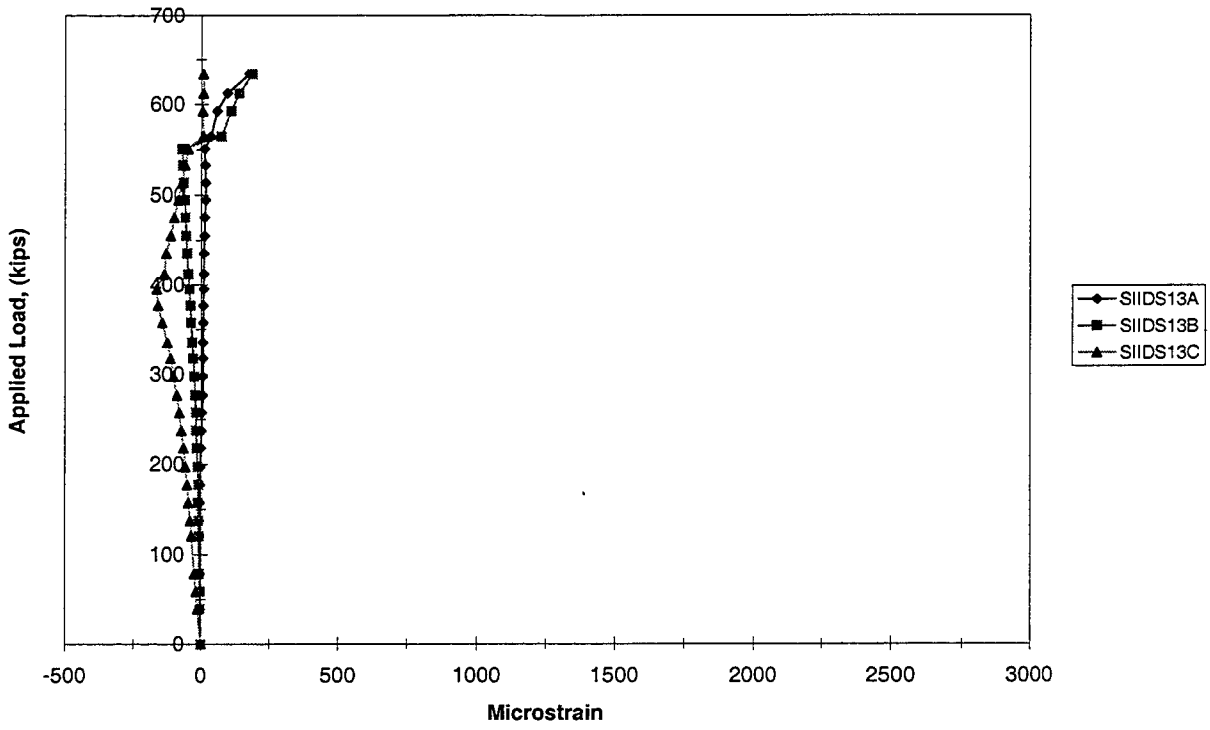

Figure 5.177 Stirrup 13 (End IID)

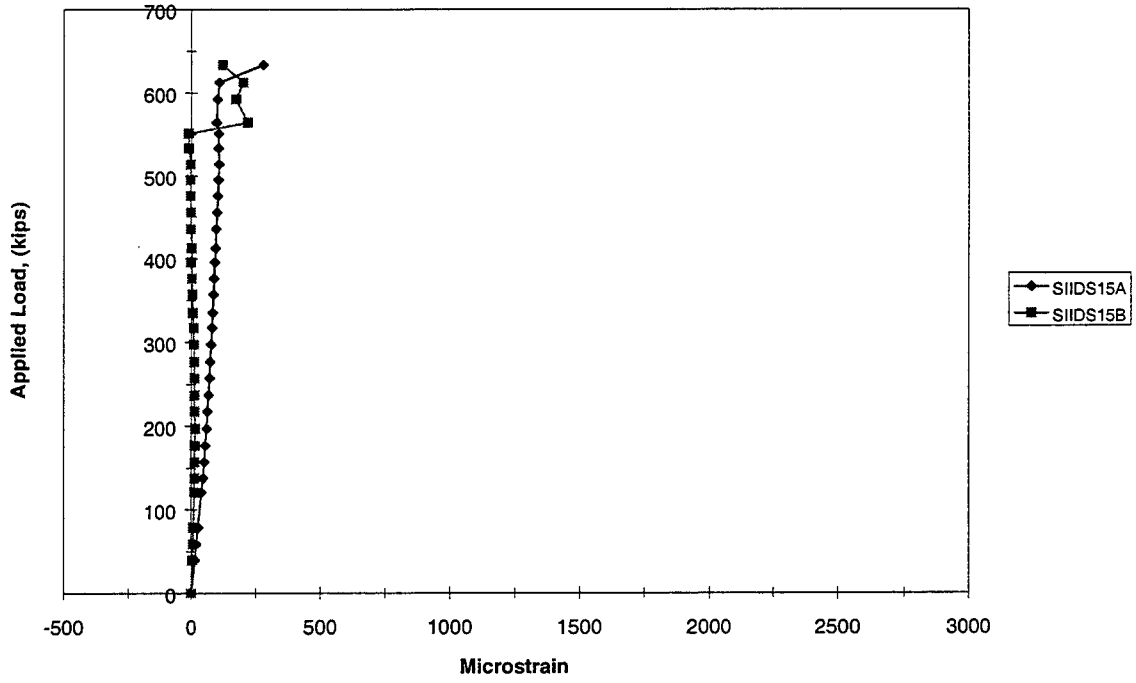

Figure 5.178 Stirrup 15 (End IID)

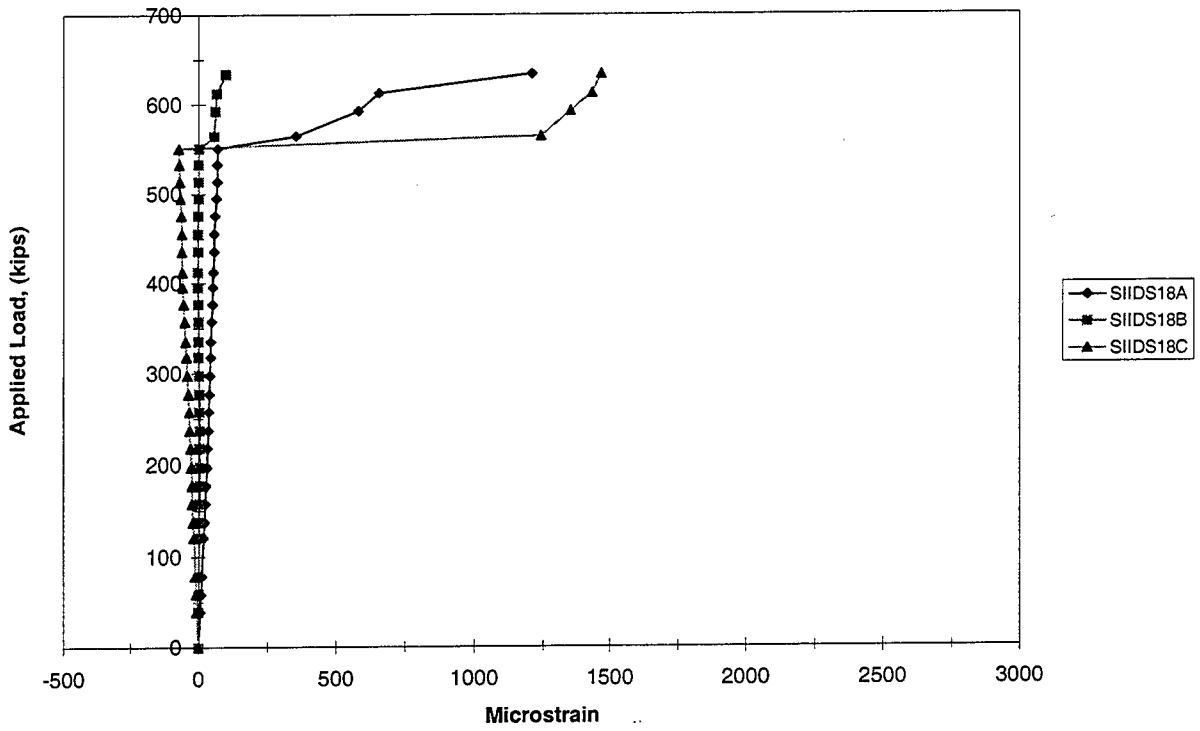

Figure 5.179 Stirrup 18 (End IID)

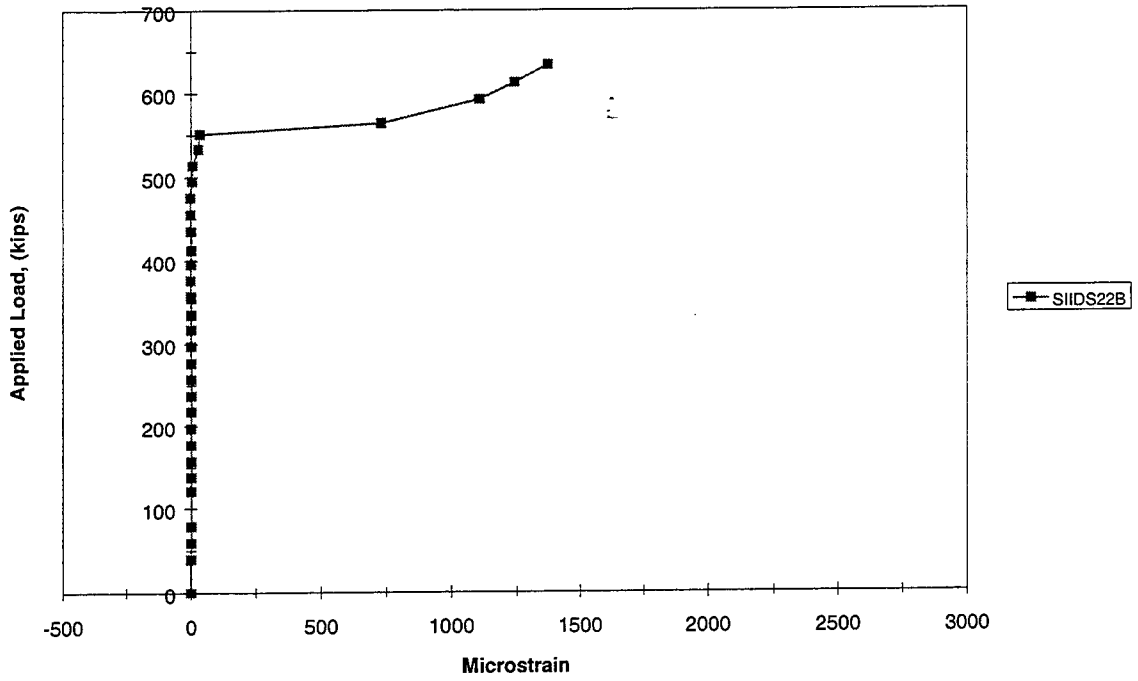

Figure 5.180 Stirrup 22 (End IID)

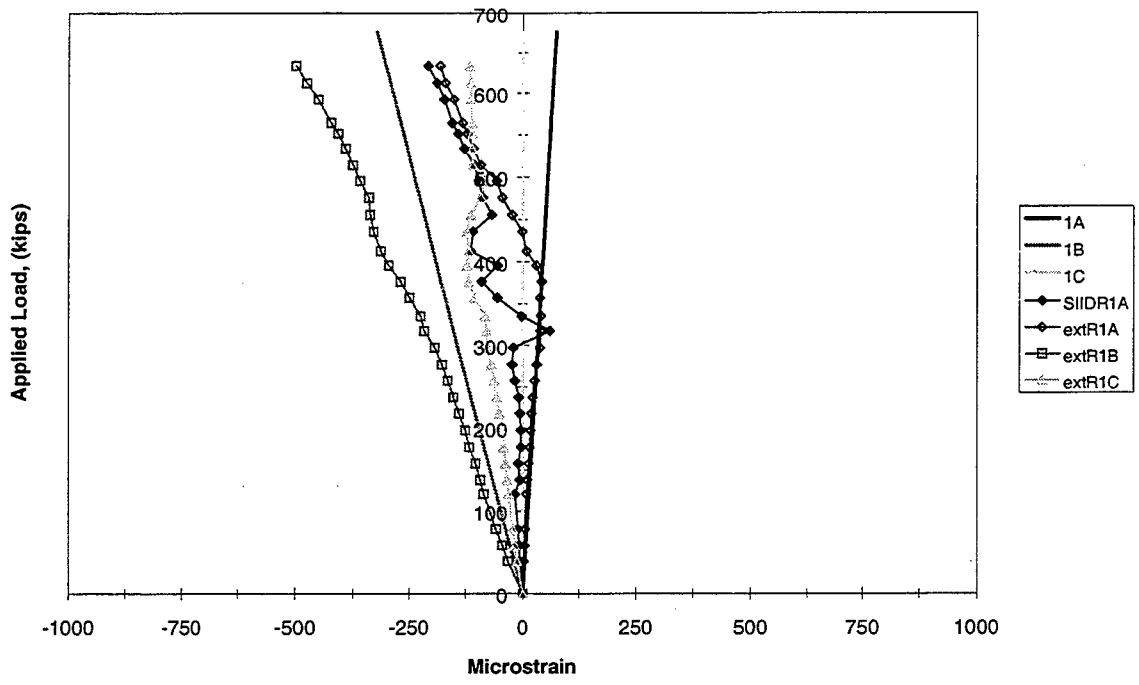

Figure 5.181 Rosette 1 (End IID)

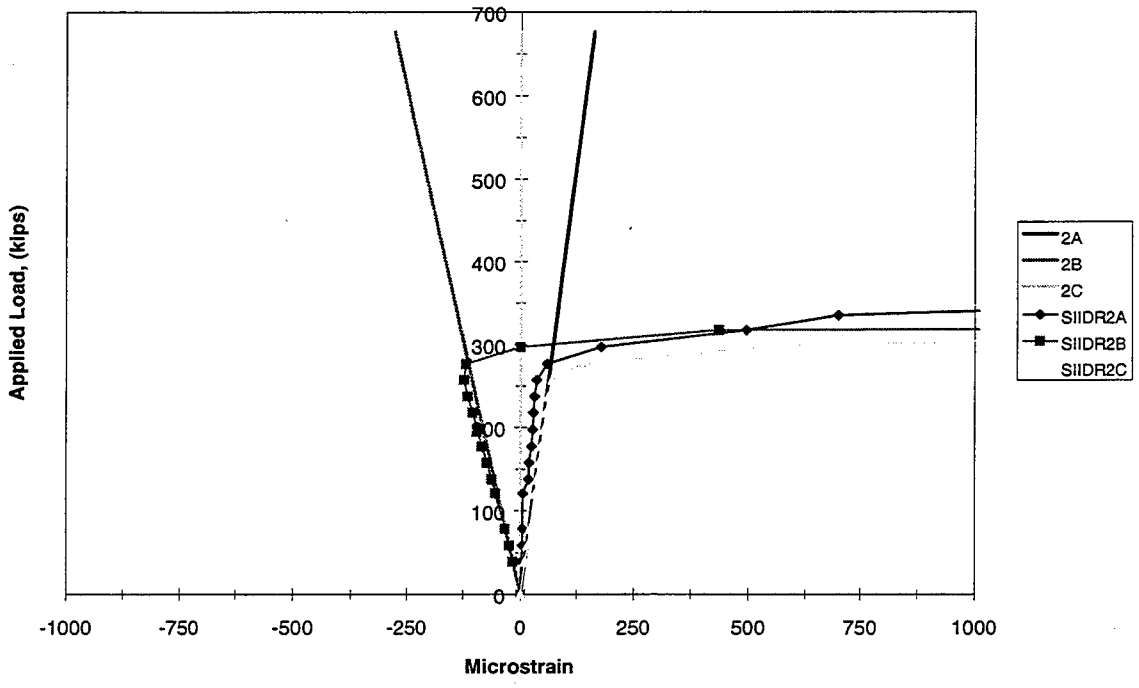

Figure 5.182 Rosette 2 (End IID)

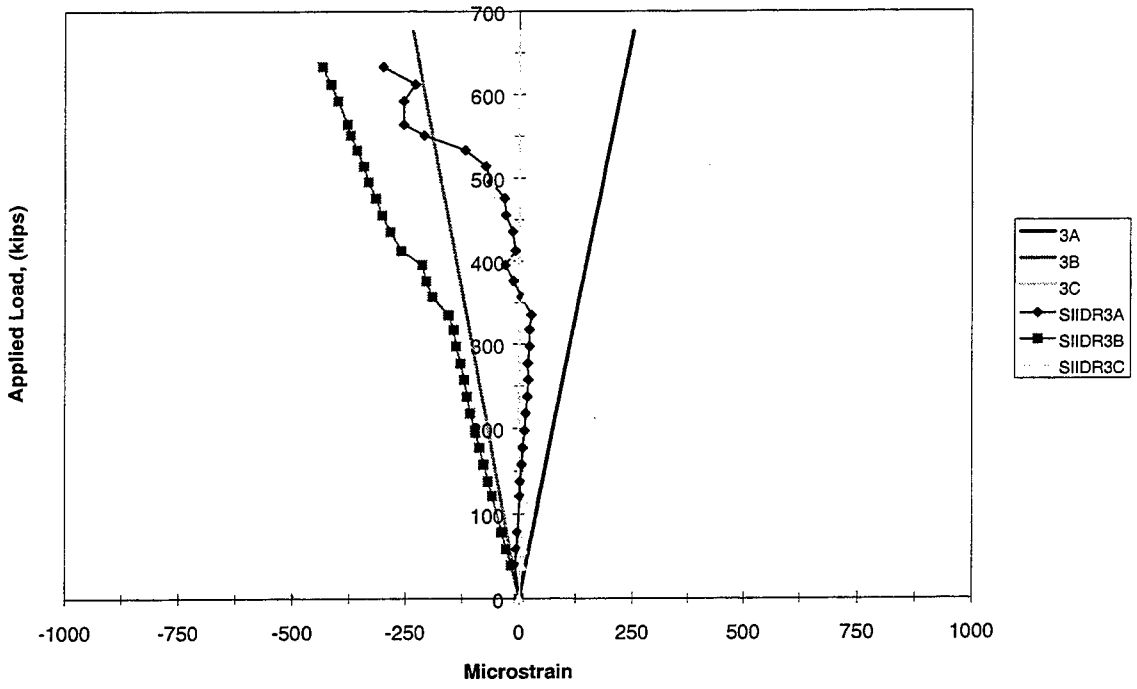

Figure 5.183 Rosette 3 (End IID)

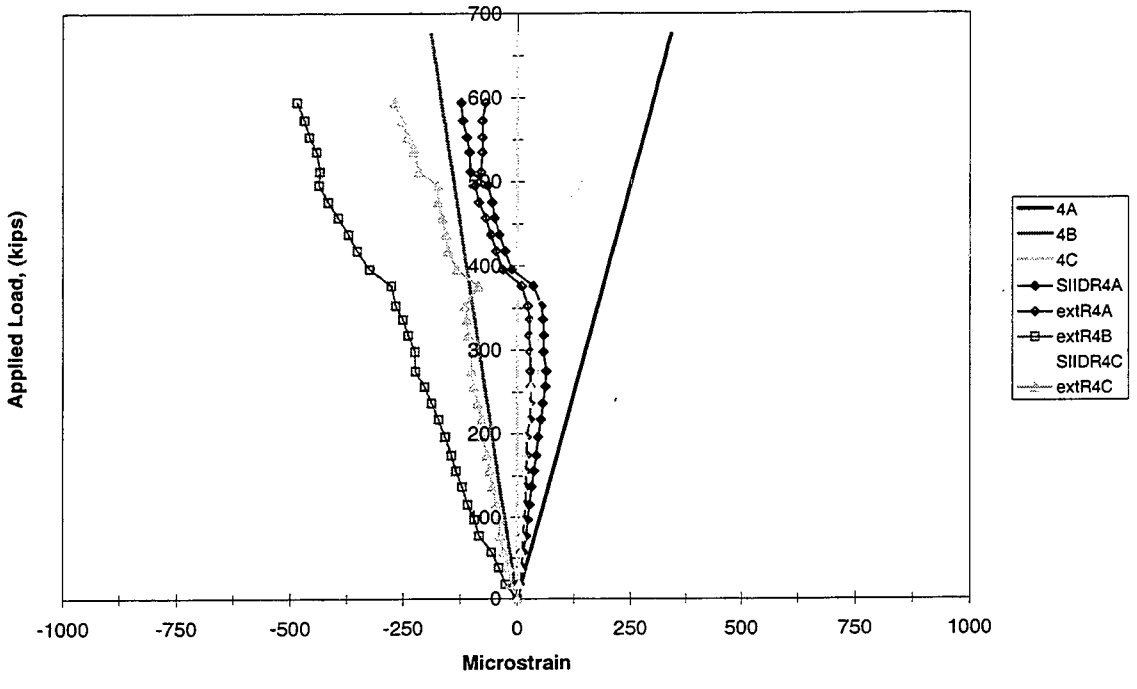

Figure 5.184 Rosette 4 (End IID)

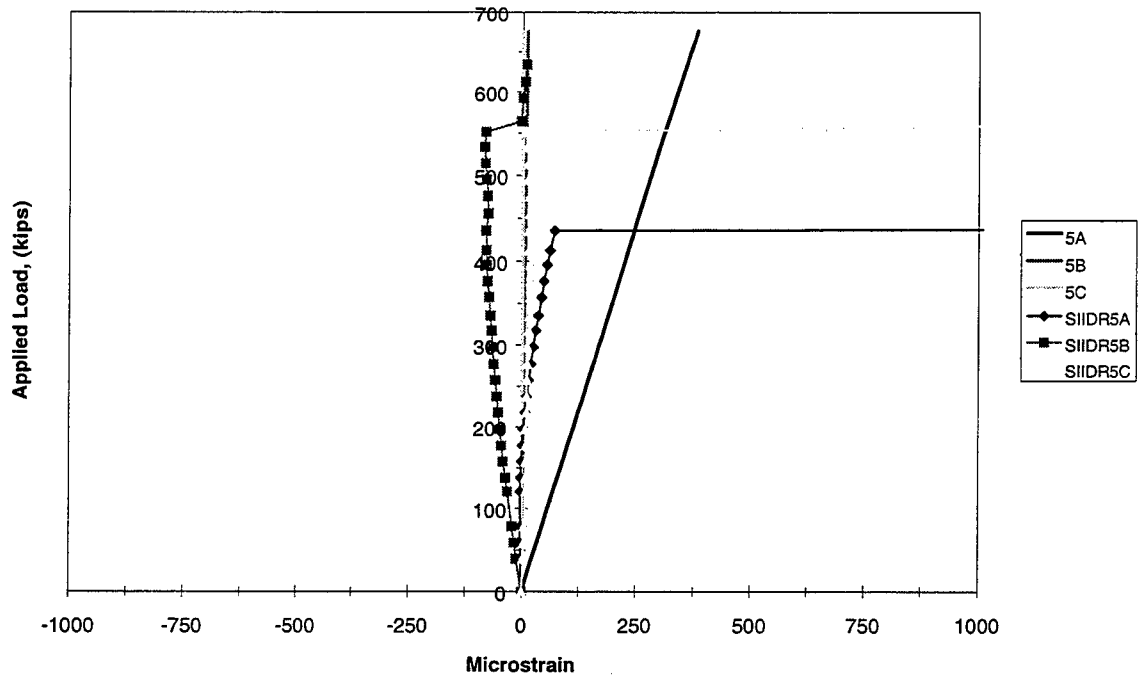

Figure 5.185 Rosette 5 (End IID)

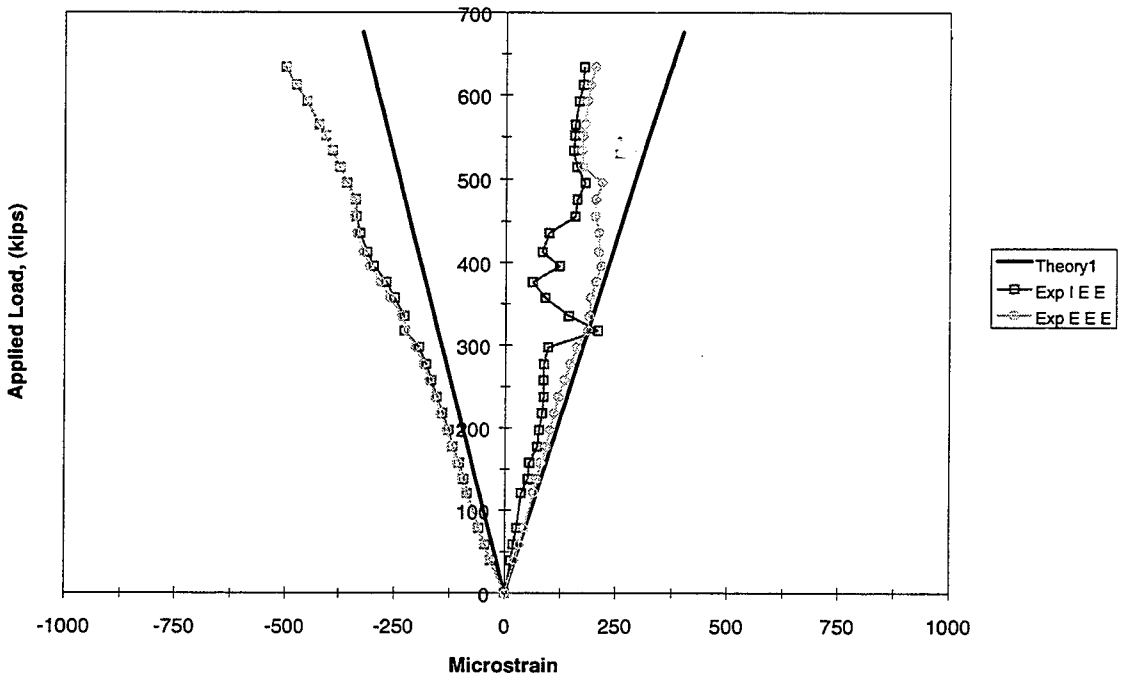

Figure 5.186 Principal Strains Rosette 1 (End IID)

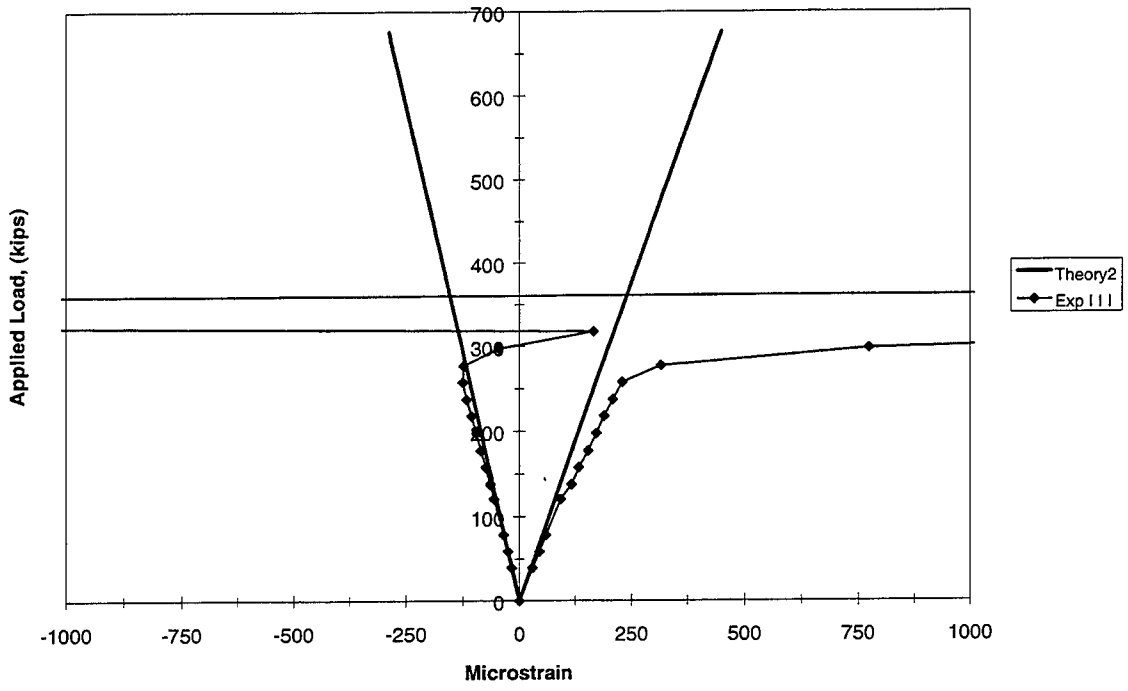

Figure 5.187 Principal Strains Rosette 2 (End IID)

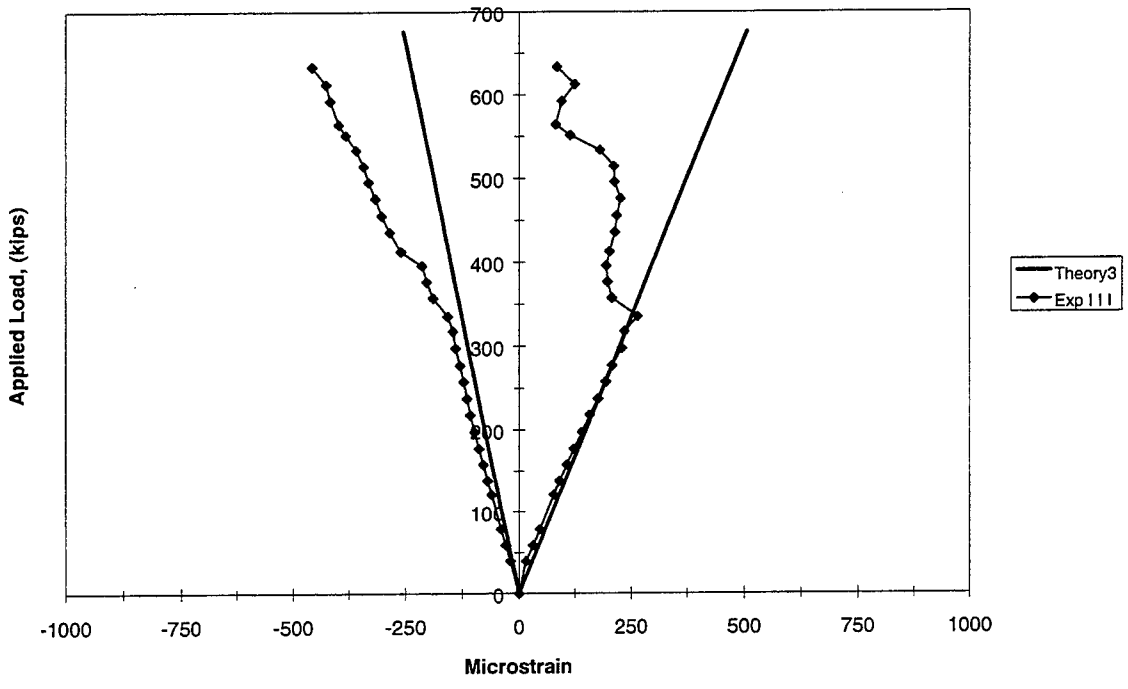

Figure 5.188 Principal Strains Rosette 3 (End IID)

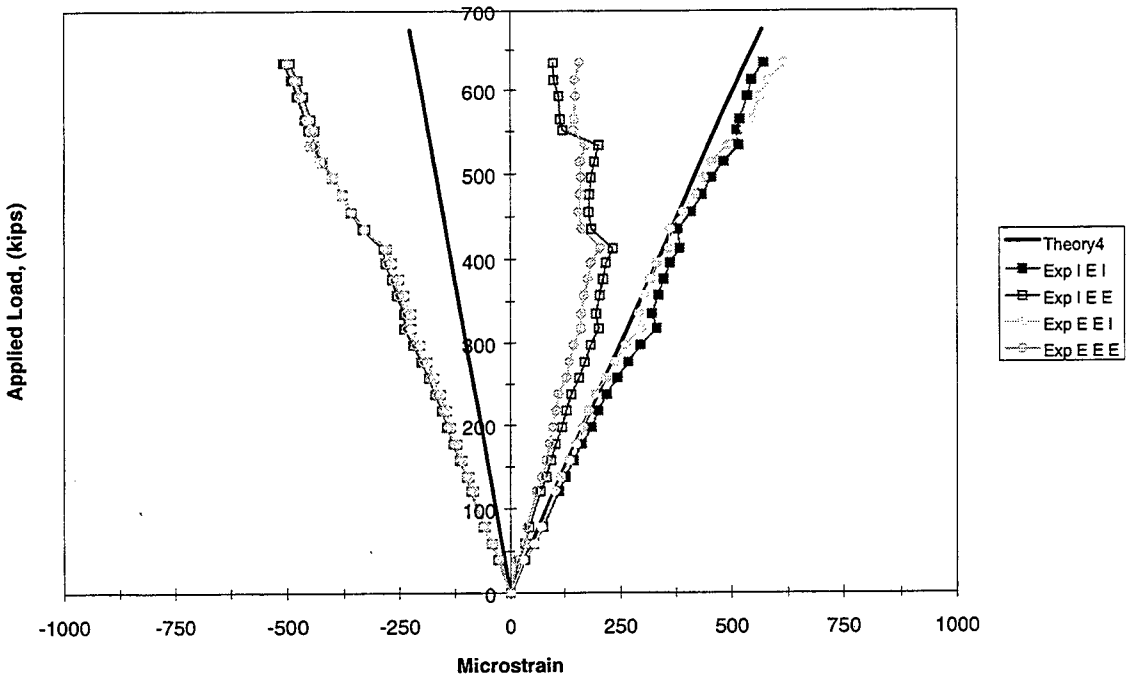

Figure 5.189 Principal Strains Rosette 4 (End IID)

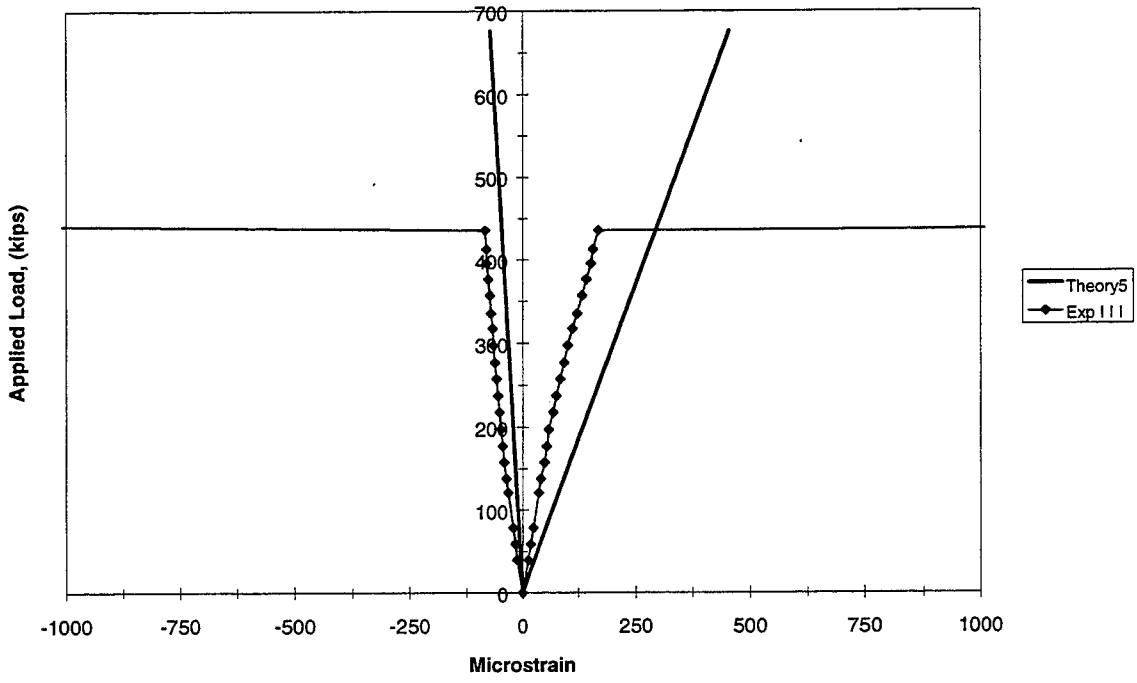

Figure 5.190 Principal Strains Rosette 5 (End IID)

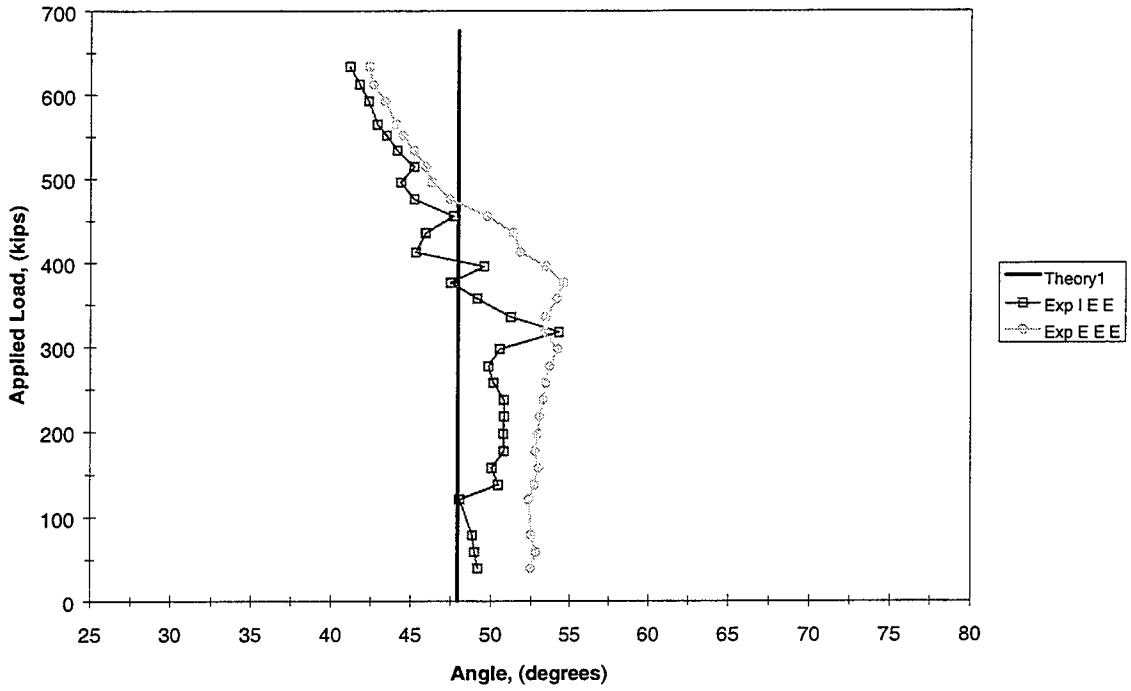

Figure 5.191 Principal Compression Angle Rosette 1 (End IID)

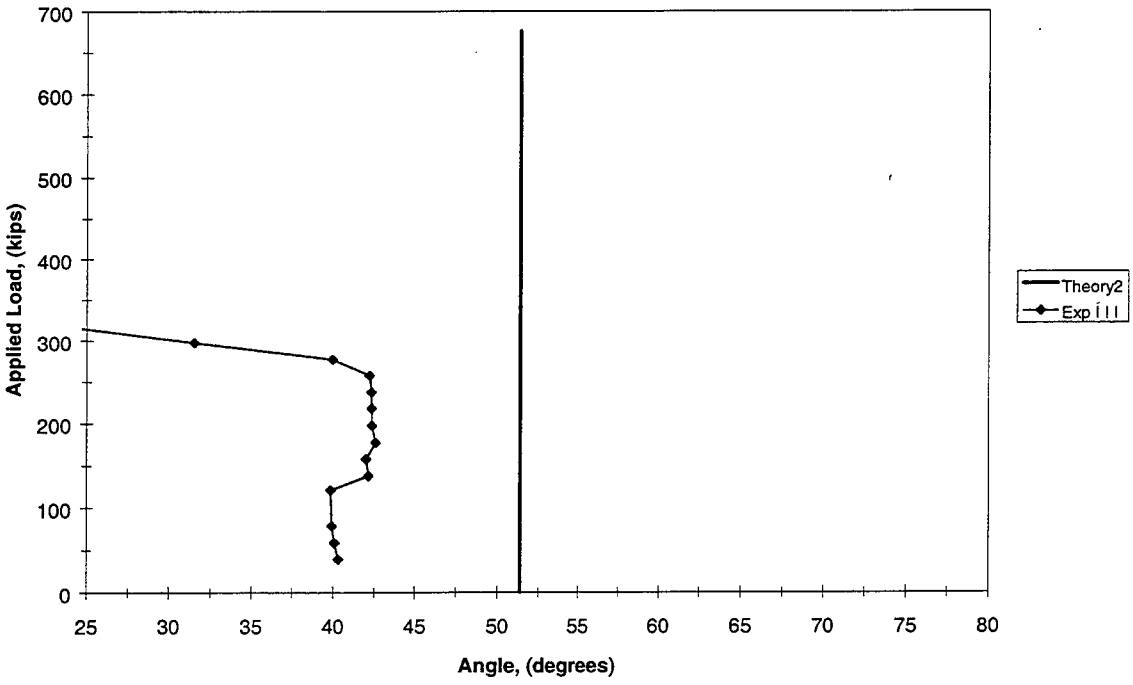

Figure 5.192 Principal Compression Angle Rosette 2 (End IID)

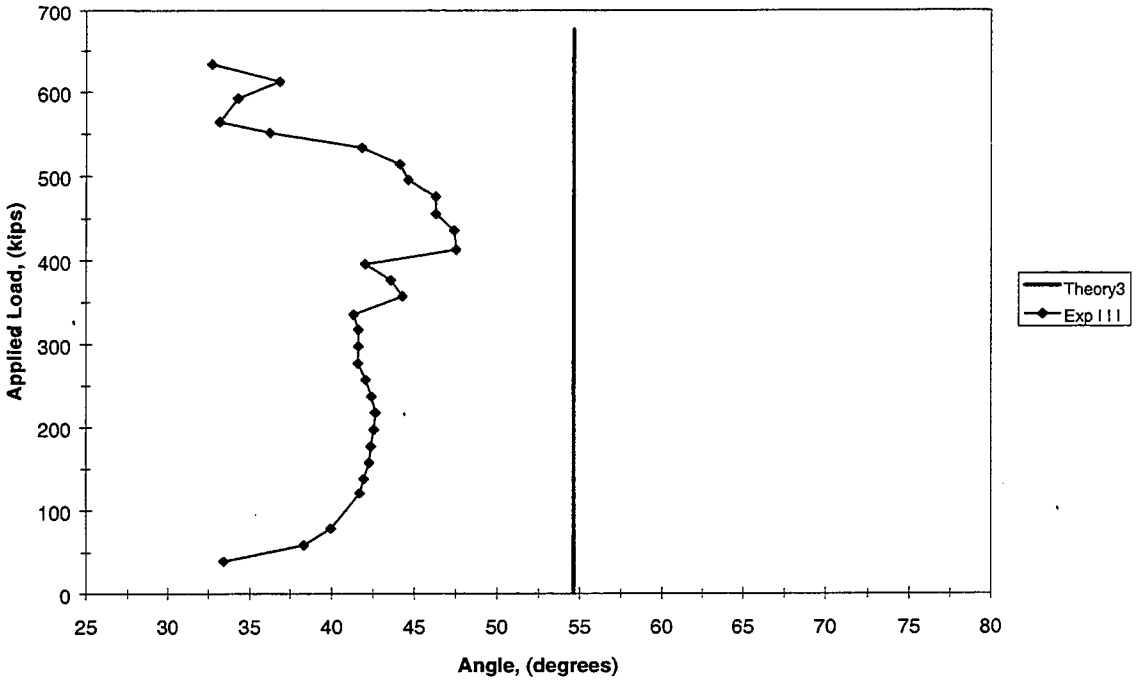

Figure 5.193 Principal Compression Angle Rosette 3 (End IID)

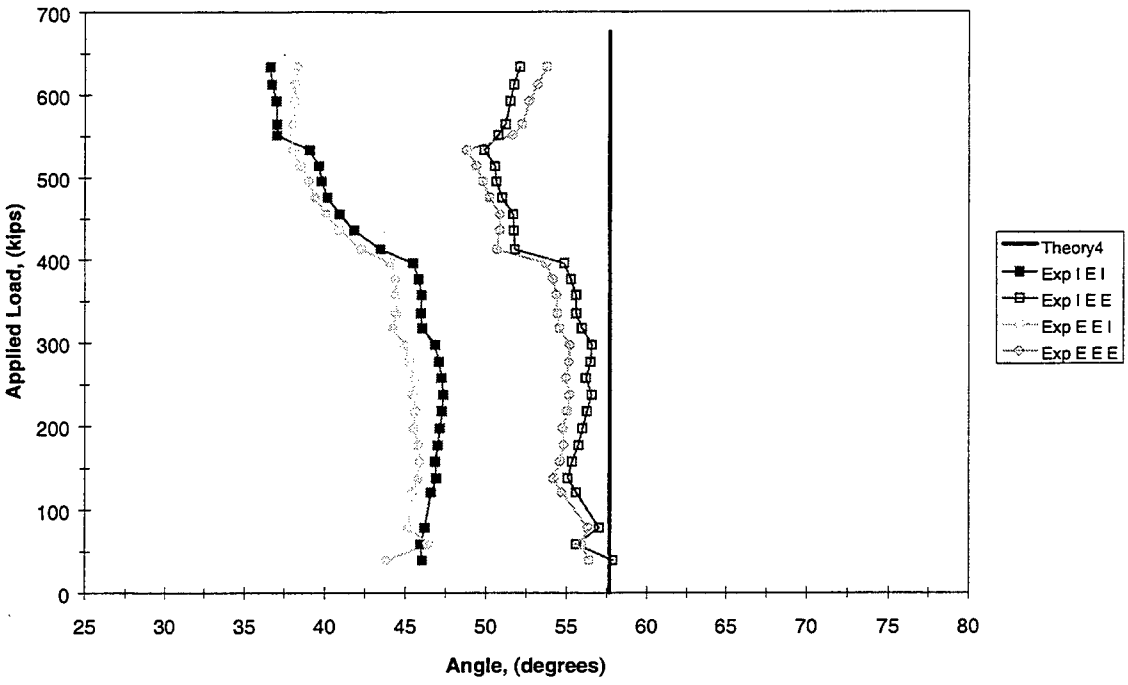

Figure 5.194 Principal Compression Angle Rosette 4 (End IID)

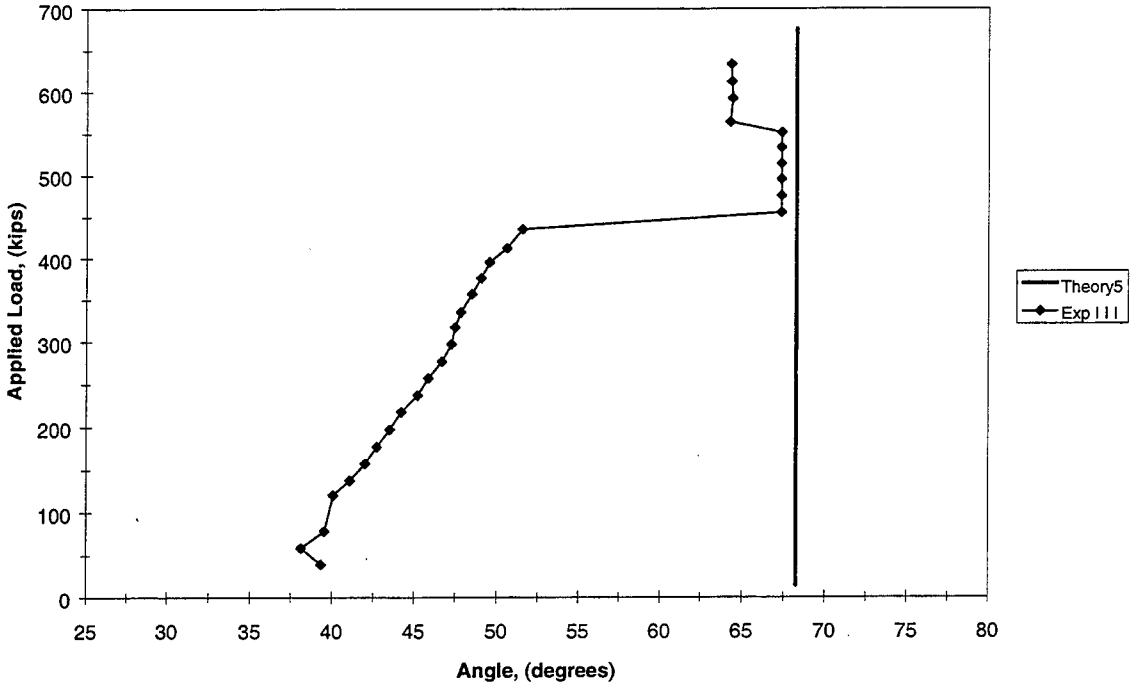

Figure 5.195 Principal Compression Angle Rosette 5 (End IID)

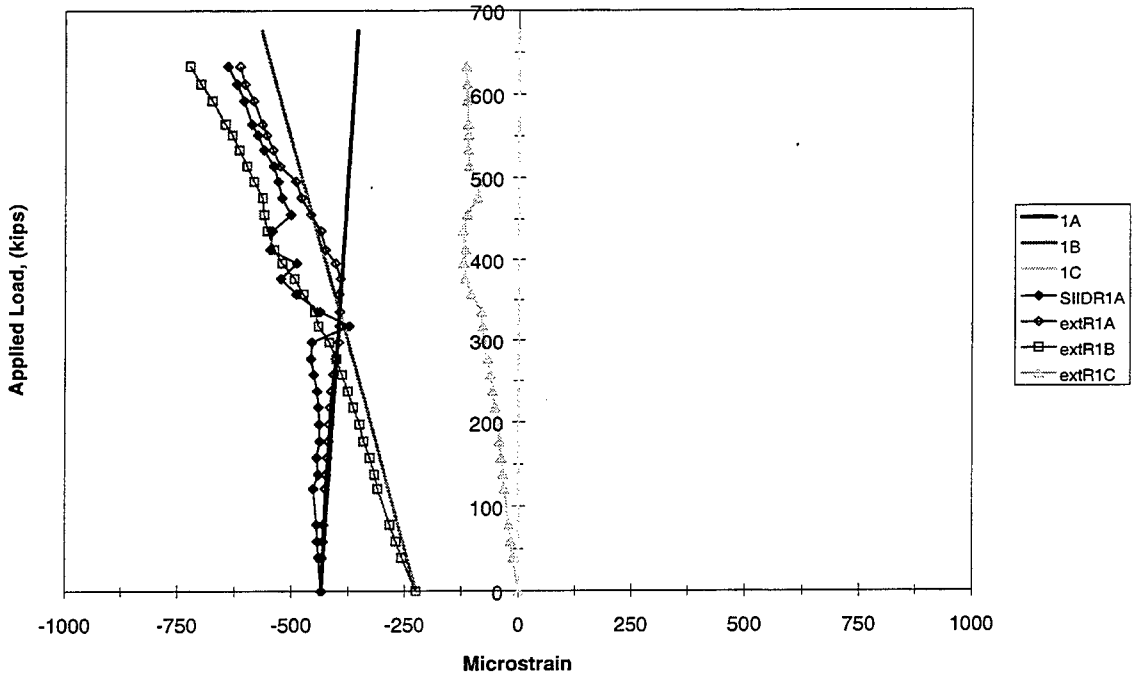

Figure 5.196 Corrected Rosette 1 (End IID)

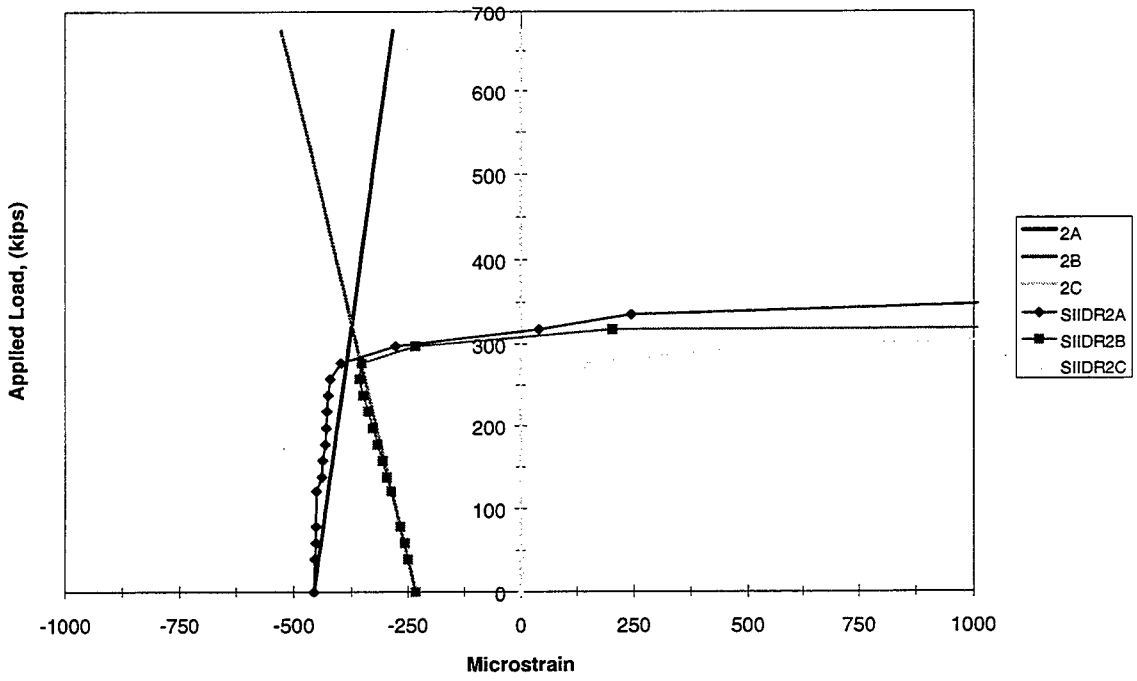

Figure 5.197 Corrected Rosette 2 (End IID)

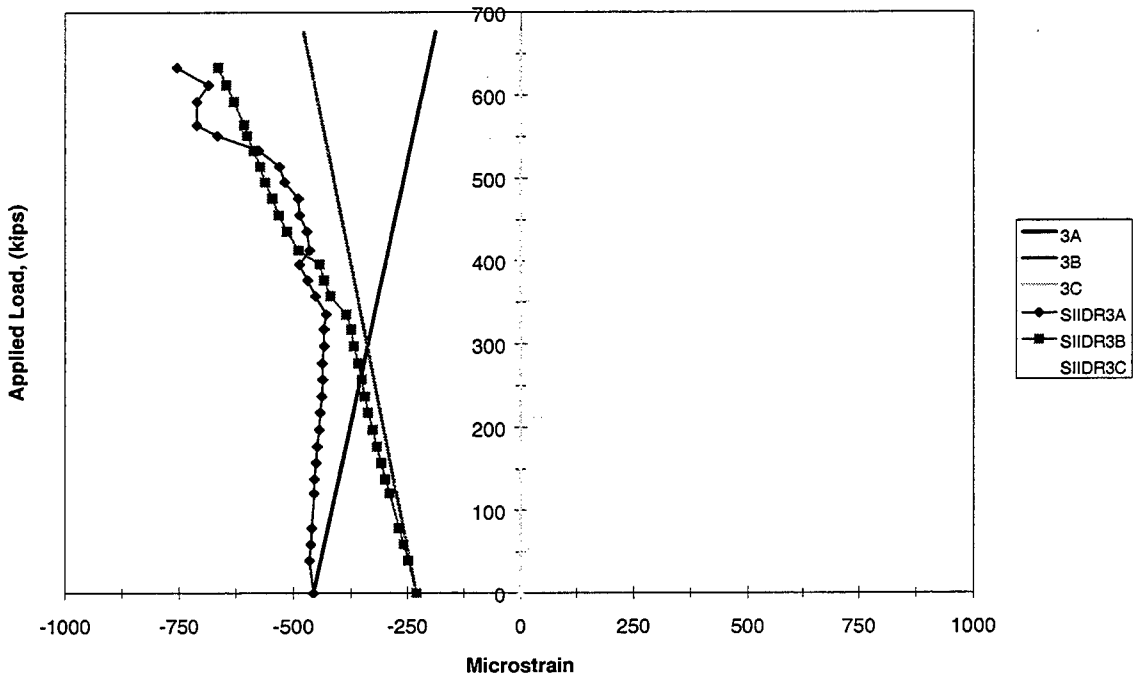

Figure 5.198 Corrected Rosette 3 (End IID)

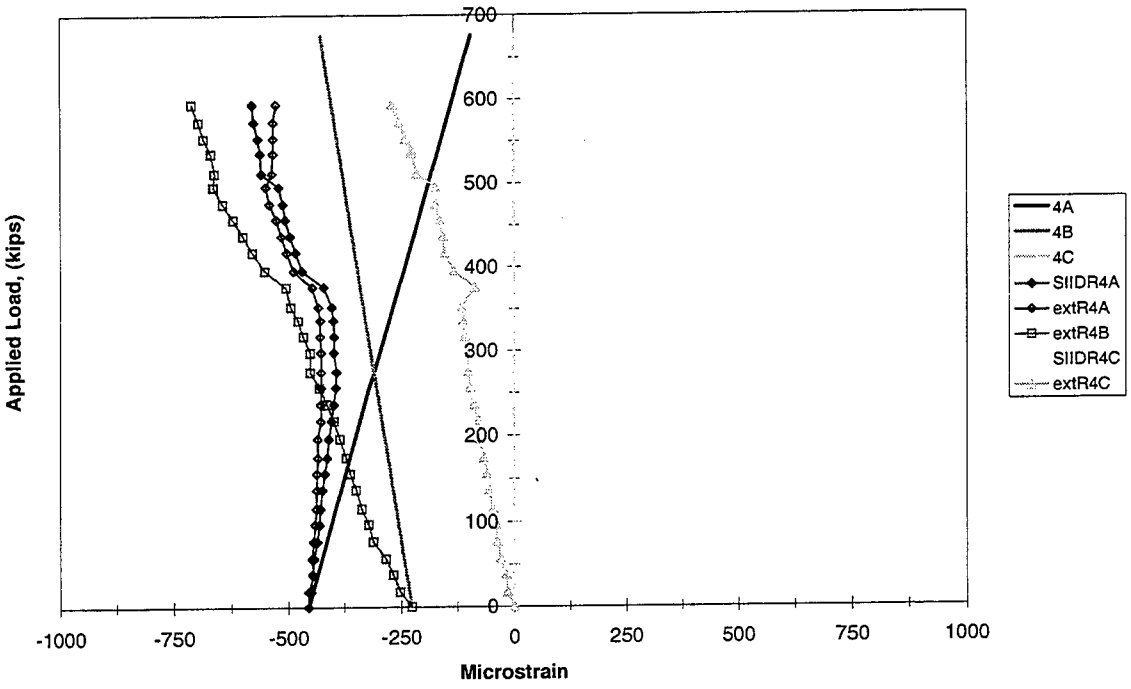

Figure 5.199 Corrected Rosette 4 (End IID)

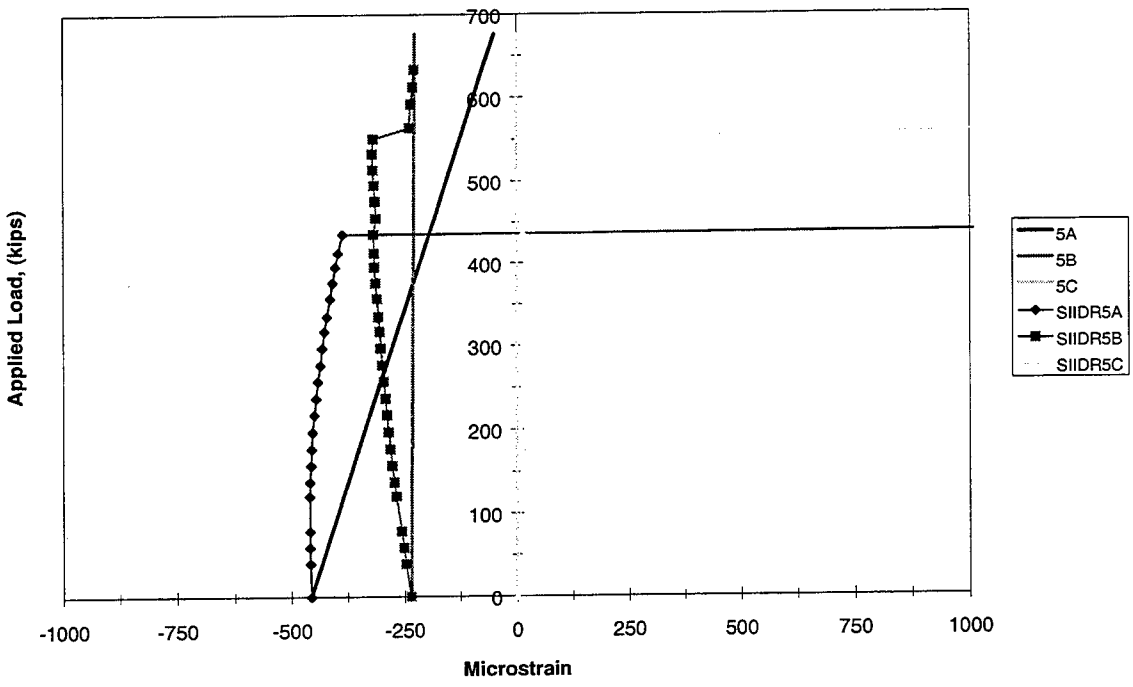

Figure 5.200 Corrected Rosette 5 (End IID)

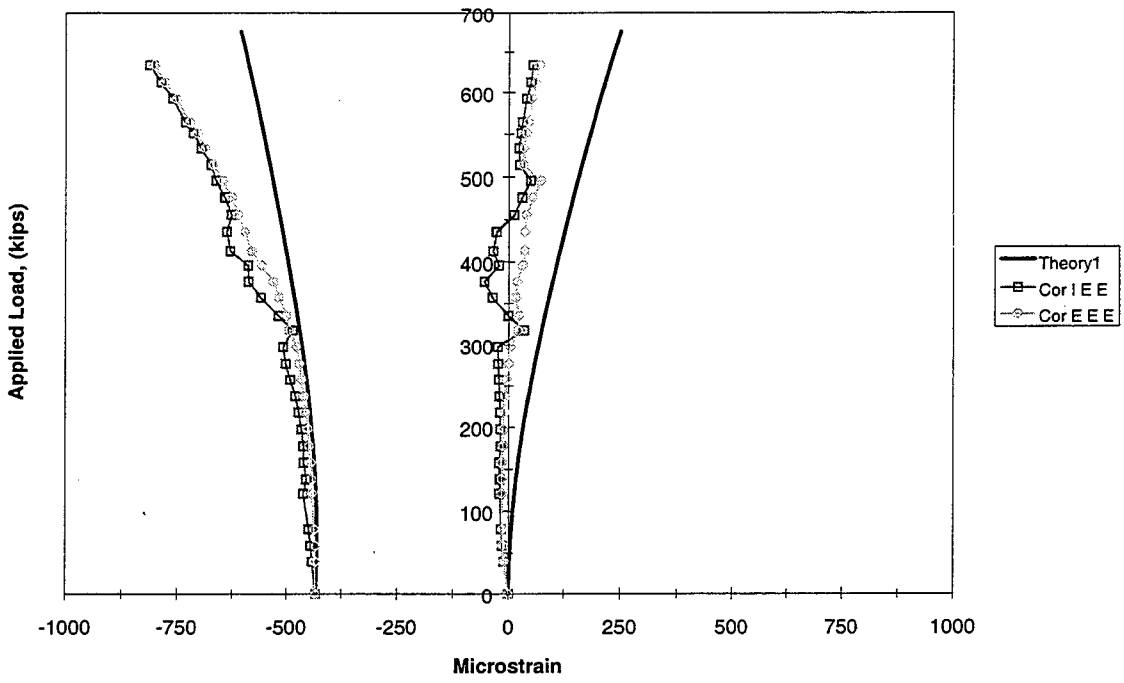

Figure 5.201 Corrected Principal Strains Rosette 1 (End IID)

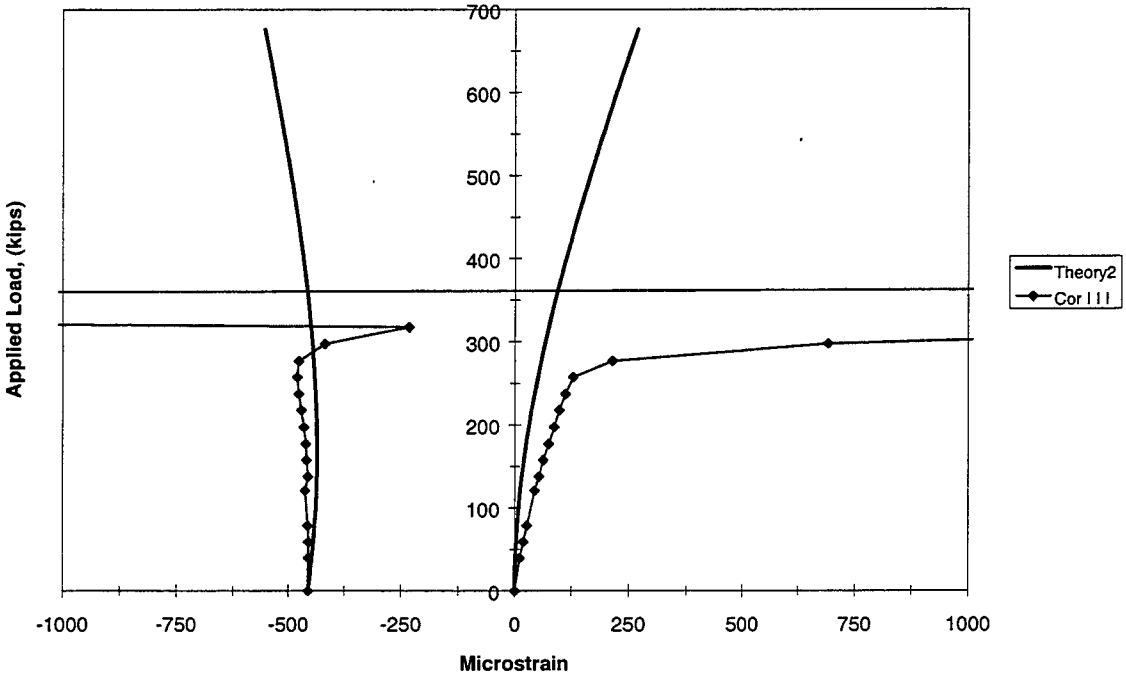

Figure 5.202 Corrected Principal Strains Rosette 2 (End IID)

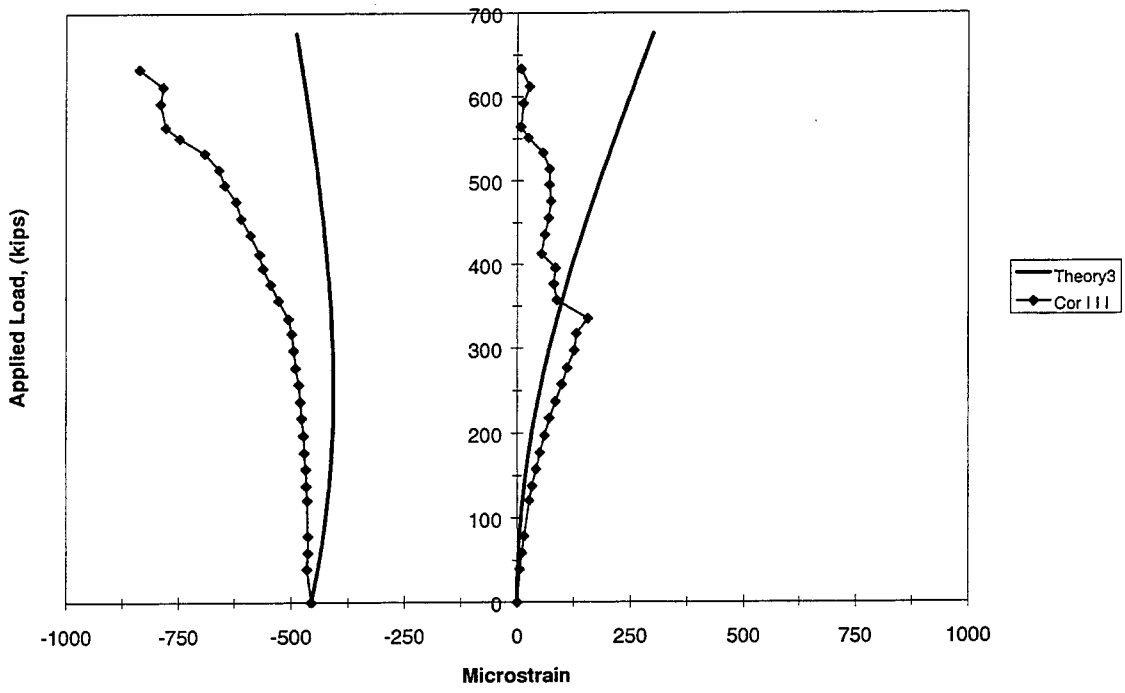

Figure 5.203 Corrected Principal Strains Rosette 3 (End IID)

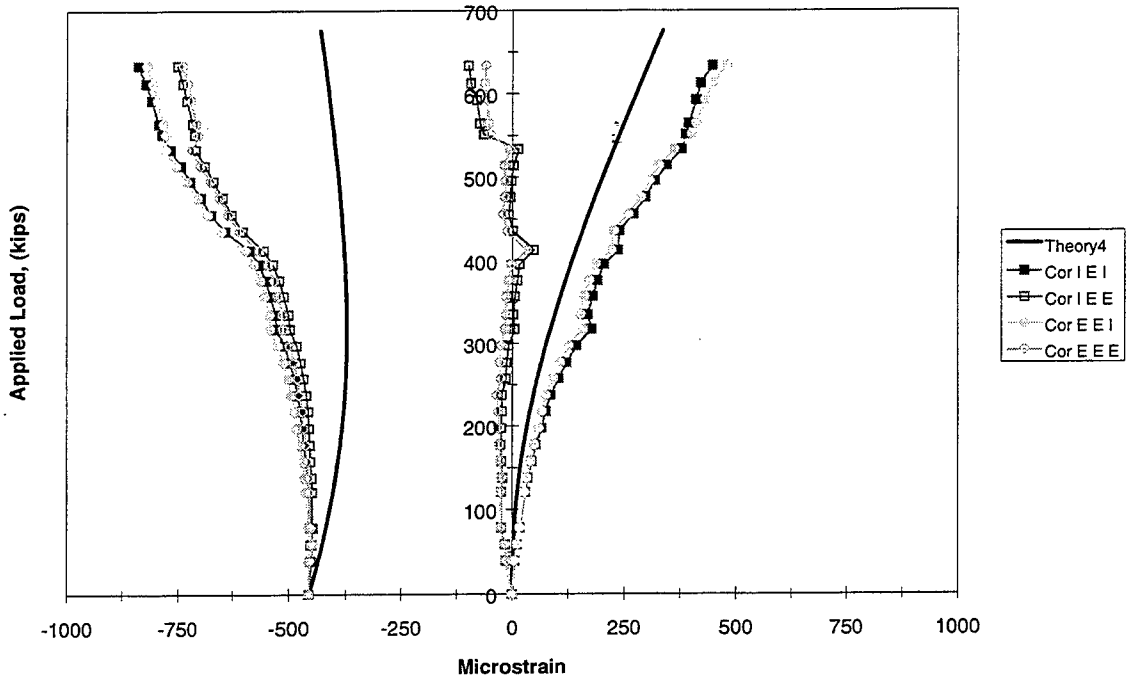

Figure 5.204 Corrected Principal Strains Rosette 4 (End IID)

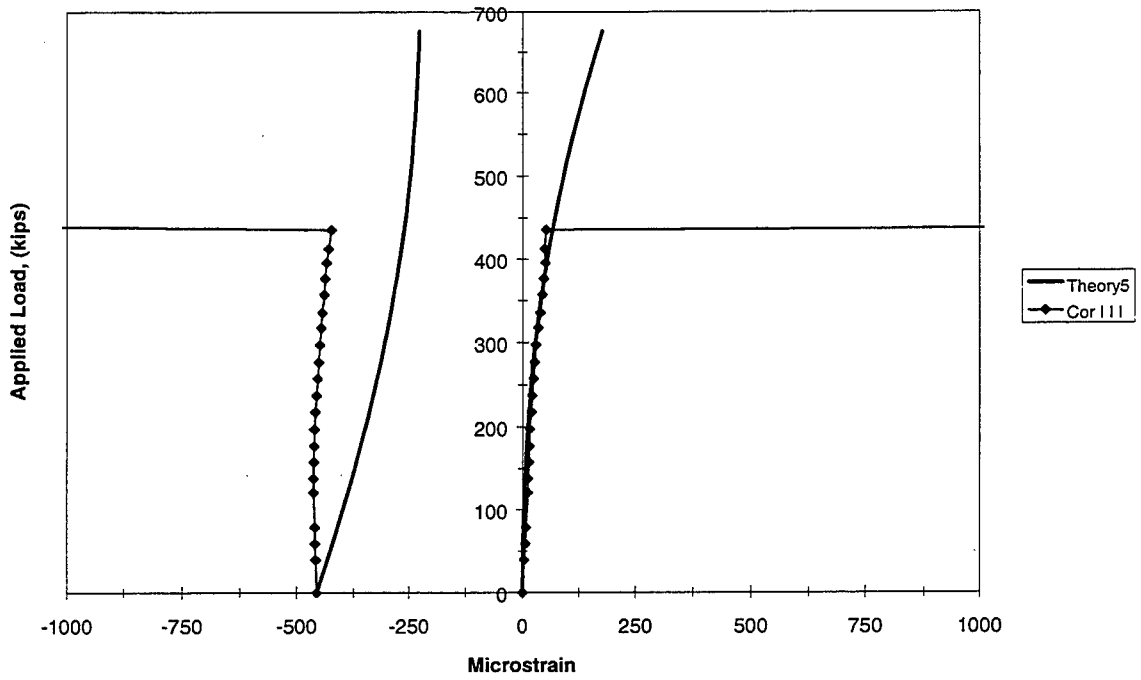

Figure 5.205 Corrected Principal Strains Rosette 5 (End IID)

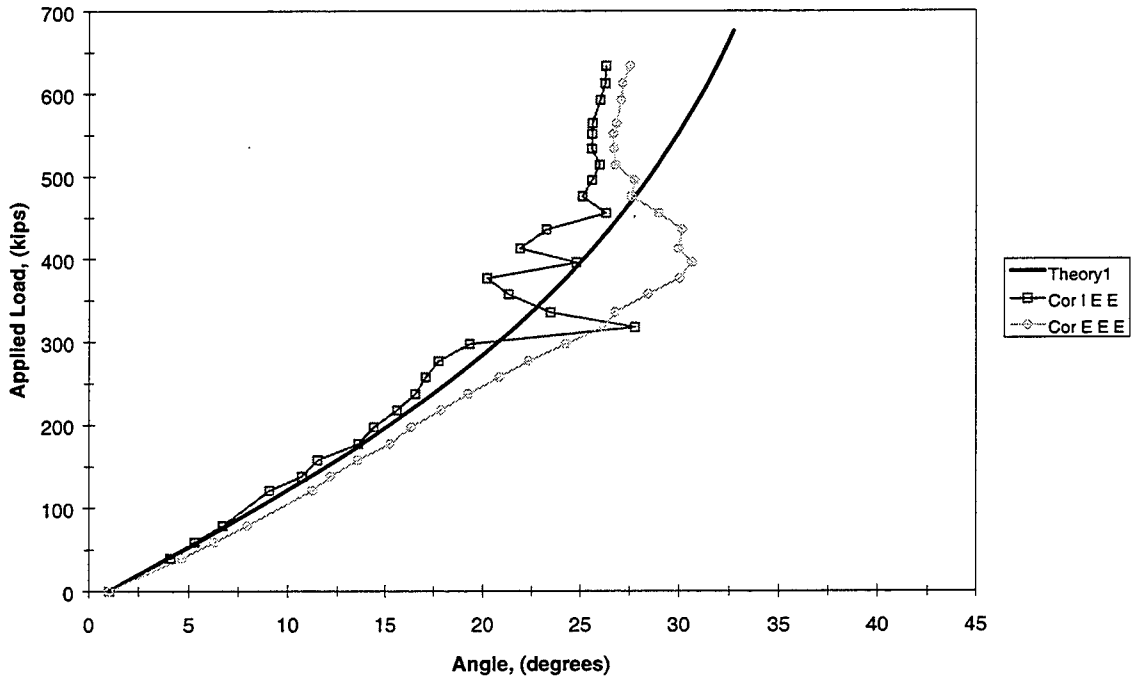

Figure 5.206 Corrected Principal Compression Angle Rosette 1 (End IID)

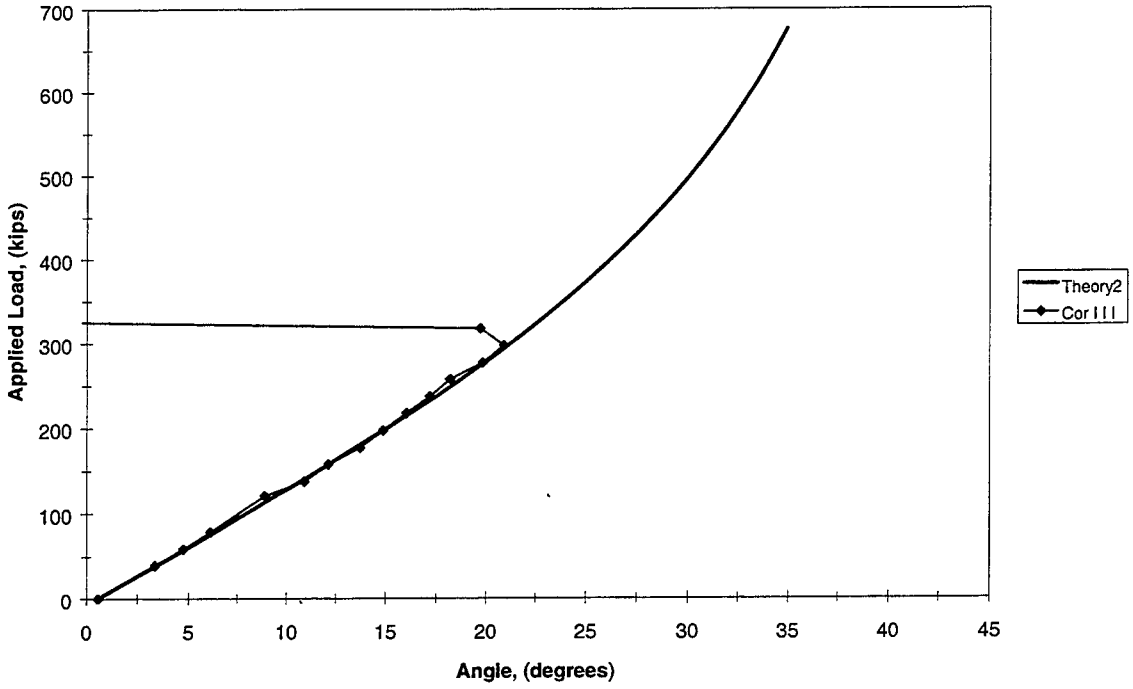

Figure 5.207 Corrected Principal Compression Angle Rosette 2 (End IID)

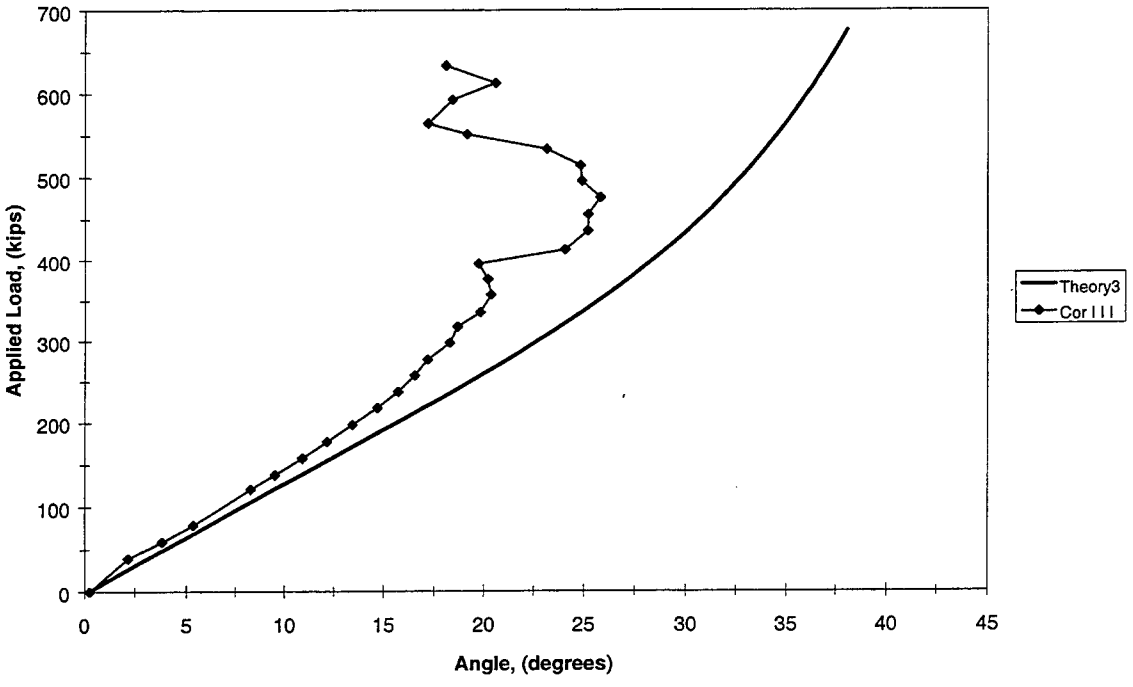

Figure 5.208 Corrected Principal Compression Angle Rosette 3 (End IID)

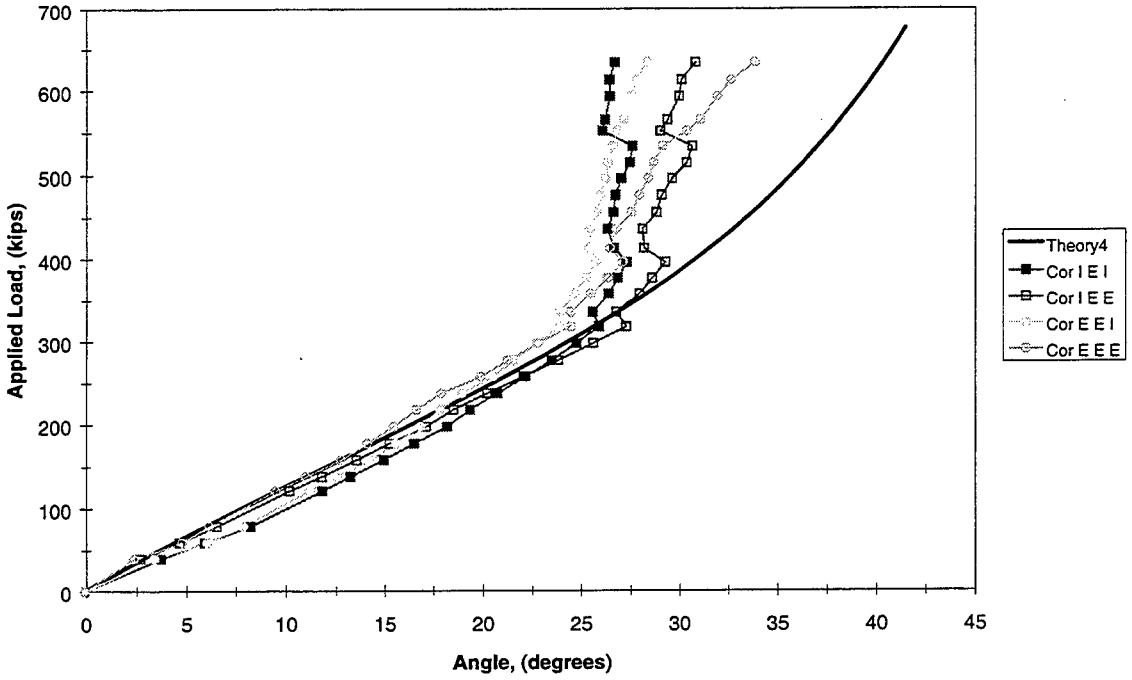

Figure 5.209 Corrected Principal Compression Angle Rosette 4 (End IID)

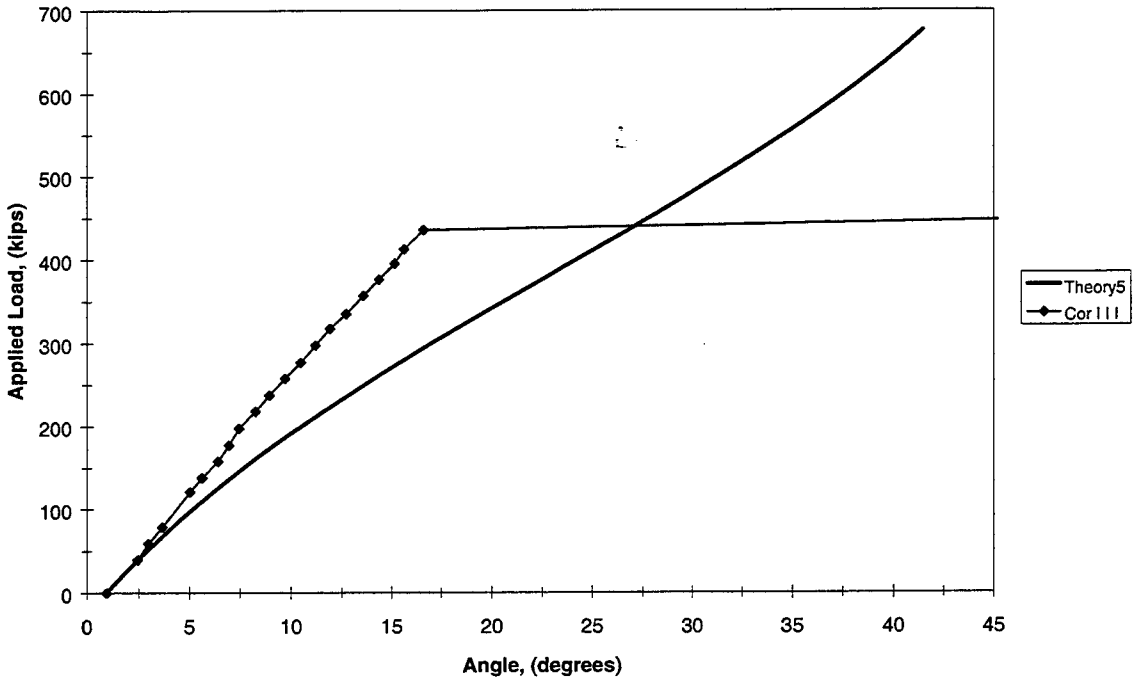

Figure 5.210 Corrected Principal Compression Angle Rosette 5 (End IID)

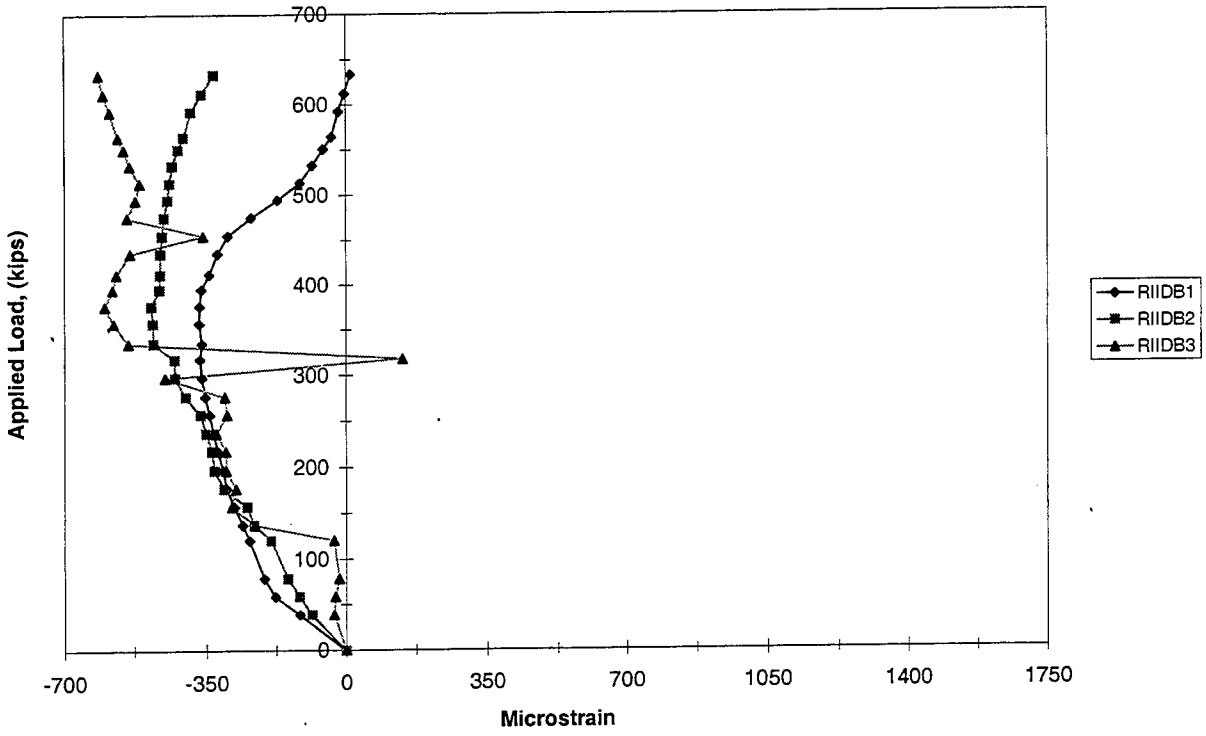

Figure 5.211 Bursting Stirrup (End IID)

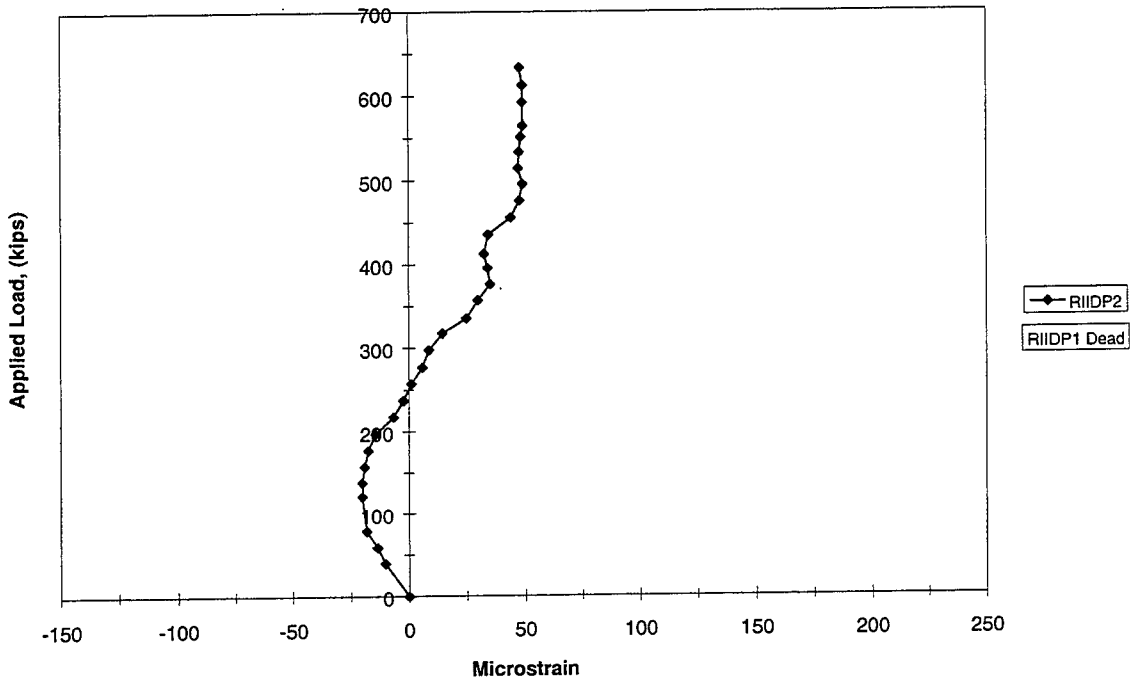

Figure 5.212 Rupture of Concrete (End IID)

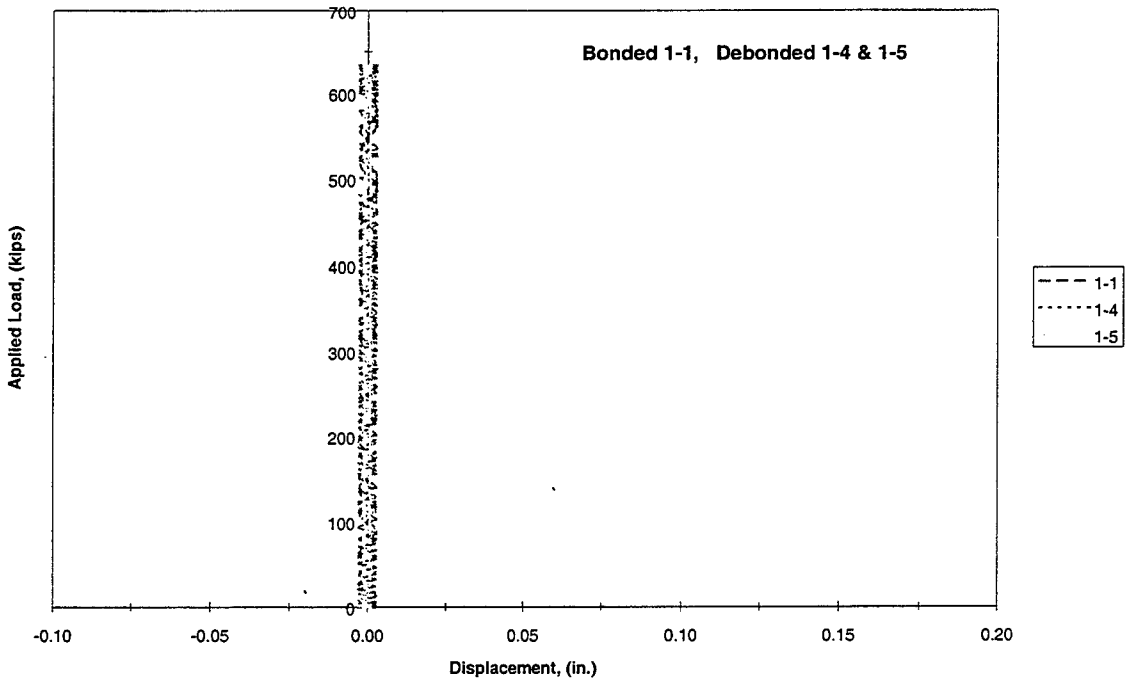

Figure 5.213 Strand Slip for 1-1, 1-4, & 1-5 (End IID)

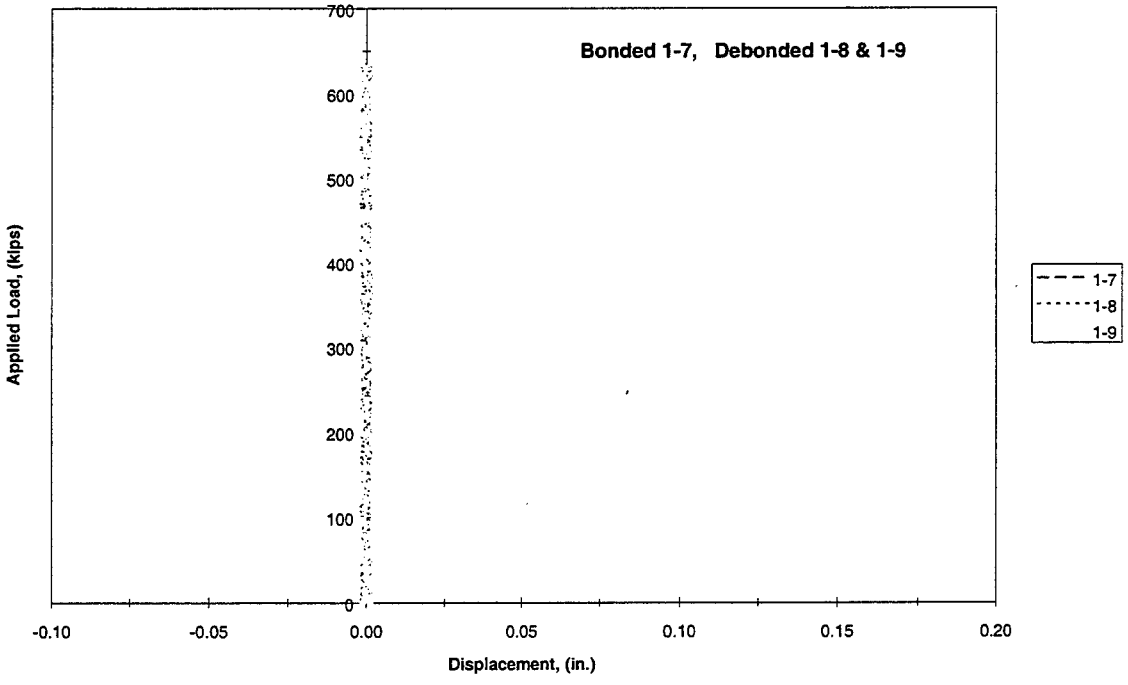

Figure 5.214 Strand Slip for 1-7, 1-8, & 1-9 (End IID)

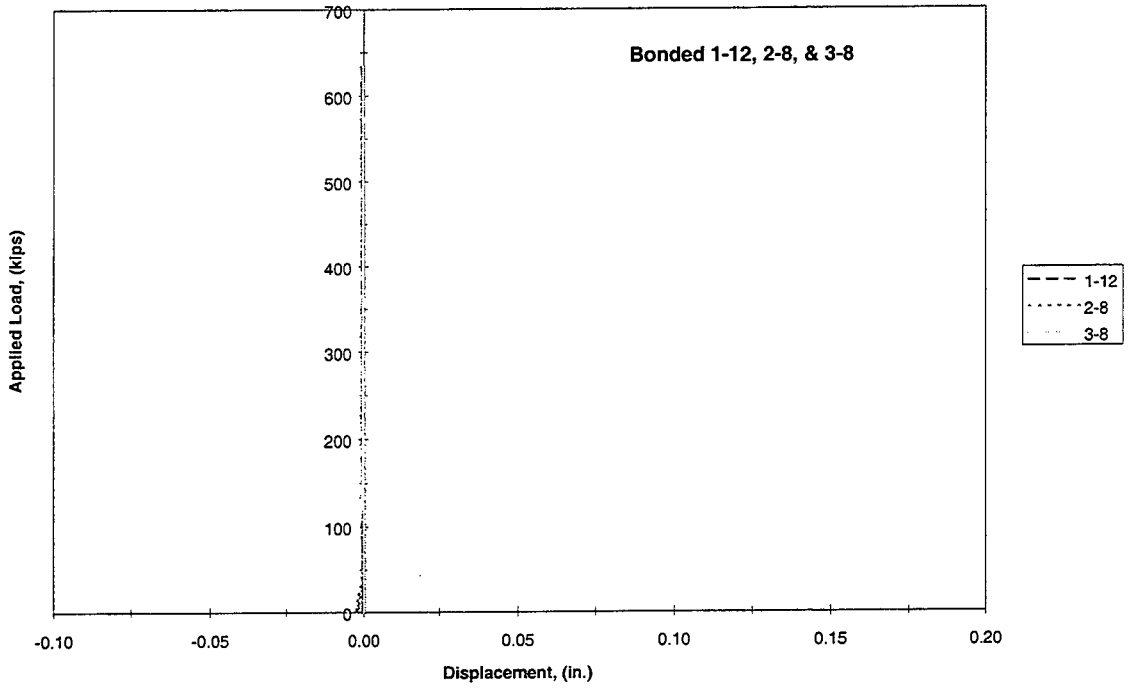

Figure 5.215 Strand Slip for 1-12, 2-8, & 3-8 (End IID)

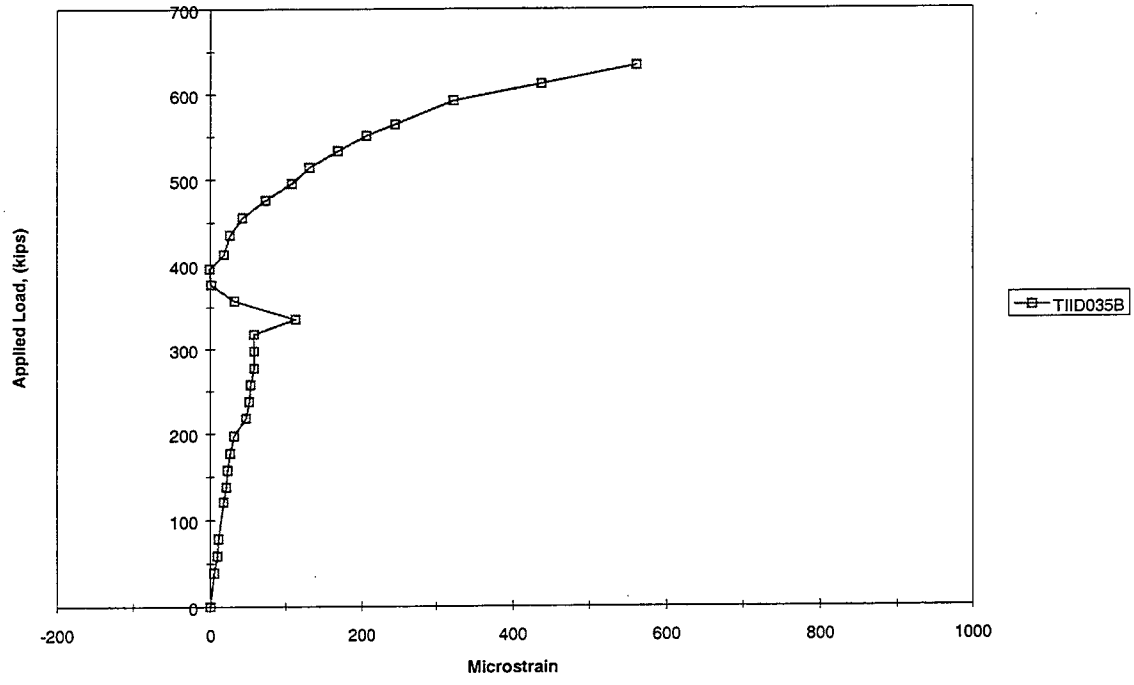

Figure 5.216 Transfer Length 0 ft. (End IID)

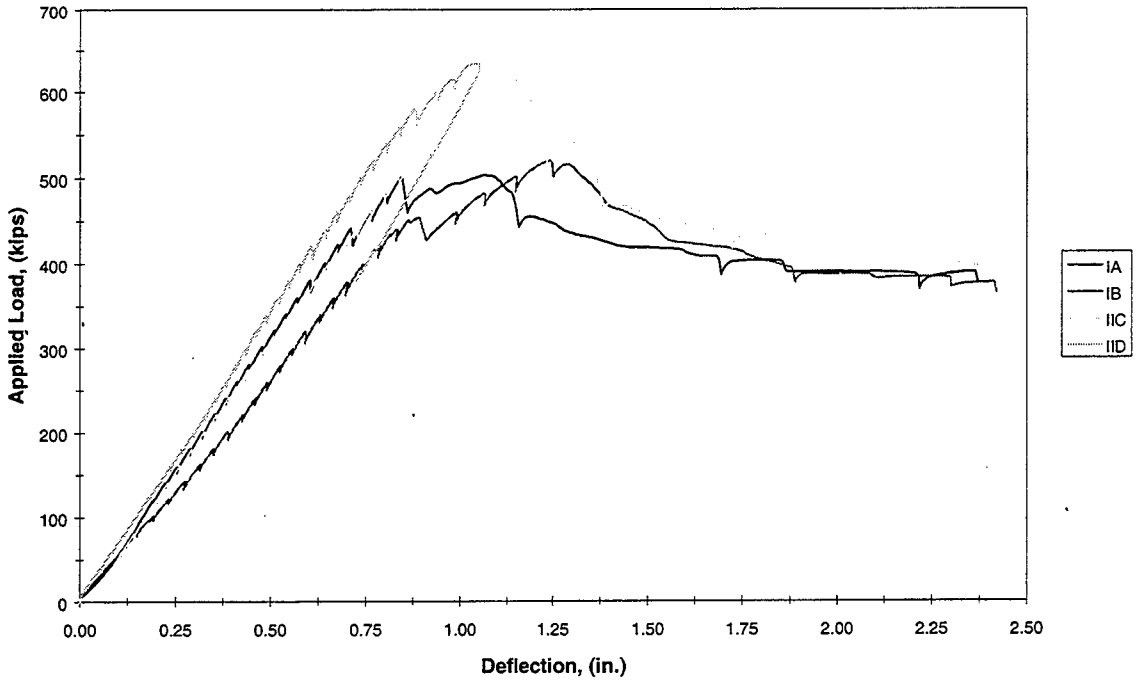

Figure 6.1 Corrected West Load Deflection

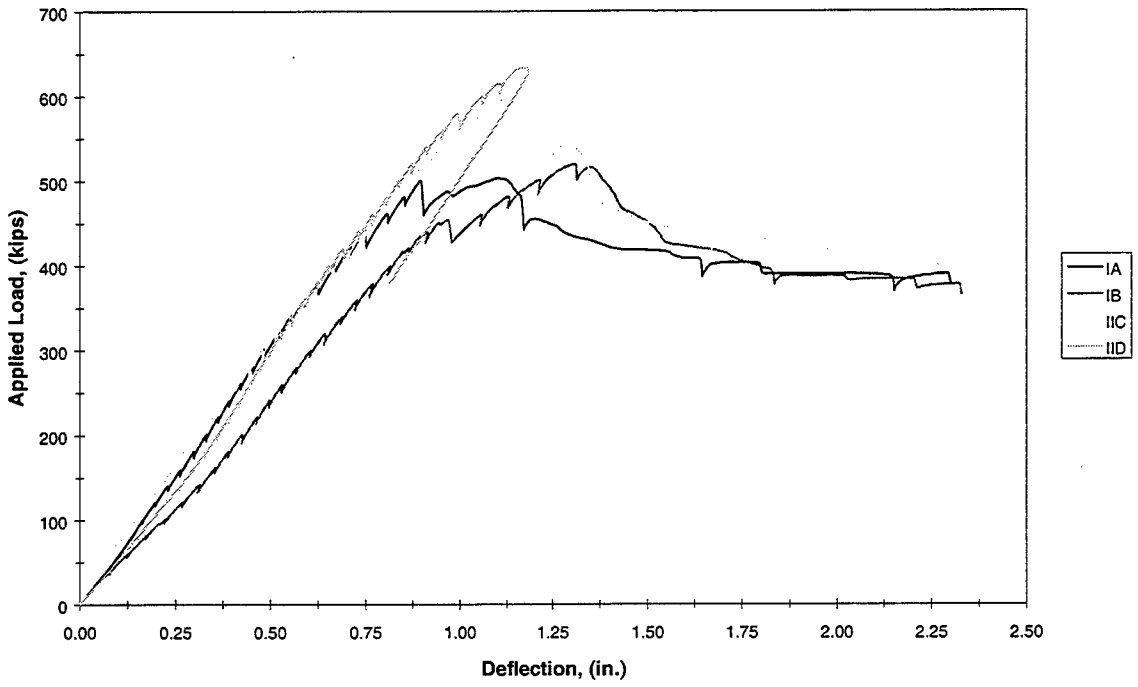

Figure 6.2 Corrected East Load Deflection

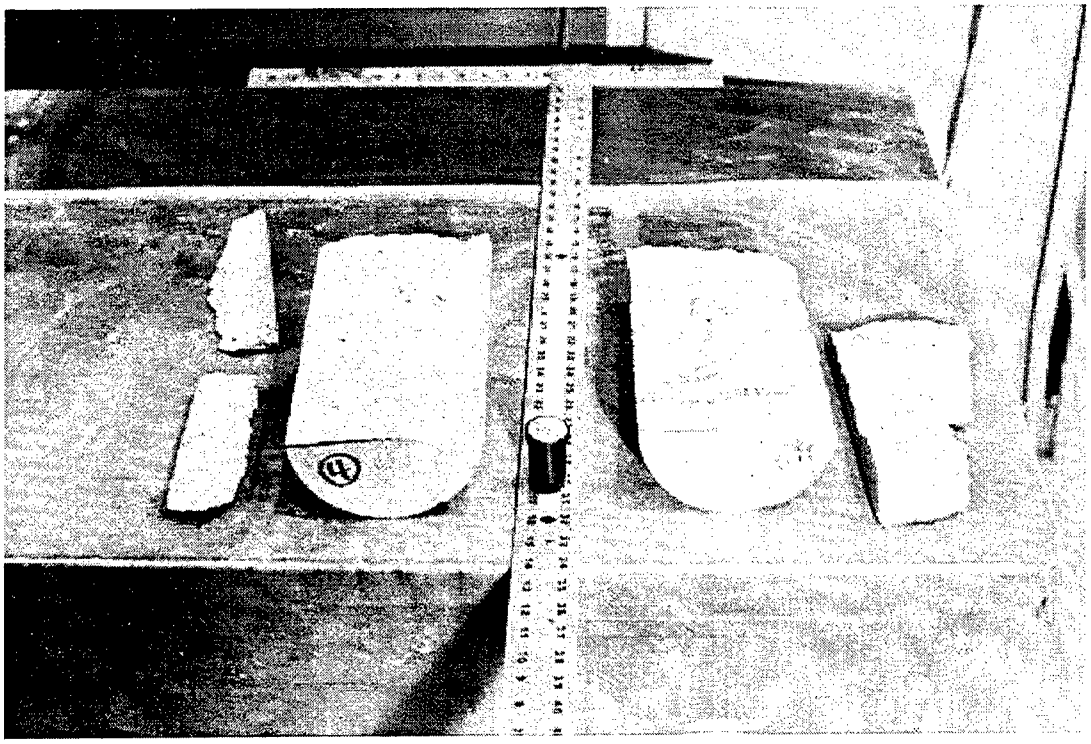

Figure 6.3 Limestone Cylinder after Split Tensile Test

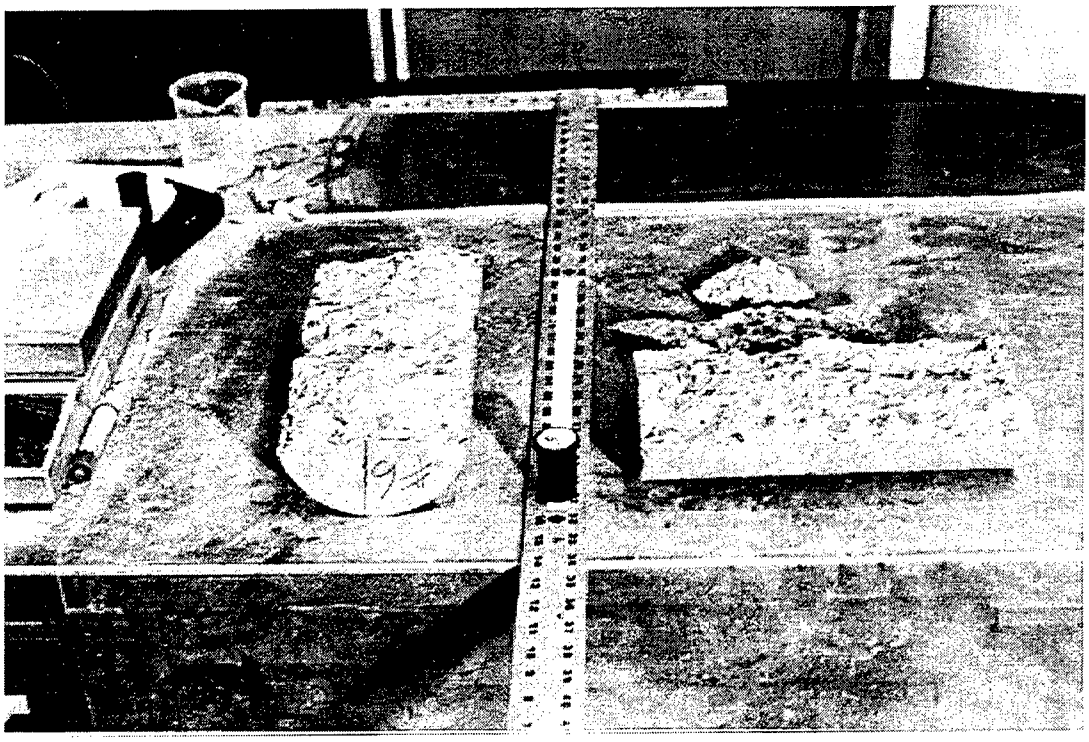

Figure 6.4 Glacial Gravel Cylinder after Split Tensile Test

Appendix A Derivations

A.1 ACI 318-95 Stirrup Contribution

See Figure A.1

Horizontal Distance

$$u = d\cot(\theta_{aci})$$

Number of Stirrups

$$n = \frac{u}{s} = \frac{d\cot(\theta_{aci})}{s}$$

Stirrup Contribution

$$V_s = \frac{d\cot(\theta_{aci})}{s} A_v f_y$$

Set $\theta_{aci} = 45°$

$$V_s = \frac{A_v f_y d}{s}\cot(45°)$$

ACI Stirrup Contribution

$$V_s = \frac{A_v f_y d}{s}$$

A.2 ACI 318-95 Concrete Contribution for Inclined Flexural Cracking

See Figure A.2

Shear-Moment Relationship

$$M - M_{cr} = \left(\frac{V + V_{cr}}{2}\right)\left(\frac{d}{2}\right)$$

Difference between V and V_{cr} usually small

$$V = V_{cr}$$

Therefore

$$M - M_{cr} = V\left(\frac{d}{2}\right)$$

Solve for M_{cr}

$$M_{cr} = M - V\left(\frac{d}{2}\right) = V\left(\frac{M}{V} - \frac{d}{2}\right)$$

Solve for V

$$V = \frac{M_{cr}}{\frac{M}{V} - \frac{d}{2}}$$

Additional component to turn flexural crack to flexural-shear crack

$$V = 0.6 b_w d \sqrt{f_c'} + \frac{M_{cr}}{\frac{M}{V} - \frac{d}{2}}$$

ACI 318-63 Concrete Contribution for inclined flexural cracking

$$V_{ci} = 0.6 b_w d \sqrt{f_c'} + \frac{M_{cr}}{\frac{M}{V} - \frac{d}{2}} + V_d$$

ACI 318-77 revised the equation (same as ACI 318-95)

$$V_{ci} = 0.6 b_w d \sqrt{f_c'} + \frac{V_i M_{cr}}{M_{\max}} + V_d$$

A.3 ACI 318-95 Concrete Contribution for Web-Shear Cracking

See Figure A.3

Mohr's Circle

$$f_t = radius - \left(\frac{f_{pc}}{2}\right)$$

Substitute for *radius*

$$f_t = \sqrt{v^2 + \left(\frac{f_{pc}}{2}\right)^2} - \left(\frac{f_{pc}}{2}\right)$$

Solve for v

$$v = \sqrt{\left(f_t + \frac{f_{pc}}{2}\right)^2 - \left(\frac{f_{pc}}{2}\right)^2}$$

Simplify

$$v = f_t\sqrt{1 + \frac{f_{pc}}{f_t}}$$

Set $f_t = 3.5\sqrt{f_c'}$

$$v = 3.5\sqrt{f_c'}\sqrt{1 + \frac{f_{pc}}{3.5\sqrt{f_c'}}}$$

ACI 318-95 simplification of above equation

$$v_{cw} = 3.5\sqrt{f_c'} + 0.3f_{pc}$$

ACI 318-95 Web Shear Equation including draping contribution

$$V_{cw} = \left(3.5\sqrt{f_c'} + 0.3f_{pc}\right)b_w d + V_p$$

A.4 Modified ACI 318-95 Concrete Contribution for Web-Shear Cracking

See Figure A.4

Mohr's Circle

$$f_t = radius - \left(\frac{f_{pd}}{2}\right)$$

Substitute for *radius*

$$f_t = \sqrt{v^2 + \left(\frac{f_{pd}}{2}\right)^2} - \left(\frac{f_{pd}}{2}\right)$$

Solve for v

$$v = \sqrt{\left(f_t + \frac{f_{pd}}{2}\right)^2 - \left(\frac{f_{pd}}{2}\right)^2}$$

Simplify

$$v = f_t\sqrt{1 + \frac{f_{pd}}{f_t}}$$

Set $f_t = 3.5\sqrt{f_c'}$

$$v = 3.5\sqrt{f_c'}\sqrt{1 + \frac{f_{pd}}{3.5\sqrt{f_c'}}}$$

From mechanics of materials

$$v = \frac{V_{mod}Q_{gc}}{I_{gc}b_w}$$

Solve for V_{mod}

$$V_{mod} = \frac{I_{gc}b_w}{Q_{gc}}v$$

Substitute for v and include draping contribution

$$V_{mod} = \frac{I_{gc}b_w}{Q_{gc}}3.5\sqrt{f_c'}\sqrt{1 + \frac{f_{pd}}{3.5\sqrt{f_c'}}} + V_p$$

A.5 Modified Truss Model Stirrup Contribution

See Figure A.5

Horizontal Distance

$$u = z\cot(\theta_{mtm})$$

Number of Stirrups

$$n = \frac{u}{s} = \frac{z\cot(\theta_{mtm})}{s}$$

Stirrup Contribution

$$V_{truss} = \frac{z\cot(\theta_{mtm})}{s} A_v f_y$$

Set $\theta_{mtm} = 25°$

$$V_{truss} = \frac{A_v f_y z}{s}\cot(25°)$$

A.6 Modified Truss Model Concrete Contribution

See Figure A.6

Mohr's Circle

$$f_t = radius - \left(\frac{f_{pc}}{2}\right)$$

Substitute for *radius*

$$f_t = \sqrt{v_{cr}{}^2 + \left(\frac{f_{pc}}{2}\right)^2} - \left(\frac{f_{pc}}{2}\right)$$

Solve for v_{cr}

$$v_{cr} = \sqrt{\left(f_t + \frac{f_{pc}}{2}\right)^2 - \left(\frac{f_{pc}}{2}\right)^2}$$

Simplify

$$v_{cr} = f_t\sqrt{1+\frac{f_{pc}}{f_t}}$$

Substitute in K

$$v_{cr} = Kf_t$$

Concrete Contribution

$$V_{cr} = Kf_t b_w d$$

where

$$f_t = 2\sqrt{f_c'} \quad \text{and} \quad K = \sqrt{1+\frac{f_{pc}}{f_t}}$$

A.7 Principal Strain and Principal Compression Angle

See Figure A.7

Experimental Strain due to Applied Load
(ε_a at 0°, ε_b at 45°, ε_c at 90°)

From Mohr's Circle

$$\varepsilon_{te} = center + radius$$
$$\varepsilon_{ce} = center - radius$$

Principal Tensile Strain and Principal Compressive Strain from Experimental Data

$$\varepsilon_{te} = \frac{\varepsilon_a + \varepsilon_c}{2} + \frac{1}{\sqrt{2}}\sqrt{(\varepsilon_a - \varepsilon_b)^2 + (\varepsilon_b - \varepsilon_c)^2}$$
$$\varepsilon_{ce} = \frac{\varepsilon_a + \varepsilon_c}{2} - \frac{1}{\sqrt{2}}\sqrt{(\varepsilon_a - \varepsilon_b)^2 + (\varepsilon_b - \varepsilon_c)^2}$$

From Mohr's Circle

$$\cos(2\theta_e) = \frac{\left(\frac{\varepsilon_a - \varepsilon_c}{2}\right)}{radius}$$

Substitute for *radius*

$$\cos(2\theta_e) = \left(\frac{(\varepsilon_a - \varepsilon_c)}{\sqrt{2}\sqrt{(\varepsilon_a - \varepsilon_b)^2 + (\varepsilon_b - \varepsilon_c)^2}}\right)$$

Angle of Principal Compression from Experimental Data

$$\theta_e = \begin{cases} +\frac{1}{2}\cos^{-1}\left(\frac{(\varepsilon_a - \varepsilon_b)}{\sqrt{2}\sqrt{(\varepsilon_a - \varepsilon_b)^2 + (\varepsilon_b - \varepsilon_c)^2}}\right), & \text{IF } \varepsilon_b \geq \frac{(\varepsilon_a + \varepsilon_c)}{2} \\ -\frac{1}{2}\cos^{-1}\left(\frac{(\varepsilon_a - \varepsilon_b)}{\sqrt{2}\sqrt{(\varepsilon_a - \varepsilon_b)^2 + (\varepsilon_b - \varepsilon_c)^2}}\right), & \text{IF } \varepsilon_b < \frac{(\varepsilon_a + \varepsilon_c)}{2} \end{cases}$$

A.7.1 Experimental Strains and Angle

Experimental strains and angle are due experimental strains of applied load only.

Experimental Strains

$$\varepsilon_a = \varepsilon_a$$
$$\varepsilon_b = \varepsilon_b$$
$$\varepsilon_c = \varepsilon_c$$

Experimental Principal Tensile and Compressive Strains

$$\varepsilon_{te} = \frac{\varepsilon_a + \varepsilon_c}{2} + \frac{1}{\sqrt{2}}\sqrt{(\varepsilon_a - \varepsilon_b)^2 + (\varepsilon_b - \varepsilon_c)^2}$$
$$\varepsilon_{ce} = \frac{\varepsilon_a + \varepsilon_c}{2} - \frac{1}{\sqrt{2}}\sqrt{(\varepsilon_a - \varepsilon_b)^2 + (\varepsilon_b - \varepsilon_c)^2}$$

Experimental Principal Angle

$$\cos(2\theta_e) = \left(\frac{(\varepsilon_a - \varepsilon_c)}{\sqrt{2}\sqrt{(\varepsilon_a - \varepsilon_b)^2 + (\varepsilon_b - \varepsilon_c)^2}} \right)$$

A.7.2 Theoretical Strains and Angle

Theoretical strains and angle are due to applied load without including self weight and prestress.

Axial Stress

$$f_{pg} = \frac{M_{pt}(y_{tc} - y_m)}{I_{gc}}$$

Shear Stress

$$\tau_g = -\frac{(V_{pt})Q_{gc}}{I_{gc}b_m}$$

Theoretical Strains

$$\varepsilon_{ag} = \frac{f_{pg}}{E_c}$$

$$\varepsilon_{bg} = \frac{f_{pg}}{2E_c} + \frac{\tau_g}{E_c}$$

$$\varepsilon_{cgg} = 0$$

Theoretical Principal Tensile and Compressive Strains

$$\varepsilon_{tg} = \frac{f_{pg}+0}{2E_c} + \frac{1}{\sqrt{2}}\sqrt{\left(\frac{f_{pg}}{2E_c} - \frac{\tau_g}{E_c}\right)^2 + \left(\frac{f_{pg}}{2E_c} + \frac{\tau_g}{E_c} - 0\right)^2}$$

$$\varepsilon_{cg} = \frac{f_{pg}+0}{2E_c} - \frac{1}{\sqrt{2}}\sqrt{\left(\frac{f_{pg}}{2E_c} - \frac{\tau_g}{E_c}\right)^2 + \left(\frac{f_{pg}}{2E_c} + \frac{\tau_g}{E_c} - 0\right)^2}$$

Simplified Theoretical Principal Tensile and Compressive Strains

$$\varepsilon_{tg} = \frac{f_{pg}}{2E_c} + \sqrt{\left(\frac{f_{pg}}{2E_c}\right)^2 + \left(\frac{\tau_g}{E_c}\right)^2}$$

$$\varepsilon_{cg} = \frac{f_{pg}}{2E_c} - \sqrt{\left(\frac{f_{pg}}{2E_c}\right)^2 + \left(\frac{\tau_g}{E_c}\right)^2}$$

Theoretical Principal Angle

$$\cos(2\theta_g) = \left(\frac{\frac{f_{pg}}{2E_c}}{\frac{1}{\sqrt{2}}\sqrt{\left(\frac{f_{pg}}{2E_c} - \frac{\tau_g}{E_c}\right)^2 + \left(\frac{f_{pg}}{2E_c} + \frac{\tau_g}{E_c}\right)^2}} \right)$$

Simplified Theoretical Principal Angle

$$\cos(2\theta_g) = \left(\frac{\frac{f_{pg}}{2}}{\sqrt{\left(\frac{f_{pg}}{2}\right)^2 + (\tau_g)^2}} \right)$$

A.7.3 Corrected Experimental Strains and Angle

Corrected experimental strains and angle are due experimental strains of applied load and initial axial stress and initial shear stress. The initial stresses are due to prestress and self weight which are superimposed onto the measured strains.

Axial Stress

$$f_{pi} = -\frac{P}{A_g} - \frac{P(y_t - y_m)e}{I_g} + \frac{(M_{gird} + M_{deck})(y_t - y_m)}{I_g}$$

Shear Stress

$$\tau_i = -\frac{(V_d - V_p)Q_g}{I_g b_m}$$

Corrected Experimental Strains

$$\varepsilon_{ai} = \varepsilon_a + \frac{f_{pi}}{E_c}$$

$$\varepsilon_{bi} = \varepsilon_b + \frac{f_{pi}}{2E_c} + \frac{\tau_i}{E_c}$$

$$\varepsilon_{cii} = \varepsilon_c + 0$$

Corrected Experimental Principal Tensile and Compressive Strains

$$\varepsilon_{tc} = \frac{\varepsilon_a + \varepsilon_c + \frac{f_{pi}}{E_c}}{2} + \frac{1}{\sqrt{2}}\sqrt{\left(\varepsilon_a - \varepsilon_b + \frac{f_{pi}}{2E_c} - \frac{\tau_i}{E_c}\right)^2 + \left(\varepsilon_b - \varepsilon_c + \frac{f_{pi}}{2E_c} + \frac{\tau_i}{E_c}\right)^2}$$

$$\varepsilon_{cc} = \frac{\varepsilon_a + \varepsilon_c + \frac{f_{pi}}{E_c}}{2} - \frac{1}{\sqrt{2}}\sqrt{\left(\varepsilon_a - \varepsilon_b + \frac{f_{pi}}{2E_c} - \frac{\tau_i}{E_c}\right)^2 + \left(\varepsilon_b - \varepsilon_c + \frac{f_{pi}}{2E_c} + \frac{\tau_i}{E_c}\right)^2}$$

Corrected Experimental Principal Angle

$$\cos(2\theta_c) = \left(\frac{\left(\varepsilon_a - \varepsilon_c + \frac{f_{pi}}{E_c}\right)}{\sqrt{2}\sqrt{\left(\varepsilon_a - \varepsilon_b + \frac{f_{pi}}{2E_c} - \frac{\tau_i}{E_c}\right)^2 + \left(\varepsilon_b - \varepsilon_c + \frac{f_{pi}}{2E_c} + \frac{\tau_i}{E_c}\right)^2}} \right)$$

A.7.4 Theoretical Strains and Angle

Theoretical strains and angle are due to applied load including self weight and prestress.

Axial Stress

$$f_{pj} = -\frac{P}{A_g} - \frac{P(y_t - y_m)e}{I_g} + \frac{(M_{gird} + M_{deck})(y_t - y_m)}{I_g} + \frac{M_{pt}(y_{tc} - y_m)}{I_{gc}}$$

Shear Stress

$$\tau_j = -\frac{(V_d - V_p)Q_g}{I_g b_m} - \frac{(V_{pt})Q_{gc}}{I_{gc} b_m}$$

Theoretical Strains

$$\varepsilon_{aj} = \frac{f_{pj}}{E_c}$$

$$\varepsilon_{bj} = \frac{f_{pj}}{2E_c} + \frac{\tau_j}{E_c}$$

$$\varepsilon_{cjj} = 0$$

Theoretical Principal Strains

$$\varepsilon_{tj} = \frac{f_{pj} + 0}{2E_c} + \frac{1}{\sqrt{2}}\sqrt{\left(\frac{f_{pj}}{E_c} - \frac{f_{pj}}{2E_c} - \frac{\tau_j}{E_c}\right)^2 + \left(\frac{f_{pj}}{2E_c} + \frac{\tau_j}{E_c} - 0\right)^2}$$

$$\varepsilon_{cj} = \frac{f_{pj} + 0}{2E_c} - \frac{1}{\sqrt{2}}\sqrt{\left(\frac{f_{pj}}{E_c} - \frac{f_{pj}}{2E_c} - \frac{\tau_j}{E_c}\right)^2 + \left(\frac{f_{pj}}{2E_c} + \frac{\tau_j}{E_c} - 0\right)^2}$$

Simplified Theoretical Principal Strains

$$\varepsilon_{tj} = \frac{f_{pj}}{2E_c} + \sqrt{\left(\frac{f_{pj}}{2E_c}\right)^2 + \left(\frac{\tau_j}{E_c}\right)^2}$$

$$\varepsilon_{cj} = \frac{f_{pj}}{2E_c} - \sqrt{\left(\frac{f_{pj}}{2E_c}\right)^2 + \left(\frac{\tau_j}{E_c}\right)^2}$$

Theoretical Principal Angle

$$\cos(2\theta_j) = \left(\frac{\frac{f_{pj}}{2E_c}}{\frac{1}{\sqrt{2}}\sqrt{\left(\frac{f_{pj}}{2E_c} - \frac{\tau_j}{E_c}\right)^2 + \left(\frac{f_{pj}}{2E_c} + \frac{\tau_j}{E_c}\right)^2}} \right)$$

Simplified Theoretical Principal Angle

$$\cos(2\theta_j) = \left(\frac{\frac{f_{pj}}{2}}{\sqrt{\left(\frac{f_{pj}}{2}\right)^2 + (\tau_j)^2}} \right).$$

A.8 Interface Shear Model

See Figure A.8

Sum of the Forces in the Vertical Direction (Assume $\theta_{ism} = 30°$)

$$R_1 + \sin(\theta_{ism})V_c = R_1 + F_{s8} + F_{s9}$$

$$R_1 = V_{con}$$

Sum of the Forces in the Horizontal Direction (Neglect Prestressing Force)

$$T + \cos(\theta_{ism})V_c = C$$

$$V_{is} = T$$

Sum of the Moment at Location A

$$Tj_T + Cj_C + F_{s8}g_8 + F_{s9}g_9 = R_1(A_1 - a)$$

Simplify Vertical Direction Equation

$$V_c = \frac{F_{s8} + F_{s9}}{\sin(\theta_{ism})}$$

Substitute for V_c in Horizontal Direction Equation

$$T + (F_{s8} + F_{s9})\cot(\theta_{ism}) = C$$

Substitute for C in Moment Equation

$$Tj_T + Tj_C + (F_{s8} + F_{s9})\cot(\theta_{ism})j_C + F_{s8}g_8 + F_{s9}g_9 = R_1(A_1 - a)$$

Substitute for T

$$V_{is}j_T + V_{is}j_C + (F_{s8} + F_{s9})\cot(\theta_{ism})j_C + F_{s8}g_8 + F_{s9}g_9 = R_1(A_1 - a)$$

Solve for V_{is}

$$V_{is} = \frac{R_1(A_1 - a)}{j_T + j_C} - \frac{(F_{s8} + F_{s9})\cot(\theta_{ism})j_C + F_{s8}g_8 + F_{s9}g_9}{j_T + j_C}$$

Shear Friction Capacity from AASHTO LRFD 1994

$$V_{sf} = \min\left(c_f A_{cv} + \mu(A_{vf} f_y + P_c),\ 0.2 f_c' A_{cv},\ 0.8 A_{cv}\right)$$

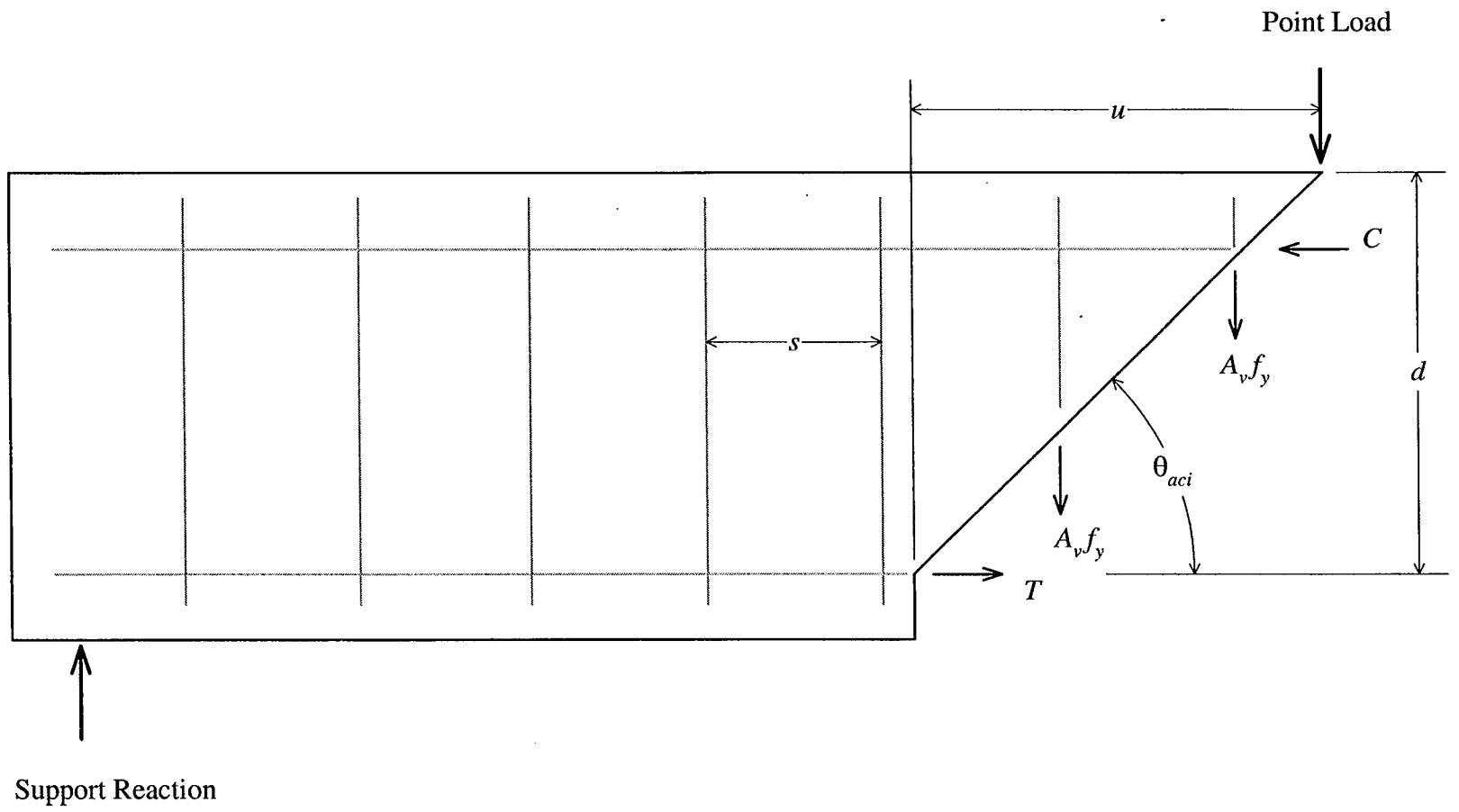

Figure A.1 ACI Stirrup Contribution Model

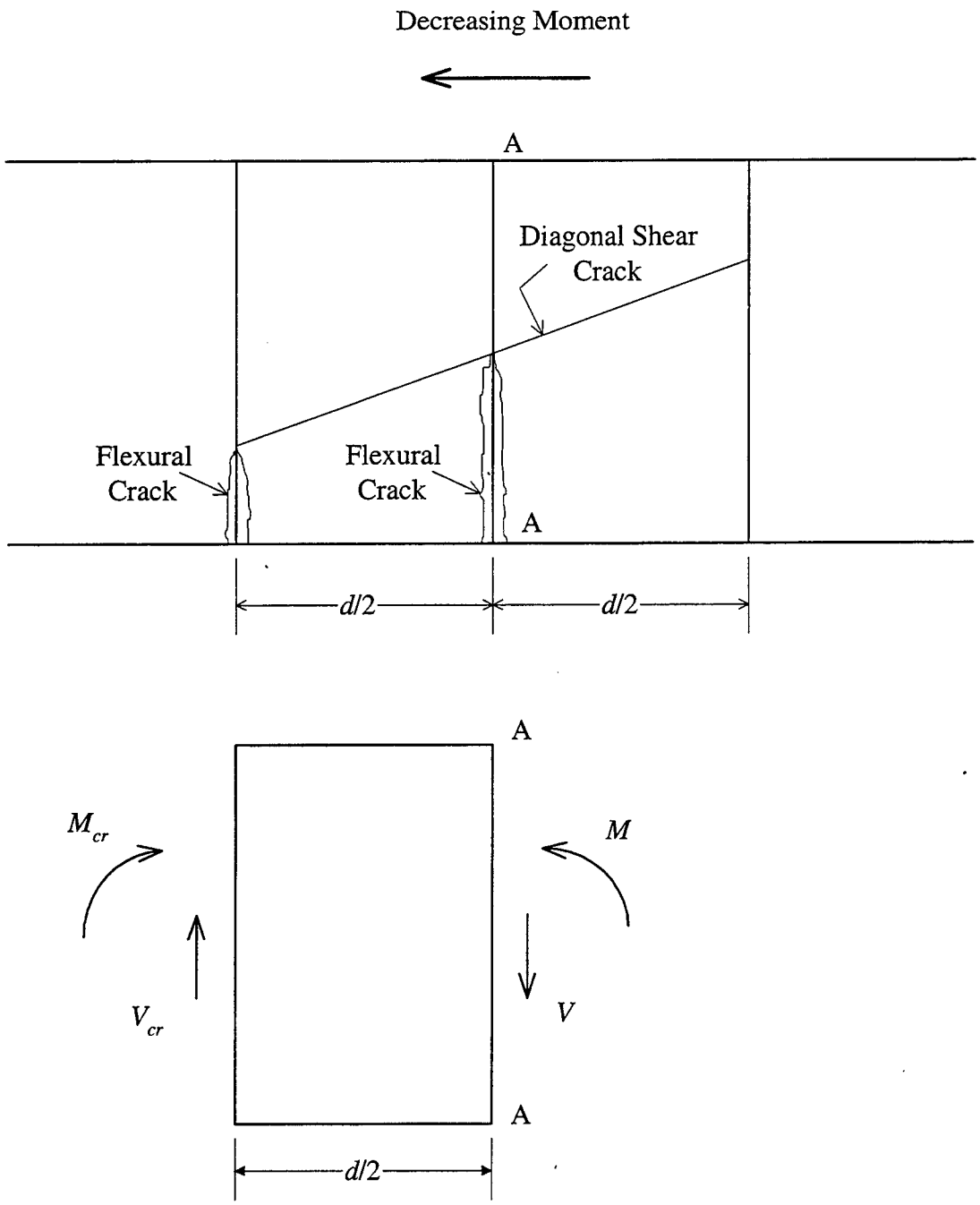

Figure A.2 Inclined Flexural Crack Initiation Model

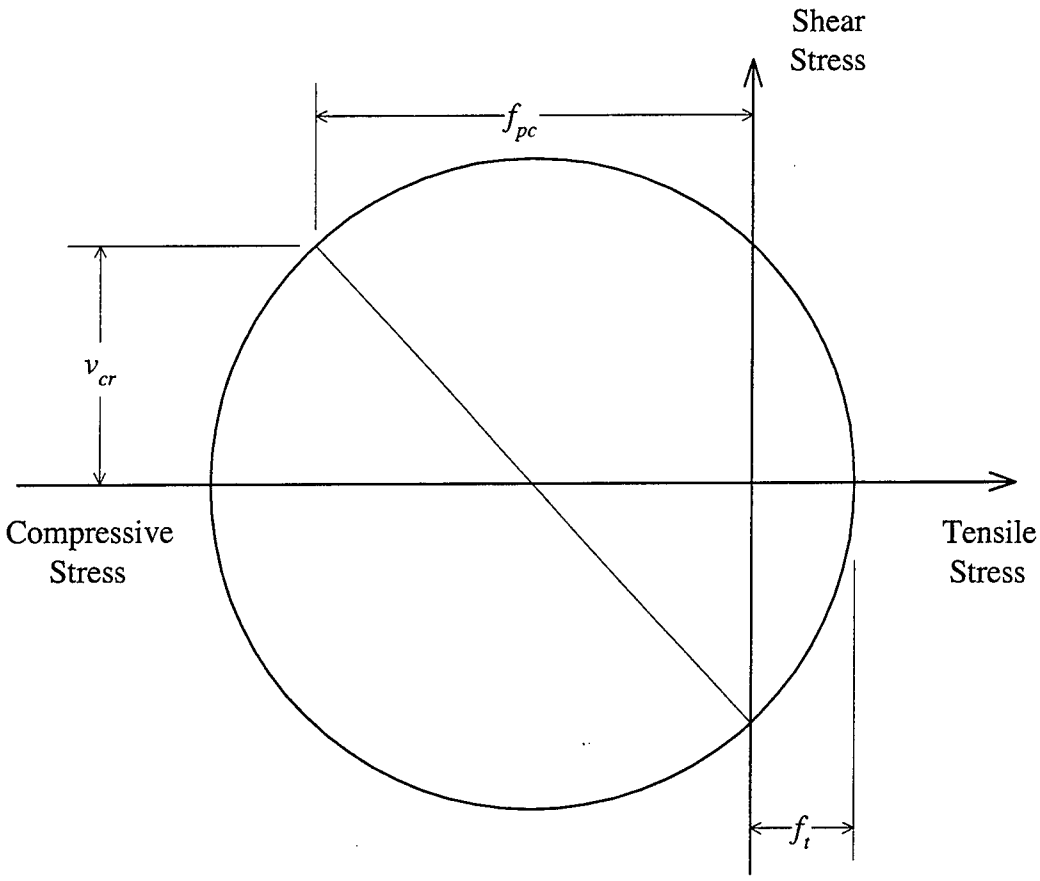

Figure A.3 Mohr's Circle for Stress State at the Composite Centroid

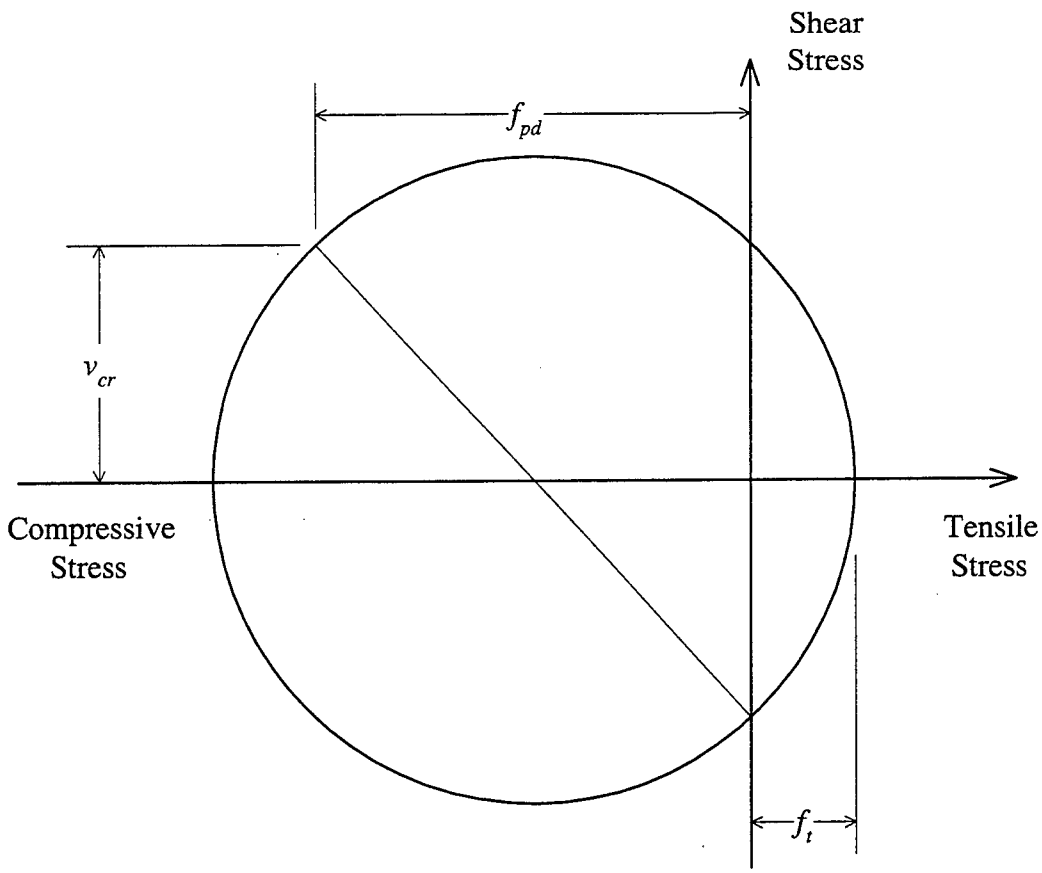

Figure A.4 Mohr's Circle for Stress State at a Given Centroid

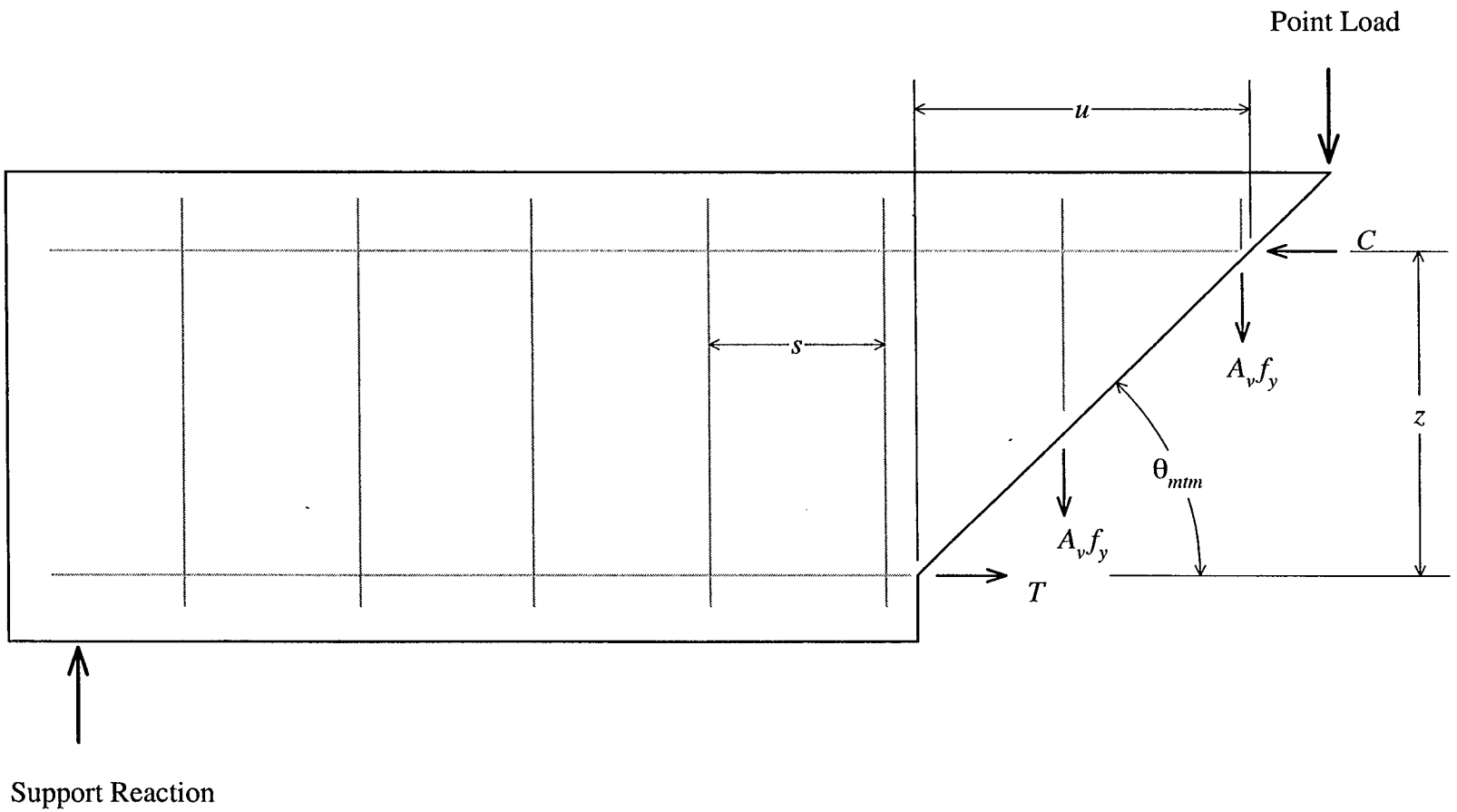

Figure A.5 Modified Truss Stirrup Contribution Model

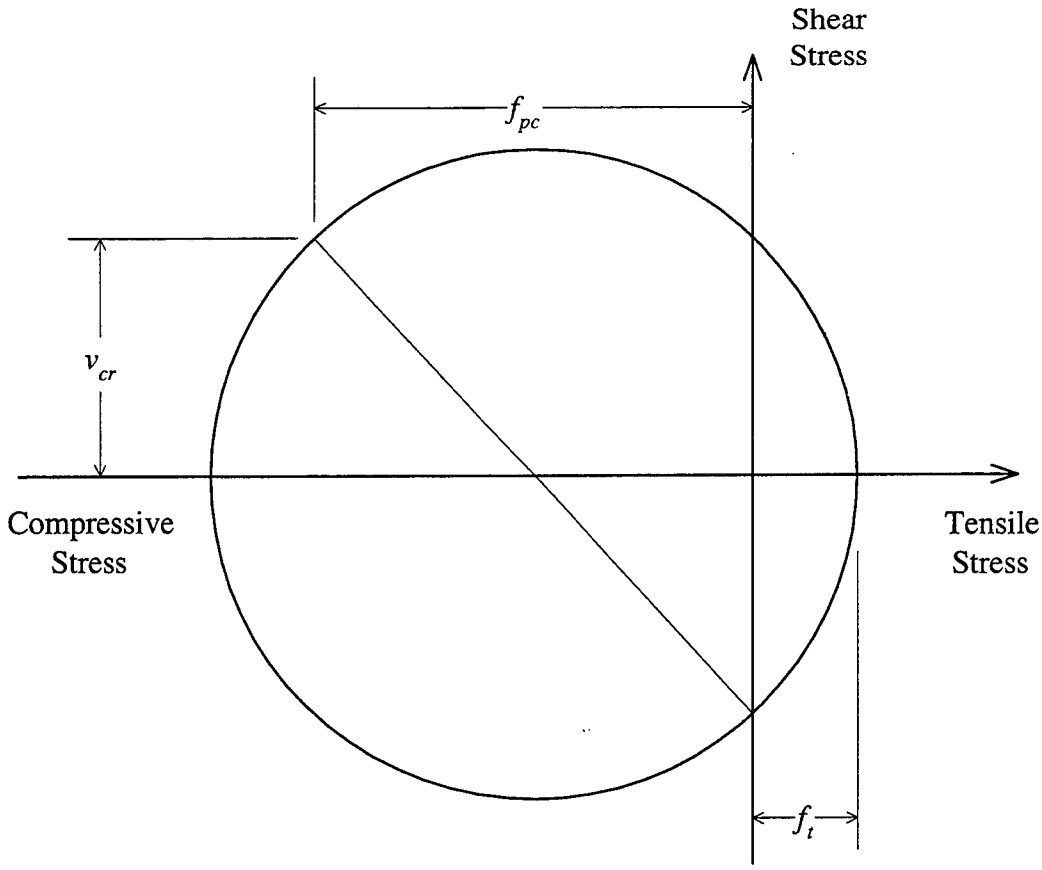

Figure A.6 Mohr's Circle for Stress State at the Composite Centroid

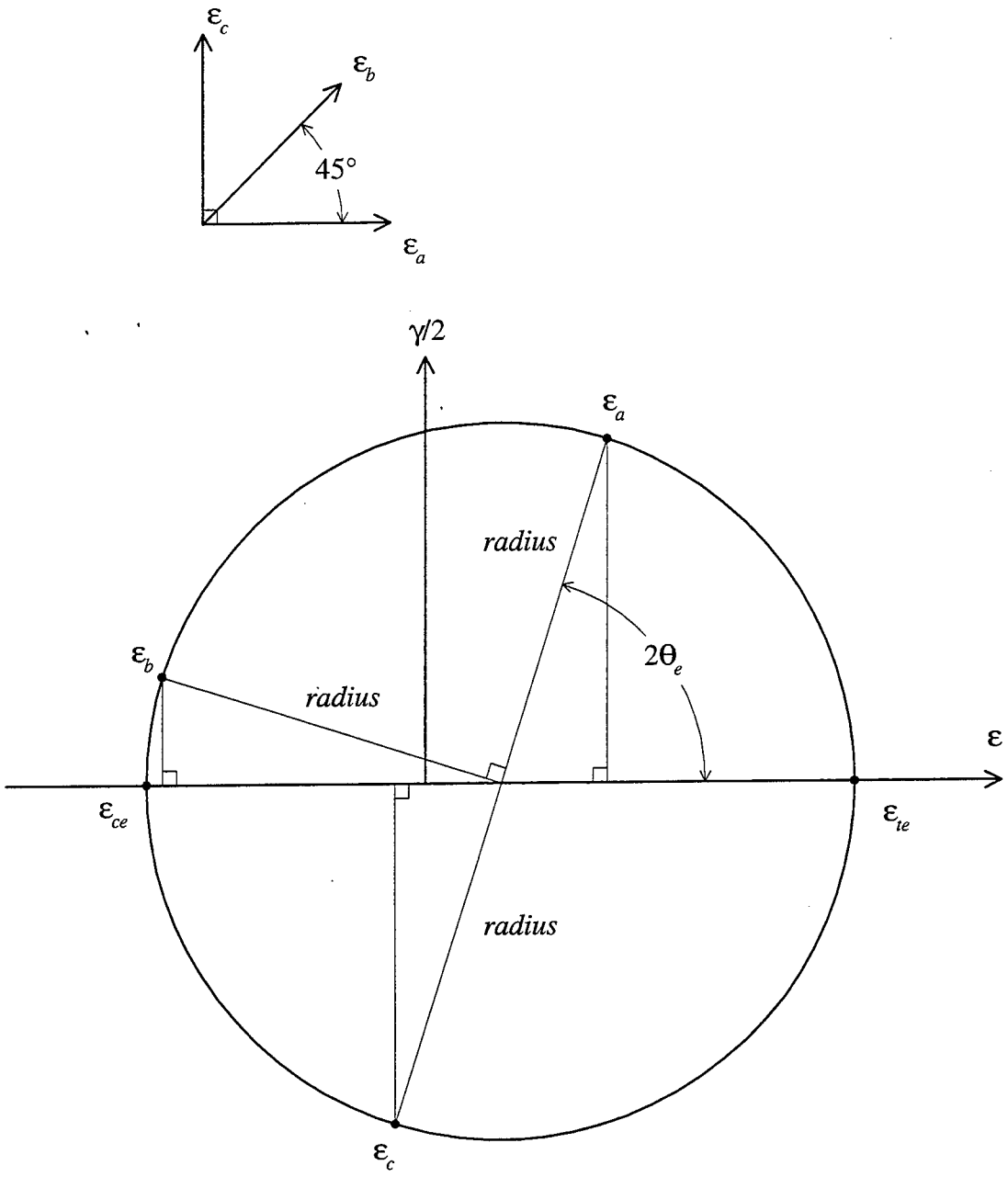

Figure A.7 Mohr's Circle for Strain State at a Rosette

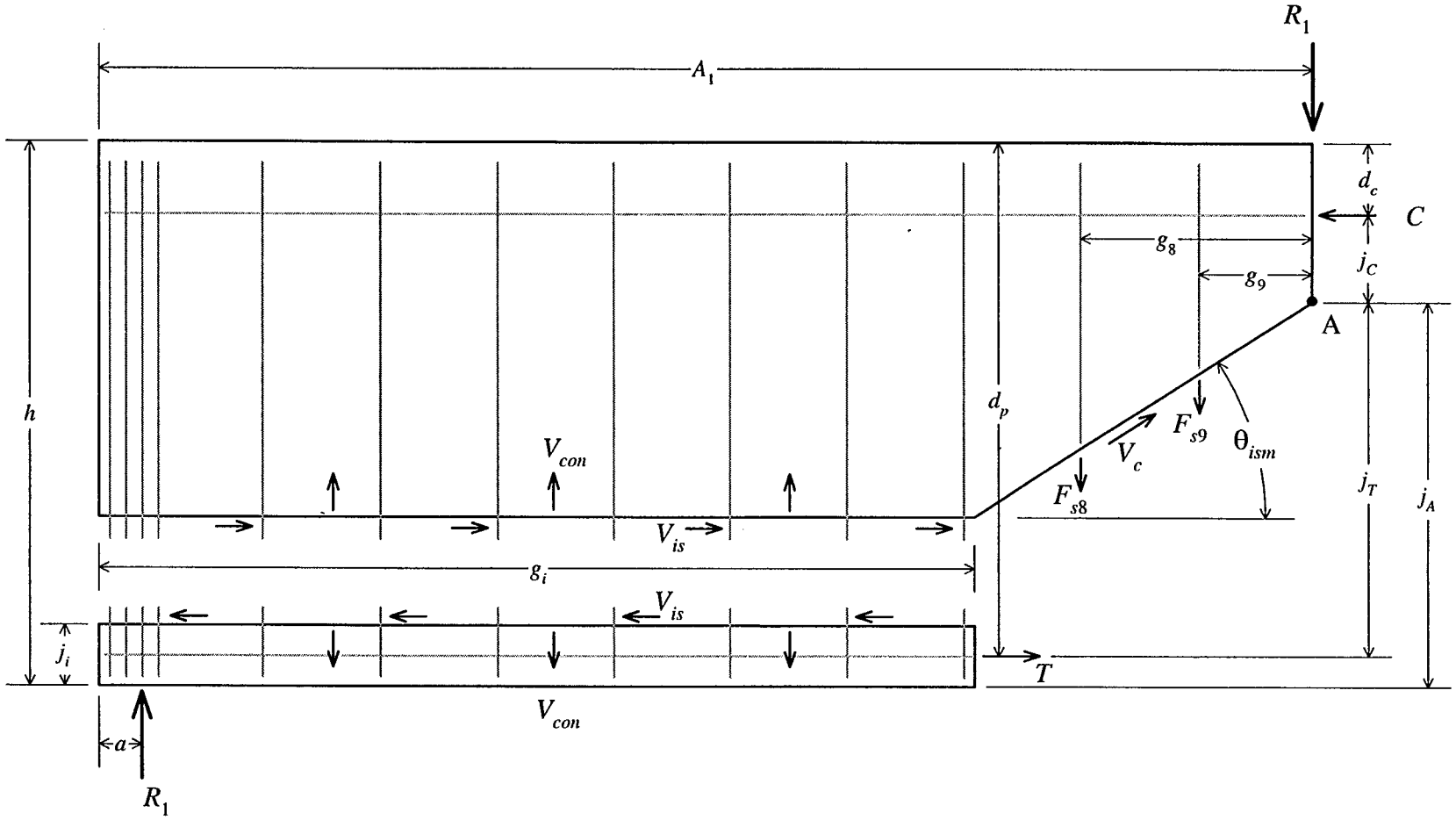

Figure A.8 Interface Shear Free Body Diagram

Appendix B Concrete Cylinder Test Results

B.1 Cylinder Test Results for Each Girder

Table B.1 Individual Cylinder Test Results for Girder I

Cylinder Number	Age (days)	Modulus of Elasticity (ksi)	Split Tensile Strength (psi)	Compressive Strength (psi)
1	1220	-	-	10830
2	1240	5000	-	10770
3	1240	5470	-	11150
4	1220	-	705	-
5	1230	-	761	-
6	1230	-	759	-
7	1220	-	-	11300
8	1240	5270	-	12210
9	1240	5190	-	11710
10	1220	-	709	-
11	1230	-	719	-
12	1230	-	723	-
Averages for Girder I =		5320	729	11330
Standard Deviation =		190	25	550

Table B.2 Cylinder Strength History for Girder I

Test	Age (days)	Elk River (psi)	Mich Tech (psi)	UMN (psi)
Compressive Strength	21 hrs	9300	-	-
	23 hrs	-	-	8400
	7	11400	-	9900
	28	12100	-	10900
	220	-	-	11600
	480	-	-	12600
	1200	-	12700	-
	1240	-	-	11330
Split Tensile Strength	28	-	-	1072
	1245	-	-	729
Modulus of Rupture	28	-	-	951
	1200	-	1283	-
Modulus of Elasticity	1	-	-	4.38×10^6
	7	-	-	4.61×10^6
	28	-	-	4.81×10^6
	1200	-	5.30×10^6	-
	1250	-	-	5.23×10^6

Table B.3 Individual Cylinder Test Results for Girder II

Cylinder Number	Age (days)	Modulus of Elasticity (ksi)	Split Tensile Strength (psi)	Compressive Strength (psi)
13	1220	-	-	8850
14	1240	4380	-	9270
15	1240	4150	-	8590
16	1220	-	523	-
17	1230	-	494	-
18	1230	-	566	-
19	1230	-	618	-
20	1220	-	610	-
21	1230	-	680	-
22	1220	-	-	9350
23	1240	4990	-	9960
24	1240	4560	-	9870
25	1230	-	624	-
26	1230	-	582	-
Averages for Girder II =		4520	587	9315
Standard Deviation =		350	60	540

Table B.4 Cylinder Strength History for Girder II

Test	Age (days)	Elk River (psi)	Mich Tech (psi)	UMN (psi)
Compressive Strength	17 hrs	-	-	9310
	24 hrs	-	-	8900
	7	11000	-	9500
	28	11100	-	9600
	220	-	-	10800
	480	-	-	11100
	1200	-	10300	-
	1240	-	-	9315
Split Tensile Strength	28	-	-	1113
	1245	-	-	587
Modulus of Rupture	28	-	-	747
	1200	-	975	-
Modulus of Elasticity	1	-	-	4.75×10^6
	7	-	-	5.34×10^6
	28	-	-	4.80×10^6
	1200	-	4.69×10^6	-
	1250	-	-	4.52×10^6

B.2 Individual Cylinder Test Results for the Deck

Table B.5 Individual Cylinder Test Results for the Deck

Cylinder Number	Age (days)	Modulus of Elasticity (ksi)	Split Tensile Strength (psi)	Compressive Strength (psi)
27	1020	-	436	-
28	1030	-	-	5610
29	1020	-	455	-
30	1040	4340	-	5920
31	1020	-	465	-
32	1040	5240	-	5910
33	1040	4470	-	5560
34	1020	-	406	-
35	1030	-	-	5500
36	1020	-	427	-
37	1040	4110	-	5400
38	1020	-	392	-
39	1040	4230	-	5720
Averages for Deck =		4480	430	5660
Standard Deviation =		450	28	200

Table B.6 Cylinder Strength History for the Deck

Test	Age (days)	Elk River (psi)	Mich Tech (psi)	UMN (psi)
Compressive Strength	7	-	-	5100
	28	-	-	5900
	1000	-	6100	-
	1040	-	-	5660
Split Tensile Strength	28	-	-	514
	1045	-	-	430
Modulus of Rupture	28	-	-	632
Modulus of Elasticity	28	-	-	3.99×10^6
	1000	-	4.46×10^6	-
	1050	-	-	4.48×10^6

Appendix C Nominal and Measured Specimen Properties

Table C.1 Nominal Properties

Nominal	IA	IB	IIC	IID	Units
Girder Dimensions					
total original girder length, g.l. =	132.75	132.75	132.75	132.75	ft.
hold down point from end, h.d. =	53.13	53.13	53.13	53.13	ft.
depth of composite section, h =	55.0	55.0	55.0	55.0	in.
width of deck, b_d =	48.0	48.0	48.0	48.0	in.
width of composite interface, b_f =	30.0	30.0	30.0	30.0	in.
width of web, b_w, b_v =	6.0	6.0	6.0	6.0	in.
Concrete Material Properties					
girder compressive strength, f_c' =	10500	10500	10500	10500	psi
deck compressive strength, f_{cd}' =	4300	4300	4300	4300	psi
girder modulus of elasticity, E_c =	5635	5635	5635	5635	ksi
deck modulus of elasticity, E_{cd} =	3975	3975	3975	3975	ksi
Stirrups					
stirrup yield strength, f_y =	60.0	60.0	60.0	60.0	ksi
bursting stirrup yield strength, f_{yb} =	60.0	60.0	60.0	60.0	ksi
stirrup area, A_v =	0.40	0.40	0.40	0.40	$in.^2$
bursting stirrup area, A_{vb} =	0.88	0.88	0.88	0.88	$in.^2$
stirrup spacing, s =	16.0	16.0	16.0	16.0	in.
bursting stirrup spacing, s_b =	3.0	3.0	3.0	3.0	in.
Support & Load Dimensions					
width of support, w.s. =	0	0	0	0	in.
left end to center of support, a =	0.625	0.625	0.625	0.625	ft.
length between supports, l =	39.78	39.78	39.78	39.78	ft.
right end to center of support, b =	2.60	2.60	2.60	2.60	ft.
total specimen length, s.l. =	43.00	43.00	43.00	43.00	ft.
applied point load from end, A_1 =	13.90	13.90	13.90	13.90	ft.
Distributed Loads					
girder dead load, w_{gird} =	672	672	672	672	plf
deck dead load, w_{deck} =	481	481	481	481	plf
distributed dead load, w_{dl} =	0	0	0	0	plf
distributed live load, w_{ll} =	0	0	0	0	plf
Gross Cross Section Properties					
girder centroid from bottom, y_t =	22.34	22.34	22.34	22.34	in.
composite centroid from bottom, y_{tc} =	31.89	31.89	31.89	31.89	in.
girder area, A_g =	624	624	624	624	$in.^2$
composite area, A_{gc} =	949.9	949.9	949.9	949.9	$in.^2$
girder moment of interia, I_g =	167048	167048	167048	167048	$in.^4$
composite moment of interia, I_{gc} =	335428	335428	335428	335428	$in.^4$

Table C.2 Measured Properties

Measured	IA	IB	IIC	IID	Units
Girder Dimensions					
total original girder length, g.*l.* =	132.75	132.75	132.75	132.75	ft.
hold down point from end, *h.d.* =	53.1	53.9	51.5	55.0	ft.
depth of composite section, h =	55.0	55.0	55.0	55.0	in.
width of deck, b_d =	48.0	48.0	48.0	48.0	in.
width of composite interface, b_f =	30.0	30.0	30.0	30.0	in.
width of web, b_w, b_v =	6.0	6.0	6.0	6.0	in.
Concrete Material Properties					
girder compressive strength, f_c' =	11330	11330	9315	9315	psi
deck compressive strength, f_{cd}' =	5659	5659	5659	5659	psi
girder modulus of elasticity, E_c =	4810	4810	4800	4800	ksi
deck modulus of elasticity, E_{cd} =	3990	3990	3990	3990	ksi
Stirrups					
stirrup yield strength, f_y =	75.0	72.7	72.7	72.7	ksi
bursting stirrup yield strength, f_{yb} =	75.0	72.7	72.7	72.7	ksi
stirrup area, A_v =	0.40	0.40	0.40	0.40	$in.^2$
bursting stirrup area, A_{vb} =	0.88	0.88	0.88	0.88	$in.^2$
stirrup spacing, s =	16.0	16.0	16.0	16.0	in.
bursting stirrup spacing, s_b =	3.0	3.0	3.0	3.0	in.
Support & Load Dimensions					
width of support, *w.s.* =	0	0	0	0	in.
left end to center of support, a =	0.641	0.625	0.599	0.698	ft.
length between supports, l =	39.81	39.73	40.10	39.60	ft.
right end to center of support, b =	2.55	2.65	2.30	2.70	ft.
total specimen length, *s.l.* =	43.00	43.00	43.00	43.00	ft.
applied point load from end, A_1 =	14.05	13.80	14.05	14.00	ft.
Distributed Loads					
girder dead load, w_{gird} =	710	710	716	716	plf
deck dead load, w_{deck} =	479	479	479	479	plf
distributed dead load, w_{dl} =	0	0	0	0	plf
distributed live load, w_{ll} =	0	0	0	0	plf
Gross Cross Section Properties					
girder centroid from bottom, y_t =	22.38	22.38	22.38	22.38	in.
composite centroid from bottom, y_{tc} =	32.97	32.97	32.98	32.98	in.
girder area, A_g =	623	623	623	623	$in.^2$
composite area, A_{gc} =	1006.2	1006.2	1007.0	1007.0	$in.^2$
girder moment of interia, I_g =	166563	166563	166563	166563	$in.^4$
composite moment of interia, I_{gc} =	352880	352880	353122	353122	$in.^4$

Table C.3 Nominal Prestressing Details

Nominal	IA	IB	IIC	IID	Units
Prestressing Properties					
ultimate strength of strand, f_{pu} =	270	270	270	270	ksi
diameter of strand, d_b =	0.600	0.600	0.600	0.600	in.
area of prestressing strand, A_p =	0.215	0.215	0.215	0.215	$in.^2$
initial prestressing stress, f_{si} =	202.5	202.5	202.5	202.5	ksi
total prestressing losses, $p.l.$ =	35.8	35.8	35.8	35.8	%
prestressing stress after losses, f_{se} =	130.0	130.0	130.0	130.0	ksi
prestressing modulus of elasticity, E_p =	28500	28500	28500	28500	ksi
transfer length of strand, l_t =	3.00	3.00	3.00	3.00	ft.
development length of strand, l_d =	8.07	8.07	8.07	8.07	ft.
Debonding					
first debonding length, l_1 =	0	0	0	0	ft.
centroid of straight, y_{n1} =	5.294	5.294	5.294	4.118	in.
straight quantity, q_{n1} =	34	34	34	34	strands
second debonding length, l_2 =	2.0	2.0	2.0	2.0	ft.
centroid of straight, y_{n2} =	2.0	2.0	2.0	0	in.
straight quantity, q_{n2} =	2	2	2	0	strands
third debonding length, l_3 =	4.0	4.0	4.0	4.0	ft.
centroid of straight, y_{n3} =	2.0	2.0	2.0	0	in.
straight quantity, q_{n3} =	2	2	2	0	strands
fourth debonding length, l_4 =	12.0	12.0	12.0	12.0	ft.
centroid of straight, y_{n4} =	2.0	2.0	2.0	0	in.
straight quantity, q_{n4} =	2	2	2	0	strands
fifth debonding length, l_5 =	20.0	20.0	20.0	20.0	ft.
centroid of straight, y_{n5} =	2.0	2.0	2.0	0	in.
straight quantity, q_{n5} =	2	2	2	0	strands
Draping					
end centroid of draped, y_{d1} =	33.0	33.0	33.0	33.0	in.
mid-span centroid of draped, y_{d1} =	13.0	13.0	13.0	9.0	in.
draped quantity, q_{d1} =	4	4	4	12	strands

Table C.4 Measured Prestressing Details

Measured	IA	IB	IIC	IID	Units
Prestressing Properties					
ultimate strength of strand, f_{pu} =	269	269	269	269	ksi
diameter of strand, d_b =	0.614	0.614	0.614	0.614	in.
area of prestressing strand, A_p =	0.228	0.228	0.228	0.228	in.^{2}
initial prestressing stress, f_{si} =	191.6	191.6	191.6	191.6	ksi
total prestressing losses, $p.l.$ =	35.8	35.8	35.8	35.8	%
prestressing stress after losses, f_{se} =	123.0	123.0	123.0	123.0	ksi
prestressing modulus of elasticity, E_p =	28800	28800	28800	28800	ksi
transfer length of strand, l_t =	3.07	3.07	3.07	3.07	ft.
development length of strand, l_d =	8.62	8.62	8.59	8.59	ft.
Debonding					
first debonding length, l_1 =	0	0	0	0	ft.
centroid of straight, y_{n1} =	5.294	5.294	5.294	4.118	in.
straight quantity, q_{n1} =	34	34	34	34	strands
second debonding length, l_2 =	2.0	2.0	2.0	2.0	ft.
centroid of straight, y_{n2} =	2.0	2.0	2.0	0	in.
straight quantity, q_{n2} =	2	2	2	0	strands
third debonding length, l_3 =	4.0	4.0	4.0	4.0	ft.
centroid of straight, y_{n3} =	2.0	2.0	2.0	0	in.
straight quantity, q_{n3} =	2	2	2	0	strands
fourth debonding length, l_4 =	12.0	12.0	12.0	12.0	ft.
centroid of straight, y_{n4} =	2.0	2.0	2.0	0	in.
straight quantity, q_{n4} =	2	2	2	0	strands
fifth debonding length, l_5 =	20.0	20.0	20.0	20.0	ft.
centroid of straight, y_{n5} =	2.0	2.0	2.0	0	in.
straight quantity, q_{n5} =	2	2	2	0	strands
Draping					
end centroid of draped, y_{d1} =	33.0	33.0	33.0	33.0	in.
mid-span centroid of draped, y_{d1} =	13.0	13.0	13.0	9.0	in.
draped quantity, q_{d1} =	4	4	4	12	strands

Appendix D Assumptions in Models

Table D.1 Model Assumptions using Nominal Properties

Nominal	IA	IB	IIC	IID	Units
Factors					
shear strength reduction factor, ϕ =	1	1	1	1	unitless
dead load factor, *d.f.* =	1	1	1	1	unitless
live load factor, *l.f.* =	1	1	1	1	unitless
Mid-Span of Original Girder Calculations					
depth of result. compression force, d_c =	6.883	6.883	6.883	6.883	in.
depth of prestressing strands, d_p =	49.609	49.609	49.609	49.609	in.
area of prestressing strands, A_{ps} =	9.890	9.890	9.890	9.890	$in.^2$
stress in prestressing reinforcement, f_{ps} =	248.1	248.1	248.1	248.1	ksi
Modified ACI 318-95 Procedure					
distance from bottom, y_m =	35.5	35.5	35.5	35.5	in.
width of interface, b_m =	6.0	6.0	6.0	6.0	in.
gross composite moment of area, Q_{gc} =	8047.1	8047.1	8047.1	8047.1	$in.^3$
Modified Truss Model					
crack angle, θ_{mtm} =	25	25	25	25	degrees
Modified Compression Field Theory (AASHTO LRFD 1994)					
mimimum stirrups provided?	yes	yes	yes	yes	
initial angle assumption, θ_1 =	30	30	30	30	degrees
tensile long. mild reinforcement, A_s =	0	0	0	0	$in.^2$
factored axial force, N_u =	0	0	0	0	kips
Truss Model					
flexural level arm, d_v =	42.39	42.39	42.39	42.39	in.
minimum crack angle, θ_{tm} =	30	30	30	30	degrees
Horizontal Shear Design (AASHTO 1989)					
minimum ties provided?	yes	yes	yes	yes	
intentionally roughened?	yes	yes	yes	yes	
Interface Shear Model					
cohesion factor, c_f =	0.15	0.15	0.15	0.15	ksi
coefficient of friction, μ =	1.0	1.0	1.0	1.0	unitless
permanent compressive force, P_c =	0	0	0	0	kips
crack angle near applied load, θ_{ism} =	30	30	30	30	degrees
area of ties across interface, A_{vf} =	6.32	6.32	6.32	6.32	$in.^2$
yield strength stirrups, F_{s8}, F_{s9} =	24.0	24.0	24.0	24.0	kips
moment arm for eighth stirrup, g_8 =	27.8	27.8	27.8	27.8	in.
moment arm for ninth stirrup, g_9 =	11.8	11.8	11.8	11.8	in.
vert. reference for moment, j_A =	35.5	35.5	35.5	35.5	in.

Table D.2 Model Assumptions using Measured Properties

Measured	IA	IB	IIC	IID	Units
Factors					
shear strength reduction factor, ϕ =	1	1	1	1	unitless
dead load factor, *d.f.* =	1	1	1	1	unitless
live load factor, *l.f.* =	1	1	1	1	unitless
Mid-Span of Original Girder Calculations					
depth of result. compression force, d_c =	5.731	5.731	5.739	5.739	in.
depth of prestressing strands, d_p =	49.609	49.609	49.609	49.609	in.
area of prestressing strands, A_{ps} =	10.448	10.448	10.448	10.488	$in.^2$
stress in prestressing reinforcement, f_{ps} =	250.5	250.5	249.9	249.9	ksi
Modified ACI 318-95 Procedure					
distance from bottom, y_m =	35.5	35.5	35.5	35.5	in.
width of interface, b_m =	6.0	6.0	6.0	6.0	in.
gross composite moment of area, Q_{gc} =	8441.4	8441.4	8446.8	8446.8	$in.^3$
Modified Truss Model					
crack angle, θ_{mtm} =	25	25	25	25	degrees
Modified Compression Field Theory (AASHTO LRFD 1994)					
mimimum stirrups provided?	yes	yes	yes	yes	
initial angle assumption, θ_1 =	30	30	30	30	degrees
tensile long. mild reinforcement, A_s =	0	0	0	0	$in.^2$
factored axial force, N_u =	0	0	0	0	kips
Truss Model					
flexural level arm, d_v =	44.06	44.06	44.06	44.06	in.
minimum crack angle, θ_{tm} =	30	30	30	30	degrees
Horizontal Shear Design (AASHTO 1989)					
minimum ties provided?	yes	yes	yes	yes	
intentionally roughened?	yes	yes	yes	yes	
Interface Shear Model					
cohesion factor, c_f =	0.15	0.15	0.15	0.15	ksi
coefficient of friction, μ =	1.0	1.0	1.4	1.4	unitless
permanent compressive force, P_c =	0	0	0	0	kips
crack angle near applied load, θ_{ism} =	30	30	30	30	degrees
area of ties across interface, A_{vf} =	6.32	6.32	6.32	6.32	$in.^2$
yield strength stirrups, F_{s8}, F_{s9} =	30.0	29.1	29.1	29.1	kips
moment arm for eighth stirrup, g_8 =	29.6	26.6	29.6	29.0	in.
moment arm for ninth stirrup, g_9 =	13.6	10.6	13.6	13.0	in.
vert. reference for moment, j_A =	35.5	35.5	35.5	35.5	in.

Appendix E Sample Calculations

Shear capacity of End IA was calculated at the critical section as defined in ACI (at x = 2.93 ft. from the west end) for an applied load of P_1 = 503 kips at A_1 = 14.05 ft. from the west end. Measured properties were used. The measured specimen properties for End IA are given in Appendix C, and the model assumptions are given in Appendix D.

The critical section for Modified Compression Field Theory is at x = 4.36 ft. from the west end; however; for illustrative purposes all sample calculations were taken at x = 2.93 ft. with an applied load of P_1 = 503 kips at A_1 = 14.05 ft. from the west end.

E.1 Forces from Ultimate Flexural Capacity at Midspan of Original Girder

This section calculates the depth of resultant compressive force and maximum tensile stress in prestressing strand. These two values were necessary for Modified Compression Field Theory presented in Appendix E.12.

Compressive force in deck

$$C_d = 0.85\left(\frac{f_{cd}'}{1000}\right)b_d h_d = 0.85\left(\frac{5659}{1000}\right)(48.0)(9.0) = 2078\,\text{kips}$$

Compressive force in deck haunch

$$C_h = 0.85\left(\frac{f_{cd}'}{1000}\right)b_f h_h = 0.85\left(\frac{5659}{1000}\right)(30.0)(1.0) = 144.3\,\text{kips}$$

Modified Eqn. 5.7.3.1.1-3 from AASHTO LRFD 1994

$$c = \frac{A_{ps}f_{pu} - C_d - C_h}{0.85f_c'\beta_1 b_f + kA_{ps}\dfrac{f_{pu}}{d_p}\left(\dfrac{h_d + h_h + c}{c}\right)}$$

Solve for depth of neutral axis measured from top of girder

$$c = \frac{A_{ps} f_{pu} - C_d - C_h - kA_{ps}\frac{f_{pu}}{d_p}(h_d + h_h)}{0.85 f_c' \beta_1 b_f + kA_{ps}\frac{f_{pu}}{d_p}}$$

$$c = \frac{10.488(269) - 2078.0 - 144.3 - 0.28(10.488)\left(\frac{269}{49.609}\right)(9.0 + 1.0)}{0.85\left(\frac{11330}{1000}\right)(0.65)(30.0) + 0.28(10.488)\left(\frac{269}{49.609}\right)} = 2.159 \text{ in.}$$

Maximum tensile stress in prestressing strands

$$f_{ps} = f_{pu}\left(1 - k\frac{h_d + h_h + c}{d_p}\right) = 269\left(1 - 0.28\left(\frac{9.0 + 1.0 + 2.159}{49.609}\right)\right) = 250.5 \text{ ksi}$$

Compressive force in girder flange

$$C_f = 0.85\beta_1\left(\frac{f_c'}{1000}\right)b_f c = 0.85(0.65)\left(\frac{11330}{1000}\right)(30.0)(2.159) = 405.4 \text{ kips}$$

Depth of resultant compressive force

$$d_c = \frac{C_d\left(\frac{h_d}{2}\right) + C_h\left(h_d + \frac{h_h}{2}\right) + C_f\left(h_d + h_h + \frac{\beta_1 c}{2}\right)}{C_d + C_h + C_f}$$

$$d_c = \frac{2078.0\left(\frac{9.0}{2}\right) + 144.3\left(9.0 + \frac{1.0}{2}\right) + 405.4\left(9.0 + 1.0 + \frac{0.65(2.159)}{2}\right)}{2078.0 + 144.3 + 405.4} = 5.731 \text{ in.}$$

E.2 Critical Sections from West End

The shear capacities given in Chapter 6 were calculated at the critical section for all methods for both nominal and measured properties.

Critical section for ACI Simplified Method, ACI Detailed Method, Modified ACI Procedure, Modified Truss Model, and Horizontal Shear AASHTO 1989

$$cs_1 = a + \frac{w.s.}{2(12)} + \frac{h}{2(12)} = 0.641 + \frac{0}{2(12)} + \frac{55}{2(12)} = 2.93\,\text{ft.}$$

Modified Compression Field Theory uses d_v which was taken at midspan of original girder

$$d_v = \max\left(0.72h\ ,\ \ d_p - d_c,\ \ 0.9d_p\right)$$

$$d_v = \max\left(0.72(55.0),\ \ 49.609 - 5.731,\ \ 0.9(49.609)\right) = 44.648\ \text{in.}$$

Critical section for Modified Compression Field Theory

$$cs_2 = a + \frac{w.s.}{2(12)} + \frac{d_v}{12} = 0.641 + \frac{0}{2(12)} + \frac{44.648}{12} = 4.36\,\text{ft.}$$

E.3 Shear Equations

Distributed dead loads were the girder and deck self weight

$$w_{dead} = \frac{1}{1000}\left(w_{gird} + w_{deck}\right) = \frac{1}{1000}(710 + 479) = 1.189\,\text{klf}$$

Shear calculation for distributed load for simply-supported beam with two overhangs

$$V_d = \begin{cases} -w_{dead}(x), & \text{IF}\ \ x < a \\ w_{dead}\left(\dfrac{l}{2} + a + \dfrac{a^2}{2l} - \dfrac{b^2}{2l} - x\right), & \text{IF}\ \ x < a+l \\ w_{dead}(a + l + b - x), & \text{IF}\ \ x \geq a+l \end{cases}$$

$$V_d = \begin{cases} -1.189(2.93), & \text{IF } 2.93 < 0.641 \\ 1.189\left(\frac{39.81}{2} + 0.641 + \frac{0.641^2}{2(39.81)} - \frac{2.55^2}{2(39.81)} - 2.93\right), & \text{IF } 2.93 < 0.641 + 39.81 \\ 1.189(0.641 + 39.81 + 2.55 - 2.93), & \text{IF } 2.93 \geq 0.641 + 39.81 \end{cases}$$

$V_d = 20.85$ kips

Shear calculation for a point load between the two supports

$$V_{pt} = \begin{cases} 0, & \text{IF } x < a \\ \frac{P_1(l - (A_1 - a))}{l}, & \text{IF } x < A_1 \\ -\frac{P_1(A_1 - a)}{l}, & \text{IF } x < a + l \\ 0, & \text{IF } x \geq a + l \end{cases}$$

$$V_{pt} = \begin{cases} 0, & \text{IF } 2.93 < 0.641 \\ \frac{503(39.81 - (14.05 - 0.641))}{39.81}, & \text{IF } 2.93 < 14.05 \\ -\frac{503(14.05 - 0.641)}{39.81}, & \text{IF } 2.93 < 0.641 + 39.81 \\ 0, & \text{IF } 2.93 \geq 0.641 + 39.81 \end{cases}$$

$V_{pt} = 333.58$ kips

Total shear is a sum of shear due to dead load and point load

$$V_u = d.f.(V_d) + l.f.(V_{pt}) = 1(20.85) + 1(333.58) = 354.43 \text{ kips}$$

E.4 Moment Equations

Moment calculation for distributed load for simply supported beam with two overhangs

$$M_{gird} = \begin{cases} -\left(\frac{w_{gird}}{1000}\right)\frac{x^2}{2}, & \text{IF } x < a \\ \left(\frac{w_{gird}}{1000}\right)\left((x-a)\left(\frac{l}{2}+\frac{a^2}{2l}-\frac{b^2}{2l}-\frac{x-a}{2}\right)-\frac{a^2}{2}\right), & \text{IF } x < a+l \\ -\frac{1}{2}\left(\frac{w_{gird}}{1000}\right)(a+l+b-x)^2, & \text{IF } x \geq a+l \end{cases}$$

$$M_{gird} = \begin{cases} -\left(\frac{710}{1000}\right)\frac{2.93^2}{2}, & \text{IF } 2.93 < 0.641 \\ \left(\frac{710}{1000}\right)\left((2.93-0.641)\left(\frac{39.81}{2}+\frac{0.641^2}{2(39.81)}-\frac{2.55^2}{2(39.81)}-\frac{2.93-0.641}{2}\right)-\frac{0.641^2}{2}\right), & \text{IF } 2.93 < 0.641+39.81 \\ -\frac{1}{2}\left(\frac{710}{1000}\right)(0.641+39.81+2.55-2.93)^2, & \text{IF } 2.93 \geq 0.641+39.81 \end{cases}$$

$M_{gird} = 30.22$ ft.-kips $= 362.6$ in.-kips

Moment calculation for distributed load for simply supported with two overhangs

$$M_{deck} = \begin{cases} -\left(\frac{w_{deck}}{1000}\right)\frac{x^2}{2}, & \text{IF } x < a \\ \left(\frac{w_{deck}}{1000}\right)\left((x-a)\left(\frac{l}{2}+\frac{a^2}{2l}-\frac{b^2}{2l}-\frac{x-a}{2}\right)-\frac{a^2}{2}\right), & \text{IF } x < a+l \\ -\frac{1}{2}\left(\frac{w_{deck}}{1000}\right)(a+l+b-x)^2, & \text{IF } x \geq a+l \end{cases}$$

$$M_{deck} = \begin{cases} -\left(\frac{479}{1000}\right)\frac{2.93^2}{2}, & \text{IF } 2.93 < 0.641 \\ \left(\frac{479}{1000}\right)\left((2.93-0.641)\left(\frac{39.81}{2}+\frac{0.641^2}{2(39.81)}-\frac{2.55^2}{2(39.81)}-\frac{2.93-0.641}{2}\right)-\frac{0.641^2}{2}\right), & \text{IF } 2.93 < 0.641+39.81 \\ -\frac{1}{2}\left(\frac{479}{1000}\right)(0.641+39.81+2.55-2.93)^2, & \text{IF } 2.93 \geq 0.641+39.81 \end{cases}$$

$M_{deck} = 20.39$ ft.-kips $= 244.7$ in.-kips

Moment calculation for a point load between the supports

$$M_{pt} = \begin{cases} 0, & \text{IF } x < a \\ \dfrac{P_1\left(l-\left(A_1-a\right)\right)}{l}\left(x-a\right), & \text{IF } x < A_1 \\ -\dfrac{P_1\left(A_1-a\right)}{l}\left(x-a\right)-P_1\left(x-A_1\right), & \text{IF } x < a+l \\ 0, & \text{IF } x \geq a+l \end{cases}$$

$$M_{pt} = \begin{cases} 0, & \text{IF } 2.93 < 0.641 \\ \dfrac{503\left(39.81-\left(14.05-0.641\right)\right)}{39.81}\left(2.93-0.641\right), & \text{IF } 2.93 < 14.05 \\ -\dfrac{503\left(14.05-0.641\right)}{39.81}\left(2.93-0.641\right)-503\left(2.93-14.05\right), & \text{IF } 2.93 < 14.05+39.81 \\ 0, & \text{IF } 2.93 \geq 14.05+39.81 \end{cases}$$

$M_{pt} = 763.56$ ft.-kips $= 9162.7$ in.-kips

Total moment is a sum of shear due to girder, deck and point load

$$M_u = d.f.\left(M_{gird}\right)+d.f.\left(M_{deck}\right)+l.f.\left(M_{pt}\right)$$

$$M_u = 1(362.6)+1(244.7)+1(9162.7) = 9770 \text{ in.-kips}$$

E.5 Transfer Equations

It was assumed that the effective quantity of strands varied from zero at the end of the specimen or at the end of debonding to the total number of strands at the end of the transfer length. The critical section for shear was within the transfer length of many of the strands and required calculation of effective strand quantities.

Transfer length of a strand

$$l_t = 60d_b = 60(0.614) = 36.8\,\text{in} = 3.07\,\text{ft.}$$

Effective quantity of draped strands at given section

$$q_{td} = \begin{cases} 0, & \text{IF } x < 0 \\ q_{d1}\left(\dfrac{x}{l_t}\right), & \text{IF } x < l_t \\ 4, & \text{IF } x \geq l_t \end{cases}$$

$$q_{td} = \begin{cases} 0, & \text{IF } 2.93 < 0 \\ 4\left(\frac{2.93}{3.07}\right), & \text{IF } 2.93 < 3.07 \\ 4, & \text{IF } 2.93 \geq 3.07 \end{cases}$$

$$q_{td} = 3.818$$

Distance from centroid of draped prestressed reinforcement measured from the extreme tension fiber

$$y_d = y_{d1} - (y_{d1} - y_{d2})\left(\frac{x}{h.d.}\right) = 33.0 - (33.0 - 13.0)\left(\frac{2.93}{53.1}\right) = 31.90\,\text{in.}$$

Effective quantity of straight strand with no debonding at given section

$$q_{tn1} = \begin{cases} 0, & \text{IF } x < l_1 \\ q_{n1}\left(\frac{x - l_1}{l_t}\right), & \text{IF } x < l_1 + l_t \\ q_{n1}, & \text{IF } x \geq l_1 + l_t \end{cases}$$

$$q_{tn1} = \begin{cases} 0, & \text{IF } 2.93 < 0 \\ 34\left(\frac{2.93 - 0}{3.07}\right), & \text{IF } 2.93 < 0 + 3.07 \\ 34, & \text{IF } 2.93 \geq 0 + 3.07 \end{cases}$$

$$q_{tn1} = 32.450$$

Effective quantity of straight strand debonded for 2 ft. at given section

$$q_{tn2} = \begin{cases} 0, & \text{IF } x < l_2 \\ q_{n2}\left(\frac{x - l_2}{l_t}\right), & \text{IF } x < l_2 + l_t \\ q_{n2}, & \text{IF } x \geq l_2 + l_t \end{cases}$$

$$q_{tn2} = \begin{cases} 0, & \text{IF } 2.93 < 2.0 \\ 2\left(\frac{2.93 - 2.0}{3.07}\right), & \text{IF } 2.93 < 2.0 + 3.07 \\ 2, & \text{IF } 2.93 \geq 2.0 + 3.07 \end{cases}$$

$$q_{tn2} = 0.606$$

Effective quantity of straight strand debonded for 4 ft. at given section

$$q_{tn3} = \begin{cases} 0, & \text{IF } x < l_3 \\ q_{n3}\left(\dfrac{x - l_3}{l_t}\right), & \text{IF } x < l_3 + l_t \\ q_{n3}, & \text{IF } x \geq l_3 + l_t \end{cases}$$

$$q_{tn3} = \begin{cases} 0, & \text{IF } 2.93 < 4.0 \\ 2\left(\dfrac{2.93 - 4.0}{3.07}\right), & \text{IF } 2.93 < 4.0 + 3.07 \\ 2, & \text{IF } 2.93 \geq 4.0 + 3.07 \end{cases}$$

$$q_{tn3} = 0$$

Effective quantity of straight strand debonded for 12 ft. at given section

$$q_{tn4} = \begin{cases} 0, & \text{IF } x < l_4 \\ q_{n4}\left(\dfrac{x - l_4}{l_t}\right), & \text{IF } x < l_4 + l_t \\ q_{n4}, & \text{IF } x \geq l_4 + l_t \end{cases}$$

$$q_{tn4} = \begin{cases} 0, & \text{IF } 2.93 < 12.0 \\ 2\left(\dfrac{2.93 - 12.0}{3.07}\right), & \text{IF } 2.93 < 12.0 + 3.07 \\ 2, & \text{IF } 2.93 \geq 12.0 + 3.07 \end{cases}$$

$$q_{tn4} = 0$$

Effective quantity of straight strand debonded for 20 ft. at given section

$$q_{tn5} = \begin{cases} 0, & \text{IF } x < l_5 \\ q_{n5}\left(\dfrac{x - l_5}{l_t}\right), & \text{IF } x < l_5 + l_t \\ q_{n5}, & \text{IF } x \geq l_5 + l_t \end{cases}$$

$$q_{tn5} = \begin{cases} 0, & \text{IF } 2.93 < 20.0 \\ 2\left(\dfrac{2.93-20.0}{3.07}\right), & \text{IF } 2.93 < 20.0+3.07 \\ 2, & \text{IF } 2.93 \geq 20.0+3.07 \end{cases}$$

$$q_{tn5} = 0$$

Total effective quantity of straight strands reduced due to transfer at given section

$$q_{tn} = q_{tn1} + q_{tn2} + q_{tn3} + q_{tn4} + q_{tn5} = 32.450 + 0.606 + 0 + 0 + 0 = 33.055$$

Distance from centroid of straight prestressed reinforcement measured from the extreme tension fiber

$$y_n = \frac{q_{tn1}y_{n1} + q_{tn2}y_{n2} + q_{tn3}y_{n3} + q_{tn4}y_{n4} + q_{tn5}y_{n5}}{q_{tn}}$$

$$y_n = \frac{32.4827(5.294) + 0.6078(2) + 0(2) + 0(2) + 0(2)}{33.0906} = 5.234 \text{ in.}$$

Effective area of prestressed reinforcement reduced due to transfer

$$A_{pst} = (q_{td} + q_{tn})A_p = (3.818 + 33.055)0.228 = 8.407 \text{ in.}^2$$

Eccentricity from the center of gravity of the gross girder cross section to the centroid of the prestressing strands

$$e = y_t - \frac{q_{td}y_d + q_{tn}y_n}{q_{td} + q_{tn}} = 22.38 - \frac{3.818(31.90) + 33.055(5.234)}{3.818 + 33.055} = 14.386 \text{ in.}$$

Distance from the extreme compression fiber to the centroid of the prestressed reinforcement

$$d_p = h - \frac{q_{td}y_d + q_{tn}y_n}{q_{td} + q_{tn}} = 55.0 - \frac{3.818(31.90) + 33.055(5.234)}{3.818 + 33.055} = 47.006 \text{ in.}$$

Limitation for d_p

$$d = \max\left(d_p,\quad 0.8h\right) = \max\left(47.006,\quad 0.8(55.0)\right) = 47.006 \text{ in.}$$

E.6 Development Equations

It was assumed that the effective quantity of strands varied from zero at the end of the specimen or at the end of debonding to the total number of strands at the end of the development length according to a bilinear relation. The given section was within the development length of many of the strands and required calculation of effective strand quantities. This section was only necessary for Modified Compression Field Theory presented in Appendix E.12.

Development length of a strand

$$l_d = \left(f_{ps} - \frac{2}{3}f_{se}\right)d_b = \left(250.5 - \frac{2}{3}(123.0)\right)(0.614) = 103.4 \text{ in.} = 8.62 \text{ ft.}$$

Effective quantity of draped strands at given section

$$q_{dd} = \begin{cases} 0, & \text{IF } x < 0 \\ q_{d1}\left(\dfrac{f_{se}}{f_{ps}}\right)\left(\dfrac{x}{l_t}\right), & \text{IF } x < l_t \\ q_{d1}\left(\dfrac{f_{se}}{f_{ps}} + \dfrac{\left(\dfrac{f_{ps} - f_{se}}{f_{ps}}\right)(x - l_t)}{l_d - l_t}\right), & \text{IF } x < l_d \\ q_{d1}, & \text{IF } x \geq l_d \end{cases}$$

$$q_{dd} = \begin{cases} 0, & \text{IF } 2.93 < 0 \\ 4\left(\frac{123.0}{250.5}\right)\left(\frac{2.93}{3.07}\right) & \text{IF } 2.93 < 3.07 \\ 4\left(\frac{123}{250.5} + \frac{\left(\frac{250.5-123.0}{250.5}\right)(2.93-3.07)}{8.62-3.07}\right) & \text{IF } 2.93 < 8.62 \\ 4, & \text{IF } 2.93 \geq 8.62 \end{cases}$$

$q_{dd} = 1.875$

Effective quantity of straight strand with no debonding at given section

$$q_{dn1} = \begin{cases} 0, & \text{IF } x < l_1 \\ q_{n1}\left(\frac{f_{se}}{f_{ps}}\right)\left(\frac{x - l_1}{l_t}\right), & \text{IF } x < l_1 + l_t \\ q_{n1}\left(\frac{f_{se}}{f_{ps}} + \frac{\left(\frac{f_{ps}-f_{se}}{f_{ps}}\right)(x - l_1 - l_t)}{l_d - l_t}\right), & \text{IF } x < l_1 + l_d \\ q_{n1}, & \text{IF } x \geq l_1 + l_d \end{cases}$$

$$q_{dn1} = \begin{cases} 0, & \text{IF } 2.93 < 0 \\ 34\left(\frac{123.0}{250.5}\right)\left(\frac{2.93-0}{3.07}\right), & \text{IF } 2.93 < 0+3.07 \\ 34\left(\frac{123.0}{250.5} + \frac{\left(\frac{250.5-123.0}{250.5}\right)(2.93-0-3.07)}{8.62-3.07}\right), & \text{IF } 2.93 < 0+8.62 \\ 34, & \text{IF } 2.93 \geq 0+8.62 \end{cases}$$

$q_{dn1} = 15.933$

Effective quantity of straight strand debonded for 2 ft. at given section

$$q_{dn2} = \begin{cases} 0, & \text{IF } x < l_2 \\ q_{n2}\left(\frac{f_{se}}{f_{ps}}\right)\left(\frac{x - l_2}{l_t}\right), & \text{IF } x < l_2 + l_t \\ q_{n2}\left(\frac{f_{se}}{f_{ps}} + \frac{\left(\frac{f_{ps} - f_{se}}{f_{ps}}\right)(x - l_2 - l_t)}{l_d - l_t}\right), & \text{IF } x < l_2 + l_d \\ q_{n2}, & \text{IF } x \geq l_2 + l_d \end{cases}$$

$$q_{dn2} = \begin{cases} 0, & \text{IF } 2.93 < 2.0 \\ 2\left(\frac{123.0}{250.5}\right)\left(\frac{2.93 - 2.0}{3.07}\right), & \text{IF } 2.93 < 2.0 + 3.07 \\ 2\left(\frac{123.0}{250.5} + \frac{\left(\frac{250.5 - 123.0}{250.5}\right)(2.93 - 2.0 - 3.07)}{8.62 - 3.07}\right), & \text{IF } 2.93 < 2.0 + 8.62 \\ 2, & \text{IF } 2.93 \geq 2.0 + 8.62 \end{cases}$$

$q_{dn2} = 0.298$

Effective quantity of straight strand debonded for 4 ft. at given section

$$q_{dn3} = \begin{cases} 0, & \text{IF } x < l_3 \\ q_{n3}\left(\frac{f_{se}}{f_{ps}}\right)\left(\frac{x - l_3}{l_t}\right), & \text{IF } x < l_3 + l_t \\ q_{n3}\left(\frac{f_{se}}{f_{ps}} + \frac{\left(\frac{f_{ps} - f_{se}}{f_{ps}}\right)(x - l_3 - l_t)}{l_d - l_t}\right), & \text{IF } x < l_3 + l_d \\ q_{n3}, & \text{IF } x \geq l_3 + l_d \end{cases}$$

$$q_{dn3} = \begin{cases} 0, & \text{IF } 2.93 < 4.0 \\ 2\left(\frac{123.0}{250.5}\right)\left(\frac{2.93-4.0}{3.07}\right), & \text{IF } 2.93 < 4.0+3.07 \\ 2\left(\frac{123.0}{250.5}+\frac{\left(\frac{250.5-123.0}{250.5}\right)(2.93-4.0-3.07)}{8.62-3.07}\right), & \text{IF } 2.93 < 4.0+8.62 \\ 2, & \text{IF } 2.93 \geq 4.0+8.62 \end{cases}$$

$$q_{dn3} = 0$$

Effective quantity of straight strand debonded for 12 ft. at given section

$$q_{dn4} = \begin{cases} 0, & \text{IF } x < l_4 \\ q_{n4}\left(\frac{f_{se}}{f_{ps}}\right)\left(\frac{x-l_4}{l_t}\right), & \text{IF } x < l_4+l_t \\ q_{n4}\left(\frac{f_{se}}{f_{ps}}+\frac{\left(\frac{f_{ps}-f_{se}}{f_{ps}}\right)(x-l_4-l_t)}{l_d-l_t}\right), & \text{IF } x < l_4+l_d \\ q_{n4}, & \text{IF } x \geq l_4+l_d \end{cases}$$

$$q_{dn4} = \begin{cases} 0, & \text{IF } 2.93 < 12.0 \\ 2\left(\frac{123.0}{250.5}\right)\left(\frac{2.93-12.0}{3.07}\right), & \text{IF } 2.93 < 12.0+3.07 \\ 2\left(\frac{123.0}{250.5}+\frac{\left(\frac{250.5-123.0}{250.5}\right)(2.93-12.0-3.07)}{8.62-3.07}\right), & \text{IF } 2.93 < 12.0+8.62 \\ 2, & \text{IF } 2.93 \geq 12.0+8.62 \end{cases}$$

$$q_{dn4} = 0$$

Effective quantity of straight strand debonded for 20 ft. at given section

$$q_{dn5} = \begin{cases} 0, & \text{IF } x < l_5 \\ q_{n5}\left(\frac{f_{se}}{f_{ps}}\right)\left(\frac{x - l_5}{l_t}\right), & \text{IF } x < l_5 + l_t \\ q_{n5}\left(\frac{f_{se}}{f_{ps}} + \frac{\left(\frac{f_{ps} - f_{se}}{f_{ps}}\right)(x - l_5 - l_t)}{l_d - l_t}\right), & \text{IF } x < l_5 + l_d \\ q_{n5}, & \text{IF } x \geq l_5 + l_d \end{cases}$$

$$q_{dn5} = \begin{cases} 0, & \text{IF } 2.93 < 20.0 \\ 2\left(\frac{123.0}{250.5}\right)\left(\frac{2.93 - 20.0}{3.07}\right), & \text{IF } 2.93 < 20.0 + 3.07 \\ 2\left(\frac{123.0}{250.5} + \frac{\left(\frac{250.5 - 123.0}{250.5}\right)(2.93 - 20.0 - 3.07)}{8.62 - 3.07}\right), & \text{IF } 2.93 < 20.0 + 8.62 \\ 2, & \text{IF } 2.93 \geq 20.0 + 8.62 \end{cases}$$

$$q_{dn5} = 0$$

Total effective quantity of strands reduced due to development at given section

$$q_{dn} = q_{dn1} + q_{dn2} + q_{dn3} + q_{dn4} + q_{dn5} = 15.933 + 0.298 + 0 + 0 + 0 = 16.231$$

Effective area of prestressed reinforcement reduced due to development

$$A_{psd} = (q_{dd} + q_{dn})A_p = (1.875 + 16.231)0.228 = 4.128\,\text{in.}^2$$

E.7 ACI 318-95 Simplified Method

The shear capacity for this method is based on the sum of a concrete contribution and a stirrup contribution. The concrete contribution given by ACI 318-95 Eqn. 11-10 must be

between the minimum and maximum concrete limits. The stirrup contribution given by ACI 318-95 Eqn. 11-17 must be less than the maximum stirrup limit.

Minimum concrete contribution

$$V_{c\,min} = 2\frac{\sqrt{f_c'}}{1000} b_w d = 2\frac{\sqrt{11330}}{1000}(6.0)(47.006) = 60.0 \text{ kips}$$

This term, a ratio of shear to moment, is necessary for the concrete contribution

$$\left(\frac{V_u d_p}{M_u}\right) = \min\left(\left|\frac{V_u d_p}{M_u}\right|,\ 1\right) = \min\left(\left|\frac{354.43(47.006)}{9770}\right|,\ 1\right) = 1$$

Concrete contribution given by ACI 318-95 Eqn. 11-10

$$V_{c\,Eq11\text{-}10} = \left(0.6\frac{\sqrt{f_c'}}{1000} + \frac{700}{1000}\left(\frac{V_u d_p}{M_u}\right)\right) b_w d$$

$$V_{c\,Eq11\text{-}10} = \left(0.6\frac{\sqrt{11330}}{1000} + \frac{700}{1000}(1)\right)(6.0)(47.006) = 215.4 \text{ kips}$$

Maximum concrete contribution

$$V_{c\,max} = 5\frac{\sqrt{f_c'}}{1000} b_w d = 5\frac{\sqrt{11330}}{1000}(6.0)(47.006) = 150.1 \text{ kips}$$

Actual concrete contribution

$$V_c = \begin{cases} V_{c\,min}, & \text{IF } V_{c\,Eq11\text{-}10} < V_{c\,min} \\ V_{c\,Eq11\text{-}10}, & \text{IF } V_{c\,Eq11\text{-}10} < V_{c\,max} \\ V_{c\,max}, & \text{IF } V_{c\,Eq11\text{-}10} \geq V_{c\,max} \end{cases}$$

$$V_c = \begin{cases} 60.04, & \text{IF } 215.4 < 60.04 \\ 215.4, & \text{IF } 215.4 < 150.1 \\ 150.1, & \text{IF } 215.4 \geq 150.1 \end{cases}$$

$V_c = 150.1$ kips

Stirrup contribution given by ACI 318-95 Eqn. 11-17

$$V_{s\,Eq11\text{-}17} = \frac{A_v f_y d}{s} = \frac{0.4(75.0)(47.006)}{16.0} = 88.1\,\text{kips}$$

Maximum stirrup contribution given below

$$V_{s\,max} = 8\frac{\sqrt{f_c'}}{1000} b_w d = 8\frac{\sqrt{11330}}{1000}(6.0)(47.006) = 240.2\,\text{kips}$$

Actual stirrup contribution

$$V_s = \min\left(V_{s\,Eq11\text{-}17},\ V_{s\,max}\right) = \min(88.1,\ 240.2) = 88.1\,\text{kips}$$

Shear capacity of ACI Simplified Method using measured properties

$$\phi V_n = \phi(V_c + V_s) = 1(150.1 + 88.1) = 238.2\,\text{kips}$$

E.8 ACI 318-95 Detailed Method

The shear capacity for this method is based on the sum of a concrete contribution and a stirrup contribution. The concrete contribution is the minimum of the capacity as determined by web-shear or flexure-shear cracking. The stirrup contribution given by ACI 318-95 Eqn. 11-17 must be less than the maximum stirrup limit.

Minimum flexure-shear contribution

$$V_{ci\,min} = 1.7\frac{\sqrt{f_c'}}{1000} b_w d = 1.7\frac{\sqrt{11330}}{1000}(6.0)(47.006) = 51.0\,\text{kips}$$

Horizontal prestressing force used for stress calculation

$$P = f_{se} A_{pst} = 123.0(8.407) = 1034.1\,\text{kips}$$

Compressive stress due to the effective prestressing force at the extreme fiber used for cracking moment calculation

$$f_{pe} = \frac{P}{A_g} + \frac{P y_t e}{I_g} = \frac{1034.1}{623} + \frac{1034.1(22.38)(14.386)}{166563} = 3.659\,\text{ksi}$$

Stress due to dead load at the extreme fiber of the given cross section used for cracking moment calculation

$$f_d = \frac{(M_{gird} + M_{deck})y_t}{I_g} = \frac{(362.6 + 244.7)22.38}{166563} = 0.082 \text{ ksi}$$

Moment causing flexural cracking at the given cross section used to calculate flexure-web cracking

$$M_{cr} = \frac{I_{gc}}{y_{tc}}\left(6\frac{\sqrt{f_c'}}{1000} + f_{pe} - f_d\right) = \frac{352880}{32.97}\left(6\frac{\sqrt{11330}}{1000} + 3.659 - 0.082\right) = 45120 \text{ in.-kips}$$

Ratio of shear to moment at the given cross section due to externally applied loads which is used to calculate flexure-shear cracking

$$\left(\frac{V_i}{M_{max}}\right) = \left|\frac{V_u - V_d}{M_u - M_{gird} - M_{deck}}\right| = \left|\frac{354.43 - 20.85}{9770 - 362.6 - 244.7}\right| = 0.0364 \text{ 1/in.}$$

Flexure-shear concrete contribution given by ACI 318-95 Eqn. 11-11

$$V_{ci\,Eq11\text{-}11} = 0.6\frac{\sqrt{f_c'}}{1000}b_w d + V_d + \left(\frac{V_i}{M_{max}}\right)M_{cr}$$

$$V_{ci\,Eq11\text{-}11} = 0.6\frac{\sqrt{11330}}{1000}(6.0)(47.006) + 20.85 + 0.0364(45120) = 1681.6 \text{ kips}$$

Actual flexure-shear concrete contribution

$$V_{ci} = \max\left(V_{ci\,min},\ V_{ci\,Eq11\text{-}11}\right) = \max(51.0,\ 1681.6) = 1681.6 \text{ kips}$$

Vertical component of effective prestressing force at the given cross section used to calculate web-shear cracking

$$V_p = \begin{cases} q_{td} A_p f_{se} \left(\dfrac{y_{d1} - y_{d2}}{12h.d.} \right), & \text{IF } x \leq h.d. \\ 0, & \text{IF } x > h.d. \end{cases}$$

$$V_p = \begin{cases} 3.818(0.228)(123.0) \left(\dfrac{33.0 - 13.0}{12(53.1)} \right), & \text{IF } 2.93 \leq 53.1 \\ 0, & \text{IF } 2.93 > 53.1 \end{cases}$$

$$V_p = 3.36 \text{ kips}$$

Compressive stress at the neutral axis due to effective prestressing force and due to applied flexural stresses

$$f_{pc} = \frac{P}{A_g} - \frac{P(y_{tc} - y_t)e}{I_g} + \frac{(M_{gird} + M_{deck})(y_{tc} - y_t)}{I_g}$$

$$f_{pc} = \frac{1034.1}{623} - \frac{1034.1(32.97 - 22.38)(14.386)}{166563} + \frac{(362.6 + 244.7)(32.97 - 22.38)}{166563}$$

$$f_{pc} = 0.753 \text{ ksi}$$

Web-shear concrete contribution given by ACI 318-95 Eqn. 11-13

$$V_{cw} = \left(3.5 \frac{\sqrt{f_c'}}{1000} + 0.3 f_{pc} \right) b_w d + V_p$$

$$V_{cw} = \left(3.5 \frac{\sqrt{11330}}{1000} + 0.3(0.753) \right) (6.0)(47.006) + 3.36 = 172.1 \text{ kips}$$

Actual concrete contribution is the lesser of web-shear and flexure-shear contributions

$$V_c = \min(V_{ci}, \ V_{cw}) = \min(1681.6, \ 172.1) = 172.1 \text{ kips}$$

Stirrup contribution given by ACI Eqn. 11-17

$$V_{s\,Eq11\text{-}17} = \frac{A_v f_y d}{s} = \frac{0.4(75.0)(47.006)}{16.0} = 88.1\,\text{kips}$$

Maximum stirrup contribution

$$V_{s\,max} = 8\frac{\sqrt{f_c'}}{1000} b_w d = 8\frac{\sqrt{11330}}{1000}(6.0)(47.006) = 240.2\,\text{kips}$$

Actual stirrup contribution

$$V_s = \min\left(V_{s\,Eq11\text{-}17},\ V_{s\,max}\right) = \min(88.1,\ 240.2) = 88.1\,\text{kips}$$

Shear capacity of ACI Detailed Method using measured properties

$$\phi V_n = \phi(V_c + V_s) = 1(172.1 + 88.1) = 260.2\,\text{kips}$$

E.9 Modified ACI 318-95 Procedure

The shear capacity for this method is based on the sum of a concrete contribution and a stirrup contribution. The concrete contribution is based on the modified web-shear cracking relationship which was derived in Appendix A.4. The stirrup contribution given by ACI 318-95 Eqn. 11-17 must be less than the maximum stirrup limit.

Horizontal prestressing force used for stress calculation

$$P = f_{se} A_{pst} = 123.0(8.407) = 1034.1\,\text{kips}$$

Vertical component of effective prestressing force at the given cross section used in modified web-shear cracking calculation

$$V_p = \begin{cases} q_{td} A_p f_{se}\left(\dfrac{y_{d1} - y_{d2}}{12h.d.}\right), & \text{IF } x \le h.d. \\ 0, & \text{IF } x > h.d. \end{cases}$$

$$V_p = \begin{cases} 3.818(0.228)(123.0)\left(\dfrac{33.0-13.0}{12(53.1)}\right), & \text{IF } 2.93 \le 53.1 \\ 0, & \text{IF } 2.93 > 53.1 \end{cases}$$

$V_p = 3.36$ kips

Compressive stress at the depth of interest due to effective prestressing force and due to applied flexural stresses, used in modified web-shear cracking calculation

$$f_{pd} = \frac{P}{A_g} - \frac{P(y_m - y_t)e}{I_g} + \frac{(M_{gird} + M_{deck})(y_m - y_t)}{I_g}$$

$$f_{pd} = \frac{1034.1}{623} - \frac{1034.1(35.5-22.38)(14.386)}{166563} + \frac{(362.6+244.7)(35.5-22.38)}{166563} = 0.536\,\text{ksi}$$

Modified web-shear concrete contribution

$$V_{mod} = \frac{I_{gc} b_m}{Q_{gc}} 3.5 \frac{\sqrt{f_c'}}{1000} \sqrt{1 + \frac{1000 f_{pd}}{3.5\sqrt{f_c'}}} + V_p$$

$$V_{mod} = \frac{352880(6.0)}{8441.4} 3.5 \frac{\sqrt{11330}}{1000} \sqrt{1 + \frac{1000(0.536)}{3.5\sqrt{11330}}} + 3.36 = 149.3\,\text{kips}$$

Stirrup contribution given by ACI 318-95 Eqn. 11-17

$$V_{s\,Eq11\text{-}17} = \frac{A_v f_y d}{s} = \frac{0.4(75.0)(47.006)}{16.0} = 88.1\,\text{kips}$$

Maximum stirrup contribution

$$V_{s\,max} = 8\frac{\sqrt{f_c'}}{1000} b_w d = 8\frac{\sqrt{11330}}{1000}(6.0)(47.006) = 240.2\,\text{kips}$$

Actual stirrup contribution

$$V_s = \min\left(V_{s\,Eq11\text{-}17},\ V_{s\,max}\right) = \min(88.1,\ 240.2) = 88.1\,\text{kips}$$

Shear capacity of Modified ACI Procedure using measured properties

$$\phi V_n = \phi(V_{mod} + V_s) = 1(149.3 + 88.1) = 237.4 \text{ kips}$$

E.10 Modified Truss Model

The shear capacity for this method is based on the sum of a concrete contribution, a stirrup contribution, and a draping contribution. The shear capacity must be less than the maximum shear capacity limit.

Effective truss depth used in concrete and stirrup contribution calculations

$$z = 0.9d = 0.9(47.006) = 42.305 \text{ in.}$$

Horizontal prestressing force used for stress calculation

$$P = f_{se} A_{pst} = 123.0(8.407) = 1034.1 \text{ kips}$$

Compressive stress at the neutral axis due to effective prestressing force and due to applied flexural stresses

$$f_{pc} = \frac{P}{A_g} - \frac{P(y_{tc} - y_t)e}{I_g} + \frac{(M_{gird} + M_{deck})(y_{tc} - y_t)}{I_g}$$

$$f_{pc} = \frac{1034.1}{623} - \frac{1034.1(32.97 - 22.38)(14.386)}{166563} + \frac{(362.6 + 244.7)(32.97 - 22.38)}{166563}$$

$$f_{pc} = 0.753 \text{ ksi}$$

Maximum tensile stress, used in concrete contribution calculation

$$f_t = 2\frac{\sqrt{f_c'}}{1000} = 2\frac{\sqrt{11330}}{1000} = 0.213 \text{ ksi}$$

Effect of the prestressing force on the shear cracking load

$$K = \sqrt{1 + \frac{f_{pc}}{f_t}} = \sqrt{1 + \frac{0.753}{0.213}} = 2.13$$

Concrete contribution

$$V_{cr} = Kf_t b_w z = 2.13(0.213)(6.0)(42.305) = 115.08 \text{ kips}$$

Stirrup contribution

$$V_{truss} = \frac{A_v f_y z}{s}\cot(\theta_{mtm}) = \frac{0.4(75.0)(42.305)}{16.0}\cot(25^\circ) = 170.11 \text{ kips}$$

Vertical component of effective prestressing force at the given cross section

$$V_p = \begin{cases} q_{td} A_p f_{se}\left(\dfrac{y_{d1} - y_{d2}}{12h.d.}\right), & \text{IF } x \le h.d. \\ 0, & \text{IF } x > h.d. \end{cases}$$

$$V_p = \begin{cases} 3.818(0.228)(123.0)\left(\dfrac{33.0 - 13.0}{12(53.1)}\right), & \text{IF } 2.93 \le 53.1 \\ 0, & \text{IF } 2.93 > 53.1 \end{cases}$$

$$V_p = 3.36 \text{ kips}$$

Nominal shear capacity is the sum concrete, stirrup, and draping contributions

$$V_n = V_{cr} + V_{truss} + V_p = 115.08 + 170.11 + 3.36 = 288.6 \text{ kips}$$

Nominal shear capacity is the sum concrete, stirrup, and draping contributions

$$V_{n\,max} = 30\frac{\sqrt{f_c'}}{1000}\sin(\theta_{mtm})\cos(\theta_{mtm}) b_w z$$

$$V_{n\,max} = 30\frac{\sqrt{11330}}{1000}\sin(25^\circ)\cos(25^\circ)(6.0)(42.305) = 310.5 \text{ kips}$$

Shear capacity of Modified Truss Model using measured properties

$$\phi V_n = \min\left(\phi V_n,\ \phi V_{n\,max}\right) = \min\left(1(288.6),\ 1(310.5)\right) = 288.6 \text{ kips}$$

E.11 Horizontal Shear Capacity (AASHTO 1989)

The horizontal shear capacity for this method is based on the sum of a tie contribution and a concrete interface contribution. The method is to calculate the shear capacity at the interface of the deck and the top of the girder.

Minimum required tie area for composite action

$$A_{mt} = \frac{50 b_f s}{1000 f_y} = \frac{50(30.0)(16.0)}{1000(75.0)} = 0.32 \text{ in.}^2$$

Additional shear capacity provided when ties are greater than minimum required

$$V_v = \begin{cases} \dfrac{16000(A_v - A_{mt}) f_y}{40000 s} d, & \text{IF } A_{mt} < A_v \\ 0, & \text{IF } A_{mt} \geq A_v \end{cases}$$

$$V_v = \begin{cases} \dfrac{16000(0.40 - 0.32)(75.0)}{40000(16.0)}(47.006), & \text{IF } 0.32 < 0.40 \\ 0, & \text{IF } 0.32 \geq 0.40 \end{cases}$$

$$V_v = 7.05 \text{ kips}$$

Interface concrete contribution when minimum ties are provided, free of laitance, and intentionally roughened to 1/4 in.

$$V_{in} = \frac{350}{1000} b_f d = \frac{350}{1000}(30.0)(47.006) = 493.56 \text{ kips}$$

Horizontal Shear Capacity (AASHTO 1989) using measured properties

$$\phi V_{nh} = \phi(V_v + V_{in}) = 1(7.05 + 493.56) = 500.6 \text{ kips}$$

E.12 Modified Compression Field Theory

The shear capacity for this method is based on the sum of concrete, stirrup, and draping contributions. The sum of those three has a maximum limit. In addition, the shear capacity is limited by an anchorage-bond failure. Modified Compression Field Theory is given in AASHTO LRFD 1994. Tables 3.2 and 3.4 are referenced for determination of β and θ.

The concrete and stirrup contribution is a function of the crack angle. The crack angle is determined by an iterative process. An assumption is made for the first angle, θ_1. This angle was set as 30°. A total of three iterations are illustrated.

Flexural level arm

$$d_v = \max\left(0.72h,\quad d_p - d_c,\quad 0.9d_p\right)$$

$$d_v = \max\left(0.72(55.0),\quad 47.006 - 5.731,\quad 0.9(47.006)\right) = 42.305 \text{ in.}$$

Vertical component of effective prestressing force at the given cross section

$$V_p = \begin{cases} q_{td} A_p f_{se}\left(\dfrac{y_{d1} - y_{d2}}{12h.d.}\right), & \text{IF} \quad x \le h.d. \\ 0, & \text{IF} \quad x > h.d. \end{cases}$$

$$V_p = \begin{cases} 3.818(0.228)(123.0)\left(\dfrac{33.0 - 13.0}{12(53.1)}\right), & \text{IF} \quad 2.93 \le 53.1 \\ 0, & \text{IF} \quad 2.93 > 53.1 \end{cases}$$

$$V_p = 3.36 \text{ kips}$$

Ratio of shear stress to compressive strength used to determine crack angle according to AASHTO LRFD Eqn. 5.8.3.4.2-1

$$\frac{v}{f_c'} = \frac{\left(V_u - \phi V_p\right)}{\phi b_v d_v}\left(\frac{1000}{f_c'}\right) = \frac{(354.43 - 1(3.36))}{1(6.0)(42.305)}\left(\frac{1000}{11330}\right) = 0.122$$

Horizontal prestressing force used for stress calculation

$$P = f_{se} A_{pst} = 123.0(8.407) = 1034.1 \text{ kips}$$

Compressive stress at the centroid of the prestressed reinforcement due to effective prestressing force and due to flexural stresses

$$f_{pcm} = \frac{P}{A_g} + \frac{Pe^2}{I_g} - \frac{\left(M_{gird} + M_{deck}\right)e}{I_g}$$

$$f_{pcm} = \frac{1034.1}{623} + \frac{1034.1(14.386)^2}{166563} - \frac{(362.6 + 244.7)(14.386)}{166563} = 2.892 \text{ ksi}$$

Stress in the prestressing steel when the stress in the surrounding concrete is zero at the depth of the longitudinal reinforcement

$$f_{po} = f_{se} + \frac{f_{pcm} E_p}{E_c} = 123.0 + \frac{2.892(28800)}{4810} = 140.3 \text{ ksi}$$

Longitudinal strain in the reinforcement on the flexural tension side of the member for first iteration according to AASHTO LRFD Eqn. 5.8.3.4.2-2

$$\varepsilon_{x1} = \frac{\frac{M_u}{d_v} + 0.5N_u + 0.5V_u \cot(\theta_1) - A_{psd} f_{po}}{E_s A_s + E_p A_{psd}}$$

$$\varepsilon_{x1} x 1000 = \frac{\left(\frac{9770}{42.305}\right) + 0.5(0) + 0.5(354.43)\cot(30^\circ) - 4.128(140.3)}{0(0) + 28800(4.128)}(1000) = -0.348$$

Factor to reduce the strain in the tensile reinforcement according to AASHTO LRFD Eqn. 5.8.3.4.2-3 due to the concrete section being in compression at the level of reinforcement

$$F_e = \frac{E_s A_s + E_p A_{psd}}{E_c A_{gc} + E_s A_s + E_p A_{psd}} = \frac{0(0) + 28800(4.128)}{4810(1006.2) + 0(0) + 28800(4.128)} = 0.0240$$

If the value of ε_{x1} is positive, then the value is unchanged. If the value of ε_{x1} is negative, then the concrete section is in compression and ε_{x1} magnitudes will be reduced by the factor F_e.

$$\varepsilon_{x1}x1000 = \begin{cases} F_e\varepsilon_{x1}x1000, & \text{IF } \varepsilon_{x1}x1000 < 0 \\ \varepsilon_{x1}x1000, & \text{IF } \varepsilon_{x1}x1000 \geq 0 \end{cases}$$

$$\varepsilon_{x1}x1000 = \begin{cases} 0.0240(-0.348), & \text{IF } -0.348 < 0 \\ -0.0659, & \text{IF } -0.348 \geq 0 \end{cases}$$

$$\varepsilon_{x1}x1000 = -0.0084$$

Table 3.4 is used to determine the second crack angle

$$\theta_2 = 23.5^\circ$$

Longitudinal strain in the reinforcement on the flexural tension side of the member for second iteration

$$\varepsilon_{x2} = \frac{\frac{M_u}{d_v} + 0.5N_u + 0.5V_u \cot(\theta_2) - A_{psd} f_{po}}{E_s A_s + E_p A_{psd}}$$

$$\varepsilon_{x2}x1000 = \frac{\left(\frac{9770}{42.305}\right) + 0.5(0) + 0.5(354.43)\cot(23.5^\circ) - 4.128(140.3)}{0(0) + 28800(4.128)}(1000) = 0.498$$

If the value of ε_{x2} is positive, then the value is unchanged. If the value of ε_{x2} is negative, then the concrete section is compression and ε_{x2} magnitudes will be reduced by the factor F_e.

$$\varepsilon_{x2}x1000 = \begin{cases} F_e\varepsilon_{x2}x1000, & \text{IF } \varepsilon_{x2}x1000 < 0 \\ \varepsilon_{x2}x1000, & \text{IF } \varepsilon_{x2}x1000 \geq 0 \end{cases}$$

$$\varepsilon_{x2}x1000 = \begin{cases} 0.0240(0.498), & \text{IF } 0.498 < 0 \\ 0.498, & \text{IF } 0.498 \geq 0 \end{cases}$$

$$\varepsilon_{x2}x1000 = 0.498$$

Table 3.4 is used to determine the third crack angle

$$\theta_3 = 31.5^\circ$$

Longitudinal strain in the reinforcement on the flexural tension side of the member for third iteration

$$\varepsilon_{x3} = \frac{\frac{M_u}{d_v} + 0.5N_u + 0.5V_u \cot(\theta_3) - A_{psd} f_{po}}{E_s A_s + E_p A_{psd}}$$

$$\varepsilon_{x3}x1000 = \frac{\left(\frac{9770}{42.305}\right) + 0.5(0) + 0.5(354.43)\cot(31.5^\circ) - 4.128(140.3)}{0(0) + 28800(4.128)}(1000) = -0.498$$

If the value of ε_{x3} is positive, then the value is unchanged. If the value of ε_{x3} is negative, then the concrete section is compression and ε_{x3} magnitudes will be reduced by the factor F_e.

$$\varepsilon_{x3}x1000 = \begin{cases} F_e\varepsilon_{x3}x1000, & \text{IF } \varepsilon_{x3}x1000 < 0 \\ \varepsilon_{x3}x1000, & \text{IF } \varepsilon_{x3}x1000 \geq 0 \end{cases}$$

$$\varepsilon_{x3}x1000 = \begin{cases} 0.0240(-0.498), & \text{IF } -0.498 < 0 \\ -0.498 & \text{IF } -0.498 \geq 0 \end{cases}$$

$$\varepsilon_{x3}x1000 = -0.012$$

Table 3.4 is used to determine the fourth and final crack angle used to calculate stirrup contribution and anchorage capacity

$$\theta_4 = 23.5^\circ$$

Table 3.2 is used to determine the β factor used to calculate concrete contribution

$$\beta = 2.60$$

Concrete contribution according to AASHTO LRFD Eqn. 5.8.3.3-3

$$V_c = 0.0316\beta\sqrt{\frac{f_c'}{1000}}b_v d_v = 0.0316(2.60)\sqrt{\frac{11330}{1000}}(6.0)(42.305) = 70.2\,\text{kips}$$

Stirrup contribution according to AASHTO LRFD Eqn. C 5.8.3.3-1

$$V_s = \frac{A_v f_y d_v}{s}\cot(\theta_4) = \frac{0.4(75.0)(42.305)}{16.0}\cot(23.5^\circ) = 182.43\,\text{kips}$$

Total shear capacity according to AASHTO LRFD Eqn. 5.8.3.3-1

$$V_n = V_c + V_s + V_p = 70.20 + 182.43 + 3.36 = 256.0\,\text{kips}$$

Maximum shear capacity according to AASHTO LRFD Eqn. 5.8.3.3-2

$$V_{max} = 0.25\frac{f_c'}{1000}b_v d_v + V_p = 0.25\left(\frac{11330}{1000}\right)(6.0)(42.305) + 3.36 = 722.3\,\text{kips}$$

Anchorage or bond failure shear according to AASHTO LRFD Eqn. 5.8.3.5-1

$$V_{bond} = \frac{A_s f_y + A_{psd} f_{ps} - \dfrac{M_u}{d_v} - 0.5N_u}{\cot(\theta_4)} + 0.5V_s + V_p$$

$$V_{bond} = \frac{0(0) + 4.128(250.5) - \left(\dfrac{9770}{42.305}\right) - 0.5(0)}{\cot(23.5^\circ)} + 0.5(182.43) + 3.36 = 443.8\,\text{kips}$$

Shear Capacity of Modified Compression Field Theory using measured properties

$$\phi V_n = \min(\phi V_n,\ \phi V_{max},\ \phi V_{bond}) = \min(1(256.0),\ 1(722.3),\ 1(443.8)) = 256.0\,\text{kips}$$

Compare shear capacity with ultimate shear

$$(V_u = 354.4) > (\phi V_n = 256.0)$$

When the Modified Compression Field Theory is used for analytical purposes rather than design, another iteration process is required because the shear capacity is a function of the applied load.

When the ultimate shear is greater than shear capacity, the applied load will have to be reduced and the shear capacity will increase. When the ultimate shear is less than the shear capacity, the applied load will have to be increased and the shear capacity will reduce.

Therefore two iterative processes are required with the Modified Compression Field Theory to calculate shear capacity. The first iterative process is with the crack angle, and second iterative process is with applied load.

E.13 Interface Shear Model

This model uses a free body diagram given in Figure A.8. Shear capacity of the horizontal interface at the lower web and flange is calculated and compared with the applied force. The self weight and prestressing force were neglected.

Interface Shear Due to Load

Vertical moment arm between the location of interest and resultant compressive force

$$j_C = h - j_A - d_c = 55.0 - 35.5 - 5.731 = 13.77 \text{ in.}$$

Vertical moment arm between the location of interest and resultant tensile force

$$j_T = j_A - \left(h - d_p\right) = 35.5 - (55.0 - 49.609) = 30.11 \text{in.}$$

Shear at the interface due to applied load and stirrup yielding

$$V_{is} = \frac{12R_1(A_1 - a)}{j_T + j_C} - \frac{(F_{s8} + F_{s9})\cot(\theta_{ism})j_C + F_{s8}g_8 + F_{s9}g_9}{j_T + j_C}$$

$$V_{is} = \frac{12R_1(14.05 - 0.641)}{30.11 + 13.77} - \frac{\left(30.0 + 30.0\right)\cot\left(30^\circ\right)13.77 + 30.0(29.6) + 30.0(13.6)}{30.11 + 13.77}$$

$$V_{is} = 3.667R_1 - 62.1 \text{ kips}$$

Interface Shear Capacity by Shear Friction

Length of horizontal interface

$$g_i = 12A_1 - (j_A - j_i)\cot(\theta_{ism}) = 12(14.05) - (35.5 - 11.0)\cot(30^\circ) = 126.2\,\text{in.}$$

Area of horizontal interface

$$A_{cv} = g_i b_w = 126.2(6.0) = 757.0\,\text{in.}^2$$

Shear capacity of interface using Shear Friction AASHTO LRFD Eqn. 5.8.4.1-1

$$V_{sf} = \min\left(c_f A_{cv} + \mu\left(A_{vf} f_y + P_c\right),\ 0.2 f_c' A_{cv},\ 0.8 A_{cv}\right)$$

$$V_{sf} = \min\left(0.15(757.0) + 1.0(6.32(75.0) + 0),\ 0.2\left(\frac{11330}{1000}\right)(757.0),\ 0.8(757.0)\right)$$

$$V_{sf} = 587.5 \text{ kips}$$

Solve for reaction force for the Interface Shear Model using measured properties

$$V_{is} = V_{sf}$$

$$3.667R_1 - 62.1 = 587.5$$

$$R_1 = 177.2 \text{ kips}$$

Applied load for the Interface Shear Model using measured properties

$$P_1 = \frac{R_1 l}{\left(l - (A_1 - a)\right)} = \frac{177.2(39.81)}{(39.81 - (14.05 - 0.641))} = 267.1\,\text{kips}$$

Appendix F Shear Test Log

F.1 End IA

Load:	Observation:	Slides:	B&W:
no load	acoustic emission ground problem corrected	8	12
20	no new cracks	-	-
40	no new cracks	-	-
60	no new cracks	-	-
80	no new cracks	-	-
100	cracks reopening	-	-
120	little acoustic emission activity during hold	-	-
140	new crack at 6 ft. marked in green	-	-
160	acoustic emission active at 5 ft. new crack at 5-8 ft., 0.002 in.	-	-
180	acoustic emission between 5 and 10 ft. new crack at 8 ft. top of the web, 0.002 in.	-	-
200	new cracks at base of web, noncontinuous, 0.002 in.	13	15
220	main diagonal crack still 0.002 in.	-	-
240	-	-	-
260	crack width increase with no growth in length	-	-
280	-	-	-
300	-	16	19
320	no new diagonal cracks	-	-

340		-	-	-
360		new crack at end near the base of web new diagonal crack	-	-
380		acoustic emission active between 5 and 10 ft.	18	
	21	sound of concrete cracking all new diagonals cracks		
400		no new cracks, little growth in length	-	-
420		-	-	-
440		loud sound, new diagonal cracks	23	25
460		loud sound	-	-
480		new diagonal crack near load point	-	-
500		loud sound, large crack at the base of the web	-	-
503		cracks in the upper flange & deck load loss	-	-

F.2 End IB

Load:	Observation:	Slides:	B&W:
330	-	1	15
380	diagonal crack starting from 280 kip crack	2,3	16
400	-	4	17
420	-	5,6	18
435	loud sound	7	-
450	-	8-11	-
460	-	-	19,20
480	-	12	-
500	-	13,14	21,22
520	-	15	-
load loss	-	16-24	-
no load	-	1-7	-

F.3 End IIC

Load:	Observation:	Slides:	B&W:
no load	acoustic emission wired incorrectly	11	11
20	pad under load point still not in full contact	-	-
40	pad in full contact	-	-
60	no sounds or new cracking	-	-
80	no sounds or new cracking	-	-
100	no sounds, cracks checked closely slight crack growth in length	12	12
120	no sounds or new cracking	-	-
140	no sounds or new cracking	-	-
160	no sounds, cracks checked closely crack growth in length, one new crack	13	13
180	no sounds	14	14
200	no sounds	0	16
220	no sounds	-	-
240	no sounds	3	17
260	no sounds	4	18
280	no sounds	-	-
300	no sounds	7	21
320	no sounds	8	-
340	no sounds, few new cracks	-	-

360	no sounds	9	22
380	no sounds, few new cracks	-	-
400	no sounds, few new cracks	11	23
420	-	12	24
440	few cracks	-	-
460	growth width in diagonal cracks	-	-
480	few new cracks	17	4
500	start spalling at base of web	-	-
520	continued spalling at base of web	19	5
540	loud sounds, continued spalling	21	6
560	loud sounds	-	-
580	nothing new	-	-
600	nothing new	-	-
620	peak load	35	18
430	past peak load	4	26

F.4 End IID, Day 1

Load:	Observation:	Slides:	B&W:
40	almost full connection of neoprene and steel	-	-
60	acoustic emission started and nothing active	-	-
80	nothing	-	-
120	checked for new crack, nothing	-	-
140	existing cracks are not growing in length	-	-
160	same	-	-
180	growth of cracks from 0-2 ft. at top of web acoustic emission between 0-2 ft. and 7-10 ft.	-	-
200	no new growth in length	-	-
220	more growth in 180 kip crack at 0-2 ft.	-	-
240	-	20	-
260	little to no growth in cracks	-	-
280	nothing has changed	-	-
300	new crack from 0-2 ft. at top of web new diagonal cracks from 5-7 ft. in web	-	-
320	diagonal crack on both sides	21,22	-
340	diagonal crack growth in length and size	-	-
360	multiple diagonal cracks	-	-
380	same	-	-
400	same	-	-

420	crack at base of the web	1-5	-
440	-	-	-
460	video tape changed	7	4
480	sound of cracking during loading	-	-
500	-	-	-
520	-	9	5,6
540	finished with crack mapping lighting moved	-	-
560	new sound near load point	-	-
580	another sound near load point	-	-
600	spalling at 440 kip crack at base of web	-	-
620	load reset	12	9
630	-	13	-
no load	test ended at 4:30 PM		

F.4 End IID, Day 2

Load:	Observation:	Slides:	B&W:
no load		16	13
100	nothing	-	-
200	nothing	-	-
300	nothing	-	-
400	nothing	-	-
450	spalling of existing cracks	-	-
500	long time break	-	-
550	no visible slip of strand	-	-
600	-	-	-
620	sounds	-	-
640	flaking of concrete, long time break	-	-
650	sounds	-	-
660	sounds	-	-
670	loud sound	-	-
672	loud sound	-	-
555	unloaded	-	-
740	reloaded	-	-